Instituto de Agrobiotecnología

Consejo Superior de Investigaciones Científicas-Gobierno de Navarra

Departamento de Agronomía, Biotecnología y Alimentación

Universidad Pública de Navarra

Implicación del metabolismo bacteriano en la interacción de *Haemophilus influenzae* con el sistema respiratorio humano: bases moleculares y explotación terapéutica

TESIS DOCTORAL presentada por:

Nahikari López López

Directores:

Dra. Junkal Garmendia García

Dr. Roberto Díez-Martínez

Pamplona, 2021

https://doi.org/10.48035/Tesis/2454/42510

La Dra. Junkal Garmendia García, Científico Titular del Consejo Superior de Investigaciones Científicas (CSIC), adscrita al grupo de Biología Molecular de Patógenos Bacterianos del Instituto de Agrobiotecnología, y el Dr. Roberto Díez-Martínez, CEO de Telum Therapeutics,

INFORMAN,

Que la presente memoria de Tesis Doctoral "Implicación del metabolismo bacteriano en la interacción de *Haemophilus influenzae* con el sistema respiratorio humano: bases moleculares y explotación terapéutica", elaborada por Nahikari López López bajo su dirección, cumple las condiciones exigidas por la legislación vigente para optar al grado de Doctor.

Y para que así conste, firma la presente en Pamplona, a 24 de noviembre de 2021.

GARMENDIA GARCIA JUNCAL - 15258061E
Firmado digitalmente por GARMENDIA GARCIA JUNCAL - 15258061E
Fecha: 2021.11.24 09:44:57 +01'00'

Fdo. Junkal Garmendia García

DIEZ MARTINEZ ROBERTO - 71929420W
Digitally signed by DIEZ MARTINEZ ROBERTO - 71929420W
Date: 2021.11.24 10:56:35 +01'00'

Roberto Díez-Martínez

Este trabajo de Tesis Doctoral se ha desarrollado mediante el disfrute de los siguientes contratos: Gobierno de Navarra ha subvencionado la contratación de Nahikari López López en el marco de la convocatoria de ayudas "Doctorados industriales 2018-2020", referencia 0011-1408-2017-000000. Contrato con cargo a proyecto Retos Investigación de la Agencia Estatal de Investigación, referencia RTI2018-096369-B-I00, cuya Investigadora Principal es la Dra. Junkal Garmendia.

Agradecimientos

En primer lugar, quiero agradecer al Gobierno de Navarra y a la Agencia Estatal de Investigación la financiación que ha posibilitado el desarrollo de esta Tesis Doctoral. Gracias a la Universidad Pública de Navarra (Upna), al Departamento de Agronomía, Biotecnología y Alimentación, al grupo de Biotecnología y a mi tutora de la Upna, la Dra. Inmaculada Farran.

Sin duda, mi mayor gracias a nivel profesional es para mi Directora de Tesis, la Dra. Junkal Garmendia, por creer que era capaz de lograrlo desde el principio, por apoyarme y dirigirme en esta etapa en la que no han faltado los obstáculos, pero que hemos logrado superar de la mejor manera posible. Gracias por el tiempo que me has dedicado. Has sido mi mayor referente estos años y por fín puedo decir que el esfuerzo que hemos hecho ha dado sus frutos. Gracias. Por supuesto, gracias a mi co-director de Tesis, el Dr. Roberto Díez-Martínez, CEO de Telum Therapeutics. Te estoy infinitamente agradecida por permitirme realizar esta Tesis.

Quiero agradecer a todas las personas que han permitido la realización de cada parte de esta Tesis. Especialmente a la Dra. Mariette Barbier, de la West Virginia University y al Dr. Juan Nogales, del Centro Nacional de Biotecnología (CNB), por acogerme durante mis estancias como a una más de vuestro equipo, gracias por vuestro tiempo y por todo lo que me habéis enseñado. Gracias a los Doctores: Ulrike Kappler, de The University of Queensland; Margarita Menéndez, del Instituto de Química Física Rocasolano (IQFR); María José Camarasa, del Instituto de Química Médica (IQM); José Leiva, de la Universidad de Navarra; Jeroen Langereis, de Radboud University Medical Center; José Ramos Vivas, del Instituto de Investigación Sanitaria Valdecilla (Idival); y Lars M. Blank, de Institute of Applied Biotechnology, RWTH Aachen University. Gracias también a Emel Sen-Kilic y a David San León por vuestro trabajo.

Gracias a todo el personal del IdAB, especialmente a Víctor y Mari Jose, gracias por todo lo que me habéis ayudado estos años. Por supuesto, gracias a mis compañeros de laboratorio, Bea, María, Javi y especialmente a Begoña, Celia y Ari. Habéis sido fundamentales estos años y tengo mucho que agradeceros. Gracias por TODO.

Gracias a mis amigas, Sara, Sonia, Nat y Ainara. Gracias por escucharme, por entender mis horarios locos, por preocuparos por mí y animarme de principio a fin. Sois muy importantes para mí.

Gracias a mi familia. Gracias mamá y Patri, por quererme tanto y creer en mí siempre, por vuestros ánimos, por darme todo lo que sois. Esto no habría sido posible sin tí, mamá. Os quiero más que a nada en el mundo. Gracias también a mi yaya Rosa porque, aunque estemos lejos, sé que te preocupas mucho por mí.

Gracias a ti, Adrián, gracias por tantas cosas que no caben aquí. Gracias por ser mi principal apoyo en esto, por hacerme ver siempre el vaso medio lleno, por hacerme creer que puedo con esto y más. Por aguantarme en los días malos y disfrutar conmigo en los buenos. Gracias a tus padres, por su apoyo. Por fín podemos decirlo: lo hemos conseguido.

A mi madre.

A mi hermana.

A Adrián.

Lista de Abreviaturas.....1
Lista de Figuras.....13
Lista de Tablas.....19
Resumen & Abstract.....23
Introducción General.....29
1. Sistema respiratorio humano.....31
1.1. Características anatómicas.....31
1.2. Inmunidad del sistema respiratorio humano.....31
1.2.1. Barreras mecánicas.....31
1.2.2. Elementos celulares y reconocimiento de patógenos.....32
1.2.3. Elementos humorales.....33
1.2.4. Inmunidad nutricional.....35
1.3. Microbioma: composición, funciones y señalización.....35
1.3.1. El microbioma del aparato respiratorio humano.....35
1.3.2. El eje intestino-pulmón.....38
1.3.3. Patógenos oportunistas colonizadores en el sistema respiratorio humano.....40
2. *Haemophilus influenzae*: patógeno oportunista colonizador del sistema respiratorio humano.....41
2.1. Características generales de *H. influenzae*.....41
2.2. Características genómicas y adaptativas de HiNT.....43
2.2.1. Competencia natural.....44
2.2.2. Características metabólicas de *H. influenzae* y su relevancia durante la infección.....49
2.2.2.1. Metabolismo de azúcares en *H. influenzae*.....51
2.2.2.2. Metabolismo de ácidos grasos en *H. influenzae*.....53
2.3. Interacción de *H. influenzae* con el sistema respiratorio humano: mecanismos de colonización y estilos de vida.....55
2.3.1. Factores de HiNT implicados en la evasión de elementos de la inmunidad respiratoria.....55
2.3.1.1. Formación de biopelículas de HiNT.....58
2.3.2. Infección del epitelio respiratorio.....59
2.3.2.1. Adhesión de HiNT al epitelio respiratorio.....60
2.3.2.2. Invasión y vida intracelular de HiNT en el epitelio respiratorio.....60
3. Estrategias terapéuticas frente a *H. influenzae*: situación actual y nuevas oportunidades.....61
3.1. Terapias empleadas frente HiNT y problemas asociados.....61
3.2. Desarrollo de nuevas terapias antimicrobianas frente a la infección por *H. influenzae*.....63
3.1.1. Enzimas de la ruta FASII como dianas antimicrobianas frente a la infección por HiNT.....64
Hipótesis y Objetivos.....67
Resultados.....71
Capítulo 1. Learning from -omics strategies applied to uncover *Haemophilus influenzae* host-pathogen interactions: Current status and perspectives.....77
1.1. Abstract.....81
1.2. Introduction.....82
1.3. Constantly evolving information from *H. influenzae* whole genome sequencing.....82
1.3.1. *H. influenzae* population structure.....82
1.3.2. NTHi isolates from COPD patients: genetic signatures and pathoadaptive traits.....85
1.3.3. WGS insights into DNA uptake, natural transformation and natural genetic variation by *H. influenzae*.....86
1.3.4. Single-molecule real-time (SMRT) sequencing contribution to *H. influenzae* phase-variable methylome analyses.....87

1.3.5. Genome-scale microevolution and genetic screening approaches shed light on NTHi adaptation and pathogenesis……89
1.4. Unraveling features of the *H. influenzae*-host interplay by genome-wide gene expression profiling…90
1.5. Update on *H. influenzae* protein and metabolite profiling……...92
1.6. Future Outlook……94
Capítulo 2. Multi-omic analysis of *Haemophilus influenzae* metabolic requirements during murine lung infection by combining RNA-seq and Tn-seq technologies……..95
2.1. Abstract……99
2.2. Introduction …….. 100
2.3. Material & Methods……...101
2.3.1. Bacterial strains and growth conditions……...101
2.3.2. Generation of *H. influenzae* mutant strains……102
2.3.3. Generation of the RdKW20 transposon mutant library……103
2.3.4. Animal handling……103
2.3.5. Animal procedures…….. 103
2.3.6. RNA extraction, purification and further processing……..105
2.3.7. Readout transposon mutant libraries……107
2.3.8. Data analysis……108
2.3.8.1. RNA-seq data analysis……..108
2.3.8.2. Tn-seq data analysis……..108
2.3.9. Statistical analysis…….. .109
2.4. Results……... 109
2.4.1. Airway infection triggers both host and pathogen transcriptional reprogramming – global gene expression analyses of *H. influenzae* and the murine lung……109
2.4.2. *H. influenzae* gene expression changes during infection……111
2.4.3. Establishing a correlation between gene up-regulation and virulence……114
2.4.4. Analysis of the effect of *sBHI to BALF* and *sBHI to MIV* transitions sheds light on *in vivo* natural competence requirements……..115
2.4.5. Identification of *H. influenzae* genes required for *in vivo* fitness by transposon insertion sequencing screening……...117
2.5. Supplementary Material……120
Capítulo 3. *Haemophilus influenzae* glucose catabolism leading to production of the immunometabolite acetate has a key contribution to the host airway-pathogen interplay……..131
3.1. Abstract……...135
3.2. Introduction …….. 136
3.3. Material & Methods……...138
3.3.1. Bacterial strains and growth conditions……...138
3.3.2. Generation of *H. influenzae* mutant strains……139
3.3.3. Western blotting……..140
3.3.4. Determination of bacterial metabolite concentrations……140
3.3.5. Transmission electron microscopy (TEM)……..141
3.3.6. Immunofluorescence microscopy……141
3.3.7. Bacteria and host gene expression analyses……141
3.3.8. NTHi mouse lung infection……142
3.3.9. Statistical analysis……... 143
3.4. Results……... 143
3.4.1. Metabolic end products produced by *H. influenzae* persistent isolates from chronic lung disease are similar to those detected in reference strains……143

3.4.2. Inactivation of genes involved in the production of metabolic end products affects the growth of NTHi with glucose as the main carbon source……..145
3.4.3. *H. influenzae ackA*, *pflA*, and *frdA* gene inactivation modifies the production of metabolic end products in response to changing oxygen tensions……146
3.4.4. Mutations in genes involved in NTHi central carbon metabolism alter gene expression patterns, revealing complex adaptations……..149
3.4.5. The inability to produce large amounts of acetate reduces NTHi survival in a mouse model of lung infection……151
3.4.6. *H. influenzae* metabolic end products have a proinflammatory effect on airway epithelial cells..153
3.5. Supplementary Material……155
Capítulo 4. Interrogation of essentiality in the reconstructed *Haemophilus influenzae* metabolic network identifies lipid metabolism antimicrobial targets: preclinical evaluation of a FabH β-ketoacyl-ACP synthase inhibitor……...161
4.1. Abstract……165
4.2. Introduction……...166
4.3. Material & Methods……...167
4.3.1. Bacterial strains, media, growth conditions, and drugs……167
4.3.2. Determination of bacterial dry weight……167
4.3.3. Constraints-based analysis…….. 168
4.3.4. Model constraints……168
4.3.5. Essentiality analysis…… 168
4.3.6. Synthesis of FabHi……...169
4.3.7. FabHi docking studies……169
4.3.8. Determination of FabHi antimicrobial effects……169
4.3.9. Bacteria gene expression analyses……...169
4.3.10. Infection of cultured cells……..169
4.3.11. NTHi adult zebrafish infection……..169
4.3.12. Statistical analyses……170
4.4. Results…….. ……..170
4.4.1. Construction, main features and consistence of *i*NL638, a high-quality model of *H. influenzae* RdKW20……...……170
4.4.2. *i*NL638 accurately predicts *H. influenzae* RdKW20 main metabolic features……172
4.4.3. Defining condition independent gene essentiality in *H. influenzae*……172
4.4.4. Model-based search of *H. influenzae* essential genes highlights lipid metabolism targets……173
4.4.5. *In silico* envisioning of FabHi binding mode……...179
4.4.6. FabHi has an antimicrobial effect on *H. influenzae* growth……180
4.4.7. Heterogeneity of FabHi antimicrobial effect among strains: assesing possible causes……...184
4.4.8. FabHi antimicrobial effect does not exclusively relate to the *fabH* gene allelic variant……185
4.4.9. FabHi does not induce bacterial resistance, antibiotic synergies or cytotoxicity……186
4.4.10. FabHi efficacy preclinical testing reveals a protective effect on zebrafish systemic infection with NTHi……187
4.5. Supplementary Material……190
4.5.1. Bacterial strains, media, growth conditions, and drugs……190
4.5.2. Determination of FabHi antimicrobial effects…… 190
4.5.2.1. Dose dependent FabHi antibacterial effect under bacterial planktonic or biofilm growth…..190
4.5.2.2. Antimicrobial synergic effects……..191
4.5.2.3. Serial passage experiments with FabHi……191
4.5.3. Inactivation of the *fabH* gene……..191
4.5.4. Model construction and manual curation……192

4.5.5. Biomass Objetive Function (BOF) formulation……..193
4.5.6. Constraints used to simulate *in silico* CDM medium……..193
4.5.7. FabHi docking studies……197
4.5.8. Bacteria gene expression analyses……...198
4.5.9. Infection of cultured cells……198
Discusión General……225
1. *In vivo* multi-omics approach us to understand genetics traits associated with NTHi bacterial infection…..228
2. The importance of NTHi glucose catabolism as a potential enhancer of chronic lung disease……231
3. The increasing focus on fatty acid biosynthesis as a therapeutic target……234
Conclusiones……239
Referencias……..243
Anexo I. Tablas Suplementarias……283
Anexo II. Publicaciones que Avalan esta Tesis Doctoral……341
Anexo III. Otras Publicaciones en las que la Doctoranda ha participado……383

Lista de Abreviaturas

µg	Microgramo
µL	Microlitro
µm	Micrómetro
H NMR	Del inglés, *proton nuclear magnetic resonance*, resonancia magnética nuclear de protones
Å	Ångström
A1	Alelo 1
A2	Alelo 2
A3	Alelo 3
A4	Alelo 4
A5	Alelo 5
A6	Alelo 6
A7	Alelo 7
A8	Alelo 8
A9	Alelo 9
A10	Alelo 10
A11	Alelo 11
A12	Alelo 12
A13	Alelo 13
A14	Alelo 14
Ab	Del inglés, *antibody*, anticuerpo
Acet	Ácido acético
ACP	Del inglés, *acyl carrier protein*, proteína transportadora de acilo
ADN	Ácido desoxirribonucleico
ADNe	ADN extracelular
AECOPD	Del inglés, *acute exacerbations of COPD*, exacerbaciones agudas de EPOC
AI-2	Del inglés, *autoinducer-2*, autoinductor-2
AICAR	Ribonucleótido 5-aminoimidazol-4-carboxamida
AIN	Asociación de la Industria Navarra
Ala	Alanina
Amp	Ampicilina
AMPc	Adenosín monofosfato cíclico
AMPs	En inglés, *antimicrobial peptides*, péptidos antimicrobianos
ANOVA	Análisis de la varianza
Arg	Arginina
ARN	Ácido ribonucleico
ARNm/mRNA	ARN mensajero
ARNt	ARN de transferencia
ASL	En inglés, *airway surface liquid*, líquido de la superficie de las vías respiratorias
Asn	Asparagina
ATP	Adenosín trifosfato
BALF	Del inglés, *bronchoalveolar lavage fluid*, lavado broncoalveolar
BCCP	Del inglés, *biotin carboxyl carrier protein*, proteína transportadora de biotina carboxilo
B-H	Benjamin-Hochberg
BHI	Del ingles, *brain-heart infusion medium*, medio infusión cerebro-corazón
BLNAR	Del inglés, *β-lactamase-negative ampicillin resistance*, β-lactamasa negativa ampicilina-resistente
BOF	Del inglés, *biomass objective function*, función objetivo de biomasa
C	Carbono
c.f.u.	Del inglés, *colony-forming unit*, unidad formadora de colonias
C2	Dos átomos de carbono

Lista de Abreviaturas

C3	Tres átomos de carbono
C4	Cuatro átomos de carbono
C4BP	Proteína de unión C4b
CC	Quimiocina C-C
CCD	Del inglés, *charge-coupled device*, dispositivo de carga acoplada
CDH	Cadherina
CDM	Del inglés, *chemically defined medium*, medio químicamente definido
cDNA	ADN complementario
CEACAM-1	Del inglés, *carcinoembryonic antigen-related cell adhesion molecule 1*, molécula 1 de adhesión celular relacionada con el antígeno carcinoembrionario
CEIN	Centro Europeo de Empresas e Innovacion de Navarra
CFTR	Del inglés, *cystic fibrosis transmembrane conductance regulator*, regulador de la conductancia transmembrana de la fibrosis quística
FQ/CF	Fibrosis quística/del inglés, *cystic fibrosis*, fibrosis quística
cCDM	CDM completo
ChoP/PCho	Fosforilcolina
CI	Del inglés, *competitive index*, índice de competencia
CIBERES	Centro de Investigación Biomédica en Red de Enfermedades Respiratorias
CLDN	Claudina
CLR	Del inglés, *C-type lectin receptor*, receptor tipo C-lectina
CNB	Centro Nacional de Biotecnología
CO_2	Dióxido de carbono
CoA	Coenzima A
Com	Complementado
COX	Ciclooxigenasa
CRE	Del inglés, *competence regulatory element*, elemento regulador de competencia
CRP	cAMP *receptor protein*
CRP-N	Sitio de unión a CRP canónico
CRP-S	Sitio de unión a CRP dependiente de Sxy
Cs	Del inglés, *carbon source*, fuente de carbono
CSIC	Consejo Superior de Investigaciones Científicas
Ct	Del inglés, *cycle threshold*, ciclo umbral comparativo
CT	Del inglés, *clonal type*, tipo clonal
Cu_2	Cobre
CXCL	Quimiocina C-X-C
Cy2	Cianina 2
Cys	Del inglés, *cysteine*, cisteína
dH_2O	Agua destilada
DMSO	Dimetilsulfóxido
DW	Del inglés, *dry weight*, peso seco
dNTP	Del inglés, *deoxynucleoside triphosphate*, trifosfato de desoxinucleósido
DTT	Ditiotreitol
EBSS	Del inglés, *Earle´s balanced salts medium*
EC	Del inglés, *enzyme commission number*, número de la comisión de enzimas
ECM	Del inglés, *extracellular matrix*, matriz extracelular
EDGE	Del inglés, *extraction of differential gene expression*, extracción de expresión genética diferencial
EDTA	Acido etilendiaminotetraacético
EPOC/COPD	Enfermedad Pulmonar Obstructiva Crónica/del inglés, *Chronic Obstructive Pulmonary Disease*

Erm	Eritromicina
EX_4abz(e)	Intercambio de aminobenzoato con el medio externo
EX_4hpro_DC(e)	Intercambio de hidroxiprolina con el medio externo
EX_arg_L(e)	Intercambio de arginina con el medio externo
EX_asn_L(e)	Intercambio de aspargina con el medio externo
EX_asp_L(e)	Intercambio de aspartato con el medio externo
EX_btn(e)	Intercambio de biotina con el medio externo
EX_ca2(e)	Intercambio de calcio con el medio externo
EX_chol(e)	Intercambio de colina con el medio externo
EX_cl(e)	Intercambio de cloro con el medio externo
EX_cobalt2(e)	Intercambio de cobalto con el medio externo
EX_cu2(e)	Intercambio de cobre con el medio externo
EX_cys_L(e)	Intercambio de cisteína con el medio externo
EX_dhf(e)	Intercambio de dihidroxifolato con el medio externo
EX_fe2(e)	Intercambio de hierro ferroso con el medio externo
EX_fe3(e)	Intercambio de hierro férrico con el medio externo
EX_glc(e)	Intercambio de glucosa con el medio externo
EX_gln_L(e)	Intercambio de glutamina con el medio externo
EX_glu_L(e)	Intercambio de glutamato con el medio externo
EX_gly(e)	Intercambio de glicina con el medio externo
EX_gthrd(e)	Intercambio de glutatión reducido con el medio externo
EX_his_L(e)	Intercambio de histidina con el medio externo
EX_ile_L(e)	Intercambio de isoleucina con el medio externo
EX_inost(e)	Intercambio de mioinositol con el medio externo
EX_ins(e)	Intercambio de inosina con el medio externo
EX_k(e)	Intercambio de potasio con el medio externo
EX_leu_L(e)	Intercambio de leucina con el medio externo
EX_lys_L(e)	Intercambio de lisina con el medio externo
EX_met_L(e)	Intercambio de metionina con el medio externo
EX_mg2(e)	Intercambio de magnesio con el medio externo
EX_mn2(e)	Intercambio de manganeso con el medio externo
EX_mobd(e)	Intercambio de molibdeno con el medio externo
EX_na1(e)	Intercambio de sodio con el medio externo
EX_nad_(e)	Intercambio de NAD con el medio externo
EX_ni2(e)	Intercambio de niquel con el medio externo
EX_nmn(e)	Intercambio de nicotinamida mononucleótido con el medio externo
EX_no3(e)	Intercambio de nitrato con el medio externo
EX_o2(e)	Intercambio de oxígeno con el medio externo
EX_phe_L(e)	Intercambio de fenilalanina con el medio externo
EX_pheme(e)	Intercambio de protohemina con el medio externo
EX_pi(e)	Intercambio de fósforo inorgánico con el medio externo
EX_pnto_R(e)	Intercambio de pantotenato con el medio externo
EX_pro_L(e)	Intercambio de prolina con el medio externo
EX_pydxn(e)	Intercambio de piridoxina con el medio externo
EX_pyr(e)	Intercambio de piruvato con el medio externo
EX_rbf(e)	Intercambio de riboflavina con el medio externo
EX_ser_L(e)	Intercambio de serina con el medio externo
EX_so4(e)	Intercambio de sulfato con el medio externo
EX_spmd(e)	Intercambio de espermidina con el medio externo
EX_thm(e)	Intercambio de tiamina con el medio externo
EX_thr_L(e)	Intercambio de treonina con el medio externo
EX_trp_L(e)	Intercambio de triptófano con el medio externo
EX_tyr_L(e)	Intercambio de tirosina con el medio externo
EX_ura(e)	Intercambio de uracilo con el medio externo

Lista de Abreviaturas

EX_val_L(e)	Intercambio de valina con el medio externo
EX_zn2(e)	Intercambio de zinc con el medio externo
FabHi	Inhibidor de FabH
$FADH_2$	Flavín adenín dinucleótido reducido
FAK	Del inglés, *focal adhesion kinase*, quinasa de adhesión focal
FASII	Del inglés, *fatty acid biosynthesis* II, biosíntesis de ácidos grasos II
FBA	Del inglés, *flux balance analysis*, análisis del balance de flujo
FCS	Del inglés, *fetal calf serum*, suero de ternera fetal
FDH	Formato deshidrogenasa
Fe	Hierro
$Fe2^+$	Ion ferroso
$Fe3^+$	Ion férrico
FeHm	Hierro-hemina
FET	Del inglés, *fish embryo acute toxicity*, toxicidad aguda en embriones de pez
FFARs	Del inglés, *free fatty acids receptors*, receptores de ácidos grasos
FIC	Del inglés, *fractional inhibitory concentration*, concentración inhibitoria fraccionada
Form	Ácido fórmico
Fw/F	Del inglés, *forward*, delantero
GAM	Del inglés, *growth-associated maintenance*, mantenimiento asociado al crecimiento
gDNA	ADN genómico
GEM	Del inglés, *genome-scale metabolic model*, modelo metabólico a escala genómica
Gln	Glutamina
Glu	Glutamato
GLUTs	Del inglés, *facilitative glucose transporters*, transportadores facilitadores de glucosa
Gly	Glicina
GPC	Del inglés, *glycerophosphocholine*, glicerofosforilcolina
GPR	Del inglés, *gene-protein-association*, asociación gen-proteína
GWAS	Del inglés, *pan-genome-wide association studies*, asociación del genoma completo
h	Hora
H	Hidrógeno
H_2O	Agua
H_2O_2	Peróxido de hidrógeno
HCl	Ácido clorhídrico
HDAC	Histona deacetilasa
HF	Del inglés, *high-fidelity*, alta fidelidad
HGT	Del inglés, *horizontal gene transfer*, transferencia horizontal de genes
Hia	*H. influenzae* serotipo a
Hib	*H. influenzae* serotipo b
Hif	*H. influenzae* serotipo f
HiNT/NTHi	*H. influenzae* no tipificable/del inglés, *nontypeable H. influenzae*
HiNT-CVs	Del inglés, *HiNT-containing vacuole,* vacuola que contiene HiNT
His	Histidina
HITS	Del inglés, *high-throughput insertion tracking by deep sequencing*, seguimiento de inserción de alto rendimiento mediante secuenciación profunda
HK	Del inglés, *heat-killed*, inactivado por calor
hpi	Hora post-infección

HPLC	Del inglés, *high performance liquid chromatography*, cromatografía líquida de alta eficacia
HPLC-MS	HPLC acoplada a espectrometría de masas
HRV	Del inglés, *human rhinovirus*, rinovirus humano
HTM	Del inglés, *Haemophilus Test Medium*, medio de prueba de Haemophilus
Hypo	Hipoxantina
Hz	Hercio
IAV	Del inglés, *Influenza A virus*, Virus de la influenza A
IBCs	Del inglés, *intracellular bacterial communities*, comunidades bacterianas intracelulares
IC	Del inglés, *inhibitory concentration*, concentración inhibitoria
ICAM-1	Del inglés, *intercellular adhesion molecule 1*, molécula de adhesión intercelular 1
ID	Identificador
IdAB	Instituto de Agrobiotecnología
IdiSNA	Instituto de Investigación Sanitaria de Navarra
IDIVAL	Instituto de Investigacion Marqués de Valdecilla
IFN-γ	Interferón
Ig	Inmunoglobulina
IHF	Del inglés, *integration host factor*, factor de integración del huésped
IL	Interleucina
Ile	Isoleucina
IMP	Inosina monofosfato
IN-seq	Del inglés, *insertion sequencing*, secuenciación por inserción
IQFR	Instituto de Física Química Rocasolano
IQM	Instituto de Química Médica
IR	Del inglés, *inverted repeats*, repeticiones invertidas
IRF	Del inglés, *interferon regulatory factor*, factores de regulación de interferón
K	Potasio
kb	Kilobase
KDa	Kilodalton
Kdo	Ácido 3-desoxi-d-mano-octulosónico
kV	Kilovoltio
LAMP1	Del inglés, *lysosome-associated membrane protein 1*, proteína 1 asociada a la membrana del lisosoma
LB	Medio Luria−Bertani
LCFAs	Del inglés, *long chain fatty acids*, ácidos grasos de cadena larga
Leu	Leucina
Log10	Logaritmo en base 10
LOS	Lipooligosacárido
LPS	Lipopolisacárido
Lys	Del inglés, *lysine*, lisina
M	Molar
MALDI-TOF	Del inglés, *matrix-assisted laser desorption ionization time-of flight*, desorción-ionización mediante láser asistida por matriz acoplada a tiempo de vuelo
MAPKs	Del inglés, *mitogen-activated protein kinases*, proteínas quinasas activadas por mitógenos
Mb	Megabase
mbar	Milibar
mCDM	CDM mínimo
MDB	Del inglés, *membrane desalting buffer*, tampón de desalación de membrana

Lista de Abreviaturas

MEM	Del inglés, *minimum essential medium*, medio esencial mínimo
Met	Metionina
mg	Miligramos
Mg	Magnesio
MH-F	Medio Mueller Hinton-Fastidioso
MHz	Megahercios
MIC	Del inglés, *minimal inhibitory concentration*, concentración mínima inhibitoria
min	Minuto
MIV	Medio de inducción de competencia de *H. influenzae*
mL	Mililitro
Mla	Del inglés, *maintenance of the lipid asymmetry*, mantenimiento de la asimetría lipídica
MLST	Del inglés, *multilocus sequence typing*, tipificación multilocus de secuencia
mM	Milimolar
mm	Milímetro
MM	Medio mínimo
mmol.gDW-1.h-1	Milimoles por gramo de peso seco por hora
MMP-9	Metaloproteinasa de matriz-9
Mn2	Manganeso
MOI	Del inglés, *multiplicity of infection*, multiplicidad de infección
MOMA	Del inglés, *minimization of metabolic adjustments*
MUC5AC	Mucina 5C
MUC5B	Mucina 5B
Mϕ	Macrófago
N	Nitrógeno
N	Normal
N_2	Nitrógeno
NAD	Nicotinamida-adenina-dinucleótido
NAD^+	Nicotinamida-adenina-dinucleótido oxidado
NADH	Nicotinamida-adenina-dinucleótido reducido
NADP	Nicotinamida-adenina-dinucleotido fosfato
NaOH	Hidróxido sódico
NCBI	Del inglés, *National Center for Biotechnology Information*, Centro Nacional de Información Biotecnológica
NETs	Del inglés, *neutrophil extracellular traps*, trampas extracelulares de neutrófilos
NF-κB	Factor nuclear-κB
ng	Nanogramos
NGAM	Del inglés, *non-growth-associated maintenance*, mantenimiento no asociado al crecimiento
Ni_2	Niquel
NLR	Del inglés, *NOD-like receptors*, receptores de tipo NOD
nm	Nanómetro
NMN	Mononucleótido de nicotinamida
No.	Número
Nov	Novobiocina
NP	Del inglés, *nasopharynx*, nasofaringe
O_2	Oxígeno
OD	Del inglés, *optical density*, densidad óptica
OECD	Del inglés, *Organisation for economic co-operation and development*
OFF	Apagado
OM	Otitis media

OMP	Del inglés, *outer membrane protein*, proteína de membrana externa
OMS/WHO	Organización Mundial de la Salud/del inglés, *World Health Organization*
ON	Encendido
P	Fósforo
p. ej./ i. e.	Por ejemplo/del latin, *in exempla*
PAF	Del inglés, *platelet activating factor*, factor activador de plaquetas
PAFr	Receptor de PAF
PAMPs	Del inglés, *pathogen-associated molecular patterns*, patrones moleculares asociados a patógenos
Pb/bp	Pares de bases/del inglés, *base pairs*
PBPs	Del inglés, *penicillin-binding proteins*, proteínas de unión a penicilina
PBS	Del inglés, *phosphate buffered saline*, solución salina con tampón fosfato
PC	Del inglés, *phosphatidyl choline*, fosfatidilcolina
PCDH	Protocadherina
pCO_2	Presión de dióxido de carbono
PCR	Del inglés, *polymerase chain reaction*, reacción en cadena de la polimerasa
PDH	Piruvato deshidrogenasa
PE	Del inglés, *phosphatidyl ethanolamine*, fosfatidiletanolamina
PFL	Piruvato formato liasa
PG	Del inglés, *phosphatidyl glycerol*, fosfatidilglicerol
Phe	Del inglés, *phenylanaline*, fenilalanina
PI	Del inglés, *phosphatidyl inositol*, fosfatidilinositol
Pi	Fosfato inorgánico
PLA_2	Del inglés, *phospholipase* A_2, fosfolipasa A_2
PMN	Leucocito polimorfonuclear
pO_2	Presión de oxígeno
PPE	Del inglés, *porcine pancreatic elastase*, elastasa pancreática porcina
PPIX	Protoporfirina IX
PPRP	Fosforribosil pirofosfato
Pro	Del inglés, *proline*, prolina
PRRs	En inglés, *pathogen recognition receptors*, receptores de reconocimiento de patógenos
PTA	Fosfato acetiltransferasa
PTS	Del inglés, *phosphotransferase system*, sistema fosfotransferasa
PVX	PolyViteX
Q	Queuosina
qCML	Del inglés, *quantile-adjusted conditional maximum likelihood method*, método de máxima verosimilitud condicional ajustado por cuantiles
QRDRs	Del inglés, *quinolone resistance–determining regions*, regiones determinantes de la resistencia a quinolonas
r.p.m.	Revoluciones por minuto
REIPI	Red Española de Investigacion en Patología Infecciosa
RH	Del inglés, *relative humidity*, humedad relativa
RI	Del inglés, *refractive index*, índice de refracción
RIN	Del inglés, *RNA integrity numbers*, números de integridad del ARN
R-M	Del inglés, *restriction-modification system*, sistema de restricción-modificación
RNA-seq	Del inglés, *RNA sequencing*, secuenciación del transcriptoma
RPKM	Del inglés, *reads per kilo base per million mapped reads*, lecturas por kilo de base por millón de lecturas asignadas
RPMI	Del inglés, *Roswell Park Memorial Institute medium*, medio Instituto Conmemorativo de Roswell Park
rRNA	RNA ribosomal

Lista de Abreviaturas

RT	Del inglés, *reverse transcription*, transcripción reversa o retrotranscripción
RT-qPCR	Del inglés, *real time-quantitative PCR*, PCR cuantitativa en tiempo real
Rv/R	Del inglés, *reverse*, reverso
s	Segundo
SCFAs	Del inglés, *short chain fatty acids*, ácidos grasos de cadena corta
SD	Del inglés, *standard deviation*, desviación estándar
SDS-PAGE	Del inglés, *sodium dodecyl sulfate polyacrylamide gel eletrophoresis*, electroforesis en gel de poliacrilamida con dodecilsulfato sódico
SEM	Del inglés, *standard error of mean*, error estándar de la media
Ser	Serina
SGLT	Del inglés, *sodium coupled glucose transport isoform*, transportador facilitador de glucosa acoplado a sodio
SMRT	Del inglés, *single-molecule real-time sequencing*, secuenciación a tiempo real de una única molécula de ADN
SMX	Sulfametoxazol
SNPs	Del inglés, *single nucleotide polymorphism*, polimorfismo de un solo nucleótido
SP	Del inglés, *surfactant protein*, proteína del surfactante
Spec	Del inglés, *spectinomycin*, espectinomicina
SSR	Del inglés, *simple/short sequence repeats*, repeticiones de secuencias simples/cortas
Str	Del inglés, *streptomycin*, estreptomicina
Succ	Ácido succínico
TCA	Del inglés, *tricarboxylic acid cycle*, ciclo del ácido tricarboxílico o ciclo de Krebs
TEM	Del inglés, *transmission electron microscopy*, microscopía electrónica de transmisión
Tfp/T4P	Del inglés, *type IV pili*, pili tipo IV
Thr	Del inglés, *threonine*, treonina
TLC	Del inglés, *thin-layer chromatography*, cromatografía de capa fina
TLR	Del inglés, *Toll-like receptor*, receptor tipo-Toll
TMM	Del inglés, *trimmed mean of M values*, media recortada de los valores M
TMP	Trimetroprim
TNF-α	Del inglés, *tumor necrosis factor-α*, factor de necrosis tumoral-α
Tn-seq	Del inglés, *transposon sequencing*, secuenciación de transposones
TraDIS	Del inglés, *transposon-directed insertion sequencing*, secuenciación por inserción dirigida por transposones
TREP	Del ingles, *transformed recombinant enrichment profiling*, perfil de enriquecimiento recombinante transformado
TxS	Cotrimoxazol
Tyr	Del inglés, *tyrosine*, tirosina
UNAV	Universidad de Navarra
UPNA	Universidad Pública de Navarra
USA	Del inglés, *United States of America*, Estados Unidos de América
USS	Del inglés, *uptake signal sequence*, secuencia señal de captación
UV	Ultravioleta
V	Vehículo
Val	Valina
VCAM-1	Del inglés, *vascular cell adhesion molecule 1*, molécula de adhesión celular vascular 1
VIH	Virus de la inmunodeficiencia adquirida
vol	Volúmen
w/v	Del inglés, *weight/volume*, peso/volumen

WB	Del inglés, *Western Blot*
WGS	Del inglés, *whole-genome sequencing*, secuenciación del genoma completo
WT	Del inglés, *wild type*, cepa silvestre o parental

Lista de Figuras

Figuras Principales:

- **Figura 1.** Gradientes fisiológicos y microbianos del aparato respiratorio humano.
- **Figura 2.** Factores que determinan la composición del microbioma respiratorio.
- **Figura 3.** Características del eje intestino-pulmón.
- **Figura 4.** Hipótesis del círculo vicioso en la progresión de la EPOC.
- **Figura 5.** Mecanismo de transformación natural de HiNT.
- **Figura 6.** Regulación de la competencia natural de HiNT.
- **Figura 7.** Incorporación y biosíntesis de purinas en HiNT.
- **Figura 8.** Características del metabolismo central de HiNT.
- **Figura 9.** Mecanismos de evasión del sistema inmune de HiNT.
- **Figura 10.** Elementos de interacción de *H. influenzae* con el hospedador.
- **Figura 11.** Summarized landscape of –omics contribution to our understanding of the interactions between *H. influenzae* and the human host.
- **Figura 12.** *Mus musculus* and *H. influenzae* global gene expression profiling upon airway infection.
- **Figura 13.** Differential expression of *H. influenzae* genes upon mice infection.
- **Figura 14.** Part of the *H. influenzae* natural competence machinery is up-regulated *in vivo*.
- **Figura 15.** Identification of *H. influenzae in vivo* fitness related genes.
- **Figura 16**. Schematic representation of *H. influenzae* glucose catabolism.
- **Figura 17.** Changes in metabolite concentrations in cultures of *H. influenzae* NTHi411, NTHi584, and NTHi1104 grown in CDM under aerobic and anaerobic conditions.
- **Figura 18.** Effect of carbon metabolism perturbation by gene inactivation on bacterial growth.
- **Figura 19.** Inactivation of the *ackA*, *pflA*, and *frdA* genes modifies *H. influenzae* production of glucose catabolism end products.
- **Figura 20.** Effect of inactivating glucose metabolic gene encoding enzymes on bacterial gene expression.
- **Figura 21.** Glucose metabolic gene encoding enzymes are key contributors to *H. influenzae* lung infection.
- **Figura 22.** Bacterially produced glucose catabolism end products have a proinflammatory effect.
- **Figure 23.** Roadmap for using *H. influenzae* metabolic reconstruction as a screening platform.
- **Figure 24.** Analysis of *i*NL638 main features and capabilities.
- **Figure 25.** FabHi mode of binding.
- **Figure 26.** FabHi has an antimicrobial effect on *H. influenzae* upon planktonic and biofilm growth.

Lista de Figuras

- **Figure 27.** FabHi effect on *H. influenzae* does not merely relate to *fabH* gene allelic variant or expression levels.
- **Figure 28.** FabHi *in vitro* characterization and preclinical evaluation.
- **Figure 29.** Summary of the metabolic aspects of the host-NTHi interplay analyzed in this PhD Thesis work.
- **Figure 30.** Model proposing the biological significance of *H. influenzae* glucose catabolism during infection within the COPD lung.
- **Figure 31.** Genome-scale metabolic network reconstructions for bacterial pathogenesis.

Figuras Suplementarias:

- **Figura S1.** Expression of *H. influenzae* genes determined by qRT-PCR.
- **Figura S2.** Growth rates of generated mutant strains.
- **Figura S3.** Global gene expression and fitness profiling analyses are complementary to uncover *H. influenzae* virulence factors.
- **Figura S4.** Growth medium modifies the expression of *H. influenzae* genes involved in central carbon metabolism and respiration.
- **Figura S5.** Changes in metabolite concentrations in cultures of *H. influenzae* NTHi411, NTHi584 and NTHi1104, grown under microaerophilic conditions.
- **Figura S6.** Expression of genes involved in central carbon metabolism and respiration in strain NTHi411.
- **Figura S7.** Effect of inactivating the *ackA*, *pflA* and *frdA* genes on *H. influenzae* growth and morphology.
- **Figura S8.** Supportive information on approaches employed for *H. influenzae* Δ*ackA* mutant complementation.
- **Figura S9.** Inactivation of the *ackA*, *pflA* and *frdA* genes modifies *H. influenzae* production of glucose catabolism endproducts.
- **Figure S10.** Synthesis of FabHi.
- **Figure S11.** *In vivo/in silico* comparison of essential genes.
- **Figure S12.** Quantitative comparison of available experimental datasets of essential genes in *H. influenzae.*
- **Figure S13.** Schematic representation of *H. influenzae* lipid metabolism.
- **Figure S14.** Multiple alignment of FabH variants identified in a previously whole-genome sequenced NTHi clinical isolate collection.

- **Figure S15.** FabHi:$FabH_{RdKW20}$ interaction mode compared with crystal structures of the *E. coli* enzyme in complex with close structural analogues of the inhibitor.
- **Figure S16**. Structure of FabHi and its sodium, potassium and hydrochloride salts.
- **Figure S17.** Distribution of FabH variants A1 to A14 among previously established clonal types (CT) in a genome-sequenced NTHi clinical strain collection.
- **Figure S18.** Growth of *H. influenzae* selected strains carrying FabH variants A1 to A14 in two different media.
- **Figure S19.** Antimicrobial effect of FabHi on *H. influenzae*.
- **Figure S20.** Antimicrobial effect of FabHi on strains A2-P62, A7-P665, A9-P645, A13-P590.
- **Figure S21.** Polymorfisms of FabH may affect FabH stability and activity.
- **Figure S22.** Distribution of AcrA variants among the 14 selected NTHi isolates.
- **Figure S23.** Distribution of AcrB variants among the 14 selected NTHi isolates.
- **Figure S24.** Distribution of TolC variants among the 14 selected NTHi isolates.
- **Figure S25.** Distribution of AcrR variants among the 14 selected NTHi isolates.
- **Figure S26.** Cytotoxicity measured by the release of lactate dehydrogenase by A549 cells incubated for 16 h with increasing doses of FabHi in serum-starved medium.

Lista de Tablas

Tablas Principales:

- **Tabla 1.** Genes de *H. influenzae* pertenecientes al regulón CRP-S.
- **Tabla 2.** Inhibidores naturales de FASII.
- **Tabla 3.** Summary of –omics studies contributing to the *H. influenzae*-host interplay.
- **Tabla 4.** Strains used in Chapter 3.
- **Table 5.** Genes predicted to be essential by *i*NL638-screening commonly found by (Gawronski et al., 2009; Mobegi et al., 2014; Wong & Akerley, 2012).
- **Table 6**. Distribution of FabH variation across a previously whole-genome sequenced (WGS) collection of NTHi clinical isolates.

Tablas Suplementarias:

- **Tabla S1.** Bacterial strains used in Chapter 2.
- **Tabla S2.** Plasmids used in Chapter 2.
- **Tabla S3.** Transformation frequency *in vitro* of RdKW20 or NTHi375-WT and mutants strains by MIV medium using MAP-7 gDNA.
- **Tabla S4.** Fifty common genes up-regulated in BALF (current RNA-seq analysis) and MIV compared to sBHI.
- **Tabla S5.** Number of genes associated to functional categories obtained from RNA-seq and Tn-seq analyses.
- **Tabla S6.** Plasmids used in Chapter 3.
- **Tabla S7.** Key metabolites detected by HPLC in culture supernatants of CDM grown *H. influenzae* RdKW20 WT and mutant strains.
- **Table S8.** Bacterial cultures dry weight.
- **Table S9**. Metabolic content of *i*NL638 compared with its antecessor.

Tablas Anexas:

- **Tabla A1.** Composición del medio de inducción de competencia de *Haemophilus influenzae*, MIV.
- **Tabla A2.** Primers used in Chapter 2.
- **Table A3.** Up-regulated genes in infected lungs compared to non-infected lungs (2,078).
- **Table A4.** Down-regulated genes in infected lungs compared to non-infected lung (2,229).
- **Table A5.** Up-regulated *H. influenzae* genes (316) *in vivo* compared to *in vitro* in RNA-seq analysis.

Lista de Tablas

- **Table A6.** Up-regulated genes (280) *in vitro* compared to *in vivo* in RNA-seq analysis.
- **Table A7.** Underrepresented genes in *output* samples compared to *input* library in Tn-seq analysis.
- **Table A8.** Primers used in Chapter 3.
- **Table A9.** Primers used in Chapter 4.

Resumen & Abstract

Este trabajo de **Tesis Doctoral** aborda el papel de tres aspectos del metabolismo bacteriano (síntesis de purinas, catabolismo de glucosa, síntesis de ácidos grasos) en la interacción entre el patógeno *Haemophilus influenzae* no tipificable (HiNT) y el sistema respiratorio humano. Mediante análisis de expresión génica global, inactivación génica y caracterización fenotípica *in vitro* e *in vivo*, modelado computacional, química médica, y evaluación antimicrobiana a nivel preclínico, estudiamos los perfiles transcripcionales de patógeno y hospedador durante la infección respiratoria (**Capítulo 2**), la contribución del catabolismo de glucosa en la patogénesis de *H. influenzae* (**Capítulo 3**), y el potencial antimicrobiano de la inhibición de la ruta de biosíntesis de ácidos grasos de esta bacteria (**Capítulo 4**).

H. influenzae fue el primer organismo de vida libre cuyo genoma completo fue secuenciado, haciéndolo pionero en el desarrollo y empleo de técnicas -ómicas. El **Capítulo 1** de este trabajo ha revisado la contribución de abordajes -ómicos incluyendo genómica, transcriptómica, proteómica y metabolómica, al estudio de la interacción entre HiNT y el sistema respiratorio humano.

En el **Capítulo 2** de este trabajo realizamos un estudio multi-ómico *in vivo*, consistente en la utilización de RNA-seq dual y Tn-seq durante el proceso de infección respiratoria murina por HiNT. El perfil de expresión génica diferencial entre bacterias cultivadas *in vitro* y bacterias recuperadas de lavado broncoalveolar murino mostró la sobre-expresión de genes que codifican enzimas implicadas en la síntesis de purinas y aminoácidos, así como de genes que codifican parte de la maquinaria de competencia natural de la bacteria.

El aumento de los niveles de glucosa en las vías respiratorias de pacientes que sufren enfermedades respiratorias crónicas facilita la proliferación de patógenos que metabolizan este azúcar. HiNT cataboliza glucosa mediante una fermentación asistida por respiración que conlleva la excreción de acetato, formato y succinato. En el **Capítulo 3** de este trabajo, diseñamos, generamos y caracterizamos un panel de cepas mutantes que no producen acetato, formato o succinato mediante la inactivación de los genes *ackA*, *pflA* y *frdA*, respectivamente. La inactivación de *ackA* limitó la producción de acetato y el crecimiento bacteriano, y estimuló tanto la producción de lactato en anaerobiosis como la atenuación bacteriana *in vivo*. El acetato excretado estimuló la expresión de genes pro-inflamatorios en células de epitelio respiratorio en cultivo, lo que sugiere que el catabolismo de glucosa contribuye no sólo al crecimiento de HiNT sino también a la inmunomodulación del sistema respiratorio humano.

La resistencia de *H. influenzae* a antibióticos β-lactámicos ha llevado a su inclusión en la lista de patógenos bacterianos para los que la OMS considera prioritaria la búsqueda y desarrollo de nuevos antimicrobianos. En el **Capítulo 4** de este trabajo, desarrollamos y validamos un modelo metabólico de *H. influenzae* a escala genómica, que utilizamos como herramienta de escrutinio *in silico* de genes esenciales de este patógeno, para su explotación como dianas terapéuticas. Este modelo predijo la

esencialidad de un gran número de genes implicados en la síntesis de lípidos. Nos centramos en la enzima FabH, que cataliza la condensación descarboxilativa de malonil-ACP y acil-CoA en la iniciación de la biosíntesis de ácidos grasos. Nuestro modelado computacional mostró la idoneidad de la interacción de la molécula ácido 1- (5- (2-fluoro-5- (hidroximetil) fenil) piridin-2-il) piperidin-4-acético y la proteína FabH. Este inhibidor redujo la viabilidad bacteriana de forma dosis-dependiente. El efecto inhibitorio observado fue variable entre aislados clínicos portadores de distintas variantes alélicas del gen *fabH*, e independiente de su expresión. El inhibidor empleado no generó sinergias, no favoreció el desarrollo de resistencias, y no alteró la dinámica de infección epitelial por HiNT, mostrado además un efecto protector frente a la infección por HiNT *in vivo*.

En conjunto, este trabajo de Tesis Doctoral proporciona conocimiento nuevo sobre el papel del metabolismo bacteriano en la interacción HiNT-sistema respiratorio humano, que esperamos sea de utilidad en el desarrollo de estrategias anti-infectivas que mejoren el manejo clínico de las enfermedades infecciosas asociadas a este patógeno.

This **PhD Thesis** work addresses the role of three aspects of bacterial metabolism (purine synthesis, glucose catabolism, fatty acid synthesis) in the interaction between nontypeable *Haemophilus influenzae* (NTHi) and the human airways. Global gene expression analysis, gene inactivation and phenotypic characterization *in vitro* and *in vivo*, computational modeling, medical chemistry, and antimicrobial evaluation at the preclinical level, led us to study pathogen and host transcriptional profiles during respiratory infection (**Chapter 2**), the contribution of glucose catabolism to *H. influenzae* pathogenesis (**Chapter 3**), and the antimicrobial potential of inhibiting this bacterial fatty acid biosynthesis pathway (**Chapter 4**).

H. influenzae was the first free-living organism whose genome was fully sequenced, thus pioneering in the development and use of -omics techniques. **Chapter 1** of this work reviewed the contribution of -omic approaches including genomics, transcriptomics, proteomics and metabolomics, to the study of this host-pathogen interplay.

In **Chapter 2,** we carried out an *in vivo* multi-omic study, using dual RNA-seq and Tn-seq during murine respiratory infection by NTHi. Differential gene expression profiling of bacteria grown *in vitro* compared to those recovered from murine bronchoalveolar lavage fluid samples showed over-expression of genes that encode enzymes involved in purine and amino acids synthesis, as well as of genes encoding part of the bacterial natural competence machinery.

The increase of glucose levels in the respiratory tract of patients suffering chronic respiratory diseases facilitates the proliferation of pathogens able to metabolize this sugar. NTHi catabolizes glucose through respiration-assisted fermentation involving the excretion of acetate, formate, and succinate. In **Chapter 3** of this work, we designed, generated, and characterized a panel of mutant strains that did not produce acetate, formate, or succinate by inactivating the *ackA*, *pflA*, and *frdA* genes, respectively. Inactivation of the *ackA* gene limited acetate production and bacterial growth, and stimulated both anaerobic lactate production and bacterial attenuation *in vivo*. The excreted acetate stimulated the expression of pro-inflammatory genes by cultured respiratory epithelial cells, which suggests that glucose catabolism contributes not only to the growth of NTHi but also to immunomodulation within the human respiratory system.

The *H. influenzae* resistance to β-lactam antibiotics led to its inclusion in the list of bacterial pathogens for which the WHO considers a priority the search and development of new antimicrobials. In **Chapter 4** of this work, we developed and validated a *H. influenzae* genome-scale metabolic model, which we used as an *in silico* screening tool to identify bacterial essential genes suitable as therapeutic targets. This model predicted the essentiality of a large number of genes involved in lipid synthesis. We focused on the enzyme FabH, which catalyzes the decarboxylative condensation of malonyl-ACP and acyl-CoA in the initiation of fatty acid biosynthesis. Computational modeling showed the suitability of the interaction of the chemical inhibitor 1- (5- (2-

Fluoro-5- (hydroxymethyl) phenyl) pyridin-2-yl) piperidine-4-acetic acid with FabH. Likewise, this inhibitor reduced bacterial viability in a dose-dependent manner. The inhibitory effect observed was variable among clinical isolates carrying different allelic variants of the *fabH* gene, and independent of this gene expression. The inhibitor did not generate synergies, did not favor the development of resistance, and did not alter the dynamics of epithelial infection by NTHi. Notably, this chemical inhibitor showed a protective effect against NTHi infection *in vivo*.

Altogether, this **PhD Thesis** work provides novel knowledge on the role of bacterial metabolism in the NTHi-human respiratory system interplay, intended to be useful in the development of anti-infective strategies that will improve the clinical management of infectious diseases associated to this pathogen.

Introducción General

1. Sistema respiratorio humano

1.1. Características anatómicas

El sistema respiratorio humano se divide en vías altas, formadas por la cavidad nasal y la faringe, constituída a su vez por nasofaringe, orofaringe y laringofaringe, y vías bajas, formadas por la laringe, la tráquea, los bronquios, bronquiolos y alveolos, estos tres últimos formando parte de los pulmones (**Figura 1A**). La orofaringe presenta epitelio escamoso estratificado. La cavidad nasal, nasofaringe, laringe, tráquea, bronquios y bronquiolos de mayor tamaño están revestidos por mucosa respiratoria que secreta mucinas (moco). La mucosa está formada por epitelio pseudoestratificado cilíndrico ciliado y tejido conjuntivo laxo formado por colágeno y fibras elásticas que dan soporte y elasticidad (lámina propia). Los bronquiolos presentan epitelio cubiodal simple no ciliado. Los alveolos están cubiertos por epitelio escamoso simple, formado por: (i) neumocitos tipo I, células planas implicadas en el intercambio gaseoso con los capilares sanguíneos contiguos; (ii) neumocitos tipo II, células cúbicas con microvellosidades que mantienen la tensión superficial mediante la secreción de surfactante pulmonar. La barrera alveolo-capilar tiene una gran superficie que permite la difusión rápida de gases con la sangre (hematosis). Esta barrera está formada por surfactante pulmonar, neumocitos tipo I, endotelio capilar y láminas basales fusionadas de neumocitos y células endoteliales capilares. Las uniones estrechas (en inglés, *tight junctions*) contribuyen a la integridad del epitelio respiratorio, formando canales paracelulares (Baker & Baines, 2018; Schlingmann et al., 2015) a través de los cuales se produce la difusión de moléculas, como es el caso de la glucosa, entre la sangre y el líquido de la superficie de las vías respiratorias (en inglés, *airway surface liquid*, ASL) (**Figura 1B**) (Baker & Baines, 2018).

1.2. Inmunidad del sistema respiratorio humano

Las vías respiratorias están constantemente expuestas a una amplia gama de material particulado y de microoganismos, que son inhalados durante la respiración y pueden resultar tóxicos o patógenos. Por ello, el aparato respiratorio está dotado de un sistema defensivo multifactorial, que se resume a continuación.

1.2.1. Barreras mecánicas

La barrera mucociliar atrapa partículas extrañas (>5 μm) (Zhang et al., 2000), expulsa material mediante el barrido mucociliar y la tos (Knowles & Boucher, 2002), y humedece e hidrata el sistema respiratorio (Chilvers & O'Callaghan, 2000). El barrido mucociliar es un movimiento coordinado de los cilios para crea un flujo turbulento que propulsa el moco desde los pulmones hacia la orofaringe para su posterior expectoración (Chilvers & O'Callaghan, 2000; Pérez et al., 2014). El moco está formado por un 90-95% agua y 10-5% sólidos (Bansil & Turner, 2018), que consisten en una mezcla compleja de mucinas, proteínas antimicrobianas, metabolitos, fluidos y electrolitos cuya abundancia

y composición varían a lo largo del sistema respiratorio, y en función de las condiciones ambientales o la posible inflamación sistémica o local (Whitsett, 2018). Las mucinas son glicoproteínas aniónicas con propiedades viscoelásticas, antimicrobianas y anti-inflamatorias (Bonser & Erle, 2017; Voynow & Mengr, 2009), decoradas con ácido siálico (Thornton et al., 1996). Las principales mucinas son MUC5B y MUC5AC, producidas por células de glándulas submucosas o epiteliales de las vías respiratorias, respectivamente (Knowles & Boucher, 2002; Whitsett, 2018). Las patologías respiratorias alteran la abundancia de mucinas, incrementando la viscoelasticidad del moco, lo que dificulta su transporte hacia el exterior obstruyendo las vías respiratorias (Bonser & Erle, 2017).

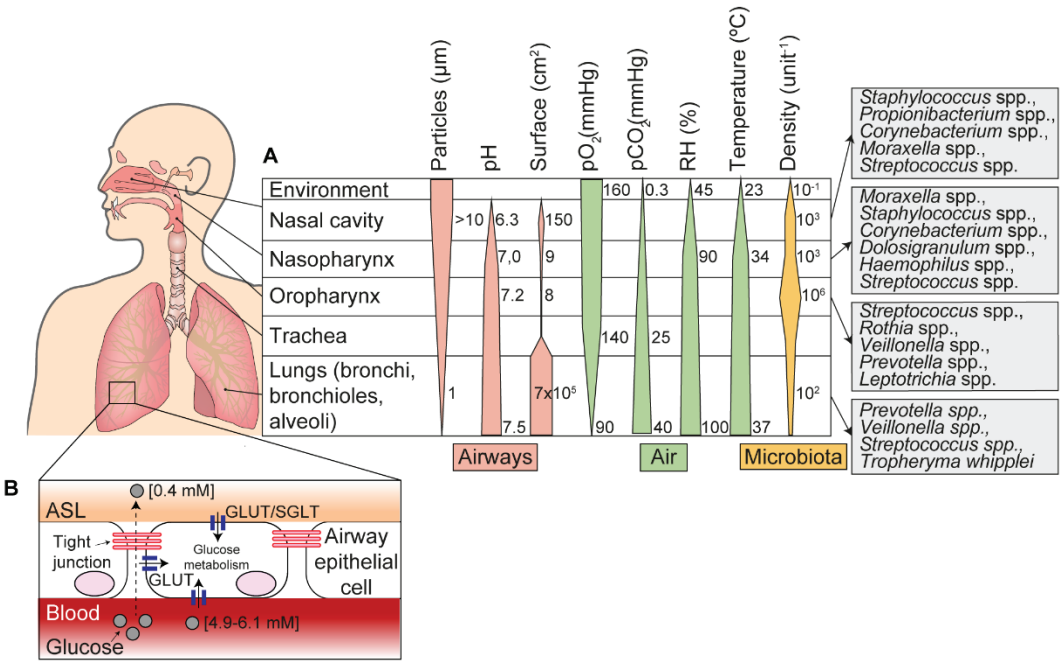

Figura 1. Gradientes fisiológicos y microbianos del aparato respiratorio humano. (A) Los parámetros indicados varían a lo largo del tracto respiratorio de individuos adultos condicionando la presencia de una microbiota específica en cada nicho. **(B)** En individuos con un sistema respiratorio sano se mantiene la homeostasis de la glucosa entre el ASL y la sangre mediante el correcto funcionamiento de las uniones estrechas celulares y el transporte a través de las células epiteliales. Panel **(A)** adaptado de Man et al., 2017; panel **(B)** adaptado de Baker & Baines, 2018.

1.2.2. Elementos celulares y reconocimiento de patógenos

El epitelio alveolar está formado por: **neumocitos tipo I,** células escamosas con función estructural, forman el componente epitelial que cubre el 93-97% de la superficie alveolar, sin capacidad para dividirse; **neumocitos tipo II,** células cuboides, cubren el 3-7% de la superficie, con capacidad de división. Los neumocitos tipo II tienen varias funciones: (i) participan en la regeneración pulmonar, su división permite reemplazamiento celular (Féréol et al., 2008); (ii) secretan proteínas del surfactante pulmonar (Casals et al., 2018); (iii) transportan electrolitos y fluidos desde la superficie apical al intersticio (Mason, 2006).

Los **macrófagos alveolares** poseen plasticidad natural adaptando su fenotipo al entorno. Constituyen una respuesta celular innata residente que es clave frente a la infección, a través de la fagocitosis, y la señalización vía liberación de citocinas y quimiocinas al espacio alveolar, que facilita el reclutamiento de neutrófilos (Bhattacharya & Westphalen, 2016; Garbi & Lambrecht, 2017; Yamasaki & Van Eeden, 2018). Los **neutrófilos**, leucocitos polimorfonucleares (PMN) reclutados a través de la señalización pro-inflamatoria, y activados en su migración al nicho infectado, liberan gránulos que contienen enzimas y péptidos antimicrobianos (en inglés, *antimicrobial peptides*, AMPs) como serín proteasas, defensinas, mieloperoxidasas y lisozimas, claves en la eliminación de microorganismos patógenos, si bien su acción desregulada puede causar daño pulmonar (Pechous, 2017).

Las células respiratorias expresan en su superficie receptores de reconocimiento de patrones (en inglés, *Pathogen Recognition Receptors*, PRRs) que reconocen patrones moleculares asociados a patógenos (en inglés, *Pathogen-Associated Molecular Patterns*, PAMPs) (Zhang et al., 2021). Los principales PRRs son: (i) receptores tipo-Toll (en inglés, *Toll-like Receptor*, TLR) (Opitz et al., 2010); (ii) receptores de oligomerización de nucleótidos (en inglés, *Nucleotide-binding Oligomerization Domain-like* (NOD)-*Receptor*, NLR) (Opitz et al., 2010); (iii) receptores C-lectinas (en inglés, *C-type Lectin Receptor*, CLR) (Campuzano & Wormley, 2018). Los PRR, al activarse, desencadenan una cascada de señalización celular que lleva a la producción de diferentes citocinas pro-inflamatorias y moléculas antimicrobianas. Entre otros, se activa el factor nuclear-κB (NF-κB), las quinasas activadas por mitógenos (en inglés, *mitogen-activated protein kinases*, MAPKs), los factores de regulación de interferón (en inglés, *Interferon Regulatory Factor*, IRF), o rutas autofágicas (Leiva-Juárez et al., 2018). Esto hace que se liberen interleucinas (IL) (IL-1, IL-6, IL-8), factor de necrosis tumoral-α (en inglés, *Tumor Necrosis Factor-α*, TNF-α), interferón (IFN)-γ, quimiocinas CXC (CXCL1-8, CXCL12) y CC (CCL2, CCL17, CCL18) (Galeas-Pena et al., 2019; Hartl et al., 2018), proteasas, AMPs, lipasas, glicosidasas, H_2O_2 o otras especies reactivas de oxígeno (Martin & Frevert, 2005). También se induce la expresión de proteínas inflamatorias como metaloproteinasa de matriz-9 (MMP-9), molécula de adhesión intercelular-1 (ICAM-1), molécula de adhesión vascular-1 (VCAM-1), ciclooxigenasa-2 (COX-2) y fosfolipasa A_2 (PLA_2) (Lee & Yang, 2013).

1.2.3. Elementos humorales

El **sistema del complemento** elimina patógenos y células dañadas, promueve la inflamación y ataca las membranas de patógenos (Kleczko et al., 2019), a través de sus tres vías, clásica, de las lectinas, y alternativa. La activación del sistema del complemento provoca lisis celular por formación de poros, opsonización y quimioatracción de fagocitos (Pandya & Wilkes, 2014; Sarma & Ward, 2011). Las proteínas del sistema del complemento son sintetizadas por macrófagos (Hartung &

Hadding, 1983), neumocitos tipo II (Strunk et al., 1988), y células bronquiales (Varsano et al., 2000). La expresión del sistema del complemento aumenta cuando se produce una lesión pulmonar y las células reciben estímulos inflamatorios mediante IL-1, IL-6 y IFN-γ (Volanakis, 1995).

Los **AMPs** son moléculas anfipáticas catiónicas, con 12-50 aminoácidos, de los cuales 2-9 son residuos de lisina o arginina, y hasta un 50% son aminoácidos hidrófobos. Los AMPs presentan actividad antibacteriana (Brown & Hancock, 2006; Zanetti, 2004). Los principales AMPs en el tracto respiratorio son defensinas y catelicidinas que, junto a su efecto antimicrobiano, tienen actividad quimioatrayente de células inmunitarias, incrementan la respuesta inflamatoria epitelial, y participan en la reparación tisular promoviendo la angiogénesis y proliferación celular (Hiemstra, 2007).

El **surfactante pulmonar** es una mezcla compleja de lípidos, siendo los fosfolípidos los más abundantes, y proteínas, en proporción 9:1 (Griese, 1999), que: (i) reduce la tensión superficial alveolar evitando el colapso pulmonar durante la espiración (Griese, 1999; Whitsett & Weaver, 2002), (ii) facilita el intercambio gaseoso (Mason, 2006), (iii) tiene propiedades antimicrobianas y anti-inflamatorias (Mason, 2006; Wright, 2005), y (iv) reduce la invasión celular por patógenos como *Haemophilus influenzae* (García-Fojeda et al., 2019). Los fosfolípidos más abundantes son fosfatidilcolina (PC), fosfatidilglicerol (PG) o fosfatidilinositol (PI), y fosfatidiletanolamina (PE), en proporciones 8:1:1 (Bernhard, 2016). Las proteínas del surfactante pulmonar son: SP-A, SP-B, SP-C y SP-D. SP-A y SP-D, colectinas hidrofílicas que: (i) unen carbohidratos presentes en la superficie de patógenos (virus, hongos y bacterias Gram-positivas y Gram-negativas como *Mycobacterium tuberculosis*, *Pseudomonas aeruginosa* y *H. influenzae*), (ii) promueven el atrapamiento bacteriano por trampas extracelulares de neutrófilos (en inglés, *neutrophil extracellular traps*, NETs), (iii) promueven la expresión de PRRs, y (iv) actuan como opsoninas (Casals et al., 2018). SP-B y SP-C son proteínas hidrofóbicas con función estructural y estabilizadora del surfactante pulmonar (Gómez-Gil et al., 2009).

Los **anticuerpos** mayoritarios del sistema respiratorio son las inmunoglobulinas IgA e IgG. IgA es predominante en el tejido bronquial, inhibe la adhesión bacteriana, inactiva toxinas y aglutina bacterias en el moco favoreciendo su eliminación (Millares et al., 2012). IgG induce la respuesta pro-inflamatoria (Gur et al., 2021) y actúa como opsonina (Reynolds, 1988).

Los **ácidos grasos**, especialmente el ácido araquidónico, son liberados de los fosfolípidos de las membranas celulares por acción hidrolítica de PLA_2 en respuesta a la inflamación. El ácido araquidónico tiene efecto antimicrobiano (Das, 2018; Fernández-Calvet et al., 2018; Moleres et al., 2018; Yoon et al., 2018), es precursor de eicosanoides a través de su oxidación por la ciclooxigenasa (COX) (Chen et al., 2019), y del factor activador de plaquetas (del inglés, *platelet activating factor*, PAF) (Meyer et al., 2005). El ácido oleico, ácido graso más abundante del cuerpo en individuos sanos, también presenta efecto antimicrobiano (Fernández-Calvet et al., 2018). Además, el ácido

oleico induce la muerte celular de neumocitos tipo I y II y células endoteliales, y activa vías de señalización intracelular a través de diferentes receptores que desencadenan la producción de citoquinas y quimocinas (Gonçalves-De-Albuquerque et al., 2015).

1.2.4. Inmunidad nutricional

La baja disponibilidad de nutrientes, conocida como inmunidad nutricional (Hood & Skaar, 2012), limita el crecimiento y supervivencia de microorganismos en el sistema respiratorio humano. La homeostasis alveolar de **glucosa** se mantiene mediante (i) la barrera creada por las uniones estrechas entre células, y (ii) el transporte de glucosa desde el ASL al epitelio a través de transportadores facilitadores de glucosa (en inglés, *facilitative glucose transporters* y *sodium coupled glucose transport isoform 1*, GLUTs y SGLT1, respectivamente), impulsado a través del gradiente generado por la velocidad de metabolismo de la glucosa intracelular (**Figura 1B**) (Baker & Baines, 2018). Esto hace que la disponibilidad de glucosa en pulmones sanos sea baja, con un 0,4 mM de glucosa en el ASL en comparación con un 4,9-6,1 mM en sangre (Baker & Baines, 2018). Los **metales de transición** son necesarios en todas las formas de vida, al ser cofactores enzimáticos y componentes estructurales de numerosas proteínas (Healy et al., 2021; Lopez & Skaar, 2019). Si bien son micronutrientes esenciales, son tóxicos en altas concentraciones por lo que controlar su disponibilidad es clave en el mantenimiento de la homeostasis tisular (Lopez & Skaar, 2019). Los mecanismos que controlan la biodisponibilidad de cationes metálicos son también empleados para limitar su disponibilidad para microorganismos patógenos. El hierro es el metal más utilizado en los procesos biológicos (Healy et al., 2021). La mayor parte del hierro está en su forma tóxica ($Fe2^{+}$), o insoluble ($Fe3^{+}$), limitando su disponibilidad (Chan et al., 2009). El $Fe3^{+}$ procedente de la dieta se une a transferrina o lactoferrina que permite su circulación sistémica y posteriormente es disociado y reducido a $Fe2^{+}$ para ser almacenado como ferritina en las células eurocariotas (Healy et al., 2021). Los macrófagos también modulan la disponibilidad de hierro mediante su importación, exportación y reciclaje (Healy et al., 2021). El zinc y el manganeso son quelados por proteínas de la familia S100, entre ellas las calprotectinas, constituyentes del ~40% de la composición proteica de los neutrófilos (Hood & Skaar, 2012).

1.3. Microbioma: composición, funciones y señalización

1.3.1. El microbioma del aparato respiratorio humano

El microbioma respiratorio de individuos sanos está formado por: (i) *Staphylococcus* spp., *Propionibacterium* spp., *Corynevacterium* spp., *Moraxella* spp., *Streptococcus* spp., *Dolosigranulum* spp., *Haemophilus* spp., *Rothia* spp., *Veillonella* spp., *Prevotella* spp. y *Leptotrichia* spp. en vías respiratorias altas; y (ii) *Prevotella* spp., *Veillonella* spp., *Streptococcus* spp. y *Tropheryma whippley* en vías respiratorias bajas (Man et al., 2017). Además de bacterias, en vias respiratorias altas también

se encuentran virus (*human rhinovirus* (HRV), *human bocavirus*, polyomaviruses, adenovirus y coronavirus entre otros (van den Bergh et al., 2012)), y micobiota que incluye *Aspergillus* spp., *Penicillium* spp., *Candida* spp. y *Alternaria* spp entre otros (Eidi et al., 2016). El microbioma respiratorio participa, entre otros, en: (i) la maduración estructural y mantenimiento de la homeostasis del sistema respiratorio (Yun et al., 2014); (ii) el desarrollo de la inmunidad local (Olszak et al., 2012); (iii) la regulación de la respuesta inmune (Segal et al., 2016); y (iv) la resistencia a la colonización por microorganismos patógenos (Man et al., 2017).

La composición del microbioma respiratorio resulta de: (i) factores genéticos (Chalmers et al., 2013; Man et al., 2017); (ii) la edad; (iii) el estilo de vida; (iv) las condiciones ambientales (Elgamal et al., 2021); (v) la inmigración microbiana, principalmente por microaspiración desde la boca, inhalación de bacterias y dispersión por la mucosa respiratoria; (vi) la eliminación microbiana, llevada a cabo por la tos y elementos del sistema inmune; (vii) las condiciones fisiológicas locales que determinan la tasa de división bacteriana, incluyendo disponibilidad de nutrientes, tensión de O_2, temperatura, pH, ventilación alveolar, estructura celular, así como la abundancia y activación de las células inflamatorias (Dickson et al., 2016; Dickson et al., 2014a; Dickson & Huffnagle, 2015). Las características físicas y fisiológicas cambian desde la cavidad nasal hasta los pulmones, con un aumento de superficie, pH, presión de CO_2, humedad relativa y temperatura, así como un descenso de la presión de O_2 y del tamaño de partículas depositadas procedentes del medio externo vía inhalación (**Figura 1A**). Además, la parte apical del pulmón tiene mayor presión de O_2, menor presión de CO_2 y un mayor pH que la parte basal (Dickson et al., 2014b; Elgamal et al., 2021; Man et al., 2017). En individuos sanos, esta estabilidad fisiológica u homeostasis hace que las distintas zonas del sistema respiratorio tengan diferente grado de habitabilidad dando ventaja selectiva a determinadas especies. Asimismo, el balance entre inmigración y eliminación es determinante en la composición del microbioma pulmonar (Dickson et al., 2017; Dickson et al., 2014b; Dickson et al., 2015a).

La composición del microbioma respiratorio cambia por la exposición del individuo a agentes externos y/o el desarrollo de patologías que alteran la homeostasis y provocan disbiosis pulmonar. El uso de fármacos anti-inflamatorios (corticosteroides) provoca un aumento de Proteobacteria sobre Firmicutes, lo que se traduce en un descenso de *Streptococcus* y un aumento de *Haemophilus* y *Moraxella* (Toraldo & Conte, 2019; Wang et al., 2016). Los antibióticos alteran la distribución y abundancia del microbioma respiratorio, en detrimento de la abundancia de microorganismos comensales (Pettigrew et al., 2012; Prevaes et al., 2016). El tabaquismo y la polución ambiental afectan la diversidad de la microbiota respiratoria (Elgamal et al., 2021; Lim et al., 2016; A. Morris et al., 2013). Las enfermedades respiratorias crónicas disminuyen la presencia de Bacteroidetes y aumentan la de Proteobacterias (Dickson & Huffnagle, 2015), y disminuyen la superficie del pulmón en un 90% lo que aumenta la concentración de microorganismos en el mismo espacio (Dickson et

al., 2016). La disfunción esofágica y el reflujo provocado por enfermedades pulmonares avanzadas aumenta la inmigración microbiana y la presencia de microorganismos procedentes del sistema gastro-intestinal (Dickson et al., 2016; Dickson et al., 2014a). La severidad de la patología favorece el crecimiento local (**Figura 2**) (Dickson et al., 2016; Dickson et al., 2014a).

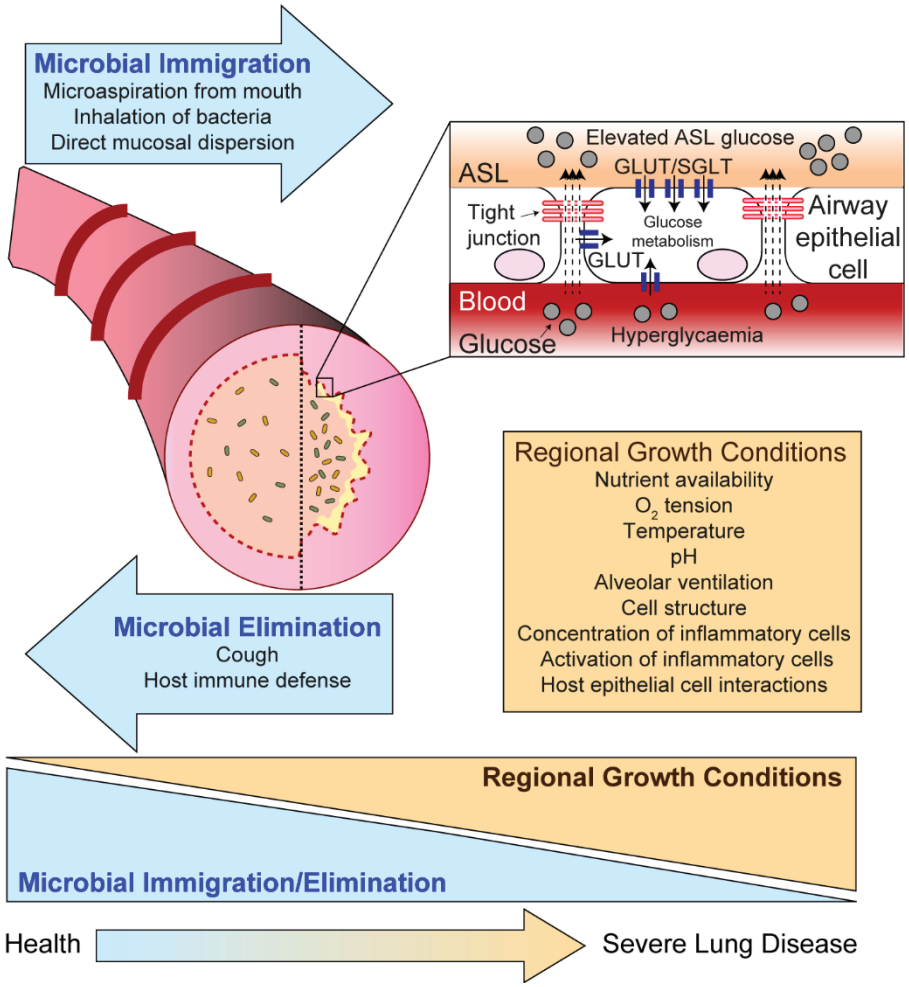

Figura 2. Factores que determinan la composición del microbioma respiratorio. La composición del microbioma en un sistema respiratorio sano viene determinada principalmente por la inmigración y eliminación bacteriana, mientras que en individuos con patologías respiratorias está influenciado por las tasas de crecimiento favorecidas por las condiciones fisiológicas locales. La inflamación de las vías respiratorias y la hiperglicemia aumentan la permeabilidad de glucosa desde la sangre al ASL. Adaptado de Dickson et al., 2014a y Baker & Baines, 2018.

El descenso de la diversidad microbiana en vías altas está asociado con la incidencia de otitis media (OM) aguda provocada por *Streptococcus pneumoniae*, *H. influenzae* y *M. catarrhalis* (Pettigrew et al., 2012). El asma, la fibrosis quística (FQ), o la enfermedad pulmonar obstructiva crónica (EPOC), cuyas principales características pato-fisiológicas son la ocurrencia de enfisema pulmonar, fibrosis, hipersecreción mucosa e hiperinflamación, modifican la topografía del tracto respiratorio, la dinámica de crecimiento bacteriano, y el microbioma pulmonar (Dickson et al., 2014a; Magryś, 2021). FQ, bronquitis crónica, bronquiectasia y asma disminuyen el barrido

mucociliar, lo que dificulta la eliminación bacteriana, provocan disminución de la concentración de O_2, y aumento de temperatura y la cantidad de moco secretado, facilitando el uso de glicoproteínas como fuente de nutrición (Dickson et al., 2015b; Dickson et al., 2014a). Las exacerbaciones de EPOC, eventos agudos de la patología en los que producen cambios de tratamiento, aumentan la abundancia de Proteobacteria y disminuyen la de Firmicutes, (Dickson et al., 2014a; Wang et al., 2016). A su vez, la inflamación respiratoria y la hiperglucemia aumentan la permeabilidad tisular, lo que aumenta la disponibilidad de nutrientes en el ASL, entre otros glucosa, favoreciendo la proliferación de bacterias que utilizan este monosacárido como fuente de carbono (Baker et al., 2007; Baker & Baines, 2018; Dickson et al., 2014a; Garnett et al., 2012). La frecuente administración de corticosteroides a pacientes que sufren EPOC también aumenta la concentración de glucosa en sangre (Hemenway & Terry, 2017). Por otra parte, los ácidos grasos de cadena corta (en inglés, *short chain fatty acids*, SCFAs), como propionato y acetato, productos del metabolismo anaerobio de microorganismos presentes en el pulmón de pacientes que sufren FQ, son utilizados como fuente de carbono por *P. aeruginosa* (Flynn et al., 2016). En conjunto, la disponibilidad de nutrientes en vías respiratorias bajas de pacientes crónicos favorece el crecimiento de patógenos oportunistas, lo que a su vez reduce la diversidad, y contribuye al desarrollo, progresión y/o exacerbación de la patología crónica (Dickson et al., 2014a; Shukla et al., 2017).

1.3.2. El eje intestino-pulmón

Existe una comunicación bilateral entre la microbiota del pulmón y del intestino denominado **eje intestino-pulmón** (en inglés, *gut-lung axis*) (**Figura 3**). Si bien las diferencias fisiológicas entre pulmón e intestino son claras; presentan características que permiten dicha comunicación bilateral (Dickson & Huffnagle, 2015). El epitelio de ambos órganos tiene el mismo orígen embrional, su microbiota (formada principalmente por los filos Firmicutes y Bacteroidetes) se desarrolla simultáneamente tras el nacimiento existiendo una comunicación constante entre ellos, y las enfermedades pulmonares o intestinales provocan cambios fisiológicos similares: reducción de mucosa, aumento de la permeabilidad tisular y menor expresión de las uniones estrechas celulares (Gui et al., 2021; Marsland et al., 2015).

La disbiosis intestinal y la alteración de la estructura epitelial del intestino aumentan la permeabilidad tisular y la liberación sistémica de metabolitos excretados por la microbiota del colon, que alcanzan otros órganos y tejidos a través de la circulación en sangre (Ratajczak et al., 2019). En este sentido, el ácido indol propiónico (IPA) es un análogo del triptófano producido por la microbiota intestinal, con efecto antimicrobiano y anti-inflamatorio frente a *M. tuberculosis* en el pulmón (Negatu et al., 2020). Los **SCFAs** son productos del metabolismo fermentativo bacteriano de residuos dietéticos no digeribles como la fibra, siendo los más abundantes acetato (C2), propionato (C3) y butirato (C4) con una concentración de 20-150 mM en el intestino y 0,1-5 mM en esputo

(Ratajczak et al., 2019; Rutting et al., 2019). Los SCFAs modulan la respuesta inmunitaria e inflamatoria mediante: (i) la unión a receptores epiteliales FFARs (del inglés, *free fatty acids receptors*), GPR43 y GPR41 (FFAR2 y FFAR3, respectivamente) que a su vez activan las proteínas heterotriméricas G, encargadas de transmitir la señal al interior de la célula; (ii) la inhibición de histonas deacetilasas (HDAC) permitendo la expresión génica; y (iii) la activación de inflamasomas (Ratajczak et al., 2019; Rutting et al., 2019).

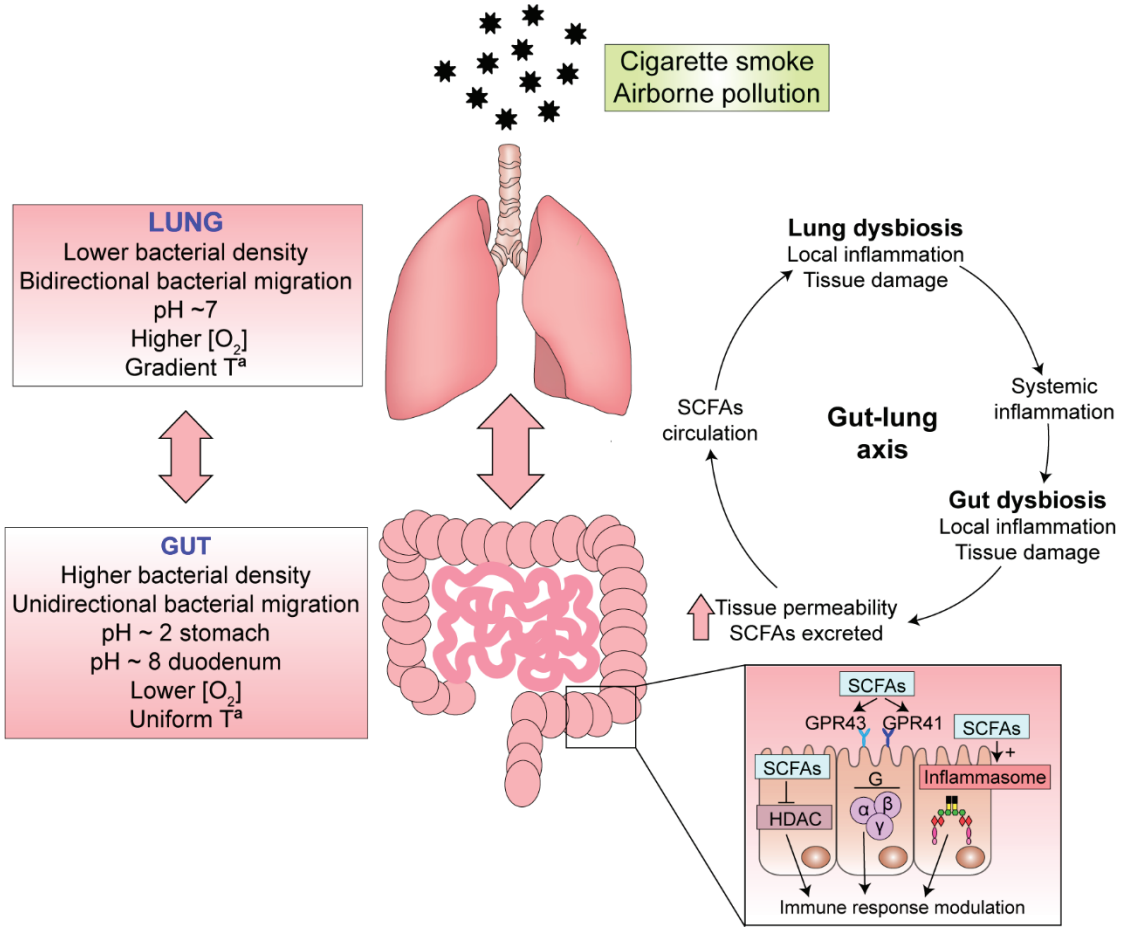

Figura 3. Características del eje intestino-pulmón. Las características fisiológicas que alteran la microbiota pulmonar producen también una disbiosis intestinal que altera la permeabilidad tisular del intestino, liberando SCFAs que llegan al pulmón agravando la disbiosis. Los SCFAs modulan la respuesta inmunitaria e inflamatoria mediante inhibición de HDAC, unión a receptores GPR43 y GRP41, que activan las proteínas G, y activación de inflamasomas.

Patologías respiratorias como asma, EPOC o FQ manifiestan alteración de la microbiota intestinal, y viceversa, por ejemplo niños que sufren disbiosis intestinal son más propensos a desarrollar asma (Marsland et al., 2015; Pambianchi et al., 2021; Price & O'Toole, 2021). La FQ es producida por modificaciones de la proteína CFTR (del inglés, *cystic fibrosis transmembrane conductance regulator,* regulador de la conductancia transmembrana de la fibrosis quística), que altera la excreción de cloruro y bicarbonato, genera un moco más espeso en pulmón e intestino, y su tratamiento (antibióticos, cambio a una dieta rica en grasas, reemplazamiento de la enzima

pancreática y terapias moduladoras de CFTR) produce cambios en la microbiota de ambos órganos (Price & O'Toole, 2021). Por otra parte, en pacientes que sufren FQ, se limita la concentración intestinal de SCFAs porque (i) se reduce la abundancia de *Faecalibacterium* y *Roseburia*, principales productores de butirato, y *Akkermansia* y *Bacteroides*, principales productores de propionato, (ii) aumenta el catabolismo de estos dos SCFAs, y (iii) disminuye la capacidad de producción tanto de butirato como de acetato bacterianos (Price & O'Toole, 2021). Esta menor presencia de SCFAs intestinales puede agravar patologías respiratorias como el asma (Price & O'Toole, 2021). Asimismo, los componentes del tabaco y las partículas tóxicas ambientales inducen inflamación, producen daño en las uniones estrechas entre células, y disbiosis, no solo en pulmón sino también en intestino (Gui et al., 2021; Pambianchi et al., 2021).

1.3.3. Patógenos oportunistas colonizadores en el sistema respiratorio humano

Los microorganismos con rango de hospedador restringido, como es el ser humano, presentan un elevado grado de adaptación al hospedador/nicho que infectan o colonizan. En determinadas condiciones, la interacción hospedador-microorganismo resulta en un proceso patogénico, lo que llamamos **patógenos oportunistas colonizadores** (en inglés, *colonizing opportunistic pathogens*) (Price et al., 2017). Estos microorganismos son hongos (p. ej. *Candida albicans*), protozoos (p. ej. *Blastocystis*), virus (p. ej. *Rhinovirus*) o bacterias, con gran relevancia clínica por la generación de resistencias antibióticas (Price et al., 2017). Entre las principales bacterias se encuentran las Gram-negativas: *Moraxella catarrhalis* y *H. influenzae*; y las Gram-positivas: *S. pneumoniae* y *Staphylococcus aureus* (Garmendia et al., 2012; Price et al., 2017; Verhaegh et al., 2013). *H. influenzae*, *M. catarrhalis* y *S. pneumoniae* son los patógenos oportunistas colonizadores más comúnmente encontrados en el sistema respiratorio humano (Riesbeck, 2020).

En el sistema respiratorio, las patologías no infecciosas crónicas (EPOC o asma), las inmunodeficiencias congénitas o adquiridas (síndrome de la inmunodeficiencia adquirida, VIH), además de hábitos (p. ej. tabaco), dieta, edad, género, microbioma basal, etc., son factores que pueden favorecer la transición colonizador asintomático-infección sintomática, así como la susceptibilidad y severidad de la misma (Garmendia et al., 2012; Price et al., 2017; Siegel & Weiser, 2015).

En el contexto de pacientes que sufren EPOC, la alteración de las barreras inmunes favorece la infección por patógenos oportunistas colonizadores o de nueva entrada, que pueden también causar exacerbaciones. La colonización crónica y las infecciones recurrentes contribuyen a la inflamación respiratoria y al deterioro de la función pulmonar, todo ello facilitando la progresión de la patología (**Figura 4**). En este sentido, nuestro grupo de investigación ha desarrollado y caracterizado un modelo murino de infección recurrente en pulmón enfisematoso que recoge características del

fenotipo exacerbador frecuente característico de la EPOC (Rodríguez-arce et al., 2021) (para mayor detalle, ver **Anexo III**).

***Haemophilus influenzae*, patógeno oportunista colonizador del sistema respiratorio humano, ha sido objeto de estudio en esta Tesis Doctoral.**

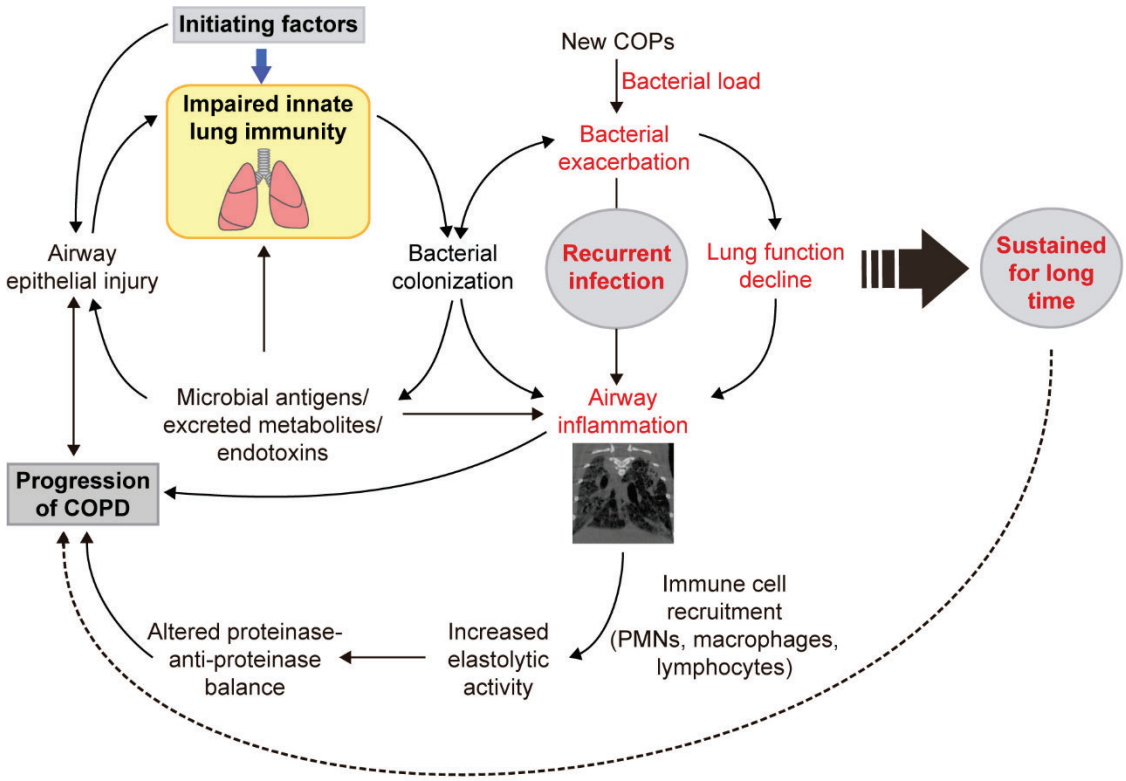

Figura 4. Hipótesis del círculo vicioso en la progresión de la EPOC. La disbiosis pulmonar provocada por la infección aguda o recurrente por patógenos colonizadores contribuye a perpetuar la patología crónica así como a su progresión irreversible. Adaptada de Rodríguez-arce et al., 2021.

2. *Haemophilus influenzae*: patógeno oportunista colonizador del sistema respiratorio humano

2.1. Características generales de *H. influenzae*

Haemophilus influenzae es un cocobacilo no móvil, Gram-negativo, pleiomórfico, catalasa positivo, con rango de hospedador restringido al ser humano, descubierto en 1892 por Richard Pfeiffer. Pertenece al filo Proteobacteria, clase γ-proteobacteria, orden Pasteurellales, familia Pasteurellaceae. Es anaerobio facultativo y presenta requerimientos nutricionales consistentes en nicotinamida adenina dinucleótido (NAD) (factor V) y hemina (factor X) (Agrawal & Murphy, 2011; Bakaletz & Novotny, 2018; Duell et al., 2016; Sriram et al., 2018). La especie *H. influenzae* se divide

en siete grupos: seis de ellos se denominan tipificables por tener cápsula polisacarídica (serotipos a-f), y uno se denomina no tipificable o desprovisto de cápsula (HiNT). En su membrana externa, *H. influenzae* posee una cadena corta de lipooligosacárido (LOS), carente de la cadena-O característica del lipopolisacárido (LPS) (Riesbeck, 2020; Schweda et al., 2007). El LOS de *H. influenzae* posee un núcleo triheptosilo sustituido con glucosa L-*α*-D-Hep*p*-(1→2)-[*P*Etn→6]-L-*α*-D-Hep*p*-(1→3)-[*β*-D-Glc*p*-(1→4)]-L-*α*-D-Hep*p* vinculado al lípido A a través de un único residuo de ácido 3-desoxi-d-mano-octulosónico (Kdo), ligado a la posición 6 del lípido A (Chung & Raetz, 2010; Schweda et al., 2007; White et al., 1997). Como estrategia de mimetismo molecular, *H. influenzae* decora la superficie del LOS con fosforilcolina (en inglés, *phosphorylcholine*, ChoP) y ácido siálico (Post et al., 2016).

H. influenzae coloniza la garganta y nasofaringe humana. Las colonización por cepas capsuladas en población infantil no vacunada es de un 3-12% de los niños menores de 3 años y se establece que a los 5 años la mayoría de los niños sin vacunar han desarrollado al menos un episodio de infección por *H. influenzae* serotipo b (Hib) (Slack, 2015). Aproximadamente 20% de la población infantil es colonizada por HiNT durante el primer año de vida, aumentando hasta 50% a los 5 años (Slack, 2015). En adultos, la colonización respiratoria por HiNT es del 20-30%, si bien este porcentaje aumenta en individuos que sufren patologías respiratorias como la EPOC (Slack, 2015). *H. influenzae* causa infecciones respiratorias agudas: OM infantil, siendo el patógeno más frecuentemente aislado en estos pacientes; sinusitis, crónica o aguda; conjuntivis en niños, ancianos y población inmunocomprometida; exacerbaciones en pacientes que sufren EPOC, bronquitis o FQ; neumonía (Agrawal & Murphy, 2011; Van Eldere et al., 2014). Asimismo, es causante de meningitis y sepsis en neonatos (Van Eldere et al., 2014). Hasta la implementación de la vacuna frente a Hib a principios de los años 90 del siglo XX, Hib fue la causa más común de infección bacteriana invasiva (infección sistémica) y meningitis bacteriana infantil en Estados Unidos (3-5% en población infantil), provocando un 3-6% de fallecimientos y 20-30% de secuelas permanentes (Agrawal & Murphy, 2011). La implementación de la vacuna frente a Hib, las mejoras en detección y serotipado de *H. influenzae*, y el aumento de virulencia de cepas HiNT, han provocado un descenso de las cepas tipificables y un aumento en la incidencia de HiNT, siendo las cepas no tipificables las que presentan mayor relevancia clínica en la actualidad por ser la principal causa de OM pediátrica y de exacerbaciones en adultos que sufren EPOC (Langereis & De Jonge, 2015; Murphy, 2015).

Este trabajo de Tesis Doctoral se ha centrado en el estudio de la interacción entre *Haemophilus influenzae* no tipificable (HiNT) y el sistema respiratorio humano.

2.2. Características genómicas y adaptativas de HiNT

El genoma de cepas HiNT presenta un tamaño medio de 1.847 Mb, contenido medio de G+C de 38% y codifica una media de 1722 proteínas (NCBI Genome ID: 165). El primer genoma secuenciado de un organismo de vida libre fue el de la cepa Hi RdKW20 (RefSeq: NC_000907.1) (Fleischmann et al., 1995), (cepa originalmente de serotipo D, sin capsula por manejo *in vitro*) con 1.830.137 pb, 1801 genes de los cuales 1604 corresponde a proteínas anotadas. Actualmente, disponemos de unos 803 genomas de *H. influenzae* en la base de datos NCBI (*National Center for Biotechnology Information*) (02/11/2021). A diferencia de las cepas tipificables, altamente clonales y con poca variabilidad genómica, las cepas no tipificables presentan alta tasa de heterogeneidad genómica (De Chiara et al., 2014; Pinto et al., 2019). Con una media de 1.813 genes por cepa, el pan genoma de HiNT presenta unos 6.453 genes, ~1.305 de los cuales se encuentran en el 95% de las cepas constituyendo el genoma central (en inglés, *core genome*), y ~4.505 genes pertenecen al genoma accesorio (Moleres et al., 2018; Pettigrew et al., 2018). El alineamiento del genoma central de HiNT permite su clasificación en 6 u 8 grupos, los cuales parecen estar relacionados con la presencia/ausencia de 17 genes, si bien no se correlacionan con la localización geográfica o el tipo de patología asociada (De Chiara et al., 2014; Pinto et al., 2019; Rajendra et al., 2020). Sin embargo, el análisis del genoma accesorio permite diferenciar cepas aisladas de pacientes EPOC respecto a cepas de otras patologías (Rajendra et al., 2020).

Los mecanismos moleculares responsables de la variación genómica observada entre cepas de HiNT consisten en: (i) polimorfismos genéticos (mutaciones puntuales, inserciones, deleciones o duplicaciones) (Gilsdorf et al., 2004); (ii) hipermutabilidad (Cardines et al., 2012; Watson et al., 2004); (iii) variación de fase por número variable de repeticiones de secuencias simples/cortas de ADN (en inglés, *simple/short sequence repeats*, SSR) en regiones codificantes y promotoras (Fernández-Calvet, et al., 2021; Moxon et al., 2006; Power et al., 2009); (iv) variación de fase por metilación del ADN y existencia de regulones de fase variable (en inglés, *phasevarions*) (Atack et al., 2015, 2019; Seib et al., 2020); (v) transferencia horizontal de genes (en inglés, *horizontal gene transfer*, HGT) mediante transformación natural (Mell et al., 2016; Poje & Redfield, 2003). Esta diversidad genómica determina la enorme plasticidad fenotípica de HiNT, que resulta clave en los procesos de evasión de la inmunidad respiratoria, pato-adaptación y evolución pato-adaptativa que favorecen la colonización del sistema respiratorio humano por este patógeno oportunista.

La secuenciación genómica temprana de *H. influenzae* permitió que esta bacteria fuera pionera en el desarrollo e implementación de técnicas –ómicas, indispensables para avanzar en el conocimiento de las características de su interacción con el sistema respiratorio humano y sus mecanismos de pato-adaptación, claves para el desarrollo de estrategias diagnósticas, preventivas y terapéuticas.

La contribución de las técnicas -ómicas al estudio de la interacción *H. influenzae*-sistema respiratorio humano ha sido revisada en el Capítulo 1 de este trabajo de Tesis Doctoral.

2.2.1. Competencia natural

La competencia natural es la capacidad de las bacterias de captar activamente ADN extracelular (**Figura 5**). Más del 85% del ADN internalizado es degradado y utilizado como fuente de carbono, nitrógeno, fósforo, energía y especialmente de nucleótidos (Macfadyen et al., 2001; Mell & Redfield, 2014; Sinha et al., 2013). La hebra de ADN incorporada puede no ser degradada y pasar a formar parte del genoma bacteriano mediante recombinación homóloga, cuyas consecuencias pueden ser (**Figura 5C**): (i) la reparación de ADN dañado, o (ii) el aumento de la variabilidad genética de la bacteria al generar intercambio alélico o incorporar material genético accesorio, lo que puede llevar asociada la incorporación de genes que proporcionan resistencia antibiótica, determinantes antigénicos o factores de virulencia (Maughan & Redfield, 2009; Mell et al., 2011; Mell & Redfield, 2014; Mora et al., 2021; Sinha et al., 2013).

H. influenzae incorpora ADN exógeno, preferentemente de especies cercanas pertenecientes a la familia Pasteurellaceae, utilizando un mecanismo de reconocimiento de secuencias (Mora et al., 2021). La maquinaria de captación de ADN de la superficie celular reconoce y une preferentemente ADN de doble cadena que contiene una secuencia conservada y específica de 9 pb, AAGTGCGGT, denominada **USS** (del inglés, *Uptake Signal Sequence*). Por ejemplo, existen unas 2.206 copias de la secuencia USS en el genoma de la cepa Hi RdKW20, ~1 USS/kb, lo que supone ~1% del genoma, la mayoría localizadas en regiones codificantes (Maughan et al., 2010; Mell & Redfield, 2014). La distribución de USS a lo largo del genoma de *H. influenzae* parece ser al azar, lo que puede hacer que diferentes genes experimenten distintas tasas de intercambio genético (Mora et al., 2021; Smith et al., 1995). Las proteínas de *H. influenzae* responsables de esta especificidad por regiones USS no han sido identificadas, si bien podría darse a través del sistema PilNOPQ (Mell & Redfield, 2014). El reconocimiento y unión de USS se produce mayoritariamente en GCGG (Mell & Redfield, 2014).

La incorporación de ADN se realiza en dos etapas secuenciales conocidas como **captación de ADN** (a través de la membrana externa) (**Figura 5A**) y **translocación** (a través de la membrana interna) (**Figura 5B**). El transporte del ADN unido a la superficie bacteriana a través de la membrana externa utiliza pseudopili tipo IV (en inglés, *type IV pili*, Tfp o T4P), fibras de pequeño tamaño que sobresalen de la superficie celular formadas por subunidades de pilina polimerizadas cuya formación depende de los genes *pilA* y *comE* (Bakaletz et al., 2005; Redfield et al., 2005).

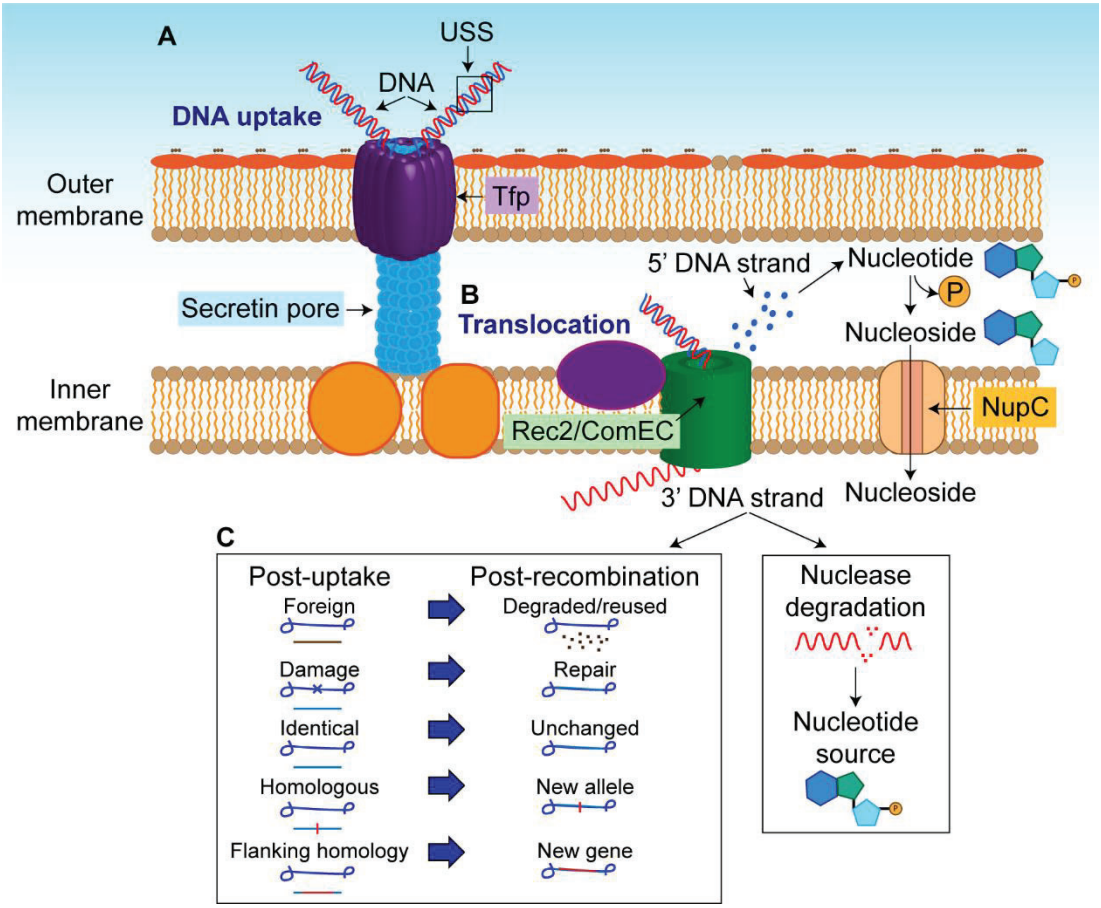

Figura 5. Mecanismo de transformación natural de HiNT. (A) Las secuencias de ADN USS son reconocidas por la maquinaria de captación permitiendo la incorporación al periplasma del fragmento de ADN a través del poro de secretina. **(B)** La hebra 5' es degradada en el periplasma y utilizada como fuente de nucleótidos; la hebra 3' es translocada hacia el citoplasma a través del poro formado por Rec2/ComEC. **(C)** Si la homología de secuencias lo permite, la hebra 3' podrá ser integrada en el genoma bacteriano mediante recombinación homóloga; sino, será degradada por nucleasas y utilizada como fuente nutricional. Adaptada de Mell & Redfield, 2014.

Tfp incorpora ADN hacia el periplasma a través del poro de secretina utilizando la fuerza creada por su capacidad retráctil (Mell & Redfield, 2014; Mora et al., 2021; Sinha et al., 2012). Durante la translocación membrana externa-membrana interna, la molécula de ADN unida se pliega sobre sí misma y las dos hebras se separan en regiones ricas en AT para pasar por el poro de secretina de la maquinaria de captación (Mora et al., 2021). Cuando un extremo de ADN está en el periplasma, ComEA controla la incorporación del resto de ADN al periplasma mediante un proceso irreversible (Mora et al., 2021). La hebra 5' es degradada en el periplasma, sus nucleótidos defosforilados e incorporados como nucleósidos a través de NupC mientras que la hebra 3' atraviesa la membrana interna a través de un poro formado por Rec2/ComEC (Mell & Redfield, 2014; Mora et al., 2021; Sinha et al., 2013). Si la homología de secuencia lo permite, esta hebra podrá ser incorporada en el genoma bacteriano mediante doble **recombinación homóloga** catalizada por RecA. Alternativamente, será degradada y utilizada como fuente de nucleótidos (Mell & Redfield, 2014).

Si bien la capacidad de unión del fragmento de ADN a la superficie bacteriana es independiente del tamaño del mismo, la eficiencia de transformación es mayor con un tamaño de fragmento de ADN > 3,5 kb (Deich & Smith, 1980; Mora et al., 2021; Pifer & Smith, 1985). En condiciones *in vitro*, la velocidad de captación de ADN se estima entre 500 y 1000 pb/s y la transformación se completa en un intervalo aproximado de 5 a 30 minutos desde que el fragmento de ADN es añadido (Deich & Smith, 1980; Mora et al., 2021).

La **regulación de la competencia natural** depende de la disponibilidad de nutrientes del medio (**Figura 6**). La privación de azúcares extracelulares PTS (del inglés, *phosphotransferase system*) activa la adenilato ciclasa (Cya) que cataliza la conversión de ATP (adenosín trifosfato) a AMPc (adenosín monofosfato cíclico) (Macfadyen et al., 1996; Sinha et al., 2013). El aumento de los niveles de **AMPc** activa el factor de transcripción **CRP** (del inglés, cAMP *receptor protein*) formando un complejo activo al unirse a su dominio N-terminal, que resulta en un cambio conformacional exponiendo el dominio C-terminal de unión a ADN (Cameron & Redfield, 2006). Para iniciar la transcripción génica, el ADN se pliega sobre CRP y recluta a la ARN polimerasa (Cameron & Redfield, 2006). La unión AMPc-CRP promueve la activación transcripcional del regulón implicado en la utilización de azúcares no PTS como fuente de carbono, que contienen un sitio de unión canónico **CRP-N** de 22 pb (TGTGA(N_6)TCACA) (Macfadyen et al., 1996; Redfield et al., 2005).

La inducción de la competencia natural de HiNT requiere, el complejo AMPc-CRP, y el regulador de competencia **Sxy** (o TfoX) (Redfield et al., 2005). El mecanismo de acción de Sxy no es bien conocido, si bien puede estabilizar la unión CRP-ADN (Cameron & Redfield, 2006). AMPc-CRP junto con Sxy activan la transcripción de unos 26 genes (*pilA*, *pilB*, *pilC*, *pilD*, *comA*, *comB*, *comC*, *comD*, *comE*, *comF*, *comN*, *comO*, *comP*, *comQ*, *comE1*, *pilF2*, *rec2*, *ligA*, *toxA*, *toxT*, *comM*, *dprA*, *radC*, *ssb*, HI0365 y HI1631) distribuídos en 13 operones pertenecientes al regulón CRE (del inglés, *competence regulatory element*) cuyos promotores contienen un sitio no canónico de unión a CRP (TGCGA(N_6)TCGCA) denominado **CRP-S** (dependiente de Sxy) o CRE (del inglés, *competence regulatory element*), que difiere en dos pares de bases de las secuencias CRP-N (Redfield et al., 2005). Diecisiete de estos genes son necesarios para que se produzca transformación natural, siendo 14 imprescindibles para la incorporación de ADN (Sinha et al., 2012) (**Tabla 1**).

La actividad de Sxy está sujeta a regulación postranscripcional condicionada por la estructura secundaria del ARNm en la región 5' UTR donde el tallo se pliega por homología de bases, forma 3 bucles, y dificulta el acceso de los ribosomas al codón de inicio (Cameron et al., 2008). La regulación de la traducción de Sxy es dependiente de la presencia de purinas, e independiente de Hfq o genes de competencia (Sinha et al., 2013).

La incorporación y biosíntesis de purinas se resume a continuación. Los nucleótidos extracelulares son convertidos en sus respectivos nucleósidos en el periplasma, transportados al

citosol mediante NupC (**Figura 7A**), y convertidos en sus respectivas bases, o de nuevo a nucleótidos a través de las HPRT y APRT fosforibosil transferasas (Sinha et al., 2013). La biosíntesis *de novo* de

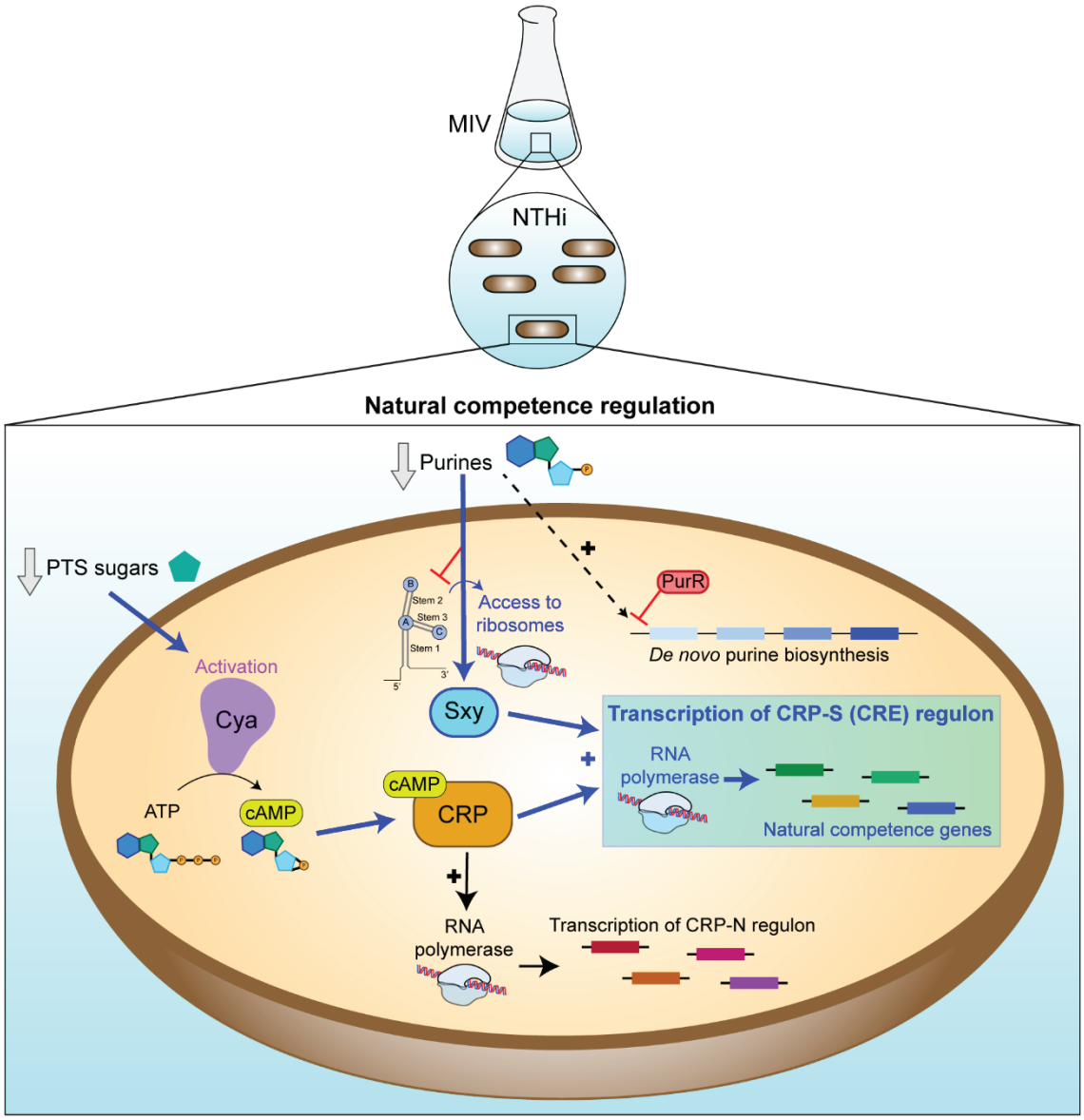

Figura 6. Regulación de la competencia natural de HiNT. La baja disponibilidad de azúcares PTS activa la adenilato ciclasa que eleva la concentación de AMPc lo que permite la formación del complejo CRP-AMPc. La baja disponibilidad de purinas ralentiza la formación de la estructura secundaria del ARN de sxy, facilitando el acceso de los ribosomas. CRP-AMPc, junto con Sxy, permite la transcripción del regulón de genes de competencia natural, denominado regulón CRP-S o CRE.

purinas convierte la ribosa-5-fosfato en fosforribosil pirofosfato (PPRP), ribonucleótido 5-aminoimidazol-4-carboxamida (AICAR) y finalmente inosina monofosfato (IMP), en un proceso relacionado con la biosíntesis de histidina a través de PRPP y AICAR, y regulado por la disponibilidad de nucleótidos extracelulares mediante el represor PurR (Sinha et al., 2013) (**Figura 7B**). La presencia de nucleótidos, incorporados o sintetizados, promueve una rápida transcripción y

formación de la estructura secundaria de ARNm de *sxy*, dificultando el acceso de los ribosomas (Cameron et al., 2008). Sin embargo, la baja disponibilidad de purinas ralentiza este proceso y facilita el acceso de los ribosomas a los nuevos transcritos formados aumentando la traducción de proteína (Cameron et al., 2008). La inactivación de PurR reduce los niveles de competencia natural ya que aumenta la biosíntesis de purinas (Sinha et al., 2013). Asimismo, el intermediario de la síntesis de purinas PRPP desempeña un papel en la traducción de Sxy, a través de un mecanismo no conocido (Sinha et al., 2013).

Tabla 1. Genes de *H. influenzae* pertenecientes al regulón CRP-S.

Gen	Locus en RdKW20	Necesario para la captación	Necesario para la transformación
pilA	HI0299	Sí	Sí
pilB	HI0298	Sí	Sí
pilC	HI0297	Sí	Sí
pilD	HI0296	Sí	Sí
comA	HI0439	Sí	Sí
comB	HI0438	Sí	Sí
comC	HI0437	Sí	Sí
comD	HI0436	Sí	Sí
comE	HI0435	Sí	Sí
comF	HI0434		Sí
comN	HI0938	Sí	Sí
comO	HI0939	Sí	Sí
comP	HI0940	Sí	Sí
comQ	HI0941	Sí	Sí
comE1	HI1008		
HI0365	HI0365		
pilF2	HI0366	Sí	Sí
rec2	HI0061		Sí
ligA	HI1182, HI1183		
toxA	HI0659		Sí
toxT	HI0660		
HI1631	HI1631		
comM	HI1117		
dprA	HI0985		
radC	HI0952		
ssb	HI0250	Mutación letal	Mutación letal

La competencia natural de *H. influenzae* se induce de manera eficiente al transferir un cultivo bacteriano crecido hasta fase exponencial en medio infusión cerebro corazón (del inglés, *brain heart infusion*, BHI) a medio mínimo MIV, carente de los precursores de nucleótidos, cofactores y fuentes de carbono necesarios para el crecimiento (Herriott et al., 1970) (**Tabla A1**).

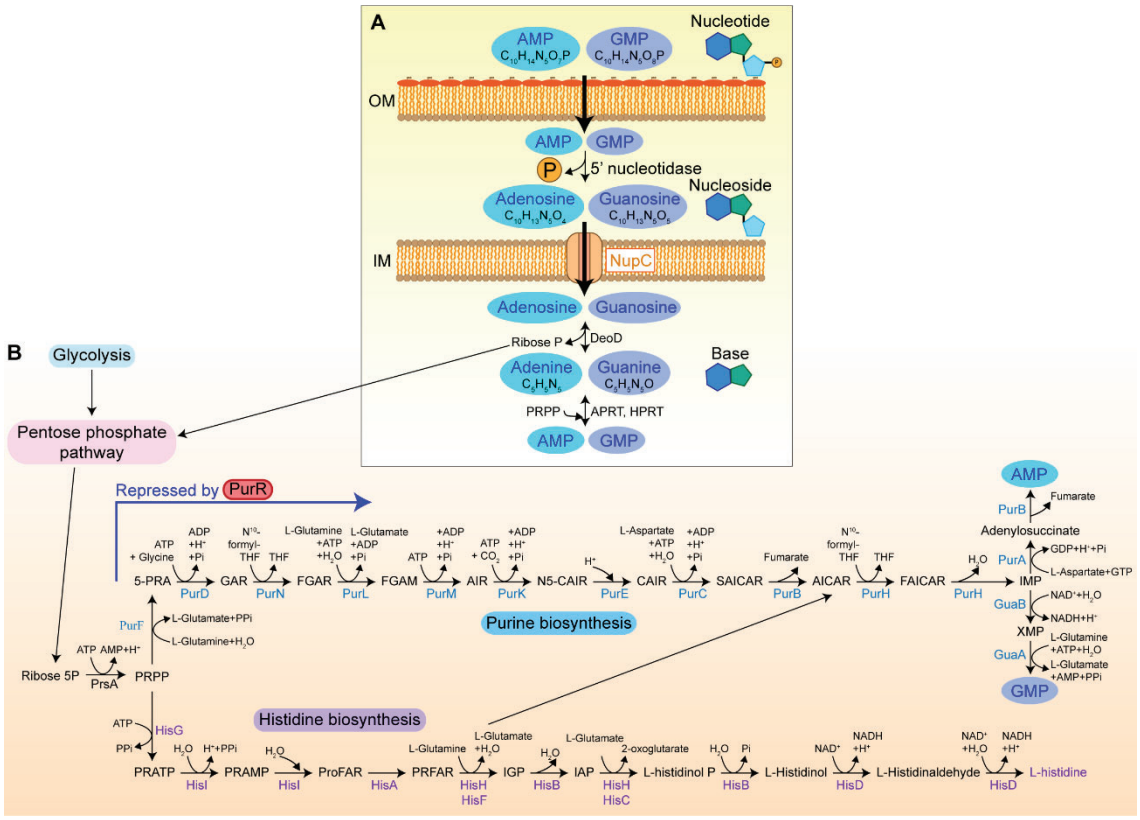

Figura 7. Incorporación y biosíntesis de purinas en HiNT. (A) Los nucléotidos AMP y GMP son desfosforilados en el periplasma e incorporados al citoplasma a través del transportador NupC. **(B)** La biosíntesis de purinas deriva de la ruta de las pentosas fosfato, está controlada mediante el represor PurR, y está relacionada con la biosíntesis de histidina a través de PRPP y AICAR.

La inducción de la expresión de genes de competencia natural y biosíntesis de purinas durante la infección respiratoria por *H. influenzae* ha sido estudiada en el Capítulo 2 de esta Tesis Doctoral.

2.2.2. Características metabólicas de *H. influenzae* y su relevancia durante la infección

H. influenzae muestra rasgos de reducción genómica que lo convierten en auxótrofo para fructosa, uracilo, espermidina y putrescina, ácido pantoténico, tiamina, hemina y NAD (Macfadyen & Redfield, 1996; Schilling & Palsson, 2000). Igualmente, *H. influenzae* presenta un ciclo de Krebs incompleto, y carece de ciclo de β-oxidación de ácidos grasos (**Figura 8**). A continuación, se detallan

las características del metabolismo de azúcares (**sección 2.2.2.1**) y metabolismo de ácidos grasos (**sección 2.2.2.2**) de *H. influenzae*.

HiNT muestra rasgos genómicos de adaptación metabólica entre los que se encuentran la presencia del operón de síntesis de histidina (operón *his*) en aislados clínicos de OM, a diferencia de aislados comensales de nasofaringe que pueden ser auxótrofos (Juliao et al., 2007), o la presencia del operón ureasa, que favorece la supervivencia del patógeno en compartimentos intracelulares ácidos durante la infección, siendo prescindible en aislados de nasofaringe (Zhang et al., 2013). Por otra parte, más de 70 genes del genoma accesorio de HiNT (transporte, mantenimiento de la homeostasis redox, metabolismo de carbohidratos, biosíntesis de LOS, competencia natural y evasión de la respuesta inmune) han sido relacionados con la adaptación de HiNT a las vías respiratorias bajas de pacientes EPOC (Rajendra et al., 2020). Estas cepas HiNT persistentes adaptan además su metabolismo mediante variación de fase o polimorfismos (en inglés, *single nucleotide polymorphism*, SNPs) regulando la adherencia, la adquisición de nutrientes, modificación de proteínas de membrana, biosíntesis y modificación del LOS, y metilación (Moleres et al., 2018; Pettigrew et al., 2018). Por su parte, los aislados invasivos muestran rasgos de adaptación de su metabolismo central, utilizan de manera más eficiente glucosa y ácido siálico, y excretan mayor cantidad de ácido succínico con efecto inmunomodulador (Muda et al., 2019a). La limitación transitoria de hemina también genera cambios metabólicos patoadaptativos en HiNT mediante la inactivación del gen *icc*, que codifica una AMPc fosfodiesterasa, lo que aumenta la persistencia bacteriana (Harrison et al., 2019).

A nivel transcripcional, HiNT activa la expresión de genes que codifican sistemas de captación y utilización de hierro, sistemas de transporte de aminoácidos, vitaminas, iones y sodio en las primeras etapas de la infección; sin embargo, posteriormente reprime su metabolismo central (glicólisis, gluconeogénesis, pentosas fosfato y biosíntesis de ácidos grasos), y activa genes implicados en captación y utilización de lactato como fuente de carbono y mecanismos de respuesta a estrés (sistemas de toxina-antitoxina y transporte de glutatión), para adaptarse metabólicamente a las condiciones del medio (Baddal et al., 2015).

La secuenciación de la cepa Hi RdKW20 (Fleischmann et al., 1995) permitió el desarrollo del primer modelo metabólico computacional a escala genómica (en inglés, *genome-scale metabolic model*, GEM) (Edwards & Palsson, 1999; Schilling & Palsson, 2000). Este modelo permitió (i) conocer características estructurales básicas del metabolismo de HiNT, (ii) mejorar la anotación de secuencias, (iii) predecir co-regulación o co-expresión de conjuntos de genes, (iv) predecir el sustrato mínimo necesario para la producción de biomasa de HiNT, y (v) la identificación de posibles dianas terapéuticas mediante simulación de inactivación génica (Schilling & Palsson, 2000). No obstante, este modelo presenta una aplicabilidad limitada al no poder emplearse en estudios de biología complejos ya que dista mucho de los nuevos GEMs desarrollados en otras bacterias (Monk et al.,

2014). El número de reacciones y genes que contempla este modelo es bajo, y carece de la especificación del compartimento celular así como de la función objetiva de biomasa detallada (en inglés, *biomass objetive function*, BOF). Con el objetivo de generar un GEM actualizado de HiNT, **este modelo ha sido completamente actualizado en el Capítulo 4 de esta Tesis Doctoral.**

2.2.2.1. Metabolismo de azúcares en *H. influenzae*

H. influenzae es anaerobio facultativo y fermenta azúcares (fructosa, glucosa, galactosa, ribosa, xilosa, fucosa, glicerol y ácido siálico) disponibles en el nicho respiratorio (Macfadyen & Redfield, 1996). El sistema PTS de *H. influenzae* transporta preferentemente fructosa que, si bien no es el azúcar más abundante en el cuerpo humano, es incorporado por HiNT de manera prioritaria ya que sus gradientes de concentración son un indicador de nichos colonizables y no genera competencia con el hospedador (Macfadyen & Redfield, 1996). La limitación de fructosa en el medio induce Cya y eleva los niveles de AMPc, lo que activa CRP y posibilita la formación del complejo activo AMPc-CRP. Este complejo induce la activación transcripcional de genes implicados en la captación y catabolismo de azúcares no PTS que contienen en sus regiones promotoras el sitio de unión CRP-N (Macfadyen & Redfield, 1996; Macfadyen et al., 1996). Los azúcares del sistema CRP-N, dependientes de AMPc y reprimidos por fructosa, son galactosa, ribosa, xilosa y fucosa, cuyo sitio de unión CRP-N se encuentra en los promotores de los genes *mglB*, *rbsD*, *xylH* y *fucP*, respectivamente (Macfadyen & Redfield, 1996). El glicerol es incorporado a través del sistema facilitador de difusión, GlpF, y del transporador GlpT (Macfadyen & Redfield, 1996); el ácido siálico es transportado al interior mediante la permeasa NanT, o los transportadores SiaT y SiaP (Allen et al., 2005; Macfadyen & Redfield, 1996; Post et al., 2016); el transportador de glucosa no es conocido, si bien HiNT incorpora este azúcar y lo fosforila a través de una quinasa dependiente de ATP (Macfadyen & Redfield, 1996).

HiNT modula su metabolismo de azúcares para adaptarse a las condiciones cambiantes del nicho de manera que (i) compite con las células del hospedador por la incorporación de glucosa (Baker & Baines, 2018), que puede sustituir a la fructosa como fuente de carbono (Edwards & Palsson, 1999; Macfadyen & Redfield, 1996; Schilling & Palsson, 2000); y (ii) sobrevive en condiciones aerobias y anaerobias, requiriendo hemina únicamente durante el crecimiento aerobio (Ghorbani et al., 2015; Man et al., 2017; Muda et al., 2019a; O'Reilly et al., 1992; Osgood et al., 2015; Othman et al., 2014; Raghunathan et al., 2004).

Como principales vías de catabolismo de glucosa a piruvato, *H. influenzae* utiliza la glicólisis y la ruta de las pentosas fosfato, con todas sus enzimas presentes a excepción de la glucoquinasa (**Figura 8**) (Othman et al., 2014). Si bien son rutas conservadas, la degradación de la glucosa principalmente a través de la glicólisis o ruta de las pentosas fosfato es cepa-dependiente (Othman et al., 2014). HiNT posee dos enzimas de la ruta Entner Doudoroff, KdgK y Eda, sin embargo la

utilización de esta ruta es exclusiva para la utilización del gluconato como fuente de carbono, y no está unida con el catabolismo de glucosa mediante la vía de las pentosas fosfato (Fleischmann et al., 1995; Ishak et al., 2014). La bacteria posee un ciclo de Krebs incompleto ya que carece de las enzimas de la rama oxidativa, citrato sintasa, isocitrato deshidrogenasa y aconitasa. Esta ausencia conlleva a la utilización de esta ruta como generador de precursores biosintéticos (Othman et al., 2014). El oxalacetato es precursor de serina, glicina, cisteína, fenilalanina, tirosina, triptófano, aspartato y asparagina; el oxoglutarato es precursor de glutamato, glutamina, prolina y arginina. La incorporación de glutamato permite la producción de oxoglutarato, y la del aspartato posibilita la generación de oxalacetato y fumarato (Edwards & Palsson, 1999; Raghunathan et al., 2004). Las unidades de carbono procedentes de la glicólisis pueden ser incorporadas al ciclo de Krebs desde fosfoenolpiruvato a oxalacetato a través de la fosfoenolpiruvato carboxiquinasa PckA, y desde piruvato a malato mediante la enzima málica dependiente de NADP MaeB (Othman et al., 2014). Si bien el metabolismo de *H. influenzae* es mayoritariamente fermentativo, utiliza una cadena de transporte de electrones que consta de 5 deshidrogenasas: NADH deshidrogenasas (Ndh y Nqr), lactato deshidronasas (LldL y Dld) y formato deshidroganasa (Fdx), y 6 reductasas terminales que transfieren los electrones al oxígeno, DMSO o productos nitrogenados, para oxidar el NADH y $FADH_2$ producido durante el catabolismo de las fuentes de carbono (Othman et al., 2014). A este tipo de metabolismo se le denomina "fermentación asistida por respiración". La fermentación de la glucosa genera acetato, lactato, formato y succinato como productos finales excretados (Muda et al., 2019a; Othman et al., 2014; Raghunathan et al., 2004). En aerobiosis, se produce principamente acetato a través del complejo piruvato deshidrogenasa (AceF, AceA y LpdA), que produce NADH, y las enzimas fosfato acetiltransferasa (Pta) y acetato quinasa (AckA) (Othman et al., 2014). La producción de acetato a través del sistema Pta-AckA es reversible, lo que permite la utilización de acetato como fuente de carbono (Raghunathan et al., 2004; Wolfe, 2005). En anaerobiosis hay una menor actividad de la cadena de transporte de electrones, y *H. influenzae* produce un cambio en el catabolismo del piruvato, sintetizando menos acetato y más formato y succinato (Muda et al., 2019a; Othman et al., 2014; Wolfe, 2005). El formato se produce a partir de piruvato mediante la piruvato-formato liasa PflB (Othman et al., 2014; Raghunathan et al., 2004). El succinato se sintetiza en el ciclo de Krebs a partir de succinil-CoA mediante la enzima succinil-CoA sintetasa SucDC, o bien a través de la fumarato reductasa FrdAB, que reduce el fumarato y oxida la quinona a quinol en la cadena de transporte de electrones (Othman et al., 2014; Raghunathan et al., 2004).

El Capítulo 3 de esta Tesis Doctoral ha analizado el efecto del desbalance del catabolismo de glucosa por inactivación génica en la infección respiratoria por *H. influenzae*.

2.2.2.2. Metabolismo de ácidos grasos en *H. influenzae*

H. influenzae utiliza el **sistema FASII** (del inglés, *fatty acid biosynthesis* II) para la biosíntesis de ácidos grasos, que una vez sintetizados pasan a formar parte de integral de los fosfolípidos y el lípido A de la molécula de LOS (Lu et al., 2004) (**Figura 8**). El genoma de *H. influenzae* contiene los genes biosintéticos *accABCD*, *fabABDGHIZ*, y el regulador *fadR* (Fleischmann et al., 1995; Sutrina & Scocca, 1976), y así como *plsB* y *plsC*, responsables de la síntesis de ácido fosfatídico, precursor de los fosfolípidos presentes en HiNT, PE y PG (85:15). La bacteria carece de *fabF*, no pudiendo regular la composición de ácidos grasos por temperatura ni elongar el ácido palmitoleico (16:1) para producir ácido cis-vaccénico (18:1), y su ausencia no es compensada por *fabB* (Parsons & Rock, 2013; Wang & Cronan, 2003). FASII es un proceso esencial debido, entre otros, a que la estructura del lípido A contiene un ácido 3-hidroxi que no puede ser incorporado desde el exterior (McKinney et al., 2016). La esencialidad de esta ruta metabólica ha identificado las enzimas integrantes de la misma como posibles dianas terapéuticas (ver **sección 3.3.1**). FASII posee un módulo de iniciación formado por: (i) el complejo acetil-CoA carboxilasa (ACC), formado por biotina carboxilasa AccC, proteína transportadora de biotina carboxilo (en inglés, *biotin carboxyl carrier protein*, BCCP) AccB, y carboxiltransferasa AccAD, que forma malonil-CoA a partir de la carboxilación de acetil-CoA utilizando la hidrólisis de una molécula de ATP como fuente de energía y biotina, y y cuya producción es proporcional a la cantidad de ácidos grasos producidos (Broussard et al., 2015; Davis et al., 2000; Parsons & Rock, 2013); (ii) FabD, que transfiere ACP (del inglés, *acyl carrier protein*) al grupo malonato del malonil-CoA (Parsons & Rock, 2013); (iii) β-cetoacil-ACP sintasa III (KASIII) o FabH, que posee un sitio catalítico formado por Cys-His-Asn, contiene 22 residuos que conforman el tunel de unión a CoA bien conservados, y cataliza la condensación de tipo Claisen entre malonil-ACP y acetil-CoA, donde el grupo acilo del acil-CoA se transfiere a la cisteína del sitio activo y libera CoA, mientras que el malonil-ACP se une posteriormente, liberando bicarbonato y β-cetoacil-ACP (Gajiwala et al., 2009; Parsons & Rock, 2013). Por su parte, el módulo de elongación de ácidos grasos recibe el producto de la reacción catalizada por FabH y en cada ciclo elonga el acil-ACP en dos carbonos. La enzima β-cetoacil-ACP reductasa o FabG, reduce el producto de FabH produciendo β-hidroxiacil-ACP y $NADP^+$, que deriva hacia la síntesis del lípido A, o continua su ciclo de elongación vía β-hidroxiacil-ACP deshidratasas o FabZ/FabA, mediante deshidratación a *trans*-2-enoil-ACP, siendo FabA la enzima que permite la isomerización *cis-trans* para la síntesis de ácidos grasos insaturados (Parsons & Rock, 2013). La enzima *trans*-2-enoil-ACP reductasa, FabI, cataliza la reducción del doble enlace C2-C3 de *trans*-2-enoil-ACP a acil-ACP, en una reacción limitante de velocidad ya que determina bien la compleción del ciclo o la acumulación de β-hidroxiacil-ACP, y es inhibible por su producto (Parsons & Rock, 2013). El acil-ACP formado es sustrato para la síntesis de ácido fosfatídico y fosfolípidos mediante PlsBC, o para otro ciclo de elongación (Parsons & Rock, 2013), comenzado por FabB, que cataliza una reacción de

condensación idéntica a FabH pero contiene un sitio catalítico diferente, His-His-Cys, que la diferencia del módulo de iniciación y no utiliza acetil-CoA como sustrato (Parsons & Rock, 2013).

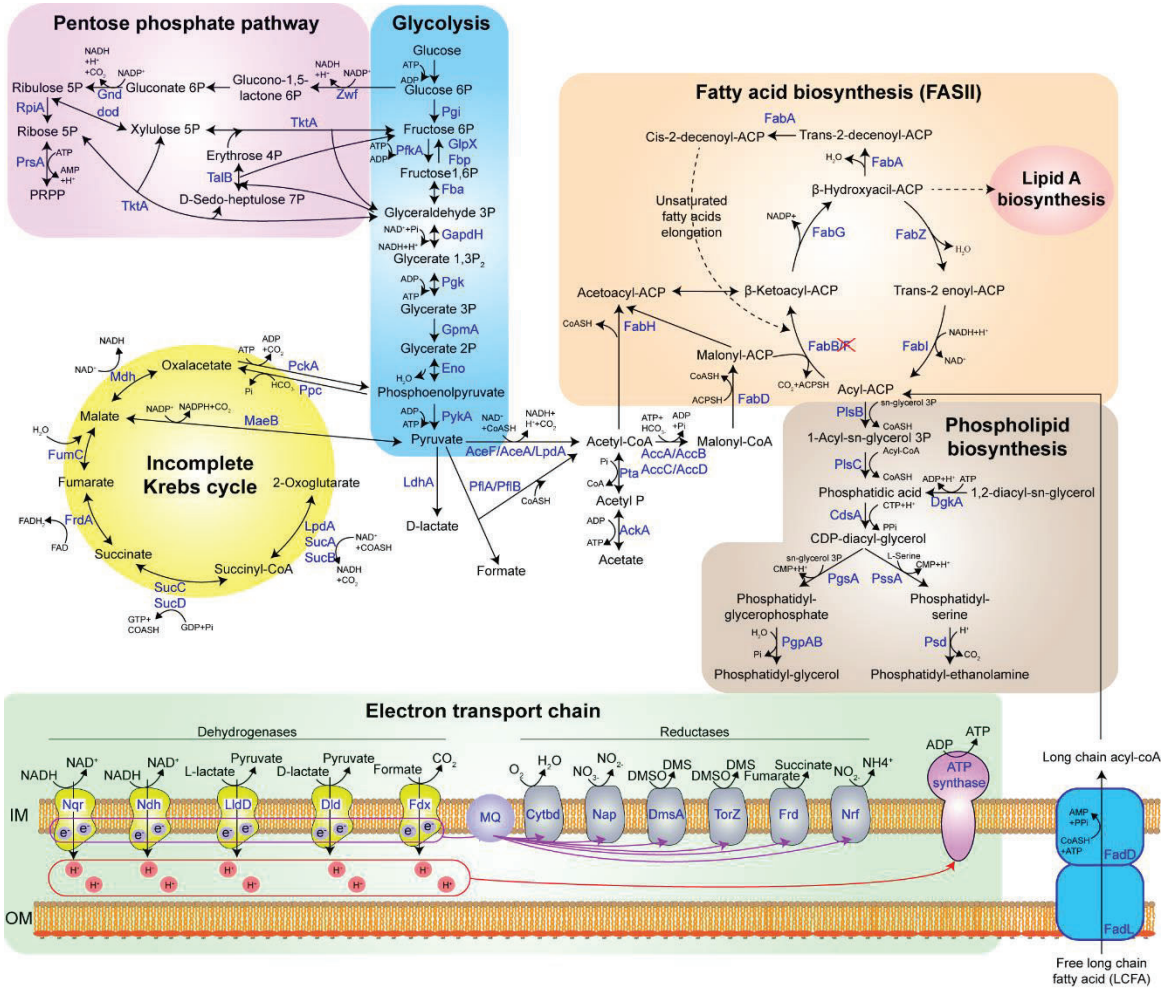

Figura 8. Características del metabolismo central de HiNT. El catabolismo de azúcares (parte izquierda) de HiNT consiste en una "fermentación asistida por respiración", conectada con la ruta de biosíntesis de ácidos grasos (parte derecha) mediante acetil-CoA. La cadena de transporte de electrones (parte de abajo), que consta de 5 deshidrogenasas y 6 reductasas, alivia el exceso de poder reductor producido en el catabolismo de la glucosa. Los productos principales de la ruta de biosíntesis de ácidos grasos son la síntesis del lípido A, y fosfolípidos, los cuales también pueden sintetizarse mediante la incorporación de ácidos grasos de cadena larga a través de FadL.

Por otra parte, HiNT dispone del transportador de ácidos grasos exógenos de cadena larga (en inglés, *long chain fatty acids*, LCFAs), OMP P1 o **FadL**, y de la LCFAs-CoA ligasa FadD, que activa y transporta los ácidos grasos incorporados al citoplasma (Fleischmann et al., 1995; Kunau et al., 1995). Estos ácidos grasos exógenos, convertidos a acil-CoA por FadD, son utilizados por PlsBC en la síntesis de fosfolípidos, si bien no entran en el ciclo de elongación de FASII debido a la falta de las enzimas acil-CoA:ACP transacilasa o 2-acilglicerofosfoetanolamina aciltransferasa bifuncional (*aas*) (Fleischmann et al., 1995; Yao & Rock, 2015).

En términos regulatorios, FadR reprime *fadL* y *fadD*, activa *fabA* y *fabB*, y es regulado por acil-CoA (Iram & Cronan, 2005; Parsons & Rock, 2013). FabR reprime *fabA* y *fabB* uniéndose a regiones del promotor en posición 3' a la secuencia de reconocimiento de FadR, y es regulado por acil-CoA y acil-ACP (Parsons & Rock, 2013).

El metabolismo de ácidos grasos de *H. influenzae* tiene varias derivadas que han sido abordadas en nuestro grupo de investigación. El desbalance en el metabolismo de lípidos observado en el sistema respiratorio de pacientes que sufren EPOC genera un entorno rico en ácidos grasos, por liberación de ácido araquidónico (C20) vía PLA_2 en respuesta a la inflamación, y aumento de los niveles de esfingolípidos (Chen et al., 2019). LCFAs como el ácido araquidónico tienen efecto bactericida frente a HiNT (Knapp & Mellyt, 1986) que a su vez puede compensarse por la inactivación de FadL (Moleres et al., 2018). Por otra parte, el mantenimiento de la asimetría de la membrana externa define la permeabilidad bacteriana, y protege a la bacteria de la acción bactericida de moléculas hidrofóbicas. El sistema **MlaA** (del inglés, *maintenance of the lipid asymmetry*)**,** formado por la lipoproteína MlaA/VacJ, la chaperona MlaC y el transportador ABC de membrana interna MlaBDEF, juega un papel clave, previniendo la acumulación de fosfolípidos en la superficie bacteriana mediante su transporte retrógrado y subsiguiente reciclaje (Henderson et al., 2016; Malinverni & Silhavy, 2009). Trabajo previo de nuestro grupo de investigación abordó la participación de VacJ/MlaA en el mantenimiento de la composición fosfolipídica en HiNT, así como su papel protector frente al efecto bactericida de moléculas hidrofóbicas como LCFAs (Fernández-Calvet et al., 2018).

El Capítulo 4 de esta Tesis Doctoral ha explorado el metabolismo de lípidos de *H. influenzae* como fuente de dianas terapéuticas, centrándose en la inhibición farmacológica de la enzima β-cetoacil-ACP sintasa III, FabH, que forma parte de la ruta de biosíntesis de ácidos grasos FASII.

2.3. Interacción de *H. influenzae* con el sistema respiratorio humano: mecanismos de colonización y estilos de vida

2.3.1. Factores de HiNT implicados en la evasión de elementos de la inmunidad respiratoria

H. influenzae dispone de varios mecanismos de defensa que contribuyen a la evasión inmunitaria en el sistema respiratorio (**Figura 9**):

(i) Factor de supervivencia de macrófagos (Figura 9A). La presencia de los genes *msfA1-4* (del inglés, *macrophage survival factor*) favorecen la supervivencia intracelular de *H. influenzae* en macrófagos (Kress-Bennett et al., 2016).

(ii) Formación de biopelículas (Figura 9B), (desarrollado en la **sección 2.3.1.1**). Contribuye a la evasión de la fagocitosis por macrófagos y neutrófilos y favorece la resistencia a NETs.

(iii) Producción de proteínas antioxidantes (Figura 9C). HiNT produce catalasa, codificada por el gen *hktE*, y peroxirredoxina-glutarredoxina codificada por el gen *pdgX*, con función protectora frente a estrés oxidativo y NETs, y contribuyen ambas proteínas a la persistencia *in vivo* (Juneau et al., 2015).

(iv) Supervivencia en ambientes con pH ácido (Figura 9D). HiNT contiene un operón ureasa (*ureA-ureH*) cuya expresión es dependiente de la disponibilidad de nitrógeno, facilita la supervivencia bacteriana en el microambiente ácido de las vías respiratorias inflamadas, y en el bajo pH intracelular de células epiteliales o macrófagos (Murphy & Brauer, 2011; Zhang et al., 2013).

(v) Evasión del sistema de complemento (Figura 9E). HiNT inhibe: (i) la vía clásica mediante la unión de C4BP a través de la proteína de superficie P5 (Hallström et al., 2007; Thofte et al., 2021), (ii) la vía alternativa a través de la unión del Factor H a P5 (Langereis et al., 2014), (iii) la formación del complejo de ataque a la membrana mediante la unión de vitronectina a los receptores P4, proteína E o proteína F de la superficie bacteriana (Singh et al., 2013; Su et al., 2013, 2016, 2017), y (iv) tanto la vía clásica como la alternativa mediante la unión de la proteína E a plasminógeno que escinde y degrada C3b (Barthel et al., 2012; Singh et al., 2013).

HiNT evade el sistema del complemento utilizando señalización redox a través de ArcA, que modula la expresión de la glicosiltransferasa Lic2B, y permite modificar la estructura del LOS (Wong et al., 2011). La decoración de LOS con ChoP incrementa la adhesión epitelial al mimetizar PAF (Swords et al., 2000) facilitando la colonización nasofaríngea, si bien favorece el reconocimiento por la proteína C-reactiva y anticuerpos específicos anti-ChoP, ambos activadores de la vía clásica del complemento (Riesbeck, 2020; Weiser et al., 1998). La decoración con ChoP está regulada por variación de fase, transitando entre un estado ON ($ChoP^+$) en vías respiratorias y OFF ($ChoP^-$) en sangre, lo que facilita la resistencia al suero (Langereis et al., 2019; Riesbeck, 2020). La decoración de LOS con ácido siálico también contribuye a evadir (i) la vía clásica del complemento bloqueando la unión de IgM a la superficie bacteriana (Oerlemans et al., 2019; Riesbeck, 2020), y (ii) la vía alternativa al reclutar el factor H que previene la activación de C3b (Meri, 2016; Riesbeck, 2020).

(vi) Evasión del efecto bactericida de ácidos grasos (Figura 9F). Trabajo previo de nuestro grupo de investigación reveló que HiNT presenta al menos dos estrategias de supervivencia frente a LCFA: la inactivación del transportador de ácidos grasos FadL protege frente a su efecto detergente, lo que además parece ser un rasgo pato-adaptativo (Moleres et al., 2018); el sistema MlaA confiere

protección frente al efecto bactericida de moléculas hidrofóbicas, incluyendo LCFAs (Fernández-Calvet et al., 2018).

(vii) Resistencia a péptidos antimicrobianos (Figura 9G). La decoración de LOS con ChoP y la acilación del lípido A contribuyen a la resistencia de *H. influenzae* a AMPs. La presencia de ChoP confiere resistencia a AMP LL-37/hCAP18 (Lysenko et al., 2000), y la inactivación de la aciltransferasa HtrB, implicada en la hexaacilación del lípido A, aumenta la susceptibilidad a β-defensinas humanas (Starner et al., 2002). El sistema MlaA contribuye a la resistencia a AMPs mediante el mantenimiento de la estabilidad de la membrana (Fernández-Calvet et al., 2018). La maquinaria de captación de hierro de *H. influenzae* también participa en la resistencia a AMPs, concretamente SapA, HxuCBA y Hpe (Rodríguez-Arce et al., 2019).

(viii) Evasión de la inmunidad nutricional (Figura 9H). HiNT carece de los genes que codifican las enzimas que catalizan la conversión de ácido δ-aminolevulínico en protoporfirina IX (PPIX), precursor de la hemina, si bien expresa HemH, ferroquelatasa que inserta reversiblemente Fe^{2+} en PPIX para generar hemina (Loeb, 1995; Schlör et al., 2000). HiNT necesita incorporar hemina o Fe^{2+} en presencia de PPIX. Para compensar esta auxotrofía y la limitación de disponibilidad de hierro en el hospedador, HiNT posee un amplio repertorio de genes multifuncionales de captación (sistemas Hxu, Hpe, Sap, Dpp, Hit), almacenaje y donación de Fe-hemina que contribuyen a su patogénesis y supervivencia en el sistema respiratorio (Rodríguez-Arce et al., 2019). En respuesta a la baja disponibilidad de zinc, HiNT presenta los mecanismos de captación, ZnuABC y ZevAB (Lu et al., 1997; Rosadini et al., 2011).

(ix) Evasión de la inmunidad mediada por anticuerpos (Figura 9I). HiNT expresa 4 proteasas con distinta especificidad para la región bisagra de la inmunoglobulina IgA1 (A1, A2, B1 y B2). Además de su función proteasa, IgaA también participa en la invasión e IgaB escinde LAMP1 (del inglés, *lysosome-associated membrane protein 1*), promoviendo la persistencia intracelular de esta bacteria (Clementi et al., 2014; Murphy et al., 2017).

(x) Evasión de la inmunidad mediada por surfactante pulmonar (Figura 9J). El componente lipídico del surfactante pulmonar protege de la infección mediante (i) la unión de vesículas grandes a HiNT que forman una barrera física y dificultan la adhesión epitelial, y (ii) la inhibición de la fosforilación de Akt y de la activación de Rac1, ambos procesos necesarios en la invasión epitelial bacteriana (García-Fojeda et al., 2019). Pacientes que sufren EPOC tienen niveles reducidos del componente lipídico del surfactante pulmonar, lo que ayuda a HiNT a evadir esta barrera inmune (García-Fojeda et al., 2019). Además, la heterogeneidad en la estructura del LOS entre cepas de HiNT dificulta su reconocimiento por las proteínas SP-A y SP-D (Clark et al., 2016).

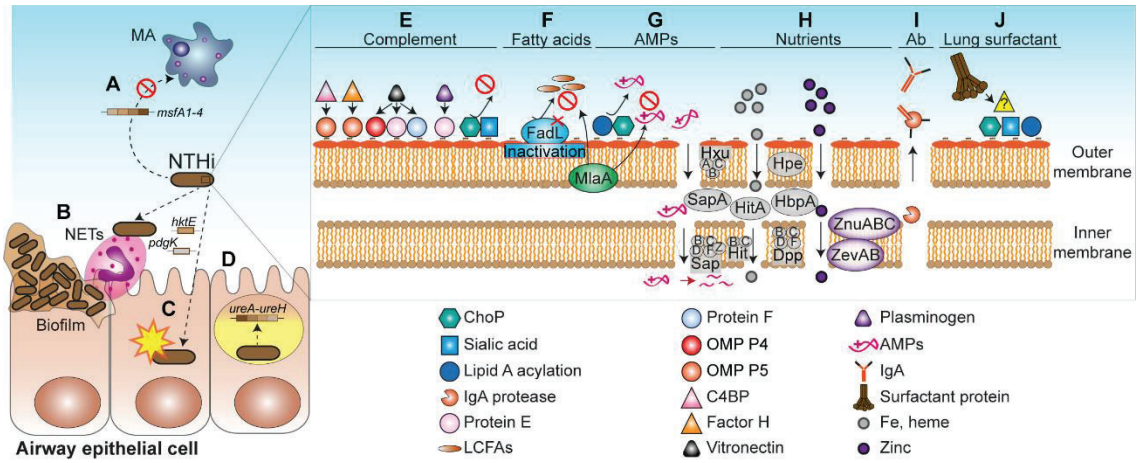

Figura 9. Mecanismos de evasión del sistema inmune de HiNT. (A) La expresión de los genes *msf*A1-4 favorece la supervivencia de HiNT en macrófagos. **(B)** La formación de biopelículas contribuye a la evasión de fagocitosis por macrófagos alveolares y neutrófilos, y confiere resistencia a NETs. **(C)** La producción de proteínas antioxidantes favorecen la supervivencia de HiNT en NETs y en condiciones de estrés oxidativo. **(D)** La actividad del operón ureasa facilita la supervivencia de HiNT en medios ácidos. **(E)** La evasión del sistema del complemento está mediada por la interacción de HiNT con C4BP, Factor H, vitronectina y plasminógeno a través de proteínas de superficie y decoración del LOS. **(F)** La inactivación de FadL y el mantenimiento de la asimietría de la membrana externa por la acción de VacJ favorecen la supervivencia de HiNT frente al efecto bactericida de ácidos grasos. **(G)** Resistencia a péptidos antimicrobianos mediante cambios en la carga y/o hidrofobicidad de la superficie bacteriana como la decoración del LOS, la acilación del lípido A, y los sistemas Mla, Sap, Hxu y Hpe. **(H)** Evasión de la inmunidad nutricional mediante múltiples sistemas de captación de hierro (Hxu, Hpe, Sap, Dpp, Hit y HbpA) y zinc (ZnuABC y ZevAB). **(I)** Producción de IgA proteasas. **(J)** Evasión del reconocimiento de proteínas del surfactante pulmonar mediante diversidad en la estructura del LOS.

2.3.1.1. Formación de biopelículas de HiNT

Las biopelículas son comunidades bacterianas con características y propiedades que confieren ventajas protectoras durante la colonización e infección (Post et al., 2014). De forma general, es un mecanismo que fomenta la persistencia bacteriana al modificar la expresión génica y la producción de matriz extracelular (del inglés, *extracellular matrix*, ECM), incrementando la virulencia, tolerancia antimicrobiana, y resistencia frente a la respuesta inmunitaria (**Figura 9B**) (Short et al., 2021).

HiNT forma biopelículas (**Figura 10A**) *in vitro* e *in vivo* en infecciones de EPOC, OM y FQ (Costerton et al., 1999; Short et al., 2021; Starner et al., 2006). La formación de biopelículas contribuye a la evasión de fagocitosis por macrófagos alveolares y neutrófilos, y confiere resistencia a NETs, favoreciendo la infección persistente por HiNT (Ahearn et al., 2017). Las proteínas que codifican los operones *pil* y *com* participan en la formación de biopelículas de HiNT (Carruthers et al., 2012). Así, ComE y PilA favorecen la formación de biopelículas al liberar ADN a la ECM y mantener la actividad de Tfp (Das et al., 2017). Asimismo, la decoración de la molécula LOS con ChoP y ácido siálico favorece la formación de comunidades estables de biopelículas y la progresión de la infección (Hong et al., 2007; Jurcisek et al., 2005). La ECM de las biopelículas de HiNT contiene (i) ADNe (ADN extracelular); (ii) proteínas: DNABII que incluyen factor de integración del huésped (en inglés, *Integration Host Factor*, IHF) y proteínas HU; proteínas Tfp, PilA; adhesinas

Hap, Hia; proteínas de membrana externa P5 y P6; (iii) ChoP y ácido siálico (Devaraj et al., 2018; Langereis & Hermans, 2013; Short et al., 2021); (iv) NETs, cuya formación está promovida por DNA, LOS y endotoxinas de HiNT (Juneau et al., 2011). La inmunidad nutricional de Fe modifica la arquitectura de la biopelícula, promoviendo una estructura de mayor magnitud (Harrison et al., 2019). La formación y maduración de biopelículas está regulada por *quorum sensing*, un mecanismo que regula la expresión génica en respuesta a la densidad poblacional. El sistema LuxS-RbsB es parte del ciclo metionina-homocisteína, dependiente de AI-2, y regula la maduración de las biopelículas aumentando su grosor y densidad (Armbruster et al., 2009). QseBC (también denominado FirRS) es un sistema de dos componentes cuyo papel en *quorum sensing*, independiente de AI-2, y formación de biopelículas en HiNT es controvertido (Steele et al., 2012; Ünal et al., 2012).

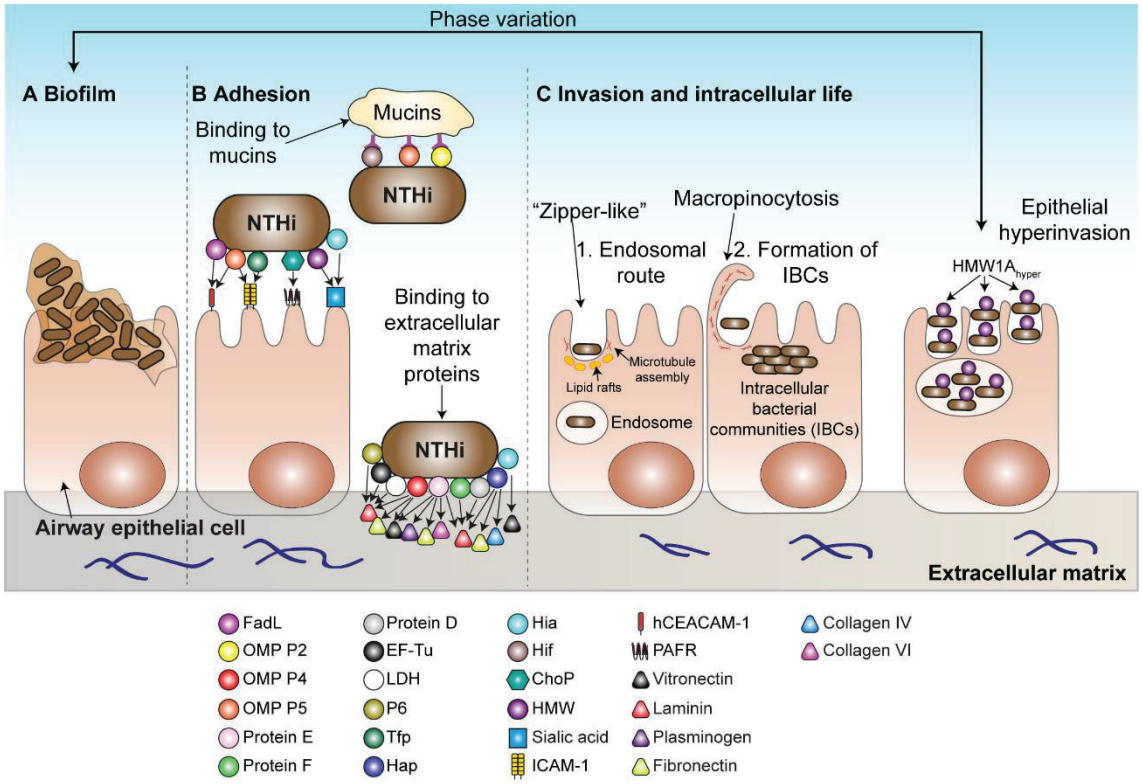

Figura 10. Elementos de interacción de *H. influenzae* con el hospedador. (A) Formación de biopelículas. **(B)** HiNT se une a células epiteliales, mucinas y proteínas de matriz extracelular mediante un amplio repertorio de adhesinas o ligandos. **(C)** La invasión epitelial de HiNT es de tipo "*zipper*" y conlleva la reorganización del citoesqueleto. HiNT se localiza intracelularmente en compartimentos de tipo endosoma y permanece en un estadío no replicativo metabólicamente activo (1). HiNT forma IBCs en el citosol tras producirse su internalización mediante macropinocitosis (2). La variación de fase de la adhesina HMW1A permite la transición entre un fenotipo hiperinvasor y una mayor capacidad de formación de biopelículas.

2.3.2. Infección del epitelio respiratorio

H. influenzae es un patógeno intracelular facultativo, con capacidad de adhesión, invasión (o hiperinvasión), y localización subcelular. Trabajo de nuestro y otros grupos de investigación ha contribuido a elucidar aspectos de la infección epitelial por *H. influenzae*, con peculiaridades que

dependen del tipo celular, cepa y/o condiciones experimentales. Estos aspectos se resumen a continuación.

2.3.2.1. Adhesión de HiNT al epitelio respiratorio

HiNT dispone de un amplio repertorio de adhesinas o ligandos (**Figura 10B**) que facilitan su interacción con receptores celulares (Short et al., 2021): (i) proteína de membrana externa (en inglés, *outer membrane protein*, OMP) **OMP P1 (FadL)**, se une a hCEACAM-1 (Moleres et al., 2018; Short et al., 2021), (ii) **OMP P2**, se une a mucinas (Reddy et al., 1996), (iii) **OMP P4**, se une a laminina (Short et al., 2021; Su et al., 2016), vitronectina y fibronectina (Osman et al., 2018a; Short et al., 2021; Su et al., 2016), (iv) **OMP P5**, se une a mucinas (Osman et al., 2018a; Reddy et al., 1996; Short et al., 2021), ICAM-1 (Short et al., 2021) y hCEACAM-1 dependiendo de la cepa (Euba et al., 2015a; Osman et al., 2018; Short et al., 2021), (v) **PD**, se une a laminina (Su et al., 2019), (vi) **PE**, se une a laminina, plasminógeno, vitronectina (Hallström et al., 2011; Short et al., 2021), fibronectina (Osman et al., 2018a) y colágeno tipo VI (Abdillahi et al., 2018), (vii) **PF**, se une a laminina (Jalalvand et al., 2013), (viii) **Tfp**, a través de su componente mayoritario PilA, se une a ICAM-1 (Novotny & Bakaletz, 2016; Short et al., 2021), (ix) **Hap**, se une a laminina (Hallström et al., 2011; Osman et al., 2018a; Short et al., 2021), fibronectina, colágeno tipo IV (Fink et al., 2002; Short et al., 2021) y colágeno tipo VI (Abdillahi et al., 2018), (x) **Hia**, se une a vitronectina (Osman et al., 2018a) y ácido siálico (Atack et al., 2020), (xi) **Hif**, se une a mucinas (Osman et al., 2018a; Short et al., 2021), (xii) **ChoP**, se une a PAFr (Johnson et al., 2011; Swords et al., 2001), (xiii) **HMW,** se une al ácido siálico**,** concretamente HMW1 se une a ácido 2-3 N-acetilneuramínico y HMW2 a 2-6 N-acetilneuramínico (Atack et al., 2018a), (xiv) **EF-Tu** (del inglés, *elongation factor thermo-unstable*), se une a laminina (Su et al., 2019), (xv) **LDH**, se une a laminina (Su et al., 2019), (xvi) **lipoproteína P6** asociada a peptidoglicano, se une a laminina (Su et al., 2019).

2.3.2.2. Invasión y vida intracelular de HiNT en el epitelio respiratorio

HiNT invade células conjuntivas Chang, nasales (RPMI 2650), faríngeas (Detroit-562), bronquiales (NCI-H292, 16HBE14, NHBE y BEAS-2B), alveolares correspondientes a neumocitos tipo II (A549), subepiteliales y del tejido adenoide (Euba et al., 2015a; Forsgren et al., 1994; Morey et al., 2011; Prasadarao et al., 1999; Singh et al., 2016; Starner et al., 2002; Vuong et al., 2013). La capacidad de invasión epitelial es una característica cepa-dependiente (Clementi & Murphy, 2011; Mell et al., 2016; Moleres et al., 2018; Morey et al., 2011). Trabajo previo de nuestro grupo de investigación determinó la existencia de cepas con elevados niveles de invasión epitelial, fenotipo de hiperinvasión epitelial, dependiente de determinadas variantes alélicas de la adhesina HMW1A ($HMW1A_{hyper}$) y regulado por la variación de fase que controla los niveles de expresión de esta adhesina, con una relación directamente proporcional expresión de $HMW1A_{hyper}$:invasión, e

inversamente proporcional expresión de HMW1A$_{hyper}$:formación de biopelículas (Fernández-Calvet et al., 2021).

El mecanismo de invasión de HiNT en las células epiteliales (**Figura 10C**) es de tipo cremallera (en inglés, *zipper-like*) e implica ensamblaje de microtúbulos, integridad de las balsas lipídicas y activación de PI3K-Akt que modula la actividad de integrinas β1, α5, quinasas de adhesión focal (en inglés, *focal adhesion kinase*, FAK) y Src, GTPasas, y factor de intercambio de nucleótidos de guanina Vab2 (López-Gómez et al., 2012; Morey et al., 2011). Las bacterias internalizadas residen intracelularmente en compartimentos subcelulares ácidos (en inglés, HiNT-*containing vacuole,* HiNT-CVs) de tipo **endosoma** en un estadío **metabólicamente activo no replicativo** (Clementi & Murphy, 2011; Morey et al., 2011). Por otra parte, HiNT puede ser internalizado mediante macropinocitosis a través de la reoganización del citoesqueleto de actina, y siguiendo una ruta endosomal (Hardison, et al., 2018a). La formación de comunidades bacterianas intracelulares (en inglés, *intracellular bacterial communities*, **IBCs**) favorece la supervivencia de HiNT (Hardison, et al., 2018a; Hardison, et al., 2018b; Szelestey et al., 2013). La formación de IBCs parece verse favorecida en episodios recurrentes de OM (Harrison et al., 2020).

3. Estrategias terapéuticas frente a *H. influenzae*: situación actual y nuevas oportunidades

3.1. Terapias empleadas frente HiNT y problemas asociados

El tratamiento de las infecciones por *H. influenzae* se basa en la **administración de antibióticos** cuya elección y dosis se fundamenta en la naturaleza y ubicación de la infección. Los principales antibióticos utilizados frente a HiNT son β-lactámicos, fluoroquinolonas, macrólidos, cloranfenicol, tetraciclinas y antagonistas de folato. El uso inadecuado y abusivo de antibióticos genera resistencia antibiótica y subsiguiente fallo terapéutico. A continuación, se presenta un resumen del uso antibiótico frente a *H. influenzae*.

Los **antibióticos β-lactámicos**, como aminopenicilinas y cefalosporinas, que actúan a nivel de la síntesis de peptidoglicano de la pared celular mediante la inhibición de proteínas de unión a penicilina (en inglés, *penicillin-binding proteins*, PBPs), son de elección habitual frente a *H. influenzae*. Los mecanismos que presenta *H. influenzae* para resistir frente a antibióticos β-lactámicos son: (i) producción de β-lactamasas TEM-1, con una prevalencia del 90-95% y distribuída mundialmente, y ROB-1, con una prevalencia del 5-10% y localizada en Canadá, EEUU y México, que catalizan la hidrólisis del anillo β-lactámico, (ii) alteración de la proteína de unión a penicilina 3 (PBP3) codificada por *ftsI*, (iii) modificaciones en la permeabilidad celular, y (iv) alteraciones en la síntesis y metabolismo de peptidoglicano (Schotte et al., 2019; Wen et al., 2020). Las cepas

resistentes a antibióticos β-lactámicos sin producción de β-lactamasas (BLNAR, del inglés, β-*lactamase-negative ampicillin resistance*), dan lugar a cepas que presentan alta resistencia localizadas en Asia, y cepas con baja resistencia distribuídas a lo largo del mundo (Schotte et al., 2019).

Las **fluoroquinolonas**, ciprofloxacino, levofloxacino y ácido nalidíxico, impiden el superenrrollamiento de las cadenas de ADN, por inhibición de las ADN topoisomerasa II y IV, y ADN girasa (Bush et al., 2020). Existe un incremento de tratamientos fallidos con levofloxacino en *H. influenzae* (Wen et al., 2020), y un aumento de resistencia a ciprofloxacino y ácido nalidíxíco (Puig et al., 2015). Estas resistencias se asocian a mutaciones en las regiones determinantes de la resistencia a quinolonas (en inglés, *quinolone resistance–determining regions*, QRDRs) de los genes *gyrA*, *gyrB*, *parC* y *parE* (Puig et al., 2015; Wen et al., 2020).

El **cloranfenicol**, las **tetraciclinas**, y los **macrólidos** como eritromicina y azitromicina, inhiben la síntesis de proteínas. Las tetraciclinas se unen a la subunidad 30S de los ribosomas bacterianos y evitan que el ARNt se una a los sitios A y P (Tristram et al., 2007). El cloranfenicol y los macrólidos se unen a 23S rRNA de la subunidad ribosomal 50S previniendo transferencia de tRNA del sitio A al P del ribosoma (Dinos, 2017; Oong & Tadi, 2021). La resistencia de *H. influenzae* a tetraciclinas está asociada a una bomba eflujo (Kostyanev & Sechanova, 2012). La resistencia a cloranfenicol está mediada por la cloranfenicol acetiltransferasa de tipo II codificada por el gen *cat*, en un plásmido conjugativo o en el cromosoma, que acetila e inactiva este antibiótico (Kostyanev & Sechanova, 2012; Powell & Livermore, 1988; Williams & Moosdeen, 1986), o bien mediante la nitroreductasa NfsB, que reduce el cloranfenicol a alcohol 4-aminofenil alílico, carente de capacidad antibacteriana (Crofts et al., 2019; Smith et al., 2007). Entre los mecanismos de resistencia a macrólidos se incluyen: (i) adquisición de bombas de eflujo codificadas por *mefA* (Roberts et al., 2011; Seyama et al., 2017), o por AcrAB TolC (Tristram et al., 2007); (ii) adquisición de metilasas 23S rARN codificadas por *ermA*, *ermB*, *ermC* y *ermD* (Roberts et al., 2011; Seyama et al., 2017; Wen et al., 2020); (iii) mutaciones en proteínas ribosomales L4, L22 y 23S rRNA (Tristram et al., 2007; Wen et al., 2020). Además de su efecto antibacteriano, los macrólidos presentan propiedades inmunomoduladoras. Por ello, la azitromicina es utilizada como profilaxis en pacientes que sufren EPOC moderada y severa, lo que favorece la aparición de resistencias (Albert et al., 2011; Euba et al., 2015b).

Otro antibiótico usado frente a *H. influenzae* es el **cotrimoxazol**, (TxS), combinación de trimetroprim (TMP) y sulfametoxazol (SMX), antagonista de ácido fólico que bloquea la síntesis de timidina. La resistencia de *H. influenzae* a TxS se asocia a cambios en la secuencia y expresión de los genes *folH* y *folP*, o adquisición de los genes *sul* (De Groot et al., 1996; Enne et al., 2002). Trabajo previo de nuestro grupo de investigación mostró que la auxotrofia a timidina mediante inactivación del gen *thyA*, que codifica la enzima timidilato sintasa, modula la susceptibilidad a TxS (Rodríguez-Arce et al., 2017).

Esta situación de creciente aparición de resistencias antibióticas ha llevado a la Organización Mundial de la Salud (OMS) a la inclusión de *H. influenzae* resistente a ampicilina en la lista de patógenos prioritarios (en inglés, *Global Priority Pathogen List*) para los que el desarrollo de nuevos antimicrobianos se considera una prioridad sanitaria (Tacconelli et al., 2018).

3.2. Desarrollo de nuevas terapias antimicrobianas frente a la infección por *H. influenzae*

El descubrimiento y desarrollo de nuevos antimicrobianos ha disminuido drásticamente en las últimas décadas, en contraste con la llamada edad de oro de los antibióticos (Stanton, 2013). Esta disminución viene dada por la dificultad de llegar a su comercialización, los altos costes del proceso, y la preferencia de la industria farmacéutica por el desarrollo de tratamientos contra el cáncer, cardiovasculares o psiconeurológicos (Stanton, 2013).

Como se ha indicado previamente, *H. influenzae* es un colonizador frecuente de las vías respiratorias bajas de pacientes que sufren patologías crónicas con un fuerte componente inflamatorio, cuyos pacientes reciben con frecuencia terapia anti-inflamatoria. Por esta razón, la búsqueda de fármacos con acción dual anti-inflamatoria y antimicrobiana es un campo en expansión. En este contexto, los polifenoles son moléculas naturales de origen vegetal con propiedades protectoras, de baja toxicidad en eucariotas, y propiedades duales. Trabajo previo de nuestro grupo de investigación evaluó el efecto terapéutico de dos polifenoles, resveratrol y quercetina, frente a la infección por HiNT con resultados prometedores en modelos preclínicos (Euba et al., 2017; Fernández-Calvet et al., 2019). Junto a los polifenoles, existen estudios con otras moléculas inmunomoduladoras, en los que no se ha explorado su dualidad antibacteriana en detalle. Entre ellos, se han evaluado inhibidores de PLA_2, que reducen la respuesta inflamatoria al bloquear las vías de señalización mediadas por eicosanoides y PAF (Meyer et al., 2005), el compuesto roflumilast, que inhibe la fosfodiesterasa 4B (en inglés, *phosphodiesterase 4B*, PDE4B), y el glucocorticoide dexametasona, que inhibe la producción de MUC5AC (Komatsu et al., 2008).

Por otra parte, el empleo de técnicas -ómicas para la identificación de **factores de virulencia** implicados en el proceso infeccioso, puede ser una herramienta útil para la identificación de nuevas dianas terapeúticas (Duell et al., 2016; Gawronski et al., 2009; Wong et al., 2013). Así, la identificación de factores de virulencia de *H. influenzae* ha posibilitado la investigación de nuevos antimicrobianos (estrategias terapéuticas anti-virulencia) (Langereis & De Jonge, 2020). Algunas de estas estrategias contemplan: (i) la inhibición de incorporación de ácido siálico al LOS mediante el compuesto SiaNAc-$3F_{ax}$ (Heise et al., 2018); (ii) la identificación de inhibidores de la proteasa IgA (Shehaj et al., 2019); (iii) la utilización de un antagonista de PAFr, WEB-2086 (Shukla et al., 2016). Igualmente, la identificación de **genes esenciales** para el crecimiento y viabilidad bacteriana es otra

estrategia de búsqueda de dianas para el desarrollo de fármacos (Duffield et al., 2010; Mobegi et al., 2014). Las técnicas -ómicas basadas en la generación de genotecas de mutantes y secuenciación de alto rendimiento (p.ej. HITS, Tn-seq), o el escrutinio *in silico* mediante el desarrollo de **modelos metabólicos a escala genómica** (en inglés, *genome-scale metabolic model*, GEM), son herramientas de búsqueda de esencialidad génica en *H. influenzae* (Gawronski et al., 2009; Mobegi et al., 2014; Wong et al., 2013; Wong & Akerley, 2012). Los GEM bacterianos son redes que conectan todas las reacciones metabólicas que pueden ocurrir en un organismo con sus metabolitos, proteínas y genes asociados, y permiten hacer predicciones matemáticas de comportamiento utilizando la reconstrucción metabólica basada en la información genómica y fenotípica disponible (Chavali et al., 2012b). La secuenciación de *H. influenzae* RdKW20 (Fleischmann et al., 1995) fue pionera para la elaboración del primer GEM (Edwards & Palsson, 1999; Schilling & Palsson, 2000). Actualmente, los GEM analizan capacidades celulares de crecimiento en distintas condiciones, predicen el efecto de mutaciones genéticas en el crecimiento bacteriano y sus flujos metabólicos asociados, y son herramientas computacionales útiles para el diseño de nuevos antimicrobianos (O'Brien et al., 2015).

En el Capítulo 4 de este trabajo de Tesis Doctoral, hemos construido y validado un nuevo modelo metabólico de HiNT a escala genómica. Este modelo ha sido empleado como herramienta de escrutinio *in silico* para la identificación de genes esenciales con potencial como dianas terapéuticas.

3.1.1. Enzimas de la ruta FASII como dianas antimicrobianas frente a la infección por HiNT

La ruta FASII (ver **sección 2.2.2.2**) contiene enzimas que son esenciales para *H. influenzae*, y por tanto posibles dianas para el desarrollo de nuevos compuestos antimicrobianos (Campbell & Cronan, 2001). Existe un panel de productos naturales que son inhibidores de enzimas FASII, resumido en la **Tabla 2**. Igualmente, existe un catálogo de compuestos sintéticos inhibidores de enzimas FASII, que se resume a continuación:

(i) Inhibidores de FabG, con un amplio espectro frente a patógenos ESKAPE *(Enterococcus faecium*, *S. aureus*, *K. pneumoniae*, *Acinetobacter baumannii, P. aeruginosa* y *Enterobacter* spp) (Vella et al., 2021), que se unen a la interfaz del dímero desplazando la triada catalítica en *P. aeruginosa* (Cukier et al., 2013), o derivados del ácido trans-cinamico en *Escherichia coli* (Kristan et al., 2009).

(ii) Inhibidores de FabF y/o FabB, derivados sintéticos del compuesto natural platencina, también con actividad frente a FabH en *S. aureus* (Li et al., 2021), derivados de platensimicina

eficaces contra *S. aureus* (Deng et al., 2018; Liu et al., 2020; Su et al., 2019) y antrabenzoxocinonas frente en *S. aureus* y *Bacillus subtilis* (Mei et al., 2018), y sulfonamidas aciladas efectivas frente a *Chlamydia trachomatis* (Mojica et al., 2017).

(iii) Inhibidores de FabI, que incluyen el carfilzomb, compuesto aprobado por la FDA (del inglés, *food and drug administration*) eficaces frente a *Klebsiella pneumoniae* y *M. tuberculosis* (Mahfuz et al., 2020), diazaborinas contra *E. coli* y *M. tuberculosis*, derivados de 1,2,3,4-tetrahidro-1H-pirido [3,4-b] indol activos frente *S. aureus* y *Moraxella catarrhalis*, derivados de 1H-imidazol contra *S. aureus* and *E. coli*, éteres de difenilo (triclosan) con un amplio espectro frente a bacterias Gram-positivas y negativas, derivados de naftiridinona (AFN-1252) eficaces frente a *S. aureus* y *H. influenzae*, derivados a base de acrilamidas activos contra *S. aureus*, 1,5,6,7-tetrahidroindeno [5,6-d] imidazol contra *S. aureus* y *E. coli*, derivados a base de cumarina contra Gram-positivas y negativas, derivados de pirona y piridona (CG400549) activos frente a Gram-positivas y negativas, inhibidores basados en pirrolidina contra *S. aureus*, *A. baumannii* y *M. tuberculosis*, aminopiridinas eficaces frente a *S. aureus* y *E. coli*, inhibidores basados en quinolina/quinoxalina contra *S. aureus*, *E. coli* y *M. tuberculosis*, derivados de N'-benzoilbenzohidrazida frente a *S. aureus* y *E. coli*, tiadiazol contra *M. tuberculosis* (Rana et al., 2020), CG400462 contra *S. aureus* (H. S. Park et al., 2007) e isoniazida frente a *M. tuberculosis* (de Faria et al., 2021).

Tabla 2. Inhibidores naturales de FASII.

Enzima FASII	Productos naturales	Referencias
ACC	Andrimid, moiramide B	(Freiberg et al., 2004; Yao & Rock, 2017)
FabG	Macrolactina, EGCC[1], galangal	(Huang et al., 2008; Parsons et al., 2011; Sohn et al., 2008; Y. M. Zhang & Rock, 2004)
FabI	EGCC, cefalocromina, kalimantacina, aquastatina A	(Parsons et al., 2011; Y. M. Zhang & Rock, 2004)
FabF	EGCC, platencina, tiolactomicina, cerulenina, platensimicina, anthrabenzoxocinones, fasamicin, antrabenzoxocinonas	(M. Das et al., 2016; Feng et al., 2012; Parsons et al., 2011; Jun Wang et al., 2006; Yao & Rock, 2017; Y. M. Zhang & Rock, 2004)
FabH	Platencina, amicomicina	(Pishchany et al., 2018; Yao & Rock, 2017)
FabB	Tiolactomicina, cerulenina, platensimicina	(Parsons et al., 2011; Jun Wang et al., 2006)

[1] Galato de epigalocatequina (*epigallocatechin gallate*, EGCG)

(iv) Inhibidores de FabH, incluyendo 27 inhibidores derivados de pirazol-bencimidazol amida eficaces frente a bacterias Gram-positivas y negativas (Wang et al., 2019); 41 compuestos seleccionados con actividad frente a FabH utilizando un ensayo de centelleo por proximidad en dos quimiotecas de AstraZeneca, **algunos con IC_{50} baja frente a HiNT** (McKinney et al., 2016); nanopartículas bimetálicas Cu:Ag también con acción frente a FabI en *S. aureus* y *A. baumannii* (Mureed et al., 2021); 2 compuestos que contienen la estructura 1,3,5- oxadiazin-2-ones, Oxa1 y

Oxa2, que modifican covalentemente la cisteína presente en el sitio activo de FabH en *S. aureus* (Wang et al., 2020); derivados de oxoindolina con acción inhibitoria dual tanto de supervivencia (FabH) como duplicación (girasa) en *S. aureus* (Yang et al., 2019a); compuestos que combinan pirazinamida con 4-feniltiazol-2-amina con actividad frente a *M. tuberculosis* (Zitko et al., 2018); 15 compuestos derivados de YKAs3003 que consisten en bases de Schiff con anillos dioxigenados y N-heterociclo con actividad frente a *E. coli* (Zhou et al., 2017).

El Capítulo 4 de este trabajo de Tesis Doctoral ha evaluado el potencial terapéutico de un inhibidor sintético de FabH, enzima iniciadora de la biosíntesis de ácidos grasos de HiNT.

Hipótesis y Objetivos

Los patógenos bacterianos son microorganismos con un alto grado de adaptación al nicho colonizado. Esta pato-adaptación implica capacidades metabólicas que permiten contrarrestar la limitación de nutrientes e inmunidad nutricional, y adaptarse a cambios en el entorno. En este contexto, la **Hipótesis General** que engloba este trabajo de Tesis Doctoral es **"*Haemophilus influenzae* es un patógeno bien adaptado al sistema respiratorio humano con rasgos metabólicos característicos que no sólo desempeñan un papel clave en su pato-adaptación, sino que también pueden ser una fuente de dianas para el desarrollo de nuevos antimicrobianos"**.

La secuenciación de genomas completos posibilitó que *H. influenzae* fuese pionero en el desarrollo y aplicación de técnicas –ómicas que, entre otros, proporcionan una visión global de la reconfiguración metabólica de la bacteria durante la infección. En el **Capítulo 2** de esta Tesis Doctoral planteamos la **Hipótesis**: **"El perfil transcriptómico de *H. influenzae* durante el proceso infeccioso en un modelo murino puede ser una herramienta útil para la identificación de rutas metabólicas importantes para la infección"**.

H. influenzae cataboliza glucosa mediante una fermentación asistida por respiración en la que los principales productos excretados son acetato, formato y succinato, a través de la participación de las enzimas AckA, PflA y FrdA, respectivamente. En el **Capítulo 3** de esta Tesis Doctoral planteamos la **Hipótesis**: **"El catabolismo de glucosa de *H. influenzae* produce inmunometabolitos en el sitio de infección que contribuyen tanto al crecimiento del patógeno como a la dinámica de la inflamación"**.

La generación de resistencias antibióticas ha llevado a la inclusión de *H. influenzae* en la lista de patógenos prioritarios de la OMS. La identificación de genes que codifican enzimas que catalizan reacciones esenciales en el metabolismo bacteriano es un abordaje de interés para el desarrollo de antimicrobianos. En este sentido, el uso de modelos metabólicos optimizados como herramienta de escrutinio *in silico* acelera la identificación de genes esenciales y la evaluación de su inhibición farmacológica. La aplicación de un modelo metabólico optimizado predijo la esencialidad de la ruta FASII de *H. influenzae*. En **el Capítulo 4** de esta Tesis Doctoral planteamos la **Hipótesis**: "**La ruta FASII de *H. influenzae* contiene enzimas que pueden ser dianas terapéuticas"**.

Objetivos

Las Hipótesis planteadas fueron abordadas mediante los siguientes **Objetivos**:

1. Análisis de la expresión génica diferencial de *H. influenzae* durante la infección respiratoria en un modelo murino mediante RNA-seq *in vivo*.
2. Estudio de la contribución de genes implicados en el catabolismo de la glucosa y sus productos excretados en la infección por *H. influenzae*.
3. Escrutinio computacional, caracterización y evaluación preclínica del efecto antimicrobiano de la inhibición farmacológica de la enzima FabH de H. *influenzae*.

El trabajo realizado para dar respuesta a los Objetivos 1 a 3 está recogido en los Capítulos 2 a 4 de esta Memoria. Con el objeto de proporcionar una visión completa del campo estudiado, el Capítulo 1 recoge una revisión del aporte realizado por el abanico de técnicas -ómicas actualmente disponibles al entendimiento de la interacción de *H. influenzae* con el sistema respiratorio humano.

Resultados

La presente Tesis Doctoral es un **compendio de Publicaciones**. Los resultados obtenidos de los Objetivos propuestos se presentan en **cuatro Capítulos**:

- **Capítulo 1:**

Nahikari López-López*, Celia Gil-Campillo*, Roberto Díez-Martínez, Junkal Garmendia. Learning from -omics strategies applied to uncover *Haemophilus influenzae* host-pathogen interactions: Current status and perspectives. Computational and Structural Biotechnology Journal. Volume 19, 2021, Pages 3042-3050. doi: 10.1016/j.csbj.2021.05.026 *Equal contribution

Revista	País	Editorial	Categoría	Factor de impacto	Cuartil
Computational and Structural Biotechnology Journal (CSBJ)	Suecia	Elsevier	Biología computacional	7.271 (2020)	Q1

- Conceptualización: JG
- Escritura: NL-L, CG-C, JG
- Revisión: NL-L, CG-C, RD-M, JG
- Recursos: JG

Trabajo de búsqueda bibliográfica realizado por NL-L:

- Transcriptómica.
- Proteómica.
- Metabolómica.

- **Capítulo 2 (Manuscrito en preparación):**

Nahikari López-López*, Begoña Euba*, Celia Gil-Campillo*, Javier Asensio-López, Irene Rodríguez-Arce, Emel Sen-Kilic, Roberto Díez-Martínez, Saioa Burgui, Jeroen Langereis, Mariette Barbier, Junkal Garmendia. Multi-omic analysis of *Haemophilus influenzae* metabolic requirements during murine lung infection by combining RNA-seq and Tn-seq technologies. *Equal contribution

- Diseño experimental: JG, MB, JL
- Realización de experimentos: NL-L, BE, CG-C, JA-L, IR-A
- Análisis de datos: NL-L, BE, CG-C, JA-L, IR-A, ES-K, ML, RD-M, JL, MB, JG
- Escritura: NL-L, BE, CG-C, JA-L, MB, JG
- Recursos: MB, JG

Trabajo experimental realizado por NL-L:

Resultados

- Generación de muestras para la secuenciación RNA-seq.
- Análisis bioinformático de los datos de secuenciación RNA-seq.
- Establecimiento manual de categorías funcionales a partir de las listas de genes diferencialmente expresados obtenidas mediante secuenciación RNA-seq.
- PCR cuantitativa a tiempo real.
- Evaluación del fenotipo de las cepas mutantes generadas (curvas de crecimiento).
- Infección respiratoria de ratones por *H. influenzae* y recuentos de la carga bacteriana en lavado broncoalveolar y pulmón murino.
- Análisis de datos.

- **Capítulo 3:**

Nahikari López-López, Begoña Euba, Julian Hill, Rabeb Dhouib, Lucía Caballero, José Leiva, Jennifer Hosmer, Sergio Cuesta, José Ramos-Vivas, Roberto Díez-Martínez, Horst Joachim Schirra, Lars M. Blank, Ulrike Kappler, Junkal Garmendia. *Haemophilus influenzae* glucose catabolism leading to production of the immunometabolite acetate has a key contribution to the host airway-pathogen interplay. ACS Infectious Diseases. Volume 6, Pages 406-421. doi: 10.1021/acsinfecdis.9b00359

Revista	País	Editorial	Categoría	Factor de impacto	Cuartil
ACS Infectious Diseases	Estados Unidos	American Chemical Society	Enfermedades infecciosas	5,084 (2020)	Q1

- Diseño experimental: NL-L, UK, JG
- Realización de experimentos: NL-L, BE, J. Hill, RD, LC, JL, J. Hosmer, SC, JR-V, HJS, LMB
- Análisis de datos: NL-L, BE, RD-M, HJS, LMB, UK, JG
- Escritura: NL-L, UK, JG
- Recursos: LMB, UK, JG

Trabajo experimental realizado por NL-L:

- Diseño y generación de construcciones de cepas mutantes de *H. influenzae.*
- SDS-PAGE de proteínas y western blot anti-HA.
- Evaluación del fenotipo de los mutantes mediante curvas de crecimiento.
- Microscopía de fluorescencia y tratamiento de imágenes.
- Determinación de concentración de metabolitos mediante kits comerciales.

- Extracción de RNA bacteriano y eucariota, retrotranscripción y PCR cuantitativa a tiempo real.
- Infección respiratoria de ratones por *H. influenzae*, recuentos de la carga bacteriana en lavado broncoalveolar y pulmón murino, así como observación y recuento de células inmunitarias.
- Cultivo de epitelio respiratorio humano (línea celular A549), ensayo inmunoestimulación.
- Análisis de datos.

- **Capítulo 4 (Manuscrito en preparación):**

Nahikari López-López, David San León, Sonia de Castro, Roberto Díez-Martínez, Manuel Iglesias-Bexiga, María José Camarasa, Margarita Menéndez, Juan Nogales, Junkal Garmendia. Interrogation of essentiality in the reconstructed *Haemophilus influenzae* metabolic network identifies lipid metabolism antimicrobial targets: preclinical evaluation of a FabH β-ketoacyl-ACP synthase inhibitor.

- Diseño experimental: NL-L, MJC, MM, JN, JG
- Realización de experimentos: NL-L, DSL, SC, RD-M, MI-B, MJC, MM, JN
- Análisis de datos: NL-L, DSL, RD-M, MJC, MM, JN, JG
- Escritura: NL-L, MJC, MM, JN, JG
- Recursos: MJC, MM, JN, JG

Trabajo experimental realizado por NL-L:

- Generación de un nuevo modelo metabólico *in silico* de *H. influenzae.*
- Análisis de secuencias de ADN y proteínas.
- Diseño y proceso de construcción de cepas mutantes de *H. influenzae*.
- Ensayos de susceptibilidad de *H. influenzae* al inhibidor de FabH, FabHi (método de microdilución en caldo, evaluación de sinergias, evaluación de generación de resistencias).
- Ensayo de formación de biopelículas en microplaca.
- Extracción de ARN bacteriano, retrotranscripción y PCR cuantitativa a tiempo real.
- Cultivo de epitelio respiratorio humano (línea celular A549), tratamientos con FabHi, ensayos de citotoxicidad, viabilidad e infección por *H. influenzae.*
- Test de toxicidad aguda de FabHi en embriones de pez cebra.
- Administración de FabHi e infección de peces cebra adultos.
- Análisis de datos.

Capítulo 1

Learning from -omics strategies applied to uncover *Haemophilus influenzae* host-pathogen interactions: Current status and perspectives

Nahikari López-López, Celia Gil-Campillo, Roberto Díez-Martínez, Junkal Garmendia. Learning from -omics strategies applied to uncover *Haemophilus influenzae* host-pathogen interactions: Current status and perspectives. Computational and Structural Biotechnology Journal. Volume 19, 2021, Pages 3042-3050. doi: 10.1016/j.csbj.2021.05.026

Capítulo 1. Learning from -omics strategies applied to uncover *Haemophilus influenzae* host-pathogen interactions: Current status and perspectives

Nahikari López-López[a,†], Celia Gil-Campillo[a,†], Roberto Díez-Martínez[b], Junkal Garmendia[a,c,*]

a. Instituto de Agrobiotecnología, CSIC-Universidad Pública Navarra-Gobierno, Navarra, Spain.
b. Telum Therapeutics, Noain, Spain.
c. Centro de Investigación Biomédica en Red de Enfermedades Respiratorias (CIBERES), Madrid, Spain.

*Corresponding author: Junkal Garmendia.

† These authors contributed equally to this work.

1.1. Abstract

Haemophilus influenzae has contributed to key bacterial genome sequencing hallmarks, as being not only the first bacterium to be genome-sequenced, but also starring the first genome-wide analysis of chromosomes directly transformed with DNA from a divergent genotype, and pioneering Tn-seq methodologies. Over the years, the phenomenal and constantly evolving development of –omic technologies applied to a whole range of biological questions of clinical relevance in the *H. influenzae*-host interplay, has greatly moved forward our understanding of this human-adapted pathogen, responsible for multiple acute and chronic infections of the respiratory tract. In this way, essential genes, virulence factors, pathoadaptive traits, and multi-layer gene expression regulatory networks with both genomic and epigenomic complexity levels are being elucidated. Likewise, the unstoppable increasing whole genome sequencing information underpinning *H. influenzae* great genomic plasticity, mainly when referring to non-capsulated strains, poses major challenges to understand the genomic basis of clinically relevant phenotypes and even more, to clearly highlight potential targets of clinical interest for diagnostic, therapeutic or vaccine development. We review here how genomic, transcriptomic, proteomic and metabolomic-based approaches are great contributors to our current understanding of the interactions between *H. influenzae* and the human airways, and point possible strategies to maximize their usefulness in the context of biomedical research and clinical needs on this human-adapted bacterial pathogen.

1.2. Introduction

The Gram-negative bacterium *Haemophilus influenzae* is a human-adapted pathogen, commonly associated with human disease in both children and adults. While asymptomatic colonisation begins in the upper airways, it can spread through the respiratory tract, and potentially lead to invasive infections. *H. influenzae* consists of capsulated strains (serotypes a to f), and non-capsulated strains designated as non-typeable (NTHi). The capsulated *H. influenzae* type b (Hib) was the predominating disease-causing serotype, with a high incidence of invasive Hib disease including meningitis and sepsis, until the introduction of the efficient polysaccharide capsule vaccine in the late 1980s/early 1990s, which has driven its almost complete disappearance in countries with established child immunisation programs (Jalalvand & Riesbeck, 2018). In contrast, other *H. influenzae* serotypes and NTHi, which are not targeted by the Hib vaccine, are currently recognised as important causes of infections. In particular, NTHi is a common coloniser of the upper airways in healthy individuals, responsible for multiple acute and chronic infections of the respiratory tract, including OM, conjunctivitis, sinusitis and lower respiratory infections in children; exacerbations of chronic obstructive pulmonary disease (COPD) and cystic fibrosis (CF) in adults; and sepsis in neonates, immunocompromised adults, and the elderly (Ahearn et al., 2017; Duell et al., 2016; Jalalvand & Riesbeck, 2018; Ladhani et al., 2010; Su et al., 2018). Furthermore, *H. influenzae* antimicrobial resistance presents an overall increased trend, in such a way that ampicillin-resistant *H. influenzae* is included in the WHO global priority list of bacteria for which new antibacterial agents are urgently needed (Tacconelli et al., 2018). Additionally, fluoroquinolone-resistant *H. influenzae* has quickly increased in recent years and spread worldwide with a variety in epidemiology (Wen et al., 2020).

The *H. influenzae* strain RdKW20 was the first free-living organism for which the complete genome sequence was established (Fleischmann et al., 1995), the first naturally transformed organism to be genome-sequenced (Mell et al., 2011), generated the first genome-scale metabolic model (Edwards & Palsson, 1999; Schilling & Palsson, 2000), and pioneered transposon sequencing methodologies (Gawronski et al., 2009). We further review the contribution of genomic, transcriptomic, proteomic and metabolomic approaches to our understanding of the interactions between *H. influenzae* and the human airways (for a summary, see **Fig. 11** and **Table 3**).

1.3. Constantly evolving information from *H. influenzae* whole genome sequencing

1.3.1. *H. influenzae* population structure

On a genomic basis, a whole range of multilocus sequence typing (MLST) and core genome-single nucleotide polymorphisms (core-SNP)-based studies, performed on different *H. influenzae*

strain sets encompassing capsulated and non-typeable clinical isolates, commonly share that capsulated strains concentrate into a small number of serotype-specific clusters or clonal populations, while NTHi strains display great genomic diversity (De Chiara et al., 2014; Pinto et al., 2019; Potts et al., 2019; Power et al., 2012; Price et al., 2015; Staples et al., 2017). About 779 *H. influenzae* genomes are found currently in publicly available databases (May 21st, 2021), and we expect this number to grow exponentially over time (Koonin et al., 2021), making genomic information dynamic as constantly evolving data requiring regular update. In this context, *H. influenzae* competence in acquiring genomic material throughout the infection process facilitates genomic plasticity (see **Section 1.3.3**) leading to an open pan-genome which, for NTHi, was recently updated to 12,249 genes where the core genome accounts for about 7% (Rajendra et al., 2020). The large accessory pan-genome confers diversity and is highly heterogeneous among strains. Many genes are phage-associated, leading to numerous isolates with distinct intact phages integrated in their genome (Pinto et al., 2019; Tanaka et al., 2020).

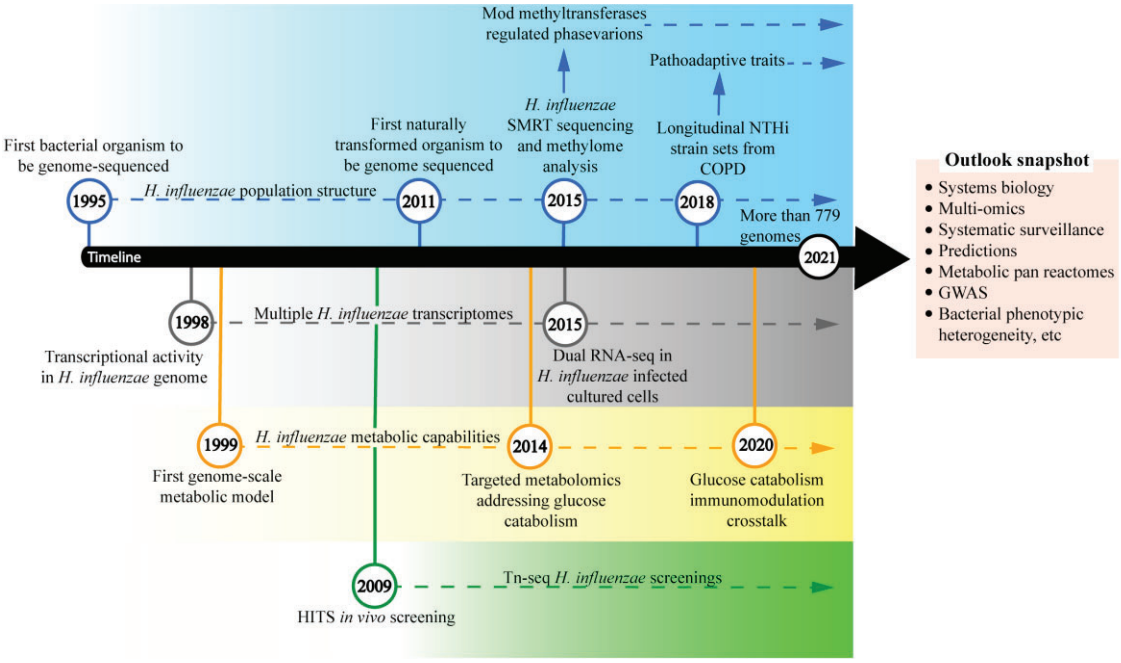

Figure 11. Summarized landscape of –omics contribution to our understanding of the interactions between *H. influenzae* and the human host. The timeline starts when the first *H. influenzae* complete genome was sequenced, as a major breakthrough on our understanding of the biology, diversity and evolution of bacteria. We highlight key genomic (labeled in blue), transcriptomic (labeled in grey), metabolomic (labeled in yellow), and Tn-seq screening (labeled in green)-based milestones and contributions over time. Information regarding *H. influenzae* population structure, genome-wide expression profiling, metabolic capabilities, and genetic screenings keeps growing along the entire timeline (indicated with dotted arrows). SMRT, single-molecule real-time; NTHi, nontypeable Haemophilus influenzae; COPD, chronic obstructive pulmonary disease; dual RNA-seq, dual RNA-sequencing; HITS, high-throughput insertion tracking by deep sequencing; Tn-seq, transposon sequencing; GWAS, genome-wide association studies.

When focusing on the capsule locus, Regions I (containing the *bexABCD* operon) and III (containing the *hcsA* and *hcsB* genes), involved in exporting the capsule polysaccharide, are

conserved among all six capsular serotypes, while Region II genes, required for polysaccharide synthesis, are unique to each serotype. Notably, in the frame of transition to whole genome sequencing (WGS)- based surveillance, bioinformatics tools for *in silico* rapid determination of *H. influenzae* serotypes from WGS data have been developed (Pinto et al., 2019; Potts et al., 2019). Moreover, capsulated strains genomic closeness has been illustrated for invasive *H. influenzae* type f (Hif) and type a (Hia) isolates (Su et al., 2014; Tsang et al., 2020). Thus, Hif may present a pattern of unique or missing genes maybe increasing the virulence, with the presence of the *sap2* operon, *aef3* fimbriae, and genes for kanamycin nucleotidyltransferase, iron-utilization and putative YadA-like trimeric autotransporters, and the absence of an operon for *de novo* histidine biosynthesis, a *hmg* locus for lipooligosaccharide (LOS) biosynthesis and biofilm formation, and a molybdate transport system (Su et al., 2014).

Table 3. Summary of –omics studies contributing to the *H. influenzae*-host interplay.

Type of study	Purpose-outcome of the study	References
A. *H. influenzae* bacterial whole genome sequencing	**A1.** Population structure of capsulated and non-capsulated (non-typeable) clinical isolates	(Aziz et al., 2019; De Chiara et al., 2014; Pinto et al., 2019; Potts et al., 2019; Power et al., 2012; E. P. Price et al., 2015; Rajendra et al., 2020; Staples et al., 2017; Y. C. Su et al., 2014; Tanaka et al., 2020; Tsang et al., 2020)
	A2. Within-host pathoadaptive traits on longitudinally collected strain sets from chronic respiratory samples – genome evolution in natural settings	(Gallo et al., 2018; Garmendia et al., 2014; Moleres et al., 2018; Pettigrew et al., 2018)
	A3. Natural transformation and recombination-driven genetic variation	(Connor et al., 2012; Mell et al., 2011, 2016; Mell, Lee, Firme, Sinha, & Redfie, 2014; Moleres et al., 2018; Mora et al., 2021; Power et al., 2012)
	A4. Methylome profiling	(Atack et al., 2015, 2019)
	A5. Microevolution in experimental settings	(Hardison, et al., 2018; Harrison et al., 2020)
B. Genome-wide genetic screening	**B1.** HITS* based *in vivo* genetic screenings	(Gawronski et al., 2009; S. M. Wong et al., 2013, 2019)
	B2. Tn-seq based *in vitro* genetic screenings	(Langereis et al., 2013, 2014; Langereis & Weiser, 2014; Marti et al., 2017; Mobegi et al., 2014)
C. Genome-wide gene expression profiling	**C1.** Bacterial transcriptomic responses to changing environmental conditions	(Jiang et al., 2016; Whitby et al., 2009, 2013; Whitby, VanWagoner, et al., 2006; S. M. S. Wong et al., 2007)
	C2. Bacterial transcriptomic responses to gene inactivation	(Atack et al., 2015, 2019; Black et al., 2020; Brockman et al. 2018; Harrison et al., 2019; Santana et al., 2014; Srikhanta et al., 2005; VanWagoner et al., 2016)
	C3. Dual RNA-seq gene expression profiling	(Baddal et al., 2015a)
D.Proteomic profiling	**D1.** Bacterial responses to changing environmental conditions	(De Souza-Hart et al., 2003; Mokrzan et al., 2020a; Post et al., 2014; Qu et al., 2010a)
	D2. Bacterial responses to gene inactivation	(Atack et al., 2015; Brockman et al., 2018; Harrison et al., 2019)
E.Metabolomic profiling	**E1.** Bacterial responses to changing environmental conditions	(López-López et al., 2020; Muda et al., 2019a; Othman et al. 2014)
	E2. Bacterial responses to gene inactivation	(Harrison et al., 2019; López-López et al., 2020)

*HITS, high-throughput insertion tracking by deep sequencing; Tn-seq, transposon sequencing; dual RNA-seq, dual RNA-sequencing

Efforts to define the structure of the NTHi population and to identify groups of related strains led to strain partitioning into six or eight groups or monophyletic clades (clades I-VI / clades I-VIII)

based on the core alignment, not predicted on the basis of MLST data, and supported by the composition of the accessory genome (De Chiara et al., 2014; Rajendra et al., 2020). The clade I-VI classification allowed proposing clade-specific signatures regarding the exclusive presence/absence of genes encoding surface-associated proteins and LOS components (De Chiara et al., 2014; Pinto et al., 2019). This sorting was further revisited on the clade I-VIII classification by applying pan-genome-wide association studies (GWAS) tools to identify genes enriched in each specific clade (Rajendra et al., 2020).

On the other hand, the molecular basis underpinning NTHi transition from commensal to pathogen is not clearly understood. Clade classification did not group strains of common clinical or geographical origin (De Chiara et al., 2014; Rajendra et al., 2020), and comparative genomics, by analysing paired isogenic strains isolated from the nasopharynx (NP) and bronchoalveolar lavage (BAL) of children with chronic lung disease, did not shed light on this matter as pairs were highly genetically similar (Aziz et al., 2019). Nevertheless, and despite NTHi heterogeneity, the previously reported association between the NTHi ST14CC-PBP3IIb/A clonal group, increased clinical virulence, antimicrobial resistance and persistence over time, together with NTHi implication in clonal invasive disease, highlights that continuous surveillance and WGS in a clinical laboratory will certainly allow to rapidly address concerns of usually virulent clones or possible outbreaks, particularly in the severe immunocompromised population (Andersson et al., 2015; John et al., 2021; Månsson et al., 2017).

1.3.2. NTHi isolates from COPD patients: genetic signatures and pathoadaptive traits

COPD is an emerging disease worldwide, and cigarette smoking is its main risk factor. The disease is characterised by dyspnea, chronic cough, sputum production and persistent airflow limitation. COPD exacerbations are often associated to bacterial pathogens, most importantly to NTHi. A main feature of COPD is, however, a chronic inflammation of the pulmonary parenchyma that is associated with bacterial persistence, and NTHi is a frequently found bacterial species in the airways of these patients (Celli & Wedzicha, 2019; Hurst et al., 2010; Ritchie & Wedzicha, 2020; Wedzicha & Seemungal, 2007). When looking for genetic distinctions between NTHi isolates from COPD with respect to other illnesses, the distribution of core genome SNPs does not separate COPD from non-COPD strains (De Chiara et al., 2014; Rajendra et al., 2020). However, this distinction is possible when applying discriminant analysis of principal components to the composition of the accessory genome, further supported by pan-GWAS identification of a repertoire of unique NTHi accessory genes significantly associated with COPD, many of them with predicted roles in virulence, transmembrane transport of metal ions and nutrients, cellular respiration and maintenance of redox homeostasis (Rajendra et al., 2020). Moreover, NTHi also alters its genome during persistence within

the lower airways of chronic respiratory patients, as stated by the analyses of longitudinally collected NTHi strains from independent cohorts of COPD patients (Garmendia et al., 2014; Moleres et al., 2018; Pettigrew et al., 2018). Pettigrew's group revealed frequent genetic variation due to slipped-strand mispairing in simple sequence repeats (SSR), and diversifying selection of several candidate vaccine antigens during NTHi persistence in the human airways (Pettigrew et al., 2018). Follow up studies on this same strain collection showed different proportions of methyltransferase-encoding *modA* alleles compared to those isolated from OM patients (Atack et al., 2019), and changes in the expression of the IgA protease variants A1, A2, B1 and B2 conferred by changes in genomes during persistent infection which, depending on the variant, could be indels or slipped-strand mispairing in mono- or heptanucleotide repeats (Gallo et al., 2018). On our part, we addressed molecular genetic changes underlying bacterial pathoadaptation by investigating genetic variants arising from within-patient evolution of NTHi in an independent cohort of COPD patients. Notably, we identified recurrent polymorphisms in several genes and provided experimental evidence for the biological significance of such convergent variation in the *ompP1-fadL* gene, whose recurrent mutations are a likely case of antagonistic pleiotropy during adaptation of NTHi to chronic lung infection associated to COPD (Moleres et al., 2018).

1.3.3. WGS insights into DNA uptake, natural transformation and natural genetic variation by *H. influenzae*

Natural competence allows bacteria to respond to environmental and nutritional cues by taking up free DNA from their surroundings, gaining both nutrients and genetic information (Mell & Redfield, 2014). *H. influenzae* intrinsic transformable nature, self-preferences caused by the uptake machinery bias for uptake signal sequences (USS), and the high rate of homologous recombination events they can undergo, have a great impact on the evolution of the genomes of this pathogen, which seems to be higher in NTHi compared to capsulated strains (Connor et al., 2012; Mora et al., 2021).

Such frequent genetic exchange also occurs among *Haemophilus* spp., (*H. influenzae*, *H. aegyptius* and *H. haemolyticus* belong to the cluster ''*Haemophilus sensu stricto*" (Hedegaard et al., 2001; Nørskov-Lauritsen et al., 2005)), causing frequent misidentifications of *H. influenzae* from clinical specimens when using selective culture methods, a limitation overcome by using matrix-assisted laser desorption/ionization time-of-flight (MALDI-TOF) mass spectrometry (Frickmann et al., 2013; Marti et al., 2016). On this matter, phylogeny studies may also allow not only seeking for *H. influenzae*-specific signatures of diagnostic potential such as the *fucP* locus (Price et al., 2015), but also speciating *Haemophilu*s isolates from COPD, further supporting that the heterogeneity of NTHi may indeed provide a genetic continuum between NTHi and *H. haemolyticus* (Osman et al., 2018b).

When focusing on bacterial genome shaping by natural transformation, it is noticeable that the first WGS characterization of recombination events was performed by using DNA from a clinical isolate of NTHi (strain 86-028NP) to transform competent cells of a laboratory strain (strain RdKW20), leading to the first genome-wide analysis of chromosomes directly transformed with DNA from a divergent genotype (Mell et al., 2011; Mell et al., 2014a). Such observations were independently supported by transformation of the same laboratory strain with donor DNA from a heterologous Hib strain (Power et al., 2012). Detailed genome-wide analyses of not only *H. influenzae* bacteria experimentally transformed with donor DNA from diverged clinical isolates, but also DNA uptake across the outer membrane of naturally competent *H. influenzae* bacteria, turned out to be extremely informative to understand the relevance and evolution of uptake sequences in the genome, and even to predict the outcome of competition between self- and non-self DNA in the respiratory tract environment (Mell et al., 2014a; Mora et al., 2021). Moreover, transformation-based experimental evolution studies showed that transformation of single competent cells is extensive, suggesting that it could be used as a tool to map traits that vary between clinical isolates. This notion was applied to develop ‘‘transformed recombinant enrichment profiling” (TREP), in which natural transformation is used to generate complex pools of recombinants, phenotypic selection is used to enrich for specific recombinants, and deep sequencing is used to survey for the genetic variation responsible. TREP was applied to investigate the genetic architecture of intracellular epithelial invasion by *H. influenzae*, and identified specific allelic variants of the HMW1 adhesin as a key factor on this matter (Mell et al., 2016). Connecting such *in vitro* transformation studies with the high levels of natural genetic variation found in NTHi, variation within closely related genomes from clinical strains collected from COPD respiratory samples shows numerous closely spaced variants which resemble natural transformation events seen in the laboratory, i.e. recombination tracts distinguishing the clinical isolates (Moleres et al., 2018).

1.3.4. Single-molecule real-time (SMRT) sequencing contribution to *H. influenzae* phase-variable methylome analyses

Formation of C-/N-methyl-cytosine and N-methyl-adenine in bacterial genomes is a postreplicative phenomenon that occurs at specific targets, has multiple roles in bacterial physiology, and can be genome-wide deciphered by using SMRT or nanopore sequencing (Flusberg et al., 2010; Sánchez-Romero et al., 2015; Sánchez-Romero & Casadesús, 2020). DNA methyltransferases can exist as part of restriction-modification (R-M) systems and be subject to phase variation, i.e. the random and reversible switching of gene expression due to the presence of inverted repeats (IR) or SSRs in their coding regions. Phase-variable methyltransferases control the expression of multiple genes via epigenetic mechanisms (Atack et al., 2018b; Phillips et al., 2019; Seib et al., 2020). Such systems, called phasevarions for phase-variable regulons, were originally identified in *H. influenzae*,

where the DNA methyltransferase ModA is a type III R-M system component containing a variable number of SSRs within its coding sequence (Srikhanta et al., 2005). ModA phase variation generates ON/OFF protein variants resulting in changes in methylation patterns, and therefore in phasevarion expression profiles and phenotypic heterogeneity. Besides phase variation, ModA also undergoes allelic variation among *H. influenzae* strains contributing to a wide range of predicted DNA methylation target sequences (Atack et al., 2018b; Phillips et al., 2019; Seib et al., 2020). By analysing *modA* allelic variation across NTHi isolates from healthy individuals, OM and COPD patients, ModA1 to ModA21 variants have been identified, whose distribution and prevalence vary depending on the strain origin, suggesting that different *modA* alleles may provide distinct advantages in the differing human body niches and even have a marker potential (Atack et al., 2015, 2019).

Several studies tackled phenotypic heterogeneity due to NTHi ModA2 phase variation, showing that (i) under alkaline conditions such as those in the middle ear during chronic disease, NTHi strains expressing ModA2 (*modA2* ON) form biofilms with greater biomass and less distinct architecture than those formed by a ModA2-deficient population (*modA2* OFF) (Brockman et al., 2018); (ii) ModA2 ON are more sensitive to oxidative stress than ModA2 OFF variants (Brockman et al., 2017). Regarding *in vivo* selection during infection of the middle ear in a chinchilla model of OM, *modA2* ON was preferentially selected compared to *mod2A* OFF (Atack et al., 2015), further supported by that the fact that a shift from OFF to ON within the middle ear results in increased disease severity (Brockman et al., 2016), and that a unique host immune response may be mounted against each discrete *modA* subpopulation (Robledo-Avila et al., 2020).

In addition, coupling of SMRT sequencing with gene and/or protein expression profiling allows combining knowledge of methylation specificity and gene expression changes proportional with methyltransferase phase variation. Thus, genome-wide gene expression profiling showed (i) differences when comparing RdKW20 WT and *modA* mutant strains for genes encoding, among others, surface-exposed proteins, transporters and heat-shock proteins (Srikhanta et al., 2005); (ii) differences when comparing R2866 WT and *modA10* mutant strains, including upregulation of membrane protein encoding genes such as *olpA2*, which is involved in host cell adhesion and invasion (VanWagoner et al., 2016); (iii) the effects of *modA2* phase variation, including those within biofilms by using an ON/OFF strain pair (Atack et al., 2015; Brockman et al., 2018); (iv) the effects of *modA15* and *modA18* phase variation, by using a single ON/OFF pair of strains for each *modA* allele. In the case of the ModA15 phasevarion, the DNA binding transcriptional regulator Fis was up-regulated in ON relative to OFF, as a likely case of regulation of a regulator (Atack et al., 2019). Conversely, proteomic analyses (i) determined relative protein abundances within the biofilms formed by each *modA2* subpopulation, with the greatest differences occurring in alkaline conditions including a significant decrease in abundance of the DNABII DNA-binding protein HU within

biofilms formed by *modA2* ON compared to those formed by *modA2* OFF bacteria (Brockman et al., 2018a), and (ii) showed differences related to changes in the expression of outer membrane proteins when comparing modA ON/OFF strain pairs (Atack et al., 2015).

1.3.5. Genome-scale microevolution and genetic screening approaches shed light on NTHi adaptation and pathogenesis

Unravelling pathoadaptive genome evolution related to chronicity in the natural setting is not only thrilling but also challenging, as it requires longitudinal and preferably prospective clinical isolate sampling (Moleres et al., 2018; Pettigrew et al., 2018). This notion, when applied to well-suited experimental settings, also allows unravelling microevolution traits contributing to the pathogen persistence. This is the case of the mutation of the *icc* gene, encoding a 3′,5′ -cyclic adenosine monophosphate phosphodiesterase, identified as a *H. influenzae* microevolution trait in response to transient nutrient limitation, which associates with increased development of intracellular bacterial communities (IBC) (Hardison, et al., 2018b). Likewise, when using a pre-clinical model of OM to assess NTHi pathoadaptation during sequential episodes of disease, microevolution of haemoglobin binding and LOS biosynthesis genes was observed in such OM-adapted strains, which in turn promoted increased biofilm formation, inflammation, stromal fibrosis, and an increased propensity to form IBCs (Harrison et al., 2020).

On the other hand, sequencing and data analysis tools have also revolutionized genome-wide gene discovery aimed to determine gene disruptions differentially represented in a mutant population upon screening. Historical limitations by the labour involved in mapping the locations of the mutations, are overcome by using random transposition insertion mutagenesis followed by deep sequencing. This is achievable by high-throughput insertion tracking by deep sequencing (HITS), insertion sequencing (IN-seq), transposon sequencing (Tn-seq), or transposon-directed insertion sequencing (TraDIS), collectively referred to as Tn-seq (Burby et al., 2017; Cain et al., 2020; van Opijnen et al., 2009; van Opijnen & Camilli, 2013; Wong & Akerley, 2012). *H. influenzae* pioneered genome-wide gene discovery by starring the original HITS proof of concept, developed to analyse genes required by *H. influenzae* to resist clearance from the lung in a murine pulmonary model, and identified a whole range of genes with reported or potential roles in survival during nutrient limitation, oxidative stress, and exposure to antimicrobial membrane perturbations (Gawronski et al., 2009). HITS was also useful to identify *H. influenzae* genes required to colonize an influenza A virus (IAV) co-infection murine model, showing genes both exclusive or commonly shared by bacterial and IAV co-infection model systems (Wong et al., 2013), or to screen genome-wide genetic interactions to unravel epistatic interaction accounting for *H. influenzae* survival in the murine lung (Wong et al., 2019). Tn-seq suitability has also been reported for *H. influenzae in vitro* genome-wide screening studies including the identification of (i) essential genes (Mobegi et al., 2014); (ii) the

carbonic anhydrase involvement in NTHi adaptation to changes in environmental CO_2 levels and intracellular survival (Langereis et al., 2013); (iii) a role for the outer membrane protein P5 in NTHi survival to complement-mediated killing (Langereis et al., 2014), and for galactose-containing oligosaccharide structures in NTHi survival to complement-dependent neutrophil-mediated killing (Langereis & Weiser, 2014); (iv) the contribution of the *mltC* and *lppB* genes to biofilm formation (Marti et al., 2017).

1.4. Unraveling features of the *H. influenzae*-host interplay by genome-wide gene expression profiling

Since the first high-density oligonucleotide probe array containing probes representing 106 *H. influenzae* genes (de Saizieu et al., 1998), microarray and later on RNA sequencing (RNA-seq) technologies have greatly contributed to broaden our understanding of NTHi physiology and host interplay. Please note that profiling of gene expression changes regulated by methyltransferases and their phase variation is reviewed in **Section 1.3.4**. Moreover, *H. influenzae* transits between niches within the host that differ in oxygen levels, and the ArcAB two-component regulatory system controls gene expression in response to different respiratory conditions of growth. Gene expression profiling contributed not only to identify the *H. influenzae* ArcA regulon upon anaerobic growth (Wong et al., 2007), but also to decipher changes in *H. influenzae* transcriptional responses upon changes in oxygen availability, showing that, in high oxygen, arginine uptake, arginine/aspartate metabolism, and glutamate pathways leading into the Krebs cycle are commonly up-regulated (Jiang et al., 2016).

Genome-wide expression profiling also identified a putative core of genes responsive to iron and heme (FeHm) availability in several NTHi strain backgrounds including RdKW20, 10810, R2866, 86-028NP or R2846. Included in the core iron/heme modulon were genes preferentially expressed under iron/heme limitation, most of which are directly involved with iron and/or heme acquisition (Whitby et al., 2006; Whitby et al., 2009, 2013). The ferric uptake regulator (Fur) regulon has also been studied, which identified the first small RNA described in any *Haemophilus* species, HrrF, overexpressed in the absence of Fur and responsive to iron levels, in turn regulating the expression of molybdate uptake, and deoxyribonucleotide and amino acid synthesis genes (Santana et al., 2014). As mentioned above, transient nutrient limitation, in particular FeHm restriction, increases the longevity of NTHi survival *in vitro* and promotes bacterial microevolution by mutation of the *icc* gene (Hardison, et al., 2018b). Such adaptive trait, besides increased development of IBCs (Hardison et al., 2018b), also relates to increased biofilm formation and gene expression changes within the *in vitro* biofilms, some of them associated to competence and therefore likely linked to the observed increased transformation efficiency of those biofilms (Harrison et al., 2019).

Regarding natural competence, changes in gene expression during competence development confirmed the existence of a competence regulon characterized by a promoter-associated competence regulatory element (CRE) closely related to the cAMP receptor protein (CRP) binding consensus, and where the essential competence gene *sxy* is induced early in competence development (Redfield et al., 2005). Such observations were further extended by differential gene expression profiling of *H. influenzae* wild-type, *crp* and *sxy* mutant strains, which also shed light on the competence-regulated toxin-antitoxin ToxTA system (Black et al., 2020). Moreover, analysis of global transcriptional changes has also been of use when assessing *H. influenzae* response to antibiotic pressure, showing increased *ponB* (encoding PBP1b) and *acrR* (negative regulator of AcrAB-TolC efflux pump) gene expression during heat stress, which may relate to the observed decrease in bacterial viability after incubation with imipenem at 42 ºC as compared to 37 ºC (Cherkaoui et al., 2017). An effort to identify convergent molecular signatures related to lung adaptation led to comparative transcriptomic analysis of paired, isogenic NTHi strains, isolated from the NP and BAL of children with chronic lung disease, showing no convergence at the gene level, but a possible trend in terms of functional enrichment among genetically unrelated NTHi strains (Aziz et al., 2019).

Although most studies have analyzed *H. influenzae* gene expression, host response to bacterial infection also needs obvious attention. Gene expression profiling identified host functions differentially expressed in NTHi-infected human type II pneumocytes, which allowed identifying a repertoire of host target candidates for pharmacological modulation (Euba et al., 2015c). In an independent study, the transcriptome of a complete episode of acute OM in mice identified sets of genes involved in regulation of immune responses, changes in epithelial and stromal cell markers, and the recruitment/function of neutrophils and macrophages (Hernandez et al., 2015). Notably, a dual RNA-seq approach was undertaken for pathogen and host genome-wide expression profiling during *H. influenzae* infection of ciliated human bronchial epithelial cells. Temporal profiling of host mRNA signatures revealed significant dysregulation of the target cell cytoskeleton elicited by bacterial infection, with a profound effect on the intermediate filament network and junctional complexes. In turn, NTHi downregulated its central metabolism, and increased the expression of transporters, suggesting a change in the metabolic regime due to the availability of host substrates (see **Section 1.5**), and of stress-induced defense mechanisms, including the transport of exogenous glutathione and activation of toxin-antitoxin family components (Baddal et al., 2015). Currently lacking, *in vivo* dual RNA-seq would likely be of great help to gather a more comprehensive view of the *H. influenzae*-host interplay.

1.5. Update on *H. influenzae* protein and metabolite profiling

Proteomic studies on the *H. influenzae*-host interaction are relatively scattered. From a diagnostic perspective, *H. influenzae* species-unique peptide biomarkers discovered by tandem mass spectrometry may be a valuable tool for clinical sample proteotyping (Karlsson et al., 2020). Protein profiling regulated by methyltransferase phase variation is reviewed in **Section 1.3.4**. Independently, proteomic expression profiling of *H. influenzae* grown in pooled human sputum revealed increased expression of antioxidant, stress-response proteins, and cofactor and nutrient uptake systems compared to media grown cells (Qu et al., 2010). Definition of the protein content of NTHi lysates identified numerous unique *H. influenzae* proteins contributing to biofilm formation, immune evasion, or epithelial inflammation, classified as outer membrane/cell surface associated, metabolic, biosynthesis mediators, proteases, chaperones/ DNA binding proteins, transporters, reductases or hydrolases (Preciado et al., 2016). Proteomic profiling was also used to demonstrate differential expression of the NTHi biofilm to planktonic samples, where ArcA showed a high level of downregulation in the biofilm (Post et al., 2014), and whose inactivation led to ArcA-regulated proteomic changes, some of them maybe involved in serum susceptibility (De Souza-Hart et al., 2003). Proteomic profiling was also useful to prove that the two bacterial populations released from a NTHi biofilm by using antibodies directed against the type IV pilus or, alternatively, against a DNABII DNA-binding protein, are different not only from planktonically grown NTHi, but also from each other despite genetic identity. Even more, each newly released population had a distinct, increased susceptibility to antibiotic killing compared to planktonic bacteria, highlighting new clues for anti-biofilm therapeutics (Mokrzan et al., 2020).

From the host side, proteomic and metabolomic signatures of NTHi-induced acute OM in a chinchilla model were delineated in infected middle ear tissue lysates, revealing that establishment of disease coincides with actin morphogenesis, suppression of inflammatory mediators, and bacterial aerobic respiration. As a first step toward identification of clinically meaningful metabolic biomarkers, decreased biogenic amines and sphingomyelin molecules, increased taurine, glutamine and ornithine were observed upon infection (Harrison et al., 2016).

Elucidating the metabolic determinants in the lung during respiratory infection is likely to be key to develop therapeutics modulating symptom and/or disease severity (Bernatchez & McCall, 2020). Lung metabolomics have not been performed on the *H. influenzae*-human airways interplay, but currently available insights on bacterial metabolism may guide us when assessing this infectious process. The *H. influenzae* RdKW20 strain drove the first genome-scale metabolic model. Besides assessing basic structural features of the *H. influenzae* metabolic network, such model facilitated addressing minimal substrates requirements for the network to allow biomass production. Minimal requirements included fructose, a likely preferred carbon source for which a phosphotransferase

system (PTS) exists in *H. influenzae* (Macfadyen & Redfield, 1996; Macfadyen et al., 1996), but fructose could also be replaced by other carbon sources including glucose (Edwards & Palsson, 1999; Schilling & Palsson, 2000). *H. influenzae* possesses complete glycolysis and pentose phosphate pathways for glucose catabolism, lacks most enzymes of the oxidative branch of the Krebs cycle, and holds a respiratory chain with several dehydrogenases transferring electrons into the menaquinone pool, and terminal reductases transferring the electrons to a variety of electron acceptors, altogether driving a so-called glucose respiration-assisted fermentation, where acetate is the main end-product under aerobic growth. When oxygen is limiting, acetate is still produced but other products arise including formate and succinate, at variable rates depending on the tested strains (López-López et al., 2020; Muda et al., 2019a; Othman et al., 2014; Raghunathan et al., 2004). End-product excretion profiling is informative not only from the bacterial perspective, but also due to their possible immunomodulatory roles. Although lung nutritional immunity keeps low glucose levels in the airway surface liquid of healthy individuals, respiratory disease generates a glucose-rich niche favorable for pathogens able to use glucose as carbon source. As this being the case for *H. influenzae,* glucose catabolism enhances bacterial growth, but also promotes the release of end-products acting as pro-inflammatory metabolites, more specifically acetate, which may contribute to lung colonization and inflammation in chronic respiratory patients (López-López et al., 2020). Besides the above described genomic flexibility (see **Section 1.3**), *H. influenzae* metabolic versatility among strains has also been reported, in terms of substrate utilization, histidine synthesis or urease activity, suggesting metabolic adaptive traits favoring differential access to throat, ear, lower airways or blood niches (Juliao et al., 2007; Muda et al., 2019; Murphy & Brauer, 2011; Zhang et al., 2013).

Finally, and considering that *H. influenzae* metabolic machinery adapts to the host-imposed milieu, transcriptome signatures upon cell infection showed that the genes encoding the bacterial biosynthesis pathways of carbohydrates, lipids, amino acids, nucleotides, and energy metabolism were mostly downregulated, although the shikimate pathway for precursor chorismate production and the consequent tryptophan biosynthesis pathway was upregulated after initial bacterial-cell contact (Baddal et al., 2015). Increased tryptophan biosynthetic pathway was also observed in biofilms formed by strain variants adapted to transient FeHm restriction where, moreover, amino acids and enzymes associated with central metabolism, and metabolites associated with the urea cycle were also increased (Harrison et al., 2019). Linked to the metabolic machinery, attention should also be paid to bacterial metabolite transport systems. In fact, lactate, arginine, tryptophan, cysteine/glutathione, thiamine, thiamine pyrophosphate, iron and polyamines uptake and transport systems were highly expressed during *H. influenzae* cell infection (Baddal et al., 2015). Likewise, increased production of serine, sialic acid and tryptophan transporters was observed in biofilms formed by strain variants adapted to transient FeHm restriction (Harrison et al., 2019), together

suggesting that changes in central metabolism combined with increased nutrient stores may help counteracting nutritional immunity at the colonizing niches.

1.6. Future Outlook

The last twenty five years, since the *H. influenzae* RdKW20 strain was genome sequenced, have gone a long way, greatly propelled by the unstoppable –omics technologies. As a human-adapted pathogen, integrative systems biology approaches to the interactions between *H. influenzae* and the human airways, are instrumental in the discovery of specific bacterial recognition, host signal transduction or immune tolerance, together with multi-omics approaches to decipher the genetic, immunologic, (post)transcriptional, (post)translational, and metabolic mechanisms underlying the outcome of such interactions. Those approaches will be enormously enriched by bacterial single-cell resolution methodologies such as microfluidics, or single-cell sorting, microscopy and genome/RNA sequencing, to allow overlooking the remarkable bacterial phenotypic heterogeneity, and shed light on complex phenotypes such as antibiotic persistence or metabolic specialization. Guidance of such integrative work by the human specificity of the infection will provide meaningful information on *H. influenzae* patho-adaptive evolution within the human host. Furthermore, we are collecting a wealth of genomic and epigenomic data, and this will continue to grow with the introduction of routine sequencing for disease surveillance. These data will be of great use to predict how changes in genome sequence lead to different host-pathogen interaction outcomes by applying machine learning approaches, or to build genome-scale metabolic network reconstructions assessing core and pan reactomes. Also, combination of deep bacterial phenotyping and pan-GWAS methodologies will allow not only predicting bacterial genotype-phenotype associations, but also deciphering genetic determinants of resistance to antimicrobials, virulence or niche adaptation. Altogether, therapeutic/vaccination target and biomarker discovery will be moved forward, to be eventually translated to the clinical settings and reach end users.

Capítulo 2

Multi-omic analysis of *Haemophilus influenzae* metabolic requirements during host lung infection by combining RNA-seq and Tn-seq technologies

Nahikari López-López, Begoña Euba, Celia Gil-Campillo, Javier Asensio-López, Irene Rodríguez-Arce, Emel Sen-Kilic, Roberto Díez-Martínez, Saioa Burgui, Jeroen Langereis, Mariette Barbier, Junkal Garmendia. Multi-omic analysis of *Haemophilus influenzae* metabolic requirements during host lung infection by combining RNA-seq and Tn-seq technologies. (Manuscript in preparation).

Capítulo 2. Multi-omic analysis of *Haemophilus influenzae* metabolic requirements during host lung infection by combining RNA-seq and Tn-seq technologies

Nahikari López-López[a,†], Begoña Euba[a,†], Celia Gil-Campillo[a,†], Javier Asensio-López[a,b], Irene Rodríguez-Arce[a], Emel Sen-Kilic[c,d], Roberto Díez-Martínez[e], Saioa Burgui[b], Jeroen Langereis[f], Mariette Barbier[b,c,*], Junkal Garmendia[a,g,*].

a. Instituto de Agrobiotecnología, CSIC-Universidad Pública Navarra-Gobierno, Navarra, Spain.
b. Asociación de la Industria Navarra (AIN)-Gobierno de Navarra, Spain
c. Vaccine Development Center, West Virginia University Health Sciences Center, Morgantown, West Virginia, USA.
d. Department of Microbiology, Immunology, and Cell Biology, West Virginia University School of Medicine, Morgantown, West Virginia, USA.
e. Telum Therapeutics, Noain, Spain.
f. Section Pediatric Infectious Diseases, Laboratory of Medical Immunology, Radboud Institute for Molecular Life Sciences and Radboud Center for Infectious diseases, Radboudumc, Nijmegen, The Netherlands.
g. Centro de Investigación Biomédica en Red de Enfermedades Respiratorias (CIBERES), Madrid, Spain.

*Corresponding author: Mariette Barbier and Junkal Garmendia.

† These authors contributed equally to this work.

2.1. Abstract

Nontypeable *Haemophilus influenzae* (NTHi) is a human-adapted bacterial pathogen causing lower airway infections of chronic obstructive pulmonary disease (COPD) patients. Bacteria and host elements dictating the complexity and fitness of NTHi within the host lung are not well understood. *In vivo* systems multi-omics analyses are powerful approaches to explore the host–microbe complex, particularly when using technologies offering fundamentally distinct but complementary insights. In this study, we used RNA and transposon sequencing, RNA-seq and Tn-seq, to profile NTHi genome-wide gene expression and mutant fitness during mouse lung infections. Differential gene expression profiling of bacteria grown *in vitro* and recovered from bronchoalveolar lavage fluid (BALF) samples showed up-regulation of genes involved in purine and several non-aromatic amino acid biosynthetic processes, and of part of the natural competence machinery, insufficient however to trigger measurable *in vivo* natural transformation. Notably, bacterial gene inactivation allowed establishing a correlation between gene up-regulation and its involvement in the infectious process. From the host side, differential gene expression analysis of infected lungs compared to non-infected lungs lungs highlighted up-regulation of inflammatory response as well as down-regulation of cell adhesion and cytoskeleton. Profiling of Tn-mutant fitness by screening bacterial genes whose mutants were underrepresented in lung samples compared to *in vitro* growth revealed only few genes correlated to those differentially expressed revealing the complementarity of these two *in vivo*-omic methodologies. Our results provide novel insights into *H. influenzae* metabolic requirements for lung infection, and demonstrate the power of using both gene expression and fitness profiling for probing bacterial virulence.

2.2. Introduction

Haemophilus influenzae is a human-adapted Gram-negative bacterial pathogen. Asymptomatic colonization begins in the upper airways, but it can spread through the respiratory tract and potentially lead to invasive infections. Successful introduction to the *H. influenzae* type b (Hib) vaccine has driven its almost complete disappearance in countries with established child immunization programs (Jalalvand & Riesbeck, 2018; Slack et al., 2021), while nontypeable strains (NTHi) gain ground as important causes of infections including otitis media, conjunctivitis, sinusitis and lower respiratory infections in children; exacerbations of chronic obstructive pulmonary disease (COPD) and cystic fibrosis (CF) in adults; and invasive disease in neonates, immunocompromised adults, and the elderly (Ahearn et al., 2017; Duell et al., 2016; Jalalvand & Riesbeck, 2018; Su et al., 2018). A major gap in understanding infectious diseases is the lack of information about molecular interaction networks occurring between pathogens and their host at the infection site. This gap applies to *H. influenzae*, as bacteria and host elements that dictate the complexity and fitness of NTHi within the host lung are not well understood. Moreover, *H. influenzae* antimicrobial resistance shows an overall increasing trend, with ampicillin-resistant *H. influenzae* being included in the WHO global priority list of bacteria for which new antibacterials are urgently needed (Tacconelli et al., 2018). Therefore, target identification and drug discovery against *H. influenzae* will contribute to expand the so much needed global antibacterial pipeline. In this context, delineation of host-pathogen interplay mechanisms leading to *H. influenzae* lower airway infection by applying complementary –omic approaches on suitable *in vivo* model systems of infection will pave the way to inform the development of new therapeutic approaches.

Since the completion of the first *H. influenzae* genome sequence in 1995, the sequenced genomes of almost 800 *H. influenzae* isolates have been made publicly available (López-López et al., 2021), becoming an exponentially increasing data set to tackle the host-pathogen interplay in a genome-wide manner. When focusing on *in vivo*-omic studies, pioneer methodologies were developed for genome-wide screening of *H. influenzae* genes required in the lower airway by using a murine model of lung infection or of coinfection with influenza A virus (Gawronski et al., 2009; Wong et al., 2013). Later on, the use of a chinchilla model of otitis media contributed to delineate global changes in gene, protein and metabolite profiles during experimentally induced disease (Harrison et al., 2016; Whitby et al., 2013). However, multi-omic studies are currently scattered, mostly focused on *in vitro H. influenzae* biofilm communities (Brockman et al., 2018; Harrison et al., 2019). Notably however, joint proteome, transcriptome and metabolome analyses on biofilm cultures revealed key *H. influenzae* metabolic traits, emphasizing that identification of new therapeutic strategies requires a detailed molecular description of the NTHi physiology during disease (Harrison et al., 2019). Conversely, although host responses to bacterial infection also need understanding, host genome

expression profiling upon *H. influenzae* infection has been mostly tackled on cultured cells (Baddal et al., 2015; Euba et al., 2015c). Of note, a dual RNA-seq approach under taken during *H. influenzae* infection of ciliated human bronchial epithelial cells allowed temporal profiling of host and bacterial mRNA signatures, also shedding light on bacterial metabolic traits likely to be major contributors during infection (Baddal et al., 2015).

Overall, the current lack of *in vivo* complementary multi-omic studies precludes us from getting a comprehensive landscape of the *H. influezae* host-pathogen interplay within the lower airway. The aim of this work was to understand more clearly the host and bacterial factors that influence lower airway infection by *H. influenzae*. We used a previously characterized murine model system (Rodríguez-Arce et al., 2021) and two complementary genomic technologies, RNA sequencing (RNA-seq) and transposon insertion mutagenesis coupled to next-generation sequencing (Tn-seq). Transcriptional responses were studied in a dual manner, for both the pathogen and the host lung. Regarding host lung global responses to infection, inflammatory response and ribosomal organization genes were shown to be up-regulated and cell adhesion and cytoskeleton genes down-regulated.

Genome-wide gene expression and mutant fitness analyses were performed for *H. influenzae* upon grown *in vitro* and *in vivo* in an aiway infection model, rendering fundamentally distinct insights, as gene expression and mutant fitness did not correlate for most genes. Besides shedding light on the host lung global responses to infection, the integration of these complementary data sets drawed a comprehensive landscape regarding bacterial metabolic requirements during infection, where purine biosynthesis and the natural competence machinery are likely to have key roles. Biological significance and potential implications for target identification and drug discovery are further discussed.

2.3. Material & Methods

2.3.1. Bacterial strains and growth conditions

Strains used in this study are listed in **Table S1**. NTHi strains were grown at 37ºC, 5% CO_2 on PolyViteX agar (PVX, Biomérieux), or on *Haemophilus* Test Medium agar (HTM, Oxoid) supplemented with 10 µg/mL hemin and 10 µg/mL nicotinamide adenine dinucleotide (NAD) (Sigma, ref. N0632), referred to as sHTM agar. NTHi liquid cultures were grown at 37ºC, 5% CO_2 in: (i) brain-heart infusion (BHI, Conda) supplemented with 10 µg/mL hemin and 10 µg/mL NAD, referred to as sBHI, or alternatively (ii) chemically defined medium (CDM). In detail, 235 mL of CDM contains 191 mL of RPMI (del inglés, *Roswell Park Memorial Institute medium*, medio Instituto Conmemorativo de Roswell Park) 1640 (Life Technologies, ref. 11879-020), 5.8 mL of 1

M Hepes (pH 7.2− 7.5, Life Technologies, ref. 15630-080), 2 mL of 100 mM MEM (del inglés, *minimum essential medium*, medio esencial mínimo) sodium pyruvate (Life Technologies, ref. 113600-070), 10 mL of uracil (2 mg/mL), 20 mL of inosine (20 mg/mL), 2 mL of NAD (1 mg/mL), 4 mL of hemin (1 mg/mL), and 2.35 mL of 1 M glucose (final concentration, 10 mM) (López-López et al., 2020; Muda et al., 2019a; Othman et al., 2014). When necessary, CDM were supplemented with L-α-glycerophosphocholine (GPC) 10 mM (Merck, ref. G5291), stock solution was disolved in distilled water at 190 mM. For growth in sBHI, NTHi strains grown on chocolate agar for 16 h were inoculated (2 to 5 colonies) in 10 mL of sBHI and incubated for 11 h with shaking (100 r.p.m.). Cultures were then diluted to OD_{600}=0.07 in sBHI, incubated in sterile 250 mL flasks with 25 mL sBHI and shaking (180 r.p.m.). OD_{600} were recorded every 1 h for up to 8 h. Assays were performed on at least three independent occasions ($n \geq 3$). Erythromycin 11 µg/mL (Erm_{11}), Spectinomycin 50 µg/mL ($Spec_{50}$) for Spec mutant generation or 150 µg/mL ($Spec_{150}$) for Tn-seq mutant library generation, Novobiocin 2.5 µg/mL ($Nov_{2.5}$) or Streptomycin 100 µg/mL ($Strep_{100}$) were used to supplemented media when required. *Escherichia coli* was grown on Luria Bertani (LB) or LB agar at 37ºC, with Ampicillin 100 µg/mL (Amp_{100}), Erm 150 µg/mL (Erm_{150}) or Spec 50 µg/mL ($Spec_{50}$), when necessary.

2.3.2. Generation of *H. influenzae* mutant strains

Plasmids and primers are shown in **Tables S2** and **A2**, respectively. Two genetic *H. influenzae* backgrounds strains were used: NTHi375 and RdKW20. NTHi375 is a genome sequenced otitis media clinical isolate, previously used in host-pathogen interplay studies (Bouchet et al., 2003; López-Gómez et al., 2012; Mell et al., 2014b; Morey et al., 2011). RdKW20 is a genome sequenced capsule-deficient laboratory strain (Fleischmann et al., 1995b). For generation of *H. influenzae* mutant strains, a DNA fragment containing each gene/operon and its respective flanking regions was PCR amplified with Phusion polymerase (ThermoScientific) using NTHi375 genomic DNA as template and primers gene+flanking region-F1 and gene+flanking region-R1, and cloned into pJET1.2/blunt (ThermoScientific), generating a collection of pJET1.2-*gene* plasmids. Two gene disruption strategies were employed: (i) an ermC-based disruption strategy: in each case, the cloned PCR product was disrupted by inverse PCR with Phusion polymerase, using primers *gene*-F2 and *gene*-R2. For each gene, an internal fragment was replaced by a blunt-ended ermC resistance cassette excised by *Sma*I digestion from pBSLerm (Allen et al., 2005), generating the respective collection of pJET1.2-*gene*::*ermC* plasmids, used as a template to amplify each *gene*::*ermC* disruption cassettes with primers gene+flanking region-F1 and gene+flanking region-R1. Disruption cassettes were independently used to transform *H. influenzae* strains by using the MIV method (Herriott et al., 1970). Transformants were selected on sHTM agar with Erm_{11} to obtain NTHi375Δ*purH*, NTHi375Δ*comD*, NTHi375Δ*rec2*, NTHi375Δ*dprA*, NTHi375Δ*comB*, NTHi375Δ*comE* and

NTHi375Δ*qseBC* mutant strains. NTHi375Δ*licBC* is a mutant strain that has been described previously (Martí-Lliteras et al., 2009); (ii) a Spec-based disruption strategy: for each gene, a Spec resistance gene was independently PCR amplified from pRSM2832 using *gene*-specific mutagenic primers *gene*-F2 and *gene*-R2. *E. coli* SW102 cells were prepared for recombineering, co-electroporated with pJET1.2-*gene* (Amp^r) (50 ng), and the *gene*-specific mutagenic cassette ($Spec^r$) (200 ng) (Tracy et al., 2008). Mutagenized clones containing pJET1.2-*gene::spec* were selected on LB agar with Amp_{100} and $Spec_{50}$. This plasmid was used as a template to amplify the *gene::spec* disruption cassette with primers *gene*-F1 and *gene*-R1, used to transform *H. influenzae* strains by using the MIV method. Transformants were selected on sHTM agar with $Spec_{50}$ to obtain NTHi375Δ*glpQ* mutant strain. In all cases, mutations were confirmed by PCR. When needed, the MIV method was used to determine strain natural transformation efficiency, by using 1 µg of *ad hoc* DNA carrying a selectable antibiotic resistance marker and serial dilution plating on sHTM agar in the absence/presence of antibiotic to calculate the following ratio: c.f.u. (colony-forming units)/mL on sHTM+antibiotic/ c.f.u./mL on sHTM were carried out (Poje & Redfield, 2003) (**Table S3**).

2.3.3. Generation of the RdKW20 transposon mutant library

Transposon mutant library in *H. influenzae* strain RdKW20 was made as previously described (Langereis et al., 2013). A mutant library with an estimated number of 30,000 mutants was selected to prevent random loss of mutants with a minimal number of bacteria collected from the lungs being ~$2x10^6$ c.f.u. at 12 hpi and ~$5x10^5$ c.f.u. at 24 hpi. *H. influenzae* strain RdKW20 mutant library stock vial was thawed, grown in 15 mL sBHI at 37ºC while shaking with 225 rpm to OD_{620} of 0.5 and 1 mL aliquots were stored with 15% glycerol at -80ºC for use in mice experiments. C.f.u. count was determined for a single aliquot by making 10-fold serial dilutions on sBHI agar plates and growth overnight at 37ºC + 5% CO_2. The mutants were collected from sBHI agar with $Spec_{150}$, grown on sBHI with $Spec_{150}$ to OD_{600}=0.3 and used for mouse infection.

2.3.4. Animal handling

CD1 female mice (18-20 g) aged 4 to 5 weeks (Charles River Laboratories) were housed under pathogen-free conditions at the IdAB-CSIC or CIMA animal facilities (registration numbers ES/31-2016-000002-CR-SU-US and ES31-2010000132). Animal handling and procedures were in accordance with European (Directive 2010/63/EU) and National (RD53/2013) legislation, with the approval of the Universidad Pública de Navarra (UPNa) and CSIC Animal Experimentation Committees and local Government authorization (Protocol PI007/19).

2.3.5. Animal procedures

When necessary, porcine pancreatic elastase (PPE, Elastin Products Company) was administered in mouse previously anesthetized with isoflurane (Zoetis) for emphysema induction, with matching

vehicle solution control groups as described (Rodríguez-arce et al., 2021). *H. influenzae* strains were used for mouse lung infection. Bacteria were grown and collected as indicated below. For intranasal infection, 20 µL of a bacterial suspension containing ~$3x10^7$–$1x10^8$ c.f.u. (depending on the assay, see below) was placed at the entrance of the nostrils until complete inhalation by each mouse, previously anesthetized with ketamine (Imalgene®, Merial) and xylazine (Rompun®, Bayer AG) (3:1). When indicated, mice were euthanized by cervical dislocation, and lungs were aseptically removed. The left lung was individually weighed in sterile bags (Stomacher80, Seward Medical) and homogenized 1:10 (w/v) in PBS. Each homogenate was serially 10-fold diluted in PBS and plated in triplicate on sHTM agar to determine the number of viable bacteria (c.f.u. counts). When indicated, the right lung was used for RNA extraction. When needed, bronchoalveolar lavage fluid (BALF) samples were obtained and processed as described below.

A. NTHi infection for *in vivo* dual RNA-seq. Two assays were performed. In the first one, to generate material for murine host RNA-seq, 12 CD1 animals were divided into two groups, non-infected (n=6) and infected (n=6), and each group was divided in three subgroups (n=2). NTHi375 was grown on PVX agar for 12 h, 2 to 5 colonies were inoculated in 20 mL sBHI, and incubated for 11 h with shaking (100 r.p.m.). Cultures were diluted to OD_{600}=0.07 in sBHI, and grown in triplicate in sterile 250 mL flasks with 25 mL of medium and shaking (200 r.p.m.) to OD_{600}=0.3 prior collection. Approximately, ~$5x10^9$ c.f.u. of these cultures were used for RNA extraction (see below). Mice in the infected group were administered 20 µL (~$1x10^8$ c.f.u./mouse) of each of the three collected bacterial suspensions. Mice in each subgroup were sampled 12 h post-infection (hpi), and underwent right lung processing for RNA extraction. Lung RNA samples from each subgroup were pulled. The left lung of the infected group was processed for c.f.u. counts. In the second assay, aimed at generating material for bacterial RNA-seq, 84 CD1 mice were divided into three groups (n=28) and infected with 20 µL (~$1x10^8$ c.f.u./mouse) of each of the three collected bacterial suspensions. Mice were sampled at 12 hpi and BALF samples were obtained by injecting 3 mL PBS 1X per mouse. BALF samples corresponding to each group were pulled, filtered using a 5.0µm syringe filter, and then used for serial dilution plating to quantify viable bacteria in BALF, and for RNA extraction.

B. NTHi infection for *in vivo* Tn-seq. Forty CD1 animals were divided into two groups: mice instilled with vehicle solution, NTHi infected (n=20) and mice with lung emphysema, NTHi infected (n=20). The previously grown RdKW20 transposon mutant library was used for infection, by using 20 µL, ~$3x10^7$ c.f.u./mouse. Mice in each group were sampled at 12 and 24 hpi (n=10 animals/group/sampling time point). For each animal, both lungs were processed together in 7.5 mL PBS/homogenate. The entire homogenate volume was plated on sBHI agar with $Spec_{50}$ on 5 Petri dishes (20 cm diameter, 1.5 mL homogenate/plate), for further pulling and collection in sBHI with glycerol 15% and freezing. In parallel, 100 µL aliquots of each homogenate were used for serial

dilution and plating to determine c.f.u. counts.

C. NTHi infection for *in vivo* screenings validation. Single bacterial strain infections were performed. For this purpose, 74 CD1 mice were divided into 10 groups (n=7), except for NTHi375 (n=11), and infected with bacterial suspensions prepared as described in **A.**, with ~1x10^8 c.f.u./mouse. At 12 hpi, mice were euthanized, BALF and lung samples obtained, and processed to determine the number of viable bacteria. BALF samples were obtained by perfusion and collection of 0.7 mL of PBS, with help of a sterile 20G (1.1 mm diameter) VialonTM intravenous catheter (Becton-Dickinson) inserted into the trachea. Recovered BALF was serially diluted in PBS, and plated in triplicate on sHTM agar. By following standardized published procedures (Grilló et al., 2012), we considered that we could have a minimum of 3.3 c.f.u. in 1 mL sample without detecting bacteria (limit of detection < 3-4 c.f.u./mL BALF), rendering $\log_{10}$=0.52.

D. NTHi infection for assessing natural transformation. Three assay types were performed. In the first one, mice (n=7) were intranasally co-infected (10:1) for 12 hpi with NTHi375 WT strain heat-killed (HK) and a previously shown attenuated mutant NTHi375Δ*opsX*, (Morey et al., 2013), and then processed for lung homogenate c.f.u. counting to assess reversion of the attenuation. In the second one, four CD1 mice were intranasally co-infected (1:1) with two RdKW20 derivative strains carrying different antibiotic resistance markers (RdKW20-Str^R, P193; RdKW20-Nov^R, P194) (Mell et al., 2016), with ~1x10^8 c.f.u./mouse. At 12 hpi, BALF samples were obtained by perfusion and collection of 3 mL PBS, pulled, filtered using a 5.0µm syringe filter, pelleted by centrifugation at 14,000 r.p.m. for 10 min, and resuspended in 3 mL PBS for plating of the entire volume on sHTM+$Strep_{100}$+$Nov_{2,5}$ agar. In the third one, CD1 mice (n=10) were infected with RdKW20, with ~1x10^8 c.f.u./mouse, for 12 h. BALF samples were then obtained by perfusion and collection of 3 mL MIV solution, pulled, filtered using a 5.0µm syringe filter, pelleted by centrifugation at 14,000 r.p.m. for 10 min, and resuspended in 1 mL MIV. Then, BALF-MIV bacterial suspensions were used for *ex vivo* natural transformation by using 1 µg of *ad hoc* DNA carrying a a PCR amplicon spanning the Str^R allele of the *rpsL* gene from strain MAP7 produced with primers 1497 + 1498 described in (Mell et al., 2016), and plating of the entire volume on sHTM+$Strep_{100}$, as described (Poje & Redfield, 2003).

2.3.6. RNA extraction, purification and further processing

For RNA-seq samples generation, RNA was isolated from two different sample types. First, bacterial RNA was isolated from sBHI grown bacterial cultures (OD_{600}=0.3) using NucleoSpin RNA kit (Macherey-Nagel, Düren, Germany) as specified by the instructions of the manufacturer. Briefly, ~5x10^9 c.f.u. were pelleted by centrifugation at 14,000 r.p.m., 5 min. and resuspended in 100 µL of 10 mM Tris-HCl (pH 8), 1 mM EDTA (pH 8), treated with 1 mg/mL lisozyme for 10 min at 37ºC. Cells were lysed with 350 µL Buffer RA1 and 3.5 mL β-mercaptoethanol. Lysates were filtered

through NucleoSpin Filter units to reduce viscosity, and mixed with 350 µL of 70% ethanol. RNA was applied to NucleoSpin RNA columns, salt was removed using membrane desalting buffer (MDB), one on-column rDNase treatment step was included, samples were cleaned with RAW2 and RA3 buffers, and RNAwas eluted. Secondly, BALF and lung samples were processed using the same kit with the following modifications: (i) for BALF, samples were filtered using a 5.0µm syringe filter before pelleted; (ii) for lungs, fresh lung tissue up to 30 mg was disrupted in 600 µL Buffer RA1 with 6 mL β-mercaptoethanol, and homogenized using arotor-stator homogenizer (IKA Ultra-turrax T10 basic homogenizer and dispersing element S10N-5G) for subsequent RNA extraction. To prevent any DNA interference, a second DNase digestion was performed in RNA solutions using RNase-free DNase (Qiagen) and cleaned on another RNeasy Mini column (Qiagen).

For RNA-seq validation by qRT-PCR in sBHI and MIV cultures, NTHi375 and RdKW20 strains were grown on chocolate agar for 16 h, inoculated (2 to 5 colonies) in 10 mL of sBHI and incubated for 11 h with shaking (100 r.p.m.). Cultures were then diluted to OD_{600}=0.07 in sBHI, incubated in sterile 250 mL flasks with 25 mL sBHI and shaking (180 r.p.m.) to OD_{600}=0.3. Bacterial total RNA was isolated using TRIzol reagent (Invitrogen). These bacterial cultures were then transferred to 25 mL MIV, incubated for 100 min and shaking (180 r.p.m.). Bacterial total RNA was isolated using TRIzol reagent (Invitrogen).

In all cases, purified RNA was quantified on a Nanodrop One^{C} (Thermofisher Scientific). Total RNA integrity was determined using RNA 6000 Nano LabChips (Agilent 2100 Bioanalyzer, Santa Clara, CA, USA).

Next, purified RNA was used as it follows:

(1) RNA-seq Illumina library preparation and sequencing. The presence and quantity of eukaryotic and bacterial genes on RNA samples was tested by RT-qPCR analysis. Samples were then submitted to eukaryotic and prokaryotic Ribo-zero rRNA depletion and reassessed for RNA integrity. rRNA depleted mRNA samples were fragmented and prepared using Illumina TruSeq RNA SMARTer Strander V3 library preparation. Libraries were checked for quality control with Bioanalyzer (Agilent), and sequenced on an Illumina HiSeq platform with 2x150bp reads by Admera Health (https://www.admerahealth.com). Sample types: (i) non-infected lung; (ii) infected lung; (iii) NTHi375 strain grown in sBHI (OD_{600}=0.3); (iv) BALF from mice infected with NTHi375 strain previously grown in sBHI (OD_{600}=0.3). Biological triplicates were performed for all samples.

(2) RT-qPCR. Reverse transcription was performed using 1 µg RNA by PrimerScript RT Reagent kit (Takara). cDNA diluted 1:10 was used as template in a 20 µL reaction mixture containing 1X SYBR Premix Ex Taq II (Tli RNaseH Plus) (Takara), and specific primers pairs for each gene (**Table A2**), designed with Primer3 or Vector NTI (Life Technologies) software. Fluorescence was analyzed with AriaMx Real-Time PCR System (Agilent Technologies). The comparative threshold cycle (Ct)

method was used to obtain relative quantities of mRNA that were normalized using *gyrA* or mouse *gapdh*, for bacteria or mouse lung samples, respectively, as endogenous controls. Technical triplicates were processed for all samples ($n \geq 3$).

2.3.7. Readout transposon mutant libraries

Transposon insertion sequencing (Tn-seq) was performed as previously described for *H. influenzae* (Langereis & Weiser, 2014) with some modifications. For NextSeq sequencing, a modified primer (PBGSF23_NextSeq) was used (**Table A2**). In total, 20 adapters with unique barcodes (A through X) were used to multiplex Tn-seq libraries. PCR products were gel purified and sequenced on an Illumina NextSeq 500 according to the manufacturer's protocol.

Genomic DNA was isolated from the recovered mutant libraries with a QIAgen Genomic-tip 20/G (Qiagen). A 200 µL solution with 2 µg of mutant library genomic DNA in CutSmart buffer (New England BioLabs) with 50 µM *S*-adenosylmethionine was digested with 10 U of MmeI (New England BioLabs) for 4 h at 37°C and dephosphorylated with 1 U of calf intestine alkaline phosphatase (Invitrogen) for 30 min at 50°C. Next, the reaction product was extracted with 200 µL of phenol-chloroform-isoamyl alcohol (25:24:1), subsequently extracted with 200 µL of chloroform-isoamyl alcohol (24:1), and ethanol precipitated, and the dried DNA pellet was dissolved in 20 µL of H_2O. Tn-seq adapters with a 6-bp barcode were prepared by combining 5 nmol of two matching oligonucleotides in 1x Tris-EDTA (TE) buffer and 50 mM NaCl in a total volume of 50 µL and subjecting the mixture to a 10-min denaturation step at 95°C and an annealing step in which the reaction mixture was slowly cooled to room temperature. A 20 µL solution with a 200-pmol adapter was phosphorylated with T4 polynucleotide kinase (3' phosphatase minus) (New England BioLabs) in T4 DNA ligase buffer (New England BioLabs) for 5 min at 37°C and heat inactivated for 10 min at 70°C. Ligation of 100 ng of dephosphorylated MmeI restriction fragments with 2 pmol of phosphorylated adapter was performed in the presence of T4 DNA ligase buffer with 2 U of T4 DNA ligase (New England BioLabs) in a total volume of 20 µL for 1 h at 16°C. Immediately after the ligation, Tn-seq DNA probes were generated by PCR with 2.5 µL of the ligation reaction mixture as the template, 20 pmol of PBGSF23_NextSeq and PBGSF31 primers, high-fidelity (HF) buffer, 0.2 mM deoxynucleoside triphosphate (dNTP) mix, and 1 U of Phusion DNA polymerase in a total volume of 50 µL. PCR cycling conditions were as follows: 72°C for 1 min and 98°C for 30s, followed by 28 cycles of 98°C for 30s, 57°C for 30s, and 72°C for 10 s, with a final step at 72°C for 5 min. The resulting PCR product of 130 bp was purified from the PCR with a Minelute Reaction Cleanup Kit (Qiagen). After samples with up to 24 different 6-bp barcodes were pooled and sequenced in a round of 35 cycles on the Illumina Nextseq500.

2.3.8. Data analysis

2.3.8.1. RNA-seq data analysis

RNA-seq reads were analyzed with the software CLC Genomics workbench 21.0.5 (Qiagen) by using the *H. influenzae* strains NTHi375, and the *Mus musculus* genomes as references. RNA reads were trimmed and mapped in pairs against the gene regions of the reference genomes using the following settings for mapping: mismatch cost = 2, insertion cost = 3, deletion cost = 3, length fraction = 0.8, similarity fraction = 0.8. RPKM were calculated using default parameters for CLC Genomics to determine relative changes in gene expression (p-value <0.05). Fold changes in gene expression and statistical analyses were performed using an Extraction of Differential Gene Expression (EDGE) test with Bonferroni correction. Differentially expressed genes, pathways or biological functions were searched in KEGG, Pubmed and Uniprot; in addition, BLASTn was performed using the sequence of each differentially expressed bacterial gene as query against all *H. influenzae* genomes available at NCBI. Remaining unidentified genes were grouped as hypothetical. For functional analysis of host transcriptome only genes with Bonferroni-corrected p-value <0.05 with fold change >2 were used for analysis. rRNA genes were discarded during the analysis. GO Term biological processes analysis was performed using WebGestalt online tool (Y. Liao et al., 2019). Only GO terms statistically significant with a Bonferroni-corrected p-value<0.05 were used for analysis. Affinity propagation was used to cluster similar gene sets to reduce redundancy in report. STRING analysis of differentially regulated genes were performed and visualized by using Cytoscape 3.7.1 (Shannon et al., 2003; Szklarczyk et al., 2019).

2.3.8.2. Tn-seq data analysis

For Tn-seq data analysis, FASTQ files with 35-bp sequences were imported in the web-based interface Essentials (Zomer et al., 2012). Of note, the first nucleotide of the sequence reads often had a poor quality and was omitted. As a result, only the last 5 bp of the 6-bp barcode sequence were available for data analysis. To identify these barcodes, a mismatch of 2 bp was allowed. After removal of the barcode and transposon sequences, the length of the remaining transposon-flanking genomic sequence was set at 17 bp. Alignment of this sequence with the forward strand of the *H. influenzae* RdKW20 reference genome should give a match of at least 15 bp. Count data (i.e., pseudoreads) were generated per unique sequence read and per gene. Normalization factors were calculated using the trimmed mean of *M* values (TMM). Pseudoreads in the control and target samples were tested for significant differences (*P* 0.001) by the quantile-adjusted conditional maximum likelihood (qCML) method assuming moderated tag-wise dispersion of replicates. The prior.n value to determine the amount of smoothing of tag-wise dispersions was set at 10. A Benjamin-Hochberg (B-H) adjusted *P* value (adjusted *P* of 0.05) was used. Gene essentiality was determined by comparing the expected number of reads per gene (based on the number of insertion

sites per gene, the mutant library size, and the sequencing depth) and the measured number of reads per gene. Significantly underrepresented genes were considered essential and omitted from the data analysis.

Under- and over-represented bacterial genes, pathways or biological functions were searched in KEGG, Pubmed and Uniprot; in addition, BLASTn was performed using the sequence of each differentially represented bacterial gene as query against all *H. influenzae* genomes available at NCBI. Remaining unidentified genes were grouped as hypothetical.

2.3.9. Statistical analysis

In all cases, $p<0.05$ value was considered statistically significant. Analyses were performed using Prism software, version 7 for Mac (GraphPad Software) statistical package and are detailed in each Figure legend.

2.4. Results

2.4.1. Airway infection triggers both host and pathogen transcriptional reprogramming – global gene expression analyses of *H. influenzae* and the murine lung

Transition from the environment to the host triggers vast changes in gene expression in bacterial pathogens (Damron et al., 2016). To gain insights into how *H. influenzae* adapts to the host environment, we attempted to perform dual RNA-seq of the pathogen and the host during acute lung infection in mice. The schematic representation of the experimental design is shown in **Figure 12A**. NTHi375 was grown on sBHI at 37ºC and 10^8 c.f.u. were used to infect CD1 mice by intranasal administration. Lung from infected animals were collected 12 hpi for RNA purification. As controls, RNA was purified from non-infected animals and from NTHi375 grown on sBHI (**Figure 12A**). For all samples, rRNA was depleted, and three libraries were prepared and sequenced. Read data were mapped to *H. influenzae* and *Mus musculus* genomes independently with CLC Genomics. A total of 70 to 75 milion 2x150bp reads were obtained for each sample. Differential gene expression analysis highlighted that a greater number of genes were statistically up-regulated in infected lungs compared to non-infected lungs (2,078 up-regulated versus 2,229 down-regulated) (**Tables A3** and **A4**). The great majority of the genes with statistical changes in expression were protein-coding genes (**Figure 12B**). Strikingly, 5.6% of the genes up-regulated in the lung in response to infection are predicted to encode non-coding RNAs. The STRING and GO Term analysis highlighted that genes associated with inflammatory response are up-regulated during infection with associated biological GO terms such as neutrophil chemotaxis, regulation of defense response and cytokine production (**Figure 12 C-D**). Among these genes, chemokines and genes encoding serum amyloid A were the most

differentially up-regulated genes (**Table A3**). On the other hand, we observed the genes associated with cell adhesion and cytoskeleton to be down-regulated (**Table A4** and **Figure 12 C-D**).

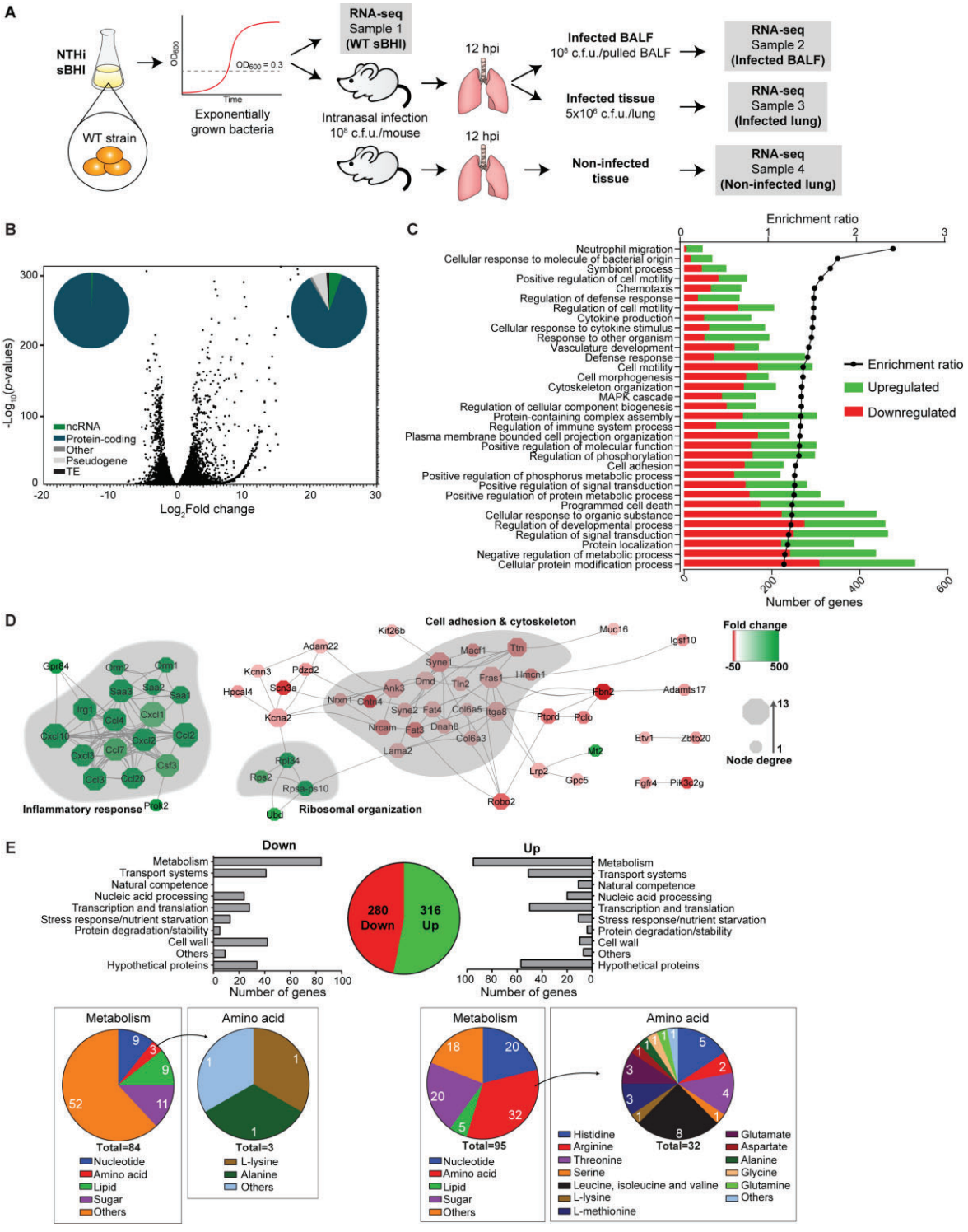

Figure 12. *Mus musculus* and *H. influenzae* global gene expression profiling upon airway infection. (A) Schematic representation of samples generated for RNA-seq. *In vitro* growth of NTHi375-WT in sBHI generated sample 1, and the *input* material for mice infection. At 12 hpi, BALF samples were recovered from infected mice, together with lung samples from both infected and uninfected mice to generate *output* samples, 2, 3 and 4, respectively. **(B)** Volcano plot that represents the fold change of murine genes differentially expressed (DE) upon *H. influenzae* infection. **(C)** Ingenuity Pathway Analysis (IPA) of canonical pathways significantly up-regulated (green) or down-regulated (red) in mice during

H. influenzae infection. **(D)** STRING analyses of mice DE genes upon *H. influenzae* infection representing inflammatory response, ribosomal organization and cell adhesion and cytoskeleton pathways. **(E)** *H. influenzae* genes significantly up-regulated (green) and down-regulated (red) *in vivo* versus *in vitro*, and their classification into functional categories.

To gain insights into the bacterial transcriptome during infection, the reads obtained from the NTHi infected lung were mapped to the pathogen. Unfortunately, only approximately 0.25% of the reads in each sample mapped to the pathogen, indicating that the amount of bacterial RNA in the infected tissue was too low for analysis. These data indicate that the methodology described above only provides RNA in sufficient quantity to study the transcriptome of the host, but not of the pathogen in the same sample. To increase bacterial RNA yield from *in vivo* samples, mice were infected as described above, bacteria were recovered from pulled BALF samples, and total RNA was purified (for details, see Methods section). After rRNA depletion, library preparation and HiSeq sequencing, 150 million to 179 million 2x150bp reads were obtained for each BALF sample. Read mapping to the pathogen was greater than in lung tissue, with 13.4 to 15.2% of the reads mapped in pairs to the pathogen. These data indicate that this methodology provides quality RNA in sufficient quantity for *in vivo* profiling of the *H. influenzae* transcriptome.

2.4.2. *H. influenzae* gene expression changes during infection

Global changes in H. influenzae gene expression. EDGE statistical analysis was used to measure differences in gene expression. A total of 316 *H. influenzae* genes were found to be up-regulated (**Table A5**) and 280 down-regulated *in vivo* compared to *in vitro* growth in sBHI (**Table A6**) (p value < 0.001). Such differential expression was further validated by RT-qPCR for a subset of genes (**Figure S1**). To define the systems differentially regulated in each experimental condition, data were analyzed using a range of metagenomics analysis tools including GO term analysis of the biological processes, hypergeometric tests on annotations, KEGG pathways and STRING analyses. Additional manual curation of the annotation was made by the means of Pubmed and Uniprot searches, and BLASTn was performed using the sequence of each differentially expressed gene as query against all *H. influenzae* genomes available at NCBI. Remaining unidentified genes were grouped as hypothetical (**Tables A5, A6**).

Changes in gene expression associated with bacterial metabolism. Data analysis based on our curated annotation highlighted that a large proportion of the genes differentially expressed during infection compared to *in vitro* growth encode products involved in bacterial metabolism (**Figure 12E**). In particular, purine and amino acid (histidine, arginine, threonine, serine, leucine, isoleucine, valine, methionine, glutamate, aspartate, glycine) biosynthesis processes, together with genes involved in sugar catabolism processes, were significantly up-regulated during infection (**Figure 13A**). On the other hand, genes involved in fermentative reactions leading to acetate production (*pta-ackA*) were significantly up-regulated *in vitro*, maybe unexpected given the previously observed

effect of such gene inactivation upon airway infection (López-López et al., 2020). Genes involved in peptidoglycan biosynthesis were also down-regulated *in vivo*. Furthermore, genes involved in glycerol and GPC metabolism processes, including the GPC link with phosphorylcholine (PCho) decoration of the lipooligosaccharide (LOS) molecule were also expressed at higher levels *in vitro* compared to *in vivo* samples (**Figure 13B**).

Changes in bacterial gene expression associated with transport. We also observed differential expression of a wide range of transport systems. As reported for other bacterial pathogens such as *P. aeruginosa*, the distinct mechanisms used for iron and heme uptake systems were differentially regulated in each condition. For example, the TonB-independent HbpA-DppBCDF and SapABCDFZ heme uptake systems were up-regulated *in vitro* (**Table A6**). However, the TonB-independent iron HitABC, and TonB-dependent transferrin TbpAB and hemopexin HxuCBA uptake systems, together with TonB-ExbBD itself, were up-regulated *in vivo* (**Table A5**). Although complex due to the moonlighting features of some of these systems (Rodríguez-Arce et al., 2019), expression differences may relate to the sources of iron availability encountered by NTHi in the host lung. Also likely related to iron sensing, the QseBC/FirRS system was up-regulated *in vivo*. When looking at amino acid transport, we observed down-regulation of the serine permease SdaC *in vivo*, together with the serine to pyruvate converting enzyme SdaA serine deaminase (**Figure 13A**), likely to be in one single transcriptional unit *sdaCA*. It is also worth mentioning up-regulation of glycerol transport *in vitro*, aligned with the above cited glycerol metabolic processes, and also linked to PCho decoration. In fact, genes encoding enzymes involved in LOS decoration by the means of di-galactose and sialic acid, or lipid A acylation, were up-regulated *in vitro*, altogether suggesting down-regulation of bacterial surface decoration *in vivo* to evade the host immunity (**Figure 13B** and **Table A6**).

Changes in gene expression associated with bacterial natural competence. H. influenzae can actively transport environmental DNA fragments across their cell envelope (uptake across the outer- and translocation across the inner membrane) and into their cytoplasm. As incoming DNA fragments can recombine with and replace homologous segments of the chromosome, competence provides cells with a potent mechanism of horizontal gene transfer, and access to the nutrients in extracellular DNA (**Figure 14A**) (Mell & Redfield, 2014). Competence machinery is regulated, as cells respond to a lack of phosphotransferase system (PTS) sugars and purine precursors, by inducing expression of a regulon under the control of the catabolite regulator cyclic AMP receptor protein (CRP) and its competence-specific cofactor Sxy, known as the CRP-S regulon (Mell & Redfield, 2014; Redfield et al., 2005; Sinha et al., 2012). Eleven genes known to be involved in *H. influenzae* natural competence were found to be up-regulated *in vivo* (*comC*, *comD*, *rec2*, *dprA*, *comB*, *comE*, *pilA*, *toxT*, *toxA*, *comF* and *ssb*) (**Figure 14B** and **Table A5**).

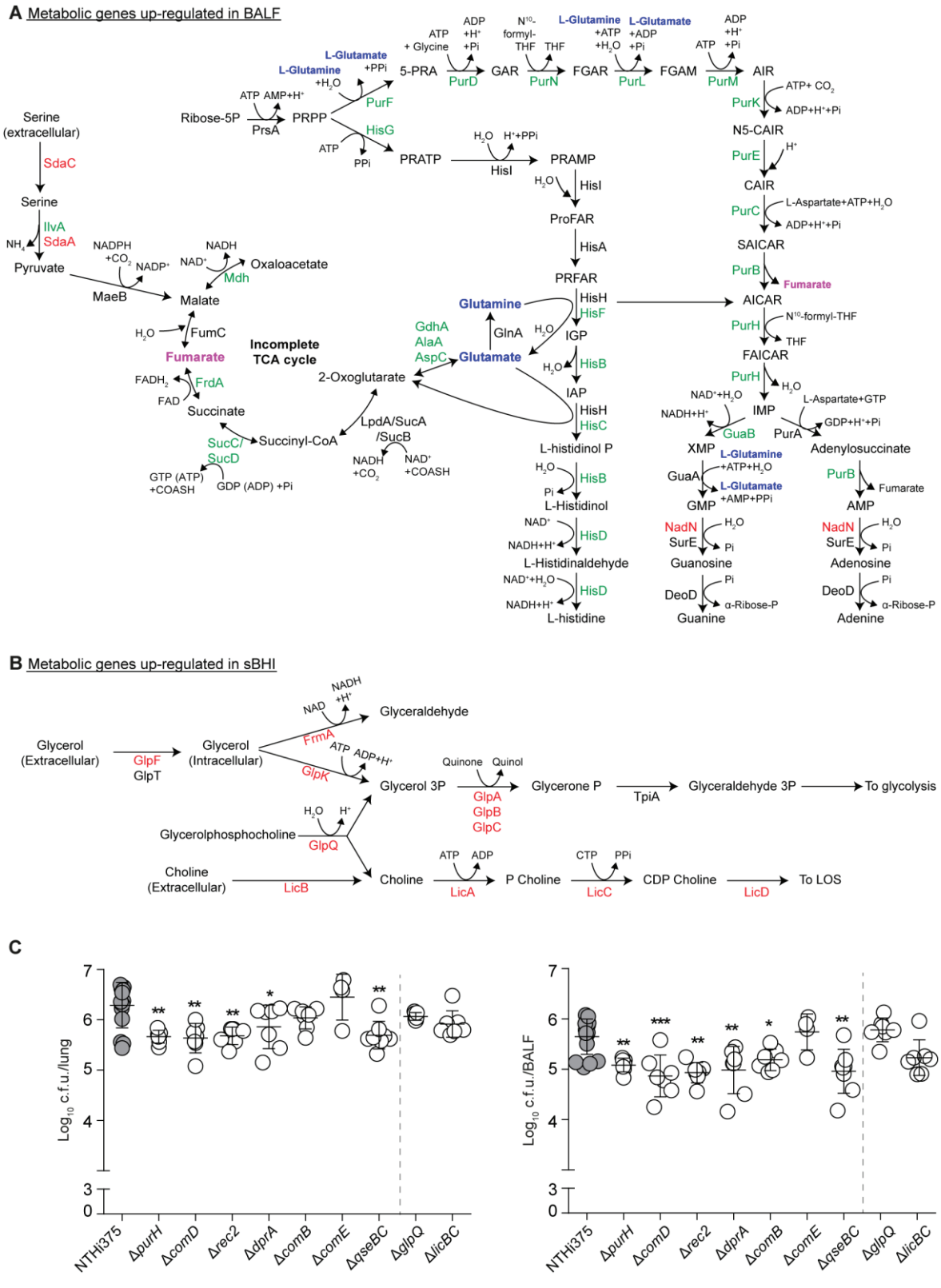

Figure 13. Differential expression of *H. influenzae* genes upon mice infection. (A) Purine biosynthesis and related pathways in this process, such as histidine biosynthesis and the Krebs cycle, are overexpressed *in vivo* (green); red: down-regulated *in vivo*. **(B)** Glycerol and PCho metabolism related to LOS decoration are down-regulated *in vivo*. **(C)** CD1 mice were intranasally infected with NTHi37-WT and mutant strains grown in sBHI. Bacterial counts were determined at 12 hpi in lungs (log_{10} c.f.u./lung) and BALF (log_{10} c.f.u./mL BALF) (left and right panels, respectively) samples. A significant reduction on bacterial loads was observed for mutants lacking the *purH*, *comD*, *rec2*, *dprA*, *comB* or *qseBC* genes compared

to NTHi375-WT strain. Statistical comparisons of means were performed by one-way ANOVA and Dunnett's multiple comparisons test (* $p < 0.05$; ** $p<0.005$; *** $p <0.0001$).

In conclusion, under the conditions tested, the infectious process stimulates *H. influenzae* natural competence machinery, as well as purines and non-aromatic amino acids biosynthesis, and on the other hand, it represses fermentative metabolism and LOS decoration. Also, our *in vivo* study revealed bacterial regulation of iron transport systems and repression of both serine transport and entry into *H. influenzae* central metabolism.

2.4.3. Establishing a correlation between gene up-regulation and virulence

RNA-seq analysis of the transcriptome of *H. influenzae* in the lung allowed for the identification of major changes in expression of genes involved in bacterial metabolism. To gain insights into the importance of these processes in the pathogenesis of *H. influenzae,* we selected genes involved in purine biosynthesis (*purH*), iron uptake-sensing (*qseBC*/*firRS*), and natural competence (*comD*, *rec2*, *dprA*, *comB*, *comE*) whose expression was up-regulated *in vivo*, and generated inactivation mutants for each gene. None of these mutants presented growth defects in sBHI (**Figure S2A**) and, as expected, the Δ*comD*, Δ*rec2*, Δ*dprA*, Δ*comB* and Δ*comE* mutants showed decreased transformation frequency, compared to the WT strain (**Table S3**). To assess the role of these genes in the pathogenesis of *H. influenzae,* animals were independently infected with each strain as described above, and processed at 12 hpi. Lower counts were observed in both lung and BALF samples upon infection with the NTHi375Δ*purH*, Δ*comD*, Δ*rec2*, Δ*dprA*, and Δ*qseBC* mutants than with the WT strain; also, lower counts were observed in BALF samples upon infection with the Δ*comB* mutant than with the WT strain (**Figure 13C**). Attenuation was not observed for the Δ*comE* strain. We also tested the effect of inactivating genes down-regulated *in vivo*, by using the previously generated NTHi375Δ*licBC* (Morey et al., 2013), and the newly generated NTHi375Δ*glpQ* strain which, as expected, showed impaired growth in CDM upon use of GPC as carbon source (**Figure S2B)** (Johnson et al., 2011). Inactivation of the *licBC* and *glpQ* genes did not have significant effects on lung and BALF bacterial counts (**Figure 13C**).

In summary, we observed a correlation between up-regulation of gene expression during *in vivo* airway infection and gene contribution to the infectious process, suggesting that *in vivo* RNA-seq can be a useful tool to identify novel genes involved in the virulence and pathogenesis of *H. influenzae*.

2.4.4. Analysis of the effect of *sBHI to BALF* and *sBHI to MIV* transitions sheds light on *in vivo* natural competence requirements

As indicated above, profiling bacterial gene expression *in vivo* showed up-regulation of eleven genes belonging to the natural competence machinery. In a previous study, Redfield et al., characterized gene expression changes during competence development by sampling the *H. influenzae* RdKW20 strain during exponential growth in sBHI and after transition to the starvation medium MIV, suitable to develop natural competence *in vitro* (Redfield et al., 2005). This genome-wide study laid the foundation to define the CRE, later on renamed CRP-S regulon, and identified other starvation-induced genes such as the PurR-regulon, also found to be up-regulated in our *in vivo* analysis. Detailed comparison between our current NTHi375 differential gene expression analysis of BALF versus sBHI samples, and the previous RdKW20 differential gene expression analysis of MIV versus sBHI samples (Redfield et al., 2005), required normalizing genomic content between strains. When looking at genes commonly shared by both strains, differences and similarities are summarized in **Figure 14B** and **Table S4**. From the 50 genes commonly up-regulated *in vivo* and in MIV compared to sBHI, 11 were involved in natural competence (**Figure 14B**) and 12 in purine biosynthesis, in addition to other CRP-regulated genes involved in sugar metabolism or transport (**Table S4**). Differences were also found, as those involving the rest of genes (15) involved in natural competence in MIV (*pilB*, *pilC*, *pilD*, *comA*, *comN*, *comO*, *comP*, *comQ*, *comE1*, HI0365, *pilF2*, *ligA*, HI1631, *comM*, *radC*), and the competence regulator encoding gene *sxy* (Redfield et al., 2005). A subset of genes up-regulated *in vivo* was validated by RT-qPCR for the NTHi375 strain, by comparing gene expression of bacteria grown in sBHI upon transition to BALF (*in vivo*) or to MIV (*in vitro*) (**Figure 14C,** upper and middle panel). Expression of the same subset of genes was tested by sampling *H. influenzae* RdKW20 grown in sBHI and after transition to MIV (**Figure 14C**, bottom panel). Up-regulation of purine biosynthesis genes in BALF and MIV compared to sBHI was commonly observed, although in some cases to a different extent between strains. Up-regulation of natural competence genes in BALF versus sBHI was actually clearer than upon bacterial transition from sBHI to MIV. Indeed, we acknowledge that a differentiation should be likely made between CRP-S genes (Redfield et al., 2005) of which we have 11/26 genes, and genes needed for natural competence (Sinha et al., 2012), with whom we share 8/17. Nine of seventeen genes were not up-regulated in our *in vivo* study: *pilB, pilC, pilD, comA, comN, comO, comP, comQ, pilF2*. In contrast, *toxT* belongs to CRP-S regulon but is not essential for natural competence.

As we observed that genes involved in natural competence machinery were up-regulated both in BALF and MIV compared to rich sBHI medium, we hypothesized that the murine airway conditions may favour natural competence of *H. influenzae* (**Figure 14D**). To test this, we first co-administered intranasally a mixed bacterial inoculum containing heat-killed NTHi375-WT bacteria:alive

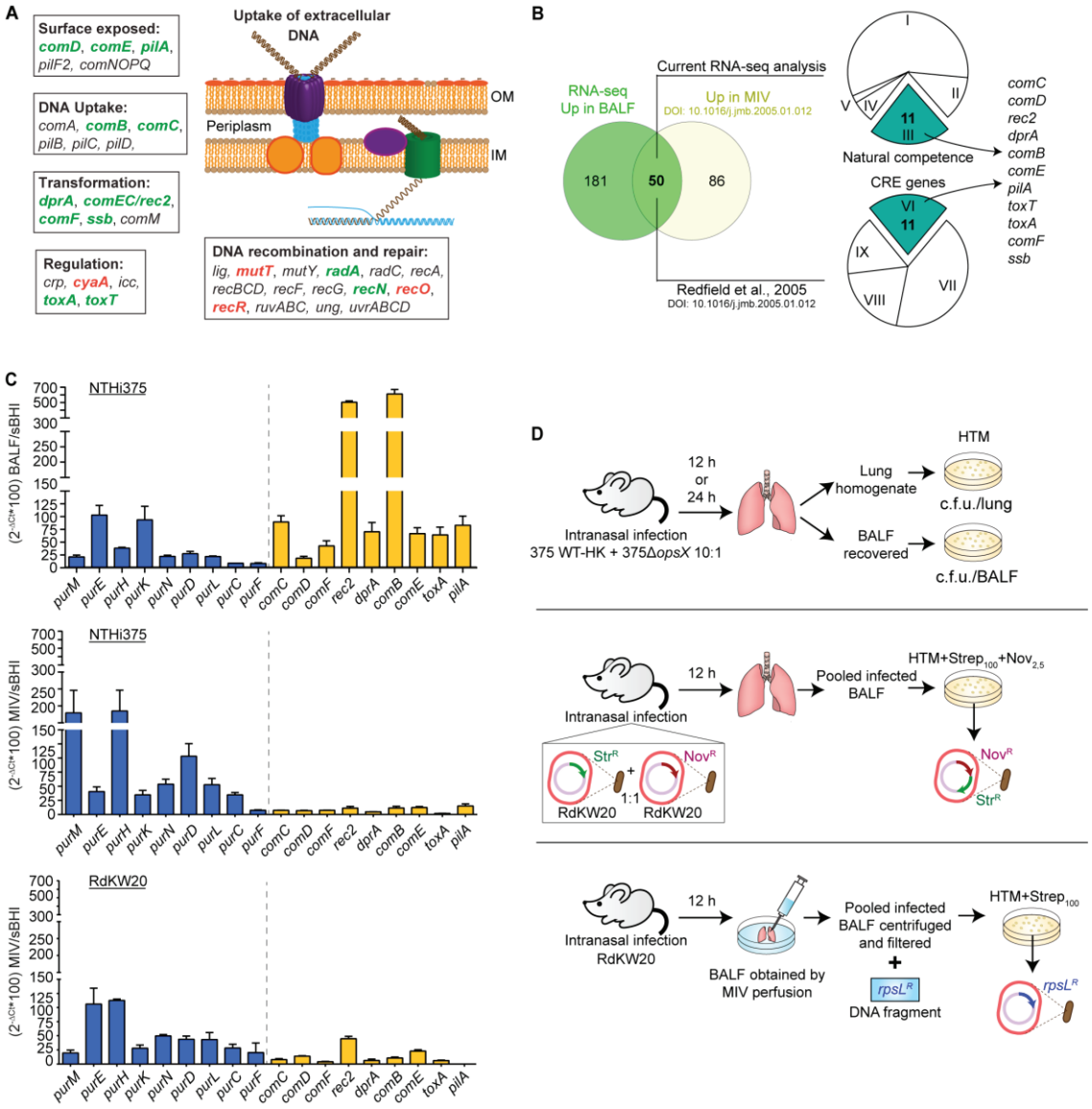

Figure 14. Part of the *H. influenzae* natural competence machinery is up-regulated *in vivo*. (A) Schematic representation of *H. influenzae* natural competence machinery. Green: up-regulated *in vivo*; red: down-regulated *in vivo*. **(B)** Venn diagram showing fifty *H. influenzae* genes commonly up-regulated *in vivo* in the current RNA-seq analysis and in a previous analysis of *H. influenzae* genes up-regulated genes upon induction of natural competence (Redfield et al., 2005). Of these, 11 genes are part of the previously described natural competence machinery. Categories established in our study: (i) metabolism, (ii) transport systems, (iii) natural competence, (iv) stress response/nutrient starvation, (v) hypothetical proteins; Categories established in (Redfield et al., 2005): (vi) CRE genes, (vii) CRP-regulated genes, (viii) PurR regulon, (ix) other. **(C)** NTHi375 and RdKW20-WT strains were grown in sBHI and collected in exponential phase, or incubated in MIV for 100 min. after reaching OD_{600}=0.3 in sBHI; NTHi375 BALF samples were recovered from CD1 mice at 12 hpi. Gene expression was determined by qRT-PCR and showed as the ratio between BALF/sBHI in NTHi375 (upper panel), and MIV/sBHI in NTHi375 (middle panel) or RdKW20 (bottom panel). Blue: purine biosynthesis genes; yellow: natural competence genes. **(D)** *In vivo* assays performed to assess *H. influenzae* natural transformation during infection. CD1 mice were co-infected for 12 or 24 h with NTHi375-WT and the attenuated mutant NTHiΔ*opsX* (10:1 ratio) to assess reversion of the attenuated phenotype (upper panel). Mice were co-infected for 12 h with RdKW20-Str^R and RdKW20-Nov^R (1:1) to search for acquisition of double resistance (middle panel). Mice were infected with RdKW20 for 12 h; bacteria recovered from BALF samples were incubated with a linear DNA fragment containg a Strep resistance cassette, and further plated on antibiotic containing sHTM agar (bottom panel).

NTHi375Δ*opsX*, a previously shown attenuated mutant (Morey et al., 2013), aiming to recover WT infection levels (**Figure 14D**, upper panel). However, NTHi375Δ*opsX* infectious capacity was not

restored to levels similar to the parental strain, suggesting that the mutant was unable to acquire genetic material from the heat-killed bacteria by natural competence. Given that RdKW20 natural transformation frequency is higher than that of NTHi375 (**Table S3**), we co-administered a mix containing two RdKW20 derivative strains (Mell et al., 2016) containing two different antibiotic resistance markers ($Strep^R$ and Nov^R), but were unable to recover double $Strep^RNov^R$ colonies after infection (**Figure 14D**, middle panel). Finally, BALF samples obtained by MIV perfusion in lungs from RdKW20 infected mice, were directly used for transformation with a *rpsL* gene containing DNA fragment, but $Strep^R$ resistant colonies could not be obtained (**Figure 14D**, bottom panel).

In conclusion, under the conditions tested, *in vivo* up-regulation of genes belonging to the natural transformation machinery *in vitro* did not correlate with measurable DNA uptake, translocation and selectable homologous recombination within the host lung.

2.4.5. Identification of *H. influenzae* genes required for *in vivo* fitness by transposon insertion sequencing screening

Our gene expression profiling data suggest that bacterial gene expression is regulated during infection, and that differentially expressed genes can play a role in *in vivo* fitness. To further identify and characterize genes involved in *H. influenzae in vivo* fitness, we complemented our RNA-seq studies with *in vivo* Tn-seq (Powell et al., 2016; Turner et al., 2014) (**Figure 15A**). We used the RdKW20 strain due to its high *in vitro* natural transformation frequency to generate a transposon (Tn) library (**Table S3**). A library of 30,000 RdKW20 Tn mutants was grown in sBHI and in both normal lung function or lung emphysema murine models, and mutant abundance was profiled by Tn-seq either 12 or 24 hpi. Data were analyzed using the manual curation methodology described above.

Tn-seq data analysis revealed differences in number of underrepresented genes obtained among all conditions tested: 41 genes for normal lung function 12 hpi, 64 for emphysema lung 12 hpi, 58 for normal lung function 24 hpi, and 58 for emphysema lung 24 hpi (**Figure 15B-E, Table A7**). In normal lung function 12 hpi and emphysema lung both 12 and 24 hpi, most of the underrepresented genes are part of amino acid metabolism, mostly belonging to tryptophan biosynthesis, with *trpA* commonly shared among these three conditions. Upon infection of mice with normal lung function, 41 and 58 *H. influenzae* genes were found to be underrepresented at 12 and 24 hpi respectively, compared to *in vitro* growth on sBHI, being 12 of shared between both conditions. When testing mice with lung emphysema, 65 and 58 *H. influenza*e genes were found to be underrepresented at 12 and 24 hpi respectively, compared to *in vitro* growth on sBHI, being 32 of them shared between both conditions (**Figure 15F**). Six genes were commonly underrepresented in the four *in vivo* tested conditions, 17 genes commonly underrepresented at 12 hpi, and 38 at 24 hpi (**Figure 15F, Table**

A7). Some genes had been previously found to contribute to *H. influenzae in vivo* lung infection,

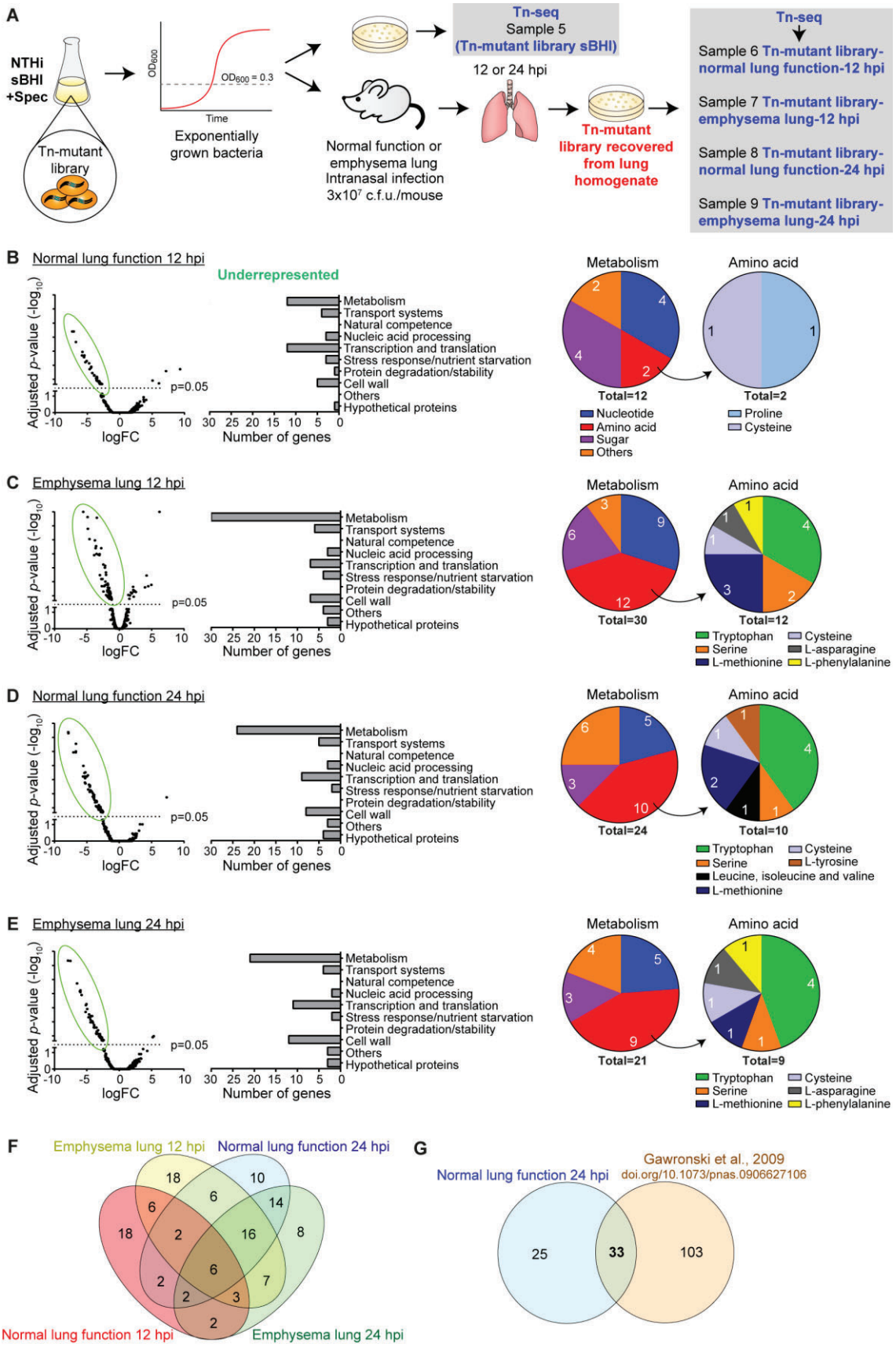

Figure 15. Identification of *H. influenzae in vivo* fitness related genes. (A) Schematic representation of *H. influenzae* samples generation for Tn-seq analysis. *In vitro* growth of RdKW20-WT in sBHI generates sample no. 5 and the *input* for mice infection. Lung homogenates were recovered from infected mice at 12 hpi (normal or elastase lung function samples generated *output* samples 6 and 7, respectively), or at 24 hpi (normal or elastase lung function samples generated *output* samples 8 and 9, respectively). **(B-E)** Volcano plots showing fold-change of under- and overrepresented genes when comparing *output* versus *input* Tn libraries (left panels). Functional categories of underrepresented genes (middle panels), and detail of the amino acid metabolism in underrepresented genes (left panels) in: normal lung function at 12 hpi **(B)**, elastase lung function at 12 hpi **(C)**, normal lung function at 24 hpi **(D),** and elastase lung function at 24 hpi **(E)**. **(F)** Venn diagram showing the intersections between underrepresented genes at 12 and 24 hpi in normal or elastase lung function. We found 6 common genes among all these conditions. **(G)** Venn diagram indicating 33 common genes between underrepresented genes in current Tn-seq analysis and a previous study performed by (Gawronski et al., 2009) using high-throughput insertion tracking by deep sequencing HITS to screen *H. influenzae* genes required during infection.

such as *galU*, *galE*, *thyA* (Gawronski et al., 2009; Rodríguez-Arce et al., 2017; Wong et al., 2019), or invasive infection such as *dam* (Watson et al., 2004b). Also, we found 33 genes, including *galE*, *hel*, *dam*, *atpD*, *atpG*, *trpA* and *trpB* which were commonly shared with a previous high-throughput insertion tracking by deep sequencing HITS screen for *H. influenzae* genes required in the lung (Gawronski et al., 2009) (**Figure 15G**).

Differentially expressed or underrepresented genes obtained from RNA-seq and Tn-seq analysis, respectively, grouped into functional categories, are summarized in **Table S5**. As previously shown for *P. aeruginosa* or *Snodgrassella alvi in vivo* multi-omics (Powell et al., 2016; Turner et al., 2014), poor correlation was found between our *H. influenzae* RNA-seq and Tn-seq results. As above, detailed comparison between both data sets required normalizing genomic content between the RdKW20 and NTH375 strains, summarized in **Figure S3**. Then, we observed that only 230 of the 316 NTHi375 genes of up-regulated *in vivo*, only 230 were present in the RdKW20 genome somehow expected as the NTHi375 genome is larger than that of RdKW20. However, genome normalization of RdKW20 when compared to NTHi375 reduced the number of genes to be considered: 39/41 genes, normal lung function at 12 hpi; 61/64 genes, emphysema lung at 12 hpi; 57/58 genes, normal lung function at 24 hpi; 57/58 genes, emphysema lung at 24 hpi. Few genes were commonly found in the two *in vivo* screening procedures carried out, summarized in **Figure S3**.

In conclusion, under the conditions tested, comparison of the results obtained by RNA-seq or Tn-seq reveals that there is little correlation between these two -omic techniques, shedding light on their complementarity and generating a global vision of the bacterial factors used by *H. influenzae* during infection.

2.5. Supplementary Material

Table S1. Bacterial strains used in this study.

Strain	Description	Source
E. coli		
TOP10	Cloning strain. F- *mcrA* Δ(*mrr-hsd*RMS-*mcr*BC) Φ80*lac*ZΔM15 Δ*lac*X74 *rec*A1 *ara*D139 Δ(*araleu*)7697 *gal*U*gal*K*rps*L (Str^R) *end*A1 *nup*G	Thermofisher Scientific
SW102	Derived from DY380; it contains a defective λ prophage with the recombination proteins *exo*, *bet*, and *gam* being controlled by the temperature-sensitive repressor *cI857*	(Tracy et al., 2008)
H. influenzae		
NTHi375	Wild-type, otitis media clinical isolate	(Bouchet et al., 2003)
RdKW20	Laboratory strain, capsule-deficient serotype d	(R D Fleischmann et al., 1995a)
NTHi375Δ*purH*/P993	*purH::ermC*, Erm^R	This study
NTHi375Δ*comD*/P987	*comD::ermC*, Erm^R	This study
NTHi375Δ*rec2*/P984	*rec2::ermC*, Erm^R	This study
NTHi375Δ*dprA*/P985	*dprA::ermC*, Erm^R	This study
NTHi375Δ*comB*/P986	*comB::ermC*, Erm^R	This study
NTHi375Δ*comE*/P1166	*comE::ermC*, Erm^R	This study
NTHi375Δ*qseBC*/P1084	*qseBC::ermC*, Erm^R	This study
NTHi375Δ*glpQ*/P908	*glpQ::spec*, Spec^R	This study
NTHi375 Δ*licBC*/1227	*licBC:: ::ermC*, Erm^R	(Martí-Lliteras et al., 2009)
NTHi375Δ*opsX*/P350	*opsX::ermC*, Erm^R	(Pau Morey et al., 2013)
P192 (MAP7)	Rd Nov^R Nal^R Str^R Spec^R Kan^R Rif^R Erm^R (aka RR666)	(Catlin et al., 1972)
P193	Rd Str^R, made as above but selecting for Str^R (aka RR514)	(Mell et al., 2016)
P194	Rd Nov^R, made as above but selecting for Nov^R (aka RR3148)	(Mell et al., 2016)

Table S2. Plasmids used in this study.

Plasmid	Description	Source
pJET1.2/blunt	Cloning vector	Life Technologies
pBSLerm	Plasmid containing an Erm resistance cassette (Erm^R)	(Simon Allen et al., 2005)
pRSM2832	pKD13 derivative carrying a cassette containing a Spec resistance gene flanked by FRT sites	(Tracy et al., 2008)
pJET1.2-*purH*	pJET1.2 derivative containing a 3,523 bp DNA fragment carrying the *purH* gene (1,599 bp) and its upstream (924 bp) and downstream (1,000 bp) flanking regions	This study
pJET1.2-*purH*::*ermC*	pJET1.2-*purH* derivative containing a 3,358 bp DNA fragment carrying a *purH::ermC* disruption cassette	This study
pJET1.2-*comD*	pJET1.2 derivative containing a 2,414 bp DNA fragment carrying the *comD* gene (414 bp) and its upstream (1,000 bp) and downstream (1,000 bp) flanking regions	This study

pJET1.2-*comD*::*ermC*	pJET1.2-*comD* derivative containing a 3,354 bp DNA fragment carrying a *comD::ermC* disruption cassette	This study
pJET1.2-*rec2*	pJET1.2 derivative containing a 4,367 bp DNA fragment carrying the *rec2* gene (2,367 bp) and its upstream (1,000 bp) and downstream (1,000 bp) flanking regions	This study
pJET1.2-*rec2*::*ermC*	pJET1.2-*rec2* derivative containing a 3,768 bp DNA fragment carrying a *rec2::ermC* disruption cassette	This study
pJET1.2-*dprA*	pJET1.2 derivative containing a 3,122 bp DNA fragment carrying the *dprA* gene (1,122 bp) and its upstream (1,000 bp) and downstream (1,000 bp) flanking regions	This study
pJET1.2-*dprA*::*ermC*	pJET1.2-*dprA* derivative containing a 3,441 bp DNA fragment carrying a *dprA::ermC* disruption cassette	This study
pJET1.2-*comB*	pJET1.2 derivative containing a 2,266 bp DNA fragment carrying the *comB* gene (507 bp) and its upstream (859 bp) and downstream (900 bp) flanking regions	This study
pJET1.2-*comB*::*ermC*	pJET1.2-*comB* derivative containing a 3,130 bp DNA fragment carrying a *comB::ermC* disruption cassette	This study
pJET1.2-*comE*	pJET1.2 derivative containing a 3,247 bp DNA fragment carrying the *comE* gene (1,338 bp) and its upstream (1,000 bp) and downstream (909 bp) flanking regions	This study
pJET1.2-*comE::ermC*	pJET1.2-*comE* derivative containing a 3,541 bp DNA fragment carrying a *comE::ermC* disruption cassette	This study
pJET1.2-*qseBC*	pJET1.2 derivative containing a 4,009 bp DNA fragment carrying the *qseBC* gene (2,018 bp) and its upstream (991 bp) and downstream (1,000 bp) flanking regions	This study
pJET1.2-*qseBC*::*ermC*	pJET1.2-*qseBC* derivative containing a 3,350 bp DNA fragment carrying a *qseBC::ermC* disruption cassette	This study
pJET1.2-*glpQ*	pJET1.2 derivative containing a 3,094 bp DNA fragment carrying the *glpQ* gene (1,095 bp) and its upstream (1,000 bp) and downstream (999 bp) flanking regions	This study
pJET1.2-*glpQ::spec*	pJET1.2-*glpQ* derivative containing a 4,090 bp DNA fragment carrying a *glpQ::spec* disruption cassette	This study

Table S3. Transformation frequency *in vitro* of RdKW20 or NTHi375-WT and mutants strains by MIV medium using MAP-7 gDNA.

Strains	**Transformation efficiency by MIV using gDNA MAP-7**	
	RdKW20	NTHi375
WT	10^{-3}	10^{-4}
Δ*comB*	10^{-7}-10^{-8}	10^{-9}-0
Δ*comD*	10^{-7}-10^{-8}	0
Δ*comE*	0	0
Δ*comF*	10^{-7}	ND*
Δ*rec2*	10^{-8}-10^{-9}	0
Δ*dprA*	10^{-6}-10^{-7}	10^{-7}-10^{-8}
Δ*purH*	ND*	10^{-5}-10^{-6}

ND*: Not determined

Table S4. Fifty common genes up-regulated in BALF (current RNA-seq analysis) and MIV (Redfield et al., 2005) compared to sBHI.

Pathway	Sub-category	EC no.	Gene	Categorization by (Redfield et al., 2005)	Enzyme description
Metabolism	Purine	6.3.3.1	*purM*	PurR regulon	Phosphoribosylformylglycinamidine cyclo-ligase
		5.4.99.18	*purE*	PurR regulon	N5-carboxyaminoimidazole ribonucleotide mutase
		2.1.2.3 3.5.4.10	*purH*	PurR regulon	Bifunctional purine biosynthesis protein
		6.3.4.18	*purK*	PurR regulon	N5-carboxyaminoimidazole ribonucleotide synthase
		2.1.2.2	*purN*	PurR regulon	Phosphoribosylglycinamide formyltransferase
		6.3.4.13	*purD*	PurR regulon	Phosphoribosylamine--glycine ligase
		6.3.5.3	*purL*	PurR regulon	Phosphoribosylformylglycinamidine synthase
		6.3.4.20	*queC*	Other	7-cyano-7-deazaguanine synthase
		6.3.2.6	*purC*	PurR regulon	Phosphoribosylaminoimidazole-succinocarboxamide synthase
		4.1.2.50	*queD*	Other	6-carboxy-5,6,7,8-tetrahydropterin synthase
		2.4.2.14	*purF*	PurR regulon	Amidophosphoribosyltransferase
		4.3.99.3	*queE*	Other	7-carboxy-7-deazaguanine synthase
	Amino acid	3.5.2.9	*pxpA*	Other	5-oxoprolinase subunit A
		2.6.1.1	*aspC*	Other	Aspartate aminotransferase
	Sugar	5.3.1.5	*xylA*	CRP-regulated genes	Xylose isomerase
		1.1.1.37	*mdh*	CRP-regulated genes	Malate dehydrogenase
		5.1.3.29	*fucU*	CRP-regulated genes	L-fucose mutarotase
			fucP	CRP-regulated genes	L-fucose-proton symporter
		5.3.1.25	*fucI*	CRP-regulated genes	L-fucose isomerase
		4.1.2.17	*fucA*	CRP-regulated genes	L-fuculose phosphate aldolase
		2.7.1.51	*fucK*	CRP-regulated genes	L-fuculokinase
		3.2.1.-	*glgX*	CRP-regulated genes	Glycogen operon protein GlgX homolog
		1.3.5.4	*frdA*	CRP-regulated genes	Fumarate reductase flavoprotein subunit
		2.4.1.21	*glgA*	CRP-regulated genes	Glycogen synthase
		2.7.7.27	*glgC*	CRP-regulated genes	Glucose-1-phosphate adenylyltransferase
		2.4.1.1	*glgP*	CRP-regulated genes	Glycogen phosphorylase
	Molybdopterin		*moaD*	CRP-regulated genes	Molybdopterin synthase sulfur carrier subunit
		4.6.1.17	*moaC*	CRP-regulated genes	Cyclic pyranopterin monophosphate synthase
		2.8.1.12	*moaE*	CRP-regulated genes	Molybdopterin synthase catalytic subunit
Transport systems			HI0125	Other	Putative permease
			yidE	CRP-regulated genes	Putative transport protein
			ycsG	Other	Uncharacterized membrane protein

	oppA	CRP-regulated genes	Periplasmic oligopeptide-binding protein
	HI0052	CRP-regulated genes	TRAP transporter substrate-binding protein
	HI0608	CRP-regulated genes	DASS family sodium-coupled anion symporter
Natural competence	*comC*	CRE genes	Competence protein C
	comD	CRE genes	Competence protein D
	rec2	CRE genes	Recombination protein 2
	dprA	CRE genes	DNA-processing protein A
	comB	CRE genes	Competence protein B
	comE	CRE genes	Competence protein E
	pilA/ppdD	CRE genes	Prepilin peptidase-dependent protein D homolog
	toxT	CRE genes	Type II toxin-antitoxin system
	toxA	CRE genes	Uncharacterized HTH-type transcriptional regulator
	comF	CRE genes	Competence protein F
	ssb	CRE genes	Single-stranded DNA-binding protein
Stress response / nutrient starvation	*uspA*	CRP-regulated genes	Universal stress protein A homolog
	cvpA	PurR regulon	Colicin V production protein homolog
	impA	Other	LexA family transcriptional regulator
Hypothetical proteins	HI1316	CRP-regulated genes	

Table S5. Number of genes associated to functional categories obtained from RNA-seq and Tn-seq analyses.

Main category	Sub-category	Sub-category	RNA-seq		Tn-seq			
			Up in sBHI compared to BALF	Up in BALF compared to sBHI	Normal lung function 12 hpi	Emphysema lung 12 hpi	Normal lung function 24 hpi	Emphysema lung 24 hpi
Metabolism	Nucleotide	Purine	5	16	2	7	4	4
		Pyrimidine	4	1	2	2	1	1
		Ribonucleoside-triphosphate reductases	0	3	0	0	0	0
	Amino acid	Histidine	0	5	0	0	0	0
		Arginine	0	2	0	0	0	0
		Tryptophan	0	1	0	4	4	4
		Threonine	0	4	0	0	0	0
		Serine	1	1	0	2	1	1
		Leucine, isoleucine and valine	0	8	0	0	1	0
		L-lysine via DAP pathway	1	1	0	0	0	0
		L-methionine, S-adenosyl-L-methionine	1	3	0	3	2	1
		Glutamate	0	3	0	0	0	0
		Aspartate	0	1	0	0	0	0
		Alanine	1	1	0	0	0	0
		Glycine	0	1	0	0	0	0
		Glutamine	0	1	0	0	0	0
		Proline	0	0	1	0	0	0
		Cysteine	0	0	1	1	1	1
		L-asparagine	0	0	0	1	0	1

		L-phenylalanine	0	0	0	1	0	1
		L-tyrosine	0	0	0	0	1	0
	Lipid		9	5	0	0	0	0
	Sugar	Hexoses	3	12	2	5	3	3
		Pentoses	1	3	2	1	0	0
		Krebs cycle	0	5	0	0	0	0
		Fermentative reactions	6	0	0	0	0	0
	Molybdopterin		3	4	0	0	0	0
	Protein (lipoproteins) metabolism		2	0	0	0	1	1
	Coenzyme A biosynthesis		1	1	0	0	0	0
	Glycerol		4	0	0	0	1	1
	Quinol/quinone metabolism		2	0	0	0	0	0
	Vitamins biosynthesis		5	3	0	1	1	1
	Isopentenyl diphosphate biosynthesis		3	0	0	0	0	0
	ATP synthase		0	0	2	1	3	1
	Other metabolism genes		32	10	0	1	0	0
Transport systems	Uptake/uptake systems	Iron	11	19	0	1	2	2
		Oligopeptides	0	5	0	0	0	0
		Amino acids	8	2	1	1	0	0
		Zinc	1	1	0	2	0	1
		Molybdenum	0	1	0	0	0	0
		Magnesium	0	1	0	0	0	0
		Purine nucleobase	0	1	0	0	0	0

		Vitamins	3	0	0	0	0	0
		Polyamines	1	0	0	0	0	0
		Phosphate (Pi)	2	0	0	0	0	0
		Nucleosides	1	0	0	0	0	0
		Queuosine (Q) precursors	0	1	0	0	0	0
		Glycerol	1	0	0	0	0	0
		Long chain fatty acids	1	0	0	0	0	0
		Mercury	0	0	1	0	0	0
		Other intake systems	2	3	0	0	0	0
	Export systems		7	4	1	1	1	0
	Bidirectional transport systems or transporters with unknown function		3	13	1	1	2	1
Natural competence			0	11	0	0	0	0
Nucleic acids processing, restriction and modification			24	20	3	3	3	2
Transcription and translation machinery	Transcription factors		0	5	2	1	1	1
	RNA polimerase		0	3	1	0	0	1
	Ribosome related things		5	22	4	2	5	3
	tRNA		12	8	5	2	1	4
	Regulators		11	12	0	2	2	2
Stress response/ nutrient starvation			13	11	3	4	2	2
Protein degradation/ stability	Protein degrading machinery		2	4	1	0	0	0
	Chaperone		3	0	0	0	0	0

Cell wall	LOS biosynthesis-modification-decoration	17	0	3	2	0	1
	Cell Wall biosynthesis	12	2	0	2	3	5
	Cell division	5	1	1	3	5	5
	OMP	8	7	1	0	0	1
Others		9	7	0	4	3	3
Hypothetical proteins		34	57	1	3	4	3
Total genes		**280**	**316**	**41**	**64**	**58**	**58**

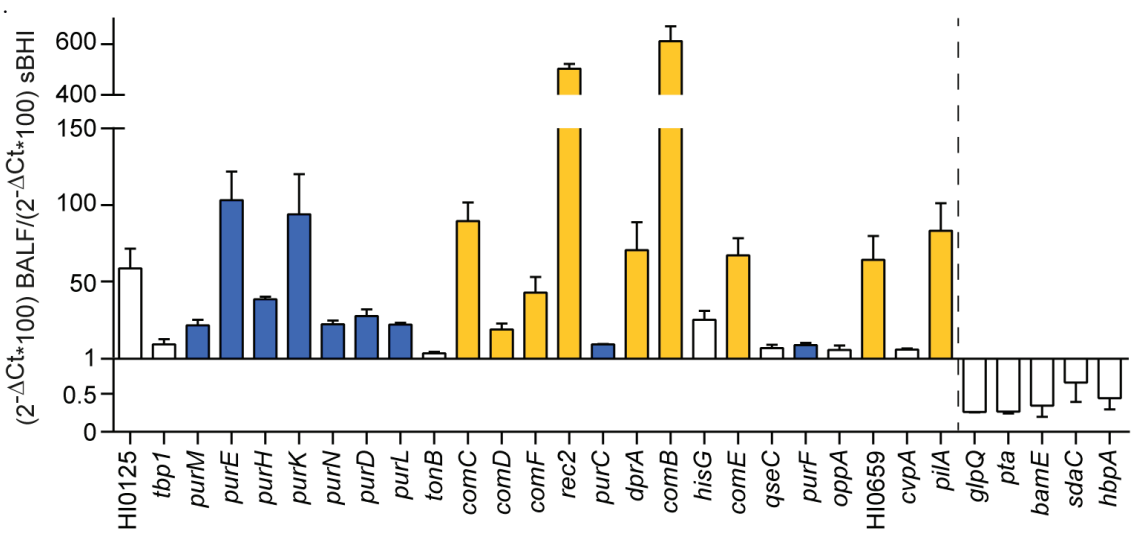

Figure S1. **Expression of *H. influenzae* genes determined by qRT-PCR**. Genes to be checked were selected based on their RNA-seq differential expression upon bacterial recovery from BALF samples versus *in vitro* growth in sBHI. NTHi375 was grown in sBHI and collected in exponential phase; NTHi375 BALF samples were recovered from CD1 mice at 12 hpi. The ratio of gene expression was determined for NTHi375 recovered from BALF versus grown sBHI. From left to right, genes are shown based on their respective observed expression fold change upon RNA-seq analysis. Blue bars: purine biosynthesis genes; yellow bars: natural competence genes; white bars: other non-purine and non-competence genes.

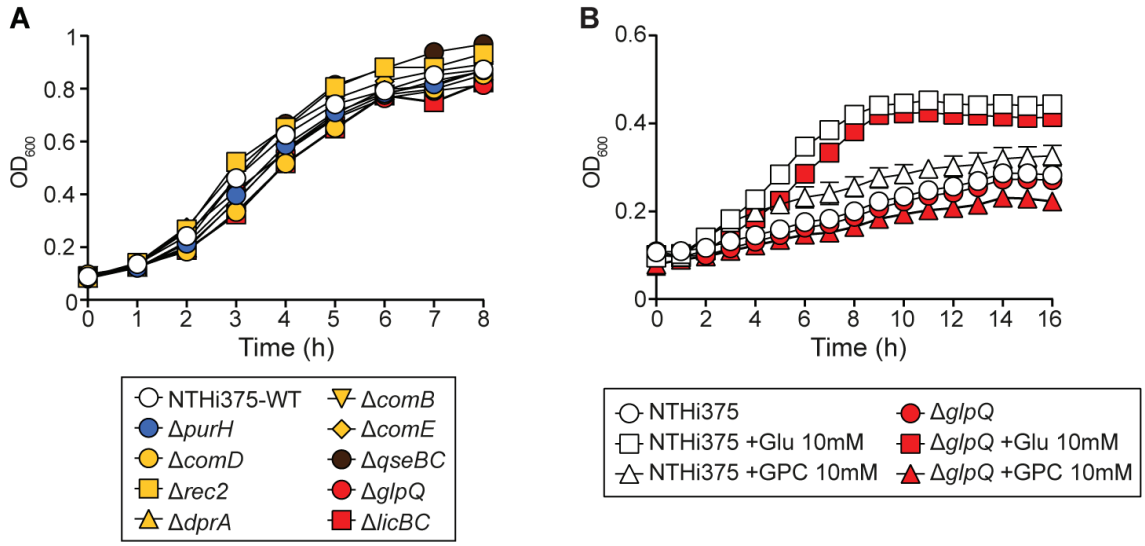

Figure S2. **Growth rates of generated mutant strains. (A)** Growth of generated *H. influenzae* mutant strains in sBHI is shown as OD_{600} measure at the indicated time points. Blue: purine biosynthesis genes; yellow: natural competence genes; red: down-regulated genes *in vivo* versus *in vitro*. **(B)** Growth of NTHi375-WT and Δ*glpQ* strains in CDM, using glucose (Glu) or L-α-glycerophosphocholine (GPC) as carbon source.

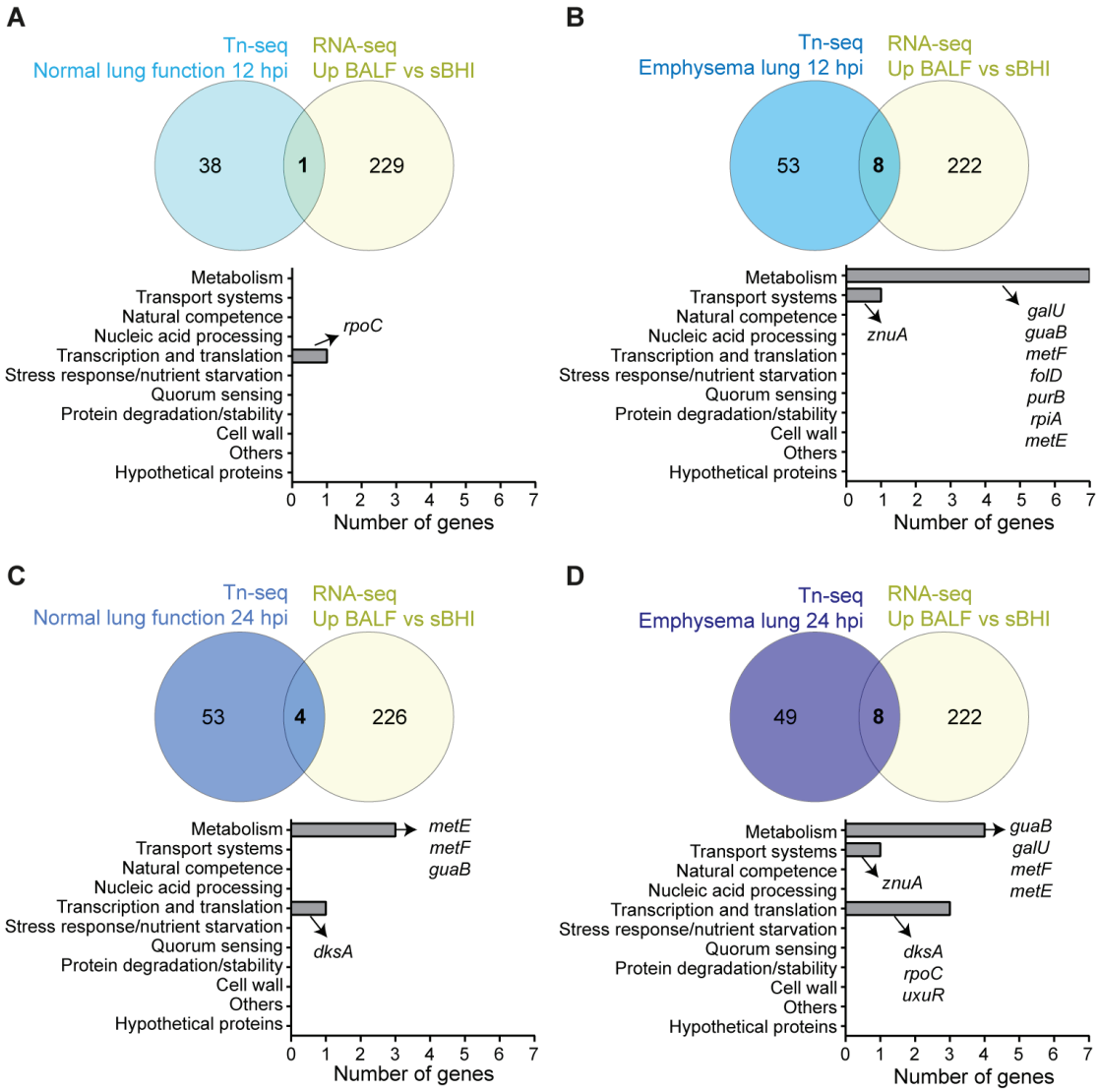

Figure S3. Global gene expression and fitness profiling analyses are complementary to uncover *H. influenzae* virulence factors. Genes commonly shared between upon analysis of genes up-regulated *in vivo* and genes whose mutants are underrepresented in normal lung function animals at 12 hpi **(A)**; emphysema lung at 12 hpi **(B)**; normal lung function at 24 hpi **(C)**; emphysema lung at 24 hpi **(D)**. Gene classification into functional categories is shown. Only genes present in both the NTHi375 and RdKW20 genomes are shown.

Capítulo 3

Haemophilus influenzae glucose catabolism leading to production of the immunometabolite acetate has a key contribution to the host airway-pathogen interplay

Nahikari López-López, Begoña Euba, Julian Hill, Rabeb Dhouib, Lucía Caballero, José Leiva, Jennifer Hosmer, Sergio Cuesta, José Ramos-Vivas, Roberto Díez-Martínez, Horst Joachim Schirra, Lars M. Blank, Ulrike Kappler, Junkal Garmendia. *Haemophilus influenzae* glucose catabolism leading to production of the immunometabolite acetate has a key contribution to the host airway-pathogen interplay. ACS Infectious Diseases. Volume 6, Pages 406-421. doi: 10.1021/acsinfecdis.9b00359

Capítulo 3. *Haemophilus influenzae* glucose catabolism leading to production of the immunometabolite acetate has a key contribution to the host airway-pathogen interplay

Nahikari López-López[a], Begoña Euba[a, b], Julian Hill[c], Rabeb Dhouib[c], Lucía Caballero[a], José Leiva[d, e], Jennifer Hosmer[c], Sergio Cuesta[a], José Ramos-Vivas[f, g], Roberto Díez-Martínez[h], Horst Joachim Schirra[i], Lars M. Blank[j], Ulrike Kappler[c, *], Junkal Garmendia[a, b, *]

a. Instituto de Agrobiotecnología, CSIC-Universidad Pública Navarra-Gobierno, Navarra, Spain.
b. Centro de Investigación Biomédica en Red de Enfermedades Respiratorias (CIBERES), Madrid, Spain.
c. Australian Infectious Diseases Research Centre, School of Chemistry and Molecular Biosciences, The University of Queensland, St. Lucia, Queensland 4072, Australia.
d. Servicio de Microbiología, Clínica Universidad de Navarra, 31008 Pamplona, Spain .
e. Instituto de Investigación Sanitaria de Navarra (IdiSNA), 31008 Pamplona, Spain .
f. Servicio Microbiología, Hospital Universitario Marqués de Valdecilla and Instituto de Investigación Marqués de Valdecilla (IDIVAL), 39011 Santander, Spain.
g. Red Española de Investigación en Patología Infecciosa (REIPI), ISCIII, Madrid, Spain.
h. Telum Therapeutics, Centro Europeo de Empresas e Innovación de Navarra (CEIN), 31110 Noáin, Spain.
i. Centre for Advanced Imaging, The University of Queensland, 4072 St Lucia, Queensland, Australia.
j. Institute of Applied Biotechnology, RWTH Aachen University, 52074 Aachen, Germany.

*Corresponding authors: Junkal Garmendia y Ulrike Kappler

3.1. Abstract

Chronic obstructive pulmonary disease (COPD) is characterized by abnormal inflammatory responses and impaired airway immunity, which provides an opportunistic platform for nontypeable *Haemophilus influenzae* (NTHi) infection. Clinical evidence supports that the COPD airways present increased concentrations of glucose, which may facilitate proliferation of pathogenic bacteria able to use glucose as a carbon source. NTHi metabolizes glucose through respiration-assisted fermentation, leading to the excretion of acetate, formate, and succinate. We hypothesized that such specialized glucose catabolism may be a pathoadaptive trait playing a pivotal role in the NTHi airway infection. To find out whether this is true, we engineered and characterized bacterial mutant strains impaired to produce acetate, formate, or succinate by inactivating the *ackA*, *pflA*, and *frdA* genes, respectively. While the inactivation of the *pflA* and *frdA* genes only had minimal physiological effects, the inactivation of the *ackA* gene affected acetate production and led to reduced bacterial growth, production of lactate under low oxygen tension, and bacterial attenuation *in vivo*. Moreover, bacterially produced acetate was able to stimulate the expression of inflammatory genes by cultured airway epithelial cells. These results back the notion that the COPD lung supports NTHi growth on glucose, enabling production of fermentative end products acting as immunometabolites at the site of infection. Thus, glucose catabolism may contribute not only to NTHi growth but also to bacterially driven airway inflammation. This information has important implications for developing nonantibiotic antimicrobials, given that airway glucose homeostasis modifying drugs could help prevent microbial infections associated with chronic lung disease.

3.2. Introduction

Nontypeable *Haemophilus influenzae* (NTHi) is a human pathobiont that exists as a commensal of the human upper airways, but it is also a common opportunistic pathogen within the lower airways of patients suffering chronic obstructive pulmonary disease (COPD) (Ahearn et al., 2017; Bandi et al., 2001; Finney et al., 2014; Sethi et al., 2002, 2008). COPD is associated with an abnormal pulmonary inflammatory response after exposure to noxious gases such as cigarette smoke. Airway inflammation persists even after smoking cessation and can be exacerbated by other factors such as bacterial infections. Indeed, persistent NTHi infections contribute to COPD airway inflammation, resulting in a worsening of symptoms and disease progression (Anzueto, 2010; Desai et al., 2014; Finney et al., 2014; Murphy et al., 2004).

Host environments that pathogens colonize have been proposed to drive their evolution to maximize nutritional opportunities (Rohmer et al., 2011). However, an incompletely explored question is how nutrient availability affects survival and host interplay of colonizing opportunistic pathogenic bacteria such as *H. influenzae*. Glucose concentrations are 3−20 times lower in the fluid that lines the lung epithelium (airway surface liquid, ASL) than in the plasma (<1 mM in nasal ASL, ~0.4 mM in lower respiratory tract ASL) (Garnett et al., 2012a). Low glucose concentrations in the ASL contribute to the maintenance of a nutrient-depleted environment, thus limiting the growth of pathogens as part of the lung nutritional immunity (Baker & Baines, 2018; Hood & Skaar, 2012; Nairz et al., 2018; Weinberg, 1975). However, ASL glucose concentrations are higher in respiratory disease associated with airway inflammation, likely due to the increased permeability and glucose flux (Baker et al., 2007; Garnett et al., 2012b). Increased glucose concentrations have been observed in sputum samples of patients with stable COPD and are further increased during exacerbations (Mallia et al., 2018). Besides acting as a metabolic energy source for bacterial growth, glucose in the airways can impair host immunity through glycosylation of innate and acquired immune proteins and by reducing epithelial resistance to bacterial invasion through glycosylation of epithelial cells (Philips et al., 2003). This is supported by clinical evidence where increased glucose levels in patients' blood and airway samples have been associated with an increasing likelihood of pathogen isolation (Baker et al., 2006; Loukides & Polyzogopoulos, 1996; Mallia et al., 2018). Dysregulation of glucose homeostasis in the COPD lung may thus facilitate infection by persistent pathogens such as *Haemophilus influenzae*, for which the use of glucose as a carbon source is well documented (Muda et al., 2019a; Othman et al., 2014; Tatusov et al., 1996).

Genomic analyses show that *H. influenzae* possess complete Embden-Meyerhof-Parnass (glycolysis) and pentose phosphate pathways for glucose degradation, combined with a functional minimization of the tricarboxylic acid (TCA) cycle where most enzymes of the oxidative branch are absent (**Figure 16**). In keeping with this partial TCA cycle, metabolomic studies of four NTHi strains

have revealed that glucose catabolism consistently leads to production of acetate during aerobic growth and to production of acetate, formate, and succinate during anaerobic growth (Muda et al., 2019; Othman et al., 2014). Additionally, hypxanthine is produced, as inosine is included in the medium (Muda et al., 2019; Othman et al., 2014). Incomplete TCA cycles are often found in fermentative bacteria, but *H. influenzae* possesses a versatile respiratory chain, indicating that it uses a specialized type of metabolism termed respiration-assisted fermentation (Harrison et al., 2016; Othman et al., 2014).

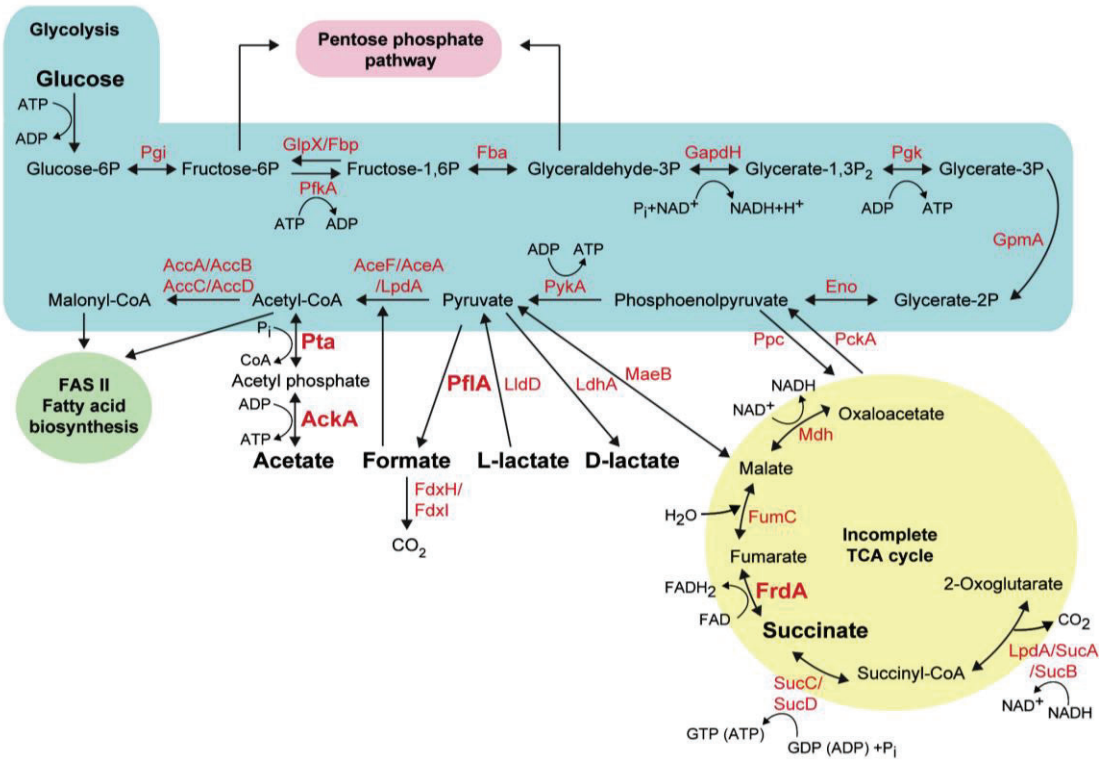

Figure 16. Schematic representation of *H. influenzae* glucose catabolism. Glycolysis, fermentative reactions, and incomplete TCA cycle are shown. Pgi, phosphoglucose isomerase; Fbp/GlpX, fructose-1,6-bisphosphatase; PfkA, 6-phosphofructokinase; Fba, fructose-bisphosphate aldolase; GapdH, glyceraldehyde-3-phosphate dehydrogenase; Pgk, phosphoglycerate kinase; GpmA, 2,3-bisphosphoglycerate-dependent phosphoglycerate mutase; Eno, phosphopyruvate hydratase; PykA, pyruvate kinase; AceF/AceA/LpdA, pyruvate dehydrogenase complex; AccABCD, acetyl-CoA carboxylase; PckA, phosphoenolpyruvate (PEP) carboxykinase; Ppc, PEP carboxylase; MaeB, malate dehydrogenase; PflA, pyruvate formate lyase activating enzyme; LldD, L-lactate dehydrogenase; LdhA, D-lactate dehydrogenase; Pta, phosphate acetyltransferase; AckA, acetate kinase; FdxHI, formate dehydrogenase; Mdh, malate dehydrogenase; FumC, fumarate hydratase; FrdA, fumarate reductase; SucCD, succinyl-CoA synthetase; LpdA, dihydrolipoamide dehydrogenase; SucAB, 2-oxoglutarate dehydrogenase.

In this study, we hypothesized that NTHi glucose catabolism may be a pathoadaptive trait. If glucose provided by the COPD lung is a main source of NTHi nutrition when colonizing this niche, any perturbations in its utilization and in the production of glucose-related metabolic end products may impact NTHi fitness and virulence. Additionally, NTHi fermentative end products might influence the host physiology and potentially act as immunometabolites (Ghorbani et al., 2015; Rutting et al., 2019), which could in turn contribute to the COPD chronic cycle (Rangelov & Sethi,

2014). To investigate this, we engineered NTHi mutant strains with impaired abilities to produce the main end products of glucose catabolism, acetate, formate, or succinate, both in a reference strain and in a chronic lung disease clinical isolate, and compared their fitness *in vitro* and *in vivo* across different assays and model systems. Our results highlight the importance of AckA for a successful interaction of *H. influenzae* with the host airways. The potential of modulating airway glucose and its bacterial use as a means to fight respiratory infections is discussed.

3.3. Material & Methods

3.3.1. Bacterial strains and growth conditions

Strains used in this study are detailed in **Table 4**. NTHi strains were grown at 37 °C, 5% CO_2 on chocolate agar (Biomerieux), brain-heart infusion (BHI, Oxoid) agar supplemented with 10 µg/mL hemin and 10 µg/mL nicotinamide adenine dinucleotide (NAD), referred to as sBHI agar, or Mueller Hinton Fastidious (MH-F) agar. NTHi liquid cultures were grown at 37 °C, 5% CO_2 in sBHI or in a chemically defined medium (CDM) (Othman et al., 2014). In detail, 235 mL of CDM contains 191 mL of RPMI 1640 (Life Technologies, ref 11879-020), 5.8 mL of 1 M Hepes (pH 7.2− 7.5, Life Technologies, ref 15630-080), 2 mL of 100 mM MEM sodium pyruvate (Life Technologies, ref 113600-070), 10 mL of uracil (2 mg/mL), 20 mL of inosine (20 mg/mL), 2 mL of NAD (1 mg/mL), 4 mL of hemin (1 mg/mL), and 2.35 mL of 1 M glucose (final concentration, 10 mM) (Othman et al., 2014). For growth in sBHI, NTHi strains grown on chocolate agar for 16 h were inoculated (2 to 5 colonies) in 20 mL of sBHI and incubated for 11 h with shaking (100 r.p.m.). Cultures were then diluted to an OD_{600} of 0.07 in sBHI, incubated as indicated below (aerobic growth), and OD_{600} was recorded every 2 h for up to 8 h. For growth in CDM, NTHi strains grown on chocolate agar for 16 h were inoculated (2 to 5 colonies) in 20 mL of CDM and incubated for 11 h with shaking (100 r.p.m.). Cultures were then diluted to an OD_{600} of 0.07 in CDM, incubated as indicated below, and OD_{600}, c.f.u./mL, and pH (pH indicator strips, Merck) were recorded every 2 h for up to 8 h. For aerobic growth, sterile 250 mL flasks with 25 mL of medium and shaking (200 r.p.m.) were used; for anaerobic growth, completely filled 50 mL tubes and shaking (200 r.p.m.) were used. When needed, microaerophilic conditions were tested by using sterile 250 mL flasks with 150 mL of medium and shaking (200 r.p.m.). Bacterial growth was monitored using at least three independent biological replicates ($n \geq 3$). Spectinomycin [30 µg/mL ($Spec_{30}$)] and erythromycin [11 µg/mL (Erm_{11})] were used to supplement media when required.

Escherichia coli was grown on Luria−Bertani (LB) broth or LB agar at 28 or 37 °C, supplemented with ampicillin [100 µg/ mL (Amp_{100})], Spec [50 µg/mL ($Spec_{50}$)], or Erm [150 µg/ mL (Erm_{150})] when necessary.

Table 4. Strains used in this study.

Strain	Description	Reference
H. influenzae		
RdKW20	Laboratory strain, capsule-deficient serotype b	(Fleischmann et al., 1995)
RdKW20Δ*ackA*-P868	*ackA::spec,* $Spec^R$	This study
RdKW20 Δ*ackA*-com *ackA* / P930	*ackA::spec,* complemented with *Pr::ackA-ermC*, $Spec^R$ Erm^R	This study
RdKW20 Δ*ackA*-com *ackA-pta* / P1020	*ackA::spec,* complemented with *Pr::pta-ackA-ermC*, $Spec^R$ Erm^R	This study
RdKW20Δ*pflA* / P865	*pflA::spec,* $Spec^R$	This study
RdKW20Δ*frdA* / P918	*frdA::ermC*, Erm^R	This study
NTHi411Δ*ackA* / P866	*ackA::spec,* $Spec^R$	This study
NTHi411Δ*pflA* / P867	*pflA::spec,* $Spec^R$	This study
NTHi411Δ*frdA* / P919	*frdA::ermC,* Erm^R	This study
E. coli		
TOP10	Used for cloning assays	Thermofisher
SW102	Derived from DY380, it contains a defective λ prophage with the recombination proteins *exo*, *bet*, and *gam* being controlled by the temperature-sensitive repressor *cI*857	(Tracy et al., 2008)

3.3.2. Generation of *H. influenzae* mutant strains

Plasmids and primers are shown in **Tables S6** and **A8**, respectively. For disruption of the *ackA* (gene accession numbers HI1204 and CK45_05190 in RdKW20 and NTHi411, respectively) and *pflA* (gene accession numbers HI0179 and CK45_08725) genes, DNA fragments containing the *ackA* gene and its respective adjacent regions (3326 bp) and the *pflA* gene and its respective adjacent regions (2815 bp) were PCR amplified with Phusion polymerase (Thermofisher Scientific) using NTHi411 genomic DNA as a template and primer pairs *ackA*-F1 and *ackA*-R1 or *pflA*-F1 and *pflA*-R1, respectively. Gene-containing fragments were cloned into pJET1.2/blunt (Thermofisher Scientific), generating pJET1.2-*ackA* and pJET1.2-*pflA*, respectively. $Spec^r$ cassettes were PCR amplified from pRSM2832 using gene-specific mutagenic primers *ackA*-F2 and *ackA*-R2 or *pflA*-F2 and *pflA*-R2. *E. coli* SW102 cells were prepared for recombineering, coelectroporated with (i) pJET1.2-*ackA* (Amp^r) (50 ng) and the *ackA*-specific mutagenic cassette ($Spec^r$) (200 ng); (ii) pJET1.2-*pflA* (Amp^r) (50 ng) and the *pflA*-specific mutagenic cassette ($Spec^r$) (200 ng). Mutagenized clones containing pJET1.2-*ackA*::spec or pJET1.2-*pflA*::spec were selected on LB agar with Amp_{100}, $Spec_{50}$ (Sinha et al., 2012; Tracy et al., 2008). These plasmids were used as a template to amplify the *ackA*::spec and *pflA*::spec disruption cassettes with primers *ackA*-F1 and *ackA*-R1 and *pflA*-F1 and *pflA*-R1, respectively, which were used to independently transform RdKW20 and NTHi411 strains using the MIV method (Herriott et al., 1970). Transformants were selected on sBHI agar with $Spec_{30}$ to obtain RdKW20Δ*ackA*, NTHi411Δ*ackA*, RdKW20Δ*pflA*, and NTHi411Δ*pflA* mutants. For *frdA*

disruption (gene accession numbers HI0835 and CK45_05995), a DNA fragment containing the *frdA* gene and its respective adjacent regions (2823 bp) was PCR amplified using NTHi411 strain genomic DNA as template and primers *frdA*-F1 and *frdA*-R1. This gene-containing fragment was cloned into pJET1.2/blunt, generating pJET1.2-*frdA*. This cloned PCR product was disrupted by inverse PCR with Phusion polymerase, using primers *frdA*-F2 and *frdA*-R2. An internal 673-bp fragment was replaced by a blunt-ended Erm resistance cassette excised by SmaI digestion from pBSLerm (Allen et al., 2005), generating pJET1.2- *frdA*::ermC. This plasmid was used as a template to amplify the *frdA*::ermC disruption cassette with primers *frdA*-F1 and *frdA*-R1, which was used to transform RdKW20 and NTHi411 strains using the MIV method. Transformants were selected on sBHI agar with Erm_{11} to obtain RdKW20Δ*frdA* and NTHi411Δ*frdA* mutants. In all cases, mutations were confirmed by PCR.

RdKW20Δ*ackA* mutant complemented strain (RdKW20Δ*ackA*-com) was generated as follows: the *ackA-pta* operon was inserted into open reading frame (ORF) HI0601.1; HI0601.1 contains a frameshift (Morey et al., 2013). The *ackA-pta* operon with its promoter region was amplified from RdKW20 genomic DNA using primers *ackA-pta*-COMP-XhoI-Fw and *ackA-pta*-HA-COMP-XhoI-Rv. Primer *ackA-pta*-HA-COMP-XhoI-Rv introduced a HA tail in the 3′end of the *pta* gene. This PCR product (3936 bp) was XhoI digested and cloned into XhoI-digested pUC19-HI0601.1-Erm (Fernández-Calvet et al., 2018), generating pUC19-HI0601.1-Erm-Pr::*ackA-pta*. This plasmid was used as a template to amplify a 7462 bp DNA fragment containing HI0601.1-flanked Pr::*ackA-pta*-HA by using primers HI0601.1- F1 and HI0601.1-R1, which was used to naturally transform RdKW20Δ*ackA*. Transformants were selected on sBHI agar with $Spec_{30}$ and Erm_{11} and confirmed by PCR and Western blotting.

3.3.3. Western blotting

Whole cell extracts were prepared from bacterial suspensions adjusted to an OD_{600} of 1 in PBS, lysed by sonication, 2-fold diluted with 2× loading buffer (Tris-HCl, 62.5 mM, pH 6.8, SDS, 2% w/v, glycerol, 10%, DTT, 50 mM; Bromophenol Blue, 0.01% w/v), and heated to 95 °C for 5 min. Proteins were separated on 12% SDS-PAGE gels (BioRad, MINI PROTEAN Tetra System) and transferred to a nitrocellulose membrane. The Pta protein (~77.6 kDa) was detected with a primary rabbit anti-HA antibody (Sigma-Aldrich), diluted to 1:4000, and a secondary goat antirabbit IgG (whole molecule, Sigma-Aldrich) antibody conjugated to horseradish peroxidase, diluted 1:1000 (**Figure S8A**, bottom panel).

3.3.4. Determination of bacterial metabolite concentrations

Three complementary procedures were employed. (i) For nuclear magnetic resonance (NMR) spectroscopy, samples for 1D 1 H NMR were collected and processed exactly as previously described (Othman et al., 2014). (ii) For enzymatic measures, ~1 mL of 8 and 24 h *H. influenzae* cultures was

pelleted (3 min, 4 °C, 14 000 r.p.m.); the supernatants were transferred into new tubes and stored at −20 °C until use. Acetate, formate, succinate, and D-lactate concentrations were determined using kits purchased from Megazyme (K-ACETRM, K-FORM, K-SUCC, and K-DATE, respectively) according to the manufacturer's instructions. These metabolites were not detected in the CDM control samples (data not shown). (iii) For high performance liquid chromatography (HPLC), metabolite concentrations for selected samples were determined by HPLC using an Ultimate 3000 HPLC system (Thermofisher Scientific) equipped with a UV detector and an RI detector (Shodex RI-101). Samples were separated (total runtime: 20 min) using a Metab-AAC column (300 × 7.8 mm; Isera, Dueren) at 30 °C, a flow rate of 0.8 mL/min, and 5 mM sulfuric acid as the running buffer. All samples were prepared as described under (ii) and filtered using a nonsterile 0.2 µm filter (Roth, Laboratory Supplies) prior to separation on the HPLC system. Data were analyzed using Chromeleon (Thermofisher Scientific).

3.3.5. Transmission electron microscopy (TEM)

As described (Rodríguez-Arce et al., 2019), bacteria growth on chocolate agar were applied to Formvar-coated grids, air-dried, negatively stained with 1% phosphotungstic acid in distilled water for 10 s, and examined with a JEM-1011 transmission electron microscope (JEOL) operating at 80 kV and equipped with an Orius SC1000 charge-coupled device (CCD) camera (Gatan). Bacterial length was calculated by using the measurement tool provided by the Gatan digital micrograph v2.11 software.

3.3.6. Immunofluorescence microscopy

After growth on CDM to half of each strain's respective maximal OD_{600} for ~5 h, bacteria were fixed with 3.7% paraformaldehyde in PBS, pH 7.4, for 15 min at room temperature, and stained with rabbit anti-NTHi serum diluted to 1:800 (Morey et al., 2011) and donkey anti-rabbit conjugated to Cy2 (Jackson Immunoresearch) diluted to 1:200. Samples were analyzed with a Carl Zeiss Axioskop 2 plus fluorescence microscope and a Carl Zeiss Axio Cam MRm monochrome camera.

3.3.7. Bacteria and host gene expression analyses

RNA was isolated from three sample types. (i) For bacterial cultures grown in sBHI or CDM, NTHi strains grown on chocolate agar for 16 h were inoculated (2 to 5 colonies) in 20 mL of sBHI or CDM, incubated for 11 h with shaking (100 r.p.m.), then diluted into 25 mL of fresh sBHI or CDM in a 250 mL flask (aerobiosis) or 50 mL of fresh CDM in 50 mL tubes (anaerobiosis) to an OD_{600} of 0.07, and grown to half of each strain's respective maximal OD_{600} for ~5 h. Bacterial total RNA was isolated using either TRIzol reagent (Invitrogen) or RNAprotect Bacteria Reagent (Qiagen) and RNAspin mini RNA isolation Kits (GE Healthcare). (ii) For cultured human epithelial cells, A549 human alveolar basal epithelial cells (ATCC CCL-185) were maintained as described

(Morey et al., 2011), seeded on 24-well tissue culture plates to 1.5 × 105 cells/well for 32 h, and serum-starved 16 h before infection. When indicated, cells were incubated with acetic acid (20 mM), formic acid (1 mM), succinic acid (1 mM), or hypoxanthine (7 mM) for 6 h in 0.3 mL of CDM. Vehicle solutions were water (acetic, formic, and succinic acids) or 0.1 N NaOH (hypoxanthine). Alternatively, cells were incubated for 6 h with 0.3 mL bacterial culture supernatants previously recovered by centrifugation of CDM cultures grown for 8 h. A549 cytotoxicity was not observed (data not shown). Total RNA from A549 cells was isolated using a Nucleospin RNAII kit (Macherey-Nagel) as recommended by the manufacturer and including an on-column DNase treatment step. (iii) For mouse lung samples, mouse lung total RNA was isolated using TRIzol reagent (Invitrogen). In all cases, total RNA quality was evaluated using RNA 6000 Nano LabChips (Agilent 2100 Bioanalyzer, Santa Clara, CA). All samples had intact 23S and 16S (prokaryotic samples) or 18S and 28S (eukaryotic samples) and rRNA bands with RNA integrity numbers (RIN) between 7.2 and 10. Reverse transcription (RT) was performed using 0.5 or 1 μg of RNA by PrimeScript RT Reagent kit (Takara) or Superscript III (Life Technologies). PCR amplification was performed by using SYBR Premix Ex TaqII (Tli RNaseH Plus) (Takara) or Power SYBR Green Master Mix (Applied Biosystems). Fluorescence was analyzed with a AriaMx Real-Time PCR System (Agilent Technologies) or a Quantstudio 5 Real-Time PCR machine (Applied Biosystems). The comparative threshold cycle (Ct) method was used to obtain relative quantities of mRNA that were normalized using *gyrA*, human *gapdh*, or mouse *gapdh* for bacteria, cultured cells, or mouse lung samples, respectively, as endogenous controls. Primers, listed in **Table A8**, were designed with Primer3 or Vector NTI (Life Technologies) software. Bacterial cultures were grown at least three times, and samples were processed with technical triplicates (n ≥ 3). A549 cell assays were performed in triplicate at three independent occasions (n = 3). Homogenized lung samples were independently obtained from groups containing 5 infected mice per strain (n = 5).

3.3.8. NTHi mouse lung infection

A mouse model of NTHi lung infection was used, as described previously (Euba et al., 2017; Euba et al., 2015c; Fernández-Calvet et al., 2018; Rodríguez-Arce et al., 2017, 2019). CD1 female mice were purchased from Charles River Laboratories (France), housed under pathogen-free conditions at the Institute of Agrobiotechnology facilities (registration number 365 ES/31-2016-000002-CR-SU-US), and used at 22−25 g (6−7 weeks). Animal handling and procedures were in accordance with the current European (Directive 2010/63/ EU) and National (RD 53/2013) legislations, with the approval of Universidad Publica de Navarra (UPNA) and CSIC Animal Experimentation Committees (PI 007/19). Mouse infection was performed with RdKW20 WT and mutant strains. The NTHi411 genetic background could not be used because the infection rate was low and poorly reproducible (data not shown). Bacterial strains were grown in CDM under aerobic

or anaerobic conditions and collected to half of each strain's respective maximal OD_{600} for ~5 h. For intranasal infection, 20 µL of a bacterial suspension containing 5×10^9 c.f.u./mL (1×10^8 c.f.u./mouse) was placed at the entrance of the nostrils until complete inhalation by the mouse, previously anesthetized (ketamine−xylazine, 3:1). At 24 or 30 h postinfection (hpi), mice were euthanized using cervical dislocation. Bronchoalveolar lavage fluid (BALF) samples were obtained by perfusion and collection of 0.7 mL of PBS with the help of a sterile 20G (1.1 mm diameter) VialonTM intravenous catheter (Becton-Dickinson) inserted into the trachea. Recovered BALF was serially 10-fold diluted in PBS and plated in triplicate on sBHI agar to determine the number of viable bacteria. By following standardized published procedures (Grilló et al., 2012), we considered that we could have a minimum of 3.3 c.f.u. in 1 mL of sample without detecting bacteria (limit of detection < 3−4 c.f.u./mL BALF), rendering $\log_{10} = 0.52$. For cell counting, the remaining volume of the BALF samples was centrifuged at 5000 r.p.m. for 3 min at 4 °C. Each pellet was resuspended in 1 mL of RPMI 1640 with 10% FCS (del inglés, *fetal calf serum*, suero de ternera fetal), Hepes (10 mM), and antibiotics (penicillin and streptomycin). A 10 µL aliquot was stained with an equal volume of 0.4% trypan blue (Sigma-Aldrich) for total cell count on a hemocytometer. 5×10^4 cells in 200 µL of RPMI 1640 with 10% FCS, Hepes (10 mM), and antibiotics (penicillin and streptomycin) were used for cytospin preparation (1500 r.p.m. for 10 min at room temperature, Thermo Shandon Cytospin). May−Grünwald− Giemsa stains were performed with an automated hematology slide preparation unit (SP-10, Sysmex Cosporation) according to the manufacturer's instructions. Preparations were examined in a double-blinded manner with an optical microscope (BX, Olympus). The left lung was individually weighed in sterile bags (Stomacher80, Seward Medical) and homogenized 1:10 wt/vol) in PBS. Each homogenate was serially 10-fold diluted in PBS and plated in triplicate on sBHI agar to determine the number of c.f.u. per lung. The right lung was homogenized with TRIzol reagent for subsequent RNA extraction as indicated above. Infections were performed in groups of at least 5 mice per strain and time point ($n \geq 5$).

3.3.9. Statistical analysis

In all cases, a p value < 0.05 was considered statistically significant. Analyses were performed using Prism software, version 7 for Mac (GraphPad Software) statistical package, and are detailed in each figure caption.

3.4. Results

3.4.1. Metabolic end products produced by *H. influenzae* persistent isolates from chronic lung disease are similar to those detected in reference strains

As the aim of this study was to perturb NTHi glucose metabolism in chronic respiratory disease

associated strains, the initial experiments were used to establish whether any systematic differences existed in the metabolic profiles of *H. influenzae* clinical isolates and reference strains such as RdKW20. NTHi411, NTHi584, and NTHi1104 are three persistent, genome sequenced, clonal strains, longitudinally isolated from one patient suffering from chronic obstructive lung disease (Garmendia et al., 2014). The analysis of the three genomes revealed the presence of gene encoding enzymes of the glycolysis and pentose phosphate pathways as well as fermentative reactions and an incomplete TCA cycle (**Figure 16**). Unlike the supplemented brain-heart infusion (sBHI) complex medium that is regularly used for *H. influenzae* growth but contains varying and unknown types of C, N, and P sources as well as inorganic ions, the composition of the chemically defined medium (CDM) is known and does not include complex organic ingredients, making it well suited for metabolomic analyses (Muda et al., 2019a; Othman et al., 2014). CDM is a modification of the RPMI 1640 tissue culture medium, also making it a suitable medium for analyzing cultured cell infection processes (Dhouib et al., 2016). Not unexpectedly, the differing composition of the two media causes some alterations in central carbon metabolism gene expression when comparing bacteria grown in sBHI or CDM (**Figure S4**). In this study, we used CDM unless otherwise indicated.

Given that physiological gradients exist along the airways and the partial pressures of oxygen (pO_2) and carbon dioxide (pCO_2) have opposing gradients (Huffnagle et al., 2017; Man et al., 2017), we then determined metabolite production by NTHi411, NTHi584, and NTHi1104 in CDM, as a function of time and oxygen tension, by ^{1}H NMR. Utilization rates for the three major carbon substrates present in CDM, glucose, pyruvate, and inosine, did not differ significantly with decreasing oxygen tension. Pyruvate was metabolized completely within the first few hours of growth, while glucose and inosine were consumed more slowly (**Figures 17** and **S5A**). Acetate was the major metabolite produced by all strains, with the highest concentrations present following aerobic growth where hypoxanthine, a byproduct of inosine breakdown, was another significant product. At decreasing oxygen tensions, acetate concentrations decreased, while formate and succinate started to accumulate with the highest succinate concentrations observed under anaerobic conditions (**Figures 17 and S5B**). This end product spectrum is comparable to previously reported ones (Muda et al., 2019; Othman et al., 2014).

The metabolic changes seen were supported by the underlying changes in bacterial gene expression (**Figure S6**), which again were similar to what has been previously reported for other NTHi strains (Muda et al., 2019; Othman et al., 2014).

In summary, under the conditions tested, substrate utilization and metabolite end products of NTHi411, NTHi584, and NTHi1104 were typical for bacterial fermentative metabolism and comparable to previously defined ones for *H. influenzae*, highlighting the strong conservation of NTHi central metabolism. As these three clinical strains showed essentially the same metabolic

profile, further work focused on NTHi411 as a representative persistent isolate, together with the RdKW20 reference strain.

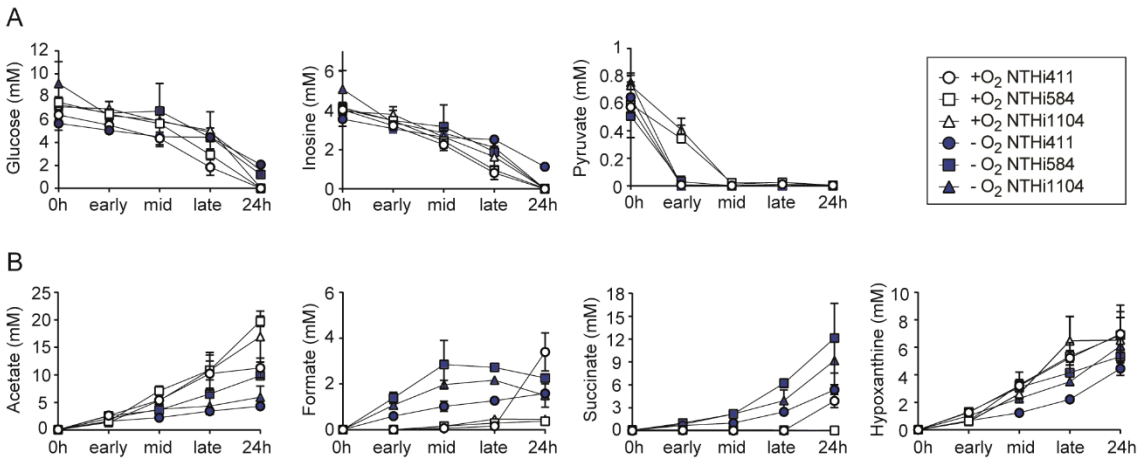

Figure 17. Changes in metabolite concentrations in cultures of *H. influenzae* NTHi411, NTHi584, and NTHi1104 grown in CDM under aerobic and anaerobic conditions. Strains and growth conditions are indicated in the right inset. NMR data shown is for three growth substrates, glucose, inosine, and pyruvate **(A)**, and for four metabolites produced during growth, acetate, formate, succinate, and hypoxanthine **(B)**.

3.4.2. Inactivation of genes involved in the production of metabolic end products affects the growth of NTHi with glucose as the main carbon source

To create perturbations of NTHi glucose metabolism, we generated mutants in the *ackA* gene, encoding the acetate kinase involved in the conversion of acetyl phosphate to acetate, the *pflA* gene, encoding the pyruvate formate lyase activating enzyme involved in converting pyruvate to formate and acetyl-CoA, and the *frdA* gene, encoding a subunit of the fumarate reductase catalyzing the conversion of fumarate to succinate (**Figure 16**). Following standard procedures, *H. influenzae* mutants were selected on sBHI agar with adequate antibiotics. RdKW20Δ*ackA* and NTHi411Δ*ackA* rendered small colonies compared to the respective wild-type (WT) strains, but changes in bacterial size or morphology were not detected (average length for RdKW20 WT and derivative strains, 1.388 ± 0.024 μm; NTHi411 WT and derivative strains, 1.276 ± 0.061 μm). Bacterial growth in sBHI also showed that inactivation of the *ackA* gene reduced the final OD_{600} (**Figure S7**).

Due to the observed effect of *ackA* gene inactivation on bacterial growth, Δ*ackA* complementation was attempted using ORF HI0601.1 for chromosomal integration of the complementation cassette (Fernández-Calvet et al., 2018; Morey et al., 2013). The *ackA* gene with its own promoter region and a HA tail introduced in its 3′-end was inserted into HI0601.1, generating the complemented strain RdKW20Δ*ackA*-com *ackA* (**Figure S8A**, upper panel) which, however, rendered only partial complementation of Δ*ackA*-associated phenotypes (data not shown). This could be linked to a polar effect of the *ackA* gene inactivation on the expression of the *pta* gene (**Figure**

S8B). For this reason, a second Δ*ackA* complementation approach was used by inserting the *ackA-pta* operon with its promoter region and a HA tail introduced at the 3′-end of the *pta* gene into ORF HI0601.1 to generate RdKW20Δ*ackA*-com, which resulted in full complementation of Δ*ackA*-associated phenotypes (**Figures S8A**, lower panel, and **S7A** and the Results section). For unknown reasons, a NTHi411Δ*ackA* complemented strain could not be generated.

We next assessed the growth of WT and mutants in CDM, where glucose is the main carbon source, under aerobic and anaerobic conditions. For both RdKW20 and NTHi411 genetic backgrounds, the inactivation of the *ackA* gene, and to a lower extent of the *frdA* gene, reduced the final bacterial OD_{600} (**Figure 18 A,C**, left panels). The growth deficiency associated with the inactivation of the *ackA* gene was reversed in RdKW20Δ*ackA*-com. Compared to the respective WT strains, bacterial cell counts were lower only for the Δ*ackA* mutants (**Figure 18 A,C**, middle panels). This cell count reduction was lower during anaerobic growth (WT versus Δ*ackA*, differences of ~50- and 10-fold in aerobiosis and anaerobiosis, respectively). Despite the reduced OD_{600} observed for the Δ*frdA* mutant strains, no difference in cell counts was observed, suggesting that it might have an effect on NTHi cell morphology. However, this could not be substantiated, as we did not observe changes in bacterial size or morphology among strains (**Figure 18B**). Interestingly, measurements of glucose concentrations in CDM following growth showed that the RdKW20Δ*frdA* mutant only partially utilized glucose present in the growth medium during anaerobiosis (**Table S7**).

We also monitored bacterial culture pH, which decreased over time, more markedly when cultures were grown without oxygen (**Figure 18 A,C**, right panels). During anaerobic growth, more reduced carbon compounds and potentially stronger acids are excreted, thus contributing to pH reduction. Stronger acidification could at least partially explain why anaerobic growth stops earlier, as *H. influenzae* growth is slowed down at a pH between 6 and 7 (U. Kappler, unpublished data).

In summary, inactivation of AckA, and to a lower extent of FrdA, reduced *H. influenzae* fitness when grown in CDM.

3.4.3. *H. influenzae ackA*, *pflA*, and *frdA* gene inactivation modifies the production of metabolic end products in response to changing oxygen tensions

Inactivation of the *ackA*, *pflA*, and *frdA* genes was expected to lead to adjustments in NTHi metabolic carbon fluxes, resulting in changes in the spectrum of excreted metabolites. The key end products, acetate, formate, and succinate, were quantified enzymatically in the supernatants of CDM grown cultures as a function of time (8 and 24 h grown cultures) and oxygen tension (aerobic and anaerobic growth). The general metabolite profiles of WT strains agreed with the data collected by NMR above, with acetate being the most abundant metabolite under both conditions and formate and succinate being produced in increased amounts anaerobically (**Figures 19** and **S9**). For the *pflA*

mutant after 8 h of growth, no significant changes of the product spectrum other than a reduced production of formate in anaerobiosis were detected (**Figure 19**).

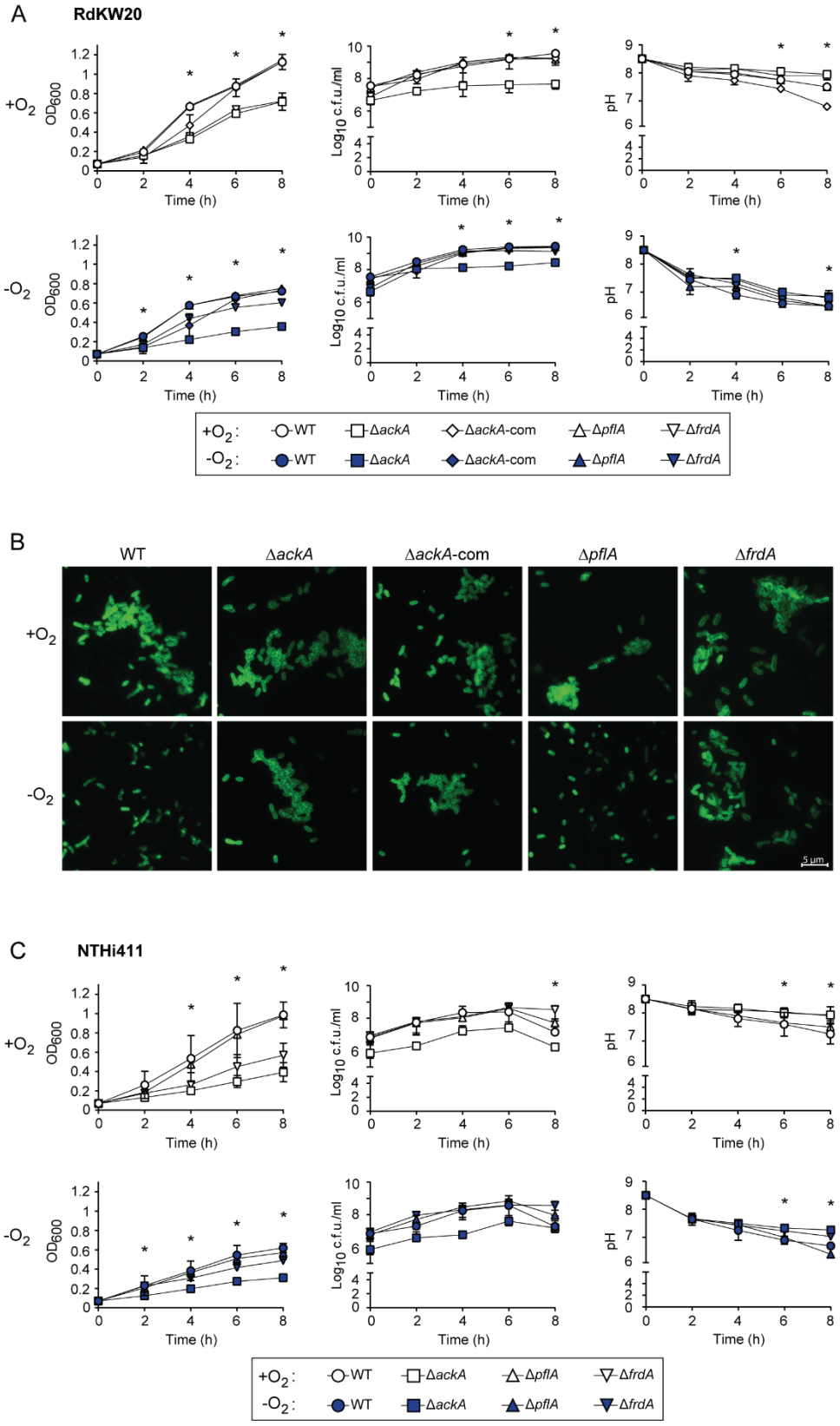

Figure 18. Effect of carbon metabolism perturbation by gene inactivation on bacterial growth. Bacterial growth in CDM is shown as a means of OD_{600} (left panels), log_{10} c.f.u./mL (middle panels), and pH (right panels) at the indicated time points (mean ± SD) for RdKW20 **(A)** and NTHi411 **(C)** strains. Strains and growth conditions are indicated in the insets. RdKW20Δ*ackA* and RdKW20Δ*frdA* showed lower OD_{600} than the WT strain (under aerobiosis: at 4, 6, and 8 h, $p < 0.0001$; under anaerobiosis: at 2 h, Δ*ackA*, $p < 0.05$; at 4 h, $p < 0.0001$ and $p = 0.01$; at 6 h, $p < 0.0001$ and $p < 0.05$; at 8 h, $p < 0.0001$ and $p < 0.05$, respectively). RdKW20Δ*ackA* deficient growth was restored in the complemented strain. NTHi411Δ*ackA* and Δ*frdA* displayed lower OD_{600} than the WT strain (in aerobiosis: at 4 h, $p < 0.005$ and $p = 0.01$; at 6 h, $p < 0.0001$ and $p < 0.0005$; at 8 h, $p < 0.0001$; in anaerobiosis: Δ*ackA*, at 2 h, $p < 0.05$; at 4 h, $p < 0.0001$; at 6 h $p < 0.0001$; at 8 h, $p < 0.0001$; Δ*frdA*, at 6 h, $p < 0.005$; at 8 h, $p < 0.005$). We quantified lower bacterial counts for RdKW20Δ*ackA* than for the WT strain at 6 and 8 h under aerobic growth and at 4, 6, and 8 h under anaerobic growth ($p < 0.0001$). RdKW20Δ*ackA* and Δ*frdA* showed higher pH than the WT strain (in aerobiosis, at 6 h, RdKW20Δ*ackA*, $p < 0.05$; at 8 h, $p < 0.001$; in anaerobiosis, at 4 h, $p < 0.01$ and $p < 0.001$; at 8 h, RdKW20Δ*frdA*, $p < 0.05$). In aerobiosis, Δ*ackA*-com showed lower pH at 8 h compared to WT ($p < 0.0001$). NTHi411Δ*ackA* and Δ*frdA* also presented higher pH than the WT strain (in aerobiosis, at 6 h, RdKW20Δ*frdA*, $p < 0.05$; at 8 h, $p < 0.001$ and $p < 0.001$; in anaerobiosis, at 6 h, $p < 0.001$ and $p < 0.01$; at 8 h, $p < 0.0001$ and $p < 0.01$). Statistical comparisons of the means were carried out with a two-way ANOVA (Dunnett's multiple comparisons test). **(B)** Representative immunofluorescence microscopy images of RdKW20 WT and mutant strains. Microscopic observation did not render significant differences among strains and growth conditions.

In contrast, both the *frdA* and *ackA* mutants showed significant alterations in the spectrum of excreted metabolites. The *frdA* mutation gave rise to an approximately 6−8-fold reduction of succinate excretion in anaerobiosis with the observed remaining levels below 0.3 mM. Additionally, formate production was reduced by 50%, and there was also a small but significant reduction in acetate excretion by RdKW20Δ*frdA*. Interestingly, production of small amounts of D-lactate was also observed (~0.4−0.7 mM). D-Lactate was not detected during the NMR-based metabolomics here or in previous work (Muda et al., 2019a; Othman et al., 2014). Production of D-lactate would involve the LdhA lactate dehydrogenase, known to be present in NTHi (Denicola-Seoane & Anderson, 1990).

For the *ackA* mutation, a very significant reduction in acetate production was observed, with no acetate detected during aerobic growth and only 2−3 mM acetate produced during anaerobic growth (WT levels: 10−13 mM). The pyruvate oxidase (PoxB) presents a possible route for acetate generation when inactivating the *pta-ackA* system (Chang et al., 1994), but our genomic search did not reveal *poxB* gene presence in *H. influenzae* genomes. Moreover, succinate excretion was reduced by about 50% under both aerobic and anaerobic conditions, as was anaerobic formate production. Again, D-lactate was also produced, with amounts increasing to over 2 mM during anaerobic growth, a noticeable increase compared to the *frdA* mutant strain (**Figure 19**). After 24 h of growth, overall similar profiles were obtained with higher final concentrations of all metabolites (**Figure S9**). These results were further confirmed by HPLC on the RdKW20 derivative strain 8 h culture supernatants (Table S12).

The production of D-lactate by the NTHi *ackA* and *frdA* mutants may be an indicator of metabolic stress and significant rerouting of metabolic fluxes, which is particularly apparent when bacteria were less able to produce acetate. Overall, the *ackA* gene inactivation led to the strongest perturbation of NTHi glucose metabolism and associated metabolite excretion, which is in keeping with acetate being the main metabolic end product excreted by NTHi.

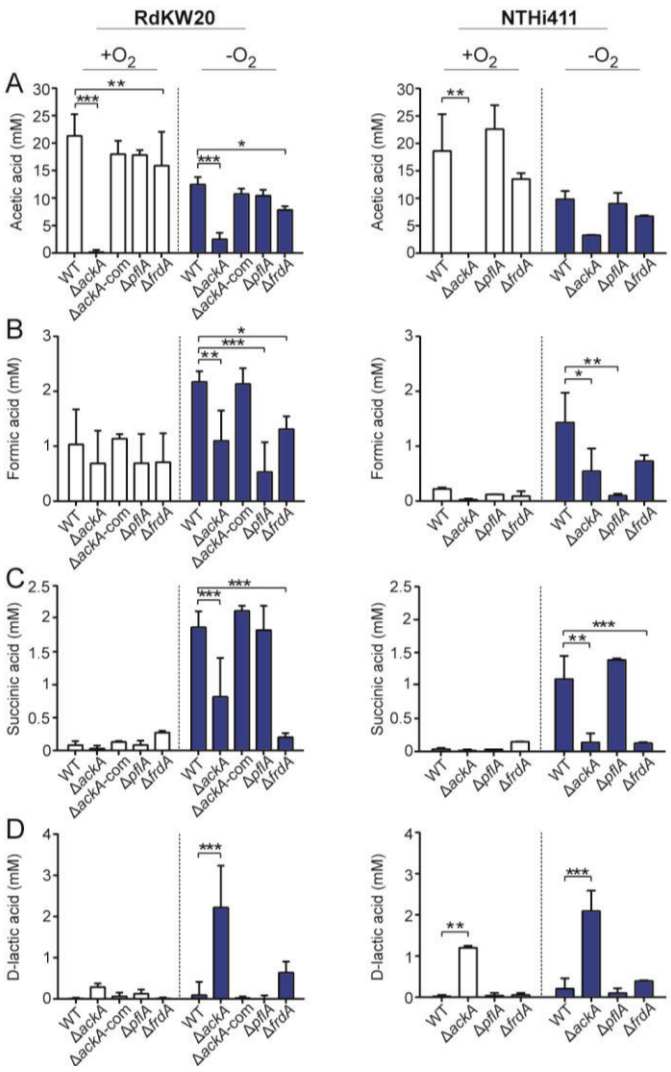

Figure 19. Inactivation of the *ackA*, *pflA*, and *frdA* genes modifies *H. influenzae* production of glucose catabolism end products. Enzymatic measure of acetic **(A)**, formic **(B)**, succinic **(C)**, and D-lactic **(D)** acids, determined on CDM bacterial culture supernatants grown for 8 h. Each metabolite concentration is shown as mM (mean ± SD). Data for RdKW20 and NTHi411 strains are shown on the left and right columns, respectively. Compared to the WT strain, reduced acetic acid levels were observed for the RdKW20Δ*ackA* and Δ*frdA* mutants grown in aerobic and anaerobic conditions; decreased formic acid was determined in culture supernatants of Δ*ackA*, Δ*pflA*, and Δ*frdA* mutants grown in anaerobiosis; a lower succinic acid level was measured for the Δ*ackA* and Δ*frdA* strains grown in anaerobiosis; increased D-lactic acid was determined in culture supernatants of the Δ*ackA* mutant grown in anaerobiosis. Also, compared to the respective WT strain, reduced acetic acid was monitored in culture supernatants of the NTHi411Δ*ackA* mutant grown in aerobiosis; decreased formic acid was determined for the Δ*ackA* and Δ*pflA* mutants grown in anaerobiosis; a lower succinic acid level was measured in culture supernatants of Δ*ackA* and Δ*frdA* strains grown without oxygen; increased D-lactic acid was determined for the Δ*ackA* mutant grown in aerobiosis and anaerobiosis. Statistical comparisons of the means were performed with a two-way ANOVA (Dunnett's multiple comparisons test). *p < 0.01, **p < 0.001, and ***p < 0.0001.

3.4.4. Mutations in genes involved in NTHi central carbon metabolism alter gene expression patterns, revealing complex adaptations

Alterations of metabolic networks can lead to compensatory changes in gene expression, and here, we monitored expression of *ackA*, *pflA*, and *frdA* as well as the genes encoding the LdhA lactate dehydrogenase and the pyruvate dehydrogenase subunit AceF. In the WT strains, expression of the

aceF pyruvate dehydrogenase subunit was high, while *ackA* and *frdA* were expressed at intermediate levels, and *pflA* and *ldhA* were expressed at low to very low levels (**Figure 20**), independent of NTHi genetic backgrounds and oxygen conditions. Gene expression levels were generally slightly lower for anaerobic conditions, except for the *frdA* gene whose expression increased during anaerobiosis, in keeping with anaerobic production of succinate.

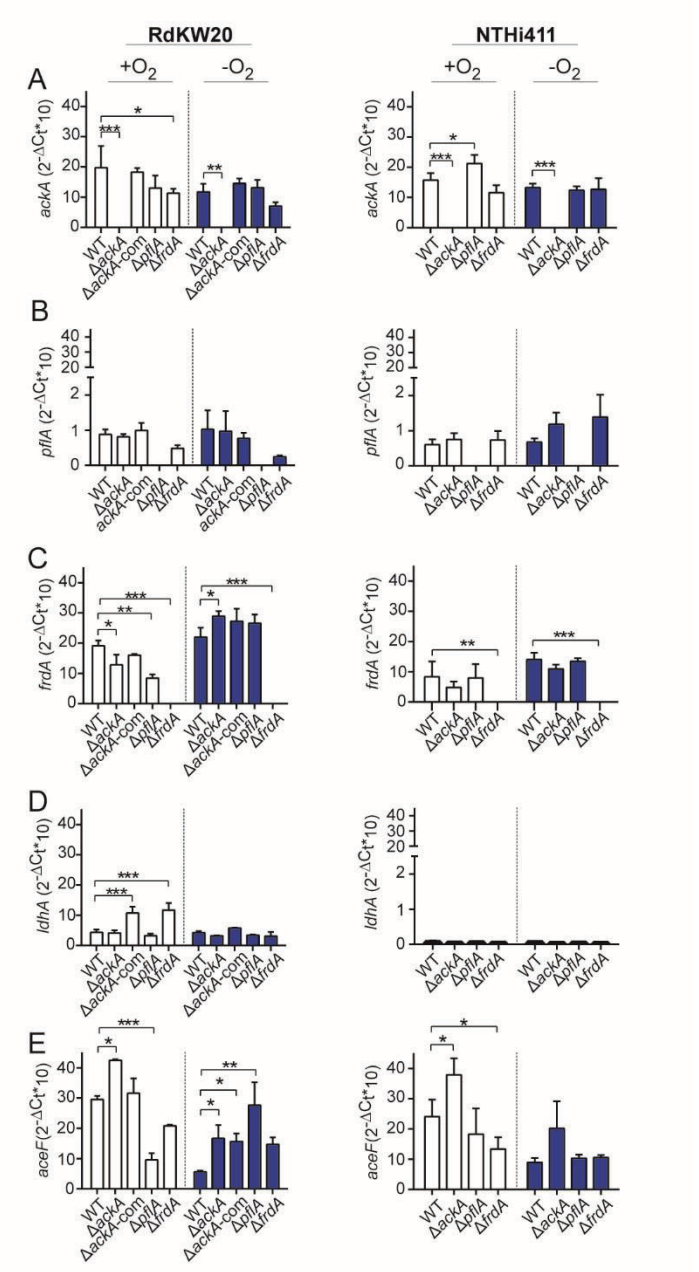

Figure 20. Effect of inactivating glucose metabolic gene encoding enzymes on bacterial gene expression. Expression of the *ackA* (**A**), *pflA* (**B**), *frdA* (**C**), *ldhA* (**D**) and *aceF* (**E**) genes in RdKW20 (left columns) and NTHi411 (right columns) strains grown in CDM, shown as mean ± SD. In RdKW20, compared to the WT strain, we observed lower *ackA* gene expression in Δ*ackA* and Δ*frdA* mutants; in aerobiosis, lower *frdA* gene expression in Δ*ackA*, Δ*pflA*, and Δ*frdA* mutants; in anaerobiosis, higher *frdA* gene expression in Δ*ackA* and lower *frdA* expression in Δ*frdA* strains; in aerobiosis, increased *ldhA* expression in Δ*ackA*-com and Δ*frdA* strains; in aerobiosis, higher *aceF* gene expression in Δ*ackA* and lower in Δ*pflA* strains, compared to WT; in anaerobiosis, higher *aceF* gene expression in Δ*ackA*, Δ*ackA*-com, and Δ*pflA* strains. In NTHi411, compared to the WT strain, we observed lower *ackA* gene expression in Δ*ackA* and higher in Δ*pflA* mutants; lower *frdA* gene expression in Δ*frdA* strain; in aerobiosis, higher *aceF* gene expression in Δ*ackA* and lower in Δ*frdA*.

Statistical comparisons of the means with a two-way ANOVA (Sidak's multiple comparisons test). *p < 0.01, **p < 0.001, and ***p < 0.0001.

As expected, in each of the mutant strains, expression of the mutated gene was not detected. Expression of the *ackA* gene showed a small adjustment with slightly lower expression in RdKW20Δ*frdA*. This is interesting as AckA is required for acetate production and given the fact that the *frdA* mutants tend to excrete less acetate, but also to excrete a noticeable amount of D-lactate, suggesting problems with the typical metabolic routing. The *pflA* gene was low throughout in all strains. Expression of *frdA* was comparatively higher, with some slight variations in expression.

On the basis of the metabolite patterns reported above, increased *ldhA* gene expression would have been expected for the *ackA* and *frdA* mutations, but that was not observed except for RdKW20Δ*frdA*. In all other cases, *ldhA* expression was low throughout, with very low expression in NTHi411. This suggests that the amount of LdhA protein present in the NTHi cell was sufficient to mediate the observed lactate production. Interestingly, pyruvate dehydrogenase expression (*aceF* gene) was increased in both *ackA* mutant strains by about 20−30%. This could be caused by an oversupply of pyruvate and could lead to increased acetyl-CoA concentrations. Increased pyruvate concentrations could also explain the excretion of D-lactate, which is formed from pyruvate.

3.4.5. The inability to produce large amounts of acetate reduces NTHi survival in a mouse model of lung infection

Next, we assessed whether the defects in metabolite production identified *in vitro* translate to *in vivo* attenuation of infection. A mouse respiratory infection model system was used (Euba et al., 2017; Euba et al., 2015c; Fernández-Calvet et al., 2018; Rodríguez-Arce et al., 2017, 2019). As in previous assays, the *ackA* mutant strain showed reduced fitness, with lower cell numbers recovered at 24 and 30 hpi, in lung tissue and bronchoalveolar lavage fluid (BALF) samples (**Figure 21A**). For the RdKW20Δ*ackA*-com strain, cell numbers were similar to those of the WT. Similar observations were made when infecting inocula were prepared by growing bacteria under aerobic or anaerobic conditions. A milder infectious defect was observed for the *pflA* mutant strain with significant decreases (∼1 order of magnitude) of bacterial counts at several data points.

RdKW20Δ*ackA* attenuation led us to next assess the expression of the *kc* proinflammatory gene in infected mouse lungs, which was lower in lung samples from animals infected with Δ*ackA* bacteria and restored to WT levels upon infection by RdKW20Δ*ackA*-com (**Figure 21B**). In parallel, we quantified the accumulation of immune cells in the collected BALF samples. When using bacteria previously grown under aerobiosis, the RdKW20 WT pulmonary infection increased the accumulation of macrophages ($p < 0.05$) and polymorphonuclear leukocytes (PMNs) compared to that observed in BALF samples of Δ*ackA* infected mice, which was restored upon infection by

RdKW20Δ*ackA*-com. In contrast, differences among animal groups were not observed upon infection with bacteria previously grown anaerobically (**Figure 21C**).

Together, these results confirmed that the fitness defect resulting from the *ackA* gene mutation impaired airway infection by NTHi and also suggested that the *H. influenzae* ability to produce formate may be of more relevance *in vivo* than *in vitro*.

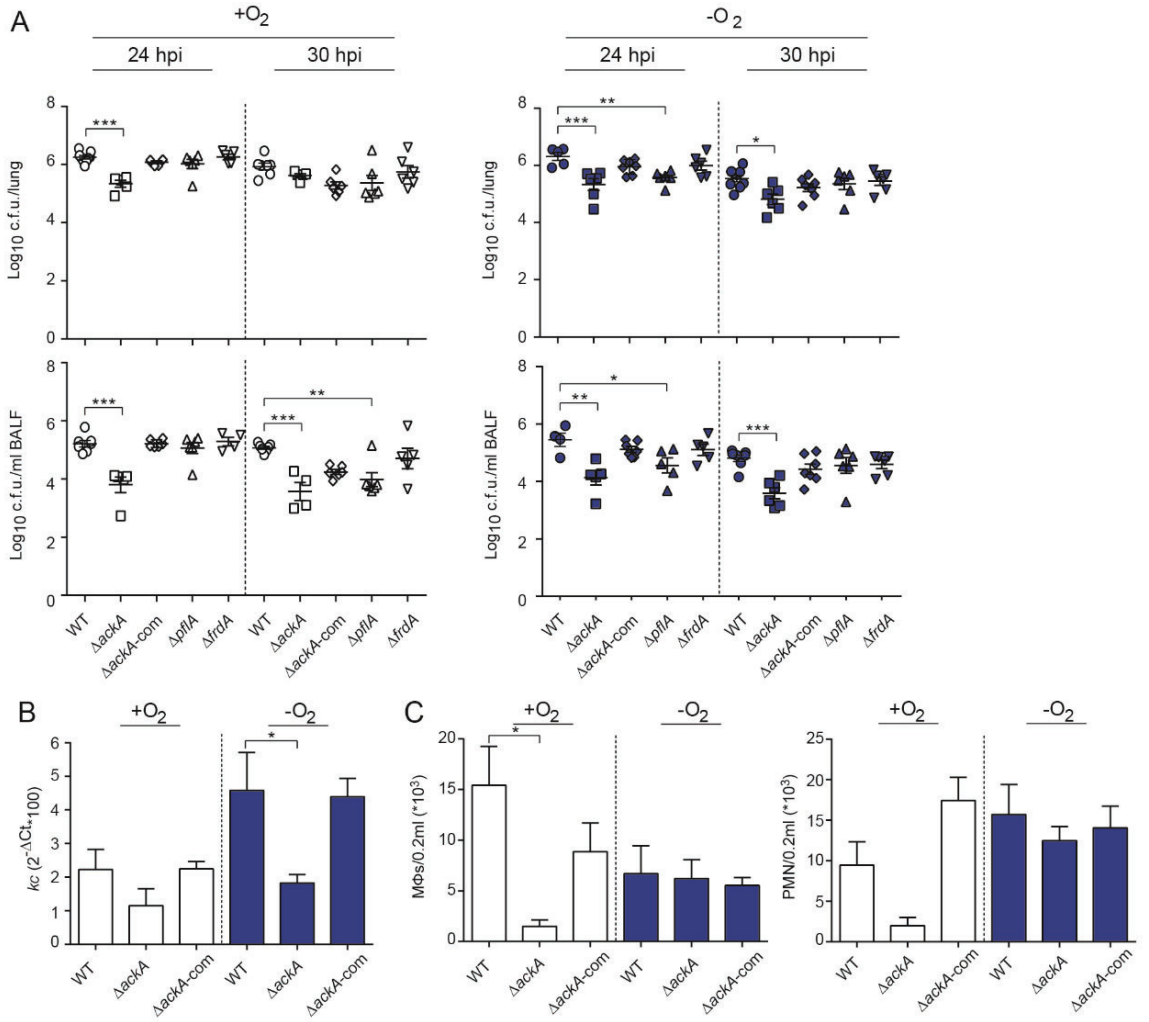

Figure 21. Glucose metabolic gene encoding enzymes are key contributors to *H. influenzae* lung infection. (**A**) CD1 mice were intranasally infected with RdKW20 WT and mutant strains grown in CDM under aerobic or anaerobic (left side, white; right side, blue, respectively) conditions. Bacterial counts were determined at 24 and 30 hpi in lungs (log10 c.f.u./lung) and BALF (log10 c.f.u./mL BALF) (upper and lower panels, respectively) samples. Inactivation of the *ackA* gene lowered bacterial counts when compared to the WT strain, observed for both aerobically and anaerobically grown bacteria. The *ackA* gene mutant deficiency was restored by complementation. Inactivation of the *pflA* gene lowered bacterial counts in several data points. Statistical comparisons were performed using one-way ANOVA (Dunnett's multiple comparisons test). (**B**) Relative quantities of mouse *kc* mRNA were measured by RT-qPCR on lung samples corresponding to RdKW20 WT, Δ*ackA*, and Δ*ackA*-com infected groups at 24 hpi. Expression of *kc* was lower in lung samples from animals infected with Δ*ackA* than with WT bacteria. Such a decrease was significant upon infection with bacteria previously grown in anaerobiosis. Statistical comparisons of the means were performed with one-way ANOVA (Sidak's multiple comparisons test). (**C**) BALF samples corresponding to RdKW20 WT, Δ*ackA*, and Δ*ackA*-com infected groups were analyzed for alveolar macrophage (left) and PMN (right) counts at 24 hpi. Lower numbers were observed in samples from animals infected with aerobically grown Δ*ackA* than with WT bacteria. Statistical comparisons of the means were performed with a one-way ANOVA (Dunnett's multiple comparisons test). In all cases, data are shown as mean ± SEM. *p < 0.01, **p < 0.001, and ***p < 0.0001.

3.4.6. *H. influenzae* metabolic end products have a proinflammatory effect on airway epithelial cells

H. influenzae growing on CDM excrete acetate in the millimolar range, and this ability is limited in the *ackA* mutant strain. Interestingly, short-chain fatty acids (SCFAs) such as acetate, propionate, and butyrate have been proposed to regulate numerous functions including inflammation (Mortensen & Clausen, 1996; Ratajczak et al., 2019).

Evidence also indicates that the hypoxic environment of cystic fibrosis (CF) airways allows the persistence of facultative anaerobic bacteria, which can produce millimolar concentrations of SCFAs and affect airway epithelial proinflammatory responses (Ghorbani et al., 2015). A proinflammatory effect of SCFAs in lung mesenchymal cells has also been reported (Rutting et al., 2019). As *H. influenzae* strains also excrete acetate in the millimolar range and the expression of the *kc* gene was lower in lung samples from animals infected with RdKW20Δ*ackA* than with WT bacteria, we tested if NTHi culture supernatants may indeed have immunomodulatory effects. A549 airway epithelial cells were incubated with CDM culture supernatants of RdKW20 WT and mutant strains, and expression of the human *il-8* and *cxcl-1* proinflammatory markers was quantified. Acetic, formic, and succinic acids together with hypoxanthine were used as controls, confirming the proinflammatory effect of acetic acid (Ghorbani et al., 2015) and excluding proinflammatory effects of formic and succinic acids as well as hypoxanthine (**Figure 22**). RdKW20 WT culture supernatants from aerobic growth stimulated expression of the *il-8* gene ~30-fold and expression of the *cxcl-1* gene ~4-fold. The observed effect was dependent on the presence of a functional *ackA* gene, i.e., the excretion of large amounts of acetate. Comparable results were obtained when testing culture supernatants of anaerobically grown strains except for the stimulation of *il-8* gene expression by the Δ*frdA* strain, which was lower than for the WT strain. This is likely due to the lower acetic acid concentration determined in Δ*frdA* supernatant samples (**Figures 22** and **19A**). In conclusion, *H. influenzae* CDM metabolic end products have a proinflammatory effect on cultured human airway epithelial cells, likely related to acetic acid levels present in the bacterial culture supernatants.

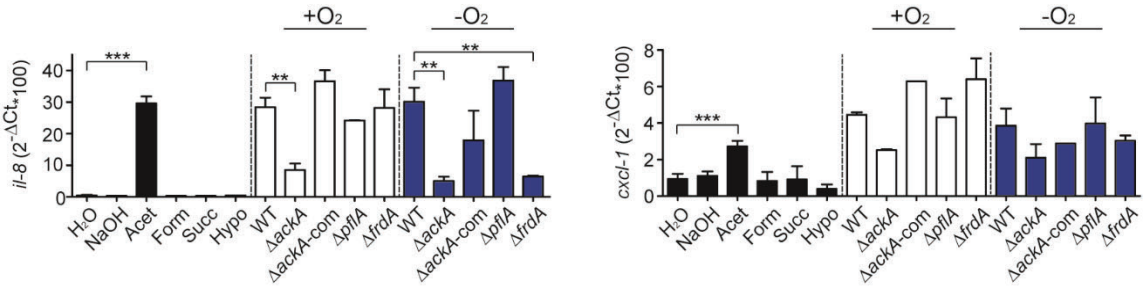

Figure 22. Bacterially produced glucose catabolism end products have a proinflammatory effect. A549 cells were incubated with acetic acid (20 mM), formic acid (1 mM), succinic acid (1 mM), hypoxanthine (7 mM), or vehicle solution (H_2O or 0.1 N NaOH) for 6 h in 0.3 mL of CDM (black bars). Alternatively, cells were incubated under the same conditions with 0.3 mL of CDM bacterial culture supernatants previously grown in aerobiosis (white bars) or anaerobiosis (blue bars) for 8 h. Relative quantities of human *il-8* (left panel) and *cxcl-1* (right panel) ($2^{-\Delta Ct} \times 100$) mRNA were measured by qRT-

PCR. Cell incubation with acetic acid increased *il-8* and *cxcl-1* gene expression, compared to the vehicle solution. Expression of the *il-8* and *cxcl-1* genes was lower when A549 cells were incubated with culture supernatants obtained from RdKW20Δ*ackA* than from WT bacteria. This effect was significant for *il-8* gene expression. This mutant deficiency was restored to WT levels by using culture supernatants of the complemented strain. Expression of the *il-8* gene was also lower in A549 cells incubated with culture supernatants of RdKW20Δ*frdA* than of WT bacteria grown in anaerobiosis. Data are shown as mean ± SD. Statistical comparisons of the means were performed with a one-way ANOVA (Tukey's multiple comparisons test). **$p < 0.001$, and ***$p < 0.0001$.

3.5. Supplementary Material

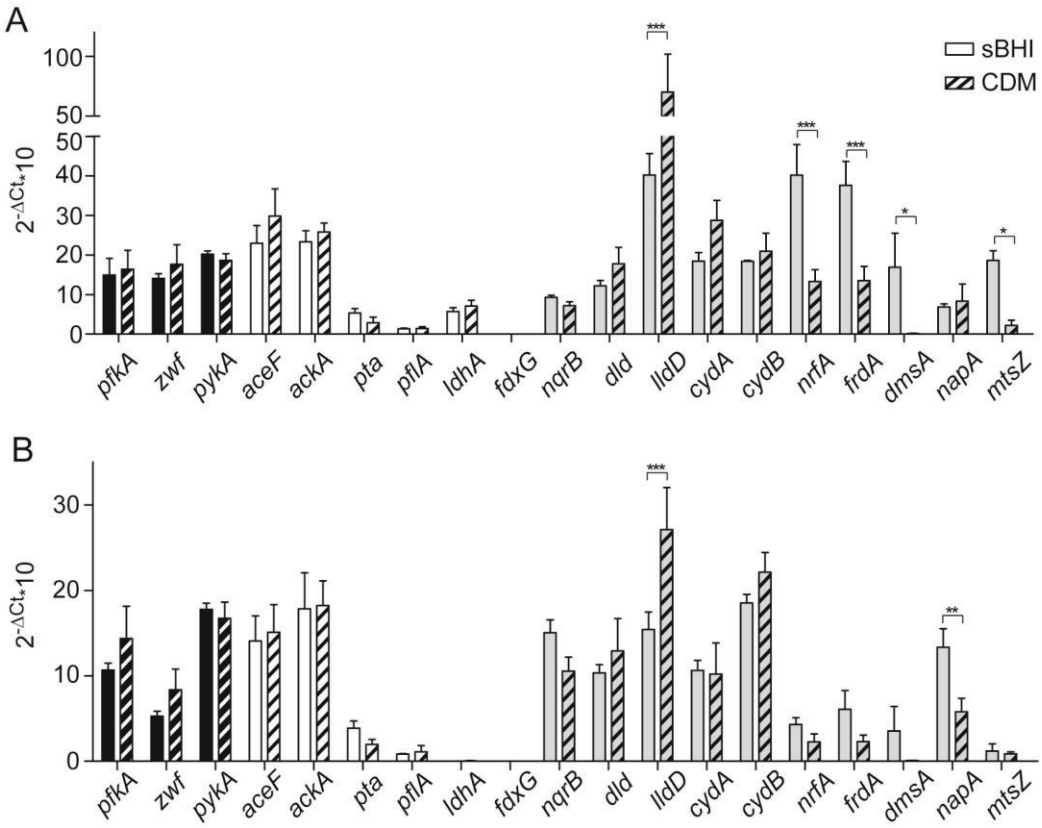

Figure S4. Growth medium modifies the expression of *H. influenzae* genes involved in central carbon metabolism and respiration. Expression of the *pfkA*, *zwf*, *pykA*, *aceF*, *ackA*, *pta*, *pflA*, *ldhA*, *fdxG*, *nqrB*, *dld*, *lldD*, *cydA*, *cydB*, *nrfA*, *frdA*, *dmsA*, *napA* and *mtsZ* genes in HiRdKW20 **(A)** and NTHi411 **(B)** strains, grown in sBHI or CDM, under aerobic conditions. Black bars: genes involved in glucose catabolism; white bars: genes relevant for pyruvate conversions; gray bars: genes relevant for respiratory metabolism. In both RdKW20 and NTHi411, the *lldD* gene expression was higher in CDM than in sBHI. In RdKW20, expression of the *nrfA*, *frdA*, *dmsA* and *mtsZ* genes was lower in CDM than in sBHI. In NTHi411, the *napA* gene expression was lower in CDM than in sBHI. Data are shown as mean±SD. Statistical comparisons of the means were performed with two-way ANOVA (Sidak´s multiple comparisons test). *p < 0.01, **p < 0.001, ***p < 0.0001.

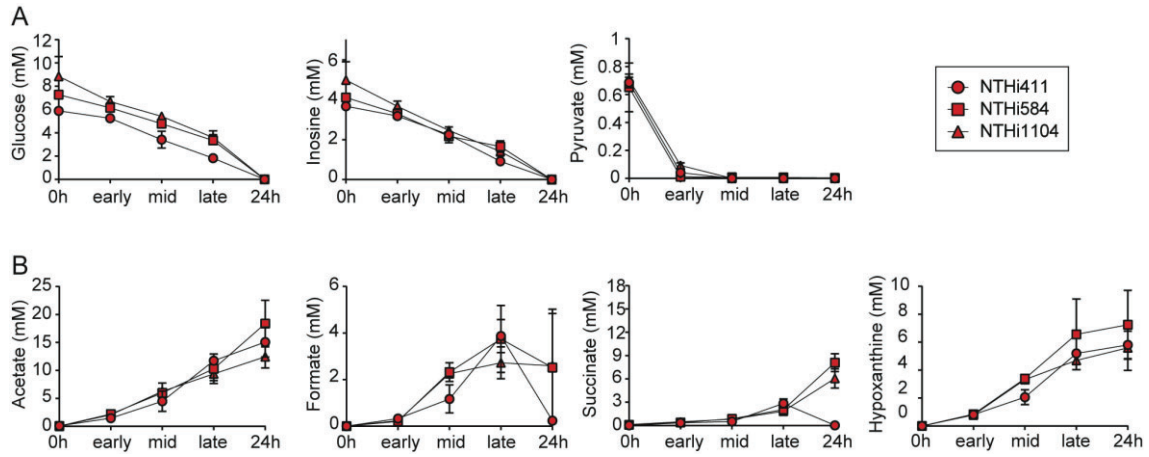

Figure S5. Changes in metabolite concentrations in cultures of *H. influenzae* NTHi411, NTHi584 and NTHi1104, grown under microaerophilic conditions. Strains are indicated in the right insert. NMR data shown is for three CDM growth substrates, glucose, inosine and pyruvate **(A)**, and for four metabolites produced during growth, acetate, formate, succinate and hypoxanthine **(B)**.

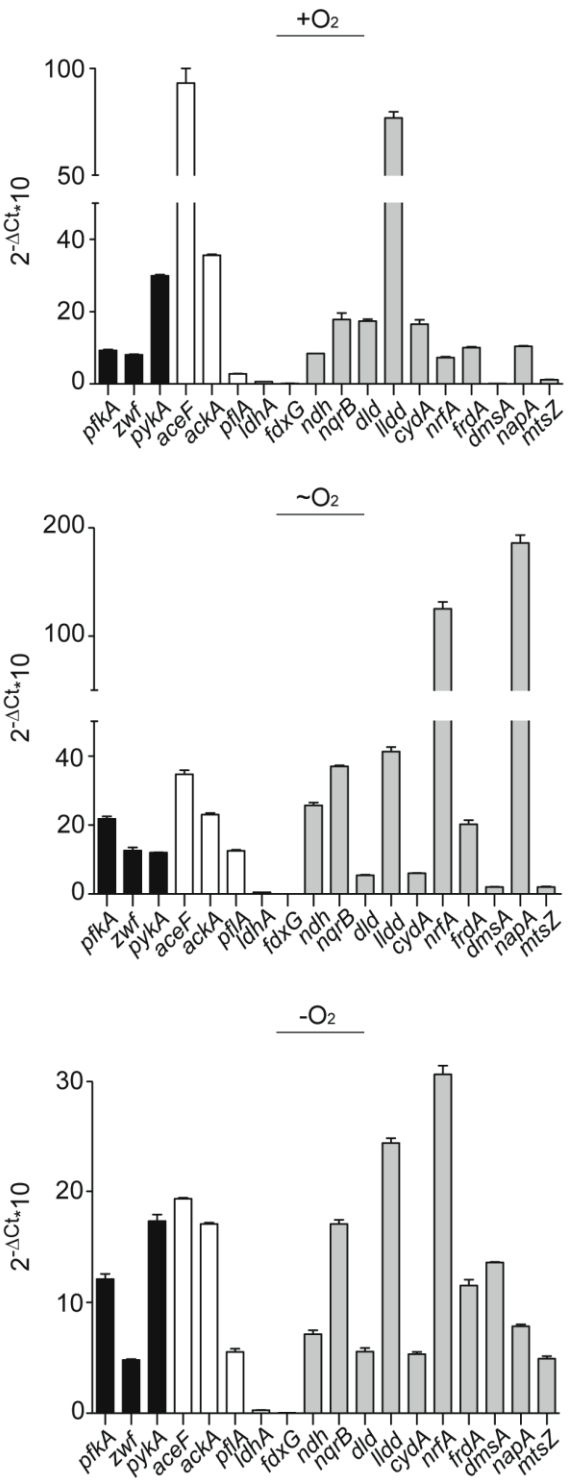

Figure S6. Expression of genes involved in central carbon metabolism and respiration in strain NTHi411. Expression of the *pfkA*, *zwf*, *pykA*, *aceF*, *ackA*, *pflA*, *ldhA*, *fdxG*, *ndh*, *nqrB*, *dld*, *lldD*, *cydA*, *nrfA*, *frdA*, *dmsA*, *napA*, *mtsZ* genes in NTHi411 grown in CDM medium under aerobic **(A)** microaerophilic **(B)** and anaerobic **(C)** conditions. Black bars: genes relevant for glucose catabolism; white bars: genes relevant for pyruvate conversion; gray bars: genes relevant for respiratory metabolism. Data are shown as mean±SD.

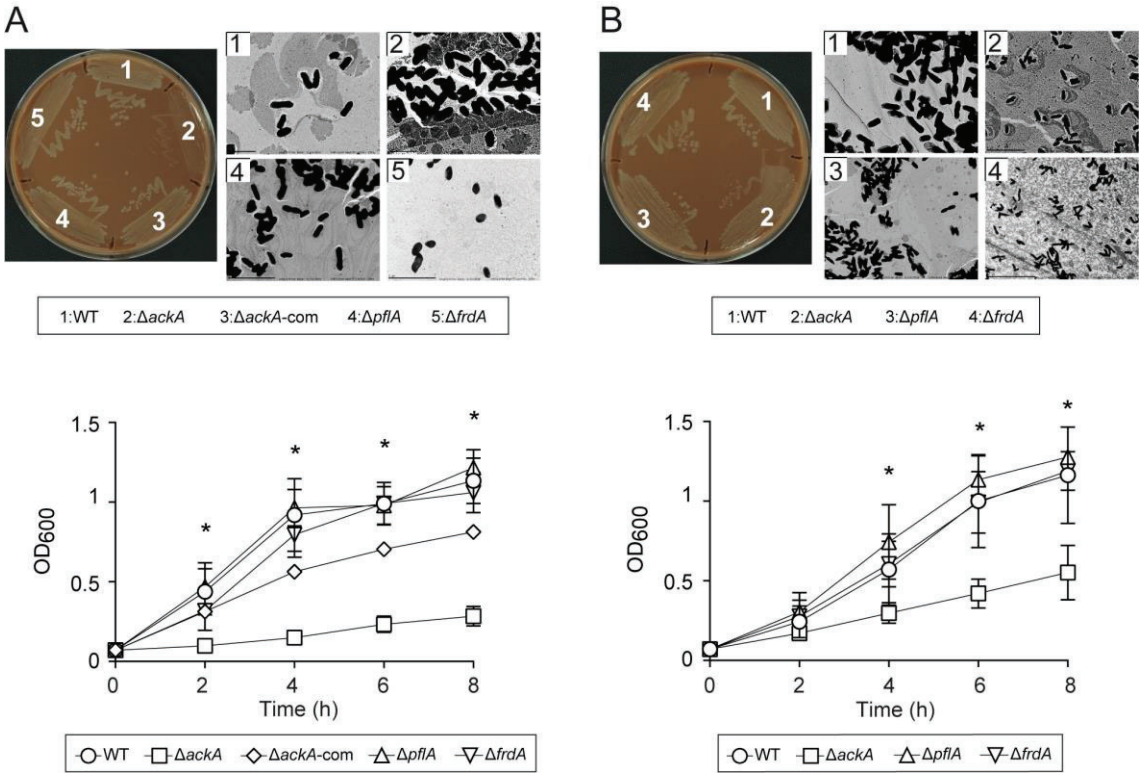

Figure S7. Effect of inactivating the *ackA*, *pflA* and *frdA* genes on *H. influenzae* growth and morphology. Data for RdKW20 and NTHi411 WT and mutant strains are shown in **(A)** and **(B)**, respectively. **(A)** Morphology at colony (left) and single bacteria (right) level, upon growth on chocolate agar. Data are shown for RdKW20 WT (1), Δ*ackA* (2), Δ*ackA*-com (3), Δ*pflA* (4), and Δ*frdA* (5) strains. Single bacterial morphology is shown by TEM. Magnification: WT, 15000x; Δ*ackA*, 15000x; Δ*pflA*, 10000x; Δ*frdA*, 10000x. Bottom panel: bacterial growth in sBHI shown as a mean of OD_{600}, at the indicated time points (mean±SD). RdKW20Δ*ackA* and Δ*frdA* showed lower OD_{600} than the WT strain (Δ*ackA*, $p<0.0001$ at all datapoints; Δ*frdA*, at 4 h, 6 h and 8 h, $p<0.005$). **(B)** Morphology at colony (left) and single bacteria (right) level, upon growth on chocolate agar. Data are shown for NTHi411 WT (1), Δ*ackA* (2), Δ*pflA* (3), and Δ*frdA* (4) strains. Single bacterial morphology is shown by TEM. Magnification: WT, 15000x; Δ*ackA*, 8000x; Δ*pflA*, 8000x; Δ*frdA*, 5000x. Bottom panel: bacterial growth in sBHI shown as a mean of OD_{600}, at the indicated time points (mean±SD). NTHi411Δ*ackA* showed lower OD_{600} than the WT strain (at 4 h $p<0.005$ and 6 h and 8 h, $p<0.0001$).

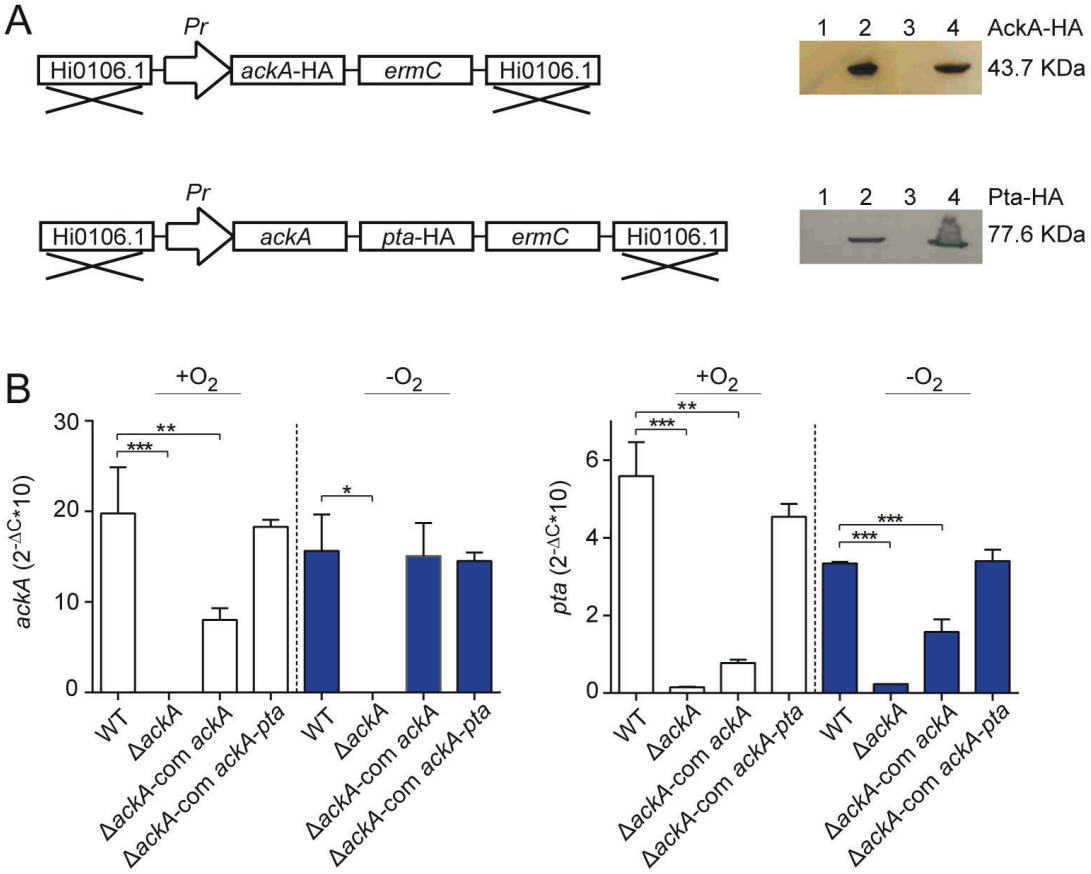

Figure S8. Supportive information on approaches employed for *H. influenzae* Δ*ackA* mutant complementation. (A) Upper panel: Δ*ackA* complementation cassette with the *ackA* gene and its promoter region, generated as it follows: the *ackA* gene with its promoter region was amplified from NTHi411 genomic DNA using primers *ackA*-COMP-*XhoI*-Fw and *ackA*-HA-COMP-*XhoI*-Rv. Primer *ackA*-HA-COMP-*XhoI*-Rv introduced a HA tail in the 3´end of the *ackA* gene. This PCR product (1,757 bp) was *Xho*I digested and cloned into *Xho*I-digested pUC19-HI0601.1-Erm (Fernández-Calvet et al., 2018), generating pUC19-HI0601.1-Erm-*Pr::ackA*. This plasmid was used as a template to amplify a 5,285 bp DNA fragment containing HI0601.1-flanked *Pr::ackA* by using primers HI0601.1-F1 and HI0601.1-R1, which was used to naturally transform RdKW20Δ*ackA*. Transformants were selected on sBHI agar with $Spec_{30}$ and Erm_{11}. AckA-HA (43.7 KDa) was monitored by western blot (WB). WB lanes: 1. *E. coli* Top10; 2. *E. coli* Top10 (pUC19-HI0601.1-Erm-*Pr::ackA*); 3. RdKW20 WT strain; 4. RdKW20Δ*ackA*-com *ackA*. Lower panel: RdKW20Δ*ackA* complementation cassette with the *ackA-pta* operon and its promoter region (for construct details, see Methods section). Pta-HA (77.6 KDa) was monitored by WB. WB lanes: 1. *E. coli* Top10; 2. *E. coli* Top10 (pUC19-HI0601.1::Erm-*Pr::ackA-pta*); 3. RdKW20 WT strain; 4. RdKW20Δ*ackA*-com *ackA-pta*. **(B)** Expression of the *ackA* and *pta* genes in RdKW20 WT, Δ*ackA* and Δ*ackA* complemented strains, exponentially grown in CDM, under aerobic and anaerobic conditions (mean±SEM). The *ackA* gene expression was not detected in RdKW20Δ*ackA* strain. Complementation with *Pr::ackA*-HA partially restored *ackA* gene expression in aerobiosis. The *pta* gene expression was lower in RdKW20Δ*ackA* and RdKW20Δ*ackA*-com *ackA* than in the WT strain. Complementation with *Pr::ackA-pta*-HA restored *ackA* and *pta* gene expression. RdKW20Δ*ackA*-com *ackA-pta* (from now on, named as RdKW20Δ*ackA*-com) was used in all phenotypic assays shown in this study. *p < 0.01, **p < 0.001, ***p < 0.0001.

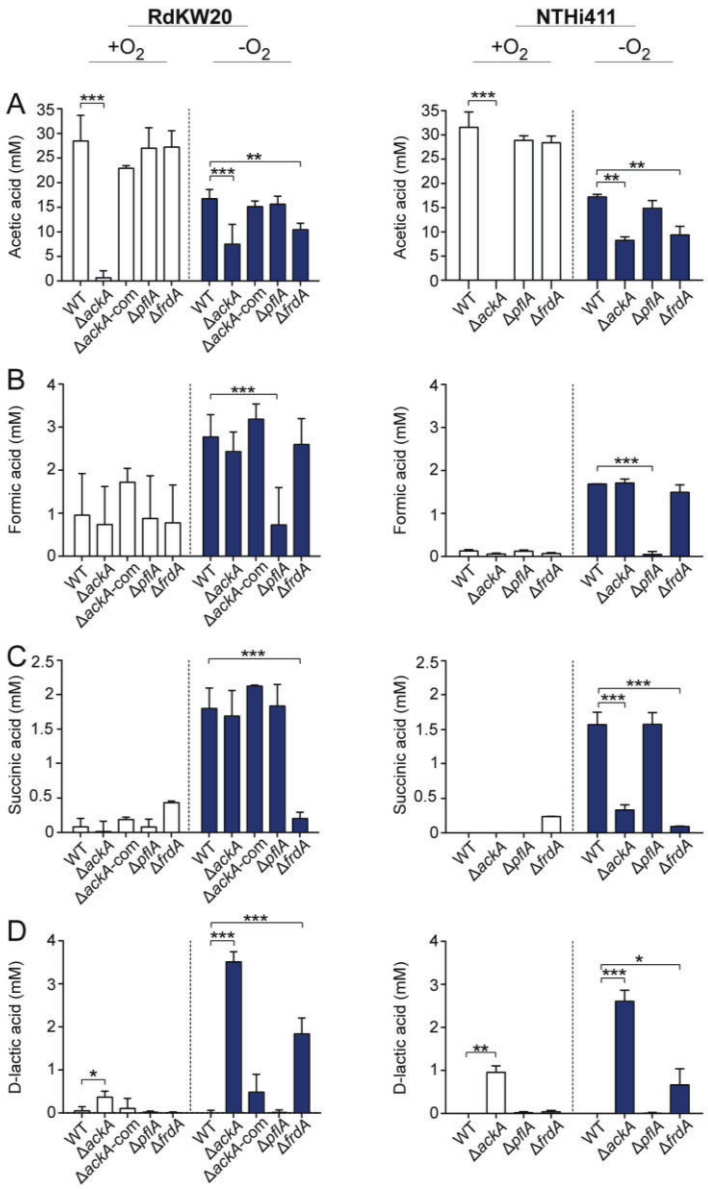

Figure S9. Inactivation of the *ackA*, *pflA* and *frdA* genes modifies *H. influenzae* production of glucose catabolism endproducts. Enzymatic measure of acetic (**A**), formic (**B**), succinic (**C**) and D-lactic (**D**) acid, determined on CDM bacterial culture supernatants grown for 24 h. Each metabolite concentration is shown as mM (mean±SD). Data for RdKW20 and NTHi411 strains are shown on the left and right columns, respectively. In RdKW20, reduced acetic acid levels were observed for the Δ*ackA* and Δ*frdA* mutants grown in aerobic and anaerobic conditions; decreased formic acid concentration was determined for Δ*pflA* grown in anaerobiosis; decreased succinic acid was found for Δ*frdA* under anaerobiosis; increased D-lactic acid level was measured for Δ*ackA*, and for Δ*frdA* (anaerobiosis) strains, compared to WT. In NTHi411, reduced acetic acid levels were measured for Δ*ackA* and Δ*frdA* mutants grown in aerobic and anaerobic conditions; decreased formic acid was quantified for Δ*pflA* bacteria grown in anaerobiosis; decreased succinic acid was measured for Δ*ackA* and Δ*frdA* mutants grown in anaerobiosis; increased D-lactic acid level was determined in Δ*ackA*, and for Δ*frdA* (anaerobiosis) strains, compared to WT. Statistical comparisons of the means with Two-way ANOVA (Dunnett's multiple comparisons test). *$p < 0.01$, **$p < 0.001$, ***$p < 0.0001$.

Table S6. Plasmids used in this study.

Plasmids	Description	Source
pJET1.2/blunt	Cloning vector	Thermofisher
pJET1.2-*ackA*	pJET1.2 derivative containing a 3,188 bp DNA fragment carrying the *ackA* gene (1,206 bp) and its upstream (1,000 bp) and downstream (982 bp) flanking regions	This study
pJET1.2-*pflA*	pJET1.2 derivative containing a 2,705 bp DNA fragment carrying the *pflA* gene (741 bp) and its upstream (964 bp) and downstream (995 bp) flanking regions	This study
pJET1.2-*frdA*	pJET1.2 derivative containing a 2,823 bp DNA fragment carrying the *frdA* gene (1800bp) and its upstream (510 bp) and downstream (513 bp) flanking regions	This study
pJET1.2-*ackA::spec*	pJET1.2-*ackA* derivative containing a 4,079 bp DNA fragment carrying an *ackA::spec* disruption cassette	This study
pJET1.2-*pflA::spec*	pJET1.2-*pflA* derivative containing a 4,050 bp DNA fragment carrying a *pflA::spec* disruption cassette	This study
pJET1.2-*frdA::ermC*	pJET1.2-*frdA* derivative containing a 3,337 bp DNA fragment carrying a *frdA::ermC* disruption cassette	This study
pUC19-HI0601.1-Erm-*Pr::ackA*	A 1,757 bp PCR fragment containing *Pr*::*ackA*-HA was *Xho*I digested and cloned into pUC19/Hi0601.1::*ermC* previously *Xho*I digested and de-P	This study
pUC19-HI0601.1-Erm	Cloning vector to generate mutant complementation cassettes to be inserted into the *H. influenzae* HI0601.1 pseudogene	(Fernández-Calvet et al., 2018)
pUC19-HI0601.1-Erm-*Pr::ackA-pta*	A 3,936 bp PCR fragment containing *Pr*::*ackA-pta*-HA was *Xho*I digested and cloned into pUC19/Hi0601.1::*ermC* previously *Xho*I digested and de-P	This study
pSBLerm	Source of an Erm^R cassette.	(Simon Allen et al., 2005)
pRSM2832	pKD13 derivative carrying a cassette containing a Spec resistance gene flanked by FRT sites	(Tracy et al., 2008)

Table S7. Key metabolites detected by HPLC in culture supernatants of CDM grown *H. influenzae* RdKW20 WT and mutant strains.

Strain		Glucose (mM)		Acetate (mM)		Succinate (mM)		Lactate (mM)	
		+O_2	**-O_2**	**+O_2**	**-O_2**	**+O_2**	**-O_2**	**+O_2**	**-O_2**
RdKW20	WT	n.d.	3.05±0.07	24.35±2.19	9.2±0.04	n.d.	13.03±0.3	n.d.	n.d.
	Δ*ackA*	6.24±0.15	3.93±0.18	1.17±0.23	8.38±0.38	n.d.	5.96±0.15	1.19±0.07	3.47±0.31
	Δ*pflA*	n.d.	1.11±0.13	21.51±0.76	10.4±2.53	n.d.	14.29±1.58	n.d.	n.d.
	Δ*frdA*	n.d.	7.26±0.52	21.52±0.05	5.6±0.47	0.4±0.01	n.d.	n.d.	1.67±0.19

Capítulo 4

Interrogation of essentiality in the reconstructed *Haemophilus influenzae* metabolic network identifies lipid metabolism antimicrobial targets: preclinical evaluation of a FabH β-ketoacyl-ACP synthase inhibitor

Nahikari López-López, David San León, Sonia de Castro, Roberto Díez-Martínez, Manuel Iglesias-Bexiga, María José Camarasa, Margarita Menéndez, Juan Nogales, Junkal Garmendia. Interrogation of essentiality in the reconstructed *Haemophilus influenzae* metabolic network identifies lipid metabolism antimicrobial targets: preclinical evaluation of a FabH β-ketoacyl-ACP synthase inhibitor. (Manuscript in preparation).

Capítulo 4. Interrogation of essentiality in the reconstructed *Haemophilus influenzae* metabolic network identifies lipid metabolism antimicrobial targets: preclinical evaluation of a FabH β-ketoacyl-ACP synthase inhibitor

Nahikari López-López[a], David San León[b], Sonia de Castro[c], Roberto Díez-Martínez[d], Manuel Iglesias-Bexiga[e], María José Camarasa[c], Margarita Menéndez[e,f], Juan Nogales[b], Junkal Garmendia[a,f,*].

a. Instituto de Agrobiotecnología, CSIC-Universidad Pública Navarra-Gobierno, Navarra, Spain .
b. Centro Nacional de Biotecnología, Consejo Superior de Investigaciones Científicas (CNB-CSIC), Madrid, Spain.
c. Instituto de Química Médica, Consejo Superior de Investigaciones Científicas (IQM-CSIC), Madrid, Spain.
d. Telum Therapeutics, Noain, Spain.
e. Instituto de Física Química Rocasolano, Consejo Superior de Investigaciones Científicas (IQFR-CSIC), Madrid, Spain.
f. Centro de Investigación Biomédica en Red de Enfermedades Respiratorias (CIBERES), Madrid, Spain.

*Corresponding author: Junkal Garmendia.

4.1. Abstract

Systems biology tools aid expediting drug discovery to fight antibacterial resistance. In this study, we focused on the human-adapted pathogen *Haemophilus influenzae* and built, validated and employed a high-quality *H. influenzae* genome-scale metabolic reconstruction for the rational identification of metabolic drug targets in this organism. Contextualization of available gene essentiality data within *in silico* predictions identified most genes involved in lipid metabolism as promising targets. We focused on the β-ketoacyl-acyl carrier protein synthase III FabH, responsible of catalyzing the first step in the FASII fatty acid synthesis pathway and feedback inhibition. Docking studies provided a plausible three-dimensional model of FabH in complex with the synthetic inhibitor 1-(5-(2-Fluoro-5-(hydroxymethyl)phenyl)pyridin-2-yl)piperidine-4-acetic acid (FabHi) bound to the catalytic triad Cys112-His243-Asn273 at FabH catalytic cavity. FabHi reduced *H. influenzae* viability in a dose and strain dependent manner, and independent of *fabH* gene expression levels. *fabH* allelic variation was observed among clinical isolates and many of these polymorphisms, relevant for stabilization of the dimeric active form of FabH and/or activity, may modulate the inhibitory effect as part of a complex multifactorial process, with the overall metabolic context emerging as a key factor for final antimicrobial potency. Synergies with antibiotics were not observed and bacteria were not prone to develop resistance. Inhibitor administration during *H. influenzae* infection on a zebrafish septicemia infection model cleared bacteria without signs of host toxicity. Overall, we highlight the potential of *H. influenzae* metabolism as a source of drug targets, metabolic models as target-screening tools and FASII targeting suitability to counteract this bacterial infection.

4.2. Introduction

Haemophilus influenzae is a human-adapted Gram-negative bacterial pathogen. Asymptomatic colonization begins in the upper airways, but it can spread through the respiratory tract and lead to invasive infections. The polysaccharide capsule vaccine has driven the almost complete disappearance of capsulated *H. influenzae* type b (Hib) in countries with established child immunisation programs (Jalalvand & Riesbeck, 2018; Slack et al., 2021). Instead, other *H. influenzae* serotypes and nontypeable strains (NTHi), untargeted by the Hib vaccine, emerge as important causes of infections. NTHi causes otitis media, conjunctivitis, sinusitis and lower respiratory infections in children; exacerbations of chronic obstructive pulmonary disease (COPD) and cystic fibrosis (CF) in adults; and invasive disease in neonates, immunocompromised adults, and the elderly (Ahearn et al., 2017; Duell et al., 2016; Jalalvand & Riesbeck, 2018; Su et al., 2018). Ampicillin-resistant *H. influenzae* is included in the WHO global priority list of bacteria for which new antibacterials are urgently needed (Tacconelli et al., 2018), fluoroquinolone-resistant *H. influenzae* has increased in recent years spreading worldwide with a variety in epidemiology, and the use of the macrolides in severe COPD patients to reduce hospital readmissions and exacerbation frequency may lead to decrease macrolide susceptibility (Pettigrew et al., 2016; Plusa, 2020; Wen et al., 2020). The current antibiotic resistance public health crisis prompted us to evaluate novel therapeutic alternatives against *H. influenzae*.

Bacterial metabolism and the effect of antimicrobial drugs are linked at several levels, in such a way that a metabolism-based approach may counteract antibiotic tolerance by the use of exogenous metabolites inducing antibiotic internalization, inhibiting antibiotic detoxification or extrusion, inducing endogenous oxidative stress, or priming to proton motive force (Liu et al., 2019, 2020). Also, inactivation of central metabolic enzymes may contribute to develop either antibiotic susceptibility or resistance (Baquero & Martínez, 2017; Gil-Gil et al., 2019; Vestergaard et al., 2017). One strategy to develop effective antimicrobial treatments is to identify and develop inhibitors of essential biological pathways, and bacterial metabolism is a source of drug targets as metabolic genes can be unconditionally essential. In this context, genome-scale network reconstructions of bacterial metabolism can serve as computational test-bed platforms to identify metabolic enzymes as potential targets (Lee et al., 2009; Mienda, 2017; Mienda et al., 2018). Such reconstructions are structured, species-specific knowledge bases that contain detailed information on the target organism such as the exact reaction stoichiometry and reversibility, relationships between genes, proteins, and reactions, as well as the biochemical and physiological data available at the time of the reconstruction. These reconstructions can be further converted into genome-scale models (GEMs) that enable computation of the metabolic capabilities and phenotype of a given organism (Fang et al., 2020).

H. influenzae was the first organism for which a GEM was constructed, just shortly after genome sequencing (Edwards & Palsson, 1999). This pioneer GEM laid the foundations of the field, while used to study minimal substrate requirements for the network to allow biomass production (Edwards & Palsson, 1999; Macfadyen & Redfield, 1996; Macfadyen et al., 1996; Schilling & Palsson, 2000). However, this initial model is far away of the increasing metabolic complexity and accuracy of current GEMs constructed for other bacteria and, in addition to account for a reduced metabolic coverage, it lacks the proper Gene-Protein-Associations (GPRs), cellular compartmentalization, and detailed Biomass Objective Function (BOF). Therefore, the available GEM of *H. influenzae* cannot be used for complex systems biology studies and presents a limited applicability (Monk et al., 2014). Here, we fill this gap by constructing and validating a high-quality GEM of *H. influenzae* strain RdKW20 (**Figure 23**). This new model, *i*NL638, was used to screen therapeutic targets in this bacterium by means of gene essentiality analysis, identifying fatty acid metabolism as a promising one. We focused on the FabH β-ketoacyl-ACP synthase at the initiating step of fatty acid synthesis. The antimicrobial activity of a good FabH inhibitor was thoroughly characterized *in vitro* and *in vivo* at the preclinical level using a wide set of NTHi clinical strains.

4.3. Material & Methods

4.3.1. Bacterial strains, media, growth conditions, and drugs

RdKW20 is a genome sequenced capsule-deficient laboratory strain (Fleischmann et al., 1995b). NTHi375 is a genome sequenced otitis media clinical isolate (Bouchet et al., 2003; López-Gómez et al., 2012; Mell et al., 2014b; Morey et al., 2011). NTHi COPD clinical strains belong to a previously genome sequenced strain collection (Moleres et al., 2018). Bacterial growth conditions are detailed in **Supplementary Methods.**

4.3.2. Determination of bacterial dry weight

Two to 3 colonies of the RdKW20 strain grown on PVX agar for 16 h were inoculated in 10 mL CDM using 100 mL flasks, and incubated for 11 h with shaking (100 r.p.m.). Cultures were then diluted to OD_{600}=0.07 in a final volume of 55, 40 or 25 mL CDM using 250 mL flasks, grown with shaking (180 r.p.m.) for ~3, 4 or 6 h, respectively. Then, 45, 30 and 15 mL were collected at OD_{600}=0.3, 0.4 and 0.8, respectively. Bacterial suspensions were centrifuged at 20.000 x *g* for 15 min at RT, pellets were instantly frozen in liquid N_2, directly transferred to a lyophilizer (LyoQuest, Telstar), lyophilized for 24 h at 0.020 mbar and -80ºC, and weighted. Using this procedure, we established a lineal relation (R^2=0,99) between OD and DW as follows: DW (g/L) = OD_{600} x 0.9097 (**Table S8**).

4.3.3. Constraints-based analysis

The *i*NL638 model was analysed with the COBRA Toolbox v2.0 (Schellenberger et al., 2011) within the MATLAB environment (The MathWorks Inc.) Gurobi, and the GNU Linear Programming Kit (http://www.gnu.org/software/glpk) were used for solving the linear programing problems. The constrain-based model consists of a 1162 x 1385 matrix containing all the stoichiometric coefficients in the model of 1162 metabolites and 1385 reactions (S). Flux balance analysis (FBA) was used to predict growth and flux distributions (Orth et al., 2010). FBA is based on solving a linear optimization problem by maximizing or minimizing a given objective function Z subject to a set of constraints. The constraints $S \cdot v = 0$ correspond to a situation of steady-state mass conservation where the change in concentration of the metabolites as a function of time is zero. The vector v represents the individual flux values for each reaction. These fluxes are further constrained by defining lower and upper limits for flux values. For reversible reactions an upper and lower bound of -1000 $mmol.gDW^{-1}.h^{-1}$ and 1000 $mmol.gDW^{-1}.h^{-1}$ were used, respectively. A lower bound of 0 $mmol.gDW^{-1}.h^{-1}$ was used in case of irreversible reactions. For simulating condition-specific growth conditions, lower bounds of the corresponding exchange reactions were modified accordingly.

4.3.4. Model constraints

The formulation of the *in silico* CDM was based on the experimental composition of this rich medium. The uptake of pyruvate, inosine, glucose, NAD, inosine and uracil was allowed as main nutrients in all the cases (López-López et al., 2020; Muda et al., 2019; Othman et al., 2014). Furthermore, complete (c) and minimal (m) CDM formulations (cCDM and mCDM) were used. cCDM allowed the uptake of the all amino acids, vitamins and inorganic salts present in the RPMI formulation (https://www.thermofisher.com/es/es/home/technical-resources/media-formulation.116.html), whereas the mCDM formulation only allowed the uptake of the inorganic salts and essential vitamins for growth (i.e. choline, pantothenate and folate). Detailed model constrains to simulate the cCDM and mCDM media are described in **Supplementary Methods**.

4.3.5. Essentiality analysis

Reaction essentiality analysis was performed using the *singleReactionDeletion* function implemented in the COBRA Toolbox. FBA (Orth et al., 2010) and minimization of metabolic adjustments (MOMA) (Segrè et al., 2002) methods were used. A lethal deletion was defined as that yielding <10% of the original model's growth rate values. Simulations for reaction essentiality were performed using both cCDM and mCDM for *i*NL638 under aerobic conditions (**Supplementary Methods**).

4.3.6. Synthesis of FabHi

The synthetic procedure for 1-(5-(2-Fluoro-5-(hydroxymethyl)phenyl)pyridin-2-yl)piperidine-4-acetic acid (compound **31** in (McKinney et al., 2016)), was performed by Maria José Camarasa's Research Group in Instituto de Química Médica. The analysis results of all compounds were in full accordance with depicted structures.

4.3.7. FabHi docking studies

Docking studies were performed with the AutoDock 4.2 (Morris et al., 2009) and AutoDock Vina (Trott & Olson, 2010) programs using the atomic coordinates of NTHi RdKW20 protein ($FabH_{RdKW20}$ from now on; Protein Data Bank: 3IL3) as receptor and FabHi as ligand. See details in **Supplementary Methods**.

4.3.8. Determination of FabHi antimicrobial effects

Experimental procedures to determine (i) dose dependent FabHi antibacterial effect under bacterial planktonic or biofilm growth, (ii) effect of the FabH inhibitor under serial passage; (iii) synergistic effects, are detailed in **Supplementary Methods.**

4.3.9. Bacteria gene expression analyses

Expression of the *fabH* gene was determined as indicated in **Supplementary Methods**, by using primers shown in **Table A9.**

4.3.10. Infection of cultured cells

A549 human alveolar basal epithelial cells (ATCC CCL-185) were employed. For details, see **Supplementary Methods**.

4.3.11. NTHi adult zebrafish infection

Animal experiments conducted at Ikan Biotech (https://www.ikanbiotech.com) animal housing facility were performed as previously described (Euba et al., 2017), according to the approval of the Universidad de Navarra (UNAV) Ethics Committee for Animal Experimentation (Protocol 107-19). To determine the maximum tolerated dose of FabHi, a toxicity assay was performed in zebrafish embryos following the guideline OECD TG236 "Fish embryo acute toxicity (FET) test" (OECD, 2013). Afterwards, six-month-old zebrafish with 0.30±0.08 g in weight were randomly divided into 2 infected and 2 uninfected groups (n=10/group). Infected groups were intraperitoneally injected 10 µL of an exponentially grown (OD_{600}=0.3) *H. influenzae* suspension containing $7x10^{10}$ c.f.u./mL ($7x10^{8}$ c.f.u./zebrafish), prepared in PBS. At 1 hpi, one infected and one uninfected group were intraperitoneally administered FabHi at a dose of 4 µg/zebrafish in 10 µL PBS by using a 35 mg/mL FabHi stock solution; the other two groups were administered PBS or vehicle solution, respectively.

Survival rate for each group was monitored three times per day for 4 days after infection. Experiments were performed in three independent occasions.

4.3.12. Statistical analyses

In all cases, a p value < 0.05 was considered statistically significant. Statistical analyses were performed using Prism software, version 7 for Mac (GraphPad Software, San Diego, CA, USA) statistical package, and are detailed in each Figure Caption.

4.4. Results

4.4.1. Construction, main features and consistence of *i*NL638, a high-quality model of *H. influenzae* RdKW20

H. influenzae RdKW20 metabolic reconstruction was addressed by using a well-known 4-step protocol (Thiele & Palsson, 2010) and the last genomic annotation of this strain at NCBI (**Figure 23**). A detailed description of model construction and manual curation is presented in **Supplementary Methods**. The final model, *i*NL638, contains 638 genes, 1385 reactions and 1162 non-unique metabolites distributed into three cellular compartments, external, periplasm and cytosol (**Table S9**). Compared to the previous *H. influenzae* model, *i*NL638 contains a significantly larger number of reactions and metabolites (**Table S9**). Reactions were classified into eleven major categories of which transport and cell envelope biosynthesis are the largest groups with 395 and 142, respectively (**Figure 24A**). Excluding transport, *i*NL638 accounts for a low number of orphan reactions (i.e., reactions known to be present in the network but with unknown encoding gene). Exchange reactions mimic the interaction of the biological network with its surrounding environment. A high number of exchange reactions (202, 15%) is present in *i*NL638, as previously found in highly metabolic versatile bacteria such as *Pseudomonas putida* (14%) (Nogales et al., 2020) and *E. coli* (13%) (Orth et al., 2011). *i*NL638 was evaluated using the Memote tool (https://memote.io/) (Lieven et al., 2020) to define its completeness, consistence and interoperability as a model while analysing potential flaws or shortcomings. The model's overall score was 91%, which suggests very good model completeness (**Dataset S2**). A limitation was the lack of annotation to outside references for some genes, metabolites, and reactions. This will only affect when using the model with certain automated tools or scripts, but its accuracy or usability should not be affected. The model scored 99% for the critical category of consistency, which represents accuracy in stoichiometry, mass balances, charge balances, connectivity of metabolites and reaction cycles. The Memote analysis demonstrated that *i*NL638 is a highly complete and detailed model that can be used as a reference for other GEM constructions. The model and scripts used in this study are freely accessible through github (https://github.com/SBGlab/Haemophilus_influenzae_GEM).

Accompanying datasets are accessible through the following link (https://www.dropbox.com/sh/60nbstp5jqntg9c/AACWWWCtE7L8q6_spjNnjH4Ia?dl=0)

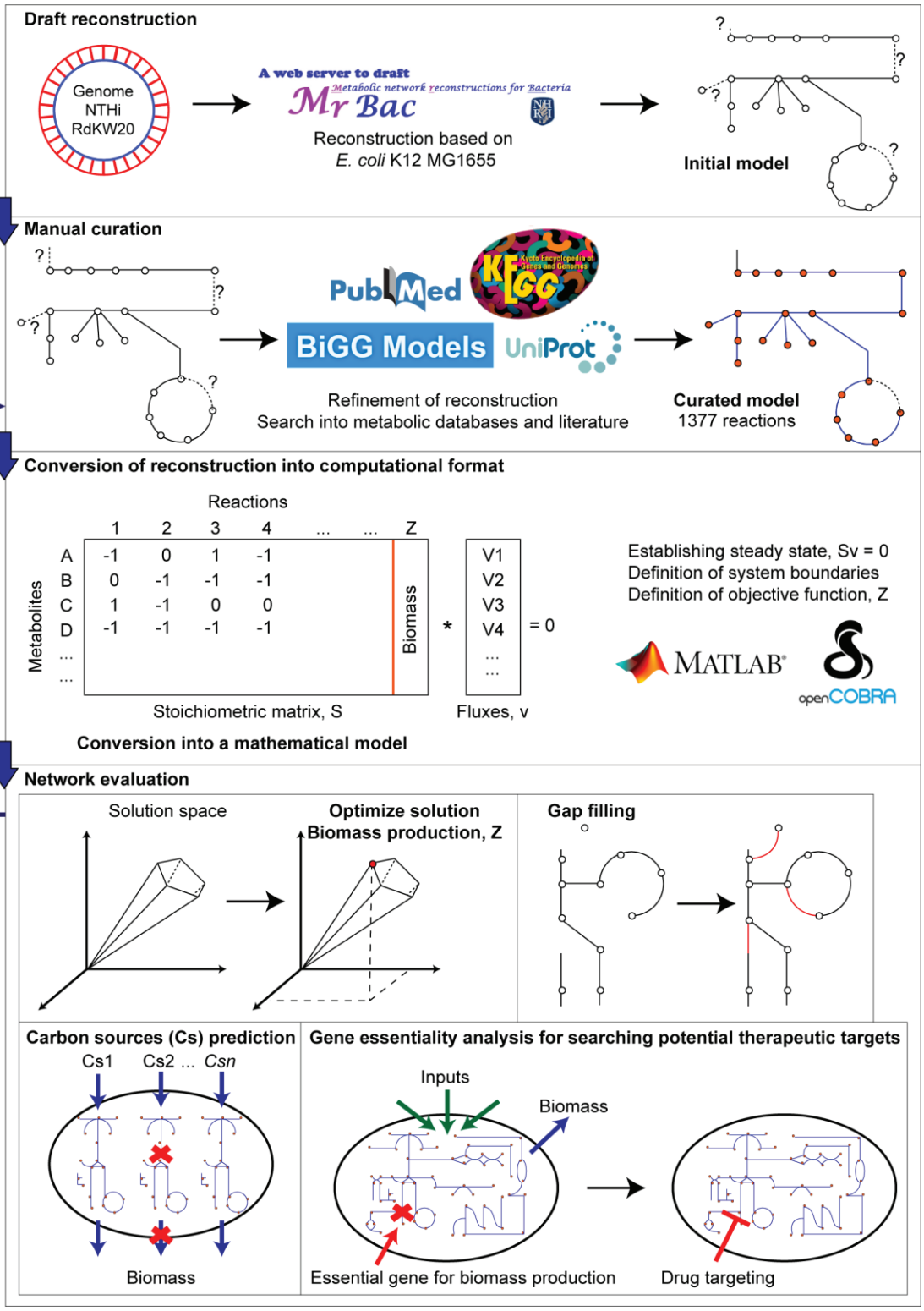

Figure 23. Roadmap for using *H. influenzae* metabolic reconstruction as a screening platform.

4.4.2. *i*NL638 accurately predicts *H. influenzae* RdKW20 main metabolic features

Large completeness and consistence does not always equate to a high-quality model and GEMs need to be validated by assessing their ability to compute physiological states (Thiele & Palsson, 2010). To validate *i*NL638, we evaluated its capability predicting well-known metabolic traits of RdKW20 such as the production of acetate and formate (López-López et al., 2020; Othman et al., 2014). In the absence of available experimental carbon flux distribution data, we addressed the ability of *i*NL638 to predict metabolic end products under changing oxygen tensions. For this, we used mCDM *in silico* media and monitored the secretion rates of acetate, formate and hypoxanthine as a function of the oxygen uptake. We identified three different steps (**Figure 24B**). In the absence of oxygen, we computed formate and acetate as main end products driving the lower growth rate. Under these conditions, formate was produced by the action of the pyruvate formate lyase (PFL) while acetate was produced from acetyl-CoA by the action of the phosphate acetyltransferase (PTA). *i*NL638 predicted PFL as major source of acetyl-CoA whereas the pyruvate dehydrogenase (PDH) only played a limited role (**Figure 24B**). Suboptimal oxygen uptake rates led a second phase characterized by an oxygen-dependent increase of the growth rate. During this phase, the flux through PFL decreased linearly; in fact, no flux was predicted at oxygen uptakes higher than 7 mmol/gDW.h^{-1}. As a consequence, formate secretion rates decreased in parallel. The role of acetyl-CoA as main source was taken by the PDH, which completely replaced PFL at oxygen uptakes higher than 7 mmol/gDW.h^{-1}. Finally, under optimal oxygen availability, we observed a stable growth rate being acetate the sole end product. These predictions fully agree with the switch in pyruvate metabolism, from PFL to PDH, observed in *H. influenzae* as oxygen become available (López-López et al., 2020). Higher levels of NADH provided by PDH are further funnelled to cytochrome bd oxidase via NADH:ubiquinone reductase, driving the generation of energy, a behaviour also accurately predicted by the model (**Figure 24B**). No flux through FDH was predicted in any condition while minor changes in the hypoxanthine secretion rate, resulting from the degradation of inosine, were monitored. These predictions are consistent with the negligible role of FDH under the conditions addressed and the little variation of inosine consumption reported for *H. influenzae* (Othman et al., 2014).

Overall, *i*NL638 predicts main carbon metabolism and energy generation in *H. influenzae* with large accuracy even under variable oxygen availability. It is ready to be used as a powerful predictive tool.

4.4.3. Defining condition independent gene essentiality in *H. influenzae*

The validated model was used to find metabolic drug targets based on gene essentiality predictions. Since gene essentiality assignment is largely dependent on culture conditions (Joyce &

Palsson, 2008; Nogales et al., 2012), we evaluated this property in well-defined situations. We first addressed RdKW20 minimal nutrient requirement in CDM and defined a minimal medium only including those nutrients required for growth (**Supplementary Methods**). Despite the presence of amino acids in the CDM composition, *i*NL638 grew in amino acid absence using nitrate as nitrogen source, thus suggesting lack of amino acid auxotrophies. *i*NL638 predicted as essential only a few additional CDM nutrients including uracil, NAD, protoheme, choline, pantothenate and thiamine. Since a robust drug target requires being condition independent, we evaluated the essentiality of *i*NL638 in this minimal CDM (mCDM) and the complete formulation (cCDM). We found 260 and 169 essential genes using minimal and complete CDM, respectively (**Dataset S3**). This analysis identified a total of 91 conditional essential genes whose requirement for growth is only visible using the mCDM formulation. We further evaluated the accuracy of *i*NL638 predictions against three available experimental gene essentiality studies (Gawronski et al., 2009; Mobegi et al., 2014; Wong et al., 2013). Overall, we found higher accuracies (0.72-0.761) and specificities (0.84-0.882) in predictions performed using cCDM (**Figure S11**). Experimental datasets were constructed using the rich medium sBHI. Therefore, most discrepancies between *in vivo* and *in silico* data are likely due to the different media composition. We found similar accuracy and sensitivities when comparing the different experimental studies to each other, thus suggesting that the gene essentiality analysis is also study-dependent (**Figure S12**).

The large diversity of gene essentiality datasets analysed and discrepancies found led us to perform an enrichment analysis for both the *in silico* and experimental datasets to identify subsystems overrepresented in all cases (**Figure 24C**). This analysis showed a significant enrichment of metabolic genes in the *in silico* datasets, while non-metabolic genes were more abundant in experimental datasets. This is due to the fact that genes other than encoding metabolic functions are not included in GEMs. Noteworthy, genes related with fatty acid metabolism were present in all available studies suggesting this subsystem as a condition-independent essential metabolic hub. Indeed, from the 89 genes predicted to be essential in all conditions, 29 were involved in lipid metabolism (**Figure 24D**, **Table 5**, **Dataset S3**). Together, the gene essentiality analysis performed using *in silico* predictions performed with *i*NL638 in the context of previous experimental studies largely shows fatty acid metabolism as containing promising *H. influenzae* drug targets.

4.4.4. Model-based search of *H. influenzae* essential genes highlights lipid metabolism targets

When focusing on lipid metabolism, our analysis predicted essentiality for 11 genes encoding fatty acid biosynthesis enzymes (FASII pathway), 6 genes encoding enzymes required for phospholipid biosynthesis, and 12 genes encoding enzymes involved in lipid A biosynthesis (**Figure S13**, **Table 5**, **Dataset S3**). The *H. influenzae* FASII pathway generates the acyl-ACP (acyl carrier

protein) and β-hydroxyacyl-ACP products, which are key components of the bacterial membrane. Acyl-ACP is used by the 1-acyl-*sn*-glycerol-3-phosphate (PslB) and 1-acyl-*sn*-glycerol-3-phosphate (PslC) acyltransferases to generate phosphatidic acid, the precursor of *H. influenzae* phospholipids phosphatidyl ethanolamine (PE) and phosphatidyl glycerol (PG) (Fernandez-Calvet et al., 2018); β-hydroxyacyl-ACP molecules are substrates for the acyltransferases catalyzing the initial steps in the lipid A biosynthesis (Raetz et al., 2007). Predicted essentiality and the selective targeting of the FASII pathway, due to significant differences in the structure of eukaryotic and bacterial fatty acid synthesis systems, make it an attractive target for drug discovery.

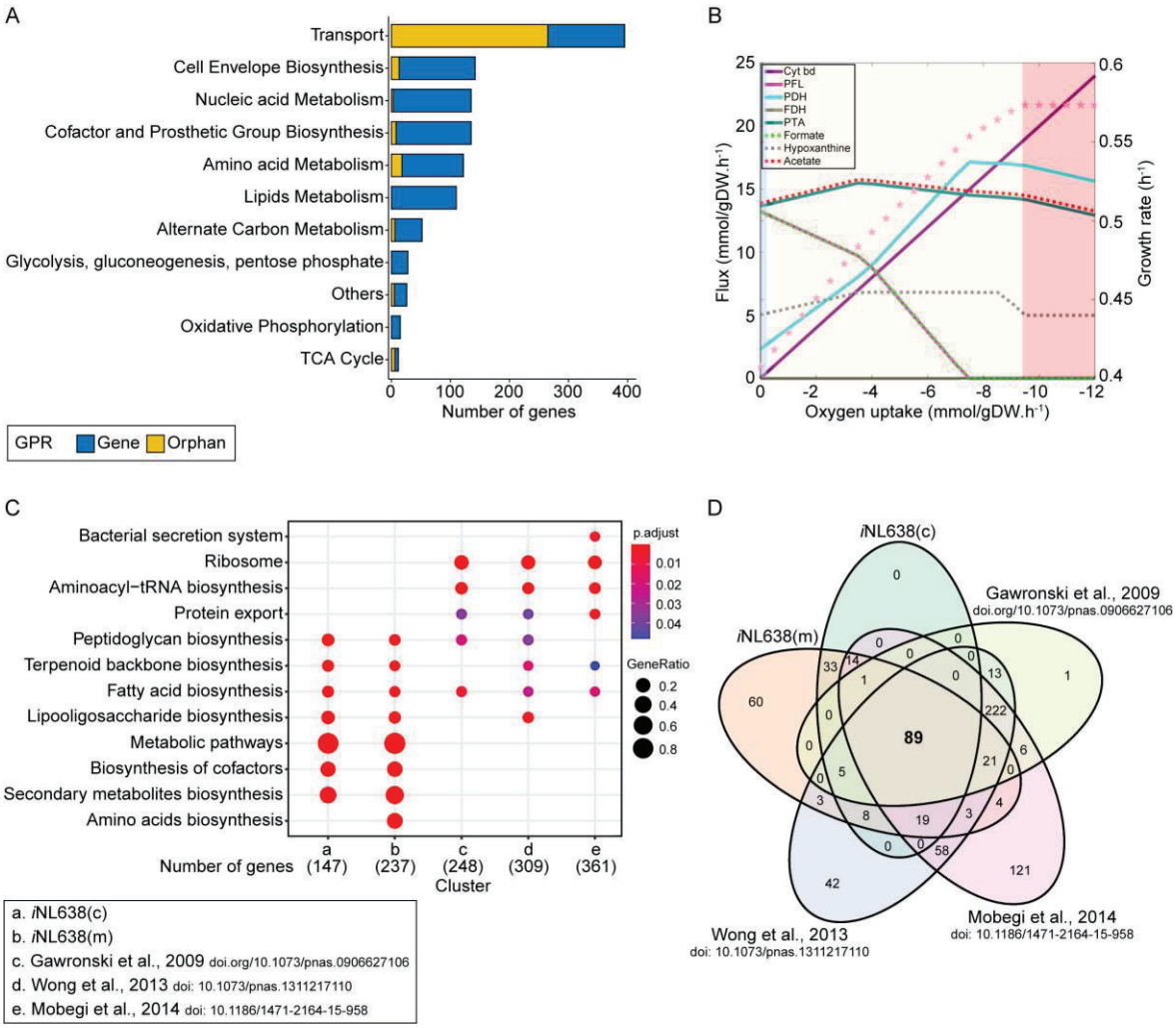

Figure 24. Analysis of *i*NL638 main features and capabilities. (A) Major categories of metabolic reactions contained in our *i*NL638 model. Reactions can be gene-associated, or orphan if there is no gene involved in process or gene is unknown. **(B)** Evolution of pyruvate metabolism and metabolic end product as a function of oxygen availability. The metabolic behaviour of *H. influenzae* was predicted under anaerobic (blue), microaerobic (yellow), and aerobic (red) conditions. Minimal CDM medium (SI) using glucose and pyruvate as carbon source was used and the fluxes thought pyruvate dehydrogenase (PDH), pyruvate formate lyase (PFL), formate dehydrogenase (FDH), phosphotransacetylase (PTA) were monitored as well as the secretion rates of formate, acetate and hypoxanthine. **(C)** KEGG-based gene essential enrichment. Only genes annotated in KEGG were used for this analysis. **(D)** Venn diagram showing the intersections between predicted essential genes commonly found when comparing our *i*NL638 model-based screening and three previous independent studies. We found 89 genes predicted to be essential among studies, mostly involved in the metabolism of fatty acids **(C)**.

Table 5. Genes predicted to be essential by *i*NL638-screening commonly found by (Gawronski et al., 2009; Mobegi et al., 2014; Wong & Akerley, 2012)

Pathway		ED no.	Gene	Enzyme
Lipid metabolism	FASII		HI0154 (*acpP*)	Acyl carrier protein
		1.1.1.100	HI0155 (*fabG*)	3-oxoacyl-[acyl-carrier-protein] reductase FabG
		2.3.1.39	HI0156 (*fabD*)	Malonyl CoA-acyl carrier protein transacylase
		2.3.1.180	HI0157 (*fabH*)	3-oxoacyl-[acyl-carrier-protein] synthase 3
		2.1.3.15	HI0406 (*accA*)	Acetyl-coenzyme A carboxylase carboxyl transferase subunit alpha
			HI0971 (*accB*)	Biotin carboxyl carrier protein of acetyl-CoA carboxylase
		6.3.4.14 6.4.1.2	HI0972 (*accC*)	Biotin carboxylase
		2.1.3.15	HI1260 (*accD*)	Acetyl-coenzyme A carboxylase carboxyl transferase subunit beta
		4.2.1.59 5.3.3.14	HI1325 (*fabA*)	3-hydroxydecanoyl-[acyl-carrier-protein] dehydratase
		2.3.1.41	HI1533 (*fabB*)	3-oxoacyl-[acyl-carrier-protein] synthase 1
		1.3.1.9	HI1734 (*fabI*)	Enoyl-[acyl-carrier-protein] reductase [NADH] FabI
	Lipid A	2.7.7.38	HI0058 (*kdsB*)	3-deoxy-manno-octulosonate cytidylyltransferase
		2.7.1.130	HI0059 (*lpxK*)	Tetraacyldisaccharide 4'-kinase
		7.5.2.6	HI0060 (*msbA*)	ATP-dependent lipid A-core flippase
		2.7.1.166	HI0260.1 (*kdkA*)	3-deoxy-D-manno-octulosonic acid kinase
		2.4.99.12	HI0652 (*kdtA*)	3-deoxy-D-manno-octulosonic acid transferase
		3.6.1.54	HI0735 (*lpxH*)	UDP-2,3-diacylglucosamine hydrolase
		2.3.1.-	HI0915 (*lpxD*)	UDP-3-O-acylglucosamine N-acyltransferase
		2.4.1.182	HI1060 (*lpxB*)	Lipid-A-disaccharide synthase
		2.3.1.129	HI1061 (*lpxA*)	Acyl-[acyl-carrier-protein]--UDP-N-acetylglucosamine O-acyltransferase
		3.5.1.108	HI1144 (*lpxC*)	UDP-3-O-acyl-N-acetylglucosamine deacetylase

		2.3.1.241	HI1527 (*htrB*)	Lipid A biosynthesis lauroyltransferase
		2.5.1.55	HI1557 (*kdsA*)	2-dehydro-3-deoxyphosphooctonate aldolase
	Phospholipids	2.7.8.5	HI0123 (*pgsA*)	CDP-diacylglycerol--glycerol-3-phosphate 3-phosphatidyltransferase
		4.1.1.65	HI0160 (*psd*)	Phosphatidylserine decarboxylase proenzyme
		2.7.1.107	HI0335 (*dgkA*)	Diacylglycerol kinase
		2.7.8.8	HI0425 (*pssA*)	CDP-diacylglycerol--serine O-phosphatidyltransferase
		2.3.1.15	HI0748 (*plsB*)	Glycerol-3-phosphate acyltransferase
		2.7.7.41	HI0919 (*cdsA*)	Phosphatidate cytidylyltransferase
Peptidoglycan biosynthesis		2.7.2.4 1.1.1.3	HI0089 (*thrA*)	Bifunctional aspartokinase/homoserine dehydrogenase
		3.5.1.18	HI0102 (*dapE*)	Succinyl-diaminopimelate desuccinylase
		4.3.3.7	HI0255 (*dapA*)	4-hydroxy-tetrahydrodipicolinate synthase
		1.3.1.98	HI0268 (*murB*)	UDP-N-acetylenolpyruvoylglucosamine reductase
		2.4.1.129 3.4.16.4	HI0440 (*ponA*)	Penicillin-binding protein 1A
		2.7.7.23 2.3.1.157	HI0642 (*glmU*)	Bifunctional protein GlmU
		1.2.1.11	HI0646 (*asd*)	Aspartate-semialdehyde dehydrogenase
		5.1.1.7	HI0750 (*dapF*)	Diaminopimelate epimerase
		2.5.1.31	HI0920 (*uppS*)	Ditrans,polycis-undecaprenyl-diphosphate synthase ((2E,6E)-farnesyl-diphosphate specific)
		2.5.1.7	HI1081 (*murA*)	UDP-N-acetylglucosamine 1-carboxyvinyltransferase
		6.3.2.13	HI1133 (*murE*)	UDP-N-acetylmuramoyl-L-alanyl-D-glutamate--2,6-diaminopimelate ligase
		6.3.2.10	HI1134 (*murF*)	UDP-N-acetylmuramoyl-tripeptide--D-alanyl-D-alanine ligase
		2.7.8.13	HI1135 (*mraY*)	Phospho-N-acetylmuramoyl-pentapeptide-transferase
		6.3.2.9	HI1136 (*murD*)	UDP-N-acetylmuramoylalanine--D-glutamate ligase
		2.4.1.227	HI1138 (*murG*)	UDP-N-acetylglucosamine--N-acetylmuramyl-(pentapeptide) pyrophosphoryl-undecaprenol N-acetylglucosamine transferase

		6.3.2.8	HI1139 (*murC*)	UDP-N-acetylmuramate--L-alanine ligase
		6.3.2.4	HI1140 (*ddl*)	D-alanine--D-alanine ligase
		1.17.1.8	HI1308 (*dapB*)	4-hydroxy-tetrahydrodipicolinate reductase
		2.3.1.117	HI1634 (*dapD*)	2,3,4,5-tetrahydropyridine-2,6-dicarboxylate N-succinyltransferase
		5.1.1.3	HI1739.2 (*murI*)	Glutamate racemase
Amino acids metabolism	Phenylalanine, tyrosine and tryptophan	4.2.3.5	HI0196 (*aroC*)	Chorismate synthase
		2.7.1.71	HI0207 (*aroK*)	Shikimate kinase
		4.2.3.4	HI0208 (*aroB*)	3-dehydroquinate synthase
		2.5.1.54	HI1547 (*aroG*)	Phospho-2-dehydro-3-deoxyheptonate aldolase
		2.5.1.19	HI1589 (*aroA*)	3-phosphoshikimate 1-carboxyvinyltransferase
	Methionine	2.5.1.6	HI1172 (*metK*)	S-adenosylmethionine synthase
		3.2.2.9	HI1216 (*mtnN*)	5'-methylthioadenosine/S-adenosylhomocysteine nucleosidase
	Alanine	5.1.1.1	HI1575 (*alr*)	Alanine racemase
Isopentenyl biosynthesis		1.17.7.3	HI0368 (*ispG*)	4-hydroxy-3-methylbut-2-en-1-yl diphosphate synthase (flavodoxin)
		4.6.1.12	HI0671 (*ispF*)	2-C-methyl-D-erythritol 2,4-cyclodiphosphate synthase
		1.1.1.267	HI0807 (*ispC*, *dxr*)	1-deoxy-D-xylulose 5-phosphate reductoisomerase
		2.5.1.90	HI0881 (*ispB*)	Octaprenyl diphosphate synthase
		1.17.7.4	HI1007 (*ispH*)	4-hydroxy-3-methylbut-2-enyl diphosphate reductase
		2.2.1.7	HI1439 (*dxs*)	1-deoxy-D-xylulose-5-phosphate synthase
		2.7.1.148	HI1608 (*ispE*)	4-diphosphocytidyl-2-C-methyl-D-erythritol kinase
Quinone biosynthesis		2.2.1.9	HI0283 (*menD*)	2-succinyl-5-enolpyruvyl-6-hydroxy-3-cyclohexene-1-carboxylate synthase
		5.4.4.2	HI0285 (*menF*)	Isochorismate synthase MenF
		2.5.1.74	HI0509 (*menA*)	1,4-dihydroxy-2-naphthoate octaprenyltransferase
		4.1.3.36	HI0968 (*menB*)	1,4-dihydroxy-2-naphthoyl-CoA synthase

		4.2.1.113	HI0969 (*menC*)	o-succinylbenzoate synthase
Transport systems			HI0139 (*ompP2*)	Outer membrane protein P2
			HI0625 (*trkA*)	Trk system potassium uptake protein TrkA
			HI1035 (*corA*)	Magnesium transport protein CorA
			HI1641 (*sapD*)	Peptide transport system ATP-binding protein SapD
Nucleotide metabolism		2.7.4.3	HI0349 (*adk*)	Adenylate kinase
		2.7.4.22	HI1065 (*pyrH*)	Uridylate kinase
		2.7.4.8	HI1743 (*gmk*)	Guanylate kinase
Iron-sulfur cluster metabolism			HI0376 (*iscA*)	Iron-binding protein IscA
			HI0377 (*iscU*)	Iron-sulfur cluster assembly scaffold protein IscU
		2.8.1.7	HI0378 (*nifS*)	Cysteine desulfurase IscS
Vitamins metabolism		1.5.1.5 3.5.4.9	HI0609 (*folD*)	Bifunctional protein FolD
		1.5.1.3	HI0899 (*folA*)	Dihydrofolate reductase
		2.7.1.26 2.7.7.2	HI0963 (*ribF*)	Bifunctional riboflavin kinase/FMN adenylyltransferase
Coenzyme A biosynthesis		2.7.1.33	HI0631 (*coaA*)	Pantothenate kinase
		2.7.1.24	HI0890m (*coaE*)	Dephospho-CoA kinase
		4.1.1.36 6.3.2.5	HI0953 (*coaBC*)	Coenzyme A biosynthesis bifunctional protein CoaBC
Protein modification		2.8.1.8	HI0026 (*lipA*)	Lipoyl synthase
		2.3.1.181	HI0027 (*lipB*)	Octanoyltransferase
NAD metabolism		2.7.1.23	HI0072 (*nadK*)	NAD kinase
Sugar metabolism		2.2.1.1	HI1023 (*tktA*)	Transketolase

A key FASII enzyme is the β-ketoacyl-acyl carrier protein synthase III FabH, which initiates the fatty acid elongation cycles by catalyzing the condensation reaction between a CoA-attached acetyl group and an ACP-attached malonyl group, yielding β-ketoacyl-ACP. This gene was found to be essential both in computational and experimental analysis (**Table 5**, **Dataset S3**). Additionally, we unsuccessfully tried to inactivate it in the RdKW20 strain (**Supplementary Material**), largely supporting its essentiality under laboratory conditions. FabH has no significant homologous proteins in humans, and small molecule inhibitors could lead to selective nontoxic antibacterials (McKinney et al., 2016; Wang et al., 2020; Wang et al., 2019). Natural products and chemically synthesized FabH inhibitors have been reported, and half-maximal inhibitory concentration (IC_{50}) determined for some of them (McKinney et al., 2016; Young et al., 2006). The previously described FabH inhibitor 1-(5-(2-Fluoro-5-(hydroxymethyl)phenyl)pyridin-2-yl)piperidine-4-acetic acid (compound **31** in (McKinney et al., 2016); from now on FabHi, **Figure 25A**) was chosen for further study because i) its potent inhibition of *H. influenzae* FabH activity (IC_{50}=0.82 μM), ii) high solubility, acceptable human plasma protein binding, and easy chemical accessibility (McKinney et al., 2016), and iii) feasibility of visualizing its mode of binding by molecular docking.

4.4.5. *In silico* envisioning of FabHi binding mode

FabH displays two similarly folded N-terminal and C-terminal halves, which differ in loops and insertion sequences (**Figure S14**) (Gajiwala et al., 2009). FabH core primarily provides a supportive structural scaffold while insertion sequences are mainly involved in substrate recognition and catalysis. To visualize the interaction mode, FabHi was docked into the active site of $FabH_{RdKW20}$. The lowest energy complex, obtained with AutoDock, placed FabHi at the substrate binding cavity with the hydroxymethyl group of the phenyl ring hydrogen bonded to Cys112–His243–Asn273 catalytic triad, and the carboxylic group of the piperidine ring forming three additional hydrogen bonds with Arg36 (**Figure 25B** and **Figure S15**). Also, the 2-fluoro-5-(hydroxymethyl)phenyl ring makes many favorable hydrophobic interactions through the ring carbon atoms (Met206, Thr211, Ala215, Ala245, Phe303), the hydroxylmethyl chain (Cys 112, Leu189, His 243, Asn273) and the fluoro group (Ala215), as depicted in **Figure S15C**. Hydrophobic contacts with Ala245 further extend to the pyridine ring, whose nitrogen atom interacts with Phe212. Besides, the piperidine ring makes additional contacts through the its carbon atoms (Asn246, Arg248, Leu156 and Arg36) and the carboxylic group (Arg36). Van der Waals interactions might also contribute to stabilize the complex. The intricate network of inhibitor-protein interactions predicted for the FabHi:$FabH_{RdKW20}$ complex fairly agrees with the contacts described for structurally related inhibitors in complex with *E. coli* FabH (McKinney et al., 2016), as also does the inhibitor disposition within the binding cavity (**Figure S15**). Besides, single point mutations at positions predicted to interact with the inhibitor (Ala215Val, Ala251Ser or Ala245Ser) significantly increased the resistance of *H. influenzae* to a

close structural analogue of FabHi (McKinney et al., 2016), supporting the plausibility our docking model.

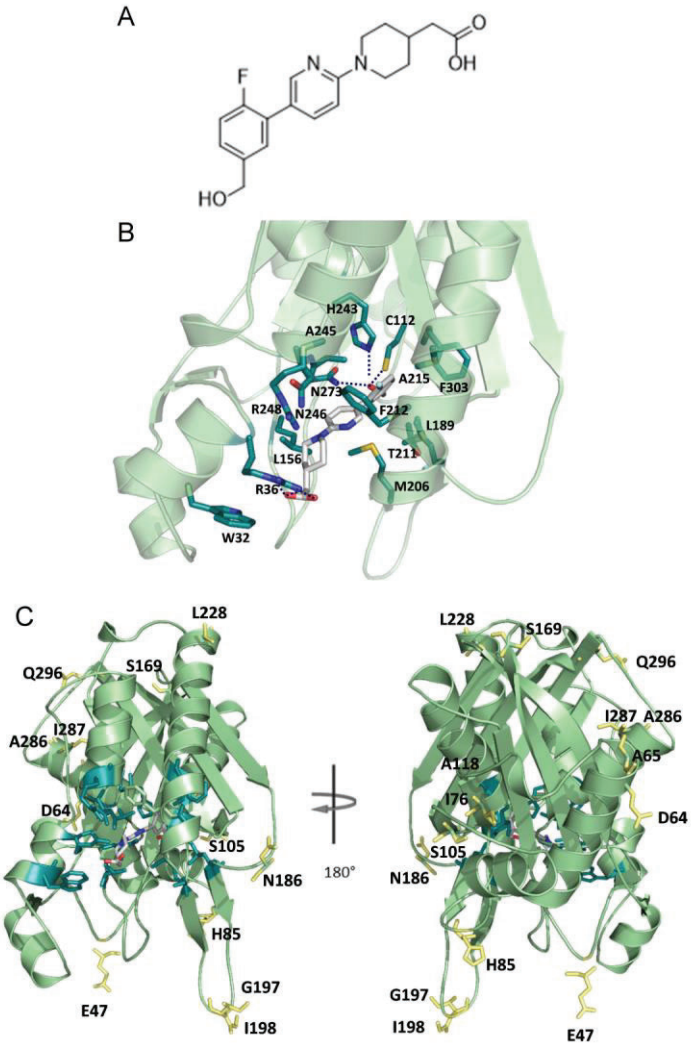

Figure 25. FabHi mode of binding. (A) Structure of FabHi. **(B)** Stick representation of FabHi in the best complex model with $FabH_{RdKW20}$, obtained with AutoDock4.2. FabH (cartoon) is depicted in light green with sides chains of residues involved in inhibitor binding in stick representation (dark green); polar contacts are represented as dotted lines. Some relevant residues are key as well in CoA binding (Trp32, Arg36, Phe212 and Asn246) and likely in ACP binding (Arg36 and Arg248), according to *E. coli* FabH structures (Qiu et al., 1999). **(C)** Residues showing polymorphism in FabH allelic variants, depicted as yellow sticks, locate out the substrate binding cavity (FabHi binding-residues in dark green).

4.4.6. FabHi has an antimicrobial effect on *H. influenzae* growth

Previous to antimicrobial effect testing, we tried to improve FabHi solubility by preparing different salts (**Figure S16**). Final assays were performed with the free acid form as it produced a higher and more homogeneous loss of *H. influenzae* viability.

Our metabolic model and $FabH_{RdKW20}$:FabHi complex structure relied on the *H. influenzae* RdKW20 genome content and $FabH_{RdKW20}$ crystal structure (Fleischmann et al., 1995; Gajiwala et al., 2009), respectively. However, *H. influenzae* strains show high genomic and phenotypic diversity

(Ahearn et al., 2017; López-López et al., 2021). To anticipate the potential role of FadHi as broad inhibitor of *H. influenzae*, we examined the sequence variability of the *fabH* locus across a well-characterized genome-sequenced set of strains collected from COPD sputum samples over time, grouped in clonal types (CTs) (Fernández-Calvet, et al., 2021; Moleres et al., 2018). Being present in all strains, best hits to *fabH* were extracted, followed by translation and multiple alignments. The NTHi375 reference strain was also included in this analysis (Bouchet et al., 2003; López-Gómez et al., 2012; Mell et al., 2014b; Morey et al., 2011). Fourteen different *fabH* allelic variants were found (alleles 1 to 14, i.e. A1-A14), with different frequency and CT distribution, although intra-CT conservation (**Table 6**, **Figures S14** and **S17**). We selected one strain per FabH allelic variant to assess the antimicrobial activity of synthesized FabHi.

Table 6. Distribution of FabH variation across a previously whole-genome sequenced (WGS) collection of NTHi clinical isolates.

FabH variant	No. of strains	Frequency (%)	NTHi WGS clinical strains	Selected representative strain
A1	29	30.9	P667, P668, P669, P594, P595, P596, P650, P676, P679, P853, P627, P628, P671, P610, P617, P634, P635, P636, P637, P661, P597, P639, P662, P663, P598, P631, P611, P606, NTHi375	NTHi375[b]
A2	17	18.1	P600, P601, P602, P612, P613, P614, P615, P616, P618, P620, P621, P622, P623, P624, P629, P632, P633	P621
A3	12	12.8	P670, P672, P674, P675, P677, P678, P646, P647, P648, P649, P592, RdKW20	RdKW20[a]
A4	6	6.4	P609, P599, P651, P652, P653, P654	P652
A5	6	6.4	P619, P640, P638, P625, P673, P630	P673
A6	5	5.3	P641, P642, P588, P604, P605	P642
A7	4	4.3	P664, P665, P666, P591	P665
A8	3	3.2	P657, P658, P660	P657
A9	3	3.2	P643, P644, P645	P645
A10	2	2.1	P603, P851	P851
A11	2	2.1	P656, P593	P593
A12	2	2.1	P607, P608	P607
A13	2	2.1	P589, P590	P590
A14	1	1.1	P626	P626

[a]RdKW20 is a reference strain, used to generate the *i*NL638 metabolic model.

[b]NTHi375 is an otitis media clinical isolate previously used in host-pathogen interplay studies (Bouchet et al., 2003; López-Gómez et al., 2012; Mell et al., 2014b; Morey et al., 2011).

We first tested the susceptibility of the 14 selected *H. influenzae* strains to FabHi upon growth in CDM, the medium used to interrogate the *i*NL638 model (strains growth shown in **Figure S18A**). We observed a significant dose-dependent reduction of bacterial viability after incubation. Such

effect was heterogeneous among strains, suggesting that FabHi may be a broad range inhibitor of $FabH_{H.influenzae}$, irrespective of the allelic variant. Based on the slope of the survival curve and the extent of bacterial viability loss upon incubation with the drug (**Figure S19A**), we established four strain categories, from higher to lower susceptibility: (i) strains showing a sharp slope reaching complete viability loss, as those carrying *fabH* allelic variants A5-P673, A11-P593, A13-P590 (blue); (ii) strains showing a sharp slope without complete viability loss (A4-P652, A6-P642, A9-P645, A10-P851 *fabH* variants; green); (iii) strains with a non-as-sharp slope but reaching complete viability loss (A2-P621, A7-P665, A12-P607, A14-P626; red); (iv) strains with a non-as-sharp slope, without complete viability loss (A1-NTHi375, A3-RdKW20, A8-P657; orange).

CDM, useful to connect our computational and experimental approaches, is not used as a standard medium for *H. influenzae* growth and antimicrobial susceptibility testing (Fernando et al., 2020). Thus, we tested susceptibility to FabHi of same strains grown in sBHI (growth shown in **Figure S18B**). We observed, again, a significant and heterogeneous dose-dependent reduction of bacterial viability after incubation (**Figure 26A**). Strain behaviour was comparable to that in CDM in most cases with some exceptions, strain P590 carrying A13 allelic variant was the clearest case (**Figures S19A** and **26A**). Detailed analysis of these curves suggests a biphasic mode with a fast initial reduction of bacterial viability followed by a second phase where viability lost drops slower, in some cases up to undetectable levels. Changes related to the FabH variant and the growth medium mainly affect the bacterial response to FabHi concentrations in this second phase (**Figure S20**).

Likewise, we assessed the effect of FabHi on bacterial biofilm growth, first defining biofilm formation for each strain, which was heterogeneous from clear biofilm formers (A6-P642) to those forming poorly detectable biofilms (A4-P652, A5-P673). FabHi 50 µg/mL (+), which allowed growth of all tested strains (**Figure 26A**), lowered biofilm growth by A1-NTHi375, A6-P642, A7-P665, A8-P657, A9-P645, and A13-P590 strains (**Figure 26B**, column +), but this inhibitory effect was not observed on strains belonging to the more susceptible category (for example, A2-P621 and A11-P593). A significant inhibitory effect was observed when using higher FabHi concentrations (**Figure 26B**, column +′).

In summary, the viability of *H. influenzae* clinical strains representative of the observed FabH variation decreased when exposed to FabHi in a dose-dependent manner and with a variable efficacy among strains. This effect was observed upon planktonic or biofilm growth. In addition, the susceptibility of *H. influenzae* to FabHi irrespective of the culture conditions argue in favour of FabH as a condition-independent drug target, and highlight our gene essentiality analysis as a robust computational approach to identify drug targets.

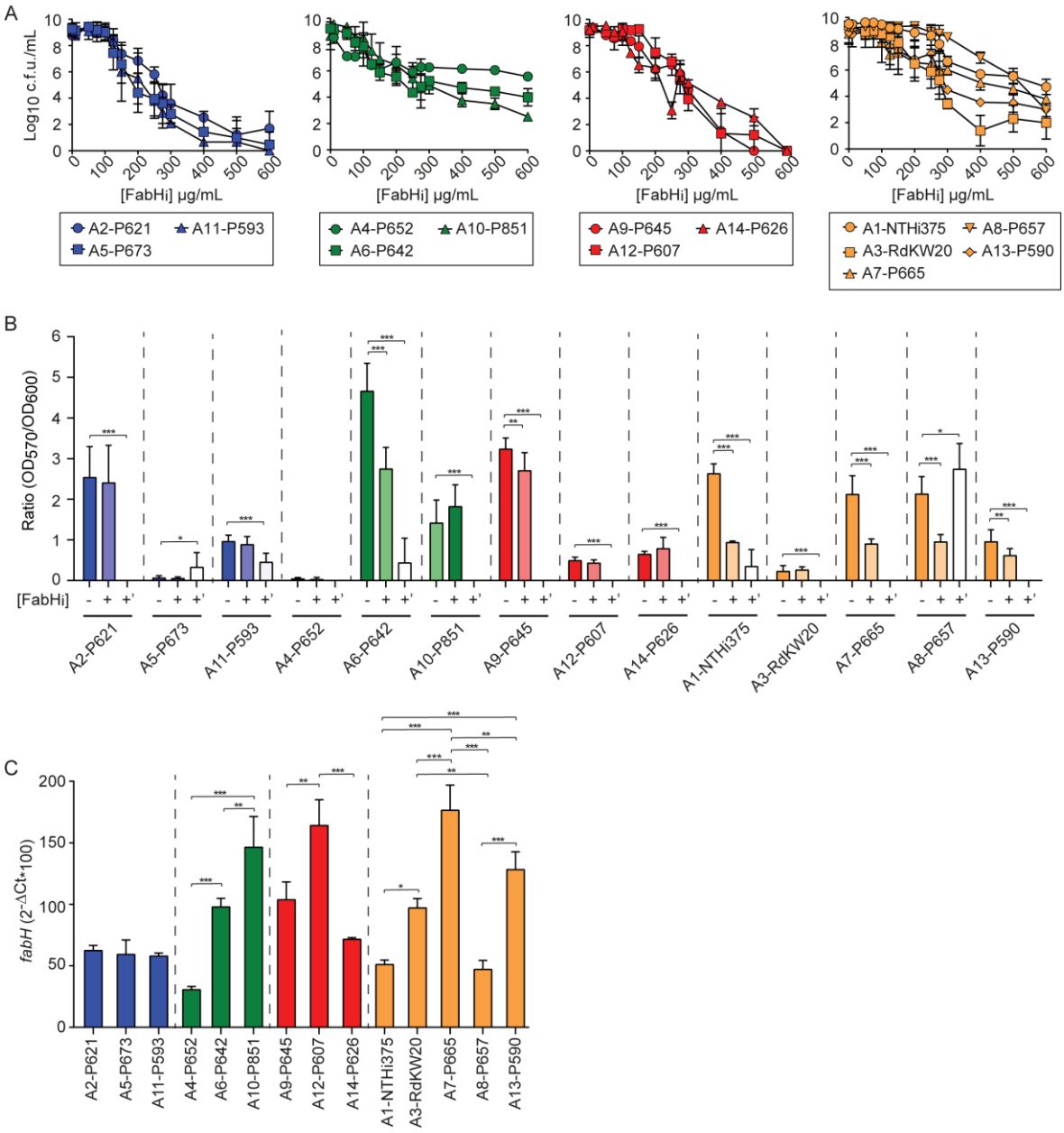

Figure 26. FabHi has an antimicrobial effect on *H. influenzae* upon planktonic and biofilm growth. (A) Determination of FabHi inhibitory effect on representative NTHi strains carrying FabH variants A1 to A14, upon planktonic growth in sBHI medium. Susceptibility to FabHi was dose-dependent. FabHi concentrations tested range from 10 to 600 µg/mL. Strains were classified into four groups (blue, green, red, orange labelling) based on increasing resistance. Results are shown as Log_{10} c.f.u./mL (mean ± SD). For each strain, statistical comparisons of means were performed by one-way ANOVA and Dunnett's multiple-comparisons test. A reduction on bacterial viability was observed as it follows: A1-NTHi375, at [FabHi] 200 µg/mL and higher, $p<0.0005$; A2-P621, at [FabHi] 200 µg/mL and higher, $p<0.0001$; A3-RdKW20, at [FabHi] 150 µg/mL and higher, $p<0.005$; A4-P652, at [FabHi] 50 µg/mL and higher, $p<0.0001$; A5-P673, at [FabHi] 125 µg/mL and higher, $p<0.0001$; A6-P642, at [FabHi] 75 µg/mL and higher, $p<0.005$; A7-P665, at [FabHi] 125 µg/mL and higher, $p<0.05$; A8-P657, at [$FabH_i$] 275 µg/mL and higher, $p<0.05$; A9-P645, at [FabHi] 150 µg/mL and higher, $p<0.05$; A10-P851, at [FabHi] 150 µg/mL and higher, $p<0.005$; A11-P593, at [FabHi] 150 µg/mL and higher, $p<0.0001$; A12-P607, at [FabHi] 200 µg/mL and higher, $p<0.0001$; A13-P590, at [FabHi] 200 µg/mL and higher, $p<0.05$; A14-P626, at [FabHi] 125 µg/mL and higher, $p<0.0001$. **(B)** Determination of FabHi inhibitory effect on biofilm growth by representative NTHi strains carrying FabH variants A1 to A14. Strains were grown in the absence (-) or presence (+, +') of FabHi. Two FabHi concentrations were used: (i) 50 µg/mL (+); (ii) a higher sub-inhibitory [FabHi] (+')close to the minimum bactericidal concentration determined in **(A)** for each strain (275 µg/mL for A1-NTHI375, A3-RdKW20, A4-P652, A7-P665, A8-P657 and A14-P626; 200 µg/mL for A2-P621, A9-P645, A10-P851, A12-P607 and A13-P590; 100 µg/mL for A5-P673, A6-P642 and A11-P593). For each strain, statistical comparisons of means were performed by one-

way ANOVA and Dunnett's multiple comparisons test (*p<0.05; **p<0.005; ***p≤ 0.0001). **(C)** The *fabH* gene expression on representative NTHi strains used for inhibition studies, grown in sBHI to half of each strain's maximal OD_{600}. Statistical comparisons of means were performed for each previously established group by one-way ANOVA and Tukey's multiple comparisons test (*p<0.05; **p<0.005; ***p<0.0001).

4.4.7. Heterogeneity of FabHi antimicrobial effect among strains: assesing possible causes

We next explored possible reasons accounting for the heterogeneity of FabHi antimicrobial effect. First, mapping of sequence polymorphisms in $FabH_{RdKW20}$ structure showed that amino acid substitutions were out of the substrate-binding cavity (**Figure 25C**). However, functional FabH is a dimer (Gajiwala et al., 2009) and several of these polymorphisms, located at the monomer-monomer interface, could be relevant for dimer stabilization and even substrate selectivity, while others might affect the monomer conformation.

The loops comprising Ser84–Ser89 and Lys185–Gln207, with polymorphisms at positions 85, 186, 197 and 198, are involved in forming the dimer interface and, more importantly, in ligand binding or active site formation (**Figure S21A**). Thus, dimerization brings Tyr87 and adjacent residues close to the catalytic Cys112 of the dimeric partner (**Figure S21B**), creating a complex network of contacts with residues from the other subunit (Thr81, Cys112, Val190, Leu191, Ala192, Gln193, Ile204 and Gly306) in which His85 itself participates. Residues at positions 197 and 198 conform the central part of the other loop turn whose pairing with the equivalent loop of the complementary subunit stabilizes the dimer interface, making contacts with Arg144, Ser201, Gly202 and Tyr203 from the other monomer (**Figure S21C**). The loop is additionally involved in CoA recognition through Leu189 and Met206 moieties (Qiu et al., 1999). Both actions could be sensitive to the polymorfism found at position 186 as well, due to its proximity to the dimer interface (**Figure S21D**). Analogously, Ser105 of $FabH_{RdKW20}$, substituted by cysteine in four variants, interacts with residues from the other subunit (**Figure S21D**), and Ala118 (substituted by valine in one allelic variant) is close too to the dimer interface. Polymorfisms potentially relevant for the monomer structural integrity comprise residue 76 (included in the hydrophobic core of the N-terminal domain hydrophobic-core); residue 169 (helping to maintain the relative dispositions of strands Nβ1 and Nβ5 of the N-terminal domain through hydrogen bonding to Asn2 and Asn171; **Figure S21E**); and residues 286, 287 and 296 (orienting Cβ2, Cα3, Cβ3, Cβ4 components of the C-terminal domain, and helping configure the loop connecting Cα3 to Cβ3; **Figure S21E**). Finally, Ser228 (substituted by cysteine in three variants) is at the C-terminus of Cα1, a long helix proposed to conform, together with Cα2, the binding surface for the ACP protein outside the active site tunnel (Qiu et al., 1999).

Therefore, sequence changes in any of these positions may have a significant impact on the functioning of the FabH enzyme, including affinities for substrates, feedback inhibitor, or FabHi, and/or catalytic efficiency and, therefore, in the inhibitory capacity of FabHi.

Second, we asked if the variable effect of FabHi would relate also to differences in the *fabH* gene expression. However, gene expression was heterogeneous and we did not observe either a correlation between resistance and *fabH* gene expression, or a defined gene expression pattern for strains belonging to the previously established categories (**Figure 26C** and **S19B**).

Third, previous evaluation of the FabHi analogue (1-(5-(2,5-dimethyl-3-(hydroxymethyl)phenyl)pyridin-2-yl)piperidine-4-carboxylic acid) showed increased susceptibility upon inactivation of the AcrAB-TolC efflux pump system (McKinney et al., 2016). AcrAB-TolC was shown to be present in the set of 14 selected strains, displaying some polymorphisms, although the AcrB hydrophobic trap (Gly142 or Ile143, Phe182, Glu594, Met599, Ile601, and Ile613) is fully conserved (Zwama et al., 2019) (**Figure S22-S24**). Inactivation of the *acrR* gene, encoding the putative repressor of the *acrAB* gene expression, leads to decreased *H. influenzae* antimicrobial susceptibility (Dean et al., 2005). Notably, examination of *acrR* revealed mutations generating truncated variants in strains A2-P621, A8-P657 and A10-P851, which may contribute at some extent to observed variability of FabHi antimicrobial effects, even though A2-P621 did not show decreased susceptibility to FabHi (**Figure S25**). Finally, although compensatory effects have been described in *Staphylococcus aureus*, by the means of *fabH* mutations conferring resistance to FabF-directed antibiotics (Parsons et al., 2015), this is unlikely for *H. influenzae* as the *fabF* gene is absent in RdKW20 (Wang & Cronan, 2003) and the rest of tested strains.

4.4.8. FabHi antimicrobial effect does not exclusively relate to the *fabH* gene allelic variant

To further assess if the observed heterogeneity would match only to *fabH* gene allelic variation, we tested strains carrying the same variant. Variants A1 (NTHi375 as reference), A3 (RdKW20 as reference), A5 (P673 as reference), A6 (P642 as reference) and A8 (P657 as reference) were used as representative examples (**Figure 27**). No significant differences were observed for strains containing variant A8, i.e. strains P657, P658 and P660 belonging all to the same CT. However, heterogeneity was observed in strain groups containing the A1, A3, A5 and A6 variants grouping different CTs. A1-containing strains P597, P639 and P606 were more susceptible, while P667 and P671 were more resistant to FabHi than NTHi375; A3-containing strains P648 and P649 were more resistant and P670, P675 and P678 more susceptible to FabHi than RdKW20; A5-containing strains P619, P640, P638 and P630 were more resistant to FabHi than P673; A6-containing strains P588 and P641 were more resistant, and P604 and P605 more susceptible to FabHi than P642. In conclusion, the extent of the FabHi antimicrobial effect could not be exclusively related to the specific FabH variant carried by each strain. Instead, the metabolic context provided by each individual strain may contribute tailoring FabHi inhibitory effect.

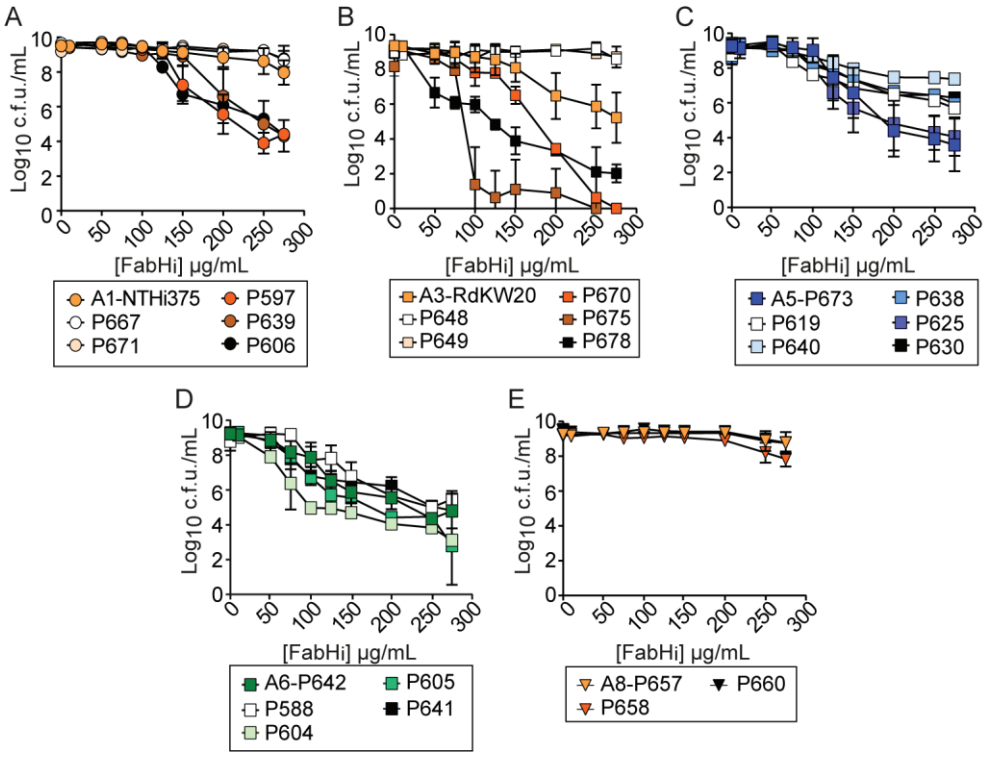

Figure 27. FabHi effect on *H. influenzae* does not merely relate to *fabH* gene allelic variant or expression levels. Determination of FabHi inhibitory effect on NTHi strains carrying FabH variants A1 (strains NTHi375, P667, P671, P597, P639, P606) **(A)**, A3 (strains RdKW20, P648, P649, P670, P675, P678) **(B)**, A5 (strains P673, P619, P640, P638, P625, P630) **(C)**, A6 (strains P642, P588, P604, P605, P641) **(D)**, or A8 (strains P657, P658, P660) **(E)** upon planktonic growth in sBHi. Strains were susceptible to FabHi in a dose-dependent manner. FabHi concentrations tested range from 10 to 275 µg/mL. Results are shown as Log_{10} c.f.u./mL (mean ± SD). For each strain set containing the same FabH variant, statistical comparisons of means were performed by two-way ANOVA and Dunnett's multiple-comparisons test, and using the previously used representative strain as a reference. A significant reduction on bacterial viability was observed as it follows: **(A)** A1 variant group: higher susceptibility than the A1-NTHi375 reference strain is shown for P606 at [$FabH_i$] ≥ 125 µg/mL, $p<0.005$; for P597 at [FabHi] ≥ 150 µg/mL, $p<0.0001$; for P639 at [$FabH_i$] ≥ 200 µg/mL, $p<0.0001$; and lower susceptibility than the A1-NTHi375 reference strain is shown for P667 and P671 at [$FabH_i$] ≥ 275 µg/mL, $p<0.05$ **(B)** A3 variant group: higher susceptibility than the A3-RdKW20 reference strain is shown for P670 at [$FabH_i$] ≥ 150 µg/mL, $p<0.005$; for P675 at [FabHi] ≥ 100 µg/mL, $p<0.0001$**;** for P678 at [FabHi] ≥ 50 µg/mL, $p<0.0001$; and lower susceptibility than the A3-RdKW20 reference strain is shown for P648 at [$FabH_i$] ≥ 200 µg/mL, $p<0.0001$; for P649 at [$FabH_i$] ≥ 200 µg/mL, $p<0.0001$; **(C)** A5 variant group: lower susceptibility than A5-P673 reference strain is shown for P619 at [FabHi] 100 and ≥200 µg/mL, $p<0.05$; for P640 at [FabHi] ≥150 µg/mL, $p<0.05$; for P638 and P630 at [FabHi] ≥200 µg/mL, $p<0.0001$; **(D)** A6 variant group: higher susceptibility than the A6-P642 reference strain is shown for P604 at [$FabH_i$] ≥ 75 µg/mL, $p<0.05$; for P605 at [FabHi] ≥ 125 µg/mL, $p<0.005$**;** and lower susceptibility than the A6-P642 reference strain is shown for P588 at [$FabH_i$] 100 and > 150 µg/mL, $p<0.05$; for P641 at [$FabH_i$] 125 µg/mL, $p<0.05$; **(E)** A8 variant group: no significant differences were found.

4.4.9. FabHi does not induce bacterial resistance, antibiotic synergies or cytotoxicity

To expand our FabHi antimicrobial effect characterization, we assessed the ability of strain P642, employed for *in vivo* assays (see below), to become resistant to FabHi through serial independent passage in sBHI broth containing three different inhibitory concentrations of FabHi. After 12 consecutive passages, no growth was detected (**Figure 28A**). Also, FabHi and the antibiotics Azm or Amp were combined at different proportion and tested against P642 by the checkerboard method;

antagonism or synergy effects were not detected. **Figure 28B** shows the MIC ± SD for each compound separately, the MIC ± SD of the combinations tested, calculated ΣFIC ± SD, and their interpretation.

FabHi effect on bacterial viability was also titrated in EBSS medium aiming to mimic cultured epithelial cell infection conditions, showing a significant dose-dependent decrease (**Figure 28C**). Based on this observation, A549 cells were pre-treated with EBSS containing FabHi for 16 h, which was then replaced by EBSS medium without drug prior infection. Under these conditions, FabHi did not show cytotoxicity (**Figure S26**). Cell exposure to increasing doses of FabHi did not modify P642 epithelial adhesion and invasion rates (**Figure 28D-E**). Therefore, FabHi does not seem to modulate NTHi infection of airway epithelial cells under the tested conditions.

4.4.10. FabHi efficacy preclinical testing reveals a protective effect on zebrafish systemic infection with NTHi

Our final goal was to evaluate drug efficacy at the preclinical level, on a FabHi protective assay in adult zebrafish infected with NTHi, by following a previously established sepsis model (Euba et al., 2017; Fernández-Calvet et al., 2019). We used strains P673 and P642, belonging to the FabHi more susceptible categories, to assess their capacity to infect zebrafish by injection of 3 animal groups (n=10) with 10 µL of bacterial suspensions containing $7x10^{10}$ c.f.u./mL, or saline solution 0.9% as a control. NTHi P642 severely reduced zebrafish survival, and an infection dose consisting of $7x10^{8}$ c.f.u./zebrafish caused progressive death of the animals after injection; however, strain P673 did not modify zebrafish survival (data not shown), precluding us from using this strain in this model system.

Next, a FabHi acute toxicity assay was performed in zebrafish embryos following the fish embryo acute toxicity (FET) test. Results showed that highest FabHi not toxic dose was 5.681 µg/embryo (data not shown). Based on these data, we tested FabHi effect on P642 infected zebrafish by using a therapeutic regimen of intraperitoneal FabHi 4 µg/zebrafish consisting of one administration 1 hpi. Survival rate for FabHi-treated and control untreated groups was monitored three times per day up to 4 days post-infection. Mortality rate in FabHi-treated infected zebrafish was significantly lower than in control animals receiving vehicle solution ($p<0.0001$); indeed, survival was similar for infected zebrafish receiving FabHi than for control non-infected animals (**Figure 28F**). This model system rendered significant FabHi-mediated increased survival upon

zebrafish NTHi infection by using P642, which did not seem to be prone to develop resistance upon serial passage.

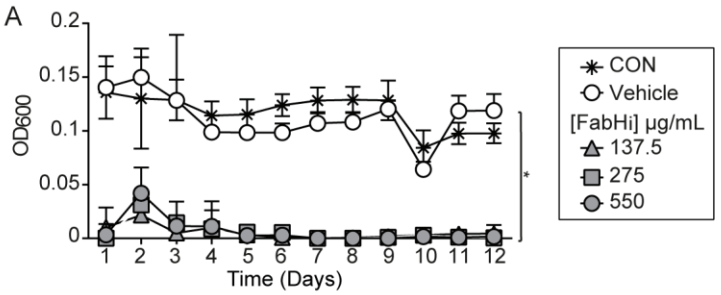

B

Combination (A + B)		MIC_A (µg/mL)	MIC_A (A + B combination)	MIC_B (µg/mL)	MIC_B (A + B combination)	ΣFIC	Result
A	B						
FabHi	Amp	150	300	4	2	2.5	Indifferent
FabHi	Azm	150	300	2	1	2.5	Indifferent

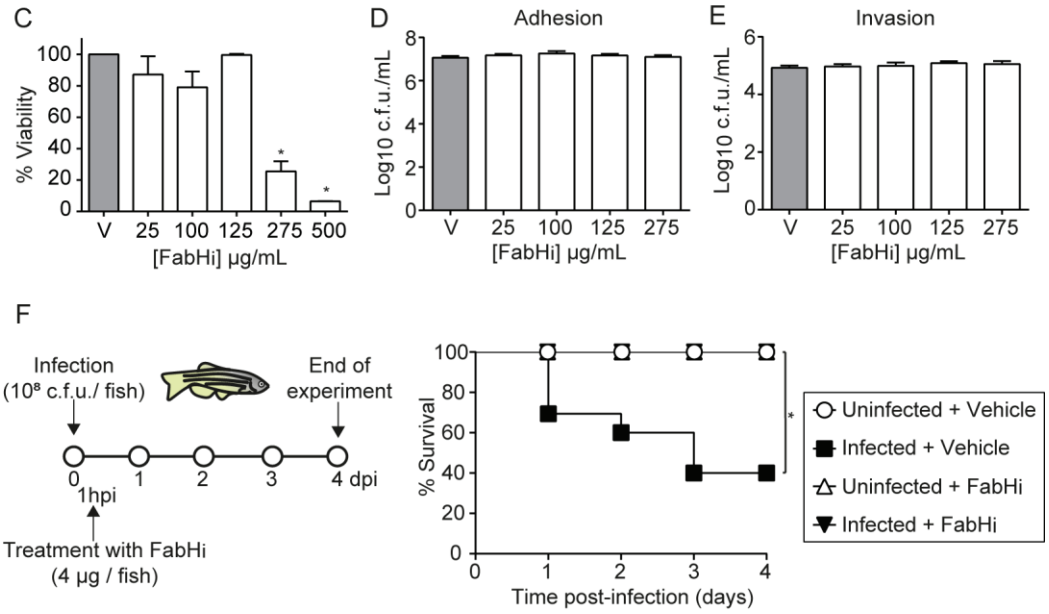

Figure 28. FabHi *in vitro* characterization and preclinical evaluation. (A) A6-P642 did not grow after 12 daily serial passages in the presence of three [FabHi] (137.5, 275 and 550 µg/mL). Data are shown as OD_{600} (mean ± SD) in every passage (*p<0.0001). Statistical comparisons of means were performed by one-way ANOVA and Dunnett's multiple comparisons test. **(B)** The checkboard method for strain P642, when combining FabHi:antibiotic molecules (mean ± SD). **(C)** The viability of NTHi strain P642 was tested by simulating host cell infection conditions (2 h at 37°C in EBSS medium, in the absence (V)/presence of FabHi). FabHi reduced (*p<0.0001) bacterial viability (mean ± SD) in a dose-dependent manner. Based on these results, cell infection assays shown in panels **D** and **E** were performed by cell pretreatment with FabHi for 16 h, and drug removal prior infection. Controls (V): cells did not receive FabHi, but did receive vehicle solution, i.e., DMSO. Adhesion **(D)** and invasion **(E)** assays did not render significant differences, Statistical comparisons of the means were performed with one-way ANOVA and Dunnett's multiple comparisons test. **(F)** Zebrafish were infected intraperitoneally with P642, $7x10^8$ CFU/zebrafish. When necessary, FabHi 4 µg/zebrafish was administered intraperitoneally at 1 hpi. Non-infected groups were administered PBS (white circle) or $FabH_i$ (white triangle); infected groups were administered PBS (black square) or $FabH_i$ (black inverted triangle). Survival rate is reported as percentage (mean ± SD) of adult individual survival up to 4 days. Survival of NTHi infected zebrafish was significantly higher in FabHi treated than in untreated animals (*p<0.0001). To draw and analyze the Kaplan-Meier survival curve, a Log-rank

(Mantel-cox) test was used (*p<0.0001). Statistical comparisons between survival rates after 4 days were performed by one-way ANOVA and Sidak's multiple comparisons test.

4.5. Supplementary Material

4.5.1. Bacterial strains, media, growth conditions, and drugs

For growth in sBHI or CDM, NTHi strains grown on PVX agar for 16 h were inoculated (2 to 3 colonies) in 10 mL sBHI or CDM using 100 mL flasks, and incubated for 11 h with shaking (100 r.p.m.). Cultures were then diluted to OD_{600}=0.07 in a final volume of 25 mL sBHI or CDM using 250 mL flasks, grown with shaking (180 r.p.m.), and OD_{600} was recorded every hour for up to 8 h. When necessary, bacterial viability upon host cell infection conditions was tested. To do so, phosphate-buffered saline (PBS)-normalized bacterial suspensions (OD_{600}=1) were prepared by using NTHi grown on PVX agar; 100 µL aliquots were incubated in 1 mL Earle´s Balanced Salts (EBSS, Gibco 24010-043) in the absence/presence of FabH inhibitor (FabHi) for 2 h at 37ºC, serially diluted, and plated on sHTM agar for c.f.u./mL determination.

FabHi was used by freshly preparing a panel of stock solutions, customized to each type of assay (7 to 35 mg/mL) in dimethyl sulfoxide (DMSO), and diluted to the working concentrations specified in each assay in CDM, sBHI or RPMI 1640 (Sigma-Aldrich R8758). Antibiotics and FabHi working concentrations are specified for each assay (see below). Amp and Azithromycin dihydrate (Azm, Zytromax) were used to assess FabHi synergic effects (see below). For this purpose, 10 mg/mL stock solutions of each antibiotic were prepared in distilled H_2O (dH_2O), filtered, and used at the indicated working concentrations.

4.5.2. Determination of FabHi antimicrobial effects

4.5.2.1. Dose dependent FabHi antibacterial effect under bacterial planktonic or biofilm growth

A 25 mg/mL FabHi stock solution in DMSO was used to prepare 40, 200, 300, 400, 500, 600, 800, 1000, 1100, 1200, 1600, 2000, 2400 µg/mL working solutions in CDM or in sBHI. Fifty µL aliquots of sBHI or CDM were transferred to individual wells. Next, 50 µL of each FabHi working solution were added, mixed, and 50 µL were discarded. A suspension of PVX agar freshly grown bacteria was generated in sBHI or CDM, adjusted to 0.5 MacFarland (OD_{600}=0.063) and diluted 1:100. Then, 50 µL bacterial aliquots were transferred to each individual well. A vehicle solution control consisting of a volume of DMSO equivalent to that of the highest FabHi concentration tested was performed in parallel (indicated as 0 [FabHi] µg/mL). Blank controls (sBHI or CDM added) were used. Plates were incubated for 24 h at 37°C, 5% CO_2, without shaking. Culture samples were serially diluted and plated on sHTM agar. Data are shown as Log c.f.u./mL; experiments were performed in duplicate at least three times ($n \geq 6$). Alternatively, FabHi antimicrobial effect was assessed upon *H. influenzae* biofilm grown in sBHI. For this purpose, assays were set as indicated above and bacterial growth was determined by measuring OD_{600} on a SpectraMAX 340 microplate

reader. The liquid portion in each well (containing planktonic bacteria) was then discarded, plates were washed 3 times through gentle submersion in distilled water and allowed to air dry. Next, 150 µL/well 0.5% crystal violet dissolved in dH_2O were added, and plates were incubated for 20 min with gentle shaking at room temperature, followed by plate washing as previously described. Finally, 150 µL/well 95% ethanol (Merck) were added, plates were incubated for 20 min with gentle shaking at room temperature, and OD_{570} was determined as a measure of biofilm growth. The OD_{570}/OD_{600} ratio for each strain and independent assay was calculated to normalize biofilm biomass to overall growth; experiments were performed in triplicate at least three times ($n \geq 9$).

4.5.2.2. Antimicrobial synergic effects

A 7 mg/mL FabHi stock solution was used to prepare 300 µg/mL working solutions in sBHI; 10 mg/mL Amp or Azm stock solutions were used to prepare 4 µg/mL and 2 µg/mL working solutions in sBHI, respectively. After generating each FabHi-Amp or $FabH_i$-Azm concentration matrix, each individual well of 96-well microtiter plates contained 80 µL final volume. A suspension of PVX agar freshly grown bacteria was generated in sBHI, adjusted to OD_{600}=0.16, diluted 1:100, and 20 µL aliquots were transferred to the plate wells. Plates were incubated for 24 h at 37ºC, 5% CO_2, without agitation. The fractional inhibitory concentration (FIC) index of each FabHi-Amp or FabHi-Azm combination was calculated to determine the existence of synergy ($\Sigma FIC \leq 0.5$), additive ($0.5 > \Sigma FIC \leq 1$), indifferent ($1 > \Sigma FIC < 2$) or antagonic ($\Sigma FIC \geq 2$) effects. Three independent assays were performed (n=3).

4.5.2.3. Serial passage experiments with FabHi

A 14 mg/mL FabHi stock solution was used to prepare 550, 1100 and 2200 µg/mL working solutions in sBHI. A vehicle solution control (indicated as V) consisting of a volume of DMSO equivalent to that of the highest FabHi concentration tested was performed in parallel. Blank controls (sBHI) were used. Fifty µL sBHI were transferred to individual wells, mixed with 50 µL of each FabHi working or vehicle control solutions, and 50 µL were discarded. A suspension of PVX agar freshly grown bacteria was generated in sBHI, adjusted to 0.5 MacFarland and diluted 1:100. Then, 50 µL bacterial aliquots were added to individual wells. Plates were incubated for 24 h at 37°C, 5% CO_2, without shaking. Cultures were then passaged (50 µL in 50 µL fresh sBHI with FabHi or vehicle solution) every day for 12 days. At each time point throughout the cycling, each well absorbance (OD_{600} at 24 h–OD_{600} at 0 h) was measured. Nine replicates per condition were made (n=9).

4.5.3. Inactivation of the *fabH* gene

For cloning purposes, *Escherichia coli* was grown on Luria Bertani (LB) broth or LB agar at 30 °C or 37 °C, supplemented with ampicillin 100 µg/mL (Amp_{100}) and/or spectinomycin 50 µg/mL ($Spec_{50}$), when necessary. For disruption of the *fabH* (gene accession number HI0157 in RdKW20

genome) gene, a DNA fragment containing the *fabH* gene and its respective adjacent regions (2,159 bp), were PCR amplified with Phusion polymerase (Thermofisher Scientific) using RdKW20 genomic DNA as a template and primer pairs *fabH*-F1 and *fabH*-R1. This gene-containing fragment was cloned into pJET1.2/blunt (Thermofisher Scientific), generating pJET1.2-*fabH*. Spec^r cassette was PCR amplified from pRSM2832 using gene-specific mutagenic primers *fabH*-F2 and *fabH*-R2. *E. coli* SW102 cells were prepared for recombineering, co-electroporated with pJET1.2-*fabH* (Amp^r) (50 ng) and the *fabH*-specific mutagenic cassette (Spec^r) (200 ng). Mutagenized clones containing pJET1.2-*fabH::spec* were selected on LB agar with Amp_{100}, $Spec_{50}$ (Sinha et al., 2012; Tracy et al., 2008). These plasmids were used as a template to amplify the *fabH::spec* disruption cassette with primers *fabH*-F1 and *fabH*-R1, which were used to transform RdKW20 using the MIV method (Herriott et al., 1970) and plated on sBHI agar with $Spec_{30}$. RdKW20Δ*fabH* mutants were not obtained.

4.5.4. Model construction and manual curation

Since the available GEM of *H. influenzae* lacks of the GPRs relationship, it could not be used as template for the draft construction. Instead we used the high-quality and well-curated GEM of *E. coli* K12 (*i*JO1366, (Orth et al., 2011)) for this purpose. GEMSiRV-MrBac server was used to construct the protein homology matrix and the initial draft (Liao et al., 2012). Briefly, the list of orthologous genes between the RdKW20 and K12 strains was obtained by Reciprocal Best Hits using BlastP (the RdKW20 (Wall et al., 2003)). This list and the corresponding model of *E. coli* in SBML format were used as input files for the GEMSiRV-MrBac server to obtain the initial model draft of RdKW20. This initial draft included the reactions present in *i*JO1366 assigned to the orthologous genes identified in RdKW20. Subsequently, the draft was subject to a detailed curation by manually reviewing all the GPR associations. The assignment of each GPR was additionally validated by BLASTP and when possible, by detailed scrutiny of available literature legacy. Pathways for well-known metabolic features of strain RdKW20 and absent in the model template such as strain specific lipooligosaccharide (LOS) and peptidoglycan biosynthesis were manually mass and charge balanced, and added to the reconstruction. Furthermore, the reactions involving strain specific cofactors were updated, such as those reactions using menaquinones or ubiquinones from *E. coli* model which were replaced by reactions accounting the cofactor usage of *H. influenzae* i.e., demetylmenaquinone and demethylmenaquinol, respectively. Finally, the network gaps across the metabolic pathways were filled out by manual gap filling by adding new reactions based on the information stored in biological databases, scientific literature and in the functional annotation of strain RdKW20. For instance, metabolic gaps in fatty acid and molybdopterin biosynthesis pathways were manually completed during this step. Additionally, transport reactions were manually curated considering the connectivity of the cognate metabolites and experimental evidences. For instance, transport reactions for certain

amino acids, fatty acids, uracil, pantothenate, biotin, dihydrofolate, protoporphyrin, pyridoxine, riboflavin, nucleotides or NAD transporters were added manually based on available biochemical and physiological evidences. Contrary, transport reactions for several compounds initially included in the automatic draft were removed due the lack of physiological evidences.

4.5.5. Biomass Objetive Function (BOF) formulation

For BOF construction, reported macromolecular composition of *H. influenzae* RdKW20 was used as base for the construction of a highly complete biomass reaction (**Dataset S1**). Protein, DNA, RNA, LOS and lipid content was taken from available literature (Flesher & Insel, 1978; Sutrina & Scocca, 1976; Zoon & Scocca, 1975). Missing information such carbohydrates, inorganic ions and soluble pool content was taken from *E. coli* model (Jasnin, 2007; Orth et al., 2011; Pramanik & Keasling, 1997) (**Dataset S1**). The stoichiometric coefficients for amino acids, DNA and RNA were further determined computationally using the *H. influenzae* available genomic information (**Dataset S1**) while the coefficients for murein and lipids were taken from experimental reports. In the absence of experimental information, growth associated ATP maintenance reaction (GAM) was estimated by determining the energy required for macromolecular synthesis as previously described (Thiele & Palsson, 2010), while non-growth associated ATP maintenance reaction (NGAM) was taken from *E. coli* model (Orth et al., 2011).

4.5.6. Constraints used to simulate *in silico* CDM medium

```
%%%%%%%%%%%%%%%%%%%%
%Complete In silico CDM medium%
%%%%%%%%%%%%%%%%%%%%

%Aerobic growth
model=changeRxnBounds(model, 'EX_o2(e)',-18.5,'l');

%Carbon Sources and main nutrients
model=changeRxnBounds(model, 'EX_pyr(e)',-1,'l');
model=changeRxnBounds(model, 'EX_ins(e)',-5,'l');
model=changeRxnBounds(model, 'EX_glc(e)',-5,'l');
model=changeRxnBounds(model, 'EX_nad_(e)',-2,'l');
model=changeRxnBounds(model, 'EX_pheme(e)',-0.1,'l');
model=changeRxnBounds(model, 'EX_ura(e)',-1,'l');

%%%%%%%%%%%%%%%%%%%%
%RPMI
```

%%%%%%%%%%%%%%%%%%%%

%Amino acids

model=changeRxnBounds(model,'EX_gln_L(e)',-1,'l');
model=changeRxnBounds(model,'EX_arg_L(e)',-1,'l');
model=changeRxnBounds(model,'EX_asn_L(e)',-1,'l');
model=changeRxnBounds(model,'EX_asp_L(e)',-1,'l');
model=changeRxnBounds(model,'EX_glu_L(e)',-1,'l');
model=changeRxnBounds(model,'EX_gly(e)',-1,'l');
model=changeRxnBounds(model,'EX_his_L(e)',-1,'l');
model=changeRxnBounds(model,'EX_ile_L(e)',-1,'l');
model=changeRxnBounds(model,'EX_leu_L(e)',-1,'l');
model=changeRxnBounds(model,'EX_lys_L(e)',-1,'l');
model=changeRxnBounds(model,'EX_met_L(e)',-1,'l');
model=changeRxnBounds(model,'EX_phe_L(e)',-1,'l');
model=changeRxnBounds(model,'EX_pro_L(e)',-1,'l');
model=changeRxnBounds(model,'EX_ser_L(e)',-1,'l');
model=changeRxnBounds(model,'EX_thr_L(e)',-1,'l');
model=changeRxnBounds(model,'EX_trp_L(e)',-1,'l');
model=changeRxnBounds(model,'EX_tyr_L(e)',-1,'l');
model=changeRxnBounds(model,'EX_val_L(e)',-1,'l');
model=changeRxnBounds(model,'EX_cys_L(e)',-1,'l');
model=changeRxnBounds(model,'EX_4hpro_DC(e)',-1,'l');

%Vitamins

model=changeRxnBounds(model,'EX_btn(e)',-0.1,'l');
model=changeRxnBounds(model, 'EX_chol(e)',-0.1,'l');
model=changeRxnBounds(model,'EX_pnto_R(e)',-0.01,'l');
model=changeRxnBounds(model,'EX_dhf(e)',-0.1,'l');
model=changeRxnBounds(model,'EX_4abz(e)',-0.1,'l');
model=changeRxnBounds(model,'EX_pydxn(e)',-0.1,'l');
model=changeRxnBounds(model,'EX_rbf(e)',-0.1,'l');
model=changeRxnBounds(model,'EX_thm(e)',-0.01,'l');
model=changeRxnBounds(model,'EX_nmn(e)',-0.1,'l');
model=changeRxnBounds(model, 'EX_inost(e)',-0.1,'l');

%Inorganic Salts

model=changeRxnBounds(model, 'EX_no3(e)',-30,'l');
model=changeRxnBounds(model, 'EX_so4(e)',-30,'l');
model=changeRxnBounds(model, 'EX_cl(e)',-1,'l');
model=changeRxnBounds(model, 'EX_k(e)',-1,'l');
model=changeRxnBounds(model, 'EX_ca2(e)',-1,'l');
model=changeRxnBounds(model, 'EX_cobalt2(e)',-1,'l');
model=changeRxnBounds(model, 'EX_cu2(e)',-1,'l');
model=changeRxnBounds(model, 'EX_mg2(e)',-1,'l');
model=changeRxnBounds(model, 'EX_mn2(e)',-1,'l');
model=changeRxnBounds(model, 'EX_na1(e)',-1,'l');
model=changeRxnBounds(model, 'EX_ni2(e)',-1,'l');
model=changeRxnBounds(model, 'EX_pi(e)',-10,'l');
model=changeRxnBounds(model, 'EX_mobd(e)',-1,'l');
model=changeRxnBounds(model, 'EX_zn2(e)',-1,'l');
model=changeRxnBounds(model, 'EX_fe2(e)',-1,'l');
model=changeRxnBounds(model, 'EX_fe3(e)',-1,'l');

%Other components

model=changeRxnBounds(model, 'EX_gthrd(e)',-0.01,'l');
model=changeRxnBounds(model,'EX_spmd(e)',-0.1,'l');

%%%%%%%%%%%%%%%%%%%%
%Minimal In silico CDM medium%
%%%%%%%%%%%%%%%%%%%%

%Aerobic growth

model=changeRxnBounds(model, 'EX_o2(e)',-18.5,'l');

%Carbon Sources and main nutrients

model=changeRxnBounds(model, 'EX_pyr(e)',-1,'l');
model=changeRxnBounds(model, 'EX_ins(e)',-5,'l');
model=changeRxnBounds(model, 'EX_glc(e)',-5,'l');

```
model=changeRxnBounds(model, 'EX_nad_(e)',-2,'l');
model=changeRxnBounds(model, 'EX_pheme(e)',-0.1,'l');
model=changeRxnBounds(model, 'EX_ura(e)',-1,'l');

%%%%%%%%%%%%%%%%%%%%
%RPMI
%%%%%%%%%%%%%%%%%%%%
%Amino acids
model=changeRxnBounds(model,'EX_gln_L(e)',0,'l');
model=changeRxnBounds(model,'EX_arg_L(e)',0,'l');
model=changeRxnBounds(model,'EX_asn_L(e)',0,'l');
model=changeRxnBounds(model,'EX_asp_L(e)',0,'l');
model=changeRxnBounds(model,'EX_glu_L(e)',0,'l');
model=changeRxnBounds(model,'EX_gly(e)',0,'l');
model=changeRxnBounds(model,'EX_his_L(e)',0,'l');
model=changeRxnBounds(model,'EX_ile_L(e)',0,'l');
model=changeRxnBounds(model,'EX_leu_L(e)',0,'l');
model=changeRxnBounds(model,'EX_lys_L(e)',0,'l');
model=changeRxnBounds(model,'EX_met_L(e)',0,'l');
model=changeRxnBounds(model,'EX_phe_L(e)',0,'l');
model=changeRxnBounds(model,'EX_pro_L(e)',0,'l');
model=changeRxnBounds(model,'EX_ser_L(e)',0,'l');
model=changeRxnBounds(model,'EX_thr_L(e)',0,'l');
model=changeRxnBounds(model,'EX_trp_L(e)',0,'l');
model=changeRxnBounds(model,'EX_tyr_L(e)',0,'l');
model=changeRxnBounds(model,'EX_val_L(e)',0,'l');
model=changeRxnBounds(model,'EX_cys_L(e)',0,'l');
model=changeRxnBounds(model,'EX_4hpro_DC(e)',0,'l');


%Vitamins
model=changeRxnBounds(model,'EX_btn(e)',0,'l');
model=changeRxnBounds(model, 'EX_chol(e)',-0.1,'l');
model=changeRxnBounds(model,'EX_pnto_R(e)',-0.01,'l');
model=changeRxnBounds(model,'EX_dhf(e)',0,'l');
model=changeRxnBounds(model,'EX_4abz(e)',0,'l');
```

```
model=changeRxnBounds(model,'EX_pydxn(e)',0,'l');
model=changeRxnBounds(model,'EX_rbf(e)',0,'l');
model=changeRxnBounds(model,'EX_thm(e)',-0.01,'l');
model=changeRxnBounds(model,'EX_nmn(e)',0,'l');
model=changeRxnBounds(model, 'EX_inost(e)',0,'l');

%Inorganic Salts
model=changeRxnBounds(model, 'EX_no3(e)',-30,'l');
model=changeRxnBounds(model, 'EX_so4(e)',-30,'l');
model=changeRxnBounds(model, 'EX_cl(e)',-1,'l');
model=changeRxnBounds(model, 'EX_k(e)',-1,'l');
model=changeRxnBounds(model, 'EX_ca2(e)',-1,'l');
model=changeRxnBounds(model, 'EX_cobalt2(e)',-1,'l');
model=changeRxnBounds(model, 'EX_cu2(e)',-1,'l');
model=changeRxnBounds(model, 'EX_mg2(e)',-1,'l');
model=changeRxnBounds(model, 'EX_mn2(e)',-1,'l');
model=changeRxnBounds(model, 'EX_na1(e)',-1,'l');
model=changeRxnBounds(model, 'EX_ni2(e)',-1,'l');
model=changeRxnBounds(model, 'EX_pi(e)',-10,'l');
model=changeRxnBounds(model, 'EX_mobd(e)',-1,'l');
model=changeRxnBounds(model, 'EX_zn2(e)',-1,'l');
model=changeRxnBounds(model, 'EX_fe2(e)',-1,'l');
model=changeRxnBounds(model, 'EX_fe3(e)',-1,'l');

%Other components
model=changeRxnBounds(model, 'EX_gthrd(e)',-0.01,'l');
model=changeRxnBounds(model,'EX_spmd(e)',-0.1,'l');
```

4.5.7. FabHi docking studies

The protein was considered rigid and the ligand flexible. FabHi structure was carefully built using the Pymol visualizer (PyMOL Molecular Graphics System, Version 1.5.0.4 Schrödinger, LLC) from the atomic coordinates of ligand cocrystallized with *E. coli* FabH in PDB entry 5BNR (compound 23 in (McKinney et al., 2016)), which lacks only the methylene unit of FabHi carboxylic moiety, followed by molecule optimization and energy minimization using the PRODRG2 server (Schüttelkopf & van Aalten, 2004). Ligand and protein files were edited and prepared with

AutoDockTools 1.5.6 program (Morris et al., 2009) after substituting de cysteine derivative at position 112 in $FabH_{RdKW20}$ structure by cysteine using Pymol. Polar hydrogens and Kollman charges were added to $FabH_{RdKW20}$ structure. Gasteiger charges were computed for the ligand, whose active torsion angles were allowed to rotate during docking. For docking simulations, 200 Lamarckian Genetic Algorithm simulation runs were performed with 25 million energy evaluations per run. The best docking solutions were selected by clustering within the default 2.0 Å rmsd value, and ranking the largest cluster solutions by the free energy AutoDock scoring function. The binding mode with lowest docking energy and best optimized configuration of catalytic triads was processed by adding hydrogens and minimizing in vacuo by 2500 cycles of conjugate gradient followed by 500 cycle of steepest descent, using the Sander program (Case DA, 2012; *PyMOL Molecular Graphics System, Version 1.5.0.4 Schrödinger, LLC*, n.d.). The minimized solution was selected as the most probable model of the $FabH_{RdKW20}$:FabHi complex.

4.5.8. Bacteria gene expression analyses

Two to three colonies of bacterial strains grown on PVX agar were inoculated in 10 mL CDM or sBHI, grown for 11 h, diluted into 25 mL fresh CDM or sBHI to OD_{600}=0.07, and grown to half of each strain's maximal OD_{600} for ~5h. Bacterial total RNA was isolated using TRIzol reagent (Invitrogen) and total RNA quality evaluated using RNA 6,000 Nano LabChips (Agilent 2,100 Bioanalyzer, Santa Clara, CA). Reverse transcription (RT) was performed using 1 µg RNA by PrimerScript RT Reagent kit (Takara). To amplify *fabH*, 1:10 diluted cDNA was used as template (including *gyrA* endogenous control). In all cases, 20 µL reaction mixtures containing 1X SYBR Premix Ex Taq II (Tli RNaseH Plus) (Takara) and the adequate primer mix were used. Fluorescence was analyzed with AriaMx Real-Time PCR System (Agilent Technologies). The comparative threshold cycle (Ct) method was used to obtain relative quantities of mRNA that were normalized using *gyrA* as endogenous control. The *fabH* gene was amplified with primers *fabH*-F and *fabH*-R in all cases except for the P851 and P642 strains, where *fabH*-P851-P642-F and *fabH*-P851-P642-R primers were used (**Table S2**). Samples were grown in triplicate and processed with technical triplicates (n=3).

4.5.9. Infection of cultured cells

A549 cells were maintained as described (Morey et al., 2011) and seeded on 24-well tissue culture plates to 1.5 x 10^5 cells/well for 32 h. To assess FabHi cytotoxicity, a 35 mg/mL FabHi stock solution was diluted in serum starved RPMI 1640 (Sigma-Aldrich) to 125, 275 and 500 µg/mL (1 mL/well), cells were incubated for 16 h at 37ºC, 5% CO_2, and cytotoxicity was determined by measuring the release of lactate dehydrogenase (CytoTox 96, Promega) and microscopy. To assess the effect of FabHi during epithelial infection by NTHi, cells were maintained and seeded as indicated above, and treated with FabHi in serum starved RPMI 1640 for 16 h before infection. For

infection, PBS-normalized bacterial suspensions (OD_{600}=1) were prepared by using NTHi grown on PVX agar. Adhesion and invasion assays were performed as previously described (López-Gómez et al., 2012; Morey et al., 2011). Controls (indicated as V in the Figures) were performed by using a DMSO volume corresponding to that of the highest FabHi concentration tested. After infection, wells were washed and cells lysed as previously described (Morey et al., 2011). Lysates were serially diluted in PBS and plated on sHTM agar for bacterial counts. Results are expressed as c.f.u./well. Experiments were performed in triplicate on at least three independent occasions (n=9).

Table S8. Bacterial cultures dry weight.

OD_{600}	Collected volume (mL)	Dry pellet weight (mg)
0.3	45	12.05
0.4	30	11.9
0.8	15	10.7

Table S9. Metabolic content of *i*NL638 compared with its antecessor.

		***i*NL638**	***H. influenzae*** (Edwards & Palsson, 1999)
Metabolites		1162	451
	Unique	746	
	Cytoplasmic	705	
	Periplasmic	250	
	Extracellular	205	
Genes		638	
Reactions		1385	471
	Metabolic	762	
	Transport	415	
	Exchange	203	
	Orphan	68	
	Blocked	234	

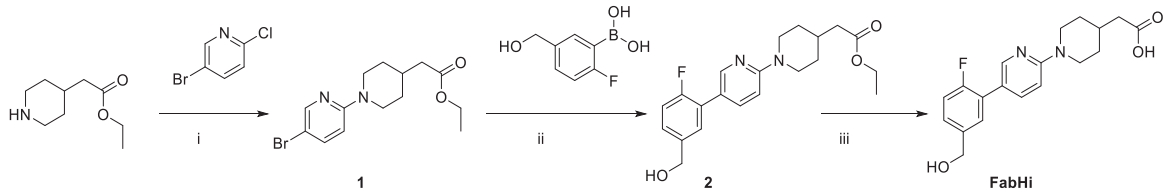

Figure S10. Synthesis of FabHi. ***Reagents and Conditions***: i) TEA, anhydrous ACN, Mw 125ºC, 2 h; ii) $Pd(ddpf)Cl_2$, K_2CO_3, anhydrous DMF, 75ºC, 16 h; iii) NaOH 1M, THF:MeOH (1:1), reflux, 4 h.

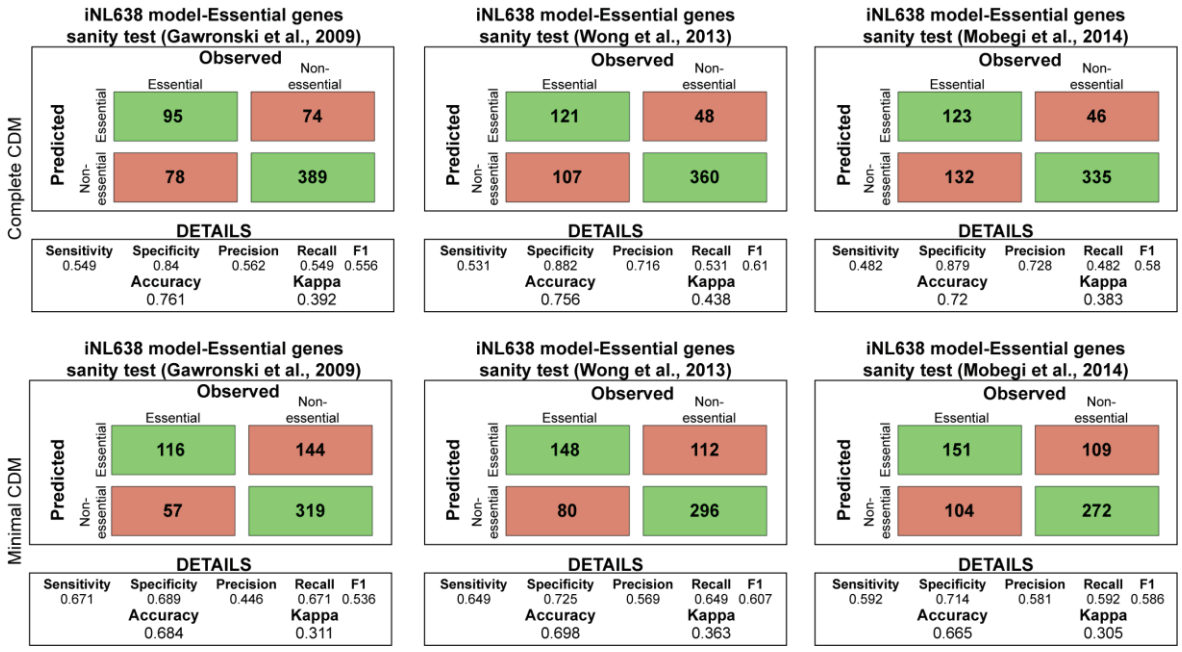

Figure S11. *In vivo/in silico* comparison of essential genes.

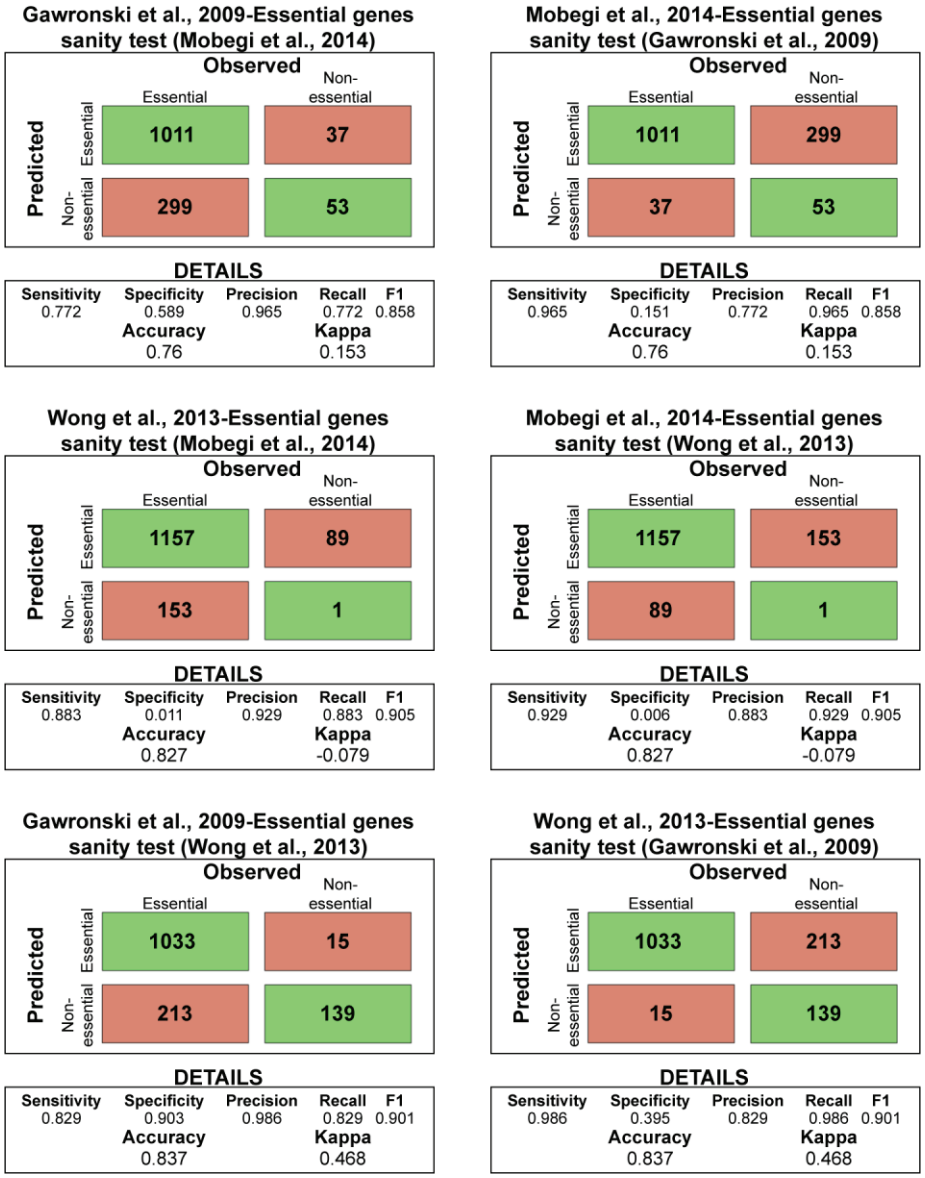

Figure S12. Quantitative comparison of available experimental datasets of essential genes in *H. influenzae.*

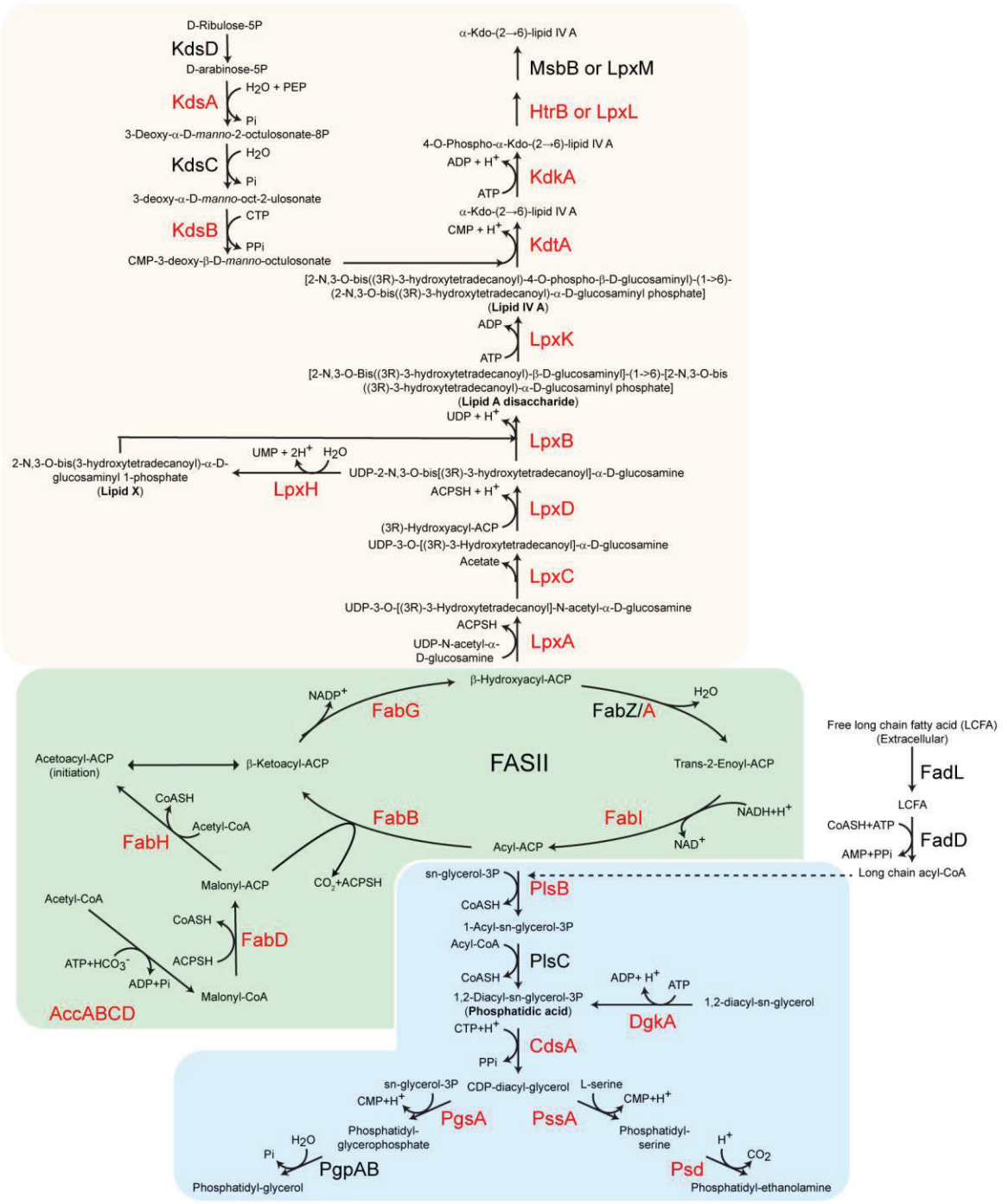

Figure S13. Schematic representation of *H. influenzae* lipid metabolism. Genes commonly predicted to be essential by the *i*NL638 model in both complete or minimal CDM, Gawronski et al., 2016, Wong et al., 2013 and Mobegi et al., 2014 (Gawronski et al., 2009; Mobegi et al., 2014; Wong et al., 2013) involved in the synthesis of fatty acids (FASII pathway, green shadow), phospholipids (blue shadow) and lipid A (orange shadow) are indicated in red.

```
Nβ1        Lβ1     Lα1         Lα2        Lβ2           Nα1

A1-NTHi375      MNSRILSTGSYLPSHIRTNADLEKMVDTSDEWIVTRSGIRERRIAAADETVATMGFEAAK    60
A2-P621         MNSRILSTGSYLPSHIRTNADLEKMVDTSDEWIVTRSGIRERRIAAEDETVATMGFEAAK    60
A3-RdKW20       MNSRILSTGSYLPSHIRTNADLEKMVDTSDEWIVTRSGIRERRIAAEDETVATMGFEAAK    60
A4-P652         MNSRILSTGSYLPSHIRTNADLEKMVDTSDEWIVTRSGIRERRIAAADETVATMGFEAAK    60
A5-P673         MNSRILSTGSYLPSHIRTNADLEKMVDTSDEWIVTRSGIRERRIAAADETVATMGFEAAK    60
A6-P642         MNSRILSTGSYLPSHIRTNADLEKMVDTSDEWIVTRSGIRERRIAAADETVATMGFEAAK    60
A7-P665         MNSRILSTGSYLPSHIRTNADLEKMVDTSDEWIVTRSGIRERRIAAADETVATMGFEAAK    60
A8-P657         MNSRILSTGSYLPSHIRTNADLEKMVDTSDEWIVTRSGIRERRIAAADETVATMGFEAAK    60
A9-P645         MNSRILSTGSYLPSHIRTNADLEKMVDTSDEWIVTRSGIRERRIAAEDETVATMGFEAAK    60
A10-P851        MNSRILSTGSYLPSHIRTNADLEKMVDTSDEWIVTRSGIRERRIAAADETVATMGFEAAK    60
A11-P593        MNSRILSTGSYLPSHIRTNADLEKMVDTSDEWIVTRSGIRERRIAAEDETVATMGFEAAK    60
A12-P607        MNSRILSTGSYLPSHIRTNADLEKMVDTSDEWIVTRSGIRERRIAAEDETVATMGFEAAK    60
A13-P590        MNSRILSTGSYLPSHIRTNADLEKMVDTSDEWIVTRSGIRERRIAAADETVATMGFEAAK    60
A14-P626        MNSRILSTGSYLPSHIRTNADLEKMVDTSDEWIVTRSGIRERRIAAADETVATMGFEAAK    60
                ********************************************** *************

                               Nβ2              Nα2         Nβ3      Nα3
A1-NTHi375      NAIEAAQINPQDIELIIVATTSHSHAYPSAACQVQGLLNIDDAISFDLAAACTGFVYALS    120
A2-P621         NAIEAAQINPQDIELIIVATTSHSHAYPSAACQVQGLLNIDDAISFDLAAACTGFVYALS    120
A3-RdKW20       NAIEAAQINPQDIELIIVATTSHSHAYPSAACQVQGLLNIDDAISFDLAAACTGFVYALS    120
A4-P652         NAIEAAQINPQDIELIIVATTSHSYAYPSAACQVQGLLNIDDAICFDLAAACTGFVYVLS    120
A5-P673         NAIEAAQINPQDIELIIVATTSHSYAYPSAACQVQGLLNIDDAICFDLAAACTGFVYALS    120
A6-P642         NAIGTAQINPQDIELVIVATTSHSHAYPSAACQVQGLLNIDDAISFDLAAACTGFVYALS    120
A7-P665         NAIEAAQINPQDIELIIVATTSHSHAYPSAACQVQGLLNIDDAISFDLAAACTGFVYALS    120
A8-P657         NAIEAAQINPQDIELIIVATTSHSHAYPSAACQVQGLLNIDDAICFDLAAACTGFVYALS    120
A9-P645         NAIEAAQINPQDIELIIVATTSHSHAYPSAACQVQGLLNIDDAISFDLAAACTGFVYALS    120
A10-P851        NAIGTAQINPQDIELVIVATTSHSHAYPSAACQVQGLLNIDDAISFDLAAACTGFVYALS    120
A11-P593        NAIEAAQINPQDIELIIVATTSHSHAYPSAACQVQGLLNIDDAISFDLAAACTGFVYALS    120
A12-P607        NAIEAAQINPQDIELIIVATTSHSHAYPSAACQVQGLLNIDDAISFDLAAACTGFVYALS    120
A13-P590        NAIEAAQINPQDIELIIVATTSHSHAYPSAACQVQGLLNIDDAISFDLAAACTGFVYALS    120
A14-P626        NAIEAAQINPQDIELIIVATTSHSHAYPSAACQVQGLLNIDDAICFDLAAACTGFVYALS    120
                *** :**********:********:*******************.************.**

                             Nβ4                          Nβ5        Cβ1
A1-NTHi375      VADQFIRAGKVKKALVIGSDLNSRKLDETDRSTVVLFGDGAGAVILEASEQEGIISTHLH    180
A2-P621         VADQFIRAGKVKKALVIGSDLNSRKLDETDRSTVVLFGDGAGAVILEASEQEGIISTHLH    180
A3-RdKW20       VADQFIRAGKVKKALVIGSDLNSRKLDETDRSTVVLFGDGAGAVILEASEQEGIISTHLH    180
A4-P652         VADQFIRAGKVKKALVIGSDLNSRKLDETDRSTVVLFGDGAGAVILEASEQEGIISTHLH    180
A5-P673         VADQFIRAGKVKKALVIGSDLNSRKLDETDRSTVVLFGDGAGAVILEASEQEGIISTHLH    180
A6-P642         VADQFIRAGKVKKALVIGSDLNSRKLDETDRSTVVLFGDGAGAVILEASEQEGIISTHLH    180
A7-P665         VADQFIRAGKVKKALVIGSDLNSRKLDETDRSTVVLFGDGAGAVILEASEQEGIISTHLH    180
A8-P657         VADQFIRAGKVKKALVIGSDLNSRKLDETDRSTVVLFGDGAGAVILEASEQEGIISTHLH    180
A9-P645         VADQFIRAGKVKKALVIGSDLNSRKLDETDRSTVVLFGDGAGAVILEANEQEGIISTHLH    180
A10-P851        VADQFIRAGKVKKALVIGSDLNSRKLDETDRSTVVLFGDGAGAVILEASEQEGIISTHLH    180
A11-P593        VADQFIRAGKVKKALVIGSDLNSRKLDETDRSTVVLFGDGAGAVILEASEQEGIISTHLH    180
A12-P607        VADQFIRAGKVKKALVIGSDLNSRKLDETDRSTVVLFGDGAGAVILEASEQEGIISTHLH    180
A13-P590        VADQFIRAGKVKKALVIGSDLNSRKLDETDRSTVVLFGDGAGAVILEASEQEGIISTHLH    180
A14-P626        VADQFIRAGKVKKALVIGSDLNSRKLDETDRSTVVLFGDGAGAVILEASEQEGIISTHLH    180
                ************************************************.***********

                       Lβ3           Lβ4       Cα1                       Cβ2
A1-NTHi375      ASADKNNALVLAQPERGIEKSGYIEMQGNETFKLAVRELSNVVEETLLANNLDKKDLDWL    240
A2-P621         ASADKNNALVLAQPERGIEKSGYIEMQGNETFKLAVRELSNVVEETLLANNLDKKDLDWL    240
A3-RdKW20       ASADKNNALVLAQPERGIEKSGYIEMQGNETFKLAVRELSNVVEETLLANNLDKKDLDWL    240
A4-P652         ASADKNNALVLAQPERAIEKSGYIEMQGNETFKLAVRELSNVVEETLLANNLDKKDLDWL    240
A5-P673         ASADKNNALVLAQPERAIEKSGYIEMQGNETFKLAVRELSNVVEETLLANNLDKKDLDWL    240
A6-P642         ASADKHNALVLAQPERGVEKSGYIEMQGNETFKLAVRELSNVVEETLLANNLDKKDLDWL    240
A7-P665         ASADKNNALVLAQPERGIEKSGYIEMQGNETFKLAVRELSNVVEETLSANNLDKKDLDWL    240
```

```
A8-P657          ASADKNNALVLAQPERAIEKSGYIEMQGNETFKLAVRELSNVVEETLLANNLDKKDLDWL    240
A9-P645          ASADKNNALVLAQPERGIEKSGYIEMQGNETFKLAVRELSNVVEETLLANNLDKKDLDWL    240
A10-P851         ASADKHNALVLAQPERGVEKSGYIEMQGNETFKLAVRELSNVVEETLLANNLDKKDLDWL    240
A11-P593         ASADKNNALVLAQPERGIEKSGYIEMQGNETFKLAVRELSNVVEETLSANNLDKKDLDWL    240
A12-P607         ASADKNNALVLAQPERGIEKSGYIEMQGNETFKLAVRELSNVVEETLLANNLDKKDLDWL    240
A13-P590         ASADKNNALVLAQPERGIEKSGYIEMQGNETFKLAVRELSNVVEETLLANNLDKKDLDWL    240
A14-P626         ASADKNNALVLAQPERGIEKSGYIEMQGNETFKLAVRELSNVVEETLSANNLDKKDLDWL    240
                 *****:**********.:***************************** ************

                              Cα2                 Lα3          Cα3              Cβ3
A1-NTHi375       VPHQANLRIITATAKKLEMDMSQVVVTLDKYANNSAATVPVALDEAIRDGRIQRGQLLLL    300
A2-P621          VPHQANLRIITATAKKLEMDMSQVVVTLDKYANNSAATVPVALDEAIRDGRIQRGELLLL    300
A3-RdKW20        VPHQANLRIITATAKKLEMDMSQVVVTLDKYANNSAATVPVALDEAIRDGRIQRGQLLLL    300
A4-P652          VPHQANLRIITATAKKLEMDMSQVVVTLDKYANNSAATVPVALDEAIRDGRIQRGQLLLL    300
A5-P673          VPHQANLRIITATAKKLEMDMSQVVVTLDKYANNSAATVPVALDEAIRDGRIQRGQLLLL    300
A6-P642          VPHQANLRIITATAKKLEMDMSQVVVTLDKYANNSAATVPVALDEAIRDGRIQRGQLLLL    300
A7-P665          VPHQANLRIITATAKKLEMDMSQVVVTLDKYANNSAATVPVALDEAIRDGRIQRGQLLLL    300
A8-P657          VPHQANLRIITATAKKLEMDMSQVVVTLDKYANNSAATVPVALDEAIRDGRIQRGQLLLL    300
A9-P645          VPHQANLRIITATAKKLEMDMSQVVVTLDKYANNSAATVPVALDEAVRDGRIQRGQLLLL    300
A10-P851         VPHQANLRIITATAKKLEMDMSQVVVTLDKYANNSAATVPVALDEAVRDGRIQRGQLLLL    300
A11-P593         VPHQANLRIITATAKKLEMDMSQVVVTLDKYANNSAATVPVALDESIRDGRIQRGQLLLL    300
A12-P607         VPHQANLRIITATAKKLEMDMSQVVVTLDKYANNSAATVPVALDEAVRDGRIQRGQLLLL    300
A13-P590         VPHQANLRIITATAKKLEMDMSQVVVTLDKYANNSAATVPVALDEAVRDGRIQRGQLLLL    300
A14-P626         VPHQANLRIITATAKKLEMDMSQVVVTLDKYANNSAATVPVALDEAIRDGRIQRGQLLLL    300
                 ********************************************::********:****

                       Cβ4
A1-NTHi375       EAFGGGWTWGSALVRF*          316
A2-P621          EAFGGGWTWGSALVRF*          316
A3-RdKW20        EAFGGGWTWGSALVRF*          316
A4-P652          EAFGGGWTWGSALVRF*          316
A5-P673          EAFGGGWTWGSALVRF*          316
A6-P642          EAFGGGWTWGSALVRF*          316
A7-P665          EAFGGGWTWGSALVRF*          316
A8-P657          EAFGGGWTWGSALVRF*          316
A9-P645          EAFGGGWTWGSALVRF*          316
A10-P851         EAFGGGWTWGSALVRF*          316
A11-P593         EAFGGGWTWGSALVRF*          316
A12-P607         EAFGGGWTWGSALVRF*          316
A13-P590         EAFGGGWTWGSALVRF*          316
A14-P626         EAFGGGWTWGSALVRF*          316
                 ****************
```

Figure S14. Multiple alignment of FabH variants identified in a previously whole-genome sequenced NTHi clinical isolate collection (Moleres et al., 2018). Polymorphisms are labeled in red except for those mapping at the FabH monomer-monomer interface labeled in green; the conserved catalytic triad Cys112-His243-Asn273 is labeled in blue. FabH comprises two similarly folded N-terminal (residues 1-170) and C-terminal halves (residues 171-316). Elements of secondary structure in $FabH_{RdKW20}$ structure are highlighted by colors. N-terminal domain core: alpha-helices (Nα1-Nα3) in light cyan and βeta-strands (Nβ1-Nβ5) in orange. C-terminal domain core: alpha-helices (Cα1-Cα3) in dark cyan and βeta-strands (Cβ1-Nβ54) in magenta. Elements of N-terminal insertions are in yellow (Lβ1-Lβ2) and light blue (Lα1-Lα2), and C-terminal ones in light pink (Lβ3-Lβ4) and green (Lα3).

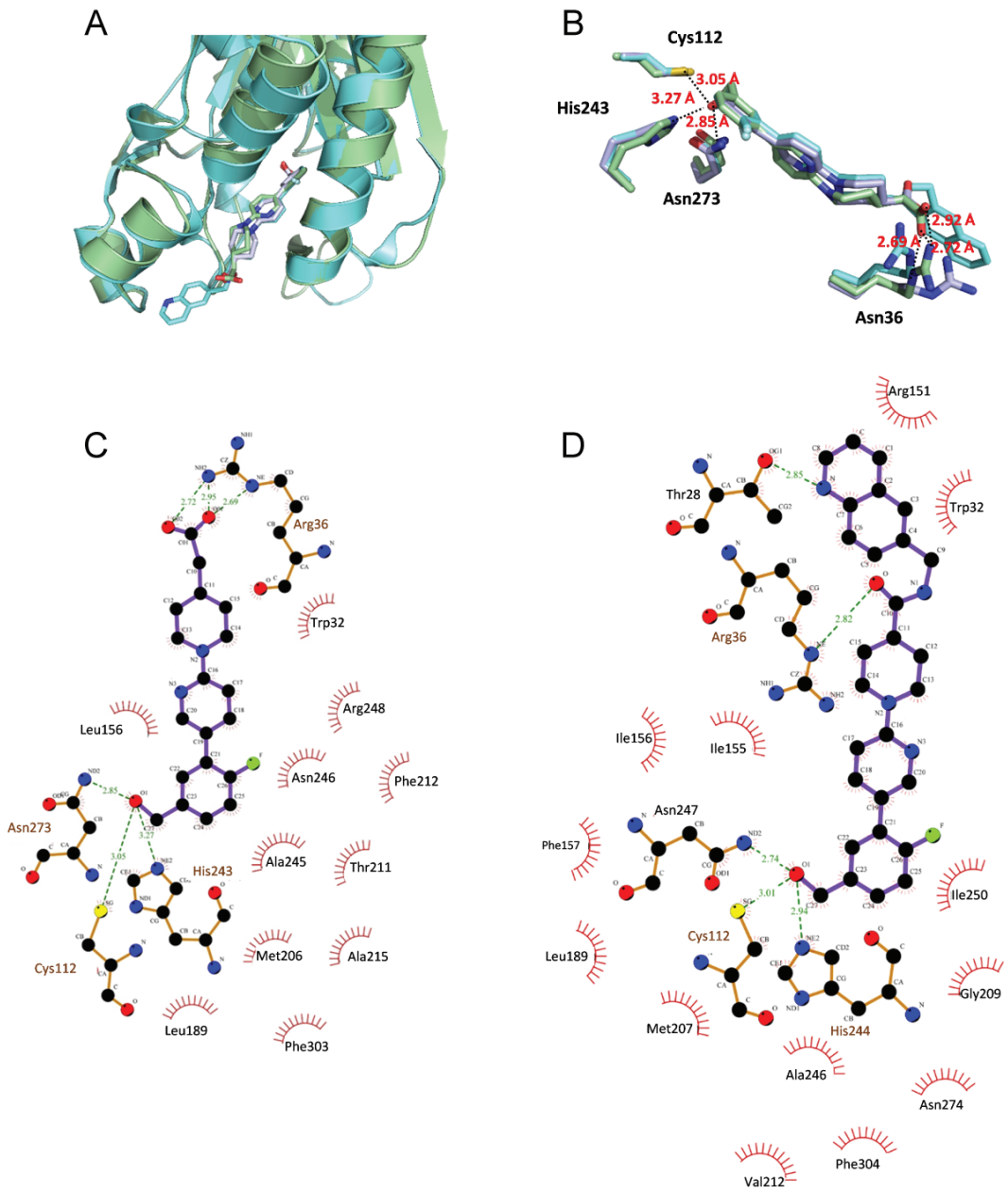

Figure S15. FabHi:FabH$_{RdKW20}$ interaction mode compared with crystal structures of the *E. coli* enzyme in complex with close structural analogues of the inhibitor. (A) FabHi bound to FabH$_{RdKW20}$ (green) superimposed to *E. coli* FabH (cyan) in complex with compounds 23 (violet) and 36 (cyan) (McKinney et al., 2016 (McKinney et al., 2016) ; ligand PDB entries: 5BNR and 5BNS, respectively). **(B)** Comparison of ligand disposition in the FabH$_{RdKW20}$ docking complex and the FabH$_{E. coli}$ complexes shown in **(A)**. Protein residues at hydrogen-bonding distance are also depicted (same color code). **(C)** and **(D)** Ligplot representation of hydrogen bonds (dashed lines) and hydrophobic contacts (brown arcs with radiating spokes) in the FabHi:FabH$_{RdKW20}$ complex, and the 5BNS *E. coli* complex, respectively.

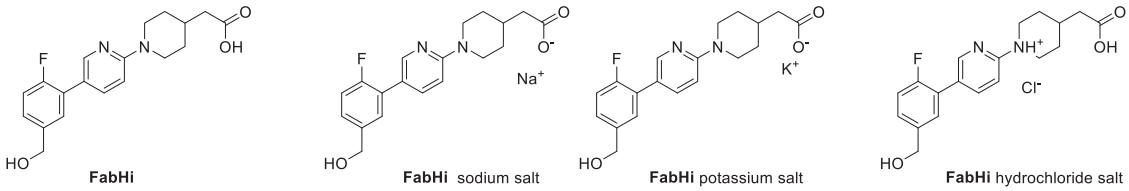

Figure S16. Structure of FabHi and its sodium, potassium and hydrochloride salts.

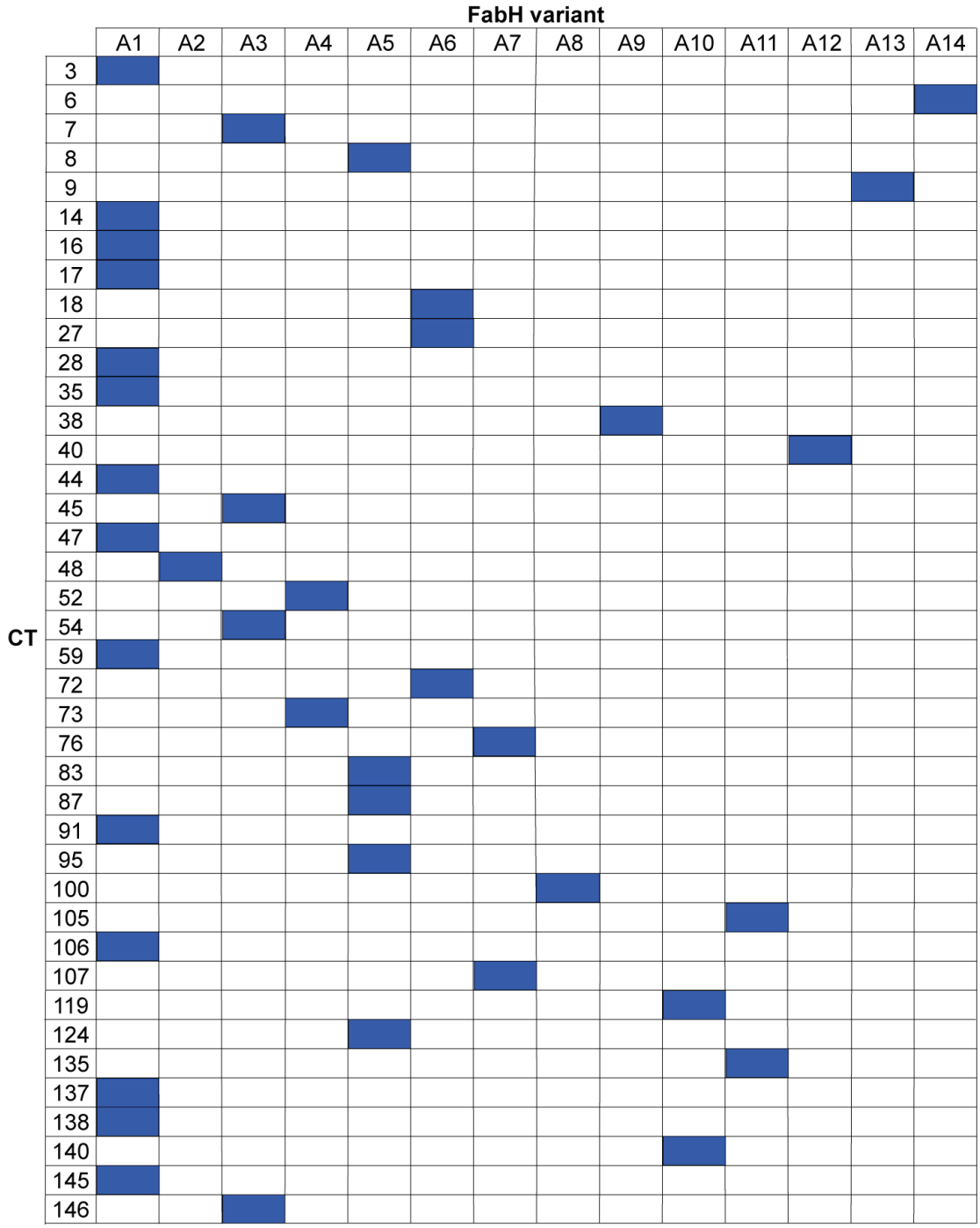

Figure S17. Distribution of FabH variants A1 to A14 among previously established clonal types (CT) in a genome-sequenced NTHi clinical strain collection (Moleres et al., 2018). Intra-CT variation was not observed

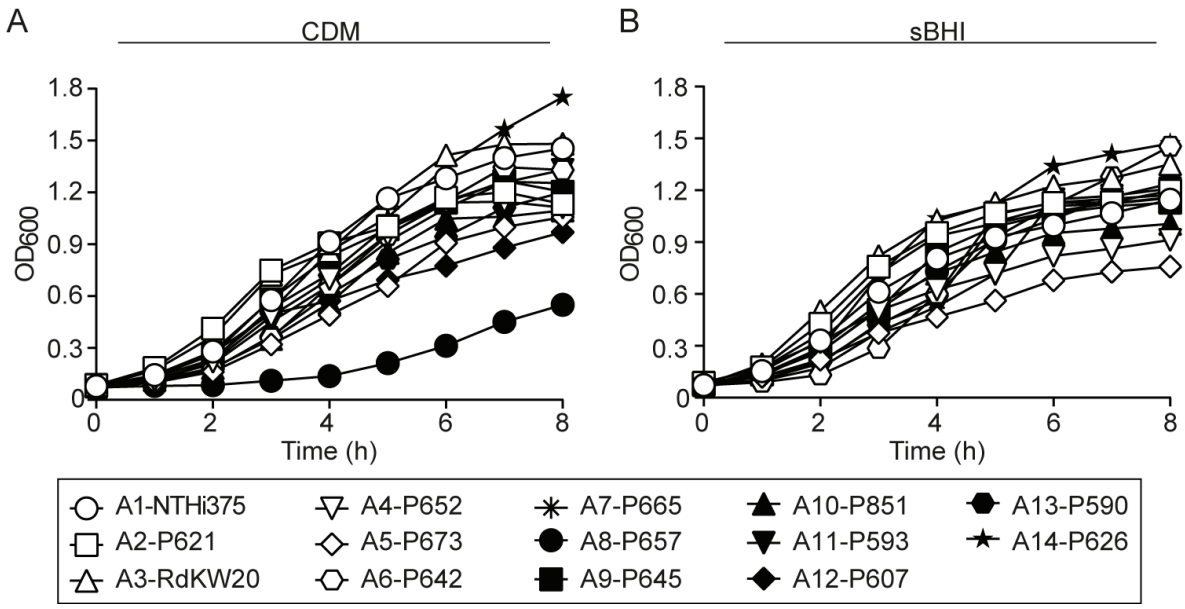

Figure S18. Growth of *H. influenzae* selected strains carrying FabH variants A1 to A14 in two different media, CDM (**A**) or sBHI (**B**). NTHi strains grown on PVX agar for 16 h were inoculated (2 to 3 colonies) in 10 mL sBHI or CDM using 100 mL flasks, and incubated for 11 h with shaking (100 r.p.m.). Cultures were then diluted to OD_{600} = 0.07 in a final volume of 25 mL sBHI or CDM using 250 mL flasks, grown with shaking (180 r.p.m.), and OD_{600} was recorded every hour for up to 8 h.

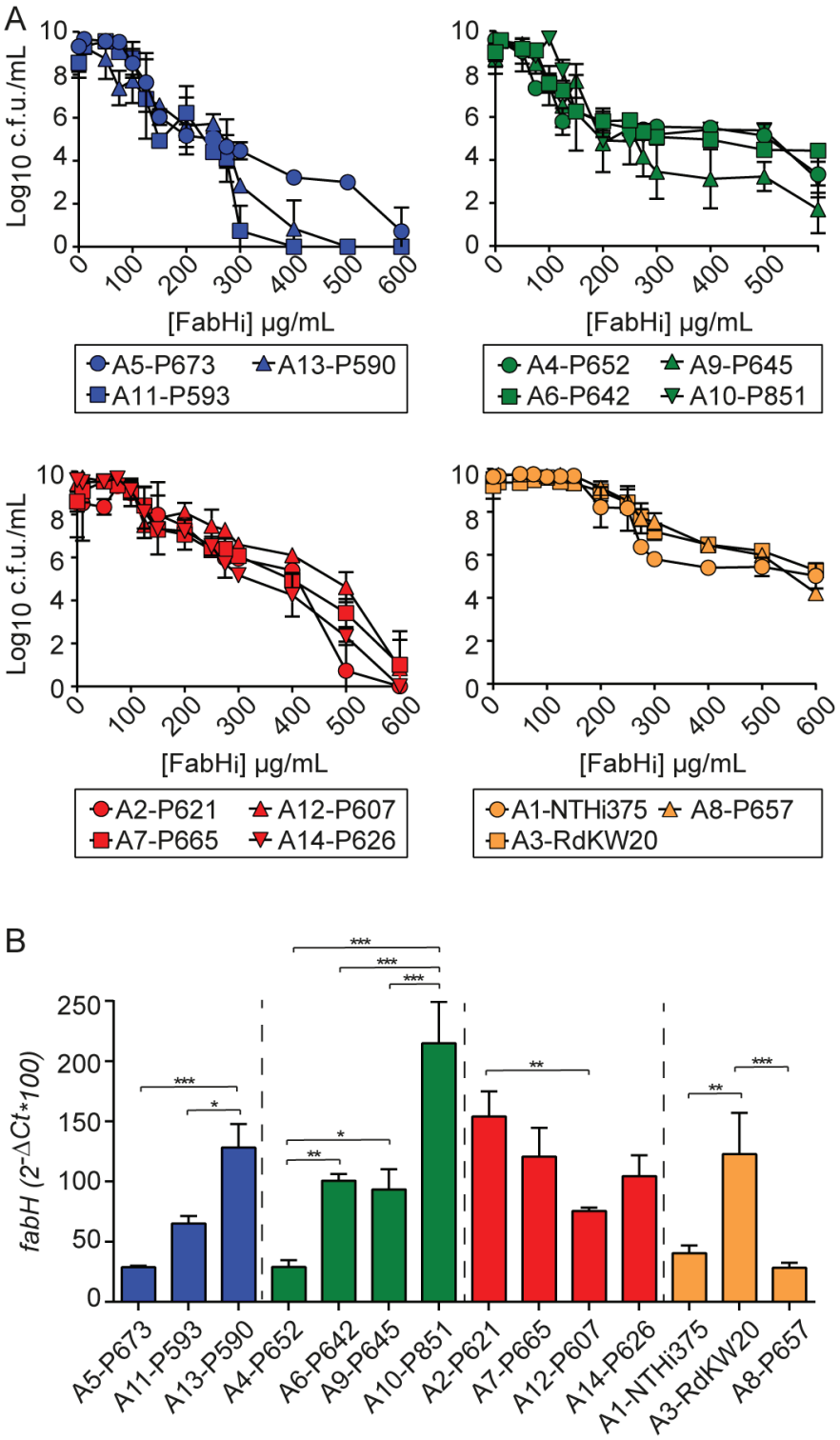

Figure S19. Antimicrobial effect of FabHi on *H. influenzae*. (A) Determination of FabHi inhibitory effect on a panel of representative NTHi strains carrying different FabH allelic variant (A1 to A14), grown in CDM. Strains were shown to be susceptible to FabHi in a dose-dependent manner, and were classified into four groups (blue, green, red, orange labeling) based on increasing resistance. FabHi concentrations tested range from 10 to 600 µg/mL. Results are shown as Log_{10} c.f.u./mL (mean ± SD). For each strain, statistical comparisons of means were performed by one-way ANOVA and Dunnett's multiple-comparisons test. A significant reduction on bacterial viability was observed as it follows: A1-NTHi375, at [FabHi] 200 µg/mL and higher, $p<0.0001$; A2-P621, at [FabHi] 250 µg/mL and higher, $p<0.0005$; A3-RdKW20, at [FabHi] 250 µg/mL and higher, $p<0.0001$; A4-P652, at [FabHi] 75 µg/mL and higher, $p<0.0001$; A5-P673, at [FabHi] 125 µg/mL and higher, $p<0.0001$; A6-P642, at [FabHi] 100 µg/mL and higher, $p<0.0001$; A7-P665, at [FabHi]

150 µg/mL and higher, p<0.05; A8-P657, at [FabHi] 200 µg/mL and higher, p<0.005; A9-P645, at [FabHi] 200 µg/mL and higher, p<0.0001; A10-P851, at [FabHi] 150 µg/mL and higher, p<0.0001; A11-P593, at [FabHi] 125 µg/mL and higher, p<0.05; A12-P607, at [FabHi] 125 µg/mL and higher, p≤0.0005; A13-P590, at [FabHi] 125 µg/mL and higher, p<0.05; A14-P626, at [FabHi] 125 µg/mL and higher, p<0.0001. **(B)** Expression of the *fabH* gene in a panel of representative NTHi strains carrying different *fabH* allelic variant, grown in CDM to half of each strain's maximal OD_{600}. This gene expression was shown to be variable among strains, and not linked to the differences observed in terms of susceptibility. Statistical comparisons of means were performed for each previously established group by one-way ANOVA and Tukey's multiple comparisons test (*p < 0.05; **p<0.005; ***p <0.0001).

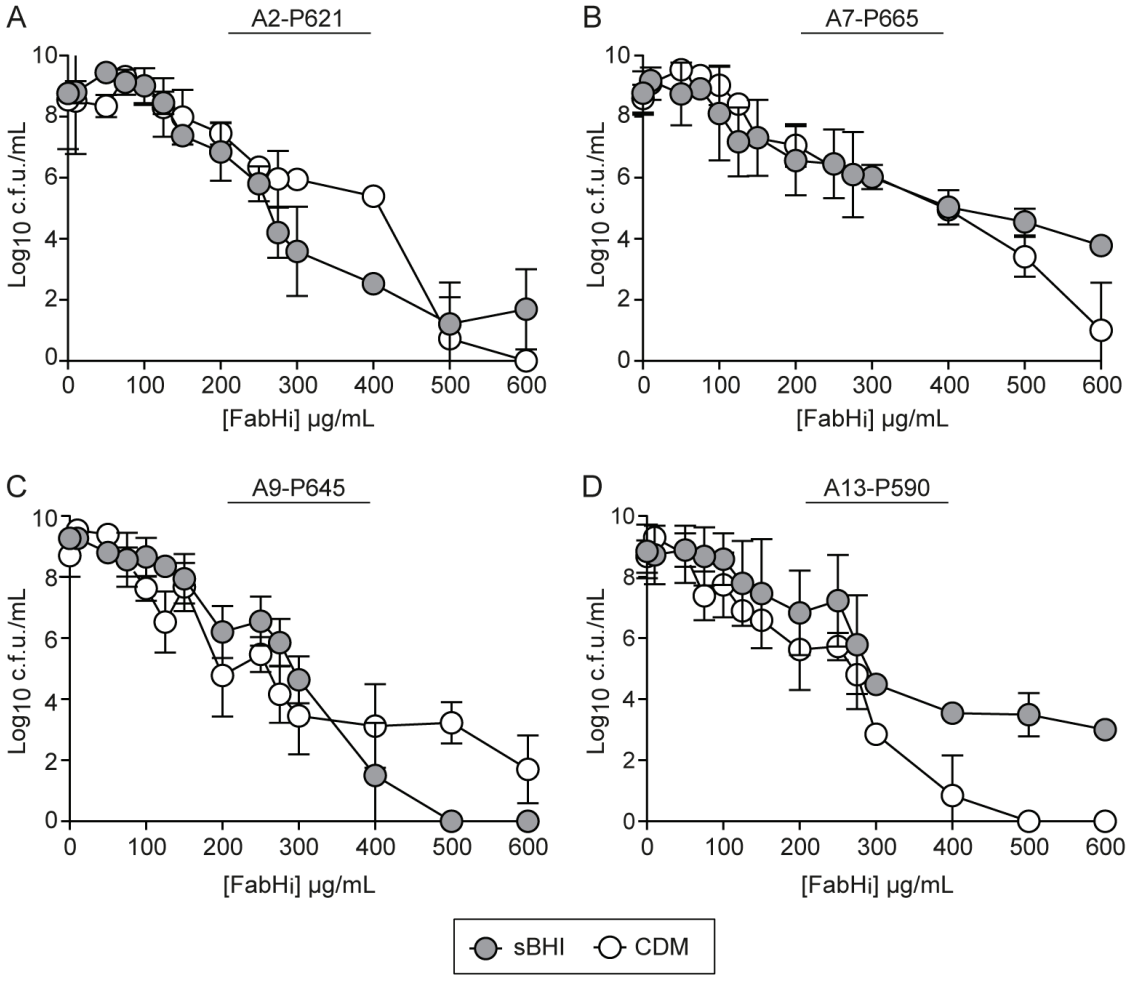

Figure S20. Antimicrobial effect of FabHi on strains A2-P621 (**A**), A7-P665 (**B**), A9-P645 (**C**), A13-P590 (**D**), grown in sBHI (gray circles) or CDM (white circles). For each strain, statistical comparisons of means were performed by two-way ANOVA and Sidak's multiple-comparisons test. A significant difference on bacterial viability was observed as it follows: A2-P621, at [FabHi] 275, 300 and 400 µg/mL, p<0.005; A7-P665, at [FabHi] 600 µg/mL, p<0.0001; A9-P645, at [FabHi] 125, 200, 275, 400 µg/mL and higher, p<0.05; and A13-P590, at [FabHi] 400 µg/mL and higher, p<0.005.

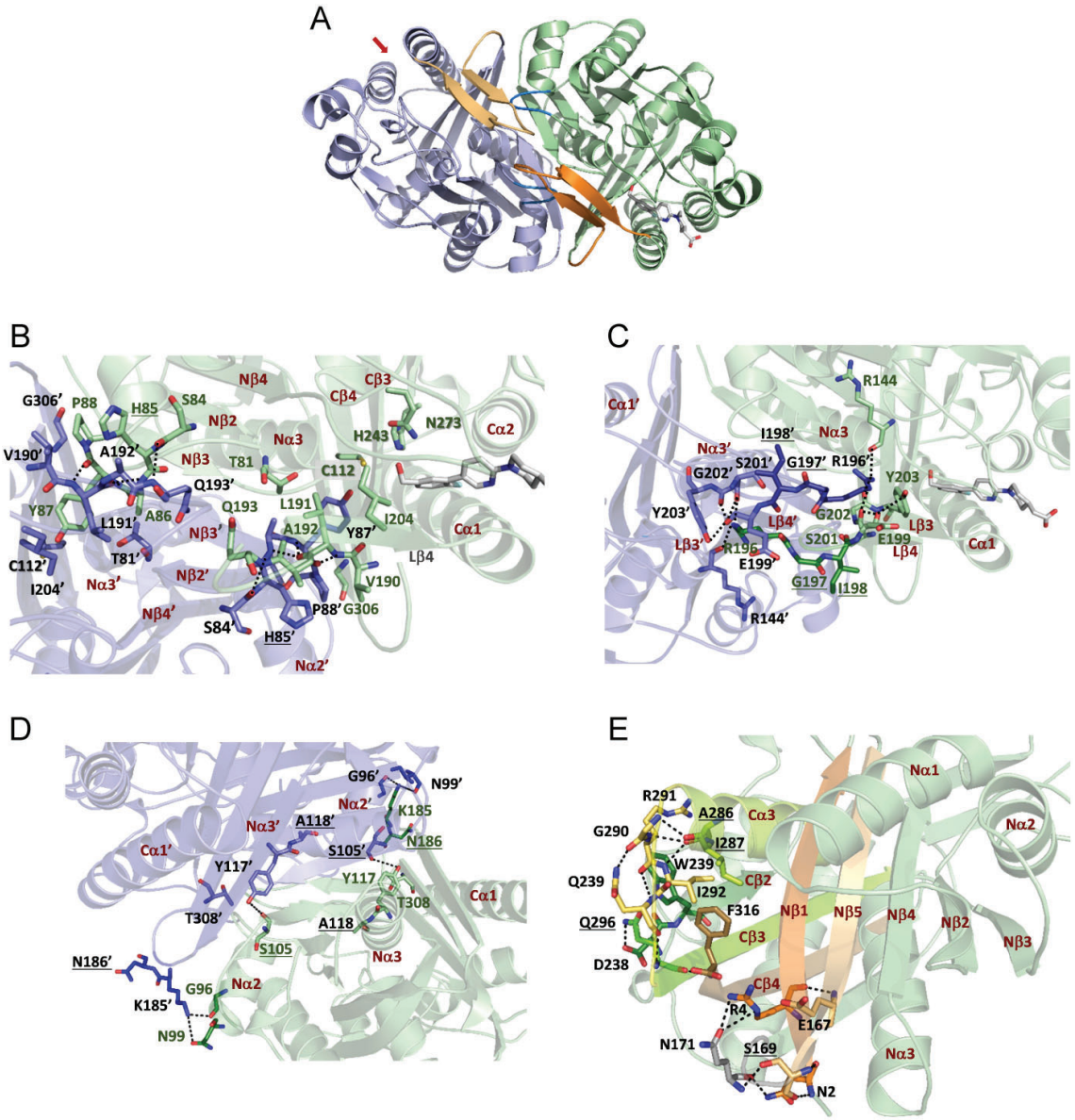

Figure S21. Polymorfisms of FabH may affect FabH stability and activity. (A) Structure of the FabH dimer with FabHi (sticks) bound to the active site of one monomer; the red arrow points to the active site of complementary subunit. Loops comprising residues 84-89 or 185-207 are colored in blue and orange, respectively. **(B)–(D)** Details of contacts at the dimer interface potentially sensitive to polymorphisms at positions 85 **(B)**, 197-198 **(C)**, 105, 118 and 186 **(D)**. **(E)** Details of contacts relevant for the monomer stability potentially affected by polymorphisms of residues 169, 286, 287 and 296. Ser169 of RdKW20, together with E167, keep the orientation of strands Nβ1 and Nβ5 (N-terminal domain) by hydrogen bonding to Asn2 and Arg4 residues. Network of hydrogen bonds participated by Ala286, Ile287 and Glu296 helping orientation of Cβ2, Cα3, Cβ3, Cβ4 and configuration of loop connecting Cα3 to Cβ3 (C-terminal domain). Residues affected by polymorphisms are underlined and catalytic residues (Cys112, H243 and N273) are shadowed. Elements of secondary structure are indicated in brown lettering (N and C refers to the N-terminal and C-terminal domains, respectively).

```
A1-NTHi375      MKIILVVFVLIFVGVIGFNIIKGVMISRAIAEMPESSSPVTALEVQPREWTPVINTTGLV    60
A2-P621         MKIILVVFVLIFVGVIGFNMIKGVMISRAIAGMPEPSSPVTALEVQPREWTPVINTTGLI    60
A3-RdKW20       MKIILVVFVLIFVGVIGFNMIKGVMISRAIAGMPESSSPVTALEVQPREWTPVINTTGLV    60
A4-P652         MKIILVVFVLIFASVIGFNMIKGIMISRAIAEMPEPSSPVTALEVQPREWTPVINTTGLV    60
A5-P673         MKIILVVFVLIFVGVIGFNMIKGVMISRAIAEMPEPSSPVTALEVQPREWTPVINTTGLV    60
A7-P665         MKIILVVFVLIFVGVIGFNMIKGVMISRAIAEMPEPSSPVTALEVQPREWTPVINTTGLV    60
A8-P657         MKIILVVFVLIFASVIGFNMIKGIMISRAIAEMPEPSSPVTALEVQPREWTPVINTTGLV    60
A9-P645         MKIILVVFVLIFVGVIGFNMIKGVMISRAIAEMPEPSSPVTALEVQPREWTPVINTTGLV    60
A10-P851        MKIILVVFVLIFVGVIGFNMIKDVMISRAIAEMPEPSSPVTALEVQPREWTPVINTTGLV    60
A11-P593        MKIILVVFVLIFVGVIGFNMIKGVMISRAIAGMPEPSSPVTALEVQPREWTPVINTTGLV    60
A12-P607        MKIILVVFVLIFVGVIGFNMIKGVMISRAIAEMPESSSPVTALEVQPREWTPVINTTGLV    60
A13-P590        MKVILAVFVLIFAGVIGFNVFKGVMTSRVIASMPEPSSPVTALEVQPREWTPVINTTGLI    60
A14-P626        MKIILVVFVLIFVGVIGFNMIKGVMISRAIAEMPEPSSPVTALEVQPREWTPVINTTGLV    60
                **:**.******..*****::*.:* **.** *** **********************:

A1-NTHi375      RPNQGALLSTQNAGTISQVLVQNGQNVKKGEVLVELDSSVERANLQAAQAQLSALRQTYQ    120
A2-P621         RPHQGAMLSAQNAGTVSQVLVQNGQNVKKGEVLVELDSSVERASLQAAQAQLSALRQTYQ    120
A3-RdKW20       RPNQGAMLSTQNAGAVSQVLVQNGQNVKKGEVLVELDSSVERANLQAAQAQLSALRQTYQ    120
A4-P652         RPNQGAMLSTQNTGAVSQVLVQNGQNVKKGEVLVELDSSVERANLQAAQAQLSALRQTYQ    120
A5-P673         RPNQGVMLSTQNAGAVSQVLVQNGQNVKKGEVLVELDSSVERANLQAAQAQLSALRQTYQ    120
A7-P665         RPNQGAMLSTQNAGAVSQVLVQNGQNVKKGEVLVELDSSVERANLQAAQAQLSALRQTYQ    120
A8-P657         RPNQGAMLSTQNAGAVSQVLVQNGQNVKKGEVLVELDSSVERANLQAAQAQLSALRQTYQ    120
A9-P645         RPNQGAMLSTQNAGTISQVLVQNGQNVKKGEVLVELDSSVERSNLQAAQAQLSALRQTYQ    120
A10-P851        RANQGAMLSTQNAGTISQVLVQNGQQVKKGDLLIELDSSVEHASLQAAQAQLPALRQTYQ    120
A11-P593        RANQGAMLSTQNAGTISQVLVQNGQNVKKGDLLIELDSSVEHASLQAAQAQLPALRQTYQ    120
A12-P607        RPNQGAMLSTQNAGTISQVLVQNGQQVKKGDLLIELDSSVEHASLQAAQAQLPALRQTYQ    120
A13-P590        RPHQGAMLSAQNAGTVSQVLVQNGQNVKKGEVLVELDNFVERASLQAAQAQLSALRQTYQ    120
A14-P626        RANQGAMLSTQNAGTISQVLVQNGQQVKKGDLLIELDSSVEHASLQAAQAQLPALRQTYQ    120
                * :**.:**:**:*::*********:****::*:***. **::.******** *******

A1-NTHi375      RYVGLLNSNAVSRQEMDNAKAAYDAQLANIESLKAVIERRKIVAPFDGKAGIVKINVGQY    180
A2-P621         RYVSLLNSNAVSRQEMDNAKAAYDAQVANIESLKAVIERRKIVAPFDGKAGIVKINIGQY    180
A3-RdKW20       RYVGLLNSNAVSRQEMDNAKAAYDAQVASIESLKAAIERRKIVAPFDGKAGIVKINVGQY    180
A4-P652         RYVGLLNSNAVSRQEMDNAKAAYDAQVASIESLKAAIERRKIVAPFDGKAGIVKVNVGQY    180
A5-P673         RYVGLLNSNAVSRQEMDNAKAAYDAQVASIESLKAAIERRKIVAPFDGKAGIVKVNVGQY    180
A7-P665         RYVGLLNSNAVSRQEMDNAKAAYDAQVASIESLKAAIERRKIVAPFDGKAGIVKVNVGQY    180
A8-P657         RYVGLLNSNAVSRQEMDNAKAAYDAQVASIESLKAAIERRKIVAPFDGKAGIVKINVGQY    180
A9-P645         RYVGLLNSNAVSRQEMDNAKAAYDAQVASIESLKAAIERRKIVAPFDGKAGIVKINVGQY    180
A10-P851        RYANLLKSNAVSRQEMDNAKAAYDAQVASIESLKAAIERRKIVAPFDGKAGIVKVNVGQY    180
A11-P593        RYANLLKSNAVSRQEMDNAKAAYDAQLANIESLKAVIERRKIVAPFDGKAGIVKVNVGQY    180
A12-P607        RYANLLKSNAVSRQEMDNAKAAYDAQLANIESLKAVIERRKIVAPFDGKAGIVKVNVGQY    180
A13-P590        RYVSLLNSNAVSRQEMDNAKAAYDAQVANIESLKAAIERRKIVAPFDGKAGIVKINIGQY    180
A14-P626        RYANLLKSNAVSRQEMDNAKAAYDAQLANIESLKAVIERRKIVAPFDGKAGIVKVNVGQY    180
                **..**:********************:*.******.******************:*:***

A1-NTHi375      VNVGTEIVRVEDTSSMKVDFALSQNDLDKLHIGQRVTATTDARLGETFSARITAIEPAIN    240
A2-P621         VNVGTEIVRVEDTSSMKVDFALSQNDLDKLHISQRVTATVDARSGETFSARITAIEPAVN    240
A3-RdKW20       VNVGTEIVRVEDTSSMKVDFALSQNDLDKLHIGQRVTATTDARLGETFSARITAIEPAIN    240
A4-P652         VNVGTEIVRVEDTSSMKVDFALSQNDLDKLHIGQRVTATTDARLGETFSARITAIEPAIN    240
A5-P673         VNVGTEIVRVEDTSSMKVDFALSQNDLDKLHIGQRVTATTDARLGETFSARITAIEPAIN    240
A7-P665         VNVGTEIVRVEDTSSMKVDFALSQNDLDKLHIGQRVTATTDARLGETFSARITAIEPAIN    240
A8-P657         VNVGTEIVRVEDTSSMKVDFALSQNDLDKLHIGQRVTATTDARLGETFSARITAIEPAIN    240
A9-P645         VNVGTEIVRVEDTSSMKVDFALSQNDLDKLHIGQRVTATTDARLGETFSARITAIEPAIN    240
A10-P851        VNVGTEIVRVEDTSSMKVDFALSQNDLDKLHIGQRVTATTDARLGETFSARITAIEPAIN    240
A11-P593        VNVGTEIVRVEDTSSMKVDFALSQNDLDKLHIGQRVTATTDARLGETFSARITAIEPAIN    240
A12-P607        VNVGTEIVRVEDTSSMKVDFALSQNDLDKLHIGQRVTATTDARLGETFSARITAIEPAIN    240
A13-P590        VNVGTEIVRVEDTSSMKVDFALSQNDLDKLHIGQRVTATVDARSGETFSARITAIEPAVN    240
```

```
A14-P626        VNVGTEIVRVEDTSSMKVDFALSQNDLDKLHIGQRVTATTDARLGETFSARITAIEPAIN    240
                ********************************.******.*** **************:*

A1-NTHi375      SSTGLVDVQATFNPEDGHKLLSGMFSRLRIALPTETNQVVVPQVAISYNMYGEIAYLLEP    300
A2-P621         AATGLVDIQATFDPEDERKLLSGMFSRLRIALSTETNQIVVPQVAISYNMYGEIAYLLTP    300
A3-RdKW20       SSTGLVDVQATFDPEDGHKLLSGMFSRLRIALPTETNQVVVPQVAISYNMYGEIAYLLEP    300
A4-P652         SSTGLVDVQATFDPEDGHKLLSGMFSRLRIALPTETNQVIVPQVAISYNMYGEIAYLLEP    300
A5-P673         SSTGLVDVQATFDPEDGHKLLSGMFSRLRIALPTETNQVVVPQVAISYNMYGEIAYLLEP    300
A7-P665         SSTGLVDVQATFDPEDGHKLLSGMFSRLRIALLTETNQVVVPQVAISYNMYGEIAYLLEP    300
A8-P657         SSTGLVDVQATFDPEDGHKLLSGMFSRLRIALPTETNQVVVPQVAISYNMYGEIAYLLEP    300
A9-P645         SSTGLVDVQATFDPEDGHKLLSGMFSRLRIALPTETNQVVVPQVAISYNMYGEIAYLLEP    300
A10-P851        SSTGLVDVQATFDPEDGHKLLSGMFSRLRIALPTETNQVVVPQVAISYNMYGEIAYLLEP    300
A11-P593        SSTGLVDVQATFDPEDGHKLLSGMFSRLRIALPTETNQVVVPQVAISYNMYGEIAYLLEP    300
A12-P607        SSTGLVDVQATFDPEDGHKLLSGMFSRLRIALPTETNQVVVPQVAISYNMYGEIAYLLEP    300
A13-P590        AATGLVDIQATFDPEDGRKLLSGMFSRLRIALSTETNQIVVPQVAISYNMYGEIAYLLTP    300
A14-P626        SSTGLVDVQATFNPEDGHKLLSGMFSRLRIALPTETNQVVVPQVAISYNMYGEIAYLLEP    300
                ::*****:****:*** :************** *****::****************** *

A1-NTHi375      LSEEEKGKMSGNEKLDRLYRAKQITVFTKDRQGVYAQLQGNEVKAGDKIITGGQQGIGNG    360
A2-P621         LSDEDKGKMSGNEKLDRLYRAKQITVFTKDRQGVYAQLQGNEVKAGDKIITGGQQGIGNG    360
A3-RdKW20       LSEEEKGKMSGNEKLDRLYRAKQITVFTKDRQGVYAQLQGNEVKVGDKIITGGQQGIGNG    360
A4-P652         LSEEEKGKMSGNEKLDHLYRAKQITVFTKDRQGVYAQLQGNEVKAGDKIITGGQQGIGNG    360
A5-P673         LSEEEKGKMSGNEKLDRLYRAKQITVFTKDRQGVYAQLQGNEVKAGDKIITGGQQGIGNG    360
A7-P665         LSEEEKGKMSGNEKLDRLYRAKQITVFTKDRQGVYAQLQGNEVKAGDKIITGGQQGIGNG    360
A8-P657         LSEEEKGKMSGNEKLDRLYRAKQITVFTKDRQGVYAQLQGNEVKAGDKIITGGQQGIGNG    360
A9-P645         LSEEEKGKMSGNEKLDRLYRAKQITVFTKDRQGVYAQLQGNEVKAGDKIITGGQQGIGNG    360
A10-P851        LSEEEKGKMSGNEKLDRLYRAKQITVFTKDRQGVYAQLQGNEVKAGDKIITGGQQGIGNG    360
A11-P593        LSEEEKGKMSGNEKLDRLYRAKQITVFTKDRQGVYAQLQGNEVKAGDKIITGGQQGIGNG    360
A12-P607        LSEEEKGKMLGNEKLDRLYRAKQITVFTKDRQGVYAQLQGNEVKAGDKIITGGQQGIGNG    360
A13-P590        LSDEDKGKMSGNEKLDRLYRAKQITVFTKDRQGVYAQLQGNEVKAGDKIITGGQQGIGNG    360
A14-P626        LSEEEKGKMSGNEKLNRLYRAKQITVFTKDRQGVYAQLQGNEVKAGDKIITGGQQGIGNG    360
                **:*:**** ***** ::****************************.***************

A1-NTHi375      SLVEWIKKDIVGAVEPAHKTPL    382
A2-P621         SLVEWIKKDIVGAVEPAHKTPL    382
A3-RdKW20       SLVEWIKKDIVGAIEPAHKTPL    382
A4-P652         SLVEWIKKDIVGAIEPAHKTPL    382
A5-P673         SLVEWIKKDIVGAIEPAHKTPL    382
A7-P665         SLVEWIKKDIVGAVEPAHKTPL    382
A8-P657         SLVEWIKKDIVGAVEPAHKTPL    382
A9-P645         SLVEWIKKDIVGAVEPAHKTPL    382
A10-P851        SLVEWIKKDIVGAVEPAHKTPL    382
A11-P593        SLVEWIKKDIVGAVEPAHKTPL    382
A12-P607        SLVEWIKKDIVGAVEPAHKTPL    382
A13-P590        SLVEWIKKDIVGAVEPAHKTPL    382
A14-P626        SLVEWIKKDIVGAVEPAHKTPL    382
                *************:********
```

Figure S22. Distribution of AcrA variants among the 14 selected NTHi isolates. Thirteen AcrA variants were found. The P642 and NTHi375 strains presented the same AcrA variant. Polymorphisms are indicated in red.

```
A1-NTHi375      MYEEIRMKFTDIFIRRPVLAVSISLLMIILGLQAISKLAVREYPKMTTTVITVSTAYPGA    60
A2-P621         MYEEIRMKFTDIFIRRPVLAVSISLLMIILGLQAISKLAVREYPKMTTTVITVSTAYPGA    60
A3-RdKW20       MYEEIRMKFTDIFIRRPVLAVSISLLMIILGLQAISKLAVREYPKMTTTVITVSTAYPGA    60
A4-P652         MYEEIRMKFTDIFIRRPVLAVSISLLMIILGLQAISKLAVREYPKMTTTVITVSTAYPGA    60
A6-P642         MYEEIRMKFTDIFIRRPVLAVSISLLMIILGLQAISKLAVREYPKMTTTVITVSTAYPGA    60
A7-P665         MYEEIRMKFTDIFIRRPVLAVSISLLMIILGLQAISKLAVREYPKMTTTVITVSTAYPGA    60
A8-P657         MYEEIRMKFTDIFIRRPVLAVSISLLMIILGLQAISKLAVREYPKMTTTVITVSTAYPGA    60
A9-P645         MYEEIRMKFTDIFIRRPVLAVSISLLMIILGLQAISKLAVREYPKMTTTVITVSTAYPGA    60
A10-P851        MYEEIRMKFTDIFIRRPVLAVSISLLMIILGLQAISKLAVREYPKMTTTVITVSTAYPGA    60
A11-P593        MYEEIRMKFTDIFIRRPILAVSISLLMIILGLQAISKLAVREYPKMTTTVITVSTAYPGA    60
A12-P607        MYEEIRMKFTDIFIRRPVLAVSISLLMIILGLQAISKLAVREYPKMTTTVITVSTAYPGA    60
A13-P590        MYEEIRMKFTDIFIRRPVLAVSISLLMIILGLQAISKLAVREYPKMTTTVITVSTAYPGA    60
A14-P626        MYEEIRMKFTDIFIRRPVLAVSISLLMIILGLQAISKLAVREYPKMTTTVITVSTAYPGA    60
                ****************:*******************************************

A1-NTHi375      DANLIQAFVTSKLEESIAQADNIDYMSSTSAPSSSTITIKMKLNTDPAGALADVLAKVNA    120
A2-P621         DANLIQAFVTSKLEESIAQADNIDYMSSTSAPSSSTITIKMKLNTDPAGALADVLAKVNA    120
A3-RdKW20       DANLIQAFVTSKLEESIAQADNIDYMSSTSAPSSSTITIKMKLNTDPAGALADVLAKVNA    120
A4-P652         DANLIQAFVTSKLEESIAQADNIDYMSSTSAPSSSTITIKMKLNTDPAGALADVLAKVNA    120
A6-P642         DANLIQAFVTSKLEESIAQADNIDYMSSTSAPSSSTITIKMKLNTDPAGALADVLAKVNA    120
A7-P665         DANLIQAFVTSKLEESIAQADNIDYMSSTSAPSSSTITIKMKLNTDPAGALADVLAKVNA    120
A8-P657         DANLIQAFVTSKLEESIAQADNIDYMSSTSAPSSSTITIKMKLNTDPAGALADVLAKVNA    120
A9-P645         DANLIQAFVTSKLEESIAQADNIDYMSSTSAPSSSTITIKMKLNTDPAGALADVLAKVNA    120
A10-P851        DANLIQAFVTSKLEESIAQADNIDYMSSTSAPSSSTITIKMKLNTDPAGALADVLAKVNA    120
A11-P593        DANLIQAFVTSKLEESIAQADNIDYMSSTSAPSSSTITIKMKLNTDPAGALADVLAKVNA    120
A12-P607        DANLIQAFVTSKLEESIAQADNIDYMSSTSAPSSSTITIKMKLNTDPAGALADVLAKVNA    120
A13-P590        DANLIQAFVTSKLEESIAQADNIDYMSSTSAPSSSTITIKMKLNTDPAGALADVLAKVNA    120
A14-P626        DANLIQAFVTSKLEESIAQADNIDYMSSTSAPSSSTITIKMKLNTDPAGALADVLAKVNA    120
                ************************************************************

A1-NTHi375      VKSALPNGIEDPSVSSSSGGSGIMYISFRSKKLDSSQVTDYINRVVKPQFFTIEGVAEVQ    180
A2-P621         VKSALPNGIEDPSVSSSSGGSGIMYISFRSKKLDSSQVTDYINRVVKPQFFTIEGVAEVQ    180
A3-RdKW20       VKSALPNGIEDPSVSSSSGGSGIMYISFRSKKLDSSQVTDYINRVVKPQFFTIEGVAEVQ    180
A4-P652         VKSALPNGIEDPSVSSSSGGSGIMYISFRSKKLDSSQVTDYINRVVKPQFFTIEGVAEVQ    180
A6-P642         VKSALPNGIEDPSVSSSSGGSGIMYISFRSKKLDSSQVTDYINRVVKPQFFTIEGVAEVQ    180
A7-P665         VKSALPNGIEDPSVSSSSGGSGIMYISFRSKKLDSSQVTDYINRVVKPQFFTIEGVAEVQ    180
A8-P657         VKSALPNGIEDPSVSSSSGGSGIMYISFRSKKLDSSQVTDYINRVVKPQFFTIEGVAEVQ    180
A9-P645         VKSALPNGIEDPSVSSSSGGSGIMYISFRSKKLDSSQVTDYINRVVKPQFFTIEGVAEVQ    180
A10-P851        VKSALPNGIEDPSVSSSSGGSGIMYISFRSKKLDSSQVTDYINRVVKPQFFTIEGVAEVQ    180
A11-P593        VKSALPNGIEDPSVSSSSGGSGIMYISFRSKKLDSSQVTDYINRVVKPQFFTIEGVAEVQ    180
A12-P607        VKSALPNGIEDPSVSSSSGGSGIMYISFRSKKLDSSQVTDYINRVVKPQFFTIEGVAEVQ    180
A13-P590        VKSALPNGIEDPSVSSSSGGSGIMYISFRSKKLDSSQVTDYINRVVKPQFFTIEGVAEVQ    180
A14-P626        VKSALPNGIEDPSVSSSSGGSGIMYISFRSKKLDSSQVTDYINRVVKPQFFTIEGVAEVQ    180
                ************************************************************

A1-NTHi375      VFGAAEYALRIWLDPQKMAAQNLSVPTVMSALSANNVQTAAGNDNGYYVSYRNKVETTTK    240
A2-P621         VFGAAEYALRIWLDPQKMAAQNLSVPTVMSALSANNVQTAAGNDNGYYVSYRNKVETTTK    240
A3-RdKW20       VFGAAEYALRIWLDPQKMAAQNLSVPTVMSALSANNVQTAAGNDNGYYVSYRNKVETTTK    240
A4-P652         VFGAAEYALRIWLDPQKMAAQNLSVPTVMSALSANNVQTAAGNDNGYYVSYRNKVETTTK    240
A6-P642         VFGAAEYALRIWLDPQKMAAQNLSVPTVMSALSANNVQTAAGNDNGYYVSYRNKVETTTK    240
A7-P665         VFGAAEYALRIWLDPQKMAAQNLSVPTVMSALSANNVQTAAGNDNGYYVSYRNKVETTTK    240
A8-P657         VFGAAEYALRIWLDPQKMAAQNLSVPTVMSALSANNVQTAAGNDNGYYVSYRNKVETTTK    240
A9-P645         VFGAAEYALRIWLDPQKMAAQNLSVPTVMSALSANNVQTAAGNDNGYYVSYRNKVETTTK    240
A10-P851        VFGAAEYALRIWLDPQKMAAQNLSVPTVMSALSANNVQTAAGNDNGYYVSYRNKVETTTK    240
A11-P593        VFGAAEYALRIWLDPQKMAAQNLSVPTVMSALSANNVQTAAGNDNGYYVSYRNKVETTTK    240
A12-P607        VFGAAEYALRIWLDPQKMAAQNLSVPTVMSALSANNVQTAAGNDNGYYVSYRNKVETTTK    240
A13-P590        VFGAAEYALRIWLDPQKMAAQNLSAPAVMSALSANNVQTAAGNDNGYYVSYRNKVETTTT    240
```

```
A14-P626        VFGAAEYALRIWLDPQKMAAQNLSVPTVMSALSANNVQTAAGNDNGYYVSYRNKVETTTK    240
                ************************.*:*********************************.

A1-NTHi375      SVEQLSNLIISSNGDDLVRLRDIATVELNKENDNSRATANGAESVVLAINPTSTANPLTV    300
A2-P621         SVEQLSNLIISSNGDDLVRLRDIATVELNKENDNSRATANGAESVVLAINPTSTANPLTV    300
A3-RdKW20       SVEQLSNLIISSNGDDLVRLRDIATVELNKENDNSRATANGAESVVLAINPTSTANPLTV    300
A4-P652         SVEQLSNLIISSNGDDLVRLRDIATVELNKENDNSRATANGAESVVLAINPTSTANPLTV    300
A6-P642         SVEQLSNLIISSNGDDLVRLRDIATVELNKENDNSRATANGAESVVLAINPTSTANPLTV    300
A7-P665         SVEQLSNLIISSNGDDLVRLRDIATVELNKESDNSRATANGAESVVLAINPTSTANPLTV    300
A8-P657         SVEQLSNLIISSNGDDLVRLRDIATVELNKESDNSRATANGAESVVLAINPTSTANPLTV    300
A9-P645         SVEQLSNLIISSNGDDLVRLRDIATVELNKENDNSRATANGAESVVLAINPTSTANPLTV    300
A10-P851        SVEQLSNLIISSNGDDLVRLRDIATVELNKESDNSRATANGAESVVLAINPTSTANPLTV    300
A11-P593        SVEQLSNLIISSNGDDLVRLRDIATVELNKENDNSRATANGAESVVLAINPTSTANPLTV    300
A12-P607        SVEQLSNLIISSNGDDLVRLRDIATVELNKENDNSRATANGAESVVLAINPTSTANPLTV    300
A13-P590        SVEQLSNLIISSNGDDLVRLRDIATVELNKESDNSRATANGAESVVLAINPTSTANPLTV    300
A14-P626        SVEQLSNLIISSNGDDLVRLRDIATVELNKENDNSRATANGAESVVLAINPTSTANPLTV    300
                ******************************.**************************

A1-NTHi375      AEKIRPLYESIKTQLPDSMESDILYDRTIAINSSIHEVIKTIGEATLIVLVVILMFIGSF    360
A2-P621         AEKIRPLYESIKTQLPDSMESDILYDRTIAINSSIHEVIKTIGEATLIVLVVILMFIGSF    360
A3-RdKW20       AEKIRPLYESIKTQLPDSMESDILYDRTIAINSSIHEVIKTIGEATLIVLVVILMFIGSF    360
A4-P652         AEKIRPLYESIKTQLPDSMESDILYDRTIAINSSIHEVIKTIGEATLIVLVVILMFIGSF    360
A6-P642         AEKIRPLYESIKTQLPDSMESDILYDRTIAINSSIHEVIKTIGEATLIVLVVILMFIGSF    360
A7-P665         AEKIRPLYESIKTQLPDSMESDILYDRTIAINSSIHEVIKTIGEATLIVLVVILMFIGSF    360
A8-P657         AEKIRPLYESIKTQLPDSMESDILYDRTIAINSSIHEVIKTIGEATLIVLVVILMFIGSF    360
A9-P645         AEKIRPLYESIKTQLPDSMESDILYDRTIAINSSIHEVIKTIGEATLIVLVVILMFIGSF    360
A10-P851        AEKIRPLYESIKTQLPDSMESDILYDRTIAINSSIHEVIKTIGEATLIVLVVILMFIGSF    360
A11-P593        AEKIRPLYESIKTQLPDSMESDILYDRTIAINSSIHEVIKTIGEATLIVLVVILMFIGSF    360
A12-P607        AEKIRPLYESIKTQLPDSMESDILYDRTIAINSSIHEVIKTIGEATLIVLVVILMFIGSF    360
A13-P590        AEKIRPLYESIKTQLPDSMESDILYDRTIAINSSIHEVIKTIGEATLIVLVVILMFIGSF    360
A14-P626        AEKIRPLYESIKTQLPDSMESDILYDRTIAINSSIHEVIKTIGEATLIVLVVILMFIGSF    360
                ************************************************************

A1-NTHi375      RAILIPILAIPISLIGVLMLLQSFNFSINLMTLLALILAIGLVVDDAIVVLENIDRHIKA    420
A2-P621         RAILIPILAIPISLIGVLMLLQSFNFSINLMTLLALILAIGLVVDDAIVVLENIDRHIKA    420
A3-RdKW20       RAILIPILAIPISLIGVLMLLQSFNFSINLMTLLALILAIGLVVDDAIVVLENIDRHIKA    420
A4-P652         RAILIPILAIPISLIGVLMLLQSFNFSINLMTLLALILAIGLVVDDAIVVLENIDRHIKA    420
A6-P642         RAILIPILAIPISLIGVLMLLQSFNFSINLMTLLALILAIGLVVDDAIVVLENVDRHIKA    420
A7-P665         RAILIPILAIPISLIGVLMLLQSFNFSINLMTLLALILAIGLVVDDAIVVLENIDRHIKA    420
A8-P657         RAILIPILAIPISLIGVLMLLQSFNFSINLMTLLALILAIGLVVDDAIVVLENIDRHIKA    420
A9-P645         RAILIPILAIPISLIGVLMLLQSFNFSINLMTLLALILAIGLVVDDAIVVLENIDRHIKA    420
A10-P851        RAILIPILAIPISLIGVLMLLQSFNFSINLMTLLALILAIGLVVDDAIVVLENIDRHIKA    420
A11-P593        RAILIPILAIPISLIGVLMLLQSFNFSINLMTLLALILAIGLVVDDAIVVLENIDRHIKA    420
A12-P607        RAILIPILAIPISLIGVLMLLQSFNFSINLMTLLALILAIGLVVDDAIVVLENIDRHIKA    420
A13-P590        RAILIPILAIPISLIGVLMLLQSFNFSINLMTLLALILAIGLVVDDAIVVLENVDRHIKE    420
A14-P626        RAILIPILAIPISLIGVLMLLQSFNFSINLMTLLALILAIGLVVDDAIVVLENIDRHIKA    420
                ************************************************:***********

A1-NTHi375      GETPFRAAIIGTREIAVPVISMTIALIAVYSPMALMGGITGTLFKEFALTLAGAVFISGV    480
A2-P621         GETPFRAAIIGTREIAVPVISMTIALIAVYSPMALMGGITGTLFKEFALTLAGAVFISGV    480
A3-RdKW20       GETPFRAAIIGTREIAVPVISMTIALIAVYSPMALMGGITGTLFKEFALTLAGAVFISGV    480
A4-P652         GETPFRAAIIGVREIAVPVISMTIALIAVYSPMALMGGITGTLFKEFALTLAGAVFISGV    480
A6-P642         GETPFRAAIIGTREIAVPVISMTIALIAVYSPMALMGGITGTLFKEFALTLAGAVFISGI    480
A7-P665         GETPFRAAIIGTREIAVPVISMTIALIAVYSPMALMGGITGTLFKEFALTLAGAVFISGV    480
A8-P657         GETPFRAAIIGTREIAVPVISMTIALIAVYSPMALMGGITGTLFKEFALTLAGAVFISGV    480
A9-P645         GETPFRAAIIGTREIAVPVISMTIALIAVYSPMALMGGITGTLFKEFALTLAGAVFISGV    480
A10-P851        GETPFRAAIIGTREIAVPVISMTIALIAVYSPMALMGGITGTLFKEFALTLAGAVFISGI    480
```

```
A11-P593        GETPFRAAIIGTREIAVPVISMTIALIAVYSPMALMGGITGTLFKEFALTLAGAVFISGV    480
A12-P607        GETPFRAAIIGTREIAVPVISMTIALIAVYSPMALMGGITGTLFKEFALTLAGAVFISGV    480
A13-P590        GETPFRAAIIGTREIAVPVISMTIALIAVYSPMALMGGITGTLFKEFALTLAGAVFISGI    480
A14-P626        GETPFRAAIIGTREIAVPVISMTIALIAVYSPMALMGGITGTLFKEFALTLAGAVFISGV    480
                ***********.**************************************************:

A1-NTHi375      VALTLSPMMSSKLLKSNAKPTWMEERVEHTLGKVNRVYEYMLDLVMLNRKSMLAFAVVIF    540
A2-P621         VALTLSPMMSSKLLKSNAKPTWMEERVEHTLGKVNRVYEYMLDLVMLNRKSMLAFAVVIF    540
A3-RdKW20       VALTLSPMMSSKLLKSNAKPTWMEERVEHTLGKVNRVYEYMLDLVMLNRKSMLAFAVVIF    540
A4-P652         VALTLSPMMSSKLLKSNAKPTWMEERVEHTLGKVNRVYEYMLDLVMLNRKSMLAFAVVIF    540
A6-P642         VALTLSPMMSSKLLKSNAKPTWMEERVEHTLGKVNRVYEYMLDLVMLNRKSMLAFAVVIF    540
A7-P665         VALTLSPMMSSKLLKSNAKPTWMEERVEHTLGKVNRVYEYMLDLVMLNRKSMLAFAVVIF    540
A8-P657         VALTLSPMMSSKLLKSNAKPTWMEERVEHTLGKVNRVYEYMLDLVMLNRKSMLAFAVVIF    540
A9-P645         VALTLSPMMSSKLLKSNAKPTWMEERVEHTLGKVNRVYEYMLDLVMLNRKSMLAFAVVIF    540
A10-P851        VALTLSPMMSSKLLKSNAKPTWMEERVEHTLGKVNRVYEYMLDLVMLNRKSMLAFAVVIF    540
A11-P593        VALTLSPMMSSKLLKSNAKPTWMEERVEHTLGKVNRVYEYMLDLVMLNRKSMLAFAVVIF    540
A12-P607        VALTLSPMMSSKLLKSNAKPTWMEERVEHTLGKVNRVYEYMLDLVMLNRKSMLAFAVVIF    540
A13-P590        VALTLSPMMSSKLLKSNAQPTWLEQKVEHTLGKVNRIYEYMLDLVMLNRKSMLAFAVVIF    540
A14-P626        VALTLSPMMSSKLLKSNAKPTWMEERVEHTLGKVNRVYEYMLDLVMLNRKSMLAFAVVIF    540
                ******************:***:*::**********:***********************

A1-NTHi375      STLPFLFNSLSSELTPNEDKGAFIAIGNAPSSVNVDYIQNAMQPYMKNVMETPEVSFGMS    600
A2-P621         STLPFLFNSLSSELTPNEDKGAFIAIGNAPSSVNVDYIQNAMQPYMKNVMETPEVSFGMS    600
A3-RdKW20       STLPFLFNSLSSELTPNEDKGAFIAIGNAPSSVNVDYIQNAMQPYMKNVMETPEVSFGMS    600
A4-P652         STLPFLFNSLSSELTPNEDKGAFIAIGNAPSSVNVDYIQNAMQPYMKNVMETPEVSFGMS    600
A6-P642         STLPFLFNALSSELTPNEDKGAFIAIGNAPSSVNVDYIQNAMQPYMKNVMETPEVSFGMS    600
A7-P665         STLPFLFNSLSSELTPNEDKGAFIAIGNAPSSVNVDYIQNAMQPYMKNVMETPEVSFGMS    600
A8-P657         STLPFLFNSLSSELTPNEDKGAFIAIGNAPSSVNVDYIQNAMQPYMKNVMETPEVSFGMS    600
A9-P645         STLPFLFNSLSSELTPNEDKGAFIAIGNAPSSVNVDYIQNAMQPYMKNVMETPEVSFGMS    600
A10-P851        STLPFLFNSLSSELTPNEDKGAFIAIGNAPSSVNVDYIQNAMQPYMKNVMETPEVSFGMS    600
A11-P593        STLPFLFNSLSSELTPNEDKGAFIAIGNAPSSVNVDYIQNAMQPYMKNVMETPEVSFGMS    600
A12-P607        STLPFLFNSLSSELTPNEDKGAFIAIGNAPSSVNVDYIQNAMQPYMKNVMETPEVSFGMS    600
A13-P590        STLPFLFNALSSELTPNEDKGAFIAIGNAPSSVNVDYIQNAMQPYMKNVMDTPEVSFGMS    600
A14-P626        STLPFLFNSLSSELTPNEDKGAFIAIGNAPSSVNVDYIQNAMQPYMKNVMETPEVSFGMS    600
                ********:****************************************:*********

A1-NTHi375      IAGAPTSNSSLNIITLKDWKERSRKQSAIMNEINEKAKSIPEVSVSAFNIPEIDTGEQGA    660
A2-P621         IAGAPTSNSSLNIITLKDWKERSRKQSAIMNEINEKAKSIPEVSVSAFNIPEIDTGEQGA    660
A3-RdKW20       IAGAPTSNSSLNIITLKDWKERSRKQSAIMNEINEKAKSIPEVSVSAFNIPEIDTGEQGP    660
A4-P652         IAGAPTSNSSLNIITLKDWKERSRKQSAIMNEINEKAKSIPEVSVSAFNIPEIDTGEQGP    660
A6-P642         IAGAPNSNGSLNIITLKDWKERSRKQSAIMNEINEKAKSIPEVSVSAFNIPEIDTGEQGA    660
A7-P665         IAGAPTSNSSLNIITLKDWKERSRKQSAIMNEINEKGKSIPEVSVSAFNIPEIDTGEQGA    660
A8-P657         IAGAPTSNSSLNIITLKDWKERSRKQSAIMNEINEKAKSIPEVSVSAFNIPEIDTGEQGA    660
A9-P645         IAGAPTSNSSLNIITLKDWKERSRKQSAIMNEINEKAKSIPEVSVSAFNIPEIDTGEQGP    660
A10-P851        IAGAPTSNSSLNIITLKDWKERSRKQSAIMNEINEKAKSIPEVSVSAFNIPEIDTGEQGA    660
A11-P593        IAGAPTSNSSLNIITLKDWKERSRKQSAIMNEINEKAKSIPEVSVSAFNIPEIDTGEQGA    660
A12-P607        IAGAPTSNSSLNIITLKDWKERSRKQSAIMNEINEKAKSIPEVSVSAFNIPEIDTGEQGA    660
A13-P590        IAGAPNSNGSLNIITLKDWKERTRKQSVVMNELNAKAKSIPEVSVSAFNFPEIDTGEQGP    660
A14-P626        IAGAPTSNSSLNIITLKDWKERSRKQSAIMNEINEKAKSIPEVSVSAFNIPEIDTGEQGA    660
                *****.**.*************:****.:***:* *.************:*********

A1-NTHi375      PVSIVLKTAQDYKSLANTAEKFLSAMKASGKFIYTNLDLTYDTAQMTISVDKEKAGTYGI    720
A2-P621         PVSIVLKTAQDYKSLANTAEKFLSAMKASGKFIYTNLDLTYDTAQMTISVDKEKAGTYGI    720
A3-RdKW20       PVSIVLKTAQDYKSLANTAEKFLSAMKASGKFIYTNLDLTYDTAQMTISVDKEKAGTYGI    720
A4-P652         PVSIVLKTAQDYKSLANTAEKFLSAMKASGKFIYTNLDLTYDTAQMTISVDKEKAGTYGI    720
A6-P642         PVSIVLKTAQDYKSLANTAEKFLSAMKASGKFIYTNLDLTYDTAQMTISVDKEKAGTYGI    720
A7-P665         PVSIVLKTAQDYKSLANTAEKFLSAMKASGKFIYTNLDLTYDTAQMTISVDKEKAGTYGI    720
```

```
A8-P657         PVSIVLKTAQDYKSLANTAEKFLSAMKASGKFIYTNLDLTYDTAQMTISVDKEKAGTYGI    720
A9-P645         PVSIVLKTAQDYKSLANTAEKFLSAMKASGKFIYTNLDLSYDTAQMTISVDKEKAGTYGI    720
A10-P851        PVSIVLKTAQDYKSLANTAEKFLSAMKASGKFIYTNLDLTYDTAQMTISVDKEKAGTYGI    720
A11-P593        PVSIVLKTAQDYKSLANTAEKFLSAMKASGKFIYTNLDLSYDTAQMTISVDKEKAGTYGI    720
A12-P607        PVSIVLKTAQDYKSLANTAEKFLSAMKASGKFIYTNLDLTYDTAQMTISVDKEKAGTYGI    720
A13-P590        PVSIVLKTAQDYKSLANTAEKFLNAMKASGKFIYSNLNLTYDTAQMTISVDKEKAGTYGI    720
A14-P626        PVSIVLKTAQDYKSLANTAEKFLSAMKASGKFIYTNLDLTYDTAQMTISVDKEKAGTYGI    720
                **********************.**********:**:*:********************

A1-NTHi375      TMQQISNTLGSFLSGATVTRVDVDGRAYKVISQVKRDDRLSPESFQNYYLTASNGQSVPL    780
A2-P621         TMQQISNTLGSFLSGATVTRVDVDGRAYKVISQVKRDDRLSPESFQNYYLTASNGQSVPL    780
A3-RdKW20       TMQQISNTLGSFLSGATVTRVDVDGRAYKVISQVKRDDRLSPESFQNYYLTASNGQSVPL    780
A4-P652         TMQQISNTLGSFLSGATVTRVDVDGRAYKVISQVKRDDRLSPESFQNYYLTASNGQSVPL    780
A6-P642         TMQQISNTLGSFLSGATVTRVDVDGRAYKVISQVKRDDRLSPESFQNYYLTASNGQSVPL    780
A7-P665         TMQQISNTLGSFLSGATVTHVDVDGRAYKVISQVKRDDRLSPESFQNYYLTASNGQSVPL    780
A8-P657         TMQQISNTLGSFLSGATVTRVDVDGRAYKVISQVKRDDRLSPESFQNYYLTASNGQSVPL    780
A9-P645         TMQQISNTLGSFLSGATVTRVDVDGRAYKVISQVKRDDRLSPESFQNYYLTASNGRSVPL    780
A10-P851        TMQQISNTLGSFLSGATVTRVDVDGRAYKVISQVKRDDRLSPESFQNYYLTASNGQSVPL    780
A11-P593        TMQQISNTLGSFLSGATVTRVDVDGRAYKVISQVKRDDRLSPESFQNYYLTASNGQSVPL    780
A12-P607        TMQQISNTLGSFLSGATVTRVDVDGRAYKVISQVKRDDRLSPESFQNYYLTASNGQSVPL    780
A13-P590        TMQQISNTLGSFLSGATVTRVDVDGRAYKVISQVKRDDRLSPESFQNYYLTASNGQSVPL    780
A14-P626        TMQQISNTLGSFLSGATVTRVDVDGRAYKVISQVKRDDRLSPESFQNYYLTASNGQSVPL    780
                ******************:***********************************:****

A1-NTHi375      SSVISMKLETQPTSLPRFSQLNSAEISAVPMPGISSGDAIAWLQQQANDNLPQGYTYDFK    840
A2-P621         SSVISMKLETQPTSLPRFSQLNSAEISAVPMPGISSGDAIAWLQQQANDNLPQGYTYDFK    840
A3-RdKW20       SSVISMKLETQPTSLPRFSQLNSAEISAVPMPGISSGDAIAWLQQQATDNLPQGYTFDFK    840
A4-P652         SSVISMKLETQPTSLPRFSQLNSAEISAVPMPGTSSGDAIAWLQQQANDNLPQGYTYDFK    840
A6-P642         SSVISMKLETQPTSLPRFSQLNSAEISAVPMPGTSSGDAIAWLQQQANDNLPQGYTYDFK    840
A7-P665         SSVISMKLETQPTSLPRFSQLNSAEISAVPMPGTSSGDAIAWLQQHATDNLPQGYTFDFK    840
A8-P657         SSVISMKLETQPTSLPRFSQLNSAEISAVPMPGTSSGDAIAWLQQHATDNLPQGYTFDFK    840
A9-P645         SSVISMKLETQPTSLPRFSQLNSAEISAVPMPGTSSGDAIAWLQQQANDNLPQGYTYDFK    840
A10-P851        SSVISMKLETQPTSLPRFSQLNSAEISAVPMPGTSSGDAIAWLQQQANDNLPQGYTYDFK    840
A11-P593        SSVISMKLETQPTSLPRFSQLNSAEISAVPMPGTSSGDAIAWLQQQANDNLPQGYTYDFK    840
A12-P607        SSVISMKLETQPTSLPRFSQLNSAEISAVPMPGTSSGDAIAWLQQQANDNLPQGYTYDFK    840
A13-P590        SSVISMKLETQPTSLPRFSQLNSAEISAVPMPGTSSGDAIAWLQQQANDNLPQGYTYDFK    840
A14-P626        SSVISMKLETQPTSLPRFSQLNSAEISAVPMPGTSSGDAIAWLQQHATDNLPQGYTFDFK    840
                ******************************* ***********:*.********:***

A1-NTHi375      SEARQLVQEGNALTTTFILAVVIIFLVLAIQFESIRDPMVIMISVPLAVSGALVSLNILS    900
A2-P621         SEARQLVQEGNALTTTFILAVVIIFLVLAIQFESIRDPMVIMISVPLAVSGALVSLNILS    900
A3-RdKW20       SEARQLVQEGNALAVTFALAVIIIFLVLAIQFESIRDPMVIMISVPLAVSGALVSLNILS    900
A4-P652         SEARQLVQEGNALTTTFILAVVIIFLVLAIQFESIRDPMVIMISVPLAVSGALVSLNILS    900
A6-P642         SEARQLVQEGNALTTTFILAVVIIFLVLAIQFESIRDPMVIMISVPLAVSGALVSLNLLS    900
A7-P665         SEARQLVQEGNALAVTFALAVIIIFLVLAIQFESIRDPMVIMISVPLAVSGALVSLNILS    900
A8-P657         SEARQLVQEGNALAVTFALAVIIIFLVLAIQFESIRDPMVIMISVPLAVSGALVSLNILS    900
A9-P645         SEARQLVQEGNALTTTFILAVVIIFLVLAIQFESIRDPMVIMISVPLAVSGALVSLNILS    900
A10-P851        SEARQLVQEGNALTTTFILAVVIIFLVLAIQFESIRDPMVIMISVPLAVSGALVSLNLLS    900
A11-P593        SEARQLVQEGNALTTTFILAVVIIFLVLAIQFESIRDPMVIMISVPLAVSGALVSLNILS    900
A12-P607        SEARQLVQEGNALTTTFILAVVIIFLVLAIQFESIRDPMVIMISVPLAVSGALVSLNILS    900
A13-P590        SEARQLVQEGNALTTTFILAVVIIFLVLAIQFESIRDPMVIMISVPLAVSGALVSLNLLS    900
A14-P626        SEARQLVQEGNALAVTFALAVIIIFLVLAIQFESIRDPMVIMISVPLAVSGALVSLNILS    900
                *************:.** ***:************************************:**

A1-NTHi375      FFSIAGTTLNIYSQVGLITLVGLITKHGILMCEVAKEEQLNYGKTRIEAITHAAKVRLRP    960
A2-P621         FFSIAGTTLNIYSQVGLITLVGLITKHGILMCEVAKEEQLNHGKTRIEAITHAAKVRLRP    960
A3-RdKW20       FFSIAGTTLNIYSQVGLITLVGLITKHGILMCEVAKEEQLNHGKTRIEAITHAAKVRLRP    960
```

```
A4-P652          FFSIAGTTLNIYSQVGLITLVGLITKHGILMCEVAKEEQLNYGKTRIEAITHAAKVRLRP    960
A6-P642          FFGIAGTTLNIYSKVGLITLVGLITKHGILMCEVAKEEQLNYGKTRIEAITHAAKVRLRP    960
A7-P665          FFSIAGTTLNIYSQVGLITLVGLITKHGILMCEVAKEEQLNHGKTRIEAITHAAKVRLRP    960
A8-P657          FFSIAGTTLNIYSQVGLITLVGLITKHGILMCEVAKEEQLNYGKTRIEAITHAAKVRLRP    960
A9-P645          FFSIAGTTLNIYSQVGLITLVGLITKHGILMCEVAKEEQLNYGKTRIEAITHAAKVRLRP    960
A10-P851         FFGIAGTTLNIYSKVGLITLVGLITKHGILMCEVAKEEQLNYGKTRIEAITHAAKVRLRP    960
A11-P593         FFSIAGTTLNIYSQVGLITLVGLITKHGILMCEVAKEEQINHGKTRIEAITHAAKVRLRP    960
A12-P607         FFSIAGTTLNIYSQVGLITLVGLITKHGILMCEVAKEEQLNYGKTRIEAITHAAKVRLRP    960
A13-P590         FFGIAGTTLNIYSKVGLITLVGLITKHGILMCEVAKEEQLNYGKTRIEAITHAAKVRLRP    960
A14-P626         FFSIAGTTLNIYSQVGLITLVGLITKHGILMCEVAKEEQLNHGKTRIEAITHAAKVRLRP    960
                 **.**********:*************************:*:*****************

A1-NTHi375       ILMTTAAMVAGLIPLLYATGAGAVSRFSIGIVIVAGLSIGTIFTLFVLPVVYSYIATEHK    1020
A2-P621          ILMTTAAMVAGLIPLLYATGAGAVSRFSIGIVIVAGLSIGTIFTLFVLPVVYSYVATEHK    1020
A3-RdKW20        ILMTTAAMVAGLIPLLYATGAGAVSRFSIGIVIVAGLSIGTIFTLFVLPVVYSYVATEHK    1020
A4-P652          ILMTTAAMVAGLIPLLYATGAGAVSRFSIGIVIVAGLSIGTIFTLFVLPVVYSYVATEHK    1020
A6-P642          ILMTTAAMVAGLIPLLYATGAGAVSRFSMGIVIVAGLSIGTIFTLFVLPVVYSYVATEHK    1020
A7-P665          ILMTTAAMVAGLIPLLYATGAGAVSRFSIGIVIVAGLSIGTIFTLFVLPVVYSYVATEHK    1020
A8-P657          ILMTTAAMVAGLIPLLYATGAGAVSRFSIGIVIVAGLSIGTIFTLFVLPVVYSYVATEHK    1020
A9-P645          ILMTTAAMVAGLIPLLYATGAGAVSRFSIGIVIVAGLSIGTIFTLFVLPVVYSYVATEHK    1020
A10-P851         ILMTTAAMVAGLIPLLYATGAGAVSRFSMGIVIVAGLSIGTIFTLFVLPVVYSYVATEHK    1020
A11-P593         ILMTTAAMVAGLIPLLYATGAGAVSRFSIGIVIVAGLSIGTIFTLFVLPVVYSYVATEHK    1020
A12-P607         ILMTTAAMVAGLIPLLYATGAGAVSRFSIGIVIVAGLSIGTIFTLFVLPVVYSYVATEHK    1020
A13-P590         ILMTTAAMVAGLIPLLYATGAGAVSRFSMGIVIVAGLSIGTIFTLFVLPVVYSYVATEHK    1020
A14-P626         ILMTTAAMVAGLIPLLYATGAGAVSRFSIGIVIVAGLSIGTIFTLFVLPVVYSYVATEHK    1020
                 ****************************:************************:*****

A1-NTHi375       PLPVFDENKTTH    1032
A2-P621          PLPVFDENKTTH    1032
A3-RdKW20        PLPVFDENKTTH    1032
A4-P652          PLPVFDENKTTH    1032
A6-P642          PLPVFDENKTTH    1032
A7-P665          PLPVFDENKTTH    1032
A8-P657          PLPVFDENKTTH    1032
A9-P645          PLPVFDENKTTH    1032
A10-P851         PLPVFDENKTTH    1032
A11-P593         PLPVFDENKTTH    1032
A12-P607         PLPVFDENKTTH    1032
A13-P590         PLPVFDENKTTH    1032
A14-P626         PLPVFDENKTTH    1032
                 ************
```

Figure S23. Distribution of AcrB variants among the 14 selected NTHi isolates. Thirteen AcrB variants were found. The P652 and P673 strains presented the same AcrB variant. Conservation of the hydrophobic pocket is labeled in blue. Polymorphisms are labeled in red.

```
A1-NTHi375      MFKMKNITLALLMSSALVGCANIGDSYQASLEDYKQYEEITKQYNVKENWWSLYDDAQLN     60
A2-P621         MFKMKNITLALLMSGALVGCANIGDSYQASLEDYKQYEEITKQYNVKENWWSLYDDAQLN     60
A3-RdKW20       MFKMKNITLALLMSGALVGCANIGDSYQASLEDYKQYEEITKQYNVKENWWSLYDDAQLN     60
A5-P673         MFKMKNITLALLMSSALVGCANIGDSYQASLEDYKQYEEITKQYNVKENWWSLYDDAQLN     60
A6-P642         MFKMKNITLALLISGALVGCANIGDSYQASLEDYKQYEEITKQYNVKENWWSLYDDAQLN     60
A7-P665         MFKMKNITLALLVSGALVGCANIGDSYQASLEDYKQYEEITKQYNVKENWWSLYDDAQLN     60
A8-P657         MFKMKNITLALLMSGALVGCANIGDSYQASLEDYKQYEEITKQYNVKENWWSLYDDAQLN     60
A9-P645         MFKMKNITLALLMSGALVGCANIGDSYQASLEDYKQYEEITKQYNVKENWWSLYNDAQLN     60
A10-P851        MFKMKNITLALLMSGALVGCANIGDSYQASLEDYKQYEAITKQYNVKENWWSLYNDAQLN     60
A11-P593        MFKMKNITLALLMSSALVGCANIGDSYQASLEDYKQYEEITKQYNVKENWWSLYDDAQLN     60
A12-P607        MFKMKNITLALLMSGALVGCANIGDSYQASLEDYKQYEEITKQYNVKENWWSLYNDAQLN     60
A13-P590        MFKMKNITLALLMSGALVGCANIGDSYQASLEDYKQYEEITKQYNVKENWWSLYDDAQLN     60
A14-P626        MFKMKNITLALLMSGALVGCANIGDSYQASLEDYKQYEEITKQYNVKENWWSLYDDAQLN     60
                ************:*.********************** ***************:*****

A1-NTHi375      RVVEQALINNKDLAKAAVAVNRALYSANLVGANLVPAFNGSTSSAAQRRVDISTNSAISH     120
A2-P621         RVIEQALTNNKDLAKAAVAVNRALYSANLVGANLVPAFNGSTSSAAQRRVDISTNSAISH     120
A3-RdKW20       RVVGQALINNKDLAKAAVAVNRALYSANLVGANLVPAFNGSTSSAAQRRVDISTNSAISH     120
A5-P673         RVVEQALINNKDLAKAAVAVNRALYSANLVGANLVPAFNGSTSSAAQRRVDTSANSAISH     120
A6-P642         RVVEQALINNKDLAKAAVAVNRALYSANLVGANLVPAFNGSTSSAAQRRVDISTNSAISH     120
A7-P665         RVIEQALTNNKDLAKAAVAVNRALYSANLVGANLVPAFNGSTSSAAQRRVDISTNSAISH     120
A8-P657         RVIEQALTNNKDLAKAAVAVNRALYSANLVGANLVPAFNGSTSSAAQRRVDISTNSAISH     120
A9-P645         RVIEQALTNNKDLAKAAVAVNRALYSANLVGANLVPAFNGSTSSAAQRRIDISTNSAISH     120
A10-P851        RVIEQALTNNKDLAKAAVAVNRALYSANLVGANLVPAFNGSTSSAAQRRVDTSANSAISH     120
A11-P593        RVVEQALINNKDLAKAAVAVNRALYSANLVGANLVPAFNGSTSSAAQRRVDISTNSAISH     120
A12-P607        RVIEQALTNNKDLAKAAVAVNRALYSANLVGANLVPAFNGSTSSAAQRRVDISTNSAISH     120
A13-P590        RVIEQALTNNKDLAKAAVAVNRALYSANLVGANLVPAFNGSTSSAAQRRVDTSANSAISH     120
A14-P626        RVVEQALINNKDLAKAAVAVNRALYSANLVGANLVPAFNGSTSSAAQRRVDISTNSAISH     120
                **: *** ****************************************:* *:******

A1-NTHi375      KGSLNVSYTLDLWQRLANTVDAAEWSHKATAEDMESARLSLINSVVTTYYQIAYLNDAIS     180
A2-P621         KGSLNVSYTLDLWQRLANTVDAAEWSHKATAEDMESARLSLINSVVTTYYQIAYLNDAIS     180
A3-RdKW20       KGSLNVSYTLDLWQRLANTVDAAEWSHKATAEDMESARLSLINSVVTTYYQIAYLNDAIS     180
A5-P673         KGSLNVSYTLDLWQRLANAADAAEWSHKATAEDMESARLSLINSVITTYYQIAYLNDAIS     180
A6-P642         KGSLNVSYTLDLWQRLANTVDAAEWSHKATAEDMESARLSLINSVVTTYYQIAYLNDAIS     180
A7-P665         KGSLNVSYTLDLWQRLANTVDAAEWSHKATAEDMESARLSLINSVVTTYYQIAYLNDAIS     180
A8-P657         KGSLNVSYTLDLWQRLANTVDAAEWSHKATAEDMESARLSLINSVVTTYYQIAYLNDAIS     180
A9-P645         KGSLNVSYTLDLWQRLANTVDAAEWSHKATAEDMESARLSLINSVVTTYYQITYLNDAIS     180
A10-P851        KGSLNVSYTLDLWQRLANTVDAAEWSHKATAEDMESARLSLINSVITTYYQIAYLNDAIS     180
A11-P593        KGSLNVSYTLDLWQRLANTVDAAEWSHKATAEDMESARLSLINSVVTTYYQIAYLNDAIS     180
A12-P607        KGSLNVSYTLDLWQRLANTVDAAEWSHKATAEDMESARLSLINSVVTTYYQIAYLNDAIS     180
A13-P590        KGSLNVSYTLDLWQRLANTADAAEWSHKASAEDMESARLSLINSVITTYYQIAYLNDAIS     180
A14-P626        KGSLNVSYTLDLWQRLANTVDAAEWSHKATAEDMESARLSLINSVVTTYYQIAYLNDAIS     180
                ******************:.*********:***************:******:*******

A1-NTHi375      TTNETIKYYTDIGNIMQTRLAQGVADAASVDQAQQAILTARNNKLNFETQRKTAEQTLRN     240
A2-P621         TTNETIKYYTDIGNIMQTRLAQGVADTASVDQAQQAILTARNNKLNFETQRKTAEQTLRN     240
A3-RdKW20       TTNETIKYYTDIGNIMQTRLVQGVADAASVDQAQQAILTARNNKLNFETQRKTAEQTLRN     240
A5-P673         TTDETIKYYTDIGNIMQTRLAQGVADAASVDQAQQAILTARNNKLNFETQRKTAEQTLRN     240
A6-P642         TTNETIKYYTDIGNIMQTRLAQGVADTASVDQAQQATLTARNNKLNFETQRKTAEQTLRN     240
A7-P665         TTNETIKYYTDIGNIMQTRLAQGVADAVSVDQAQQAILTARNNKLNFETQRKTAEQTLRN     240
A8-P657         TTNETIKYYTDIGNIMQTRLAQGVADVASVDQAQQAILTARNNKLNFETQRKTAEQTLRN     240
A9-P645         TTNETIKYYTDIGNIMQTRLAQGVADAASVDQAQQAILTARNNKLNFETQRKTAEQTLRN     240
A10-P851        TTDETIKYYTDIGNIMQTRLAQGVADAASVDQAQQAILTARNNKLNFETQRKTAEQTLRN     240
A11-P593        TTNETIKYYTDIGNIMQTRLAQGVADAASVDQAQQAILTARNNKLNFETQRKTAEQTLRN     240
A12-P607        TTNETIKYYTDIGNIMQTRLVQGVADAASVDQAQQAILTARNNKLNFETQRKTAEQTLRN     240
A13-P590        TTDETIKYYTDIGNIMQTRLAQGVADAASVDQAQQAILTARNNKLNFETQRKTAEQTLRN     240
```

```
A14-P626        TTNETIKYYTDIGNIMQTRLAQGVADAASVDQAQQAILTARNNKLNFETQRKTAEQTLRN    240
                **:*****************.******..******** ************************

A1-NTHi375      LLNLKPNEALNITFPHIMNVKTAGVNLNVPVSVIANRPDVKAAQFRLSSAFKNAKATQKS    300
A2-P621         LLNLKPNEALNITFPHIMNVKTAGVNLNVPVSVIANRPDVKAAQFRLSSAFKNAKATQKS    300
A3-RdKW20       LLNLKPNEALNITFPHIMNVKTAGVNLNVPVSVIANRPDVKAAQFRLSSAFKNAKATQKS    300
A5-P673         LLNLKPNEALNITFPHIMNVKTAGVNLNVPVSVIANRPDVKAAQFRLSSAFKNAKATQKS    300
A6-P642         LLNLKPNEALNITFPHIMNVKTAGVNLNVPVSVIANRPDVKAAQFRLSSAFKNAKATQKS    300
A7-P665         LLNLKPNEALNITFPHIMNVKTAGVNLNVPVSVIANRPDVKAAQFRLSSAFKNAKATQKS    300
A8-P657         LLNLKPNEALNITFPHIMNVKTAGVNLNVPVSVIANRPDVKAAQFRLSSAFKNAKATQKS    300
A9-P645         LLNLKPNEALNITFPHIMNVKTAGVNLNVPVSVIANRPDVKAAQFRLSSAFKNAKATQKS    300
A10-P851        LLNLKPNEALNITFPHIMNVKTAGVNLNVPVSVIANRPDVKAAQFRLSSAFKNAKATQKS    300
A11-P593        LLNLKPNEALNITFPHIMNVKTAGVNLNVPVSVIANRPDVKAAQFRLSSAFKNAKATQKS    300
A12-P607        LLNLKPNEALNITFPHIMNVKTAGVNLNVPVSVIANRPDVKAAQFRLSSAFKNAKATQKS    300
A13-P590        LLNLKPNDGLNITFPHIMNVKTAGVNLNVPVSVIANRPDVKAAQFRLSSAFKNAKATQKS    300
A14-P626        LLNLKPNEALNITFPHIMNVKTAGVNLNVPVSVIANRPDVKAAQFRLSSAFKNAKAAQKS    300
                *******:.**************************************************:***

A1-NTHi375      WFPEVNLGASLSSTASTVGTALHNPVAAGTVGISLPFLNWNTVKWNVKISEADYETARLN    360
A2-P621         WFPEVNLGASLSSTASTVGTALHNPVAAGTVGISLPFLNWNTVKWNVKISEADYETARLN    360
A3-RdKW20       WFPEVNLGASLSSTASTVGTALHNPVAAGTVGISLPFLNWNTVKWNVKISEADYETARLN    360
A5-P673         WFPEVNLGASLSSTASTVGTALHNPVAAGTVGISLPFLNWNSVKWNVKISEADYETARLN    360
A6-P642         WFPEVNLGASLSSTASTVGTALHNPVAAGTVGISLPFLNWNTVKWNVKISEADYETARLN    360
A7-P665         WFPEVNLGASLSSTASTVGTALHNPVAAGTVGISLPFLNWNTVKWNVKISEADYETARLN    360
A8-P657         WFPEVNLGASLSSTASTVGTALHNPVAAGTVGISLPFLNWNTVKWNVKISEADYETARLN    360
A9-P645         WFPEVNLGASLSSTASTVGTALHNPVAAGTVGISLPFLNWNTVKWNVKISEADYETARLN    360
A10-P851        WFPEVNLGASLSSTASTVGTALHNPVAAGTVGISLPFLNWNSVKWNVKISEADYETARLN    360
A11-P593        WFPEVNLGGSLSSTASTVGTALHNPVAAGTVGISLPFLNWNTVKWNVKISEADYETARLN    360
A12-P607        WFPEVNLGASLSSTASTIGTALHNPVAAGTVGISLPFLNWNTVKWNVKISEADYETARLN    360
A13-P590        WFPEINLGASLSSTASTVGTALHNPVAAGTVGISLPFLNWNSVKWNVKISEADYETARLN    360
A14-P626        WFPEVNLGASLSSTASTVGTALHNPVAAGTVGISLPFLNWNSVKWNVKISEADYETARLN    360
                ****:***.********:************************:******************

A1-NTHi375      YEQRITTALNNVDTNYFAFTQAQSTLSNLQQTHSYNQRITQYYRNRYNAGVSELREWLVA    420
A2-P621         YEQRITTALNNVDTNYFAFTQAQSTLSNLQQTHSYNQRITQYYRNRYNAGVSELREWLVA    420
A3-RdKW20       YEQRITTALNNVDTNYFAFTQAQSTLSNLQQTHSYNQRITQYYRNRYNAGVSELREWLVA    420
A5-P673         YEQRITTALNNVDTNYFAFTQAQSTLSNLQQTHSYNQRITQYYRNRYNAGVSELREWLVA    420
A6-P642         YEQRITTALNNVDTNYFAFTQAQSTLSNLQQTHSYNQRITQYYRNRYNAGVSELREWLVA    420
A7-P665         YEQRITTALNNVDTNYFAFTQAQSTLSNLQQTHSYNQRITQYYRNRYNAGVSELREWLVA    420
A8-P657         YEQRITTALNNVDTNYFAFTQAQSTLSNLQQTHSYNQRITQYYRNRYNAGVSELREWLVA    420
A9-P645         YEQRITTALNNVDTNYFAFTQAQSTLSNLQQTHSYNQRITQYYRNRYNAGVSELREWLVA    420
A10-P851        YEQRITTALNNVDTNYFAFTQAKSTLSNLQQTHSYNQRITQYYRNRYNAGVSELREWLVA    420
A11-P593        YEQRITTALNNVDTNYFAFTQAQSTLSNLQQTHSYNQRITQYYRNRYNAGVSELREWLVA    420
A12-P607        YEQRITTALNNVDTNYFAFTQAQSTLSNLQQTHSYNQRITQYYRNRYNAGVSELREWLVA    420
A13-P590        YEQRITTALNNVDTNYFAFTQAQSTLSNLQQTHSYNQRITQYYRNRYNAGVSELREWLVA    420
A14-P626        YEQRITTALNNVDTNYFAFTQAQSTLSNLQQTHSYNQRITQYYRNRYNAGVSELREWLVA    420
                **********************:***************************************

A1-NTHi375      ANTEKSSQLAILNAKYQVLQSENAVYSSMAGYYL  454
A2-P621         ANTEKSSQLAILNAKYQVLQSENAVYSSMAGYYL  454
A3-RdKW20       ANTEKSSQLAILNAKYQVLQSENAVYSSMAGYYL  454
A5-P673         ANTEKSSQLAILNAKYQVLQSENTVYSSMAGYYL  454
A6-P642         ANTEKSSQLAILNAKYQVLQSENAVYSSMAGYYL  454
A7-P665         ANTEKSSQLAILNAKYQVLQSENAVYSSMAGYYL  454
A8-P657         ANTEKSSQLAILNAKYQVLQSENAVYSSMAGYYL  454
A9-P645         ANTEKSSQLAILNAKYQVLQSENAVYSSMAGYYL  454
A10-P851        ANTEKSSQLAILNAKYQVLQSENAVYSSMAGYYL  454
```

```
A11-P593        ANTEKSSQLAILNAKYQVLQSENAVYSSMAGYYL   454
A12-P607        ANTEKSSQLAILNAKYQVLQSENAVYSSMAGYYL   454
A13-P590        ANTEKSSQLAILNAKYQVLQSENAVYSSMAGYYF   454
A14-P626        ANTEKSSQLAILNAKYQVLQSENAVYSSMAGYYL   454
                **********************:*********:
```

Figure S24. Distribution of TolC variants among the 14 selected NTHi isolates. Thirteen TolC variants were found. The NTHi375 and P652 strains presented the same TolC variant. Polymorphisms are labeled in red.

```
A1-NTHi375      MRQAKTDLAEQIFLATDRLMAKEGLDRLSMHKIAKEANVAAGTIYLY-FKNKDELLEQFA     59
A2-P621         MRQAKTDLAEQIFSATDRLMAKEGLNQLSMHKLAKEANVAAGTIYLY-FKNKDELLEQFA     59
A3-RdKW20       MRQAKTDLAEQIFSATDRLMAREGLNQLSMLKLAKEANVAAGTIYLY-FKNKDELLEQFA     59
A4-P652         MRQAKTDLAEQIFSATDRLMAREGLNQLSMHKLAKEANVAAGTIYLY-FKNKDELLEQFA     59
A5-P673         MRQAKTDLAEQIFSATDRLMAREGLNQLSMHKLAKEANVAAGTIYLY-FKNKDELLEQFA     59
A7-P665         MRQAKTDLAEQIFSATDGLMAREGLNQLSMHKLAKEANVAAGTIYLY-FKNKDELLEQFA     59
A8-P657         ------------------------------------------------------------     0
A9-P645         MRQAKTDLAEQIFSATDRLMAREGLNQLSMHKLAKEANVAAGTIYLY-FKNKDELLEQFA     59
A10-P851        -------------------MAKEGLNQLSMHKLAKEANVAAGTIYLYFFKNKDELLEQFA     41
A11-P593        MRQAKTDLAEQIFSATDRLMAKEGLNQLSMHKLAKEANVAAGTIYLY-FKNKDELLEQFA     59
A12-P607        MRQAKTDLAEQIFSATDRLMAKEGLNQLSMHKLAKEANVAAGTIYLY-FKNKDELLEQFA     59
A13-P590        MRQAKTDLAEQIFLATDRLMAKEGLDRLSMHKIAKEANVAAGTIYLY-FKNKDELLEQFA     59

A1-NTHi375      HRVFSMFMATLEKDFDESKPFFEQYRQMWKNIWYFLQENPTILSNLKQYESLPNFKDICK     119
A2-P621         HRVFSMFMATLEKDFDETKPFFEQYIDKCGKTFGISY------------KKIPLFYPI--     105
A3-RdKW20       HRVFSMFMATLEKDFDETKPFFEQYRQMWKNIWYFLQENPTILSNLKQYESLPNFKDICK     119
A4-P652         HRVFSMFMATLEKDFDETKPFFEQYRQMWKNIWYFLQENPTILSNLKQYESLPNFKDICK     119
A5-P673         HRVFSMFMATLEKDFDETKPFFEQYRQMWKNIWYFLQENPTILSNLKQYESLPNFKDICK     119
A7-P665         HRVFSMFMATLEKDFDETKPFFEQYRQMWKNIWYFLQENPTILSNLKQYESLPNFKDICK     119
A8-P657         ----------------------------MWKNIWYFLQENPTILSNLKQYESLPNFKDICK     33
A9-P645         HRVFSMFMATLEKDFDETKPFFEQYRQMWKNIWYFL-ENPTILSNLKQYESLPNFKDICK     118
A10-P851        HRVFSMFMATLEKDFDETKPFFEQYRQMWKNIWYFLQENPTILSNLKQYEYLPNFKDICK     101
A11-P593        HRVFSMFMATLEKDFDETKPFFEQYRQMWKNIWYFLQENPTILSNLKQYESLPNFKDICK     119
A12-P607        HRVFSMFMATLEKDFDETKPFFEQYRQMWKNIWYFLQENPTILSNLKQYEPLPNFKDICK     119
A13-P590        HRVFSMFMATLEKDFDESKPFFEQYRQMWKNIWYFLQENPTILSNLKQYESLPNFKDICK     119
                                           : : :             : :* *  *

A1-NTHi375      NVKNCRWDLFCDQAKKAGLLAELSEDILFLLSLKTAINLASDAKFIDFDLKPEILESVIE     179
A2-P621         ------------------------------------------------------------     105
A3-RdKW20       NIKNCRWDLFCHQAQKAGLLAELSEDILFLLSLKTAINLASDAKFIDFDLKPEILESVIE     179
A4-P652         NVKNCRWDLFCHQAQKAGLLAELSEDILFLLSLKTAINLASDAKFIDFDLKPEILESVIE     179
A5-P673         NIKNCRWDLFCHQAQKAGLLAELSEDILFLLSLKTAINLASDAKFIDFDLKPEILESVIE     179
A7-P665         NIKNCRWDLFCHQAQKAGLLAELSEDILFLLSLKTAINLASDAKFIDFDLKPEILESVIE     179
A8-P657         NVKNCRWDLFCHQAKKAGLLAELSEDILFLLSLKTAINLASDAKFIDFDLKPEILESVIE     93
A9-P645         NIKNCRWDLFCHQAQKAGLLAELSEDILFLLSLKTAINLASDAKFIDFDLKPEILESVIE     178
A10-P851        NIKNCRWDLFCHQAQKAGLLAELSEDILFLLSLKTAINLASDAKFIDFDLKPEILESVIE     161
A11-P593        NVKNCRWDLFCHQAQKAGLLAELSEDILFLLSLKTAINLASDAKFIDFDLKPEILESVIE     179
A12-P607        NIKNCRWDLFCHQAQKAGLLAELSEDILFLLSLKTAINLASDAKFIDFDLKPEILESVIE     179
A13-P590        NVKNCRWDLFCDQAKKAGLLAELPEDILFLLSLKTAINLVSDAKFIDFDLNPEILESVIE     179

A1-NTHi375      RSWRAIQK         187
A2-P621         --------         105
A3-RdKW20       RSWRAIQK         187
A4-P652         RSWRAIQK         187
A5-P673         RSWRAIQK         187
A7-P665         RSWRAIQK         187
A8-P657         RSWRAIQK         101
A9-P645         RSWRAIQK         186
A10-P851        RSWRAIQK         169
A11-P593        RSWRAIQK         187
A12-P607        RSWRAIQK         187
A13-P590        RSWRAIQK         187
```

Figure S25. Distribution of AcrR variants among the 14 selected NTHi isolates. Twelve AcrR variants were found. The

NTHi375 and P642 strains presented the same AcrR variant; the P673 and P626 strains presented the same AcrR variant. Polymorphisms are labeled in red.

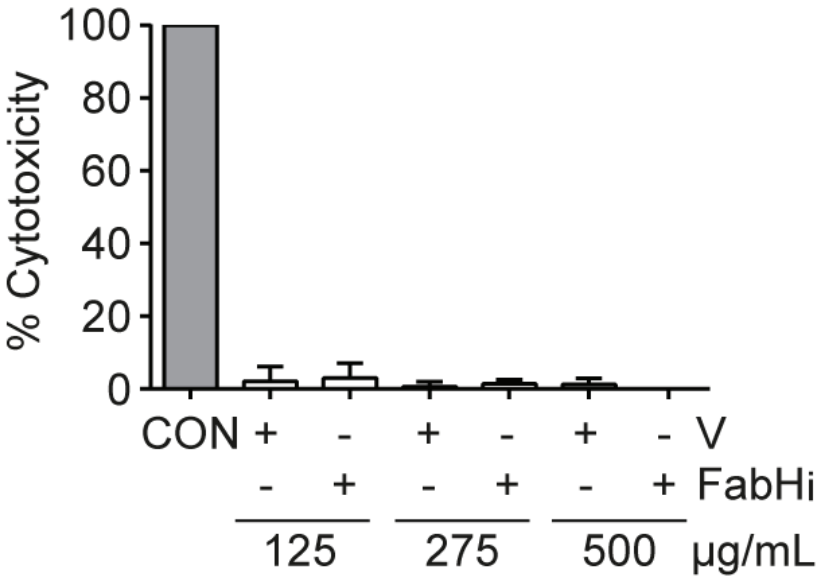

Figure S26. Cytotoxicity measured by the release of lactate dehydrogenase by A549 cells incubated for 16 h with increasing doses of FabHi in serum-starved medium. FabHi did not cause a cytotoxic effect on cells under the conditions tested (mean ± SD). Statistical comparisons of the means were performed with one-way ANOVA and Dunnett's multiple comparisons test.

Discusión General

In this PhD Thesis work, we studied the involvement of *Haemophilus influenzae* metabolism in the host airway infectious process. A myriad of complentary approaches were used, ultimately aiming to identify and propose novel therapeutic targets for further antimicrobial development. This work has three main related axes:

(1) the search for bacterial virulence factors by *in vivo* screening using multi-omic approaches (revised in **Chapter 1**, developed in **Chapter 2**);

(2) addressing features and biological meaning of NTHi glucose catabolism during infection, by using genetic engineering and mutant phenotyping approaches (**Chapter 3**);

(3) addressing the capabilities of genome-scale metabolic modelling and computational docking for therapeutic target-drug screening, followed by evaluation of NTHi fatty acid biosynthesis pharmacological inhibition up to a preclinical stage **(Chapter 4)**.

The outcome of this work is summarized in **Figure 29** and discussed below.

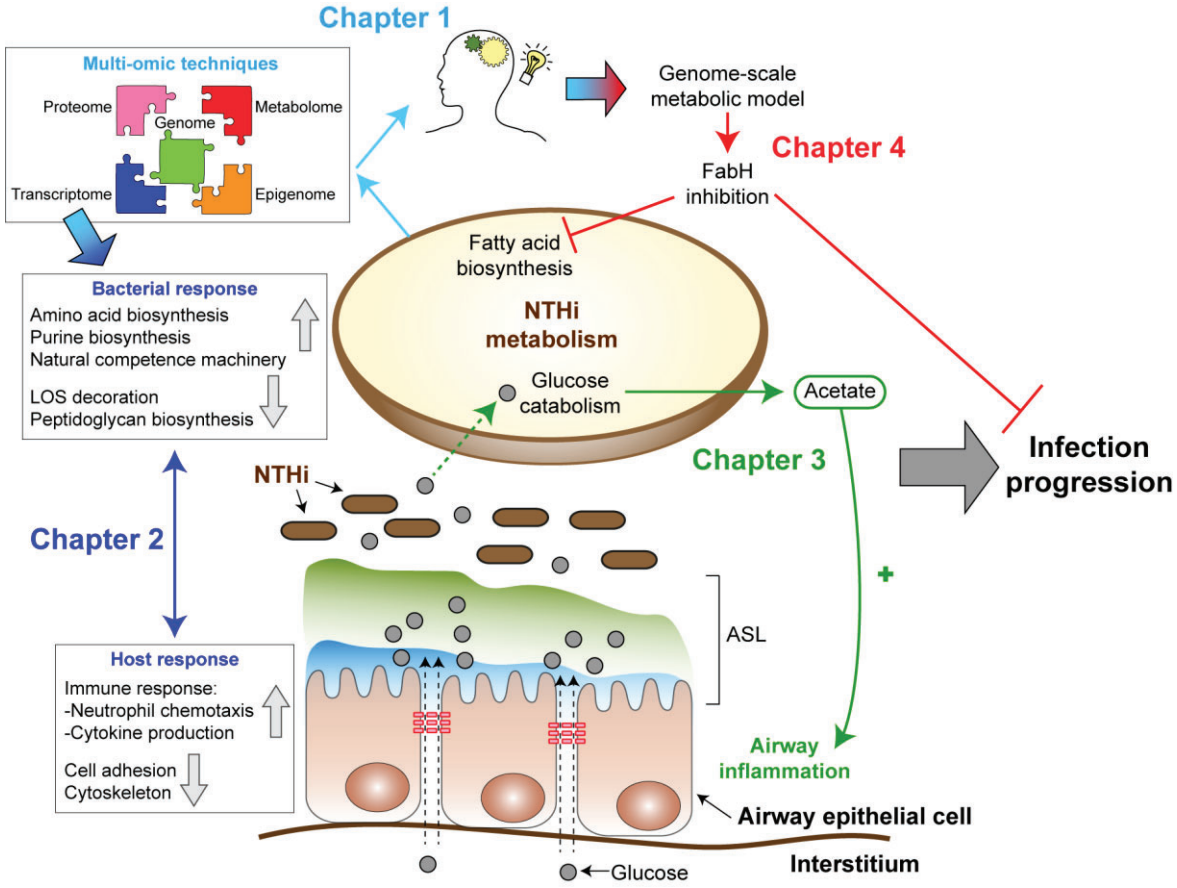

Figure 29. Summary of the metabolic aspects of the host-NTHi interplay analyzed in this PhD Thesis work through the use of -omic techniques (**Chapters 1** and **2**), analysis of glucose catabolism as a patho-adaptive mechanism (**Chapter 3**), as well blocking the biosynthesis of fatty acids from a therapeutic point of view (**Chapter 4**).

1. *In vivo* multi-omics approach us to understand genetic traits associated with NTHi bacterial infection

In this work, we combined high-throughput sequencing-mediated transcriptome profiling (RNA-seq) and genome-wide insertion mutant fitness profiling (Tn-seq) to characterize gene expression and fitness determinants upon *H. influenzae* murine lung infection.

We acknowledge some limitations: our Tn-seq assays were performed in mice with normal lung function or with lung emphysema. However, our RNA-seq analyses were carried out in mice with normal lung function only. There are several reasons for this decision: infected lung tissues did not contain enough bacterial RNA, as we found that only 0.25% of reads mapped to the bacterial genome. It was necessary to use pulled BALF samples from infected mice to gather enough material allowing to sequence bacterial RNA from infected animals. The need to use BALF samples limited our capacity for using emphysema mice for RNA-seq analysis, as our emphysema model, consisting of porcine pancreatic elastase administration to mice 21 days prior infection does not allow consistent BALF sampling (Rodríguez-arce et al., 2021). Conversely, our model does no involve bacterial replication but clearance over time, which also limits the sampling time point to obtain material for RNA-seq analyses. As a result of preliminary assays, we decided to simple bacterial transcriptome by using pulled BALF samples from infected animals euthanised 12 hpi. These limitations did not happen when preparing material for Tn-seq, and aiming to be as comprehensive as possible, we employed both normal lung function and emphysematous lungs for this purpose, at 12 and 24 hpi.

H. influenzae natural competence machinery is induced by deprivation of phosphotransferase system (PTS) sugars that activates adenylate cyclase, Cya, raising cAMP levels which promotes the activation of CRP regulator, and by Sxy (also known as TfoX) regulator whose activity depends on the deprivation of purines precursors (Cameron & Redfield, 2006; Redfield et al., 2005; Sinha et al., 2013). Our RNA-seq analysis revealed *in vivo* up-regulaton of 11 genes belonging to CRP-S regulon (Redfield et al., 2005) compared to *in vitro*, suggesting a partial activation of natural competence machinery. In addition, it is known that starvation medium MIV induces purine biosynthesis genes expression, all belonging to the PurR regulon (*cvpA*, *purC*, *purD*, *purE*, *purF*, *purH*, *purK*, *purL*, *purM* and *purN*) (Redfield et al., 2005) in response to extracellular purine deprivation. Our RNA-seq screening revealed up-regulation of all of them upon infection, and together with the observed attenuation of Δ*purH in vivo*, suggests low purines availability in the infectious environment, which is in line with previous studies (Turner et al., 2014). Both purine biosynthesis and partial natural competence machinery up-regulation *in vivo* suggested that the infection environment could induce *H. influenzae* natural transformation. We performed several *in vivo* and *ex vivo* transformation assays, but we did not get recombinants. This may be due to the fact that not all the genes of the uptake machinery were activated. Of 26 genes belonging to the CRP-S regulon (Redfield et al., 2005)

or 17 essential genes for transformation (*pilA*, *pilB*, *pilC*, *pilD*, *comA*, *comB*, *comC*, *comD*, *comE*, *comF*, *comN*, *comO*, *comP*, *comQ*, *pilF2*, *rec2* and *toxA*) (Sinha et al., 2012), only 11 or 8, respectively, showed an induction *in vivo*. Furthermore, neither *crp* and *sxy* appeared induced after mice infection. Although *sxy* did not appear up-regulated *in vivo* it is not really a lack of natural competence indicator since Sxy activity does not depend so much on its gene expression but on translational regulation enhanced on low purine availability (Cameron et al., 2008; Sinha et al., 2013).

More than 85% of internalized DNA is degraded and used as energy source (Macfadyen et al., 2001; Mell & Redfield, 2014; Sinha et al., 2013), however our experiments carried out to verify natural competence *in vivo* require both uptake and recombination. So we cannot determine if the partial activation of natural competence machinery and the entire PurR regulon only promotes uptake but not recombination. All up-regulated natural competence genes showed attenuation *in vivo* with the exception of *comE*, somehow surprising since it belongs to the *comABCDEF* operon (Redfield et al., 2005). ComE cellular location is not a differentiating element since ComD is also surface exposed, and both mutants presented a close to zero transformation frequency, although Δc*omD* was attenuated in mice.

Most mutants in genes up-regulated *in vivo* showed attenuation upon mouse infection, whereas the down-regulated ones showed a WT phenotype. While Δ*glpQ* rendered a WT phenotype in *H. influenzae*, it shows attenuation upon inactivation in *S. pneumoniae* suggesting different needs for GPC catabolism among respiratory pathogens (Chuang et al., 2015). We previously observed lack of attenuation by NTHi375Δ*licBC* (Morey et al., 2013), further completed in the current study. Down-regulation of genes involved in outer surface decoration had been seen in previous *P. aeruginosa* studies (Turner et al., 2014). Up-regulation of the *hxuCBA* locus expression *in vivo* may relate with attenuation in mice (Rodríguez-Arce et al., 2019). Conversely, some down-regulated genes showed attenuation in previous studies, such as the *hbpA*, *ackA*, *fadL* or *thyA* genes (López-López et al., 2020; Moleres et al., 2018; Rodríguez-Arce et al., 2017, 2019). This could relate to different assay conditions or other currently unknown factors. The two-component system QseBC, also called FirRS (ferrous iron responsive regulator/sensor) is part of an operon together with *ygiW* (Steele et al., 2012), although differential expression was observed for *qseBC* but not for *ygiW*. NTHi375Δ*qseBC* attenuation upon mouse infection nicely correlates with a previous observation by (Steele et al., 2012).

in vivo H. influenzae up-regulated genes showed little coincidence with a previous dual RNA-seq *in vitro* study carried out upon NTHi infection of ciliated human bronchial epitelial cells (Baddal et al., 2015). Our RNA-seq study revealed that NTHi alters its surface during murine infection, modulating the expression of adhesins, outer membrane proteins, and cell wall biosynthesis. The infection carried out by the Baddal's group showed differential expression of *H. influenzae* adhesins

and OMP, although different from those obtained in our study or with opposite results, as it is the case of *pilA* and *ompP26*. Other differences between study outcomes relied on genes encoding toxin-antitoxin systems and central metabolism enzymes. Notably, several transport systems (*artP*, *cydC*, *cydD*, and iron uptake systems) were up-regulated in both studies. Other respiratory pathogens such as *P. aeruginosa* also up-regulate genes involved in iron uptake *in vivo* (Damron et al., 2016; Turner et al., 2014), but the repertoire of regulated genes involved in iron uptake *in vivo* was larger than *in vitro*, likely due to mice nutritional immunity. Unlike lactate transport up-regulation shown in the Baddal's study, suggesting its use as a primary carbon and energy source, we did not observe up-regulation *in vivo*. Several stress response systems were represented in both studies: 11 and 13 genes were up- or down-regulated, respectively, in our current study, showing no overlap with *dppBCDF*, *OxyR*, *pgdX*, *pntAB*, *ureABCEFGH*, *ifhAB* systems up-regulated in Baddal's study. Differences obtained between both studies are likely due to the use of different bacterial strains (NTHi375 versus strain 176), or assay conditions (murine airway versus cultured cell infection).

During infection, multiple host factors come into action to control and eliminate pathogens, a response customized to the pathogen and infection site. Few studies on *in vivo* lung genome expression profiling upon bacterial infection are currently available. A seminal study was performed for *P. aeruginosa* lung infection (Damron et al., 2016), where a lower number of regulated host genes were seen *in vivo* despite using the same mouse breed as in our current study. However, Damron's group also observed an acute inflammatory response, in line with our observations. The host response observed upon *H. influenzae* infection *in vitro* (Baddal et al., 2015) is similar to that obtained in our current study, with up-regulation of pro-inflammatory immune response, and down-regulation of cytoskeleton and cell adhesion, despite different host considered in each study. Our results revealed cell death as one of the most represented categories regulated upon mice infection, with half of genes being up-regulated and the other half being down-regulated. This observation probably represents the transition between 6 to 24 hpi showed by Baddal's group, where they found up-regulation of these genes in early states of infection only, which highlights the importance of time sampling taking into account the dynamic process of infection.

We hypothesized that genes with higher *in vivo* expression could be important for fitness during infection but we actually found very little correlation between RNA-seq and Tn-seq assays. Such poor correlation is in line with previous studies (Powell et al., 2016; Turner et al., 2014). Overlapping between the two -omic methodologies occurs for *P. aeruginosa* metabolic genes (Turner et al., 2014), and more specifically for branched amino acids biosynthesis, iron uptake, and short-chain fatty acids utilization in *Snodgrassella alvi* (Powell et al., 2016). Metabolic genes constitute the majority of shared genes between our RNA-seq and Tn-seq analyses. However, all came from Tn-seq data at 24 hpi. Only *rpoC* was commonly found by RNA-seq and Tn-seq analyses under comparable conditions. Poor overlapping may be due to differences in both bacterial strain used or the mice age, the

constitutive/transient expression of many genes at a given time of infection (Powell et al., 2016), or the fact that Tn-seq uses a mixed population of mutants where compensatory event can have masking effects (West et al., 2006). These results shed light on the complementarity of data obtained using these two -omic techniques allowing to generate a global vision of the mechanisms employed by *H. influenzae* during infection.

In this work, we mostly focused on the RNA-seq part of the study. We acknowledge the lack of Tn-seq validation and further related mechanistic work. This requires additional work, currently ongoing in our research group, which hopefully provide an integrative and comprehensive landscape on the NTHi-host airway interplay.

2. The importance of NTHi glucose catabolism as a potential enhancer of chronic lung disease

The ability to access nutrients is essential for pathogen survival in the host. Airway inflammation has been related to increased glucose availability in the ASL, which seems to facilitate respiratory infections. In this study, we investigated if changes in the glucose metabolic network of *H. influenzae* alter its host interplay and virulence. Our focus was on genes whose inactivation would perturb glucose metabolism by preventing the formation of end products such as acetate, succinate, and formate. In the tested WT strains, glucose consumption followed an established pattern where acetate is the dominant metabolite during aerobic growth, while reductions in oxygen tension lead to the formation of increasing amounts of succinate and formate (**Figures 17, 19**, and S5) (Ahearn et al., 2017; Muda et al., 2019; Othman et al., 2014). Despite genomic heterogeneity (De Chiara et al., 2014; Moleres et al., 2018; Pettigrew et al., 2018; Price et al., 2015), it now appears that this end product spectrum is a stable feature of NTHi, which is supported by a high level of conservation of genes encoding relevant enzymes including the *ackA*, *pflA*, and *frdA* genes among genome sequenced strains (N. López-López, personal´ communication) (Othman et al., 2014). The removal of each of these genes led to the expected loss of gene expression and limited production of the corresponding metabolite, and interestingly, for both the *ackA* and *frdA* mutant strains, production of D-lactate could also be observed. D-Lactate is a typical byproduct of the so-called “mixed acid” fermentation in species such as *E. coli* but is not generally produced by *H. influenzae* (Ahearn et al., 2017; Muda et al., 2019; Othman et al., 2014). D-Lactate production by the *ackA* and *frdA* mutant strains is thus indicative of a perturbation of central carbon metabolism and possibly the cellular redox balance, with accumulation of pyruvate being a likely cause of the redirection of carbon flux into lactate. The perturbation of carbon metabolism also extended to glucose utilization, where particularly the *frdA* mutant only partially utilized glucose present in the growth medium (**Table S12**).

For the *ackA* mutant, we observed reduced growth on both sBHI and CDM, which likely reflects the reduced ATP yield resulting from the loss of the Pta-AckA reactions. The slightly less severe reduction in cell numbers observed during anaerobic growth of the *ackA* mutant (**Figure 18, middle panels**) may be linked to the extended spectrum of excreted products in this condition. A similar observation has been made in *Staphylococcus aureus* where, although having a complete TCA cycle and thus greater metabolic flexibility, inactivation of the *ackA-pta* genes caused milder growth defects under anaerobic conditions compared to aerobic conditions and also resulted in a redirection of carbon flux into the generation of lactate (Marshall et al., 2016; Sadykov et al., 2013).

Interestingly, in a model of NTHi lung infection, only the *ackA* mutant showed a significant reduction in survival, and a small reduction in fitness was also observed for the *pflA* mutant strain. AckA has also been linked to pathogenesis of other bacteria such as *Streptococcus mutans*, uropathogenic *E. coli*, and *Listeria monocytogenes* (Anfora et al., 2008; Gueriri et al., 2008; Kim et al., 2015), while reduced virulence was also observed in a *pflA* mutant strain of *S. pneumoniae* (Yesilkaya et al., 2009). Currently, the role of formate in *H. influenzae* virulence is unclear and may require further work. Our data increase links between NTHi central carbon metabolism and virulence, with previous studies having shown that the inactivation of *aceF*, *sucAB*, and *mtsZ* molybdenum-containing methionine sulfoxide reductase encoding genes also impair NTHi infection (Dhouib et al., 2016; Edwards & Palsson, 1999; Herbert et al., 2003; Othman et al., 2014; Papin et al., 2002; Raghunathan et al., 2004).

An interesting and previously unexplored aspect of NTHi biology is the potential of the metabolites produced during glucose catabolism to be immunomodulators. Chronic *H. influenzae* infections are often associated with persistent, high levels of inflammation, and here, we show that acetate, a key metabolite produced by this pathogen, seems to drive inflammation. While the precise composition of bacterial culture supernatants employed in our cell stimulation assays is unknown, it is that of the supernatants analyzed during growth experiments (**Figures 19 and S9**). In combination with the single compound controls, the fact that extracts from *ackA* mutant that did not produce significant amounts of acetate showed a low stimulation of inflammatory cytokine gene expression in cultured cells strongly suggests that acetate was giving rise to this effect (Ghorbani et al., 2015). Succinate, formate, and hypoxanthine did not appear to have immunomodulatory activities in this assay, although there is some evidence for their immunomodulatory properties in other infectious processes (Gallego-Delgado et al., 2014; Hughes et al., 2017; Orengo et al., 2008). This notion is supported by the *kc* gene expression data in infected murine lung samples (**Figure 21**). Also, the fact that infection by Δ*ackA* did not increase cell recruitment further backs that impaired airway infection relates to the fitness defect resulting from the *ackA* gene inactivation. In contrast, infection with anaerobically grown Δ*ackA* bacteria rendered attenuation but not differences in cell recruitment in BALF samples. Mutant produced end products could contribute to such cell recruitment, but it seems

unlikely to relate to lactic acid production given that lactic acid bacteria seem to have anti-inflammatory properties (Kuda et al., 2014; Nam et al., 2019; Park et al., 2014).

Our results thus indicate that mutations that perturb NTHi glucose metabolism have a direct effect on virulence, and body niches that are infected by this pathogen are known to contain elevated levels of glucose. A link between elevated ASL glucose and bacterial lung infection has been established *in vivo* (Garnett et al., 2013; Hunt et al., 2014; Pezzulo et al., 2011) and does not occur after infection with *S. aureus* or *P. aeruginosa* mutants unable to metabolize glucose (Gill et al., 2016; Hunt et al., 2014; Pezzulo et al., 2011). Our results suggest that these elevated glucose levels may increase not only bacterial growth but also the release of proinflammatory metabolites produced by the bacteria. Altogether, we speculate that bacterial consumption of glucose present in the COPD airway could have a direct effect on the chronic cycle of the disease, by increasing both bacterial growth and inflammation (summarized in **Figure 30**).

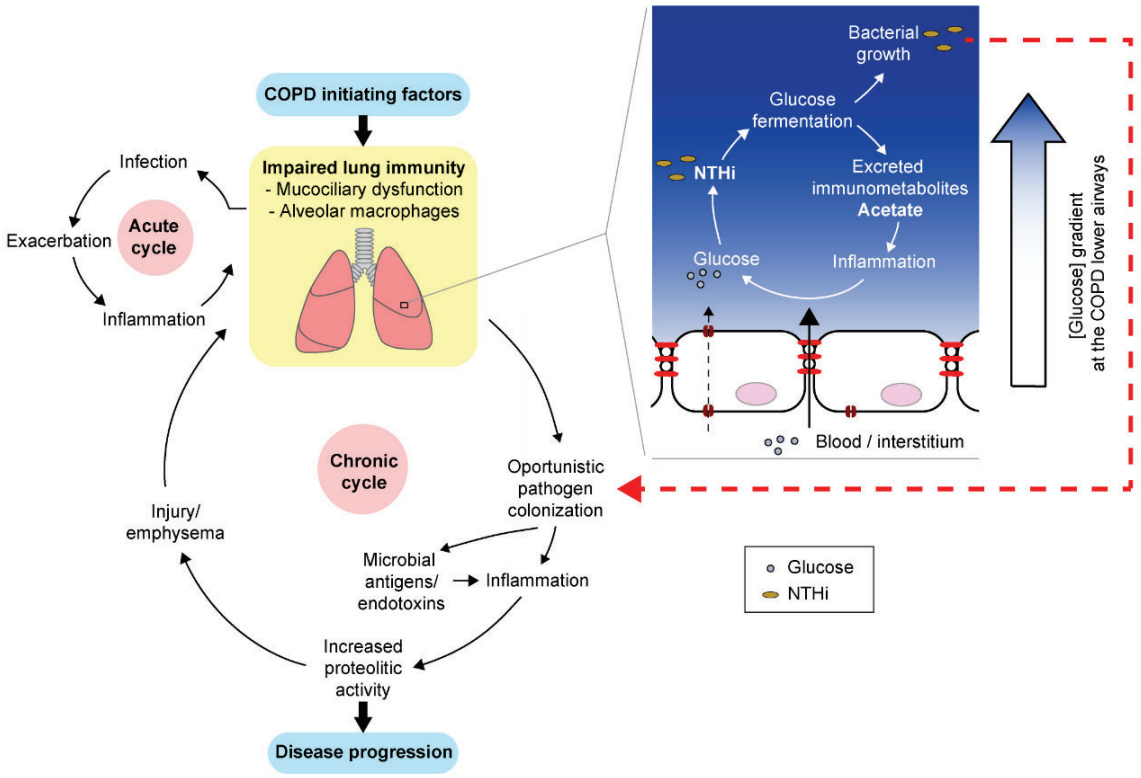

Figure 30. Model proposing the biological significance of *H. influenzae* glucose catabolism during infection within the COPD lung. Data in the current era of COPD demonstrate a bidirectional relationship between COPD and bacterial infections, with each impacting the pathogenesis of the other. COPD initiating factors impair innate lung immunity, allowing microbial pathogens to cause infectious exacerbations (acute cycle) or to persist at the lower airways (chronic cycle). Colonizing opportunistic pathogens and their proinflammatory components worsen mucus hypersecretion, mucociliary dysfunction, and emphysema, facilitating further microbial susceptibility and contributing to worsening airflow obstruction, lung parenchymal damage, and disease progression in an endless manner. NTHi may take advantage of elevated glucose levels encountered at the COPD lower airways, use it as carbon source facilitating growth and infection, and generate fermentative end products with a proinflammatory effect likely associated with the production of acetic acid. As a whole, bacterial glucose metabolism at the human airways may have a significant impact on the chronic cycle of the disease, as a means of bacterial growth and host inflammation. NTHi produced immunometabolites may add to previously known proinflammatory signals, together favoring persistent inflammation within this niche.

In this context, it is worth considering that inhaled corticosteroids, commonly used in COPD, reduce exacerbations but are associated with an increased risk of pneumonia (Finney et al., 2014). Given that corticosteroids may have a hyperglycaemic effect (Herth et al., 2015), increased airway glucose could be one mechanism whereby such drugs increase susceptibility to infection and pneumonia risk.

Finally, the link between elevated glucose and bacterial infection may open up therapeutic avenues to reduce infection. Metformin, used to treat type II diabetes, reduces epithelial permeability to glucose and improves barrier function (Kalsi et al., 2019; Patkee et al., 2016), and evidence indicates that treating diabetic mice with metformin lowers *P. aeruginosa* and *S. aureus* growth in the lungs (Garnett et al., 2013; Gill et al., 2016). A systemic reduction of blood glucose could be achieved with insulin or with sodium-glucose cotransporter inhibitors such as dapagliflozin, that lowers blood glucose by increasing its renal excretion, and has been shown to reduce airway glucose and bacterial load *in vivo* (Åstrand et al., 2017). From a bacterial perspective, therapeutic targeting of proteins involved in glucose uptake or metabolism could prevent an infection in patients with elevated airway glucose, but bacterial energy requirements are not restricted to glucose alone; therefore, elevated levels of any molecule that can be broken down to generate energy could potentially lead to increased bacterial growth. Altogether, this study highlights that understanding both host mechanisms leading to control of vital nutrients and bacterial pathways required to metabolize them, may lead to novel antibacterial strategies.

3. The increasing focus on fatty acid biosynthesis as a therapeutic target

iNL638 is a powerful tool for drug target discovery and set the bases of future H. influenzae strain-specific metabolic evaluation. Here, we constructed a high-quality GEM of *H. influenzae* as a basic computational framework to identify essential genes (among other possibilities) suitable for further exploitation as drug targets. The exponential increase of pathogen genomes and the emergence of high-throughput technologies are providing a myriad of large datasets. Among the numerous computational methods developed to generate meaningful outcomes of these data, metabolic modeling is emerging as a promising approach for the coherent organization of this information while providing insights on biological systems (**Figure 31**) (Fang et al., 2020). Thus, it is not surprising that this approach is being increasingly incorporated as a key strategy for antimicrobial target discovery at the level of preclinical research (Cesur et al., 2020; Chavali et al., 2012; Dunphy & Papin, 2018; Lee et al., 2009; Mienda et al., 2018; Presta et al., 2017; Ramos et al., 2018). Metabolic modeling has been used for the design of new drugs by informing target selection (Bartell et al., 2017; Lee et al., 2009; Mienda et al., 2018), and for the engineering of cells by rewiring

metabolism towards the production of a product of interest (Gudmundsson & Nogales, 2021; King et al., 2015). Despite the success of GEMs, the lack of a high-quality model for *H. influenzae* largely hampered the application of such approaches in this clinically relevant bacterium. *i*NL638 represents a powerful and unprecedented computational tool towards the search for novel drug targets in *H. influenzae*. In addition, the large quality of *i*NL638 in terms of consistency and interoperability paves the way for the future multi-strain modeling of the *H. influenzae* species using the strain RdKW20 as a reference. As shown by the strain dependent effect of the inhibitor tested, the impact of metabolic context is gaining relevance as a key factor driving cell behaviour (Tas et al., 2021). Therefore, a further *H. influenzae* multi-strains modeling effort could lead the identification of secondary metabolic hubs modulating the response of known and novel drugs, promoting the establishment of synergistic and more robust antibacterial treatments. Following this notion, *Salmonella* multi-strain modeling identified serovar-specific metabolic traits, including auxotrophies and catabolic pathways related with adaptations to their colonization sites (Seif et al., 2018), and strain-specific metabolic features were unravelled for *S. aureus*, *P. aeruginosa* or *A. baumannii* (Bartell et al., 2017; Bosi et al., 2016; Norsigian et al., 2018).

The potential of targeting H. influenzae fatty acid biosynthesis. Among essential genes predicted by *i*NL638, 89 also showed to be essential in three previous Tn-seq-bed screenings (Gawronski et al., 2009; Mobegi et al., 2014; Wong et al., 2013). These data do not only argue in favour of the accuracy of *i*NL638 when predicting essential genes, but give further support to the potential role of these genes as drug targets. About 33% predicted essential genes were involved in lipid metabolism. Although focused here on FASII inhibition, we acknowledge that peptidoglycan biosynthesis, accounting for over 22% of the commonly shared predicted essential genes, also deserves attention as the diversity of antimicrobials with distinct mechanisms reported to disrupt the bacterial peptidoglycan is wide (Sibinelli-Sousa et al., 2021). When focusing on FabH targeting, the antimicrobial potential of natural (Pishchany et al., 2018; Wang et al., 2006, 2007; Young et al., 2006) and synthetic (McKinney et al., 2016; Jia Wang et al., 2020; Wang et al., 2019; Yang et al., 2019b; Young et al., 2006; Zhou et al., 2017) molecules has been reported for several bacterial pathogenic species, including *H. influenzae*. Here, we went further with previously reported compound 31 in (McKinney et al., 2016), renamed FabHi for simplicity.

Several technical aspects of FabHi antibacterial effect evaluation may deserve consideration by those interested in assessing novel drugs without pre-established standardized procedures. We initially aimed to adapt regular MIC assays by measuring culture turbidity, in combination with quantifying redox activity in metabolically active bacterial cells by reduction of iodonitrotetrazolium chloride (Braissant et al., 2020) (data not shown), and with serial dilution plating for c.f.u. counting. However, the lack of consistency and correlation between methodologies, which can lead to misleading interpretations when testing new drugs, drove us

to use c.f.u. counts as rendering the clearest, more reliable and reproducible results. Another technical aspect is the culture medium of choice. Although results obtained by bacterial growth in CDM or in sBHI were relatively similar, we consistently found differences for some strains when incubated with the highest drug doses tested, which may relate to the apparently biphasic mode of action previously suggested above (**Figure S20**). Lastly, the bacterial growth type of culture may be another key aspect. Here, by following the same procedure, we monitored the effect of FabHi on both bacteria in suspension and attached to the plastic surface on 96x well plates. Differences were noticeable, as an inverse correlation was observed on the FabHi effect when assessing planktonic or biofilm grown bacteria, as the lowest inhibitor concentration tested did not alter biofilm growth by those strains considered to be more susceptible, according to planktonic studies, in comparison to the more resistant ones. In this context, strain P657 showed slow growth in CDM, although clearly grouped in the most resistant category despite low expression of the *fabH* gene, and the effect of FabHi on P657 biofilm growth could not be easily explained, as consistently unrelated to the concentration of inhibitor used.

***FabHi effects are heterogeneous among clinical* isolates.** Strain phenotypic heterogeneity when incubated with FabHi evidenced the concurrence of several factors in its killing activity on *H. influenzae*. According to the docking model, FabHi fills a large tunnel at the base of which are located the active site residues. This tunnel is the only access to the active center and, therefore, constitutes the binding cavity for the first (acyl-CoA) and second (malonyl-ACP) substrates and the feed-back inhibitor (palmitoyl-ACP), all of which will compete with FabHi binding. Hence, the antimicrobial effect of FabHi would depend on the available concentrations of all potential ligands and their respective affinities, which may vary among strains and also with growing conditions. Indeed, as shown above, several polymorfisms in FabH variants locate at regions relevant for activity and structural stability, and sequence changes at such positions may alter substrates and inhibitor binding as well as FabH catalytic efficiency. Additionally, strain variability associated to different CTs might modify, among other elements, the efflux pump system, with the subsequent impact on the amount of FabHi available to interact with FabH. Likewise, variations in expression level, conformation or potency of other components of the FASII biosynthetic pathway, including peripheral enzymes involved in production of FabH substrates (Campbell and Cronan 2001), may modify the catalytic balance of rates along FASII pathway and thus alter the FabHi antimicrobial effect. Indeed, mutations might compensate deficiencies in other enzymes of the FASII system, rescuing specific *H. influenzae* strains from FabHi antimicrobial effect or, alternatively, enhancing its outcome.

Nonetheless, variations observed among strains carrying the same FabH variant indicate that heterogeneity may be multifactorial. Strains carrying variants A1, A3, A5 or A6, although

sharing the same FabH variant, are diverse in terms of genomic content, i.e. do not cluster by clonal type (Moleres et al., 2018), and such genomic variability may contain currently unidentified elements

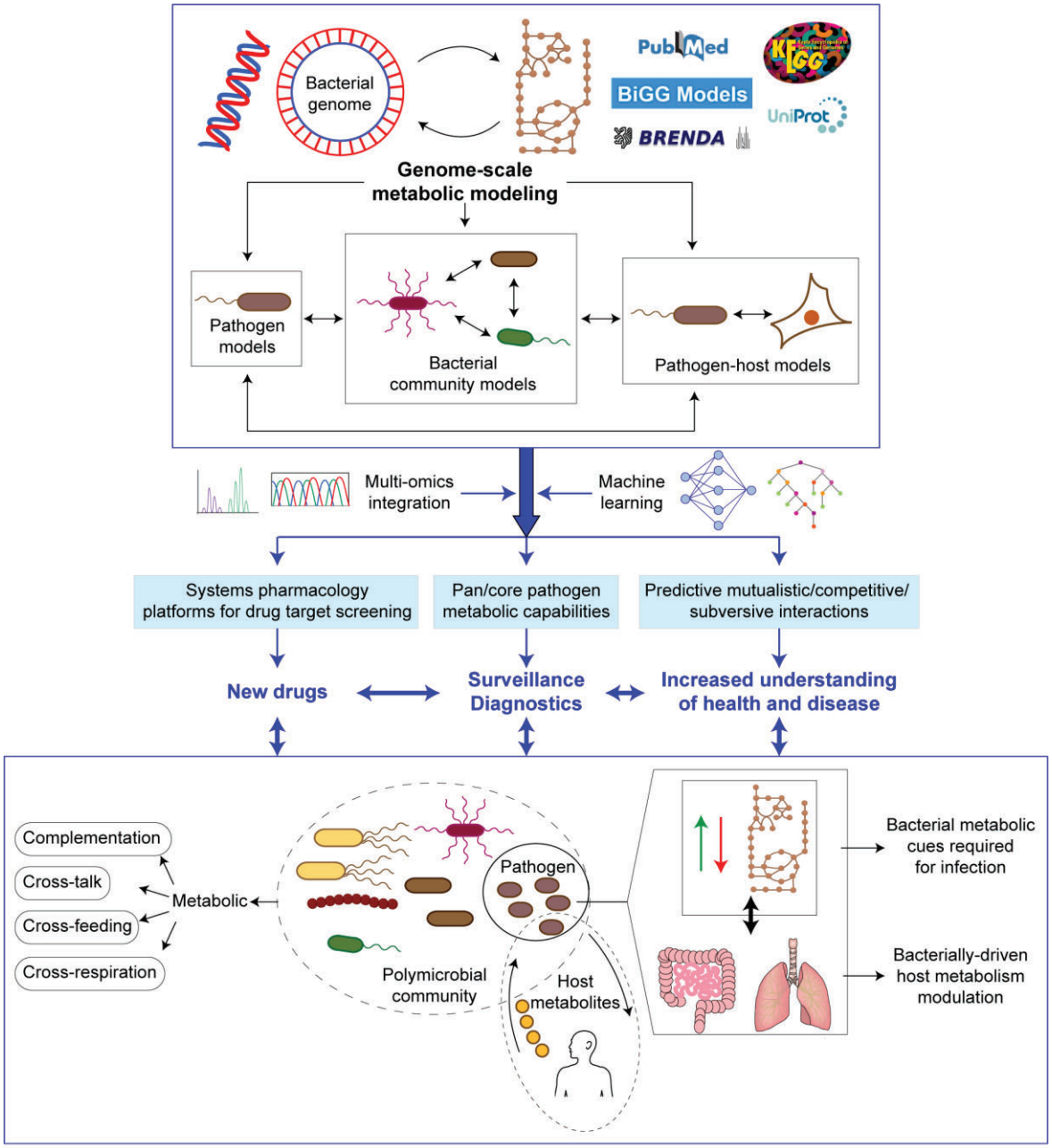

Figure 31. Genome-scale metabolic network reconstructions for bacterial pathogenesis. Fast evolving advances in the genomics and metabolomics fields facilitate metabolic modeling of priority pathogens, such as *H. influenzae*, of polymicrobial communities where key pathogens may have a starring role, and of host-pathogen systems. Metabolic reconstructions can yield significant benefits when combined with various layers of multi-omics information as part of integration strategies, further enriched by the predictive potential of machine learning computational tools. Such integrative view will guide our experimental work to understand key metabolic traits in bacteria-bacteria or bacteria-host interactions where virulence is the outcome since they can predict, among others, gene essentiality, carbon sources utilization capacity, or growth abilities in different nutritional or environmental conditions. More importantly, we foresee that such integrative view will contribute to pave the way for developing new diagnostic, treatment and surveillance procedures, seeking for their ultimate positive impact in the clinical management of bacterial infectious diseases.

also contributing to the observed phenotypes. In line with this, the three strains tested carrying variant A8 and belonging to the same clonal type (closely related genome-wise), behave all in the same manner. These strains are highly resistant, despite low *fabH* gene expression, which could be compensated by carrying a "resistant variant" together with an inactive variant of the AcrR repressor.

On the other hand, inspection of FabHi:$FabH_{RdKW20}$ complex structure indicates that FabHi affinity could be increased by introducing a hydroxyl group in ortho to the N-atom of the piperidine ring, which could lead to an extra hydrogen-bond with the side chain of Asn246 without introducing steric clashes. Of interest for further analysis, exploring the effect of FabHi modifications exceeds the scope of this study.

Overall, we present here a high-quality metabolic model of *H. influenzae* and show how *i*NL638 can be used as (i) powerful tool to better understanding the metabolism of this important pathogen; (ii) computational framework for large experimental datasets contextualization, and (iii) for the discovery of condition-independent drug targets. We shed light on the mechanism of inhibition of FabH mediated by FabHi and beyond allelic variation, we suggest the strain-specific metabolic context as a key factor modulating drugs performance. Therefore, the systematic metabolic evaluation of individual strains through computational frameworks will become of critical importance in the near future to design more precise and accurate treatments.

Conclusiones

1. La infección pulmonar murina por *H. influenzae* provoca cambios en el perfil global de expresión génica del pulmón infectado consistentes, entre otros, en una reprogramación celular que estimula la respuesta inmune pro-inflamatoria, y reprime la adhesión celular y la organización del citoesqueleto.
2. El estudio de cambios en el perfil transcriptómico de *H. influenzae* durante la infección pulmonar murina mediante su comparación con el transcriptoma de bacterias crecidas *in vitro* previo a la infección, reveló la expresión diferencial de un gran número de genes que pueden jugar papeles relevantes en el *fitness*, capacidad infectiva y/o adaptación del patógeno al nicho infectado.
3. Durante el proceso de infección respiratoria, se observó expresión diferencial significativa de genes bacterianos implicados, entre otros, en metabolismo, transporte de nutrientes y captación de ADN exógeno mediante transformación natural. Asimismo, se observó correlación entre sobre-expresión y atenuación tras inactivación génica.
4. Una parte significativa del panel de genes que codifica los elementos de la maquinaria de transformación natural de *H. influenzae* se sobre-expresan durante un proceso de infección pulmonar. Sin embargo, esta expresión diferencial no parece ser suficiente para completar de forma exitosa la translocación de ADN exógeno al citosol bacteriano y su integración genómica mediante doble recombinación homóloga.
5. El empleo de un enfoque multi-ómico en un sistema modelo *in vivo* destinado a la búsqueda de genes de *H. influenzae* con papeles relevantes en la interacción patógeno-sistema respiratorio evidencia la complementariedad y capacidad integrativa de aproximaciones globales como son RNA-seq y Tn-seq.
6. El catabolismo de glucosa de *H. influenzae* es un sistema conservado y coordinado que dirige el flujo metabólico hacia la formación de acetato, y en menor medida de formato y succinato, a través de las enzimas acetato quinasa AckA, piruvato formato liasa PflA y fumarato reductasa FrdA, respectivamente. La inactivación de *ackA* genera defectos en el crecimiento de la bacteria.
7. La perturbación en la producción de metabolitos mediante el catabolismo de glucosa re-direcciona los flujos metabólicos en *H. influenzae*. La inactivación de *ackA*, y en menor medida *frdA*, reduce la producción de acetato y conduce a la generación de D-lactato.
8. El acetato producido a través del sistema Pta-AckA es excretado durante el crecimiento de *H. influenzae* y tiene un efecto pro-inflamatorio en células de epitelio respiratorio en cultivo.
9. Las enzimas AckA, y en menor grado, PflA, juegan un papel relevante en la infección respiratoria por *H. influenzae*.
10. Un nuevo modelo metabólico a escala genómica, *i*NL638, ha sido generado mediante la integración de información genómica y fenotípica de *H. influenzae*. Este modelo presenta estándares de calidad elevados, que lo convierten en una herramienta computacional útil para el estudio de la fisiología de *H. influenzae* o el escrutinio *in silico* de dianas terapéuticas.

Conclusiones

11. El escrutinio computacional de genes metabólicos esenciales para el crecimiento y viabilidad de *H. influenzae* reveló la importancia de los genes bacterianos que codifican enzimas implicadas en el metabolismo de lípidos.
12. El modelado molecular de la interacción entre la molécula sintética ácido 1- (5- (2-fluoro-5-(hidroximetil) fenil) piridin-2-il) piperidin-4-acético y la enzima iniciadora de la síntesis de ácidos grasos β-cetoacil-ACP sintasa III FabH de *H. influenzae*, indica su unión en la triada catalítica Cys112-His243-Asn273 de FabH.
13. El inhibidor sintético de FabH reduce la viabilidad de *H. influenzae* de manera dosis-dependiente. El efecto observado es variable entre aislados clínicos, y no parece estar directa o exclusivamente relacionado con la variación alélica o niveles de expresión de su diana.
14. La incubación de *H. influenzae* con el inhibidor de FabH no genera resistencia o efectos sinérgicos con antibióticos convencionales, y no modula la interacción del patógeno con células de epitelio respiratorio en cultivo.
15. La administración intraperitoneal del inhibidor de FabH en un modelo de septicemia por *H. influenzae* en pez cebra adulto aumenta su supervivencia respecto a un grupo control de animales infectados no tratados con este inhibidor.

Referencias

Abdillahi, S. M., Tati, R., Nordin, S. L., Baumgarten, M., Hallgren, O., Bjermer, L., Erjefält, J., Westergren-Thorsson, G., Singh, B., Riesbeck, K. & Mörgelin, M. (2018). The pulmonary extracellular matrix is a bactericidal barrier against *Haemophilus influenzae* in chronic obstructive pulmonary disease (COPD): Implications for an *in vivo* innate host defense function of collagen VI. *Frontiers in Immunology*, 9, 1–14. https://doi.org/10.3389/fimmu.2018.01988

Agrawal, A. & Murphy, T. F. (2011). *Haemophilus influenzae* infections in the *H. influenzae* type b conjugate vaccine era. *Journal of Clinical Microbiology*, 49 (11), 3728–3732. https://doi.org/10.1128/JCM.05476-11

Ahearn, C. P., Gallo, M. C. & Murphy, T. F. (2017). Insights on persistent airway infection by non-typeable *Haemophilus influenzae* in chronic obstructive pulmonary disease. *Pathogens and Disease*, 75 (4), 1–18. https://doi.org/10.1093/femspd/ftx042

Albert, R. K., Connett, J., Bailey, W. C., Casaburi, R., Cooper, J. A. D. J., Criner, G. J., Curtis, J. L., Dransfield, M. T., Han, M. K., Lazarus, S. C., Make, B., Marchetti, N., Martinez, F. J., Madinger, N. E., McEvoy, C., Niewoehner, D. E., Porsasz, J., Price, C. S., Reilly, J., et al. (2011). Azithromycin for prevention of exacerbations of COPD. *The New England Journal of Medicine*, 365 (8), 689–698. https://doi.org/10.1056/NEJMoa1104623

Allen, S., Zaleski, A., Johnston, J. W., Gibson, B. W. & Apicella, M. A. (2005). Novel sialic acid transporter of *Haemophilus influenzae*. *Infection and Immun*ity, 73 (9), 5291–5300. https://doi.org/10.1128/IAI.73.9.5291-5300.2005

Andersson, M., Resman, F., Eitrem, R., Drobni, P., Riesbeck, K., Kahlmeter, G. & Sundqvist, M. (2015). Outbreak of a beta-lactam resistant non-typeable *Haemophilus influenzae* sequence type 14 associated with severe clinical outcomes. *BMC Infectious Diseases*, 15, 581. https://doi.org/10.1186/s12879-015-1319-8

Anfora, A. T., Halladin, D. K., Haugen, B. J. & Welch, R. A. (2008). Uropathogenic *Escherichia coli* CFT073 is adapted to acetatogenic growth but does not require acetate during murine urinary tract infection. *Infection and Immunity*, 76 (12), 5760–5767. https://doi.org/10.1128/IAI.00618-08

Anzueto, A. (2010). Impact of exacerbations on COPD. *European Respiratory Review : An Official Journal of the European Respiratory Society*, 19 (116), 113–118. https://doi.org/10.1183/09059180.00002610

Armbruster, C. E., Hong, W., Pang, B., Dew, K. E., Juneau, R. A., Byrd, M. S., Love, C. F., Kock, N. D. & Swords, W. E. (2009). LuxS promotes biofilm maturation and persistence of nontypeable *Haemophilus influenzae in vivo* via modulation of lipooligosaccharides on the bacterial surface. *Infection and Immunity*, 77 (9), 4081–4091. https://doi.org/10.1128/IAI.00320-09

Åstrand, A., Wingren, C., Benjamin, A., Tregoning, J. S., Garnett, J. P., Groves, H., Gill, S., Orogo-Wenn, M., Lundqvist, A. J., Walters, D., Smith, D. M., Taylor, J. D., Baker, E. H. & Baines, D. L. (2017). Dapagliflozin-lowered blood glucose reduces respiratory *Pseudomonas aeruginosa* infection in diabetic mice. *British Journal of Pharmacology*, 174 (9), 836–847. https://doi.org/10.1111/bph.13741

Atack, J. M., Day, C. J., Poole, J., Brockman, K. L., Bakaletz, L. O., Barenkamp, S. J. & Jennings, M. P. (2018a). The HMW2 adhesin of non-typeable *Haemophilus influenzae* is a human-adapted lectin that mediates high-affinity binding to 2-6 linked N-acetylneuraminic acid glycans. *Biochemical and Biophysical Research Communications*, 503 (2), 1103–1107. https://doi.org/10.1016/j.bbrc.2018.06.126

Atack, J. M., Day, C. J., Poole, J., Brockman, K. L., Timms, J. R. L., Winter, L. E., Haselhorst, T., Bakaletz, L. O., Barenkamp, S. J. & Jennings, M. P. (2020). The nontypeable *Haemophilus*

influenzae major adhesin *hia* is a dual-function lectin that binds to human-specific respiratory tract sialic acid glycan receptors. *MBio*, 11 (6), 1–15. https://doi.org/10.1128/mBio.02714-20

Atack, J. M., Murphy, T. F., Pettigrew, M. M., Seib, K. L. & Jennings, M. P. (2019). Non-typeable *Haemophilus influenzae* isolates from patients with chronic obstructive pulmonary disease contain new phase-variable *modA* methyltransferase alleles controlling phasevarions. *Scientific Reports*, 9 (1), 1–10. https://doi.org/10.1038/s41598-019-52429-6

Atack, J. M., Srikhanta, Y. N., Fox, K. L., Jurcisek, J. A., Brockman, K. L., Clark, T. A., Boitano, M., Power, P. M., Jen, F. E.-C., McEwan, A. G., Grimmond, S. M., Smith, A. L., Barenkamp, S. J., Korlach, J., Bakaletz, L. O. & Jennings, M. P. (2015a). A biphasic epigenetic switch controls immunoevasion, virulence and niche adaptation in non-typeable *Haemophilus influenzae*. *Nature Communications*, 6, 7828. https://doi.org/10.1038/ncomms8828

Atack, J. M., Tan, A., Bakaletz, L. O., Jennings, M. P. & Seib, K. L. (2018b). Phasevarions of bacterial pathogens: methylomics sheds new light on old enemies. *Trends in Microbiology*, 26 (8), 715–726. https://doi.org/10.1016/j.tim.2018.01.008

Aziz, A., Sarovich, D. S., Nosworthy, E., Beissbarth, J., Chang, A. B., Smith-Vaughan, H., Price, E. P. & Harris, T. M. (2019). Molecular signatures of nontypeable *Haemophilus influenzae* lung adaptation in pediatric chronic lung disease. *Frontiers in Microbiology*, 10, 1622. https://doi.org/10.3389/fmicb.2019.01622

Baddal, B., Muzzi, A., Censini, S., Calogero, R. A., Torricelli, G., Guidotti, S., Taddei, A. R., Covacci, A., Pizza, M., Rappuoli, R., Soriani, M. & Pezzicoli, A. (2015). Dual RNA-seq of nontypeable *Haemophilus influenzae* and host cell transcriptomes reveals novel insights into host-pathogen cross talk. *MBio*, 6 (6), 1–13. https://doi.org/10.1128/mBio.01765-15

Bakaletz, L. O., Baker, B. D., Jurcisek, J. A., Harrison, A., Novotny, L. A., Bookwalter, J. E., Mungur, R. & Munson, R. S. (2005). Demonstration of type IV pilus expression and a twitching phenotype by *Haemophilus influenzae*. *Infection and Immunity*, 73 (3), 1635–1643. https://doi.org/10.1128/IAI.73.3.1635-1643.2005

Bakaletz, L. O. & Novotny, L. A. (2018). Nontypeable *Haemophilus influenzae* (NTHi). *Trends in Microbiology*, 26 (8), 727–728. https://doi.org/10.1016/j.tim.2018.05.001

Baker, E. H., Janaway, C. H., Philips, B. J., Brennan, A. L., Baines, D. L., Wood, D. M. & Jones, P. W. (2006). Hyperglycaemia is associated with poor outcomes in patients admitted to hospital with acute exacerbations of chronic obstructive pulmonary disease. *Thorax*, 61 (4), 284–289. https://doi.org/10.1136/thx.2005.051029

Baker, E. H. & Baines, D. L. (2018). Airway Glucose Homeostasis: A New Target in the Prevention and Treatment of Pulmonary Infection. *Chest*, 153 (2), 507–514. https://doi.org/10.1016/j.chest.2017.05.031

Baker, E. H., Clark, N., Brennan, A. L., Fisher, D. A., Gyi, K. M., Hodson, M. E., Philips, B. J., Baines, D. L. & Wood, D. M. (2007). Hyperglycemia and cystic fibrosis alter respiratory fluid glucose concentrations estimated by breath condensate analysis. *Journal of Applied Physiology*, 102 (5), 1969–1975. https://doi.org/10.1152/japplphysiol.01425.2006

Bandi, V., Apicella, M. A., Mason, E., Murphy, T. F., Siddiqi, A., Atmar, R. L. & Greenberg, S. B. (2001). Nontypeable *Haemophilus influenzae* in the lower respiratory tract of patients with chronic bronchitis. *American Journal of Respiratory and Critical Care Medicine*, 164 (11), 2114–2119. https://doi.org/10.1164/ajrccm.164.11.2104093

Bansil, R. & Turner, B.S. (2018). The biology of mucus: composition, synthesis and organization. *Advanced Drug Delivery Reviews*, 124, 3-15. https://doi: 10.1016/j.addr.2017.09.023

Baquero, F. & Martínez, J. L. (2017). Interventions on metabolism: making antibiotic-susceptible

bacteria. *MBio*, 8 (6). https://doi.org/10.1128/mBio.01950-17

Bartell, J. A., Blazier, A. S., Yen, P., Thøgersen, J. C., Jelsbak, L., Goldberg, J. B. & Papin, J. A. (2017). Reconstruction of the metabolic network of *Pseudomonas aeruginosa* to interrogate virulence factor synthesis. *Nature Communications*, 8. https://doi.org/10.1038/ncomms14631

Barthel, D., Singh, B., Riesbeck, K. & Zipfel, P. F. (2012). *Haemophilus influenzae* uses the surface protein E to acquire human plasminogen and to evade innate immunity . *The Journal of Immunology*, 188 (1), 379–385. https://doi.org/10.4049/jimmunol.1101927

Bernatchez, J. A. & McCall, L. I. (2020). Insights gained into respiratory infection pathogenesis using lung tissue metabolomics. *PLoS Pathogens*, 16 (7), e1008662. https://doi.org/10.1371/journal.ppat.1008662

Bernhard, W. (2016). Lung surfactant: Function and composition in the context of development and respiratory physiology. *Annals of Anatomy*, 208, 146–150. https://doi.org/10.1016/j.aanat.2016.08.003

Bhattacharya, J. & Westphalen, K. (2016). Macrophage-epithelial interactions in pulmonary alveoli. *Seminars in Immunopathology*, 38 (4), 461–469. https://doi.org/10.1007/s00281-016-0569-x

Black, H. F., Mastromatteo, S., Sinha, S., Ehrlich, R. L., Nislow, C., Mell, J. C. & Redfield, R. J. (2020). A competence-regulated toxin-antitoxin system in *Haemophilus influenzae*. *PLoS ONE*, 15 (1), 1–23. https://doi.org/10.1371/journal.pone.0217255

Bonser, L. & Erle, D. (2017). Airway mucus and asthma: the role of MUC5AC and MUC5B. *Journal of Clinical Medicine*, 6 (12), 112. https://doi.org/10.3390/jcm6120112

Bosi, E., Monk, J. M., Aziz, R. K., Fondi, M., Nizet, V. & Palsson, B. Ø. (2016). Comparative genome-scale modelling of *Staphylococcus aureus* strains identifies strain-specific metabolic capabilities linked to pathogenicity. *Proceedings of the National Academy of Sciences of the United States of America*, 113 (26), E3801-9. https://doi.org/10.1073/pnas.1523199113

Bouchet, V., Hood, D. W., Li, J., Brisson, J. R., Randle, G. A., Martin, A., Li, Z., Goldstein, R., Schweda, E. K. H., Pelton, S. I., Richards, J. C. & Moxon, E. R. (2003). Host-derived sialic acid is incorporated into *Haemophilus influenzae* lipopolysaccharide and is a major virulence factor in experimental otitis media. *Proceedings of the National Academy of Sciences of the United States of America*, 100 (15), 8898–8903. https://doi.org/10.1073/pnas.1432026100

Braissant, O., Astasov-Frauenhoffer, M., Waltimo, T. & Bonkat, G. (2020). A review of methods to determine viability, vitality, and metabolic rates in microbiology. *Frontiers in Microbiology*, 11 (2), 1–25. https://doi.org/10.3389/fmicb.2020.547458

Brockman, K. L., Azzari, P. N., Branstool, M. T., Atack, J. M., Schulz, B. L., Jen, F. E. C., Jennings, M. P. & Bakaletz, L. O. (2018). Epigenetic regulation alters biofilm architecture and composition in multiple clinical isolates of nontypeable *Haemophilus influenzae*. *MBio*, 9 (5), 1–15. https://doi.org/10.1128/mBio.01682-18

Brockman, K. L., Branstool, M. T., Atack, J. M., Robledo-Avila, F., Partida-Sanchez, S., Jennings, M. P. & Bakaletz, L. O. (2017). The ModA2 phasevarion of nontypeable *Haemophilus influenzae* regulates resistance to oxidative stress and killing by human neutrophils. *Scientific Reports*, 7 (1), 3161. https://doi.org/10.1038/s41598-017-03552-9

Brockman, K. L., Jurcisek, J. A., Atack, J. M., Srikhanta, Y. N., Jennings, M. P. & Bakaletz, L. O. (2016). ModA2 phasevarion switching in nontypeable *Haemophilus influenzae* increases the severity of experimental otitis media. *The Journal of Infectious Diseases*, 214 (5), 817–824. https://doi.org/10.1093/infdis/jiw243

Broussard, T. C., Pakhomova, S., Neau, D. B., Bonnot, R. & Waldrop, G. L. (2015). Structural

analysis of substrate, reaction intermediate, and product binding in *Haemophilus influenzae* biotin carboxylase. *Biochemistry*, 54 (24), 3860–3870. https://doi.org/10.1021/acs.biochem.5b00340

Brown, K. L. & Hancock, R. E. W. (2006). Cationic host defense (antimicrobial) peptides. *Current Opinion in Immunology*, 18 (1), 24–30. https://doi.org/10.1016/j.coi.2005.11.004

Burby, P. E., Nye, T. M., Schroeder, J. W. & Simmons, L. A. (2017). Implementation and data analysis of Tn-seq, whole-genome resequencing, and single-molecule real-time sequencing for bacterial genetics. *Journal of Bacteriology*, 199 (1). https://doi.org/10.1128/JB.00560-16

Bush, N. G., Diez-Santos, I., Abbott, L. R. & Maxwell, A. (2020). Quinolones: mechanism, lethality and their contributions to antibiotic resistance. *Molecules*, 25 (23). https://doi.org/10.3390/molecules25235662

Cain, A. K., Barquist, L., Goodman, A. L., Paulsen, I. T., Parkhill, J. & van Opijnen, T. (2020). A decade of advances in transposon-insertion sequencing. *Nature Reviews Genetics*, 21 (9), 526–540. https://doi.org/10.1038/s41576-020-0244-x

Cameron, A. D. S. & Redfield, R. J. (2006). Non-canonical CRP sites control competence regulons in *Escherichia coli* and many other γ-proteobacteria. *Nucleic Acids Research*, 34 (20), 6001–6014. https://doi.org/10.1093/nar/gkl734

Cameron, A. D. S., Volar, M., Bannister, L. A. & Redfield, R. J. (2008). RNA secondary structure regulates the translation of *sxy* and competence development in *Haemophilus influenzae*. *Nucleic Acids Research*, 36 (1), 10–20. https://doi.org/10.1093/nar/gkm915

Campbell, J. W. & Cronan, J. E. J. (2001). Bacterial fatty acid biosynthesis: targets for antibacterial drug discovery. *Annual Review of Microbiology*, 55, 305–332. https://doi.org/10.1146/annurev.micro.55.1.305

Campuzano, A. & Wormley, F. L. (2018). Innate immunity against *Cryptococcus*, from recognition to elimination. *Journal of Fungi*, 4 (1). https://doi.org/10.3390/jof4010033

Cardines, R., Giufrè, M., Pompilio, A., Fiscarelli, E., Ricciotti, G., Di Bonaventura, G. & Cerquetti, M. (2012). *Haemophilus influenzae* in children with cystic fibrosis: antimicrobial susceptibility, molecular epidemiology, distribution of adhesins and biofilm formation. *International Journal of Medical Microbiology*, 302 (1), 45–52. https://doi.org/10.1016/j.ijmm.2011.08.003

Carruthers, M. D., Tracy, E. N., Dickson, A. C., Ganser, K. B., Munson, R. S. & Bakaletz, L. O. (2012). Biological roles of nontypeable *Haemophilus influenzae* type IV pilus proteins encoded by the *pil* and *com* operons. *Journal of Bacteriology*, 194 (8), 1927–1933. https://doi.org/10.1128/JB.06540-11

Casals, C., Campanero-Rhodes, M. A., García-Fojeda, B. & Solís, D. (2018). The role of collectins and galectins in lung innate immune defense. *Frontiers in Immunology*, 9, 1–10. https://doi.org/10.3389/fimmu.2018.01998

Case DA. (2012). *AMBER 12, University of California, San Francisco.*

Catlin, B. W., Bendler, J. W. & Goodgal, S. H. (1972). The type b capsulation locus of *Haemophilus influenzae*: map location and size. *Journal of General Microbiology*, 70 (3), 411–422. https://doi.org/10.1099/00221287-70-3-411

Celli, B. R. & Wedzicha, J. A. (2019). Update on Clinical Aspects of Chronic Obstructive Pulmonary Disease. *The New England Journal of Medicine*, 381 (13), 1257–1266. https://doi.org/10.1056/NEJMra1900500

Cesur, M. F., Siraj, B., Uddin, R., Durmuş, S. & Çakır, T. (2020). Network-based metabolism-

centered screening of potential drug targets in *Klebsiella pneumoniae* at genome scale. *Frontiers in Cellular and Infection Microbiology*, 9, 1–18. https://doi.org/10.3389/fcimb.2019.00447

Chalmers, J. D., McHugh, B. J., Doherty, C., Smith, M. P., Govan, J. R., Kilpatrick, D. C. & Hill, A. T. (2013). Mannose-binding lectin deficiency and disease severity in non-cystic fibrosis bronchiectasis: A prospective study. *The Lancet Respiratory Medicine*, 1 (3), 224–232. https://doi.org/10.1016/S2213-2600(13)70001-8

Chan, Y. R., Liu, J. S., Pociask, D. A., Zheng, M., Mietzner, T. A., Berger, T., Mak, T. W., Clifton, M. C., Strong, R. K., Ray, P. & Kolls, J. K. (2009). Lipocalin 2 is required for pulmonary host defense against *Klebsiella* infection . *The Journal of Immunology*, 182 (8), 4947–4956. https://doi.org/10.4049/jimmunol.0803282

Chang, Y. Y., Wang, A. Y. & Cronan, J. E. J. (1994). Expression of *Escherichia coli* pyruvate oxidase (PoxB) depends on the sigma factor encoded by the *rpoS*(*katF*) gene. *Molecular Microbiology*, 11 (6), 1019–1028. https://doi.org/10.1111/j.1365-2958.1994.tb00380.x

Chavali, A. K., D'Auria, K. M., Hewlett, E. L., Pearson, R. D. & Papin, J. A. (2012). A metabolic network approach for the identification and prioritization of antimicrobial drug targets. *Trends in Microbiology*, 20 (3), 113–123. https://doi.org/10.1016/j.tim.2011.12.004

Chen, H., Li, Z., Dong, L., Wu, Y., Shen, H. & Chen, Z. (2019). Lipid metabolism in chronic obstructive pulmonary disease. *International Journal of COPD*, 14, 1009–1018. https://doi.org/10.2147/COPD.S196210

Cherkaoui, A., Diene, S. M., Fischer, A., Leo, S., François, P. & Schrenzel, J. (2017). Transcriptional modulation of penicillin-binding protein 1b, outer membrane protein P2 and efflux pump (AcrAB-TolC) during heat stress is correlated to enhanced bactericidal action of imipenem on non-typeable *Haemophilus influenzae*. *Frontiers in Microbiology*, 8, 2676. https://doi.org/10.3389/fmicb.2017.02676

Chilvers, M. A. & O'Callaghan, C. (2000). Local mucociliary defence mechanisms. *Paediatric Respiratory Reviews*, 1 (1), 27–34. https://doi.org/10.1053/prrv.2000.0009

Chuang, Y. P., Peng, Z. R., Tseng, S. F., Lin, Y. C., Sytwu, H. K. & Hsieh, Y. C. (2015). Impact of the *glpQ2* gene on virulence in a *Streptococcus pneumoniae* serotype 19a sequence type 320 strain. *Infection and Immunity*, 83 (2), 682–692. https://doi.org/10.1128/IAI.02357-14

Chung, H. S. & Raetz, C. R. H. (2010). Interchangeable domains in the Kdo transferases of *Escherichia coli* and *Haemophilus influenzae*. *Biochemistry*, 49 (19), 4126–4137. https://doi.org/10.1021/bi100343e

Clark, H. W., Mackay, R. M., Deadman, M. E., Hood, D. W., Madsen, J., Moxon, E. R., Townsend, J. P., Reid, K. B. M., Ahmed, A., Shaw, A. J., Greenhough, T. J. & Shrive, A. K. (2016). Crystal structure of a complex of surfactant protein D (SP-D) and *Haemophilus influenzae* lipopolysaccharide reveals shielding of core structures in SP-D-resistant strains. *Infection and Immunity*, 84 (5), 1585–1592. https://doi.org/10.1128/IAI.01239-15

Clementi, C. F., Håkansson, A. P. & Murphy, T. F. (2014). Internalization and trafficking of nontypeable *Haemophilus influenzae* in human respiratory epithelial cells and roles of IgA1 proteases for optimal invasion and persistence. *Infection and Immunity*, 82 (1), 433–444. https://doi.org/10.1128/IAI.00864-13

Clementi, C. F. & Murphy, T. F. (2011). Non-typeable *Haemophilus influenzae* invasion and persistence in the human respiratory tract. *Frontiers in Cellular and Infection Microbiology*, 1, 1. https://doi.org/10.3389/fcimb.2011.00001

Connor, T. R., Corander, J. & Hanage, W. P. (2012). Population subdivision and the detection of

recombination in non-typable *Haemophilus influenzae*. *Microbiology*, 158 (12), 2958–2964. https://doi.org/10.1099/mic.0.063073-0

Costerton, A. J. W., Stewart, P. S. & Greenberg, E. P. (1999). Bacterial bioflims : a common cause of persistent infections. *Science*, 284 (5418), 1318–1322.

Crofts, T. S., Sontha, P., King, A. O., Wang, B., Biddy, B. A., Zanolli, N., Gaumnitz, J. & Dantas, G. (2019). Discovery and characterization of a nitroreductase capable of conferring bacterial resistance to chloramphenicol. *Cell Chemical Biology*, 26 (4), 559-570.e6. https://doi.org/10.1016/j.chembiol.2019.01.007

Cukier, C. D., Hope, A. G., Elamin, A. A., Moynie, L., Schnell, R., Schach, S., Kneuper, H., Singh, M., Naismith, J. H., Lindqvist, Y., Gray, D. W. & Schneider, G. (2013). Discovery of an allosteric inhibitor binding site in 3-oxo-acyl-ACP reductase from *Pseudomonas aeruginosa*. *ACS Chemical Biology*, 8 (11), 2518–2527. https://doi.org/10.1021/cb4005063

Damron, F. H., Oglesby-Sherrouse, A. G., Wilks, A. & Barbier, M. (2016). Dual-seq transcriptomics reveals the battle for iron during *Pseudomonas aeruginosa* acute murine pneumonia. *Scientific Reports*, 6, 39172. https://doi.org/10.1038/srep39172

Das, J., Mokrzan, E., Lakhani, V., Rosas, L., Jurcisek, J. A., Ray, W. C. & Bakaletz, L. O. (2017). Extracellular DNA and type IV pilus expression regulate the structure and kinetics of biofilm formation by nontypeable *Haemophilus influenzae*. *MBio*, 8 (6), 1–19. https://doi.org/10.1128/mBio.01466-17

Das, M., Sakha Ghosh, P. & Manna, K. (2016). A review on platensimycin: a selective FabF inhibitor. *International Journal of Medicinal Chemistry*, 2016. https://doi.org/10.1155/2016/9706753

Das, U. N. (2018). Arachidonic acid and other unsaturated fatty acids and some of their metabolites function as endogenous antimicrobial molecules: a review. *Journal of Advanced Research*, 11, 57–66. https://doi.org/10.1016/j.jare.2018.01.001

Davis, M. S., Solbiati, J. & Cronan, J. E. (2000). Overproduction of acetyl-CoA carboxylase activity increases the rate of fatty acid biosynthesis in *Escherichia coli*. *Journal of Biological Chemistry*, 275 (37), 28593–28598. https://doi.org/10.1074/jbc.M004756200

De Chiara, M., Hood, D., Muzzi, A., Pickard, D. J., Perkins, T., Pizza, M., Dougan, G., Rappuoli, R., Moxon, E. R., Soriani, M. & Donati, C. (2014). Genome sequencing of disease and carriage isolates of nontypeable *Haemophilus influenzae* identifies discrete population structure. *Proceedings of the National Academy of Sciences of the United States of America*, 111 (14), 5439–5444. https://doi.org/10.1073/pnas.1403353111

de Faria, C. F., Moreira, T., Lopes, P., Costa, H., Krewall, J. R., Barton, C. M., Santos, S., Goodwin, D., Machado, D., Viveiros, M., Machuqueiro, M. & Martins, F. (2021). Designing new antitubercular isoniazid derivatives with improved reactivity and membrane trafficking abilities. *Biomedicine and Pharmacotherapy*, 144. https://doi.org/10.1016/j.biopha.2021.112362

de Groot, R., Sluijter, M., De Bruyn, A. D., Campos, J., Goessens, W. H. F., Smith, A. L. & Hermans, P. W. M. (1996). Genetic characterization of trimethoprim resistance in *Haemophilus influenzae*. *Antimicrobial Agents and Chemotherapy*, 40 (9), 2131–2136. https://doi.org/10.1128/aac.40.9.2131

de Saizieu, A., Certa, U., Warrington, J., Gray, C., Keck, W. & Mous, J. (1998). Bacterial transcript imaging by hybridization of total RNA to oligonucleotide arrays. *Nature Biotechnology*, 16 (1), 45–48. https://doi.org/10.1038/nbt0198-45

De Souza-Hart, J. A., Blackstock, W., Di Modugno, V., Holland, I. B. & Kok, M. (2003). Two-

component systems in *Haemophilus influenzae*: a regulatory role for ArcA in serum resistance. *Infection and Immunity*, 71 (1), 163–172. https://doi.org/10.1128/IAI.71.1.163-172.2003

Dean, C. R., Narayan, S., Daigle, D. M., Dzink-Fox, J. L., Puyang, X., Bracken, K. R., Dean, K. E., Weidmann, B., Yuan, Z., Jain, R. & Ryder, N. S. (2005). Role of the AcrAB-TolC efflux pump in determining susceptibility of *Haemophilus influenzae* to the novel peptide deformylase inhibitor LBM415. *Antimicrobial Agents and Chemotherapy*, 49 (8), 3129–3135. https://doi.org/10.1128/AAC.49.8.3129-3135.2005

Deich, R. A. & Smith, H. O. (1980). Mechanism of homospecific DNA uptake in *Haemophilus influenzae* transformation. *MGG Molecular & General Genetics*, 177 (3), 369–374. https://doi.org/10.1007/BF00271475

Deng, Y., Su, M., Kang, D., Liu, X., Wen, Z., Li, Y., Qiu, L., Shen, B., Duan, Y. & Huang, Y. (2018). Semisynthesis of platensimycin derivatives with antibiotic activities in mice via Suzuki-Miyaura cross-coupling reactions. *Journal of Medicinal Chemistry*, 61 (24), 11341–11348. https://doi.org/10.1021/acs.jmedchem.8b01580

Denicola-Seoane, A. & Anderson, B. M. (1990). Purification and characterization of *Haemophilus influenzae* D-lactate dehydrogenase. *The Journal of Biological Chemistry*, 265 (7), 3691–3696.

Desai, H., Eschberger, K., Wrona, C., Grove, L., Agrawal, A., Grant, B., Yin, J., Parameswaran, G. I., Murphy, T. & Sethi, S. (2014). Bacterial colonization increases daily symptoms in patients with chronic obstructive pulmonary disease. *Annals of the American Thoracic Society*, 11 (3), 303–309. https://doi.org/10.1513/AnnalsATS.201310-350OC

Devaraj, A., Buzzo, J., Rocco, C. J., Bakaletz, L. O. & Goodman, S. D. (2018). The DNABII family of proteins is comprised of the only nucleoid associated proteins required for nontypeable *Haemophilus influenzae* biofilm structure. *MicrobiologyOpen*, 7 (3), 1–13. https://doi.org/10.1002/mbo3.563

Dhouib, R., Othman, D. S. M. P., Lin, V., Lai, X. J., Wijesinghe, H. G. S., Essilfie, A.-T., Davis, A., Nasreen, M., Bernhardt, P. V, Hansbro, P. M., McEwan, A. G. & Kappler, U. (2016). A novel, molybdenum-containing methionine sulfoxide reductase supports survival of *Haemophilus influenzae* in an *in vivo* model of infection. *Frontiers in Microbiology*, 7, 1743. https://doi.org/10.3389/fmicb.2016.01743

Dickson, R. P., Erb-Downward, J. R., Freeman, C. M., McCloskey, L., Beck, J. M., Huffnagle, G. B. & Curtis, J. L. (2015a). Spatial variation in the healthy human lung microbiome and the adapted island model of lung biogeography. *Annals of the American Thoracic Society*, 12 (6), 821–830. https://doi.org/10.1513/AnnalsATS.201501-029OC

Dickson, R. P., Erb-Downward, J. R., Freeman, C. M., McCloskey, L., Falkowski, N. R., Huffnagle, G. B. & Curtis, J. L. (2017). Bacterial topography of the healthy human lower respiratory tract. *MBio*, 8(1), e02287-16. https://doi.org/10.1128/mBio.02287-16

Dickson, R. P., Erb-Downward, J. R. & Huffnagle, G. B. (2014b). Towards an ecology of the lung: new conceptual models of pulmonary microbiology and pneumonia pathogenesis. *The Lancet. Respiratory Medicine*, 2 (3), 238–246. https://doi.org/10.1016/S2213-2600(14)70028-1

Dickson, R. P., Erb-Downward, J. R. & Huffnagle, G. B. (2015b). Homeostasis and its disruption in the lung microbiome. *American Journal of Physiology. Lung Cellular and Molecular Physiology*, 309 (10), L1047-55. https://doi.org/10.1152/ajplung.00279.2015

Dickson, R. P., Erb-Downward, J. R., Martinez, F. J. & Huffnagle, G. B. (2016). The microbiome and the respiratory tract. *Annual Review of Physiology*, 78, 481–504. https://doi.org/10.1146/annurev-physiol-021115-105238

Dickson, R. P. & Huffnagle, G. B. (2015). The lung microbiome: new principles for respiratory

bacteriology in health and disease. *PLoS Pathogens*, 11 (7), 1–5. https://doi.org/10.1371/journal.ppat.1004923

Dickson, R. P., Martinez, F. J. & Huffnagle, G. B. (2014a). The role of the microbiome in exacerbations of chronic lung diseases. *Lancet*, 384 (9944), 691–702. https://doi.org/10.1016/S0140-6736(14)61136-3

Dinos, G. P. (2017). The macrolide antibiotic renaissance. *British Journal of Pharmacology*, 174 (18), 2967–2983. https://doi.org/10.1111/bph.13936

Duell, B. L., Su, Y.-C. & Riesbeck, K. (2016). Host-pathogen interactions of nontypeable *Haemophilus influenzae*: from commensal to pathogen. *FEBS Letters*, 590 (21), 3840–3853. https://doi.org/10.1002/1873-3468.12351

Duffield, M., Cooper, I., McAlister, E., Bayliss, M., Ford, D. & Oyston, P. (2010). Predicting conserved essential genes in bacteria: *in silico* identification of putative drug targets. *Molecular BioSystems*, 6 (12), 2482–2489. https://doi.org/10.1039/c0mb00001a

Dunphy, L. J. & Papin, J. A. (2018). Biomedical applications of genome-scale metabolic network reconstructions of human pathogens. *Current Opinion in Biotechnology*, 51, 70–79. https://doi.org/10.1016/j.copbio.2017.11.014

Edwards, J. S. & Palsson, B. O. (1999). Systems properties of the *Haemophilus influenzae* Rd metabolic genotype. *Journal of Biological Chemistry*, 274 (25), 17410–17416. https://doi.org/10.1074/jbc.274.25.17410

Eidi, S., Kamali, S. A., Hajari, Z., Fata, A., Farid Hosseini, R., Naseri, A. & Bakhshaee, M. (2016). Nasal and indoors fungal contamination in healthy subjects. *Health Scope*, 5 (1). https://doi.org/10.17795/jhealthscope-30033

Elgamal, Z., Singh, P. & Geraghty, P. (2021). The upper airway microbiota, environmental exposures, inflammation, and disease. *Medicina*, 57 (8), 823. https://doi.org/10.3390/medicina57080823

Enne, V. I., King, A., Livermore, D. M. & Hall, L. M. C. (2002). Sulfonamide resistance in *Haemophilus influenzae* mediated by acquisition of *sul2* or a short insertion in chromosomal *folP*. *Antimicrobial Agents and Chemotherapy*, 46 (6), 1934–1939. https://doi.org/10.1128/AAC.46.6.1934-1939.2002

Euba, B., López-López, N., Rodríguez-Arce, I., Fernández-Calvet, A., Barberán, M., Caturla, N., Martí, S., Díez-Martínez, R. & Garmendia, J. (2017). Resveratrol therapeutics combines both antimicrobial and immunomodulatory properties against respiratory infection by nontypeable *Haemophilus influenzae*. *Scientific Reports*, 7 (1). https://doi.org/10.1038/s41598-017-13034-7

Euba, B., Moleres, J., Segura, V., Viadas, C., Morey, P., Moranta, D., Leiva, J., De-Torres, J. P., Bengoechea, J. A. & Garmendia, J. (2015c). Genome expression profiling-based identification and administration efficacy of host-directed antimicrobial drugs against respiratory infection by nontypeable *Haemophilus influenzae*. *Antimicrobial Agents and Chemotherapy*, 59 (12), 7581–7592. https://doi.org/10.1128/AAC.01278-15

Euba, B., Moleres, J., Viadas, C., Barberán, M., Caballero, L., Grilló, M. J., Bengoechea, J. A., De-Torres, J. P., Liñares, J., Leiva, J. & Garmendia, J. (2015b). Relationship between azithromycin susceptibility and administration efficacy for nontypeable *Haemophilus influenzae* respiratory infection. *Antimicrobial Agents and Chemotherapy*, 59 (5), 2700–2712. https://doi.org/10.1128/AAC.04447-14

Euba, B., Moleres, J., Viadas, C., De los Mozos, I. R., Valle, J., Bengoechea, J. A. & Garmendia, J. (2015a). Relative contribution of P5 and Hap surface proteins to nontypable *Haemophilus*

influenzae interplay with the host upper and lower airways. *PLoS ONE*, 10 (4), 1–18. https://doi.org/10.1371/journal.pone.0123154

Fang, X., Lloyd, C. J. & Palsson, B. O. (2020). Reconstructing organisms *in silico*: genome-scale models and their emerging applications. *Nature Reviews. Microbiology*, 18 (12), 731–743. https://doi.org/10.1038/s41579-020-00440-4

Feng, Z., Chakraborty, D., Dewell, S. B., Reddy, B. V. B. & Brady, S. F. (2012). Environmental DNA-encoded antibiotics fasamycins A and B inhibit FabF in type II fatty acid biosynthesis. *Journal of the American Chemical Society*, 134 (6), 2981–2987. https://doi.org/10.1021/ja207662w

Féréol, S., Fodil, R., Pelle, G., Louis, B. & Isabey, D. (2008). Cell mechanics of alveolar epithelial cells (AECs) and macrophages (AMs). *Respiratory Physiology and Neurobiology*, 163 (1–3), 3–16. https://doi.org/10.1016/j.resp.2008.04.018

Fernández-Calvet, A., Euba, B., Caballero, L., Díez-Martínez, R., Menéndez, M., Ortiz de Solórzano, C., Leiva, J., Micol, V., Barrajón-Catalán, E. & Garmendia, J. (2019). Preclinical evaluation of the antimicrobial-immunomodulatory dual action of xenohormetic molecules against *Haemophilus influenzae* respiratory infection. *Biomolecules*, 9 (12), 891. https://www.mdpi.com/2218-273X/9/12/891

Fernández-Calvet, A., Euba, B., Gil-Campillo, C., Catalan-Moreno, A., Moleres, J., Martí, S., Merlos, A., Langereis, J. D., García-del Portillo, F., Bakaletz, L. O., Ehrlich, G. D., Porsch, E. A., Menéndez, M., Mell, J. C., Toledo-Arana, A. & Garmendia, J. (2021). Phase variation in HMW1A controls a phenotypic switch in *Haemophilus influenzae* associated with pathoadaptation during persistent infection. *MBio*, 12 (3), 1–20. https://doi.org/10.1128/mbio.00789-21

Fernández-Calvet, A., Rodríguez-Arce, I., Almagro, G., Moleres, J., Euba, B., Caballero, L., Martí, S., Ramos-Vivas, J., Bartholomew, T. L., Morales, X., Ortíz-De-Solórzano, C., Yuste, J. E., Bengoechea, J. A., Conde-Álvarez, R. & Garmendia, J. (2018). Modulation of *Haemophilus influenzae* interaction with hydrophobic molecules by the VacJ/MlaA lipoprotein impacts strongly on its interplay with the airways. *Scientific Reports*, 8 (1), 1–17. https://doi.org/10.1038/s41598-018-25232-y

Fernando, S. A., Pang, S., McKew, G. L., Phan, T., Merlino, J., Coombs, G. W. & Gottlieb, T. (2020). Evaluation of the *Haemophilus influenzae* EUCAST and CLSI disc diffusion methods to recognize aminopenicillin and amoxicillin/clavulanate resistance. *The Journal of Antimicrobial Chemotherapy*, 75 (9), 2594–2598. https://doi.org/10.1093/jac/dkaa229

Fink, D. L., Green, B. A. & St. Geme, J. W. (2002). The *Haemophilus influenzae* Hap autotransporter binds to fibronectin, laminin, and collagen IV. *Infection and Immunity*, 70 (9), 4902–4907. https://doi.org/10.1128/IAI.70.9.4902-4907.2002

Finney, L., Berry, M., Singanayagam, A., Elkin, S. L., Johnston, S. L. & Mallia, P. (2014). Inhaled corticosteroids and pneumonia in chronic obstructive pulmonary disease. *The Lancet Respiratory Medicine*, 2 (11), 919–932. https://doi.org/10.1016/S2213-2600(14)70169-9

Finney, L. J., Ritchie, A., Pollard, E., Johnston, S. L. & Mallia, P. (2014). Lower airway colonization and inflammatory response in COPD: a focus on *Haemophilus influenzae*. *International Journal of Chronic Obstructive Pulmonary Disease*, 9, 1119–1132. https://doi.org/10.2147/COPD.S54477

Fleischmann, R. D., Adams, M. D., White, O., Clayton, R. A., Kirkness, E. F., Kerlavage, A. R., Bult, C. J., Tomb, J. F., Dougherty, B. A., Merrick, J. M., et al. (1995). Whole-genome random sequencing and assembly of *Haemophilus influenzae* Rd. *Science*, 269 (5223), 496 LP – 512. https://doi.org/10.1126/science.7542800

Referencias

Flesher, A. R. & Insel, R. A. (1978). Characterization of lipopolysaccharide of *Haemophilus influenzae*. *The Journal of Infectious Diseases*, 138 (6), 719–730. https://doi.org/10.1093/infdis/138.6.719

Flusberg, B. A., Webster, D. R., Lee, J. H., Travers, K. J., Olivares, E. C., Clark, T. A., Korlach, J. & Turner, S. W. (2010). Direct detection of DNA methylation during single-molecule, real-time sequencing. *Nature Methods*, 7 (6), 461–465. https://doi.org/10.1038/nmeth.1459

Flynn, J. M., Niccum, D., Dunitz, J. M. & Hunter, R. C. (2016). Evidence and role for bacterial mucin degradation in cystic fibrosis airway disease. *PLoS Pathogens*, 12 (8), 1–21. https://doi.org/10.1371/journal.ppat.1005846

Forsgren, J., Samuelson, A., Ahlin, A., Jonasson, J., Rynnel-Dagoo, B. & Lindberg, A. (1994). *Haemophilus influenzae* resides and multiplies intracellularly in human adenoid tissue as demonstrated by *in situ* hybridization and bacterial viability assay. *Infection and Immunity*, 62 (2), 673–679. https://doi.org/10.1128/iai.62.2.673-679.1994

Freiberg, C., Brunner, N. A., Schiffer, G., Lampe, T., Pohlmann, J., Brands, M., Raabe, M., Häbich, D. & Ziegelbauer, K. (2004). Identification and characterization of the first class of potent bacterial acetyl-CoA carboxylase inhibitors with antibacterial activity. *Journal of Biological Chemistry*, 279 (25), 26066–26073. https://doi.org/10.1074/jbc.M402989200

Frickmann, H., Christner, M., Donat, M., Berger, A., Essig, A., Podbielski, A., Hagen, R. M. & Poppert, S. (2013). Rapid discrimination of *Haemophilus influenzae*, *H. parainfluenzae*, and *H. haemolyticus* by fluorescence in situ hybridization (FISH) and two matrix-assisted laser-desorption-ionization time-of-flight mass spectrometry (MALDI-TOF-MS) platforms. *PloS One*, 8 (4), e63222. https://doi.org/10.1371/journal.pone.0063222

Gajiwala, K. S., Margosiak, S., Lu, J., Cortez, J., Su, Y., Nie, Z. & Appelt, K. (2009). Crystal structures of bacterial FabH suggest a molecular basis for the substrate specificity of the enzyme. *FEBS Letters*, 583 (17), 2939–2946. https://doi.org/10.1016/j.febslet.2009.08.001

Galeas-Pena, M., McLaughlin, N. & Pociask, D. (2019). The role of the innate immune system on pulmonary infections. *Biological Chemistry*, 400 (4), 443–456. https://doi.org/10.1515/hsz-2018-0304

Gallego-Delgado, J., Ty, M., Orengo, J. M., van de Hoef, D. & Rodriguez, A. (2014). A surprising role for uric acid: the inflammatory malaria response. *Current Rheumatology Reports*, 16 (2), 401. https://doi.org/10.1007/s11926-013-0401-8

Gallo, M. C., Kirkham, C., Eng, S., Bebawee, R. S., Kong, Y., Pettigrew, M. M., Tettelin, H. & Murphy, T. F. (2018). Changes in IgA protease expression are conferred by changes in genomes during persistent infection by nontypeable *Haemophilus influenzae* in chronic obstructive pulmonary disease. *Infection and Immunity*, 86 (8), 1–11. https://doi.org/10.1128/IAI.00313-18

Garbi, N. & Lambrecht, B. N. (2017). Location, function, and ontogeny of pulmonary macrophages during the steady state. *Pflugers Archiv European Journal of Physiology*, 469 (3–4), 561–572. https://doi.org/10.1007/s00424-017-1965-3

García-Fojeda, B., González-Carnicero, Z., De Lorenzo, A., Minutti, C. M., De Tapia, L., Euba, B., Iglesias-Ceacero, A., Castillo-Lluva, S., Garmendia, J. & Casals, C. (2019). Lung surfactant lipids provide immune protection against *Haemophilus influenzae* respiratory infection. *Frontiers in Immunology*, 10, 1–16. https://doi.org/10.3389/fimmu.2019.00458

Garmendia, J., Martí-Lliteras, P., Moleres, J., Puig, C. & Bengoechea, J. A. (2012). Genotypic and phenotypic diversity of the noncapsulated *Haemophilus influenzae*: adaptation and pathogenesis in the human airways. *International Microbiology*, *15*(4), 159–172.

https://doi.org/10.2436/20.1501.01.169

Garmendia, J., Viadas, C., Calatayud, L., Mell, J. C., Martí-Lliteras, P., Euba, B., Llobet, E., Gil, C., Bengoechea, J. A., Redfield, R. J. & Liñares, J. (2014). Characterization of nontypable *Haemophilus influenzae* isolates recovered from adult patients with underlying chronic lung disease reveals genotypic and phenotypic traits associated with persistent infection. *PLoS ONE*, 9 (5). https://doi.org/10.1371/journal.pone.0097020

Garnett, J. P., Baker, E. H. & Baines, D. L. (2012). Sweet talk: insights into the nature and importance of glucose transport in lung epithelium. *The European Respiratory Journal*, 40 (5), 1269–1276. https://doi.org/10.1183/09031936.00052612

Garnett, J. P., Baker, E. H., Naik, S., Lindsay, J. A., Knight, G. M., Gill, S., Tregoning, J. S. & Baines, D. L. (2013). Metformin reduces airway glucose permeability and hyperglycaemia-induced *Staphylococcus aureus* load independently of effects on blood glucose. *Thorax*, 68 (9), 835–845. https://doi.org/10.1136/thoraxjnl-2012-203178

Garnett, J. P., Nguyen, T. T., Moffatt, J. D., Pelham, E. R., Kalsi, K. K., Baker, E. H. & Baines, D. L. (2012). Proinflammatory mediators disrupt glucose homeostasis in airway surface liquid. *The Journal of Immunology*, 189 (1), 373–380. https://doi.org/10.4049/jimmunol.1200718

Gawronski, J. D., Wong, S. M. S., Giannoukos, G., Ward, D. V & Akerley, B. J. (2009). Tracking insertion mutants within libraries by deep sequencing and a genome-wide screen for *Haemophilus* genes required in the lung. *Proceedings of the National Academy of Sciences of the United States of America*, 106 (38), 16422–16427. https://doi.org/10.1073/pnas.0906627106

Ghorbani, P., Santhakumar, P., Hu, Q., Djiadeu, P., Wolever, T. M. S., Palaniyar, N. & Grasemann, H. (2015). Short-chain fatty acids affect cystic fibrosis airway inflammation and bacterial growth. *European Respiratory Journal*, 46 (4), 1033–1045. https://doi.org/10.1183/09031936.00143614

Gil-Gil, T., Corona, F., Martínez, J. L. & Bernardini, A. (2019). The inactivation of enzymes belonging to the central carbon metabolism, a novel mechanism of developing antibiotic resistance. *BioRxiv*, 5 (3), 1–19. https://doi.org/10.1101/823013

Gill, S. K., Hui, K., Farne, H., Garnett, J. P., Baines, D. L., Moore, L. S. P., Holmes, A. H., Filloux, A. & Tregoning, J. S. (2016). Increased airway glucose increases airway bacterial load in hyperglycaemia. *Scientific Reports*, 6, 27636. https://doi.org/10.1038/srep27636

Gilsdorf, J. R., Marrs, C. F. & Foxman, B. (2004). *Haemophilus influenzae*: genetic variability and natural selection to identify virulence factors. *Infection and Immunity*, 72 (5), 2457–2461. https://doi.org/10.1128/IAI.72.5.2457-2461.2004

Gómez-Gil, L., Schürch, D., Goormaghtigh, E. & Pérez-Gil, J. (2009). Pulmonary surfactant protein SP-C counteracts the deleterious effects of cholesterol on the activity of surfactant films under physiologically relevant compression-expansion dynamics. *Biophysical Journal*, 97 (10), 2736–2745. https://doi.org/10.1016/j.bpj.2009.08.045

Gonçalves-De-Albuquerque, C. F., Silva, A. R., Burth, P., Castro-Faria, M. V. & Castro-Faria-Neto, H. C. (2015). Acute respiratory distress syndrome: role of oleic acid-triggered lung injury and inflammation. *Mediators of Inflammation*, 2015. https://doi.org/10.1155/2015/260465

Griese, M. (1999). Pulmonary surfactant in health and human lung diseases: State of the art. *European Respiratory Journal*, 13 (6), 1455–1476. https://doi.org/10.1034/j.1399-3003.1999.13f36.x

Grilló, M.-J., Blasco, J. M., Gorvel, J. P., Moriyón, I. & Moreno, E. (2012). What have we learned from brucellosis in the mouse model? *Veterinary Research*, 43 (1), 29.

https://doi.org/10.1186/1297-9716-43-29

Gudmundsson, S. & Nogales, J. (2021). Recent advances in model-assisted metabolic engineering. *Current Opinion in Systems Biology*, 28, 100392. https://doi.org/https://doi.org/10.1016/j.coisb.2021.100392

Gueriri, I., Bay, S., Dubrac, S., Cyncynatus, C. & Msadek, T. (2008). The Pta-AckA pathway controlling acetyl phosphate levels and the phosphorylation state of the DegU orphan response regulator both play a role in regulating *Listeria monocytogenes* motility and chemotaxis. *Molecular Microbiology*, 70 (6), 1342–1357. https://doi.org/10.1111/j.1365-2958.2008.06496.x

Gui, X., Yang, Z. & Li, M. D. (2021). Effect of cigarette smoke on gut microbiota: state of knowledge. *Frontiers in Physiology*, 12, 1–14. https://doi.org/10.3389/fphys.2021.673341

Gur, M., Ben-David, Y., Hanna, M., Ilivitzki, A., Weichhendler, A., Bar-Yoseph, R., Toukan, Y., Masarweh, K. & Bentur, L. (2021). The association between IgG and disease severity parameters in CF patients. *Journal of Clinical Medicine*, 10 (15), 3316. https://doi.org/10.3390/jcm10153316

Hallström, T., Jarva, H., Riesbeck, K. & Blom, A. M. (2007). Interaction with C4b-binding protein contributes to nontypeable *Haemophilus influenzae* serum resistance. *The Journal of Immunology*, 178 (10), 6359–6366. https://doi.org/10.4049/jimmunol.178.10.6359

Hallström, T., Singh, B., Resman, F., Blom, A. M., Mörgelin, M. & Riesbeck, K. (2011). *Haemophilus influenzae* protein E binds to the extracellular matrix by concurrently interacting with laminin and vitronectin. *Journal of Infectious Diseases*, 204 (7), 1065–1074. https://doi.org/10.1093/infdis/jir459

Hardison, R. L., Harrison, A., Wallace, R. M., Heimlich, D. R., O'Bryan, M. E., Sebra, R. P., Pinkett, H. W., Justice, S. S. & Mason, K. M. (2018b). Microevolution in response to transient heme-iron restriction enhances intracellular bacterial community development and persistence. *PLoS Pathogens*, 14 (10), 1–25. https://doi.org/10.1371/journal.ppat.1007355

Hardison, R. L., Heimlich, D. R., Harrison, A., Beatty, W. L., Rains, S., Moseley, M. A., Thompson, J. W., Justice, S. S. & Mason, K. M. (2018a). Transient nutrient deprivation promotes macropinocytosis-dependent intracellular bacterial community development. *MSphere*, 3 (5). https://doi.org/10.1128/mSphere.00286-18

Harrison, A., Dubois, L. G., St John-Williams, L., Moseley, M. A., Hardison, R. L., Heimlich, D. R., Stoddard, A., Kerschner, J. E., Justice, S. S., Thompson, J. W. & Mason, K. M. (2016). Comprehensive proteomic and metabolomic signatures of nontypeable *Haemophilus influenzae*-induced acute otitis media reveal bacterial aerobic respiration in an immunosuppressed environment. *Molecular & Cellular Proteomics*, 15 (3), 1117–1138. https://doi.org/10.1074/mcp.M115.052498

Harrison, A., Hardison, R. L., Fullen, A. R., Wallace, R. M., Gordon, D. M., White, P., Jennings, R. N., Justice, S. S. & Mason, K. M. (2020). Continuous microevolution accelerates disease progression during sequential episodes of infection. *Cell Reports*, 30 (9), 2978-2988.e3. https://doi.org/10.1016/j.celrep.2020.02.019

Harrison, A., Hardison, R. L., Wallace, R. M., Fitch, J., Heimlich, D. R., Bryan, M. O., Dubois, L., John-Williams, L. S., Sebra, R. P., White, P., Moseley, M. A., Thompson, J. W., Justice, S. S. & Mason, K. M. (2019). Reprioritization of biofilm metabolism is associated with nutrient adaptation and long-term survival of *Haemophilus influenzae*. *Npj Biofilms and Microbiomes*, 5 (1). https://doi.org/10.1038/s41522-019-0105-6

Hartl, D., Tirouvanziam, R., Laval, J., Greene, C. M., Habiel, D., Sharma, L., Yildirim, A. Ö., Dela

Cruz, C. S. & Hogaboam, C. M. (2018). Innate immunity of the lung: from basic mechanisms to translational medicine. *Journal of Innate Immunity*, 10 (5–6), 487–501. https://doi.org/10.1159/000487057

Hartung, H. P. & Hadding, U. (1983). Synthesis of complement by macrophages and modulation of their functions through complement activation. *Springer Seminars in Immunopathology*, 6 (4), 283–326. https://doi.org/10.1007/BF02116277

Healy, C., Munoz-Wolf, N., Strydom, J., Faherty, L., Williams, N. C., Kenny, S., Donnelly, S. C. & Cloonan, S. M. (2021). Nutritional immunity: the impact of metals on lung immune cells and the airway microbiome during chronic respiratory disease. *Respiratory Research*, 22 (1), 1–44. https://doi.org/10.1186/s12931-021-01722-y

Hedegaard, J., Okkels, H., Bruun, B., Kilian, M., Mortensen, K. K. & Nørskov-Lauritsen, N. (2001). Phylogeny of the genus *Haemophilus* as determined by comparison of partial *infB* sequences. *Microbiology,* 147, 2599–2609. https://doi.org/10.1099/00221287-147-9-2599

Heise, T., Langereis, J. D., Rossing, E., de Jonge, M. I., Adema, G. J., Büll, C. & Boltje, T. J. (2018). Selective inhibition of sialic acid-based molecular mimicry in *Haemophilus influenzae* abrogates serum resistance. *Cell Chemical Biology*, 25 (10), 1279-1285.e8. https://doi.org/10.1016/j.chembiol.2018.05.018

Hemenway, A. N. & Terry, A. M. (2017). Evaluation of corticosteroid dose in acute exacerbation of chronic obstructive pulmonary disease. *Hospital Pharmacy*, 52 (8), 546–550. https://doi.org/10.1177/0018578717722540

Henderson, J. C., Zimmerman, S. M., Crofts, A. A., Boll, J. M., Kuhns, L. G., Herrera, C. M. & Trent, M. S. (2016). The power of asymmetry: architecture and assembly of the Gram-negative outer membrane lipid bilayer. *Annual Review of Microbiology*, 70, 255–278. https://doi.org/10.1146/annurev-micro-102215-095308

Herbert, M., Kraiss, A., Hilpert, A.-K., Schlör, S. & Reidl, J. (2003). Aerobic growth deficient *Haemophilus influenzae* mutants are non-virulent: implications on metabolism. *International Journal of Medical Microbiology*, 293 (2–3), 145–152. https://doi.org/10.1078/1438-4221-00261

Hernandez, M., Leichtle, A., Pak, K., Webster, N. J., Wasserman, S. I. & Ryan, A. F. (2015). The transcriptome of a complete episode of acute otitis media. *BMC Genomics*, 16 (1), 259. https://doi.org/10.1186/s12864-015-1475-7

Herriott, R. M., Meyer, E. M. & Vogt, M. (1970). Defined nongrowth media for stage II development of competence in *Haemophilus influenzae*. *Journal of Bacteriology*, 101 (2), 517–524. https://doi.org/10.1128/jb.101.2.517-524.1970

Herth, F. J. F., Bramlage, P. & Müller-Wieland, D. (2015). Current perspectives on the contribution of inhaled corticosteroids to an increased risk for diabetes onset and progression in patients with chronic obstructive pulmonary disease. *Respiration*, 89 (1), 66–75. https://doi.org/10.1159/000368371

Hiemstra, P. S. (2007). The role of epithelial β-defensins and cathelicidins in host defense of the lung. *Experimental Lung Research*, 33 (10), 537–542. https://doi.org/10.1080/01902140701756687

Hong, W., Mason, K., Jurcisek, J., Novotny, L., Bakaletz, L. O. & Swords, W. E. (2007). Phosphorylcholine decreases early inflammation and promotes the establishment of stable biofilm communities of nontypeable *Haemophilus influenzae* strain 86-028NP in a chinchilla model of otitis media. *Infection and Immunity*, 75 (2), 958–965. https://doi.org/10.1128/IAI.01691-06

Referencias

Hood, M. I. & Skaar, E. P. (2012). Nutritional immunity: transition metals at the pathogen-host interface. *Nature Reviews. Microbiology*, 10 (8), 525–537. https://doi.org/10.1038/nrmicro2836

Huang, H., Wu, D., Tian, W. X., Ma, X. F. & Wu, X. D. (2008). Antimicrobial effect by extracts of rhizome of *Alpinia officinarum* Hance may relate to its inhibition of β-ketoacyl-ACP reductase. *Journal of Enzyme Inhibition and Medicinal Chemistry*, 23 (3), 362–368. https://doi.org/10.1080/14756360701622099

Huffnagle, G. B., Dickson, R. P. & Lukacs, N. W. (2017). The respiratory tract microbiome and lung inflammation: a two-way street. *Mucosal Immunology*, 10 (2), 299–306. https://doi.org/10.1038/mi.2016.108

Hughes, E. R., Winter, M. G., Duerkop, B. A., Spiga, L., Furtado de Carvalho, T., Zhu, W., Gillis, C. C., Büttner, L., Smoot, M. P., Behrendt, C. L., Cherry, S., Santos, R. L., Hooper, L. V. & Winter, S. E. (2017). Microbial respiration and formate oxidation as metabolic signatures of inflammation-associated dysbiosis. *Cell Host & Microbe*, 21 (2), 208–219. https://doi.org/10.1016/j.chom.2017.01.005

Hunt, W. R., Zughaier, S. M., Guentert, D. E., Shenep, M. A., Koval, M., McCarty, N. A. & Hansen, J. M. (2014). Hyperglycemia impedes lung bacterial clearance in a murine model of cystic fibrosis-related diabetes. *American Journal of Physiology. Lung Cellular and Molecular Physiology*, 306 (1), L43-9. https://doi.org/10.1152/ajplung.00224.2013

Hurst, J. R., Vestbo, J., Anzueto, A., Locantore, N., Müllerova, H., Tal-Singer, R., Miller, B., Lomas, D. A., Agusti, A., Macnee, W., Calverley, P., Rennard, S., Wouters, E. F. M. & Wedzicha, J. A. (2010). Susceptibility to exacerbation in chronic obstructive pulmonary disease. *The New England Journal of Medicine*, 363 (12), 1128–1138. https://doi.org/10.1056/NEJMoa0909883

Iram, S. H. & Cronan, J. E. (2005). Unexpected functional diversity among FadR fatty acid transcriptional regulatory proteins. *Journal of Biological Chemistry*, 280 (37), 32148–32156. https://doi.org/10.1074/jbc.M504054200

Ishak, N., Tikhomirova, A., Bent, S. J., Ehrlich, G. D., Hu, F. Z. & Kidd, S. P. (2014). There is a specific response to pH by isolates of *Haemophilus influenzae* and this has a direct influence on biofilm formation. *BMC Microbiology*, 14 (1), 1–10. https://doi.org/10.1186/1471-2180-14-47

Jalalvand, F. & Riesbeck, K. (2018). Update on non-typeable *Haemophilus influenzae*-mediated disease and vaccine development. *Expert Review of Vaccines*, 17 (6), 503–512. https://doi.org/10.1080/14760584.2018.1484286

Jalalvand, F., Su, Y. C., Mörgelin, M., Brant, M., Hallgren, O., Westergren-Thorsson, G., Singh, B. & Riesbeck, K. (2013). *Haemophilus influenzae* protein F mediates binding to laminin and human pulmonary epithelial cells. *Journal of Infectious Diseases*, 207 (5), 803–813. https://doi.org/10.1093/infdis/jis754

Jasnin, M. (2007). La dynamique intracellulaire explorée par marquage isotopique et diffusion incohérente de neutrons.

Jiang, D., Tikhomirova, A. & Kidd, S. P. (2016). *Haemophilus influenzae* strains possess variations in the global transcriptional profile in response to oxygen levels and this influences sensitivity to environmental stresses. *Research in Microbiology*, 167 (1), 13–19. https://doi.org/10.1016/j.resmic.2015.08.004

John, M.-A., Beukers, A., Chan, R. & van Hal, S. (2021). Whole genome sequencing identifies opportunistic non-typeable *Haemophilus influenzae* rather than a hypervirulent clone. *Pathology*, 53 (4) 540–541. https://doi.org/10.1016/j.pathol.2020.08.011

Johnson, R. W., McGillivary, G., Denoël, P., Poolman, J. & Bakaletz, L. O. (2011). Abrogation of nontypeable *Haemophilus influenzae* Protein D function reduces phosphorylcholine decoration, adherence to airway epithelial cells, and fitness in a chinchilla model of otitis media. *Vaccine*, 29 (6), 1211–1221. https://doi.org/10.1016/j.vaccine.2010.12.003

Joyce, A. R. & Palsson, B. Ø. (2008). Predicting gene essentiality using genome-scale *in silico* models. *Methods in Molecular Biology*, 416, 433–457. https://doi.org/10.1007/978-1-59745-321-9_30

Juliao, P. C., Marrs, C. F., Xie, J. & Gilsdorf, J. R. (2007). Histidine auxotrophy in commensal and disease-causing nontypeable *Haemophilus influenzae*. *Journal of Bacteriology*, 189 (14), 4994–5001. https://doi.org/10.1128/JB.00146-07

Juneau, R. A., Pang, B., Armbruster, C. E., Murrah, K. A., Perez, A. C. & Swords, W. E. (2015). Peroxiredoxin-glutaredoxin and catalase promote resistance of nontypeable *Haemophilus influenzae* 86-028NP to oxidants and survival within neutrophil extracellular traps. *Infection and Immunity*, 83 (1), 239–246. https://doi.org/10.1128/IAI.02390-14

Juneau, R. A., Pang, B., Weimer, K. W. D., Armbruster, C. E. & Swords, W. E. (2011). Nontypeable *Haemophilus influenzae* initiates formation of neutrophil extracellular traps. *Infection and Immunity*, 79(1), 431–438. https://doi.org/10.1128/IAI.00660-10

Jurcisek, J., Greiner, L., Watanabe, H., Zaleski, A., Apicella, M. A. & Bakaletz, L. O. (2005). Role of sialic acid and complex carbohydrate biosynthesis in biofilm formation by nontypeable *Haemophilus influenzae* in the chinchilla middle ear. *Infection and Immunity*, 73 (6), 3210–3218. https://doi.org/10.1128/IAI.73.6.3210-3218.2005

Kalsi, K. K., Garnett, J. P., Patkee, W., Weekes, A., Dockrell, M. E., Baker, E. H. & Baines, D. L. (2019). Metformin attenuates the effect of *Staphylococcus aureus* on airway tight junctions by increasing PKCζ-mediated phosphorylation of occludin. *Journal of Cellular and Molecular Medicine*, 23 (1), 317–327. https://doi.org/10.1111/jcmm.13929

Karlsson, R., Thorsell, A., Gomila, M., Salvà-Serra, F., Jakobsson, H. E., Gonzales-Siles, L., Jaén-Luchoro, D., Skovbjerg, S., Fuchs, J., Karlsson, A., Boulund, F., Johnning, A., Kristiansson, E. & Moore, E. R. B. (2020). Discovery of species-unique peptide biomarkers of bacterial pathogens by tandem mass spectrometry-based proteotyping. *Molecular & Cellular Proteomics*, 19 (3), 518–528. https://doi.org/10.1074/mcp.RA119.001667

Kim, J. N., Ahn, S.-J. & Burne, R. A. (2015). Genetics and physiology of acetate metabolism by the Pta-Ack pathway of *Streptococcus mutans*. *Applied and Environmental Microbiology*, 81 (15), 5015–5025. https://doi.org/10.1128/AEM.01160-15

King, Z. A., Lloyd, C. J., Feist, A. M. & Palsson, B. O. (2015). Next-generation genome-scale models for metabolic engineering. *Current Opinion in Biotechnology*, 35, 23–29. https://doi.org/10.1016/j.copbio.2014.12.016

Kleczko, E. K., Kwak, J. W., Schenk, E. L. & Nemenoff, R. A. (2019). Targeting the complement pathway as a therapeutic strategy in lung cancer. *Frontiers in Immunology*, 10, 1–16. https://doi.org/10.3389/fimmu.2019.00954

Knapp, H. R. & Mellyt, M. A. (1986). Knapp, H. R., & Melly, M. A. (1986). Bactericidal effects of polyunsaturated fatty acids. *The Journal of Infectious Diseases,* 154 (1), 84–94. https://www.jstor.org/stable/30105256

Knowles, M. R. & Boucher, R. C. (2002). Mucus clearance as a primary innate defense mechanism for mammalian airways. *Journal of Clinical Investigation*, 109 (5), 571–577. https://doi.org/10.1172/JCI0215217

Komatsu, K., Jono, H., Lim, J. H., Imasato, A., Xu, H., Kai, H., Yan, C. & Li, J. D. (2008).

Glucocorticoids inhibit nontypeable *Haemophilus influenzae*-induced MUC5AC mucin expression via MAPK phosphatase-1-dependent inhibition of p38 MAPK. *Biochemical and Biophysical Research Communications*, 377 (3), 763–768. https://doi.org/10.1016/j.bbrc.2008.10.091

Koonin, E. V., Makarova, K. S. & Wolf, Y. I. (2021). Evolution of microbial genomics: conceptual shifts over a quarter century. *Trends in Microbiology*, 29 (7), 582–592. https://doi.org/10.1016/j.tim.2021.01.005

Kostyanev, T. S. & Sechanova, L. P. (2012). Virulence factors and mechanisms of antibiotic resistance of *Haemophilus influenzae*. *Folia Medica*, 54 (1), 19–23. https://doi.org/10.2478/v10153-011-0073-y

Kress-Bennett, J. M., Hiller, N. L., Eutsey, R. A., Powell, E., Longwell, M. J., Hillman, T., Blackwell, T., Byers, B., Mell, J. C., Post, J. C., Hu, F. Z., Ehrlich, G. D. & Janto, B. A. (2016). Identification and characterization of *msf*, a novel virulence factor in *Haemophilus influenzae*. *PLoS ONE*, 11 (3), 1–34. https://doi.org/10.1371/journal.pone.0149891

Kristan, K., Bratkovič, T., Sova, M., Gobec, S., Preželj, A. & Urleb, U. (2009). Novel inhibitors of β-ketoacyl-ACP reductase from *Escherichia coli*. *Chemico-Biological Interactions*, 178 (1–3), 310–316. https://doi.org/10.1016/j.cbi.2008.09.030

Kuda, T., Kawahara, M., Nemoto, M., Takahashi, H. & Kimura, B. (2014). *In vitro* antioxidant and anti-inflammation properties of lactic acid bacteria isolated from fish intestines and fermented fish from the Sanriku Satoumi region in Japan. *Food Research International*, 64, 248–255. https://doi.org/10.1016/j.foodres.2014.06.028

Kunau, W. H., Dommes, V. & Schulz, H. (1995). β-Oxidation of fatty acids in mitochondria, peroxisomes, and bacteria: a century of continued progress. *Progress in Lipid Research*, 34 (4), 267–342. https://doi.org/10.1016/0163-7827(95)00011-9

Ladhani, S., Slack, M. P. E., Heath, P. T., von Gottberg, A., Chandra, M. & Ramsay, M. E. (2010). Invasive *Haemophilus influenzae* disease, Europe, 1996-2006. *Emerging Infectious Diseases*, 16 (3), 455–463. https://doi.org/10.3201/eid1603.090290

Langereis, J. D., Cremers, A. J. H., Vissers, M., Van Beek, J., Meis, J. F. & De Jonge, M. I. (2019). Nontypeable *Haemophilus influenzae* invasive blood isolates are mainly phosphorylcholine negative and show decreased complement-mediated killing that is associated with lower binding of IgM and CRP in comparison to colonizing isolates from the oropharynx. *Infection and Immunity*, 87 (2), 1–11. https://doi.org/10.1128/IAI.00604-18

Langereis, J. D. & De Jonge, M. I. (2015). Invasive disease caused by nontypeable *Haemophilus influenzae*. *Emerging Infectious Diseases*, 21 (10), 1711–1718. https://doi.org/10.3201/eid2110.150004

Langereis, J. D. & De Jonge, M. I. (2020). Unraveling *Haemophilus influenzae* virulence mechanisms enable discovery of new targets for antimicrobials and vaccines. *Current Opinion in Infectious Diseases*, 33 (3), 231–237. https://doi.org/10.1097/QCO.0000000000000645

Langereis, J. D., de Jonge, M. I. & Weiser, J. N. (2014). Binding of human factor H to outer membrane protein P5 of non-typeable *Haemophilus influenzae* contributes to complement resistance. *Molecular Microbiology*, 94 (1), 89–106. https://doi.org/10.1111/mmi.12741

Langereis, J. D. & Hermans, P. W. M. (2013). Novel concepts in nontypeable *Haemophilus influenzae* biofilm formation. *FEMS Microbiology Letters*, 346 (2), 81–89. https://doi.org/10.1111/1574-6968.12203

Langereis, J. D. & Weiser, J. N. (2014). Shielding of a lipooligosaccharide IgM epitope allows evasion of neutrophil-mediated killing of an invasive strain of nontypeable *Haemophilus*

influenzae. *MBio*, *5*(4), 1–10. https://doi.org/10.1128/mBio.01478-14

Langereis, J. D., Zomer, A., Stunnenberg, H. G., Burghout, P. & Hermans, P. W. M. (2013). Nontypeable *Haemophilus influenzae* carbonic anhydrase is important for environmental and intracellular survival. *Journal of Bacteriology*, 195 (12), 2737–2746. https://doi.org/10.1128/JB.01870-12

Lee, D. S., Burd, H., Liu, J., Almaas, E., Wiest, O., Barabási, A. L., Oltvai, Z. N. & Kapatral, V. (2009). Comparative genome-scale metabolic reconstruction and flux balance analysis of multiple *Staphylococcus aureus* genomes identify novel antimicrobial drug targets. *Journal of Bacteriology*, 191 (12), 4015–4024. https://doi.org/10.1128/JB.01743-08

Lee, I. T. & Yang, C. M. (2013). Inflammatory signalings involved in airway and pulmonary diseases. *Mediators of Inflammation*, 2013. https://doi.org/10.1155/2013/791231

Leiva-Juárez, M. M., Kolls, J. K. & Evans, S. E. (2018). Lung epithelial cells: therapeutically inducible effectors of antimicrobial defense. *Mucosal Immunology*, 11 (1), 21–34. https://doi.org/10.1038/mi.2017.71

Li, Y., Weng, X., Deng, Y., Pan, J., Zhu, S., Wen, Z., Yuan, Y., Li, S., Shen, B., Duan, Y. & Huang, Y. (2021). Semisynthesis and biological evaluation of platencin thioether derivatives: dual FabF and FabH inhibitors against MRSA. *ACS Medicinal Chemistry Letters*, 12 (3), 433–442. https://doi.org/10.1021/acsmedchemlett.0c00653

Liao, Y.-C., Tsai, M.-H., Chen, F.-C. & Hsiung, C. A. (2012). GEMSiRV: a software platform for GEnome-scale metabolic model simulation, reconstruction and visualization. *Bioinformatics (Oxford, England)*, 28 (13), 1752–1758. https://doi.org/10.1093/bioinformatics/bts267

Liao, Y., Wang, J., Jaehnig, E. J., Shi, Z. & Zhang, B. (2019). WebGestalt 2019: gene set analysis toolkit with revamped UIs and APIs. *Nucleic Acids Research*, 47 (1), W199–W205. https://doi.org/10.1093/nar/gkz401

Lieven, C., Beber, M. E., Olivier, B. G., Bergmann, F. T., Ataman, M., Babaei, P., Bartell, J. A., Blank, L. M., Chauhan, S., Correia, K., Diener, C., Dräger, A., Ebert, B. E., Edirisinghe, J. N., Faria, J. P., Feist, A. M., Fengos, G., Fleming, R. M. T., García-Jiménez, B., et al. (2020). MEMOTE for standardized genome-scale metabolic model testing. *Nature biotechnology*, 38 (3), 272–276. https://doi.org/10.1038/s41587-020-0446-y

Lim, M. Y., Yoon, H. S., Rho, M., Sung, J., Song, Y. M., Lee, K. & Ko, G. (2016). Analysis of the association between host genetics, smoking, and sputum microbiota in healthy humans. *Scientific Reports*, 6, 1–9. https://doi.org/10.1038/srep23745

Liu, X., Wang, Z., Feng, X., Bai, E., Xiong, Y., Zhu, X., Zhu, X., Shen, B., Shen, B., Duan, Y., Duan, Y., Duan, Y., Huang, Y. & Huang, Y. (2020). Platensimycin-encapsulated poly(lactic- co-glycolic acid) and poly(amidoamine) dendrimers nanoparticles with enhanced anti-staphylococcal activity *in vivo*. *Bioconjugate Chemistry*, 31 (5), 1425–1437. https://doi.org/10.1021/acs.bioconjchem.0c00121

Liu, Y., Li, R., Xiao, X. & Wang, Z. (2019). Bacterial metabolism-inspired molecules to modulate antibiotic efficacy. *Journal of Antimicrobial Chemotherapy*, 74 (12), 3409–3417. https://doi.org/10.1093/jac/dkz230

Liu, Y., Yang, K., Zhang, H., Jia, Y. & Wang, Z. (2020). Combating antibiotic tolerance through activating bacterial metabolism. *Frontiers in Microbiology*, 11. https://doi.org/10.3389/fmicb.2020.577564

Loeb, M. R. (1995). Ferrochelatase activity and protoporphyrin IX utilization in *Haemophilus influenzae*. *Journal of Bacteriology*, 177 (12), 3613–3615. https://doi.org/10.1128/jb.177.12.3613-3615.1995

Referencias

López-Gómez, A., Cano, V., Moranta, D., Morey, P., del Portillo, F. G., Bengoechea, J. A. & Garmendia, J. (2012). Host cell kinases, α5 and β1 integrins, and Rac1 signalling on the microtubule cytoskeleton are important for non-typable *Haemophilus influenzae* invasion of respiratory epithelial cells. *Microbiology*, 158 (9), 2384–2398. https://doi.org/10.1099/mic.0.059972-0

López-López, N., Euba, B., Hill, J., Dhouib, R., Caballero, L., Leiva, J., Hosmer, J., Cuesta, S., Ramos-Vivas, J., Díez-Martínez, R., Schirra, H. J., Blank, L. M., Kappler, U. & Garmendia, J. (2020). *Haemophilus influenzae* glucose catabolism leading to production of the immunometabolite acetate has a key contribution to the host airway-pathogen interplay. *ACS Infectious Diseases*, 6 (3), 406–421. https://doi.org/10.1021/acsinfecdis.9b00359

López-López, N., Gil-Campillo, C., Díez-Martínez, R. & Garmendia, J. (2021). Learning from -omics strategies applied to uncover *Haemophilus influenzae* host-pathogen interactions: current status and perspectives. *Computational and Structural Biotechnology Journal*, 19, 3042–3050. https://doi.org/10.1016/j.csbj.2021.05.026

Lopez, C. A. & Skaar, E. P. (2019). The impact of dietary transition metals. *Cell Host & Microbe* 23 (6), 737–748. https://doi.org/10.1016/j.chom.2018.05.008.

Loukides, S. & Polyzogopoulos, D. (1996). The effect of diabetes mellitus on the outcome of patients with chronic obstructive pulmonary disease exacerbated due to respiratory infections. *Respiration; International Review of Thoracic Diseases*, 63 (3), 170–173. https://doi.org/10.1159/000196539

Lu, D., Boyd, B. & Lingwood, C. A. (1997). Identification of the key protein for zinc uptake in *Hemophilus influenzae*. *Journal of Biological Chemistry*, 272 (46), 29033–29038. https://doi.org/10.1074/jbc.272.46.29033

Lu, Y. J., Zhang, Y. M. & Rock, C. O. (2004). Product diversity and regulation of type II fatty acid synthases. *Biochemistry and Cell Biology*, 82 (1), 145–155. https://doi.org/10.1139/o03-076

Lysenko, E. S., Gould, J., Bals, R., Wilson, J. M. & Weiser, J. N. (2000). Bacterial phosphorylcholine decreases susceptibility to the antimicrobial peptide LL-37/hCAP18 expressed in the upper respiratory tract. *Infection and Immunity*, 68 (3), 1664–1671. https://doi.org/10.1128/IAI.68.3.1664-1671.2000

Macfadyen, L. P., Chen, D. & Vo, H. C. (2001). Competence development by *Haemophilus influenzae* is regulated by the availability of nucleic acid precursors. *Molecular Microbiology*, 40 (3), 700–707. https://doi.org/10.1046/j.1365-2958.2001.02419.x

Macfadyen, L. P. & Redfield, R. J. (1996). Life in mucus: sugar metabolism in *Haemophilus influenzae*. *Research in Microbiology*, 147 (6–7), 541–551. https://doi.org/10.1016/0923-2508(96)84010-1

Macfadyen, L. P., Dorocicz, I. R., Reizer, J., Saler, M. H. & Redfield, R. J. (1996). Regulation of competence development and sugar utilization in *Haemophilus influenzae* Rd by a phosphoenolpyruvate:fructose phosphotransferase system. *Molecular Microbiology*, 21 (5), 941–952. https://doi.org/10.1046/j.1365-2958.1996.441420.x

Magryś, A. (2021). Microbiota: A missing link in the pathogenesis of chronic lung inflammatory diseases. *Polish Journal of Microbiology*, 70 (1), 25–32. https://doi.org/10.33073/pjm-2021-013

Mahfuz, A. M. U. B., Stambuk Opazo, F., Aguilar, L. F. & Iqbal, M. N. (2020). Carfilzomib as a potential inhibitor of NADH-dependent enoyl-acyl carrier protein reductases of *Klebsiella pneumoniae* and *Mycobacterium tuberculosis* as a drug target enzyme: insights from molecular docking and molecular dynamics. *Journal of Biomolecular Structure and Dynamics*, 30, 1–17.

https://doi.org/10.1080/07391102.2020.1852966

Malinverni, J. C. & Silhavy, T. J. (2009). An ABC transport system that maintains lipid asymmetry in the Gram-negative outer membrane. *Proceedings of the National Academy of Sciences of the United States of America*, 106 (19), 8009–8014. https://doi.org/10.1073/pnas.0903229106

Mallia, P., Webber, J., Gill, S. K., Trujillo-Torralbo, M.-B., Calderazzo, M. A., Finney, L., Bakhsoliani, E., Farne, H., Singanayagam, A., Footitt, J., Hewitt, R., Kebadze, T., Aniscenko, J., Padmanaban, V., Molyneaux, P. L., Adcock, I. M., Barnes, P. J., Ito, K., Elkin, S. L., et al. (2018). Role of airway glucose in bacterial infections in patients with chronic obstructive pulmonary disease. *The Journal of Allergy and Clinical Immunology*, 142 (3), 815-823.e6. https://doi.org/10.1016/j.jaci.2017.10.017

Man, W. H., De Steenhuijsen Piters, W. A. A. & Bogaert, D. (2017). The microbiota of the respiratory tract: gatekeeper to respiratory health. *Nature Reviews Microbiology*, 15 (5), 259–270. https://doi.org/10.1038/nrmicro.2017.14

Månsson, V., Skaare, D., Riesbeck, K. & Resman, F. (2017). The spread and clinical impact of ST14CC-PBP3 type IIb/A, a clonal group of non-typeable *Haemophilus influenzae* with chromosomally mediated β-lactam resistance-a prospective observational study. *Clinical Microbiology and Infection : The Official Publication of the European Society of Clinical Microbiology and Infectious Diseases*, 23 (3), 209.e1-209.e7. https://doi.org/10.1016/j.cmi.2016.11.006

Marshall, D. D., Sadykov, M. R., Thomas, V. C., Bayles, K. W. & Powers, R. (2016). Redox imbalance underlies the fitness defect associated with inactivation of the Pta-AckA pathway in *Staphylococcus aureus*. *Journal of Proteome Research*, 15 (4), 1205–1212. https://doi.org/10.1021/acs.jproteome.5b01089

Marsland, B. J., Trompette, A. & Gollwitzer, E. S. (2015). The gut-lung axis in respiratory disease. *Annals of the American Thoracic Society*, 12, S150–S156. https://doi.org/10.1513/AnnalsATS.201503-133AW

Martí-Lliteras, P., Regueiro, V., Morey, P., Hood, D. W., Saus, C., Sauleda, J., Agustí, A. G. N., Bengoechea, J. A. & Garmendia, J. (2009). Nontypeable *Haemophilus influenzae* clearance by alveolar macrophages is impaired by exposure to cigarette smoke. *Infection and Immunity*, 77 (10), 4232–4242. https://doi.org/10.1128/IAI.00305-09

Marti, S., Puig, C., de la Campa, A. G., Tirado-Velez, J. M., Tubau, F., Domenech, A., Calatayud, L., Garcia-Somoza, D., Ayats, J., Liñares, J. & Ardanuy, C. (2016). Identification of *Haemophilus haemolyticus* in clinical samples and characterization of their mechanisms of antimicrobial resistance. *The Journal of Antimicrobial Chemotherapy*, 71 (1), 80–84. https://doi.org/10.1093/jac/dkv307

Marti, S., Puig, C., Merlos, A., Viñas, M., de Jonge, M. I., Liñares, J., Ardanuy, C. & Langereis, J. D. (2017). Bacterial lysis through interference with peptidoglycan synthesis increases biofilm formation by nontypeable *Haemophilus influenzae*. *MSphere*, 2 (1), 1–12. https://doi.org/10.1128/msphere.00329-16

Martin, T. R. & Frevert, C. W. (2005). Innate immunity in the lungs. *Proceedings of the American Thoracic Society*, 2 (5), 403–411. https://doi.org/10.1513/pats.200508-090js

Mason, R. J. (2006). Biology of alveolar type II cells. *Respirology*, 11, 12–15. https://doi.org/10.1111/j.1440-1843.2006.00800.x

Maughan, H., Wilson, L. A. & Redfield, R. J. (2010). Bacterial DNA uptake sequences can accumulate by molecular drive alone. *Genetics*, 186 (2), 613–627. https://doi.org/10.1534/genetics.110.119438

Maughan, H. & Redfield, R. J. (2009). Extensive variation in natural competence in *Haemophilus influenzae*. *Evolution*, 63 (7), 1852–1866. https://doi.org/10.1111/j.1558-5646.2009.00658.x

McKinney, D. C., Eyermann, C. J., Gu, R. F., Hu, J., Kazmirski, S. L., Lahiri, S. D., McKenzie, A. R., Shapiro, A. B. & Breault, G. (2016). Antibacterial FabH inhibitors with mode of action validated in *Haemophilus influenzae* by *in vitro* resistance mutation mapping. *ACS Infectious Diseases*, 2 (7), 456–464. https://doi.org/10.1021/acsinfecdis.6b00053

Mei, X., Yan, X., Zhang, H., Yu, M., Shen, G., Zhou, L., Deng, Z., Lei, C. & Qu, X. (2018). Expanding the bioactive chemical space of anthrabenzoxocinones through engineering the highly promiscuous biosynthetic modification steps. *ACS Chemical Biology*, 13 (1), 200–206. https://doi.org/10.1021/acschembio.7b00743

Mell, J. C., Lee, J. Y., Firme, M., Sinha, S. & Redfield, R. J. (2014a). Extensive cotransformation of natural variation into chromosomes of naturally competent *Haemophilus influenzae*. *G3: Genes, Genomes, Genetics*, 4 (4), 717–731. https://doi.org/10.1534/g3.113.009597

Mell, J. C. & Redfield, R. J. (2014). Natural competence and the evolution of DNA uptake specificity. *Journal of Bacteriology*, 196 (8), 1471–1483. https://doi.org/10.1128/JB.01293-13

Mell, J. C., Shumilina, S., Hall, I. M. & Redfield, R. J. (2011). Transformation of natural genetic variation into *Haemophilus influenzae* genomes. *PLoS Pathogens*, 7 (7), 32–34. https://doi.org/10.1371/journal.ppat.1002151

Mell, J. C., Sinha, S., Balashov, S., Viadas, C., Grassa, C. J., Ehrlich, G. D., Nislow, C., Redfield, R. J. & Garmendia, J. (2014b). Complete genome sequence of *Haemophilus influenzae* strain 375 from the middle ear of a pediatric patient with otitis media. *Genome Announcements*, 2 (6). https://doi.org/10.1128/genomeA.01245-14

Mell, J. C., Viadas, C., Moleres, J., Sinha, S., Fernández-Calvet, A., Porsch, E. A., St. Geme, J. W., Nislow, C., Redfield, R. J. & Garmendia, J. (2016). Transformed recombinant enrichment profiling rapidly identifies HMW1 as an intracellular invasion locus in *Haemophilus influenzae*. *PLoS Pathogens*, 12 (4). https://doi.org/10.1371/journal.ppat.1005576

Meri, S. (2016). Self-nonself discrimination by the complement system. *FEBS Letters*, 590, 2418–2434. https://doi.org/10.1002/1873-3468.12284

Meyer, M. C., Rastogi, P., Beckett, C. S. & Mchowat, J. (2005). Phospholipase A 2 inhibitors as potential anti-inflammatory agents. *Current Pharmaceutical Design*, 11, 1301–1312.

Mienda, B. S. (2017). Genome-scale metabolic models as platforms for strain design and biological discovery. *Journal of Biomolecular Structure and Dynamics*, 35 (9), 1863–1873. https://doi.org/10.1080/07391102.2016.1197153

Mienda, B. S., Salihu, R., Adamu, A. & Idris, S. (2018). Genome-scale metabolic models as platforms for identification of novel genes as antimicrobial drug targets. *Future Microbiology*, 13 (4), 455–467. https://doi.org/10.2217/fmb-2017-0195

Millares, L., Marin, A., Garcia-Aymerich, J., Sauleda, J., Belda, J., Monsó, E., Antó, J. M., Benet, M., de Batlle, J., Serra, I., Donaire-Gonzalez, D., Guerra, S., Gea, J., Balcells, E., Gayete, A., Orozco-Levi, M., Vollmer, I., Barberà, J. A., Gómez, F. P., et al. (2012). Specific IgA and metalloproteinase activity in bronchial secretions from stable chronic obstructive pulmonary disease patients colonized by *Haemophilus influenzae*. *Respiratory Research*, 13, 1–11. https://doi.org/10.1186/1465-9921-13-113

Mobegi, F. M., van Hijum, S. A. F. T., Burghout, P., Bootsma, H. J., de Vries, S. P. W., van der Gaast-de Jongh, C. E., Simonetti, E., Langereis, J. D., Hermans, P. W. M., de Jonge, M. I. & Zomer, A. (2014). From microbial gene essentiality to novel antimicrobial drug targets. *BMC Genomics*, 15 (1). https://doi.org/10.1186/1471-2164-15-958

Mojica, S. A., Salin, O., Bastidas, R. J., Sunduru, N., Hedenström, M., Andersson, C. D., Núñez-Otero, C., Engström, P., Valdivia, R. H., Elofsson, M. & Gylfe, Å. (2017). N-Acylated derivatives of sulfamethoxazole block *Chlamydia* fatty acid synthesis and interact with FabF. *Antimicrobial Agents and Chemotherapy*, 61 (10). https://doi.org/10.1128/AAC.00716-17

Mokrzan, E. M., Ahearn, C. P., Buzzo, J. R., Novotny, L. A., Zhang, Y., Goodman, S. D. & Bakaletz, L. O. (2020). Nontypeable *Haemophilus influenzae* newly released (NRel) from biofilms by antibody-mediated dispersal versus antibody-mediated disruption are phenotypically distinct. *Biofilm*, 2, 100039. https://doi.org/10.1016/j.bioflm.2020.100039

Moleres, J., Fernández-Calvet, A., Ehrlich, R. L., Martí, S., Pérez-Regidor, L., Euba, B., Rodríguez-Arce, I., Balashov, S., Cuevas, E., Liñares, J., Ardanuy, C., Martín-Santamaría, S., Ehrlich, G. D., Mell, J. C. & Garmendia, J. (2018). Antagonistic pleiotropy in the bifunctional surface protein Fadl (OmpP1) during adaptation of *Haemophilus influenzae* to chronic lung infection associated with chronic obstructive pulmonary disease. *MBio*, 9 (5), 1–23. https://doi.org/10.1128/mBio.01176-18

Monk, J., Nogales, J. & Palsson, B. O. (2014). Optimizing genome-scale network reconstructions. *Nature Biotechnology*, 32 (5), 447–452. https://doi.org/10.1038/nbt.2870

Mora, M., Mell, J. C., Ehrlich, G. D., Ehrlich, R. L. & Redfield, R. J. (2021). Genome-wide analysis of DNA uptake across the outer membrane of naturally competent *Haemophilus influenzae*. *IScience*, 24 (1), 102007. https://doi.org/10.1016/j.isci.2020.102007

Morey, P, Viadas, C., Euba, B., Hood, D. W., Barberan, M., Gil, C., Grillo, M. J., Bengoechea, J. A. & Garmendia, J. (2013). Relative contributions of lipooligosaccharide inner and outer core modifications to nontypeable *Haemophilus influenzae* pathogenesis. *Infection and Immunity*, 81 (11), 4100–4111. https://doi.org/10.1128/IAI.00492-13

Morey, P, Cano, V., Martí-Lliteras, P., López-Gómez, A., Regueiro, V., Saus, C., Bengoechea, J. A. & Garmendia, J. (2011). Evidence for a non-replicative intracellular stage of nontypable *Haemophilus influenzae* in epithelial cells. *Microbiology*, 157 (1), 234–250. https://doi.org/10.1099/mic.0.040451-0

Morris, A., Beck, J. M., Schloss, P. D., Campbell, T. B., Crothers, K., Curtis, J. L., Flores, S. C., Fontenot, A. P., Ghedin, E., Huang, L., Jablonski, K., Kleerup, E., Lynch, S. V., Sodergren, E., Twigg, H., Young, V. B., Bassis, C. M., Venkataraman, A., Schmidt, T. M. & Weinstock, G. M. (2013). Comparison of the respiratory microbiome in healthy nonsmokers and smokers. *American Journal of Respiratory and Critical Care Medicine*, 187 (10), 1067–1075. https://doi.org/10.1164/rccm.201210-1913OC

Morris, G. M., Huey, R., Lindstrom, W., Sanner, M. F., Belew, R. K., Goodsell, D. S. & Olson, A. J. (2009). AutoDock4 and AutoDockTools4: Automated docking with selective receptor flexibility. *Journal of Computational Chemistry*, 30 (16), 2785–2791. https://doi.org/10.1002/jcc.21256

Mortensen, P. B. & Clausen, M. R. (1996). Short-chain fatty acids in the human colon: relation to gastrointestinal health and disease. *Scandinavian Journal of Gastroenterology,* 216, 132–148. https://doi.org/10.3109/00365529609094568

Moxon, R., Bayliss, C. & Hood, D. (2006). Bacterial contingency loci: the role of simple sequence DNA repeats in bacterial adaptation. *Annual Review of Genetics*, 40, 307–333. https://doi.org/10.1146/annurev.genet.40.110405.090442

Muda, N. M., Nasreen, M., Dhouib, R., Hosmer, J., Hill, J., Mahawar, M., Schirra, H. J., McEwan, A. G. & Kappler, U. (2019). Metabolic analyses reveal common adaptations in two invasive *Haemophilus influenzae* strains. *Pathogens and Disease*, 77 (2), 1–12. https://doi.org/10.1093/femspd/ftz015

Mureed, S., Naz, S., Haider, A., Raza, A., Ul-Hamid, A., Haider, J., Ikram, M., Ghaffar, R., Irshad, M., Ghaffar, A. & Saeed, A. (2021). Development of multi-concentration Cu:Ag bimetallic nanoparticles as a promising bactericidal for antibiotic-resistant bacteria as evaluated with molecular docking study. *Nanoscale Research Letters*, 16 (1). https://doi.org/10.1186/s11671-021-03547-6

Murphy, T. F. (2015). Vaccines for Nontypeable *Haemophilus influenzae*: the Future Is Now. *Clinical and Vaccine Immunology.* 22 (5), 459–466. https://doi.org/10.1128/CVI.00089-15

Murphy, T. F. & Brauer, A. L. (2011). Expression of urease by *Haemophilus influenzae* during human respiratory tract infection and role in survival in an acid environment. *BMC Microbiology*, 11 (1), 183. https://doi.org/10.1186/1471-2180-11-183

Murphy, T. F., Brauer, A. L., Schiffmacher, A. T. & Sethi, S. (2004). Persistent colonization by *Haemophilus influenzae* in chronic obstructive pulmonary disease. *American Journal of Respiratory and Critical Care Medicine*, 170 (3), 266–272. https://doi.org/10.1164/rccm.200403-354OC

Murphy, T. F., Kirkham, C., Gallo, M. C., Yang, Y., Wilding, G. E. & Pettigrew, M. M. (2017). Immunoglobulin a protease variants facilitate intracellular survival in epithelial cells by nontypeable *Haemophilus influenzae* that persist in the human respiratory tract in chronic obstructive pulmonary disease. *Journal of Infectious Diseases*, 216 (10), 1295–1302. https://doi.org/10.1093/infdis/jix471

Nairz, M., Dichtl, S., Schroll, A., Haschka, D., Tymoszuk, P., Theurl, I. & Weiss, G. (2018). Iron and innate antimicrobial immunity-depriving the pathogen, defending the host. *Journal of Trace Elements in Medicine and Biology*, *48*, 118–133. https://doi.org/10.1016/j.jtemb.2018.03.007

Nam, B., Kim, S. A., Nam, W., Jeung, W. H., Park, S.-D., Lee, J.-L., Sim, J.-H. & Jang, S. S. (2019). Lactobacillus plantarum HY7714 restores TNF-α induced defects on tight junctions. *Preventive Nutrition and Food Science*, 24 (1), 64–69. https://doi.org/10.3746/pnf.2019.24.1.64

Negatu, D. A., Gengenbacher, M., Dartois, V. & Dick, T. (2020). Indole propionic acid, an unusual antibiotic produced by the gut microbiota, with anti-inflammatory and antioxidant properties. *Frontiers in Microbiology*, 11, 575586. https://doi.org/10.3389/fmicb.2020.575586

Nogales, J., Gudmundsson, S., Knight, E. M., Palsson, B. O. & Thiele, I. (2012). Detailing the optimality of photosynthesis in cyanobacteria through systems biology analysis. *Proceedings of the National Academy of Sciences of the United States of America*, 109 (7), 2678–2683. https://doi.org/10.1073/pnas.1117907109

Nogales, J., Mueller, J., Gudmundsson, S., Canalejo, F. J., Duque, E., Monk, J., Feist, A. M., Ramos, J. L., Niu, W. & Palsson, B. O. (2020). High-quality genome-scale metabolic modelling of *Pseudomonas putida* highlights its broad metabolic capabilities. *Environmental Microbiology*, 22 (1), 255–269. https://doi.org/10.1111/1462-2920.14843

Norsigian, C. J., Kavvas, E., Seif, Y., Palsson, B. O. & Monk, J. M. (2018). iCN718, an updated and improved genome-scale metabolic network reconstruction of *Acinetobacter baumannii* AYE. *Frontiers in Genetics*, 9, 121. https://doi.org/10.3389/fgene.2018.00121

Nørskov-Lauritsen, N., Bruun, B. & Kilian, M. (2005). Multilocus sequence phylogenetic study of the genus *Haemophilus* with description of *Haemophilus pittmaniae* sp. nov. *International Journal of Systematic and Evolutionary Microbiology*, 55 (1), 449–456. https://doi.org/10.1099/ijs.0.63325-0

Novotny, L. A. & Bakaletz, L. O. (2016). Intercellular adhesion molecule 1 serves as a primary cognate receptor for the Type IV pilus of nontypeable *Haemophilus influenzae*. *Cellular*

Microbiology, 18 (8), 1043–1055. https://doi.org/10.1111/cmi.12575

O'Brien, E. J., Monk, J. M. & Palsson, B. O. (2015). Using genome-scale models to predict biological capabilities. *Cell*, 161 (5), 971–987. https://doi.org/10.1016/j.cell.2015.05.019

O'Reilly, T., Maciver, I., Poole, R. K., Niven, D. F., Martin, P. G. & Brown, M. R. W. (1992). Effect of haemin limitation on the cytochrome complement and glucose metabolism of non-typable *Haemophilus influenzae*. *Journal of Medical Microbiology*, 37 (2), 133–140. https://doi.org/10.1099/00222615-37-2-133

OECD (2013), Test No. 236: Fish Embryo Acute Toxicity (FET) Test, OECD Guidelines for the Testing of Chemicals, Section 2, OECD Publishing, Paris, https://doi.org/10.1787/9789264203709-en.

Oerlemans, M. M. P., Moons, S. J., Heming, J. J. A., Boltje, T. J., De Jonge, M. I. & Langereis, J. D. (2019). Uptake of sialic acid by nontypeable *Haemophilus influenzae* increases complement resistance through decreasing IgM-dependent complement activation. *Infection and Immunity*, 87 (6), 1–11. https://doi.org/10.1128/IAI.00077-19

Olszak, T., An, D., Zeissig, S., Vera, M. P., Richter, J., Franke, A., Glickman, J. N., Siebert, R., Baron, R. M., Dennis, L. & Blumberg, R. S. (2012). Microbial exposure during early life has persistent effects on natural killer T cell function. *NIH Public Access*. 336 (6080), 489–493. https://doi:10.1126/science.1219328

Oong, G. C. & Tadi, P. (2021). *Chloramphenicol.* StatPearls

Opitz, B., Van Laak, V., Eitel, J. & Suttorp, N. (2010). Innate immune recognition in infectious and noninfectious diseases of the lung. *American Journal of Respiratory and Critical Care Medicine*, 181 (12), 1294–1309. https://doi.org/10.1164/rccm.200909-1427SO

Orengo, J. M., Evans, J. E., Bettiol, E., Leliwa-Sytek, A., Day, K. & Rodriguez, A. (2008). Plasmodium-induced inflammation by uric acid. *PLoS Pathogens*, 4 (3), e1000013. https://doi.org/10.1371/journal.ppat.1000013

Orth, J. D., Conrad, T. M., Na, J., Lerman, J. A., Nam, H., Feist, A. M. & Palsson, B. Ø. (2011). A comprehensive genome-scale reconstruction of *Escherichia coli* metabolism--2011. *Molecular Systems Biology*, 7, 535. https://doi.org/10.1038/msb.2011.65

Orth, J. D., Thiele, I. & Palsson, B. Ø. (2010). What is flux balance analysis? *Nature Biotechnology*, 28 (3), 245–248. https://doi.org/10.1038/nbt.1614

Osgood, R., Salamone, F., Diaz, A., Casey, J. R., Bajorski, P. & Pichichero, M. E. (2015). Effect of pH and oxygen on biofilm formation in acute otitis media associated NTHi clinical isolates. *Laryngoscope*, 125 (9), 2204–2208. https://doi.org/10.1002/lary.25102

Osman, K. L., Jefferies, J. M. C., Woelk, C. H., Devos, N., Pascal, T. G., Mortier, M.-C., Devaster, J.-M., Wilkinson, T. M. A., Cleary, D. W. & Clarke, S. C. (2018b). Patients with chronic obstructive pulmonary disease harbour a variation of *Haemophilus* species. *Scientific Reports*, 8 (1), 14734. https://doi.org/10.1038/s41598-018-32973-3

Osman, K. L., Jefferies, J. M., Woelk, C. H., Cleary, D. W. & Clarke, S. C. (2018a). The adhesins of non-typeable *Haemophilus influenzae*. *Expert Review of Anti-Infective Therapy*, 16 (3), 187–196. https://doi.org/10.1080/14787210.2018.1438263

Othman, D. S. M. P., Schirra, H., McEwan, A. G. & Kappler, U. (2014). Metabolic versatility in *Haemophilus influenzae*: a metabolomic and genomic analysis. *Frontiers in Microbiology*, 5, 1–10. https://doi.org/10.3389/fmicb.2014.00069

Pambianchi, E., Pecorelli, A. & Valacchi, G. (2021). Gastrointestinal tissue as a "new" target of

pollution exposure. *IUBMB Life*, 2021, 1–12. https://doi.org/10.1002/iub.2530

Pandya, P. H. & Wilkes, D. S. (2014). Complement system in lung disease. *American Journal of Respiratory Cell and Molecular Biology*, 51 (4), 467–473. https://doi.org/10.1165/rcmb.2013-0485TR

Papin, J. A., Price, N. D., Edwards, J. S. & Palsson B, B. Ø. (2002). The genome-scale metabolic extreme pathway structure in *Haemophilus influenzae* shows significant network redundancy. *Journal of Theoretical Biology*, 215 (1), 67–82. https://doi.org/10.1006/jtbi.2001.2499

Park, H. S., Yoon, Y. M., Jung, S. J., Yun, I. N. R., Kim, C. M., Kim, J. M. & Kwak, J. H. (2007). CG400462, a new bacterial enoyl-acyl carrier protein reductase (FabI) inhibitor. *International Journal of Antimicrobial Agents*, 30 (5), 446–451. https://doi.org/10.1016/j.ijantimicag.2007.07.006

Park, J.-E., Oh, S.-H. & Cha, Y.-S. (2014). *Lactobacillus brevis* OPK-3 isolated from kimchi inhibits adipogenesis and exerts anti-inflammation in 3T3-L1 adipocyte. *Journal of the Science of Food and Agriculture*, 94 (12), 2514–2520. https://doi.org/10.1002/jsfa.6588

Parsons, J. B., Frank, M. W., Subramanian, C., Saenkham, P. & Rock, C. O. (2011). Metabolic basis for the differential susceptibility of Gram-positive pathogens to fatty acid synthesis inhibitors. *Proceedings of the National Academy of Sciences of the United States of America*, 108 (37), 15378–15383. https://doi.org/10.1073/pnas.1109208108

Parsons, J. B. & Rock, C. O. (2013). Bacterial lipids: metabolism and membrane homeostasis. *Progress in Lipid Research*, 52 (3), 249–276. https://doi.org/10.1016/j.plipres.2013.02.002

Parsons, J. B., Yao, J., Frank, M. W. & Rock, C. O. (2015). FabH mutations confer resistance to Fabf-directed antibiotics in *Staphylococcus Aureus*. *Antimicrobial Agents and Chemotherapy*, 59 (2), 849–858. https://doi.org/10.1128/AAC.04179-14

Patkee, W. R. A., Carr, G., Baker, E. H., Baines, D. L. & Garnett, J. P. (2016). Metformin prevents the effects of *Pseudomonas aeruginosa* on airway epithelial tight junctions and restricts hyperglycaemia-induced bacterial growth. *Journal of Cellular and Molecular Medicine*, 20 (4), 758–764. https://doi.org/10.1111/jcmm.12784

Pechous, R. D. (2017). With friends like these: the complex role of neutrophils in the progression of severe pneumonia. *Frontiers in Cellular and Infection Microbiology*, *7*. https://doi.org/10.3389/fcimb.2017.00160

Pérez B., F., Méndez G., A., Lagos R., A. & Vargas M., S. L. (2014). Mucociliary clearance system in lung defense. *Revista Medica de Chile*, 142 (5), 606–615. https://doi.org/10.4067/S0034-98872014000500009

Pettigrew, M. M., Ahearn, C. P., Gent, J. F., Kong, Y., Gallo, M. C., Munro, J. B., D'Mello, A., Sethi, S., Tettelin, H. & Murphy, T. F. (2018). *Haemophilus influenzae* genome evolution during persistence in the human airways in chronic obstructive pulmonary disease. *Proceedings of the National Academy of Sciences of the United States of America*, 115 (14), E3256–E3265. https://doi.org/10.1073/pnas.1719654115

Pettigrew, M. M., Laufer, A. S., Gent, J. F., Kong, Y., Fennie, K. P. & Metlay, J. P. (2012). Upper respiratory tract microbial communities, acute otitis media pathogens, and antibiotic use in healthy and sick children. *Applied and Environmental Microbiology*, 78 (17), 6262–6270. https://doi.org/10.1128/AEM.01051-12

Pettigrew, M. M., Tsuji, B. T., Gent, J. F., Kong, Y., Holden, P. N., Sethi, S. & Murphy, T. F. (2016). Effect of fluoroquinolones and macrolides on eradication and resistance of *Haemophilus influenzae* in chronic obstructive pulmonary disease. *Antimicrobial Agents and Chemotherapy*, 60 (7), 4151–4158. https://doi.org/10.1128/AAC.00301-16

Pezzulo, A. A., Gutiérrez, J., Duschner, K. S., McConnell, K. S., Taft, P. J., Ernst, S. E., Yahr, T. L., Rahmouni, K., Klesney-Tait, J., Stoltz, D. A. & Zabner, J. (2011). Glucose depletion in the airway surface liquid is essential for sterility of the airways. *PloS One*, 6 (1), e16166. https://doi.org/10.1371/journal.pone.0016166

Philips, B. J., Meguer, J.-X., Redman, J. & Baker, E. H. (2003). Factors determining the appearance of glucose in upper and lower respiratory tract secretions. *Intensive Care Medicine*, 29 (12), 2204–2210. https://doi.org/10.1007/s00134-003-1961-2

Phillips, Z. N., Husna, A.-U., Jennings, M. P., Seib, K. L. & Atack, J. M. (2019). Phasevarions of bacterial pathogens - phase-variable epigenetic regulators evolving from restriction-modification systems. *Microbiology*, 165(9), 917–928. https://doi.org/10.1099/mic.0.000805

Pifer, M. L. & Smith, H. O. (1985). Processing of donor DNA during *Haemophilus influenzae* transformation: analysis using a model plasmid system. *Proceedings of the National Academy of Sciences of the United States of America*, 82 (11), 3731–3735. https://doi.org/10.1073/pnas.82.11.3731

Pinto, M., González-Díaz, A., Machado, M. P., Duarte, S., Vieira, L., Carriço, J. A., Marti, S., Bajanca-Lavado, M. P. & Gomes, J. P. (2019). Insights into the population structure and pan-genome of *Haemophilus influenzae*. *Infection, Genetics and Evolution*, 67, 126–135. https://doi.org/10.1016/j.meegid.2018.10.025

Pishchany, G., Mevers, E., Ndousse-Fetter, S., Horvath, D. J., Paludo, C. R., Silva-Junior, E. A., Koren, S., Skaar, E. P., Clardy, J. & Kolter, R. (2018). Amycomicin is a potent and specific antibiotic discovered with a targeted interaction screen. *Proceedings of the National Academy of Sciences of the United States of America*, 115 (40), 10124–10129. https://doi.org/10.1073/pnas.1807613115

Plusa, T. (2020). Azithromycin in the treatment of patients with exacerbation of chronic obstructive pulmonary disease. *Pol Merkur Lekarski*, 48 (283), 65–68. https://www.ncbi.nlm.nih.gov/pubmed/32218410

Poje, G. & Redfield, R. J. (2003). Transformation of *Haemophilus influenzae*. *Methods in Molecular Medicine*, 71, 57–70. https://doi.org/10.1385/1-59259-321-6:57

Post, D. M. B., Held, J. M., Ketterer, M. R., Phillips, N. J., Sahu, A., Apicella, M. A. & Gibson, B. W. (2014). Comparative analyses of proteins from *Haemophilus influenzae* biofilm and planktonic populations using metabolic labeling and mass spectrometry. *BMC Microbiology*, 14 (1), 1–16. https://doi.org/10.1186/s12866-014-0329-9

Post, D. M. B., Ketterer, M. R., Coffin, J. E., Reinders, L. M., Munson, R. S., Bair, T., Murphy, T. F., Foster, E. D., Gibson, B. W. & Apicella, M. A. (2016). Comparative analyses of the lipooligosaccharides from nontypeable *Haemophilus influenzae* and *Haemophilus haemolyticus* show differences in sialic acid and phosphorylcholine modifications. *Infection and Immunity*, 84 (3), 765–774. https://doi.org/10.1128/IAI.01185-15

Potts, C. C., Topaz, N., Rodriguez-Rivera, L. D., Hu, F., Chang, H. Y., Whaley, M. J., Schmink, S., Retchless, A. C., Chen, A., Ramos, E., Doho, G. H. & Wang, X. (2019). Genomic characterization of *Haemophilus influenzae*: a focus on the capsule locus. *BMC Genomics*, 20 (1), 1–9. https://doi.org/10.1186/s12864-019-6145-8

Powell, J. E., Leonard, S. P., Kwong, W. K., Engel, P. & Moran, N. A. (2016). Genome-wide screen identifies host colonization determinants in a bacterial gut symbiont. *Proceedings of the National Academy of Sciences of the United States of America*, 113 (48), 13887–13892. https://doi.org/10.1073/pnas.1610856113

Powell, M. & Livermore, D. M. (1988). Mechanisms of chloramphenicol resistance in *Haemophilus*

influenzae in the United Kingdom. *Journal of Medical Microbiology*, 27 (2), 89–93. https://doi.org/10.1099/00222615-27-2-89

Power, P. M., Bentley, S. D., Parkhill, J., Moxon, E. R. & Hood, D. W. (2012). Investigations into genome diversity of *Haemophilus influenzae* using whole genome sequencing of clinical isolates and laboratory transformants. *BMC Microbiology*, 12, 273. https://doi.org/10.1186/1471-2180-12-273

Power, P. M., Sweetman, W. A., Gallacher, N. J., Woodhall, M. R., Kumar, G. A., Moxon, E. R. & Hood, D. W. (2009). Simple sequence repeats in *Haemophilus influenzae*. *Infection, Genetics and Evolution*, 9 (2), 216–228. https://doi.org/10.1016/j.meegid.2008.11.006

Pramanik, J. & Keasling, J. D. (1997). Stoichiometric model of *Escherichia coli* metabolism: incorporation of growth-rate dependent biomass composition and mechanistic energy requirements. *Biotechnology and Bioengineering*, 56 (4), 398–421. https://doi.org/10.1002/(SICI)1097-0290(19971120)56:4<398::AID-BIT6>3.0.CO;2-J

Prasadarao, N. V., Lysenko, E., Wass, C. A., Kim, K. S. & Weiser, J. N. (1999). Opacity-associated protein A contributes to the binding of *Haemophilus influenzae* to chang epithelial cells. *Infection and Immunity*, 67 (8), 4153–4160. https://doi.org/10.1128/iai.67.8.4153-4160.1999

Preciado, D., Poley, M., Tsai, S., Tomney, A., Brown, K. & Val, S. (2016). A proteomic characterization of NTHi lysates. *International Journal of Pediatric Otorhinolaryngology*, 80, 8–16. https://doi.org/10.1016/j.ijporl.2015.11.016

Presta, L., Bosi, E., Mansouri, L., Dijkshoorn, L., Fani, R. & Fondi, M. (2017). Constraint-based modeling identifies new putative targets to fight colistin-resistant *A. baumannii* infections. *Scientific Reports*, 7 (1), 1–12. https://doi.org/10.1038/s41598-017-03416-2

Prevaes, S. M. P. J., De Winter-De Groot, K. M., Janssens, H. M., De Steenhuijsen Piters, W. A. A., Tramper-Stranders, G. A., Wyllie, A. L., Hasrat, R., Tiddens, H. A., Van Westreenen, M., Van Der Ent, C. K., Sanders, E. A. M. & Bogaert, D. (2016). Development of the nasopharyngeal microbiota in infants with cystic fibrosis. *American Journal of Respiratory and Critical Care Medicine*, 193 (5), 504–515. https://doi.org/10.1164/rccm.201509-1759OC

Price, C. E. & O'Toole, G. A. (2021). The gut-lung axis in cystic fibrosis. *Journal of Bacteriology*, 203 (20). https://doi.org/10.1128/jb.00311-21

Price, E. P., Sarovich, D. S., Nosworthy, E., Beissbarth, J., Marsh, R. L., Pickering, J., Kirkham, L.-A. S., Keil, A. D., Chang, A. B. & Smith-Vaughan, H. C. (2015). *Haemophilus influenzae*: using comparative genomics to accurately identify a highly recombinogenic human pathogen. *BMC Genomics*, 16 (1), 641. https://doi.org/10.1186/s12864-015-1857-x

Price, L. B., Hungate, B. A., Koch, B. J., Davis, G. S. & Liu, C. M. (2017). Colonizing opportunistic pathogens (COPs): the beasts in all of us. *PLoS Pathogens*, 13 (8), 1–8. https://doi.org/10.1371/journal.ppat.1006369

Puig, C., Tirado-Vélez, J. M., Calatayud, L., Tubau, F., Garmendia, J., Ardanuy, C., Marti, S., De La Campa, A. G. & Liñaresa, J. (2015). Molecular characterization of fluoroquinolone resistance in nontypeable *Haemophilus influenzae* clinical isolates. *Antimicrobial Agents and Chemotherapy*, 59 (1), 461–466. https://doi.org/10.1128/AAC.04005-14

PyMOL Molecular Graphics System, Version 1.5.0.4 Schrödinger, LLC.

Qiu, X., Janson, C. A., Konstantinidis, A. K., Nwagwu, S., Silverman, C., Smith, W. W., Khandekar, S., Lonsdale, J. & Abdel-Meguid, S. S. (1999). Crystal structure of β-ketoacyl-acyl carrier protein synthase III. A key condensing enzyme in bacterial fatty acid biosynthesis. *The Journal of Biological Chemistry*, 274 (51), 36465–36471. https://doi.org/10.1074/jbc.274.51.36465

Qu, J., Lesse, A. J., Brauer, A. L., Cao, J., Gill, S. R. & Murphy, T. F. (2010). Proteomic expression profiling of *Haemophilus influenzae* grown in pooled human sputum from adults with chronic obstructive pulmonary disease reveal antioxidant and stress responses. *BMC Microbiology*, 10, 162. https://doi.org/10.1186/1471-2180-10-162

Raetz, C. R. H., Reynolds, C. M., Trent, M. S. & Bishop, R. E. (2007). Lipid A modification systems in Gram-negative bacteria. *Annual Review of Biochemistry*, 76, 295–329. https://doi.org/10.1146/annurev.biochem.76.010307.145803

Raghunathan, A., Price, N. D., Galperin, M. Y., Makarova, K. S., Purvine, S., Picone, A. F., Cherny, T., Xie, T., Reilly, T. J., Munson, R., Tyler, R. E., Akerley, B. J., Smith, A. L., Palsson, B. O. & Kolker, E. (2004). *In silico* metabolic model and protein expression of *Haemophilus influenzae* strain Rd KW20 in rich medium. *OMICS A Journal of Integrative Biology*, 8 (1), 25–41. https://doi.org/10.1089/153623104773547471

Rajendra, K. C., Leong, K. W. C., Harkness, N. M., Lachowicz, J., Gautam, S. S., Cooley, L. A., McEwan, B., Petrovski, S., Karupiah, G. & O'toole, R. F. (2020). Whole-genome analyses reveal gene content differences between nontypeable *Haemophilus influenzae* isolates from chronic obstructive pulmonary disease compared to other clinical phenotypes. *Microbial Genomics*, 6 (8), 1–12. https://doi.org/10.1099/mgen.0.000405

Ramos, P. I. P., Fernández Do Porto, D., Lanzarotti, E., Sosa, E. J., Burguener, G., Pardo, A. M., Klein, C. C., Sagot, M. F., De Vasconcelos, A. T. R., Gales, A. C., Marti, M., Turjanski, A. G. & Nicolás, M. F. (2018). An integrative, multi-omics approach towards the prioritization of *Klebsiella pneumoniae* drug targets. *Scientific Reports*, 8 (1), 1–19. https://doi.org/10.1038/s41598-018-28916-7

Rana, P., Ghouse, S. M., Akunuri, R., Madhavi, Y. V., Chopra, S. & Nanduri, S. (2020). FabI (enoyl acyl carrier protein reductase) - A potential broad spectrum therapeutic target and its inhibitors. *European Journal of Medicinal Chemistry*, 208, 112757. https://doi.org/10.1016/j.ejmech.2020.112757

Rangelov, K. & Sethi, S. (2014). Role of infections. *Clinics in Chest Medicine*, 35 (1), 87–100. https://doi.org/10.1016/j.ccm.2013.09.012

Ratajczak, W., Rył, A., Mizerski, A., Walczakiewicz, K., Sipak, O. & Laszczyńska, M. (2019). Immunomodulatory potential of gut microbiome-derived shortchain fatty acids (SCFAs). *Acta Biochimica Polonica*, 66 (1), 1–12. https://doi.org/10.18388/abp.2018_2648

Reddy, M. S., Bernstein, J. M., Murphy, T. F. & Faden, H. S. (1996). Binding between outer membrane proteins of nontypeable *Haemophilus influenzae* and human nasopharyngeal mucin. *Infection and Immunity*, 64 (4), 1477–1479. https://doi.org/10.1128/iai.64.4.1477-1479.1996

Redfield, R. J., Cameron, A. D. S., Qian, Q., Hinds, J., Ali, T. R., Kroll, J. S. & Langford, P. R. (2005). A novel CRP-dependent regulon controls expression of competence genes in *Haemophilus influenzae*. *Journal of Molecular Biology*, 347 (4), 735–747. https://doi.org/10.1016/j.jmb.2005.01.012

Regueiro, V., Moranta, D., Frank, C. G., Larrarte, E., Margareto, J., March, C., Garmendia, J. & Bengoechea, J. A. (2011). *Klebsiella pneumoniae* subverts the activation of inflammatory responses in a NOD1-dependent manner. *Cellular Microbiology*, 13 (1), 135–153. https://doi.org/10.1111/j.1462-5822.2010.01526.x

Reynolds, H. Y. (1988). Immunoglobulin G and its function in the human respiratory tract. *Mayo Clinic Proceedings*, 63 (2), 161–174. https://doi.org/10.1016/s0025-6196(12)64949-0

Riesbeck, K. (2020). Complement evasion by the human respiratory tract pathogens *Haemophilus influenzae* and *Moraxella catarrhalis*. *FEBS Letters*, 594 (16), 2586–2597.

https://doi.org/10.1002/1873-3468.13758

Ritchie, A. I. & Wedzicha, J. A. (2020). Definition, causes, pathogenesis, and consequences of chronic obstructive pulmonary disease exacerbations. *Clinics in Chest Medicine*, 41 (3), 421–438. https://doi.org/10.1016/j.ccm.2020.06.007

Roberts, M. C., Soge, O. O. & No, D. B. (2011). Characterization of macrolide resistance genes in *Haemophilus influenzae* isolated from children with cystic fibrosis. *Journal of Antimicrobial Chemotherapy*, 66 (1), 100–104. https://doi.org/10.1093/jac/dkq425

Robledo-Avila, F. H., Ruiz-Rosado, J. de D., Partida-Sanchez, S. & Brockman, K. L. (2020). A bacterial epigenetic switch in non-typeable *Haemophilus influenzae* modifies host immune response during otitis media. *Frontiers in Cellular and Infection Microbiology*, 10, 512743. https://doi.org/10.3389/fcimb.2020.512743

Rodríguez-Arce, I., Al-Jubair, T., Euba, B., Fernández-Calvet, A., Gil-Campillo, C., Martí, S., Törnroth-Horsefield, S., Riesbeck, K. & Garmendia, J. (2019). Moonlighting of *Haemophilus influenzae* heme acquisition systems contributes to the host airway-pathogen interplay in a coordinated manner. *Virulence*, 10 (1), 315–333. https://doi.org/10.1080/21505594.2019.1596506

Rodríguez-Arce, I., Martí, S., Euba, B., Fernández-Calvet, A., Moleres, J., López-López, N., Barberán, M., Ramos-Vivas, J., Tubau, F., Losa, C., Ardanuy, C., Leiva, J., Yuste, J. E. & Garmendia, J. (2017). Inactivation of the thymidylate synthase *thyA* in non-typeable *Haemophilus influenzae* modulates antibiotic resistance and has a strong impact on its interplay with the host airways. *Frontiers in Cellular and Infection Microbiology*, 7. https://doi.org/10.3389/fcimb.2017.00266

Rodríguez-arce, I., Morales, X., Ariz, M., Euba, B., López-López, N., Esparza, M., Hood, D. W., Leiva, J., Ortíz-de-Solórzano, C. & Garmendia, J. (2021). Development and multimodal characterization of an elastase-induced emphysema mouse disease model for the COPD frequent bacterial exacerbator phenotype. *Virulence*, 12 (1), 1672–1688. https://doi.org/10.1080/21505594.2021.1937883

Rohmer, L., Hocquet, D. & Miller, S. I. (2011). Are pathogenic bacteria just looking for food? Metabolism and microbial pathogenesis. *Trends in Microbiology*, 19 (7), 341–348. https://doi.org/10.1016/j.tim.2011.04.003

Rosadini, C. V., Gawronski, J. D., Raimunda, D., Argüello, J. M. & Akerley, B. J. (2011). A novel zinc binding system, ZevAB, is critical for survival of nontypeable *Haemophilus influenzae* in a murine lung infection model. *Infection and Immunity*, 79 (8), 3366–3376. https://doi.org/10.1128/IAI.05135-11

Rutting, S., Xenaki, D., Malouf, M., Horvat, J. C., Wood, L. G., Hansbro, P. M. & Oliver, B. G. (2019). Short-chain fatty acids increase TNFα-induced inflammation in primary human lung mesenchymal cells through the activation of p38 mapk. *American Journal of Physiology - Lung Cellular and Molecular Physiology*, 316 (1), L157–L174. https://doi.org/10.1152/ajplung.00306.2018

Sadykov, M. R., Thomas, V. C., Marshall, D. D., Wenstrom, C. J., Moormeier, D. E., Widhelm, T. J., Nuxoll, A. S., Powers, R. & Bayles, K. W. (2013). Inactivation of the Pta-AckA pathway causes cell death in *Staphylococcus aureus*. *Journal of Bacteriology*, 195 (13), 3035–3044. https://doi.org/10.1128/JB.00042-13

Sánchez-Romero, M. A. & Casadesús, J. (2020). The bacterial epigenome. *Nature Reviews. Microbiology*, 18 (1), 7–20. https://doi.org/10.1038/s41579-019-0286-2

Sánchez-Romero, M. A., Cota, I. & Casadesús, J. (2015). DNA methylation in bacteria: from the

methyl group to the methylome. *Current Opinion in Microbiology*, 25, 9–16. https://doi.org/10.1016/j.mib.2015.03.004

Santana, E. A., Harrison, A., Zhang, X., Baker, B. D., Kelly, B. J., White, P., Liu, Y. & Munson, R. S. J. (2014). HrrF is the Fur-regulated small RNA in nontypeable *Haemophilus influenzae*. *PloS One*, 9 (8), e105644. https://doi.org/10.1371/journal.pone.0105644

Sarma, J. V. & Ward, P. A. (2011). The complement system. *Cell and Tissue Research*, 343(1), 227–235. https://doi.org/10.1007/s00441-010-1034-0

Schellenberger, J., Que, R., Fleming, R. M. T., Thiele, I., Orth, J. D., Feist, A. M., Zielinski, D. C., Bordbar, A., Lewis, N. E., Rahmanian, S., Kang, J., Hyduke, D. R. & Palsson, B. Ø. (2011). Quantitative prediction of cellular metabolism with constraint-based models: the COBRA Toolbox v2.0. *Nature Protocols*, 6 (9), 1290–1307. https://doi.org/10.1038/nprot.2011.308

Schilling, C. H. & Palsson, B. O. (2000). Assessment of the metabolic capabilities of *Haemophilus influenzae* Rd through a genome-scale pathway analysis. *Journal of Theoretical Biology*, 203 (3), 249–283. https://doi.org/10.1006/jtbi.2000.1088

Schlingmann, B., Molina, S. A. & Koval, M. (2015). Claudins: gatekeepers of lung epithelial function. *Seminars in Cell & Developmental Biology*, 42, 47–57. https://doi.org/10.1016/j.semcdb.2015.04.009

Schlör, S., Herbert, M., Rodenburg, M., Blass, J. & Reidl, J. (2000). Characterization of ferrochelatase (*hemH*) mutations in *Haemophilus influenzae*. *Infection and Immunity*, 68 (5), 3007–3009. https://doi.org/10.1128/IAI.68.5.3007-3009.2000

Schotte, L., Wautier, M., Martiny, D., Piérard, D. & Depypere, M. (2019). Detection of beta-lactamase-negative ampicillin resistance in *Haemophilus influenzae* in Belgium. *Diagnostic Microbiology and Infectious Disease*, 93 (3), 243–249. https://doi.org/10.1016/j.diagmicrobio.2018.10.009

Schüttelkopf, A. W. & van Aalten, D. M. F. (2004). PRODRG: a tool for high-throughput crystallography of protein-ligand complexes. *Acta Crystallographica. Section D, Biological Crystallography*, 60, 1355–1363. https://doi.org/10.1107/S0907444904011679

Schweda, E. K. H., Richards, J. C., Hood, D. W. & Moxon, E. R. (2007). Expression and structural diversity of the lipopolysaccharide of *Haemophilus influenzae*: implication in virulence. *International Journal of Medical Microbiology*, 297 (5), 297–306. https://doi.org/10.1016/j.ijmm.2007.03.007

Segal, L. N., Clemente, J. C., Tsay, J.-C. J., Koralov, S. B., Keller, B. C., Wu, B. G., Li, Y., Shen, N., Ghedin, E., Morris, A., Diaz, P., Huang, L., Wikoff, W. R., Ubeda, C., Artacho, A., Rom, W. N., Sterman, D. H., Collman, R. G., Blaser, M. J. & Weiden, M. D. (2016). Enrichment of the lung microbiome with oral taxa is associated with lung inflammation of a Th17 phenotype. *Nature Microbiology*, 1, 16031. https://doi.org/10.1038/nmicrobiol.2016.31

Segrè, D., Vitkup, D. & Church, G. M. (2002). Analysis of optimality in natural and perturbed metabolic networks. *Proceedings of the National Academy of Sciences of the United States of America*, 99 (23), 15112–15117. https://doi.org/10.1073/pnas.232349399

Seib, K. L., Srikhanta, Y. N., Atack, J. M. & Jennings, M. P. (2020). Epigenetic regulation of virulence and immunoevasion by phase-variable restriction-modification systems in bacterial pathogens. *Annual Review of Microbiology*, 74, 655–671. https://doi.org/10.1146/annurev-micro-090817-062346

Seif, Y., Kavvas, E., Lachance, J.-C., Yurkovich, J. T., Nuccio, S.-P., Fang, X., Catoiu, E., Raffatellu, M., Palsson, B. O. & Monk, J. M. (2018). Genome-scale metabolic reconstructions of multiple *Salmonella* strains reveal serovar-specific metabolic traits. *Nature Communications*, 9 (1),

3771. https://doi.org/10.1038/s41467-018-06112-5

Sethi, S., Evans, N., Grant, B. J. B. & Murphy, T. F. (2002). New strains of bacteria and exacerbations of chronic obstructive pulmonary disease. *The New England Journal of Medicine*, 347 (7), 465–471. https://doi.org/10.1056/NEJMoa012561

Sethi, S., Wrona, C., Eschberger, K., Lobbins, P., Cai, X. & Murphy, T. F. (2008). Inflammatory profile of new bacterial strain exacerbations of chronic obstructive pulmonary disease. *American Journal of Respiratory and Critical Care Medicine*, 177 (5), 491–497. https://doi.org/10.1164/rccm.200708-1234OC

Seyama, S., Wajima, T., Suzuki, M., Ushio, M., Fujii, T. & Noguchi, N. (2017). Emergence and molecular characterization of *Haemophilus influenzae* harbouring *mef*(A). *Journal of Antimicrobial Chemotherapy*, 72 (3), 948–949. https://doi.org/10.1093/jac/dkw501

Shannon, P., Markiel, A., Ozier, O., Baliga, N. S., Wang, J. T., Ramage, D., Amin, N., Schwikowski, B. & Ideker, T. (2003). Cytoscape: a software environment for integrated models of biomolecular interaction networks. *Genome Research*, 13 (11), 2498–2504. https://doi.org/10.1101/gr.1239303

Shehaj, L., Choudary, S. K., Makwana, K. M., Gallo, M. C., Murphy, T. F. & Kritzer, J. A. (2019). Small-molecule inhibitors of *Haemophilus influenzae* IgA1 Protease. *ACS Infectious Diseases*, 5 (7), 1129–1138. https://doi.org/10.1021/acsinfecdis.9b00004

Short, B., Carson, S., Devlin, A. C., Reihill, J. A., Crilly, A., MacKay, W., Ramage, G., Williams, C., Lundy, F. T., McGarvey, L. P., Thornbury, K. D. & Martin, S. L. (2021). Non-typeable *Haemophilus influenzae* chronic colonization in chronic obstructive pulmonary disease (COPD). *Critical Reviews in Microbiology*, 47 (2), 192–205. https://doi.org/10.1080/1040841X.2020.1863330

Shukla, S. D., Budden, K. F., Neal, R. & Hansbro, P. M. (2017). Microbiome effects on immunity, health and disease in the lung. *Clinical and Translational Immunology*, 6 (3), e133-12. https://doi.org/10.1038/cti.2017.6

Shukla, S. D., Fairbairn, R. L., Gell, D. A., Latham, R. D., Sohal, S. S., Walters, E. H. & O'Toole, R. F. (2016). An antagonist of the platelet-activating factor receptor inhibits adherence of both nontypeable *Haemophilus influenzae* and *Streptococcus pneumoniae* to cultured human bronchial epithelial cells exposed to cigarette smoke. *International Journal of COPD*, 11 (1), 1647–1655. https://doi.org/10.2147/COPD.S108698

Sibinelli-Sousa, S., Hespanhol, J. T. & Bayer-Santos, E. (2021). Targeting the achilles' heel of bacteria: different mechanisms to break down the peptidoglycan cell wall during bacterial warfare. *Journal of Bacteriology*, 203 (7). https://doi.org/10.1128/JB.00478-20

Siegel, S. J. & Weiser, J. N. (2015). Mechanisms of bacterial colonization of the respiratory tract. *Annual Review of Microbiology*, 69, 425–444. https://doi.org/10.1146/annurev-micro-091014-104209

Singh, B., Al-Jubair, T., Mörgelin, M., Thunnissen, M. M. & Riesbeck, K. (2013). The unique structure of *Haemophilus influenzae* protein E reveals multiple binding sites for host factors. *Infection and Immunity*, 81(3), 801–814. https://doi.org/10.1128/IAI.01111-12

Singh, N. K., Kunde, D. A. & Tristram, S. G. (2016). Effect of epithelial cell type on *in vitro* invasion of nontypeable *Haemophilus influenzae*. *Journal of Microbiological Methods*, 129, 66–69. https://doi.org/10.1016/j.mimet.2016.07.021

Sinha, S., Mell, J. C. & Redfield, R. J. (2012). Seventeen Sxy-dependent cyclic AMP receptor protein site-regulated genes are needed for natural transformation in *Haemophilus influenzae*. *Journal of Bacteriology*, 194 (19), 5245–5254. https://doi.org/10.1128/JB.00671-12

Sinha, S., Mell, J. & Redfield, R. (2013). The availability of purine nucleotides regulates natural competence by controlling translation of the competence activator Sxy. *Molecular Microbiology*, 88 (6), 1106–1119. https://doi.org/10.1111/mmi.12245

Slack, M. P. E, Cripps, A. W., Grimwood, K., Mackenzie, G. A. & Ulanova, M. (2021). Invasive *Haemophilus influenzae* infections after 3 decades of Hib protein conjugate Vaccine Use. *Clinical Microbiology Reviews*, 34 (3), e0002821. https://doi.org/10.1128/CMR.00028-21

Slack, M. P. E. (2015). A review of the role of *Haemophilus influenzae* in community-acquired pneumonia. *Pneumonia (Nathan),* 6, 26–43. doi: 10.15172/pneu.2015.6/520

Smith, A. L., Erwin, A. L., Kline, T., Unrath, W. C. T., Nelson, K., Weber, A. & Howald, W. N. (2007). Chloramphenicol is a substrate for a novel nitroreductase pathway in *Haemophilus influenzae*. *Antimicrobial Agents and Chemotherapy*, 51 (8), 2820–2829. https://doi.org/10.1128/AAC.00087-07

Smith, H. O., Tomb, J. F., Dougherty, B. A., Fleischmann, R. D. & Venter, J. C. (1995). Frequency and distribution of DNA uptake signal sequences in the *Haemophilus influenzae* Rd genome. *Science*, 269 (5223), 538–540. https://doi.org/10.1126/science.7542802

Sohn, M. J., Zheng, C. J. & Kim, W. G. (2008). Macrolactin S, a new antibacterial agent with FabG-inhibitory activity from *Bacillus* sp. AT28. *Journal of Antibiotics*, 61 (11), 687–691. https://doi.org/10.1038/ja.2008.98

Srikhanta, Y. N., Maguire, T. L., Stacey, K. J., Grimmond, S. M. & Jennings, M. P. (2005). The phasevarion: a genetic system controlling coordinated, random switching of expression of multiple genes. *Proceedings of the National Academy of Sciences of the United States of America*, 102 (15), 5547–5551. https://doi.org/10.1073/pnas.0501169102

Sriram, K. B., Cox, A. J., Clancy, R. L., Slack, M. P. E. & Cripps, A. W. (2018). Nontypeable *Haemophilus influenzae* and chronic obstructive pulmonary disease: a review for clinicians. *Critical Reviews in Microbiology*, 44 (2), 125–142. https://doi.org/10.1080/1040841X.2017.1329274

Stanton, T. B. (2013). A call for antibiotic alternatives research. *Trends in Microbiology*, 21 (3), 111–113. https://doi.org/10.1016/j.tim.2012.11.002

Staples, M., Graham, R. M. A. & Jennison, A. V. (2017). Characterisation of invasive clinical *Haemophilus influenzae* isolates in Queensland, Australia using whole-genome sequencing. *Epidemiology and Infection*, 145 (8), 1727–1736. https://doi.org/10.1017/S0950268817000450

Starner, T. D., Swords, W. E., Apicella, M. A. & McCray, P. B. (2002). Susceptibility of nontypeable *Haemophilus influenzae* to human β-defensins is influenced by lipooligosaccharide acylation. *Infection and Immunity*, 70 (9), 5287–5289. https://doi.org/10.1128/IAI.70.9.5287-5289.2002

Starner, T. D., Zhang, N., Kim, G. H., Apicella, M. A. & McCray, P. B. (2006). *Haemophilus influenzae* forms biofilms on airway epithelia: implications in cystic fibrosis. *American Journal of Respiratory and Critical Care Medicine*, 174 (2), 213–220. https://doi.org/10.1164/rccm.200509-1459OC

Steele, K. H., O'Connor, L. H., Burpo, N., Kohler, K. & Johnston, J. W. (2012). Characterization of a ferrous iron-responsive two-component system in nontypeable *Haemophilus influenzae*. *Journal of Bacteriology*, 194 (22), 6162–6173. https://doi.org/10.1128/JB.01465-12

Strunk, R. C., Eidlen, D. M. & Mason, R. J. (1988). Pulmonary alveolar type II epithelial cells synthesize and secrete proteins of the classical and alternative complement pathways. *Journal of Clinical Investigation*, 81 (5), 1419–1426. https://doi.org/10.1172/JCI113472

Su, M., Qiu, L., Deng, Y., Ruiz, C. H., Rudolf, J. D., Dong, L. Bin, Feng, X., Cameron, M. D., Shen,

B., Duan, Y. & Huang, Y. (2019). Evaluation of platensimycin and platensimycin-inspired thioether analogues against methicillin-resistant *Staphylococcus aureus* in topical and systemic infection mouse models. *Molecular Pharmaceutics*, 16 (7), 3065–3071 https://doi.org/10.1021/acs.molpharmaceut.9b00293

Su, Y.-C., Jalalvand, F., Thegerström, J. & Riesbeck, K. (2018). The interplay between immune response and bacterial infection in COPD: focus upon non-typeable *Haemophilus influenzae*. *Frontiers in Immunology*, 9, 2530. https://doi.org/10.3389/fimmu.2018.02530

Su, Y.-C., Resman, F., Hörhold, F. & Riesbeck, K. (2014). Comparative genomic analysis reveals distinct genotypic features of the emerging pathogen *Haemophilus influenzae* type f. *BMC Genomics*, 15 (1), 38. https://doi.org/10.1186/1471-2164-15-38

Su, Y. -C., Halang, P., Fleury, C., Jalalvand, F., Mörgelin, M. & Riesbeck, K. (2017). *Haemophilus protein* F orthologs of pathogens infecting the airways: exploiting host laminin at heparinbinding sites for maximal adherence to epithelial cells. *Journal of Infectious Diseases*, 216 (10), 1303–1307. https://doi.org/10.1093/infdis/jix467

Su, Y. -C., Jalalvand, F., Mörgelin, M., Blom, A. M., Singh, B. & Riesbeck, K. (2013). *Haemophilus influenzae* acquires vitronectin via the ubiquitous Protein F to subvert host innate immunity. *Molecular Microbiology*, 87 (6), 1245–1266. https://doi.org/10.1111/mmi.12164

Su, Y. -C., Jalalvand, F., Thegerström, J. & Riesbeck, K. (2018). The interplay between immune response and bacterial infection in COPD: focus upon non-typeable *Haemophilus influenzae*. *Frontiers in Immunology*, 9, 1–26. https://doi.org/10.3389/fimmu.2018.02530

Su, Y. -C., Mattsson, E., Singh, B., Jalalvand, F., Murphy, T. F. & Riesbeck, K. (2019). The laminin interactome: a multifactorial laminin-binding strategy by nontypeable *Haemophilus influenzae* for effective adherence and colonization. *Journal of Infectious Diseases*, 220 (6), 1049–1060. https://doi.org/10.1093/infdis/jiz217

Su, Y. -C., Mukherjee, O., Singh, B., Hallgren, O., Westergren-Thorsson, G., Hood, D. & Riesbeck, K. (2016). *Haemophilus influenzae* P4 interacts with extracellular matrix proteins promoting adhesion and serum resistance. *Journal of Infectious Diseases*, 213 (2), 314–323. https://doi.org/10.1093/infdis/jiv374

Su, Y. C., Resman, F., Hörhold, F. & Riesbeck, K. (2014). Comparative genomic analysis reveals distinct genotypic features of the emerging pathogen *Haemophilus influenzae* type f. *BMC Genomics*, 15 (1). https://doi.org/10.1186/1471-2164-15-38

Sutrina, S. L. & Scocca, J. J. (1976). Phospholipids of *Haemophilus influenzae* Rd during exponential growth and following the development of competence for genetic transformation. *Journal of General Microbiology*, 92 (2), 410–412. https://doi.org/10.1099/00221287-92-2-410

Swords, W. E., Buscher, B. A., Ver Steeg Li, K., Preston, A., Nichols, W. A., Weiser, J. N., Gibson, B. W. & Apicella, M. A. (2000). Non-typeable *Haemophilus influenzae* adhere to and invade human bronchial epithelial cells via an interaction of lipooligosaccharide with the PAF receptor. *Molecular Microbiology*, 37 (1), 13–27. https://doi.org/10.1046/j.1365-2958.2000.01952.x

Swords, W. E., Ketterer, M. R., Shao, J., Campbell, C. A., Weiser, J. N., & Apicella, M. A. (2001). Binding of the non-typeable *Haemophilus influenzae* lipooligosaccharide to the PAF receptor initiates host cell signalling. *Cellular Microbiology*, 3 (8), 525–536. https://doi.org/10.1046/j.1462-5822.2001.00132.x

Szelestey, B. R., Heimlich, D. R., Raffel, F. K., Justice, S. S. & Mason, K. M. (2013). *Haemophilus* responses to nutritional immunity: epigenetic and morphological contribution to biofilm architecture, invasion, persistence and disease severity. *PLoS Pathogens*, 9 (10).

https://doi.org/10.1371/journal.ppat.1003709

Szklarczyk, D., Gable, A. L., Lyon, D., Junge, A., Wyder, S., Huerta-Cepas, J., Simonovic, M., Doncheva, N. T., Morris, J. H., Bork, P., Jensen, L. J. & Mering, C. von. (2019). STRING v11: protein-protein association networks with increased coverage, supporting functional discovery in genome-wide experimental datasets. *Nucleic Acids Research*, 47 (1), D607–D613. https://doi.org/10.1093/nar/gky1131

Tacconelli, E., Carrara, E., Savoldi, A., Harbarth, S., Mendelson, M., Monnet, D. L., Pulcini, C., Kahlmeter, G., Kluytmans, J., Carmeli, Y., Ouellette, M., Outterson, K., Patel, J., Cavaleri, M., Cox, E. M., Houchens, C. R., Grayson, M. L., Hansen, P., Singh, N., et al. (2018). Discovery, research, and development of new antibiotics: the WHO priority list of antibiotic-resistant bacteria and tuberculosis. *The Lancet Infectious Diseases*, 18 (3), 318–327. https://doi.org/10.1016/S1473-3099(17)30753-3

Tanaka, E., Wajima, T., Nakaminami, H. & Noguchi, N. (2020). Whole-genome sequence of *Haemophilus influenzae* ST422 outbreak clone strain 2018-Y40 with low quinolone susceptibility isolated from a paediatric patient. *Journal of Global Antimicrobial Resistance*, 22, 759–761. https://doi.org/10.1016/j.jgar.2020.06.024

Tas, H., Grozinger, L., Stoof, R., de Lorenzo, V. & Goñi-Moreno, Á. (2021). Contextual dependencies expand the re-usability of genetic inverters. *Nature Communications*, 12 (1), 355. https://doi.org/10.1038/s41467-020-20656-5

Tatusov, R. L., Mushegian, A. R., Bork, P., Brown, N. P., Hayes, W. S., Borodovsky, M., Rudd, K. E. & Koonin, E. V. (1996). Metabolism and evolution of *Haemophilus influenzae* deduced from a whole-genome comparison with *Escherichia coli*. *Current Biology*, 6 (3), 279–291. https://doi.org/10.1016/s0960-9822(02)00478-5

Thiele, I. & Palsson, B. Ø. (2010). A protocol for generating a high-quality genome-scale metabolic reconstruction. *Nature Protocols*, 5 (1), 93–121. https://doi.org/10.1038/nprot.2009.203

Thofte, O., Bettoni, S., Su, Y.-C., Thegerström, J., Jonsson, S., Mattsson, E., Sandblad, L., Martí, S., Garmendia, J., Blom, A. M. & Riesbeck, K. (2021). Nontypeable *Haemophilus influenzae* P5 binds human C4b-binding protein, promoting serum resistance . *The Journal of Immunology*, 207 (6), 1566–1577. https://doi.org/10.4049/jimmunol.2100105

Thornton, D. J., Carlstedt, I., Howard, M., Devine, P. L., Price, M. R. & Sheehan, J. K. (1996). Respiratory mucins: identification of core proteins and glycoforms. *Biochemical Journal*, 316 (3), 967–975. https://doi.org/10.1042/bj3160967

Toraldo, D. M. & Conte, L. (2019). Influence of the lung microbiota dysbiosis in chronic obstructive pulmonary disease exacerbations: the controversial use of corticosteroid and antibiotic treatments and the role of eosinophils as a disease marker. *Journal of Clinical Medicine Research*, 11 (10), 667–675. https://doi.org/10.14740/jocmr3875

Tracy, E., Ye, F., Baker, B. D. & Munson, R. S. (2008). Construction of non-polar mutants in *Haemophilus influenzae* using FLP recombinase technology. *BMC Molecular Biology*, 9, 1–9. https://doi.org/10.1186/1471-2199-9-101

Tristram, S., Jacobs, M. R. & Appelbaum, P. C. (2007). Antimicrobial resistance in *Haemophilus influenzae*. *Clinical Microbiology Reviews*, 20 (2), 368–389. https://doi.org/10.1128/CMR.00040-06

Trott, O. & Olson, A. J. (2010). AutoDock Vina: improving the speed and accuracy of docking with a new scoring function, efficient optimization, and multithreading. *Journal of Computational Chemistry*, 31 (2), 455–461. https://doi.org/10.1002/jcc.21334

Tsang, R. S. W., Shuel, M., Ahmad, T., Hayden, K., Knox, N., Van Domselaar, G., Hoang, L.,

Tyrrell, G. J., Minion, J., Van Caeseele, P., Kus, J. V., Ulanova, M., Lefebvre, B., Haldane, D., Garceau, R., German, G., Zahariadis, G., Hanley, B., Kandola, K. & Patterson, M. (2020). Whole genome sequencing to study the phylogenetic structure of serotype a *Haemophilus influenzae* recovered from patients in Canada. *Canadian Journal of Microbiology*, 66 (2), 99–110. https://doi.org/10.1139/cjm-2019-0406

Turner, K. H., Everett, J., Trivedi, U., Rumbaugh, K. P. & Whiteley, M. (2014). Requirements for *Pseudomonas aeruginosa* acute burn and chronic surgical wound infection. *PLoS Genetics*, 10 (7), e1004518. https://doi.org/10.1371/journal.pgen.1004518

Ünal, C. M., Singh, B., Fleury, C., Singh, K., Chávez de Paz, L., Svensäter, G. & Riesbeck, K. (2012). QseC controls biofilm formation of non-typeable *Haemophilus influenzae* in addition to an AI-2-dependent mechanism. *International Journal of Medical Microbiology*, 302 (6), 261–269. https://doi.org/10.1016/j.ijmm.2012.07.013

van den Bergh, M. R., Biesbroek, G., Rossen, J. W. A., de Steenhuijsen Piters, W. A. A., Bosch, A. A. T. M., van Gils, E. J. M., Wang, X., Boonacker, C. W. B., Veenhoven, R. H., Bruin, J. P., Bogaert, D. & Sanders, E. A. M. (2012). Associations between pathogens in the upper respiratory tract of young children: interplay between viruses and bacteria. *PLoS ONE*, 7 (10). https://doi.org/10.1371/journal.pone.0047711

Van Eldere, J., Slack, M. P. E., Ladhani, S. & Cripps, A. W. (2014). Non-typeable *Haemophilus influenzae*, an under-recognised pathogen. *The Lancet Infectious Diseases*, 14 (12), 1281–1292. https://doi.org/10.1016/S1473-3099(14)70734-0

van Opijnen, T., Bodi, K. L. & Camilli, A. (2009). Tn-seq: high-throughput parallel sequencing for fitness and genetic interaction studies in microorganisms. *Nature Methods*, 6 (10), 767–772. https://doi.org/10.1038/nmeth.1377

van Opijnen, T. & Camilli, A. (2013). Transposon insertion sequencing: a new tool for systems-level analysis of microorganisms. *Nature reviews. Microbiology*, 11 (7), 435–442. https://doi.org/10.1038/nrmicro3033

VanWagoner, T. M., Atack, J. M., Nelson, K. L., Smith, H. K., Fox, K. L., Jennings, M. P., Stull, T. L. & Smith, A. L. (2016). The *modA10* phasevarion of nontypeable *Haemophilus influenzae* R2866 regulates multiple virulence-associated traits. *Microbial Pathogenesis*, 92, 60–67. https://doi.org/10.1016/j.micpath.2015.12.006

Varsano, S., Kaminsky, M., Kaiser, M. & Rashkovsky, L. (2000). Generation of complement C3 and expression of cell membrane complement inhibitory proteins by human bronchial epithelium cell line. *Thorax*, 55 (5), 364–369. https://doi.org/10.1136/thorax.55.5.364

Vella, P., Rudraraju, R. S., Lundbäck, T., Axelsson, H., Almqvist, H., Vallin, M., Schneider, G. & Schnell, R. (2021). A FabG inhibitor targeting an allosteric binding site inhibits several orthologs from Gram-negative ESKAPE pathogens. *Bioorganic and Medicinal Chemistry*, 30, 115898. https://doi.org/10.1016/j.bmc.2020.115898

Verhaegh, S. J. C., Flores, A. R., van Belkum, A., Musser, J. M. & Hays, J. P. (2013). Differential virulence gene expression of group A *Streptococcus* serotype M3 in response to co-culture with *Moraxella catarrhalis*. *PLoS ONE*, *8* (4), 1–8. https://doi.org/10.1371/journal.pone.0062549

Vestergaard, M., Nøhr-Meldgaard, K., Bojer, M. S., Krogsgård Nielsen, C., Meyer, R. L., Slavetinsky, C., Peschel, A. & Ingmer, H. (2017). Inhibition of the ATP synthase eliminates the intrinsic resistance of *Staphylococcus aureus* towards polymyxins. *MBio*, 8 (5). https://doi.org/10.1128/mBio.01114-17

Volanakis, J. E. (1995). Transcriptional regulation of complement genes. *Annual Review of Immunology*, 13, 277–305. https://doi.org/10.1146/annurev.iy.13.040195.001425

Voynow, J. A. & Mengr, B. K. R. (2009). Mucins, mucus, and sputum. *Chest*, 135 (2), 505–512. https://doi.org/10.1378/chest.08-0412

Vuong, J., Wang, X., Theodore, J. M., Whitmon, J., de Leon, P. G., Mayer, L. W., Carlone, G. M. & Romero-Steiner, S. (2013). Absence of high molecular weight proteins 1 and/or 2 is associated with decreased adherence among non-typeable *Haemophilus influenzae* clinical isolates. *Journal of Medical Microbiology*, 62, 1649–1656. https://doi.org/10.1099/jmm.0.058222-0

Wall, D. P., Fraser, H. B. & Hirsh, A. E. (2003). Detecting putative orthologs. *Bioinformatics*, 19 (13), 1710–1711. https://doi.org/10.1093/bioinformatics/btg213

Wang, H. & Cronan, J. E. (2003). *Haemophilus influenzae* Rd lacks a stringently conserved fatty acid biosynthetic enzyme and thermal control of membrane lipid composition. *Journal of Bacteriology*, 185 (16), 4930–4937. https://doi.org/10.1128/JB.185.16.4930-4937.2003

Wang, J., Ye, X., Yang, X., Cai, Y., Wang, S., Tang, J., Sachdeva, M., Qian, Y., Hu, W., Leeds, J. A. & Yuan, Y. (2020). Discovery of novel antibiotics as covalent inhibitors of fatty acid synthesis. *ACS Chemical Biology*, 15 (7), 1826–1834. https://doi.org/10.1021/acschembio.9b00982

Wang, J., Kodali, S., Sang, H. L., Galgoci, A., Painter, R., Dorso, K., Racine, F., Motyl, M., Hernandez, L., Tinney, E., Colletti, S. L., Herath, K., Cummings, R., Salazar, O., González, I., Basilio, A., Vicente, F., Genilloud, O., Pelaez, F., et al. (2007). Discovery of platencin, a dual FabF and FabH inhibitor with *in vivo* antibiotic properties. *Proceedings of the National Academy of Sciences of the United States of America*, 104 (18), 7612–7616. https://doi.org/10.1073/pnas.0700746104

Wang, J., Soisson, S. M., Young, K., Shoop, W., Kodali, S., Galgoci, A., Painter, R., Parthasarathy, G., Tang, Y. S., Cummings, R., Ha, S., Dorso, K., Motyl, M., Jayasuriya, H., Ondeyka, J., Herath, K., Zhang, C., Hernandez, L., Allocco, J., et al. (2006). Platensimycin is a selective FabF inhibitor with potent antibiotic properties. *Nature*, 441 (7091), 358–361. https://doi.org/10.1038/nature04784

Wang, Y. T., Shi, T. Q., Fu, J. & Zhu, H. L. (2019). Discovery of novel bacterial FabH inhibitors (Pyrazol-Benzimidazole amide derivatives): design, synthesis, bioassay, molecular docking and crystal structure determination. *European Journal of Medicinal Chemistry*, 171, 209–220. https://doi.org/10.1016/j.ejmech.2019.03.026

Wang, Z., Bafadhel, M., Haldar, K., Spivak, A., Mayhew, D., Miller, B. E., Tal-Singer, R., Johnston, S. L., Ramsheh, M. Y., Barer, M. R., Brightling, C. E. & Brown, J. R. (2016). Lung microbiome dynamics in COPD exacerbations. *European Respiratory Journal*, 47 (4), 1082–1092. https://doi.org/10.1183/13993003.01406-2015

Watson, M. E., Burns, J. L. & Smith, A. L. (2004a). Hypermutable *Haemophilus influenzae* with mutations in *mutS* are found in cystic fibrosis sputum. *Microbiology*, 150 (9), 2947–2958. https://doi.org/10.1099/mic.0.27230-0

Watson, M. E., Jarisch, J. & Smith, A. L. (2004b). Inactivation of deoxyadenosine methyltransferase (*dam*) attenuates *Haemophilus influenzae* virulence. *Molecular Microbiology*, 53 (2), 651–664. https://doi.org/10.1111/j.1365-2958.2004.04140.x

Wedzicha, J. A. & Seemungal, T. A. R. (2007). COPD exacerbations: defining their cause and prevention. *Lancet (London, England)*, 370 (9589), 786–796. https://doi.org/10.1016/S0140-6736(07)61382-8

Weinberg, E. D. (1975). Nutritional immunity. Host's attempt to withold iron from microbial invaders. *JAMA*, 231 (1), 39–41. doi:10.1001/jama.1975.03240130021018

Weiser, J. N., Pan, N., McGowan, K. L., Musher, D., Martin, A. & Richards, J. (1998).

Phosphorylcholine on the lipopolysaccharide of *Haemophilus influenzae* contributes to persistence in the respiratory tract and sensitivity to serum killing mediated by C-reactive protein. *Journal of Experimental Medicine*, 187 (4), 631–640. https://doi.org/10.1084/jem.187.4.631

Wen, S., Feng, D., Chen, D., Yang, L. & Xu, Z. (2020). Molecular epidemiology and evolution of *Haemophilus influenzae*. *Infection, Genetics and Evolution*, 80, 104205. https://doi.org/10.1016/j.meegid.2020.104205

West, S. A., Griffin, A. S., Gardner, A. & Diggle, S. P. (2006). Social evolution theory for microorganisms. *Nature Reviews Microbiology*, 4 (8), 597–607. https://doi.org/10.1038/nrmicro1461

Whitby, P. W., Seale, T. W., VanWagoner, T. M., Morton, D. J. & Stull, T. L. (2009). The iron/heme regulated genes of *Haemophilus influenzae*: comparative transcriptional profiling as a tool to define the species core modulon. *BMC Genomics*, 10, 1–19. https://doi.org/10.1186/1471-2164-10-6

Whitby, P. W., Vanwagoner, T. M., Seale, T. W., Morton, D. J. & Stull, T. L. (2006). Transcriptional profile of *Haemophilus influenzae*: effects of iron and heme. *Journal of Bacteriology*, 188 (15), 5640–5645. https://doi.org/10.1128/JB.00417-06

Whitby, P. W., VanWagoner, T. M., Seale, T. W., Morton, D. J. & Stull, T. L. (2013). Comparison of transcription of the *Haemophilus influenzae* iron/heme modulon genes *in vitro* and *in vivo* in the chinchilla middle ear. *BMC Genomics*, 14, 925. https://doi.org/10.1186/1471-2164-14-925

White, K. A., Kaltashov, I. A., Cotter, R. J. & Raetz, C. R. H. (1997). A mono-functional 3-deoxy-D-manno-octulosonic acid (Kdo) transferase and a Kdo kinase in extracts of *Haemophilus influenzae*. *Journal of Biological Chemistry*, 272 (26), 16555–16563. https://doi.org/10.1074/jbc.272.26.16555

Whitsett, J. A. (2018). Airway epithelial differentiation and mucociliary clearance. *Annals of the American Thoracic Society*, 15, S143–S148. https://doi.org/10.1513/AnnalsATS.201802-128AW

Whitsett, J. A. & Weaver, T. E. (2002). Hydrophobic surfactant proteins in lung function and disease. *The New England Journal of Medicine*, 347 (26), 2141–2148. https://doi.org/10.1056/NEJMra022387

Williams, J. D. & Moosdeen, F. (1986). Antibiotic resistance in *Haemophilus influenzae*, epidemiology, mechanisms, and therapeutic possibilities. *Reviews of Infectious Diseases*, 8, 555–561. https://doi.org/10.1093/clinids/8.Supplement_5.S555

Wolfe, A. J. (2005). The acetate switch. *Microbiology and Molecular Biology Reviews*, 69 (1), 12–50. https://doi.org/10.1128/mmbr.69.1.12-50.2005

Wong, S. M., Bernui, M., Shen, H. & Akerley, B. J. (2013a). Genome-wide fitness profiling reveals adaptations required by *Haemophilus* in coinfection with influenza A virus in the murine lung. *Proceedings of the National Academy of Sciences of the United States of America*, 110 (38), 15413–15418. https://doi.org/10.1073/pnas.1311217110

Wong, S. M., Jackson, M. D. & Akerley, B. J. (2019). Suppression of alternative lipooligosaccharide glycosyltransferase activity by UDP-galactose epimerase enhances murine lung infection and evasion of serum IgM. *Frontiers in Cellular and Infection Microbiology*, 9, 160. https://doi.org/10.3389/fcimb.2019.00160

Wong, S. M. S. & Akerley, B. J. (2012). Genome-scale approaches to identify genes essential for *Haemophilus influenzae* pathogenesis. *Frontiers in Cellular and Infection Microbiology*, 2, 23. https://doi.org/10.3389/fcimb.2012.00023

Wong, S. M. S., Alugupalli, K. R., Ram, S. & Akerley, B. J. (2007). The ArcA regulon and oxidative stress resistance in *Haemophilus influenzae*. *Molecular Microbiology*, 64 (5), 1375–1390. https://doi.org/10.1111/j.1365-2958.2007.05747.x

Wong, S. M. S., St. Michael, F., Cox, A., Ram, S. & Akerley, B. J. (2011). ArcA-regulated glycosyltransferase Lic2B promotes complement evasion and pathogenesis of nontypeable *Haemophilus influenzae*. *Infection and Immunity*, 79 (5), 1971–1983. https://doi.org/10.1128/IAI.01269-10

Wright, J. R. (2005). Immunoregulatory functions of surfactant proteins. *Nature Reviews Immunology*, 5 (1), 58–68. https://doi.org/10.1038/nri1528

Yamasaki, K. & Van Eeden, S. F. (2018). Lung macrophage phenotypes and functional responses: role in the pathogenesis of COPD. *International Journal of Molecular Sciences*, 19 (2), 1–12. https://doi.org/10.3390/ijms19020582

Yang, Y. S., Su, M. M., Xu, J. F., Liu, Q. X., Bai, L. F., Hu, X. W. & Zhu, H. L. (2019). Discovery of novel oxoindolin derivatives as atypical dual inhibitors for DNA Gyrase and FabH. *Bioorganic Chemistry*, 93, 103309. https://doi.org/10.1016/j.bioorg.2019.103309

Yao, J. & Rock, C. O. (2015). How bacterial pathogens eat host lipids: implications for the development of fatty acid synthesis therapeutics. *Journal of Biological Chemistry*, 290 (10), 5940–5946. https://doi.org/10.1074/jbc.R114.636241

Yao, J. & Rock, C. O. (2017). Bacterial fatty acid metabolism in modern antibiotic discovery. *Biochimica et Biophysica Acta. Molecular and Cell Biology of Lipids*, 1862 (11), 1300–1309. https://doi.org/10.1016/j.bbalip.2016.09.014

Yesilkaya, H., Spissu, F., Carvalho, S. M., Terra, V. S., Homer, K. A., Benisty, R., Porat, N., Neves, A. R. & Andrew, P. W. (2009). Pyruvate formate lyase is required for pneumococcal fermentative metabolism and virulence. *Infection and Immunity*, 77 (12), 5418–5427. https://doi.org/10.1128/IAI.00178-09

Yoon, B. K., Jackman, J. A., Valle-González, E. R. & Cho, N. J. (2018). Antibacterial free fatty acids and monoglycerides: biological activities, experimental testing, and therapeutic applications. In *International Journal of Molecular Sciences*, 19 (4). https://doi.org/10.3390/ijms19041114

Young, K., Jayasuriya, H., Ondeyka, J. G., Herath, K., Zhang, C., Kodali, S., Galgoci, A., Painter, R., Brown-Driver, V., Yamamoto, R., Silver, L. L., Zheng, Y., Ventura, J. I., Sigmund, J., Ha, S., Basilio, A., Vicente, F., Tormo, J. R., Pelaez, F., et al. (2006). Discovery of FabH/FabF inhibitors from natural products. *Antimicrobial Agents and Chemotherapy*, 50 (2), 519–526. https://doi.org/10.1128/AAC.50.2.519-526.2006

Yun, Y., Srinivas, G., Kuenzel, S., Linnenbrink, M., Alnahas, S., Bruce, K. D., Steinhoff, U., Baines, J. F. & Schaible, U. E. (2014). Environmentally determined differences in the murine lung microbiota and their relation to alveolar architecture. *PLoS ONE*, 9 (12), 1–24. https://doi.org/10.1371/journal.pone.0113466

Zanetti, M. (2004). Cathelicidins, multifunctional peptides of the innate immunity. *Journal of Leukocyte Biology*, 75 (1), 39–48. https://doi.org/10.1189/jlb.0403147

Zhang, H., He, F., Li, P., Hardwidge, P. R., Li, N. & Peng, Y. (2021). The role of innate immunity in pulmonary infections. *BioMed Research International*, 2021, 11–13. https://doi.org/10.1155/2021/6646071

Zhang, L., Patel, M., Xie, J., Davis, G. S., Marrs, C. F. & Gilsdorf, J. R. (2013). Urease operon and urease activity in commensal and disease-causing nontypeable *Haemophilus influenzae*. *Journal of Clinical Microbiology*, 51 (2), 653–655. https://doi.org/10.1128/JCM.03145-12

Zhang, P., Summer, W. R., Bagby, G. J. & Nelson, S. (2000). Innate immunity and pulmonary host defense. *Immunological Reviews*, 173, 39–51. https://doi.org/10.1034/j.1600-065X.2000.917306.x

Zhang, Y. M. & Rock, C. O. (2004). Evaluation of epigallocatechin gallate and related plant polyphenols as inhibitors of the FabG and FabI reductases of bacterial type II fatty-acid synthase. *Journal of Biological Chemistry*, 279 (30), 30994–31001. https://doi.org/10.1074/jbc.M403697200

Zhou, Y., Yang, Y. S., Song, X. Da, Lu, L. & Zhu, H. L. (2017). Study of Schiff-base-derived with dioxygenated rings and nitrogen heterocycle as potential β-ketoacyl-acyl carrier protein synthase III (FabH) inhibitors. *Chemical and Pharmaceutical Bulletin*, 65 (2), 178–185. https://doi.org/10.1248/cpb.c16-00772

Zitko, J., Jand'Ourek, O., Paterová, P., Navrátilová, L., Kuneš, J., Vinšová, J. & Doležal, M. (2018). Design, synthesis and antimycobacterial activity of hybrid molecules combining pyrazinamide with a 4-phenylthiazol-2-amine scaffold. *MedChemComm*, 9 (4), 685–696. https://doi.org/10.1039/c8md00056e

Zomer, A., Burghout, P., Bootsma, H. J., Hermans, P. W. M. & van Hijum, S. A. F. T. (2012). Essentials: software for rapid analysis of high throughput transposon insertion sequencing data. *PLoS ONE*, 7 (8), 1–9. https://doi.org/10.1371/journal.pone.0043012

Zoon, K. C. & Scocca, J. J. (1975). Constitution of the cell envelope of *Haemophilus influenzae* in relation to competence for genetic transformation. *Journal of Bacteriology*, 123 (2), 666–677. https://doi.org/10.1128/jb.123.2.666-677.1975

Zwama, M., Yamaguchi, A. & Nishino, K. (2019). Phylogenetic and functional characterisation of the *Haemophilus influenzae* multidrug efflux pump AcrB. *Communications Biology*, 2, 340. https://doi.org/10.1038/s42003-019-0564-6

Anexo I:

Tablas Suplementarias

Tabla A1. Composición del medio de inducción de competencia de *Haemophilus influenzae*, MIV.

Componente	**[µg/mL]**
Ácido L-aspártico	4032
Ácido L-Glutámico	314
L-Arginina	21
L-Citrulina	12
Glicina	2,5
L-Lisina	35
L-Metionina	18
L-Serina	65
L-Leucina	61
L-Tirosina	42
L-Histidina	13
L-Cistina	6
L-Fenilalanina	46
L-Treonina	20
L-Isoleucina	33
L-Valina	35
L-Alanina	48
L-Prolina, hidroxiprolina	50
Ácido fumárico	1000
Tween 80	200
	[M]
NaCl	0,08
MgSO4	5 x 10-4
CaCl2	0,001
KH2PO4-K2HPO4	0,01

Tablas Suplementarias

Table A2. Primers used in Chapter 2.

Primer name	Primer ID	Primer sequence (5'-3')	Purpose	Source
HI0125-qPCR-F	2039	CGTGAGCGATATTGGATGGT	qRT-PCR	This study
HI0125-qPCR-R	2040	GCAGTATTCTTAATGGGGGTTG	qRT-PCR	This study
tbp1-qPCR-F3	1471	AAGTAAGAGATCGTAAAGATAATGAAGTAACTG	qRT-PCR	(Whitby et al., 2013a)
tbp1-qPCR-R3	1472	ACCGCGACCTTGTTCTACAACT	qRT-PCR	(Whitby et al., 2013a)
purM-qPCR-F	2025	TTGAGCCGAGTGCGATAAG	qRT-PCR	This study
purM-qPCR-R	2026	TGCCAGGAATGTATCACGAA	qRT-PCR	This study
purE-qPCR-F	2035	CATGTGGAAATCGTCTCTGCT	qRT-PCR	This study
purE-qPCR-R	2036	ATCATGCCGGGTAAATGTG	qRT-PCR	This study
purH-qPCR-F	1835	CTGCTGGAAAGTGGCAAAA	qRT-PCR	This study
purH-qPCR-R	1836	GGAATGGGAAGAACGCATC	qRT-PCR	This study
purK-qPCR-F	2037	GAAATTGAACGCTGGGAAAA	qRT-PCR	This study
purK-qPCR-R	2038	CACCAAGGCGAGGTAGAAAG	qRT-PCR	This study
purN-qPCR-F	2027	ACGGGTTTTAGCCTCCACTT	qRT-PCR	This study
purN-qPCR-R	2028	AGATGGTGGTGCGATTGTCT	qRT-PCR	This study
purD-qPCR-F	2021	GCCTAACGCAGTCACACAAA	qRT-PCR	This study
purD-qPCR-R	2022	GCCTAAAAGTGCGGTCAAAA	qRT-PCR	This study
purL-qPCR-F	2029	AGCAGCACCACCACCTAAAC	qRT-PCR	This study
purL-qPCR-R	2030	ACAGGTTCAAAAAGGCGAAA	qRT-PCR	This study
tonB-qPCR-F	1414	GCTACCAAAAGGCGATGAAA	qRT-PCR	(Rodríguez-Arce et al., 2019)
tonB-qPCR-R	1415	TCCGTTCCACTTCCTGCTAC	qRT-PCR	(Rodríguez-Arce et al., 2019)
comC-qPCR-F	2013	ATCGAGGGGAGTTCACGTTT	qRT-PCR	This study
comC-qPCR-R	2014	TTTTCGACTTTCCGACTGCT	qRT-PCR	This study
comD-qPCR-F	1827	GCACAAACAGTAATGGAGCAAA	qRT-PCR	This study
comD-qPCR-R	1828	GAAATCACTACCCCCACCAA	qRT-PCR	This study
comF-qPCR-F	2017	GCAATATCGTAAAGCGTGTGAA	qRT-PCR	This study
comF-qPCR-R	2018	CATCATCCACCAACGCAAC	qRT-PCR	This study
rec2-qPCR-F	1829	ATTGGAAAGCGAAAGAGGTG	qRT-PCR	This study
rec2-qPCR-R	1830	TACCATTGTTGCCGATCAAA	qRT-PCR	This study
purC-qPCR-F	2023	ATAAGCGGTCAGAAGCAACC	qRT-PCR	This study
purC-qPCR-R	2024	TGACACAACAACTCCCCATTT	qRT-PCR	This study
dprA-qPCR-F	1833	TCAAGGTTGTCATCGCCTAA	qRT-PCR	This study
dprA-qPCR-R	1834	CGAGCAACTGAACAAGCAAA	qRT-PCR	This study
comB-qPCR-F	1831	GTAACGCGCAAGATCAAACA	qRT-PCR	This study
comB-qPCR-R	1832	CCCCTTGTTCCACATCAAA	qRT-PCR	This study
hisG-qPCR-F	1951	GGCGAAAATGTGTTAGAAGAGG	qRT-PCR	This study
hisG-qPCR-R	1952	GACGACAATCACCAAAATCAAG	qRT-PCR	This study
comE-qPCR-F	2015	GGTTCTCGTGTCGCTTATGG	qRT-PCR	This study
comE-qPCR-R	2016	CTTCGCTTTTCGTGATTGTG	qRT-PCR	This study

qseC-qPCR-F	1955	AAGGAGAAAATCTGGCGATG	qRT-PCR	This study
qseC-qPCR-R	1956	CATAGCTGAAGTGCGGTCAA	qRT-PCR	This study
purF-qPCR-F	2033	CACAAACTCGAAACCCACAA	qRT-PCR	This study
purF-qPCR-R	2034	AAACGTGAAGAAAATGGCAAA	qRT-PCR	This study
oppA-qPCR-F	1953	GGCTGAATTAGGCGTGGA	qRT-PCR	This study
oppA-qPCR-R	1954	GTTTTCAATGGCGAGGAATG	qRT-PCR	This study
toxA-qPCR-F	2019	CACGCATTGAAAAAGGACAA	qRT-PCR	This study
toxA-qPCR-R	2020	CTTAGAGGCACAATCGACAGG	qRT-PCR	This study
cvpA-qPCR-F	2031	TTTGCGTAAGATAAGTGGCAAG	qRT-PCR	This study
cvpA-qPCR-R	2032	ACTTGGTAGCTGGGTTGTGG	qRT-PCR	This study
pilA-qPCR-F	2011	CCACTATCGCAATTCCCTCTT	qRT-PCR	This study
pilA-qPCR-R	2012	TCCACCCGTACAGTTTGTTG	qRT-PCR	This study
glpQ-qPCR-F	1959	CCCAAATGAAATCAGACAAAATC	qRT-PCR	This study
glpQ-qPCR-R	1960	GCAACATCAGTCAAGCCATC	qRT-PCR	This study
pta-qPCR-F	1856	CTACATCAGCACCGCTACCA	qRT-PCR	(López-López et al., 2020)
pta-qPCR-R	1857	CACCACTGCAAACACCATTC	qRT-PCR	(López-López et al., 2020)
bamE-qPCR-F	2003	GCCTCGCTTCTTGTTCCAC	qRT-PCR	This study
bamE-qPCR-R	2004	CGCCTCTAAATAGTTGCCTTG	qRT-PCR	This study
sdaC-qPCR-F	2001	TTTGGTAAAACAGCGGGTAAA	qRT-PCR	This study
sdaC-qPCR-R	2002	CCGTAAATCAACAGAATAGGGAAA	qRT-PCR	This study
hbpA-qPCR-F2	1613	CTGGATCGTACGGATAATCTTGG	qRT-PCR	(Rodríguez-Arce et al., 2019
hbpA-qPCR-R2	1614	AAGGCGCAGGAATATCAGCTAA	qRT-PCR	(Rodríguez-Arce et al., 2019
gyrA-qPCR-F2	1078	ATATGTTGGTTGATGGGCAAGG	qRT-PCR	(Moleres et al., 2018)
gyrA-qPCR-R2	1079	GGCGAGAAATTGACGGTTTCT	qRT-PCR	(Moleres et al., 2018)
purH-F1	1809	CAGATCCACAAGTGCAACAGCAATTTC	Disruption cassette	This study
purH-R1	1810	CGTAGCATTATTGGCTGCGTTTCTGGA	Disruption cassette	This study
purH-F2	1811	TGGCATCTGATGCGTTCTTCCCATTCC	Disruption cassette	This study
purH-R2	1812	ACCTTGAGCAAACTCTACAATACCCGT	Disruption cassette	This study
comD-F1	1760	TGGCGTACTTATCAACATCAAAAGCGT	Disruption cassette	This study
comD-R1	1761	TAGAAATATGTGGCGTCACTTCCAAAC	Disruption cassette	This study
comD-F2	1776	CAATGTTCAATTTATGCGTAAGCTAGG	Disruption cassette	This study
comD-R2	1777	TCAAACTGAGAACGGTTACGCTGTGTT	Disruption cassette	This study
rec2-F1	1764	CACATTTTTATCATAGCGACGTGTTTG	Disruption cassette	This study
rec2-R1	1765	ACATGCTGCCATTCCACTTTGAAATTG	Disruption cassette	This study
rec2-F2	1780	CATCGACAAGTGAATACTTGCTTTCTC	Disruption cassette	This study
rec2-R2	1781	TCTCCAATGTTGCTGTGGCGATAAGCG	Disruption cassette	This study
dprA-F1	1768	AATGCCTGTACGGCCTGCATCTTCGCA	Disruption cassette	This study
dprA-R1	1769	CCAGCGTATCTGGTTTAGCAATATACA	Disruption cassette	This study
dprA-F2	1784	GTTACACGCCAGTGAGCATTGATGATT	Disruption cassette	This study
dprA-R2	1785	CAACATCATCATAATTAAGTAATTCAT	Disruption cassette	This study

Tablas Suplementarias

comB-F1	1766	AGAGACCTATGATTTGGCTGTTAAGTA	Disruption cassette	This study
comB-R1	1767	CTATCACATTGCTCTCCTAGCTTACGC	Disruption cassette	This study
comB-F2	1782	GTCAGGTTCAACCTGAACAAGATACAT	Disruption cassette	This study
comB-R2	1783	GCTAAAAGCCAACATTAAATTAATAGC	Disruption cassette	This study
comE-F1	1770	GTTCAACCTGAACAAGATACATTGTTT	Disruption cassette	This study
comE-R1	1771	CACATTCCGCATTAGGCGTACCAGGAT	Disruption cassette	This study
comE-F2	1786	CTATTGATAAACAAGAAATTAATACTC	Disruption cassette	This study
comE-R2	1787	TATATCTCCAATCACTAAATTCACATC	Disruption cassette	This study
qseBC-F1	1937	AGGCGAGGGAATTTCCCAAGAT	Disruption cassette	This study
qseBC-R1	1938	CGCTAAACACATCACCACAACA	Disruption cassette	This study
qseBC-F2 (2)	2045	TGCGAATTGCGGAATTACACGAA	Disruption cassette	This study
qseBC-R2 (2)	2046	CAAAACCAAGTTTAGTTAAACCA	Disruption cassette	This study
glpQ-F1	1575	ATTTTCTTCAGCACTCACGGTATTG	Disruption cassette	This study
*glp*Q-R1	1572	TAAATTGCCGCCAATTGCTTTTTTG	Disruption cassette	This study
glpQ -F2	1576	CTAAAAACCTCATAAAAATTTACCGCACTCTCAAGGAGAA AATACTTATGATTCCGGGGATCCGTCGACC	Disruption cassette	This study
glpQ-R2	1577	GGTATGTTTACCTACGGTTATAATGAAATTATTTTATTCCT TTTAAGAATGTAGGCTGGAGCTGCTTCG	Disruption cassette	This study
rpsL-RdKW20-F	1497	GATTACGTGTAGATCGCCTTAAAACAGGTA	Str^R allele	(Mell et al., 2016)
rpsL-RdKW20-R	1498	CCAAAATAATTTCATTTGCTAATACACGCT	Str^R allele	(Mell et al., 2016)
PBGSF29 ATCACG		TTCCCTACACGACGCTCTTCCGATCTATCACGNN	Tn-seq analysis	This study
PBGSF30 ATCACG		CGTGATAGATCGGAAGAGCGTCGTGTAGGGAAAGAGT	Tn-seq analysis	This study
PBGSF29 CGATGT		TTCCCTACACGACGCTCTTCCGATCTCGATGTNN	Tn-seq analysis	This study
PBGSF30 CGATGT		ACATCGAGATCGGAAGAGCGTCGTGTAGGGAAAGAGT	Tn-seq analysis	This study
PBGSF29 TTAGGC		TTCCCTACACGACGCTCTTCCGATCTTTAGGCNN	Tn-seq analysis	This study
PBGSF30 TTAGGC		GCCTAAAGATCGGAAGAGCGTCGTGTAGGGAAAGAGT	Tn-seq analysis	This study
PBGSF29 TGACCA		TTCCCTACACGACGCTCTTCCGATCTTGACCANN	Tn-seq analysis	This study
PBGSF30 TGACCA		TGGTCAAGATCGGAAGAGCGTCGTGTAGGGAAAGAGT	Tn-seq analysis	This study
PBGSF29 ACAGTG		TTCCCTACACGACGCTCTTCCGATCTACAGTGNN	Tn-seq analysis	This study
PBGSF30 ACAGTG		CACTGTAGATCGGAAGAGCGTCGTGTAGGGAAAGAGT	Tn-seq analysis	This study
PBGSF29 GCCAAT		TTCCCTACACGACGCTCTTCCGATCTGCCAATNN	Tn-seq analysis	This study
PBGSF30 GCCAAT		ATTGGCAGATCGGAAGAGCGTCGTGTAGGGAAAGAGT	Tn-seq analysis	This study
PBGSF29 CAGATC		TTCCCTACACGACGCTCTTCCGATCTCAGATCNN	Tn-seq analysis	This study
PBGSF30 CAGATC		GATCTGAGATCGGAAGAGCGTCGTGTAGGGAAAGAGT	Tn-seq analysis	This study
PBGSF29 ACTTGA		TTCCCTACACGACGCTCTTCCGATCTACTTGANN	Tn-seq analysis	This study
PBGSF30 ACTTGA		TCAAGTAGATCGGAAGAGCGTCGTGTAGGGAAAGAGT	Tn-seq analysis	This study
PBGSF29 GATCAG		TTCCCTACACGACGCTCTTCCGATCTGATCAGNN	Tn-seq analysis	This study
PBGSF30 GATCAG		CTGATCAGATCGGAAGAGCGTCGTGTAGGGAAAGAGT	Tn-seq analysis	This study
PBGSF29 TAGCTT		TTCCCTACACGACGCTCTTCCGATCTTAGCTTNN	Tn-seq analysis	This study
PBGSF30 TAGCTT		AAGCTAAGATCGGAAGAGCGTCGTGTAGGGAAAGAGT	Tn-seq analysis	This study
PBGSF29 GGCTAC		TTCCCTACACGACGCTCTTCCGATCTGGCTACNN	Tn-seq analysis	This study
PBGSF30 GGCTAC		GTAGCCAGATCGGAAGAGCGTCGTGTAGGGAAAGAGT	Tn-seq analysis	This study

PBGSF29 CTTGTA	TTCCCTACACGACGCTCTTCCGATCTCTTGTANN	Tn-seq analysis	This study
PBGSF30 CTTGTA	TACAAGAGATCGGAAGAGCGTCGTGTAGGGAAAGAGT	Tn-seq analysis	This study
PBGSF29 AGTCAA	TTCCCTACACGACGCTCTTCCGATCTAGTCAANN	Tn-seq analysis	This study
PBGSF30 AGTCAA	TTGACTAGATCGGAAGAGCGTCGTGTAGGGAAAGAGT	Tn-seq analysis	This study
PBGSF29 AGTTCC	TTCCCTACACGACGCTCTTCCGATCTAGTTCCNN	Tn-seq analysis	This study
PBGSF30 AGTTCC	GGAACTAGATCGGAAGAGCGTCGTGTAGGGAAAGAGT	Tn-seq analysis	This study
PBGSF29 ATGTCA	TTCCCTACACGACGCTCTTCCGATCTATGTCANN	Tn-seq analysis	This study
PBGSF30 ATGTCA	TGACATAGATCGGAAGAGCGTCGTGTAGGGAAAGAGT	Tn-seq analysis	This study
PBGSF29 CCGTCC	TTCCCTACACGACGCTCTTCCGATCTCCGTCCNN	Tn-seq analysis	This study
PBGSF30 CCGTCC	GGACGGAGATCGGAAGAGCGTCGTGTAGGGAAAGAGT	Tn-seq analysis	This study
PBGSF29 GTCCGC	TTCCCTACACGACGCTCTTCCGATCTGTCCGCNN	Tn-seq analysis	This study
PBGSF30 GTCCGC	GCGGACAGATCGGAAGAGCGTCGTGTAGGGAAAGAGT	Tn-seq analysis	This study
PBGSF29 GTGAAA	TTCCCTACACGACGCTCTTCCGATCTGTGAAANN	Tn-seq analysis	This study
PBGSF30 GTGAAA	TTTCACAGATCGGAAGAGCGTCGTGTAGGGAAAGAGT	Tn-seq analysis	This study
PBGSF29 GTGGCC	TTCCCTACACGACGCTCTTCCGATCTGTGGCCNN	Tn-seq analysis	This study
PBGSF30 GTGGCC	GGCCACAGATCGGAAGAGCGTCGTGTAGGGAAAGAGT	Tn-seq analysis	This study
PBGSF29 GTTTCG	TTCCCTACACGACGCTCTTCCGATCTGTTTCGNN	Tn-seq analysis	This study
PBGSF30 GTTTCG	CGAAACAGATCGGAAGAGCGTCGTGTAGGGAAAGAGT	Tn-seq analysis	This study
PBGSF29 CGTACG	TTCCCTACACGACGCTCTTCCGATCTCGTACGNN	Tn-seq analysis	This study
PBGSF30 CGTACG	CGTACGAGATCGGAAGAGCGTCGTGTAGGGAAAGAGT	Tn-seq analysis	This study
PBGSF29 GAGTGG	TTCCCTACACGACGCTCTTCCGATCTGAGTGGNN	Tn-seq analysis	This study
PBGSF30 GAGTGG	CCACTCAGATCGGAAGAGCGTCGTGTAGGGAAAGAGT	Tn-seq analysis	This study
PBGSF29 ACTGAT	TTCCCTACACGACGCTCTTCCGATCTACTGATNN	Tn-seq analysis	This study
PBGSF30 ACTGAT	ATCAGTAGATCGGAAGAGCGTCGTGTAGGGAAAGAGT	Tn-seq analysis	This study
PBGSF29 ATTCCT	TTCCCTACACGACGCTCTTCCGATCTATTCCTNN	Tn-seq analysis	This study
PBGSF30 ATTCCT	AGGAATAGATCGGAAGAGCGTCGTGTAGGGAAAGAGT	Tn-seq analysis	This study
PBGSF23_NextSeq	CAAGCAGAAGACGGCATACGAGATAGACCGGGGACTTAT CATCCAACCTGT	Tn-seq analysis	This study
PBGSF31	AATGATACGGCGACCACCGAGATCTACACTCTTTCCCTAC ACGACGCTCTTCCGATCT	Tn-seq analysis	This study

Table A3. Up-regulated genes in infected lungs compared to non-infected lungs (2,078).

Gene name	Fold-change	p-value
Rn7sk	2988798,334	0
Rn7s1	496987,514	0
Rn7s6	301736,387	3,421E-298
Rpl34-ps1	170804,822	0
Gm24447	151614,856	0
Rpph1	136233,521	1,526E-290
Gm15772	106685,247	9,056E-237
Rpl3-ps1	49533,769	0
Rpsa-ps10	37125,065	6,319E-54
Gm12250	30649,427	2,490E-220
Rmrp	30149,758	6,828E-69
Hist1h2al	29923,617	1,178E-114
Gm1821	27134,283	6,237E-140
Gm14292	25883,731	2,372E-210
2900097C17Rik	20342,943	8,283E-179
Gm28438	16267,131	2,560E-44
Gm8995	14888,929	1,167E-145
Gm8730	14815,165	2,324E-162
Rps24-ps3	14741,102	3,711E-80
Gm28661	12447,002	2,254E-53
Gm4332	9300,053	1,129E-100
Ear-ps2	9219,203	2,529E-112
Gm22634	9189,476	6,858E-114
Vamp7-ps	6784,577	9,508E-74
Rn7s2	6690,497	5,588E-72
Gm43085	5736,459	2,228E-72
Rps2-ps13	5550,343	1,087E-16
Gm9118	5340,984	9,328E-71
Gm15487	5305,289	2,186E-71
Gm4366	5273,146	1,203E-79
Gm10154	5225,312	1,022E-74
Gm44250	4533,406	3,127E-64
6720427I07Rik	4512,632	2,196E-57
Saa2	4359,535	2,614E-55
Saa1	4232,282	3,621E-144
Scarna2	4012,349	9,624E-54
Gm15387	3973,524	1,528E-54
Gm13736	3959,416	1,839E-48
Rnps1-ps	3916,011	2,900E-49
Gm10925	3680,893	9,812E-55
Gm7993	3609,000	1,904E-46
Gm25679	3480,408	1,312E-35
Tdg-ps2	3448,369	2,357E-53
Gm9855	3448,369	2,357E-53
Gm44751	3366,536	2,212E-44
Gm15056	3255,417	1,202E-81
Rnu2-10	3205,207	5,269E-45
Gm43814	3037,233	3,606E-44
Gm27028	2907,064	2,538E-43
Gvin-ps6	2683,516	5,348E-48
Gpr84	2680,397	8,299E-38
Gm14584	2421,080	1,349E-44
Gm24950	2368,344	9,654E-41
Gm3375	2251,475	2,930E-38
Saa3	2165,083	0
Gm23804	2149,306	4,308E-37
Gm45884	2109,834	2,718E-36
Prok2	2078,386	1,530E-36
Rpl31-ps8	2044,549	7,145E-34
Gm9616	2013,442	7,829E-33
Gm22513	1992,687	4,331E-36
Gm6969	1961,473	3,144E-33
Gm4875	1953,572	2,140E-34
Acod1	1845,083	1,794E-209
Gm12966	1817,090	1,243E-26
Gm26532	1758,471	8,882E-32
Gsta1	1681,488	2,371E-74
Gm10240	1665,271	1,959E-25
Gm37296	1648,936	1,189E-28
Gm28872	1636,492	1,421E-23
Hmgb1-ps3	1622,857	4,392E-26
Orm1	1616,003	0
Gm14539	1535,488	2,567E-23
Cxcl3	1468,191	1,661E-197
Actr3-ps	1450,956	1,012E-22
B230303A05Rik	1392,967	4,055E-24
Cxcl2	1365,964	1,998E-251
Hmgb1-ps2	1365,762	5,753E-22
Gm20300	1337,604	3,951E-23
Gm29216	1303,986	2,309E-19
Gm44950	1289,651	1,008E-22
Gm43460	1252,902	3,449E-21
Gm28439	1237,490	1,652E-21
Gm37352	1218,103	3,573E-21
Tpt1-ps3	1165,764	2,973E-19
Ccl4	1152,611	5,406E-265
2010320M18Rik	1141,604	1,021E-19
Gm4735	1138,112	8,249E-19
Gm28437	1105,857	4,669E-17
Gm13443	1095,570	1,489E-07
Gm18860	1090,226	6,209E-19
Gm5527	1070,465	5,776E-15
Gm12751	1068,220	2,848E-18
Gm4322	1065,367	1,953E-13
Gm5526	1053,614	7,304E-18
Ccl3	1053,113	1,091E-286
Gm15500	1011,213	8,972E-16
Gm12312	1010,196	1,834E-12
Gm10222	986,095	2,016E-16
Gm38244	951,092	3,338E-16
Orm2	920,939	1,386E-168
Gm27019	913,987	1,332E-15
Gm12663	911,916	9,847E-15
Gm13577	893,252	3,835E-14
Rps19-ps3	856,166	5,093E-12
1700096K18Rik	846,588	9,232E-14
1110025M09Rik	842,136	7,340E-14
Gm45138	832,585	4,025E-12
Ccl20	832,072	1,036E-128
Gm43848	822,125	1,531E-13
Gm6548	811,457	4,818E-13
Gm6485	768,176	8,376E-12
Gm6545	763,363	4,475E-12
Gm25360	743,006	4,599E-10
Gm4617	735,128	2,950E-11
Gm22973	725,174	6,522E-11
Rpl31-ps11	715,570	1,456E-09
Gm49602	708,623	6,253E-11
Gm10039	699,919	9,896E-08
Gm5586	696,950	7,771E-10
Gm47863	689,577	1,064E-10
4632415L05Rik	667,749	8,643E-10
Rpl17-ps9	654,263	5,594E-10
Gm1966	645,128	1,119E-06
2610306M01Rik	644,615	1,053E-09
Rpsa-ps9	627,612	6,540E-08
Cxcl11	622,448	4,118E-80
Nudc-ps1	620,744	4,600E-09
Rnu3a_1	606,700	8,131E-09
Rnu3a_1	606,700	8,131E-09
Gm14586	605,602	8,648E-09
Gm43719	605,338	1,190E-08
Gm43196	602,141	1,523E-08
Gm37320	599,594	1,053E-08
Gm5518	593,189	2,117E-08
Gm48496	572,867	1,773E-06
Ctdsp2-ps	565,368	2,455E-07
Mrpl48-ps	563,938	6,425E-08
2810402E24Rik	562,994	5,612E-08
Cxcl10	553,229	0
Gm5900	549,654	1,387E-07
Gm12696	546,377	8,403E-07
Gm44053	536,563	1,575E-07
Gm37305	536,418	2,549E-07
Gm20632	536,148	2,052E-07
Rpl19-ps11	534,451	2,573E-07
Gm7285	532,171	2,554E-07
Gm4540	528,716	2,176E-06
Gm13841	524,943	4,198E-07
Gm10698	520,577	7,940E-07
Gm13534	518,155	8,045E-07
Ccl2	512,277	1,293E-203
Gm28187	509,864	6,673E-07
Gm10524	500,490	9,832E-07
Gm10156	498,876	2,184E-06
2510046G10Rik	498,323	1,091E-06
Gad1-ps	496,688	1,198E-06

Gm11425	473,531	4,425E-06	Mir155hg	143,935	1,142E-34
AA467197	472,463	1,530E-148	Hpx	140,771	1,662E-52
2810405F17Rik	467,517	4,931E-06	Cxcl5	139,294	7,130E-144
Gm42528	456,614	1,172E-05	Il6	135,424	5,820E-53
Gm37238	456,523	8,423E-06	Tnfrsf9	129,138	2,755E-83
Gm48621	453,560	1,562E-05	Gm3776	124,196	1,245E-23
Rpl39-ps	448,917	1,574E-05	Cxcl13	116,604	2,417E-178
Rps13-ps1	448,005	1,525E-05	Ifng	115,678	2,144E-38
Gm6637	446,691	2,479E-05	Lcn2	106,697	0
Gm37516	431,185	3,339E-05	Tarm1	106,429	1,663E-32
Cstdc4	428,641	2,718E-153	Asprv1	101,837	8,537E-24
Gm6863	426,944	3,300E-05	Wfdc21	97,545	7,744E-170
Gm9027	426,599	3,362E-05	Gm10718	91,939	1,072E-05
Gm21781	424,444	6,038E-05	Tnf	91,649	3,364E-152
Gm45495	423,327	8,545E-05	Ccl17	87,394	2,721E-75
Gm45769	422,011	6,009E-05	Plekhs1	87,295	4,283E-03
Ubd	416,495	8,433E-83	S100a8	87,129	5,360E-134
Mt2	416,359	1,679E-234	Cstdc5	81,450	3,843E-13
Gm10420	406,161	1,341E-04	Il4i1	81,115	3,295E-78
Gm10045	406,004	3,928E-04	Mt1	78,858	6,908E-228
Gm7964	405,318	1,292E-04	BC018473	78,018	2,390E-07
Ccl7	404,489	1,318E-112	Gm17041	76,167	4,980E-06
Gm10443	400,570	2,958E-04	Il1rn	75,494	1,231E-159
Rps12-ps1	394,246	2,631E-04	Fam26f	75,168	3,311E-80
Gm43672	390,804	3,323E-04	Il1b	73,948	1,141E-139
Mirt2	386,250	2,687E-03	Ackr1	73,295	5,821E-19
Gm43461	385,149	3,860E-04	Orm3	69,963	3,803E-23
Csf3	379,934	2,475E-26	Serpina3n	68,918	4,244E-267
Gm10275	379,419	1,589E-20	Gm10801	67,878	5,478E-04
Gm19498	373,106	7,052E-04	Ifitm6	64,881	9,793E-128
Stfa2	366,532	1,647E-29	Slc36a3os	62,245	5,310E-03
Gm23444	366,290	4,599E-02	Retnla	61,891	5,071E-93
Gm37660	360,968	1,261E-03	Isg15	61,692	4,969E-85
1700008J07Rik	357,124	1,008E-03	Aqp3	57,977	1,273E-32
Gm4742	356,949	3,840E-03	Gm26602	57,922	6,278E-28
9230112E08Rik	348,917	2,117E-03	Pla1a	57,335	8,888E-51
Rps10-ps2	348,914	2,444E-03	Serpina3m	57,169	5,483E-38
Gm28913	348,747	2,490E-03	Cd14	56,853	2,663E-276
AV356131	346,537	1,934E-03	Klk10	56,639	8,734E-20
AA414768	342,371	2,142E-03	Reg3g	56,502	2,222E-31
Gm17081	341,219	2,134E-03	Ly6g	56,364	2,190E-12
Cxcl1	340,419	0	Csf2	55,432	2,288E-106
Gpx4-ps2	339,457	6,850E-03	Ch25h	55,178	2,344E-124
Gm48296	332,397	4,323E-03	Igkv6-23	55,119	3,180E-02
Gm37699	332,274	3,944E-03	Gm21738	54,029	5,980E-09
Gm45133	321,479	8,268E-03	Clec4d	53,097	1,142E-152
1300014J16Rik	316,868	9,300E-03	Gm16685	52,408	1,107E-47
Eif4a-ps4	315,752	7,522E-03	Prss22	52,061	3,570E-05
Gm21188	314,240	3,082E-02	Mrgpra2a	51,838	2,426E-16
Gm27167	313,232	8,546E-03	Tmem8c	51,577	6,190E-09
Gm18329	308,026	1,809E-02	Mir142hg	51,013	9,463E-10
Gm43457	307,406	1,505E-02	Gm2564	50,448	6,485E-34
Rps15a-ps7	305,797	3,913E-02	Il1a	49,132	7,004E-288
Stfa3	305,703	2,398E-09	Ccl19	49,067	9,700E-46
Gm4149	304,224	1,941E-02	Gm4841	46,203	3,615E-04
B930036N10Rik	304,016	1,683E-02	Mefv	45,823	2,579E-107
Gm48226	301,846	1,627E-02	Gm27252	45,133	2,888E-05
Gm2511	301,578	1,876E-02	Olfm4	45,071	4,845E-24
Gm15427	300,901	1,607E-02	Trem3	44,506	3,473E-52
Gm12715	300,771	2,576E-02	Il27	44,335	2,873E-09
Gm26982	300,598	1,743E-02	Clec4e	43,788	2,860E-143
Gm20900	299,118	3,699E-02	Sele	42,540	2,533E-53
Gm37233	294,129	2,879E-02	BC023105	42,300	1,751E-43
Wfdc17	291,160	2,826E-178	Speer4c	41,438	1,912E-23
Cxcl9	273,454	2,369E-174	Socs1	39,802	1,105E-55
Ccl12	230,821	1,136E-95	Trim30c	39,674	1,814E-26
Gm10800	228,356	7,898E-07	Gm42835	38,686	3,318E-04
Timp1	225,261	5,954E-147	Retnlg	37,699	1,129E-210
Stfa2l1	220,311	8,551E-74	Mrgpra2b	37,224	7,635E-40
Sectm1b	212,576	6,103E-07	Bcl2a1b	37,098	9,053E-234
Gm18445	199,894	5,377E-06	Gm42674	36,596	8,906E-07
4930430E12Rik	192,645	9,841E-12	Siglece	35,327	6,511E-61
Il23a	183,837	3,824E-29	Ms4a4a	34,385	3,118E-27
Il1f9	177,870	3,752E-117	Gm37468	34,069	4,587E-05
Xcl1	176,976	4,285E-26	Cfb	33,777	1,166E-101
Gm29094	174,371	1,012E-17	Lst1	33,396	5,691E-139
Ly6i	169,568	3,454E-146	Steap4	32,642	2,147E-200
Gm21370	161,870	1,463E-03	Bcl2a1a	32,238	2,559E-157
Il1r2	156,332	1,860E-66	Vnn3	32,231	4,914E-78
Gpr31b	153,059	7,366E-04	Gm14023	32,026	2,810E-27
Mab21l3	152,654	1,100E-12	Gm18342	31,929	7,771E-03
S100a9	148,751	4,201E-95	S100a4	31,209	1,304E-116

A930015D03Rik	30,576	3,968E-08	Ninj1	16,796	5,826E-39
Marcksl1	29,990	1,157E-120	Pram1	16,789	1,243E-08
Nppa	29,929	5,337E-18	D13Ertd608e	16,772	8,756E-27
Gm7592	29,772	1,571E-12	Ccl24	16,733	4,776E-11
Hcar2	29,283	8,655E-93	Dusp2	16,603	5,309E-26
Trex1	29,011	2,243E-57	Gm9973	16,417	1,047E-02
Ifitm1	28,884	5,760E-176	I830127L07Rik	16,284	2,900E-06
Rgs16	28,404	4,650E-28	Calca	16,270	2,948E-03
Gm2000	28,169	1,462E-11	Socs3	16,264	5,097E-157
Soat2	26,933	1,327E-08	Gm37335	16,106	3,836E-23
Basp1	26,820	1,128E-114	Slc7a11	16,038	9,372E-59
Slfn4	26,378	8,840E-23	Adamts4	15,917	2,707E-21
Krt87	26,069	1,526E-02	Rhov	15,897	5,461E-10
Rab20	25,606	1,192E-94	Gm17334	15,774	5,137E-28
Bcl2a1d	25,589	1,106E-191	Ccl8	15,627	1,311E-07
Tff2	25,362	8,772E-11	Apol6	15,329	1,880E-25
Ighv1-19	25,243	1,123E-06	Igsf6	15,260	2,470E-39
Ighv5-17	25,077	4,532E-03	Slc26a4	15,125	1,611E-25
Cstb	25,027	8,502E-185	Smpdl3b	15,067	2,364E-40
Ifi202b	24,974	1,349E-36	Nfkbia	15,056	3,200E-217
AW112010	24,795	3,858E-122	Agr2	14,909	2,678E-18
Apod	24,741	1,311E-28	Slamf8	14,880	1,997E-18
Arg2	24,525	7,311E-113	Gm10130	14,665	7,421E-06
Ptx3	24,479	1,888E-60	Trem1	14,649	1,188E-33
Nlrp3	24,126	9,337E-114	Epb41l4aos	14,644	8,099E-27
Lrrc25	24,074	1,935E-39	Lrg1	14,574	9,195E-99
Fcrlb	23,891	1,014E-05	Gm9733	14,548	4,474E-29
Gm6594	23,852	5,509E-13	Mmp8	14,470	2,462E-69
Scgb3a1	23,838	8,752E-19	Ifitm2	14,442	5,370E-189
Fcer1g	23,716	2,637E-177	Mreg	14,404	1,289E-67
Fpr2	23,360	1,484E-178	Slpi	14,375	9,833E-39
Il1bos	23,314	1,700E-10	Ifitm3	14,231	2,452E-100
Gm16094	23,174	6,835E-09	Bst2	14,142	5,345E-16
Ankrd22	23,158	7,464E-04	Zc3h12a	14,139	3,327E-30
Rasl10b	23,151	1,158E-30	Ms4a4c	14,022	1,006E-55
Ccl5	22,939	5,948E-75	Serpine1	13,979	1,956E-143
Tnfrsf8	22,703	5,758E-06	Gm17586	13,846	6,857E-18
Gpx2	22,700	3,091E-83	Ceacam10	13,793	1,707E-05
Cd177	22,663	1,938E-61	Hsd11b2	13,583	6,234E-05
Serpinb2	22,552	6,061E-18	Acp5	13,577	8,859E-86
Gm12840	22,232	1,169E-151	Gm13889	13,557	5,297E-69
Ebi3	22,095	1,289E-48	Tifa	13,511	2,376E-76
Gm6264	21,994	4,660E-02	Dgat2	13,496	2,173E-25
Fth1	21,956	2,673E-133	S100a11	13,059	9,113E-67
Gm16712	21,749	5,834E-03	Ccl11	12,984	6,097E-33
Ccl22	21,732	1,162E-72	Il12b	12,880	1,918E-08
Batf	21,711	1,994E-99	Gm20390	12,867	2,469E-03
Hamp	21,649	2,280E-27	Rab26os	12,822	1,017E-07
Gm15402	21,177	8,264E-04	Inhba	12,752	2,262E-30
Ppp1r14d	21,023	3,098E-09	Ccl9	12,732	5,719E-101
Marco	21,017	5,274E-33	Tnip3	12,722	1,363E-33
mt-Atp8	20,970	4,467E-27	Serpina3i	12,625	3,888E-15
Ighv1-47	20,851	3,284E-02	Mcoln2	12,586	1,371E-18
Gm10226	20,770	4,861E-07	Osm	12,430	3,947E-18
Serpina3e-ps	20,452	4,483E-15	A530032D15Rik	12,424	8,926E-11
Ighv1-55	20,220	4,098E-08	Nfkbie	12,358	7,543E-73
Serpina3h	20,138	3,274E-35	Tyrobp	12,331	5,369E-145
Ms4a6d	20,122	6,619E-122	Ighv1-64	12,328	1,023E-08
Gm21149	19,764	3,210E-02	Gadd45g	12,285	2,274E-109
Selp	19,712	3,796E-41	Tmc5	12,242	1,909E-10
Htr7	19,556	5,901E-04	Gm16602	12,181	4,086E-03
Clec5a	19,466	1,510E-77	Oas1g	12,134	2,354E-08
Apoc2	19,225	9,546E-07	Mfsd7a	12,129	6,747E-10
Gm13293	19,152	6,053E-04	Gzmb	12,075	3,863E-06
Gm21762	18,717	1,691E-03	Igkv1-117	12,035	3,880E-10
AU040972	18,680	8,993E-145	Gbp2b	12,017	8,117E-20
Gm15832	18,653	2,172E-24	Gm10076	11,973	4,594E-18
Slfn1	18,611	5,367E-86	Ifi211	11,933	2,109E-26
Oasl1	18,574	2,653E-22	Cxcr2	11,925	9,513E-51
Dynlt1a	18,337	7,582E-11	Igkv1-110	11,895	1,969E-15
Trbv5	18,265	2,688E-03	Ighv1-26	11,874	2,766E-09
Ptafr	18,120	2,037E-117	Zswim7	11,874	4,144E-08
Cxcl17	17,895	1,616E-98	Phfl1b	11,838	8,985E-10
Gm13767	17,835	4,250E-03	Gm16028	11,832	1,258E-02
Slfn2	17,726	1,605E-117	Usmg5	11,825	5,350E-114
Igkv19-93	17,588	3,633E-09	Phfl1a	11,781	3,655E-13
Cd80	17,554	1,824E-12	Apol9b	11,694	7,163E-07
F10	17,552	8,786E-101	Rgcc	11,674	6,974E-30
Gm11772	17,487	3,135E-02	Gm2396	11,630	2,010E-02
Gm45802	17,155	3,200E-04	Aldh1a3	11,617	1,188E-05
Ighv2-2	16,965	1,496E-07	Pstpip2	11,541	2,458E-43
Pglyrp1	16,874	1,334E-75	Gm9493	11,482	5,256E-04

Mx1	11,463	1,134E-29	Oas1a	8,887	5,332E-09
Apol9a	11,429	8,310E-05	Slfn10-ps	8,871	1,087E-06
Ncf4	11,417	1,003E-53	Rpl23a-ps3	8,867	1,050E-03
Gm10134	11,365	1,440E-04	Fcgr2b	8,845	1,089E-70
Acat3	11,263	2,865E-04	Pla2g7	8,807	3,645E-71
Gm6377	11,255	1,534E-49	Ltb4r1	8,780	2,789E-03
Ccr1	11,227	2,421E-50	Iglc1	8,775	2,246E-03
Trbv16	11,192	1,412E-03	Dctpp1	8,757	2,978E-04
Cldn2	11,097	3,042E-03	Cited4	8,755	2,788E-02
Snx20	11,091	3,905E-56	Cd52	8,737	1,494E-151
Gbp2	11,074	2,580E-08	Irak3	8,729	3,913E-44
Mif	11,013	2,605E-118	Rdh12	8,705	2,166E-03
Gsta2	10,997	4,118E-30	Slc11a1	8,705	1,306E-23
2410006H16Rik	10,901	1,228E-17	Fabp4	8,691	2,647E-104
Rpl27-ps3	10,863	3,656E-113	Tnfrsf12a	8,673	1,505E-48
Fcgr4	10,848	1,237E-33	Hist1h4k	8,650	3,368E-11
mt-Nd3	10,840	5,226E-38	2410004I01Rik	8,646	5,145E-22
E230013L22Rik	10,660	4,350E-14	Itgam	8,625	4,476E-98
Ms4a6c	10,625	1,193E-99	Itgam_1	8,625	4,476E-98
Cyp7b1	10,614	1,823E-45	Ifit3b	8,569	1,260E-21
Ankrd1	10,595	3,812E-153	Akr1b8	8,550	8,908E-47
Eid3	10,563	2,650E-07	Tnfaip2	8,520	7,916E-155
Clec4a1	10,553	3,646E-49	Gm26880	8,518	1,275E-11
Gm45695	10,500	1,462E-07	Hmox1	8,504	4,654E-60
Aif1	10,492	3,396E-33	Gm11808	8,487	1,105E-127
Trgv2	10,488	1,588E-02	Cyba	8,483	4,482E-89
Pim1	10,473	1,022E-169	Rplp1	8,432	7,999E-132
Fpr1	10,469	1,472E-73	Atox1	8,421	2,959E-31
Ifit3	10,382	1,404E-22	Hk3	8,415	1,451E-07
Batf3	10,377	5,550E-03	Tlr2	8,384	8,862E-60
Cd69	10,350	4,908E-25	Elob	8,360	3,957E-67
Ndufa1	10,326	3,200E-34	Polr2k	8,334	5,777E-16
Maff	10,259	8,038E-105	Cyp4f18	8,313	1,271E-09
Mmp25	10,252	6,529E-05	H2-M2	8,302	4,113E-07
Klk1	10,213	3,629E-09	Tmem173	8,284	1,080E-40
Ifi204	10,204	5,795E-62	mt-Nd6	8,276	4,966E-73
AB124611	10,126	3,615E-10	Cebpb	8,261	4,173E-44
Treml4	10,066	9,718E-28	Timm10	8,258	1,990E-21
Gm14548	9,986	9,322E-58	Gbp5	8,230	1,017E-04
Tnnc1	9,908	1,850E-28	Hist1h4d	8,218	3,610E-37
Irf7	9,882	4,759E-20	Ppp1r14b	8,215	2,023E-82
Gm43079	9,872	1,082E-21	Ifit1	8,208	8,566E-26
Rps12-ps3	9,867	7,779E-132	2310039H08Rik	8,206	4,988E-04
Upp1	9,863	7,630E-102	Oas3	8,184	4,637E-08
Tnfsf14	9,810	5,566E-07	Rpl29	8,117	2,779E-18
A530064D06Rik	9,809	1,014E-08	H2-K2	8,103	1,218E-12
Nos2	9,801	5,371E-19	Pf4	8,102	7,322E-15
Car13	9,756	7,462E-25	Pilrb2	8,100	2,032E-15
Serpina1a	9,739	2,023E-07	Glrx	8,080	8,995E-78
Rpl36	9,731	5,073E-103	Snrpd1	8,075	6,764E-84
Gm15429	9,730	1,327E-11	Cd274	8,064	5,983E-05
Atf3	9,710	7,822E-38	Tnfaip3	8,007	4,957E-118
4833407H14Rik	9,688	9,269E-07	Uchl3	7,990	3,682E-54
Ighv2-9	9,687	1,380E-11	Gm16096	7,985	1,249E-05
Gm4951	9,643	1,648E-02	Gm10131	7,976	6,173E-21
Lilr4b	9,567	2,620E-55	Tmem37	7,974	2,503E-25
Gstp2	9,550	1,304E-04	Noxo1	7,960	3,726E-12
Cldn4	9,550	3,751E-03	Bcl3	7,939	3,823E-45
Cst7	9,547	3,441E-04	Tgm1	7,931	2,112E-17
1810049J17Rik	9,495	4,306E-39	Cox8a	7,898	3,107E-67
Dydc2	9,476	4,228E-13	Polr2f	7,897	4,056E-29
BC147527	9,468	4,660E-04	Rasd1	7,860	4,071E-02
Ffar2	9,454	1,343E-14	Smim22	7,853	5,940E-21
H2-T22	9,414	3,099E-10	Psmb5	7,847	1,909E-41
Arg1	9,399	4,787E-14	Gadd45b	7,847	1,393E-95
Cfd	9,394	1,179E-06	Cd83	7,847	3,884E-51
Rps2-ps6	9,334	1,421E-22	Hist2h2ab	7,842	7,939E-21
Csf3r	9,249	2,347E-36	Gm6712	7,842	3,265E-04
Cks2	9,225	2,089E-38	Eef1e1	7,834	5,648E-37
Ifi205	9,208	4,888E-58	Bpifb1	7,814	7,254E-06
Vmn2r96	9,175	4,111E-05	Ifi47	7,801	1,648E-09
Gm8325	9,163	1,850E-03	Tubb6	7,790	5,478E-47
Mrpl52	9,159	9,289E-71	Slc2a6	7,778	2,257E-10
Fkbp1b	9,137	2,814E-13	Ikbke	7,776	1,024E-28
mt-Nd4l	9,136	1,090E-36	Arl5c	7,764	6,496E-10
Plac8	9,071	1,448E-105	Msr1	7,760	4,590E-35
Hal	9,067	5,085E-09	Irak1bp1	7,729	1,479E-06
Gm5617	9,061	1,588E-08	Gm10095	7,714	2,053E-122
Iigp1	9,021	8,958E-03	Gm17024	7,713	1,331E-02
Psmg4	9,019	2,939E-25	Gm26809	7,712	1,293E-115
Syt12	9,005	1,989E-07	Myl7	7,709	4,626E-32
Itln1	8,895	3,485E-04	Trir	7,703	2,257E-13

Fau	7,680	1,785E-72	Romo1	6,625	1,115E-05
Igkv10-96	7,672	1,801E-06	Lsm4	6,616	8,213E-17
Smim26	7,663	3,778E-17	Hist1h3i	6,600	5,980E-03
Fcgr3	7,642	2,293E-141	Gzma	6,595	3,176E-25
Mlkl	7,625	7,118E-27	Scimp	6,593	5,261E-19
Cd302	7,625	1,531E-124	Tnfrsf1b	6,563	2,459E-38
Gm9803	7,621	2,871E-09	Pigr	6,553	9,265E-84
Nedd8	7,617	2,608E-112	Rpp25l	6,524	1,536E-14
Snhg15	7,611	8,936E-10	Prdx5	6,513	1,336E-138
Igkc	7,592	3,475E-49	Srgn	6,504	1,091E-68
Ndufa2	7,587	1,152E-60	Pin4	6,497	3,902E-48
Ccdc121	7,575	1,278E-10	Hck	6,465	4,370E-40
Gm10309	7,544	8,717E-05	1700016K19Rik	6,465	9,644E-19
Pigbos1	7,542	1,656E-35	Rubcnl	6,462	3,893E-08
Scand1	7,510	1,352E-22	Sdf2l1	6,448	6,350E-29
Snrpf	7,497	2,023E-91	Gm10053	6,443	6,959E-23
Nfkbid	7,494	2,512E-06	Ighv1-53	6,436	2,168E-03
Fam183b	7,485	2,441E-78	Ier3	6,434	4,004E-25
Ndufb6	7,472	3,018E-30	Ppp1r32	6,418	1,740E-04
Capsl	7,455	1,042E-36	Sod2	6,417	1,723E-121
Ly6d	7,453	1,440E-07	A630001O12Rik	6,399	2,735E-04
1700071M16Rik	7,442	1,917E-03	Mrps16	6,393	1,190E-31
Fkbp2	7,423	8,372E-47	Ctps	6,379	2,625E-98
Atp5k	7,401	3,922E-41	Hist1h4f	6,375	3,057E-09
Chl1	7,348	6,395E-04	Ifit2	6,371	1,247E-17
Gpr65	7,301	1,204E-30	Psme2	6,351	1,008E-20
Rnaset2a	7,301	7,352E-52	Ccrl2	6,338	2,444E-66
Csrnp1	7,294	2,237E-28	Uqcr10	6,332	3,119E-25
Tlr1	7,281	2,862E-19	Malt1	6,317	8,764E-83
Rpl38	7,271	9,177E-21	Sftpd	6,312	1,015E-119
B2m	7,250	2,110E-19	Rnd1	6,308	1,638E-35
Samsn1	7,240	1,303E-48	Adm	6,303	2,898E-44
Cd300lf	7,234	2,958E-36	Alpl	6,255	4,281E-21
Efcab10	7,231	3,415E-02	Ms4a8a	6,251	2,831E-17
Iglc3	7,209	1,327E-14	Mrpl54	6,247	7,901E-52
Gm9806	7,200	7,085E-04	Nnat	6,239	4,176E-23
Pdk4	7,194	1,043E-17	Fam46b	6,236	4,609E-07
Sh2b2	7,191	4,312E-02	Rtp4	6,225	5,109E-17
Hmga1-rs1	7,179	4,573E-05	Tspo	6,215	5,412E-19
Junb	7,127	7,062E-60	Sap30	6,197	2,406E-22
Tmem213	7,122	8,210E-08	Banf1	6,172	4,394E-15
Gm45396	7,083	2,819E-12	Dancr	6,169	4,356E-03
Hcls1	7,060	1,540E-119	Adora3	6,151	1,901E-04
Hp	7,055	2,790E-132	Ppa1	6,112	3,002E-46
C1rb	7,039	2,794E-22	Vnn1	6,110	4,350E-19
Txn1	7,017	7,600E-62	Sln	6,104	7,099E-12
Ly96	6,982	1,068E-06	Sema7a	6,083	5,141E-40
Snhg8	6,964	2,087E-21	Msrb1	6,080	1,997E-65
Lgals1	6,951	1,547E-63	Psme2b	6,072	5,466E-15
Nhp2	6,945	2,445E-41	F3	6,072	3,562E-51
Tmem212	6,879	9,800E-08	Ifi207	6,064	9,536E-29
Milr1	6,865	1,068E-16	Nqo1	6,049	9,448E-09
Ltb	6,863	3,194E-11	Fscn1	6,047	7,496E-22
Lilrb4a	6,858	5,780E-35	Slfn8	6,028	1,046E-16
Lilrb4a_1	6,858	5,780E-35	Slc7a5	6,018	1,127E-11
Gm8797	6,856	3,137E-46	Trbc2	6,013	7,564E-19
Riiad1	6,853	1,189E-14	Cd53	6,011	1,713E-60
Rab32	6,815	3,485E-39	Gm867	5,991	2,600E-10
Rnf149	6,815	2,286E-48	Scgb1a1	5,972	3,294E-62
Timm8b	6,806	4,794E-80	Fkbp5	5,953	5,997E-27
Ifi27l2a	6,806	4,421E-05	Spaca9	5,953	3,831E-03
Pilrb1	6,804	8,357E-21	Tsku	5,951	6,448E-13
Mrps28	6,799	1,487E-16	H2-T23	5,940	1,572E-05
Dnajc15	6,798	2,364E-47	1700024G13Rik	5,926	1,121E-04
Casp4	6,796	4,139E-48	C5ar1	5,919	9,695E-22
Nkg7	6,778	7,683E-04	Il12a	5,912	4,693E-13
Tgfbi	6,769	6,257E-34	Sec61b	5,904	2,096E-37
Gm8909	6,760	1,067E-21	Gm9843	5,900	1,883E-33
Cisd3	6,743	1,185E-07	Mmp9	5,897	7,207E-19
Magoh	6,732	3,883E-51	Cox6a1	5,880	1,374E-41
Cd63	6,725	5,703E-55	Fbp1	5,878	8,084E-04
Hist2h2aa1	6,717	5,273E-07	Ndufa6	5,878	1,421E-40
Ctsw	6,693	3,581E-08	Gm45479	5,873	4,138E-05
Blvrb	6,678	2,967E-29	D8Ertd738e	5,871	4,026E-43
Dynlrb2	6,672	9,378E-24	Ndufs6	5,868	1,250E-14
Ly6a	6,666	2,134E-36	Ddit4	5,866	1,298E-07
2310010J17Rik	6,661	5,978E-03	Rps27l	5,857	4,324E-44
Tnip1	6,636	9,240E-36	Hmga1	5,851	9,020E-25
Fcer2a	6,629	2,885E-19	Lsm5	5,841	1,104E-26
Fas	6,627	7,607E-83	Chil1	5,840	8,642E-49
Rilpl2	6,626	3,349E-23	Gstp3	5,833	1,710E-05
Chchd1	6,626	8,357E-31	Rnf19b	5,814	1,127E-79

Myc	5,797	9,842E-14	Uqcr11	5,317	5,615E-39
P2ry13	5,781	3,691E-16	Tlr13	5,300	4,452E-27
AI662270	5,769	1,793E-34	Sntn	5,297	2,470E-22
Gm29237	5,751	2,012E-23	Cox7a1	5,285	9,945E-03
Fam174c	5,747	1,429E-14	Mmp3	5,272	9,128E-22
mt-Co2	5,745	4,851E-23	Ndufaf2	5,262	2,545E-14
Psma5	5,741	1,584E-82	Rps23	5,259	3,198E-25
F630028O10Rik	5,741	8,671E-30	Fbp2	5,240	2,931E-20
Abracl	5,739	9,542E-30	Casp1	5,228	1,771E-18
Gpr132	5,734	5,406E-05	Tnfrsf14	5,223	1,409E-16
U2af1	5,734	1,786E-46	2010016I18Rik	5,216	3,160E-08
Cdc42ep2	5,729	1,942E-28	Snhg3	5,205	2,225E-14
Gm5150	5,725	9,456E-07	Zeb2os	5,191	2,438E-08
Gm26917	5,716	1,403E-21	Hist1h4b	5,182	6,619E-05
Timm8a1	5,712	4,421E-30	Selenbp2	5,179	4,529E-18
Pam16	5,691	6,512E-05	Rps27rt	5,177	3,564E-07
Snhg6	5,676	3,035E-11	Ifi30	5,168	5,173E-55
Ass1	5,664	3,081E-11	Cd68	5,163	2,622E-40
Sphk1	5,661	2,604E-14	1110038F14Rik	5,157	3,475E-29
Ltf	5,660	4,946E-05	Srm	5,157	4,212E-13
Gadd45a	5,657	5,681E-31	Gm10557	5,151	1,424E-28
Rps15	5,655	4,114E-23	Hoatz	5,141	7,039E-04
Alox5ap	5,650	6,443E-57	Trac	5,139	1,531E-05
Pilra	5,649	5,591E-28	Nupr1	5,139	2,471E-93
Oas1b	5,646	4,630E-03	Gpr18	5,137	9,506E-11
Ctsz	5,637	2,516E-117	Ftl1-ps1	5,134	2,249E-02
Misp	5,632	4,355E-21	Sh3bgrl3	5,124	2,357E-24
Dok3	5,626	2,899E-10	Grina	5,122	2,336E-43
C3ar1	5,625	1,151E-15	B9d2	5,107	4,273E-07
Myd88	5,617	7,615E-63	Rpl8	5,099	1,537E-38
Spata24	5,602	6,394E-10	Gstp1	5,081	1,218E-35
Mir22hg	5,600	4,576E-21	Gsta4	5,080	2,031E-54
Npm3	5,595	2,112E-18	Lcp2	5,076	4,254E-30
Hist2h2ac	5,590	3,930E-25	Tnfrsf11b	5,069	6,097E-11
CAAA01180111.2	5,589	5,004E-16	Bid	5,064	9,855E-06
Rpl22l1	5,577	8,015E-16	Slc28a2	5,063	3,578E-05
Sod1	5,572	8,404E-134	Kcne4	5,059	1,756E-10
Dynlt1b	5,566	6,171E-25	AU020206	5,054	4,723E-17
Pcbd1	5,563	7,444E-03	Tctex1d4	5,047	2,256E-03
Rsad2	5,561	1,917E-05	Rpl27	5,028	9,596E-08
Gnl3	5,555	3,915E-48	Mea1	5,024	3,363E-39
Ddt	5,554	4,353E-30	Rpl23a	5,019	2,015E-32
Psma6	5,548	1,958E-129	Vcpkmt	5,016	2,832E-12
Psmb2	5,536	2,505E-70	Nfkbib	5,012	6,882E-14
Usp18	5,530	4,224E-21	Cox6a2	5,005	5,997E-14
C2cd4b	5,504	8,948E-04	Bloc1s2	4,998	2,149E-21
Tmem160	5,504	6,058E-06	1700028P14Rik	4,997	5,605E-03
Nme2	5,482	9,719E-83	Klrc1	4,995	1,276E-02
Sycp2	5,481	1,385E-02	Psmb1	4,982	1,455E-67
Rnase6	5,481	4,731E-16	Lilra6	4,974	3,660E-22
Adam8	5,480	1,326E-13	Cmss1	4,972	8,056E-04
Atp6v1f	5,480	1,393E-18	Wdr74	4,969	9,079E-17
Ptges	5,475	6,728E-31	Gar1	4,962	2,953E-03
Pira2	5,473	3,380E-20	Micos13	4,962	1,405E-22
Cfp	5,468	4,303E-13	Nudt8	4,957	4,665E-02
Eno1b	5,466	1,468E-36	Nudt8_1	4,957	4,665E-02
Rps19bp1	5,455	5,885E-18	Clec4n	4,956	4,737E-13
C1qbp	5,450	2,237E-26	Ppil6	4,951	1,212E-07
Rhoc	5,448	5,979E-48	Mien1	4,949	2,659E-14
Pfn1	5,443	3,516E-25	Slc39a4	4,944	1,756E-35
Nfkb2	5,437	2,105E-38	Gimap7	4,939	1,731E-03
Cks1b	5,435	3,776E-04	Fgr	4,936	4,975E-26
Rpp38	5,432	2,203E-07	6820408C15Rik	4,935	1,693E-05
Mapk13	5,430	4,128E-17	Mrps21	4,933	3,823E-40
Plk3	5,423	1,640E-09	Sap18b	4,921	1,213E-89
Hist1h2bg	5,410	1,883E-12	Clec4a3	4,912	4,205E-29
Ankrd66	5,403	3,662E-03	Dynlt1f	4,908	1,257E-22
1110038B12Rik	5,387	3,090E-09	Phf5a	4,901	4,907E-28
Pgf	5,383	1,747E-08	Cdkn1a	4,895	9,425E-13
Mthfd2	5,374	7,232E-13	Cotl1	4,881	9,176E-51
Rpl32	5,365	2,216E-65	Ndufb3	4,874	7,253E-11
Psmb10	5,351	7,659E-24	Lpxn	4,872	2,147E-07
Hspb7	5,349	3,645E-10	Psmb4	4,868	1,664E-41
Ndufb9	5,345	3,384E-44	Med30	4,863	3,577E-28
Fhl3	5,345	1,036E-02	Oasl2	4,862	1,401E-07
Rnf125	5,342	5,961E-24	Tuba1c	4,855	2,034E-24
Rps29	5,337	5,307E-31	Tspan4	4,855	2,424E-15
Tmem51	5,337	3,187E-11	Spi1	4,853	1,608E-23
Pifo	5,333	8,345E-09	Metrnl	4,844	4,342E-11
Hint1	5,325	1,592E-115	S100a6	4,843	9,198E-96
Mx2	5,320	2,704E-10	Ndufaf8	4,838	7,185E-07
Nfil3	5,318	4,429E-24	Cox14	4,828	1,075E-17

Sfn	4,824	2,234E-07	Pgam2	4,488	1,282E-03
Stap2	4,823	1,246E-21	Clca3a1	4,486	2,388E-03
Hist1h4h	4,820	1,627E-09	Gsdmd	4,486	2,296E-12
Pym1	4,804	1,110E-16	Mrpl27	4,485	1,107E-18
Litaf	4,803	3,284E-69	Hist1h4c	4,484	3,365E-02
Lamtor5	4,802	1,075E-29	Creld2	4,472	3,243E-44
Tcap	4,797	3,845E-03	Pim3	4,472	1,207E-16
Relb	4,793	1,784E-18	Mcub	4,471	9,110E-06
Hist2h2bb	4,792	7,268E-05	Rac2	4,471	1,452E-32
Rpl24	4,791	4,270E-64	2700062C07Rik	4,467	3,623E-11
Ly86	4,787	1,286E-11	Ripk3	4,463	3,988E-06
Mrpl55	4,786	7,083E-16	Pno1	4,460	3,660E-33
Med11	4,779	6,221E-16	Gm20417	4,459	1,054E-06
Tapbpl	4,776	1,016E-26	Psmg2	4,450	1,480E-13
Atp6v1g1	4,776	1,194E-38	Cxcl16	4,446	6,814E-48
Tfpi2	4,774	1,408E-02	Gm17066	4,442	1,157E-08
Plaur	4,772	1,060E-28	Ndufa8	4,438	2,150E-20
P2ry2	4,765	4,726E-13	Bex3	4,437	5,207E-25
Rpl37	4,749	3,276E-39	Tmem261	4,432	1,235E-20
Bhlhe40	4,745	1,931E-47	Pcbd2	4,427	1,154E-04
Ccr7	4,744	4,957E-07	Adora2b	4,426	1,376E-09
Ly6c1	4,732	2,236E-27	Cmc1	4,425	1,075E-18
S100a13	4,720	2,099E-40	Mrpl16	4,420	1,467E-23
Cox5b	4,713	2,427E-05	Rps24	4,419	8,022E-26
Hist1h4n	4,713	3,331E-13	Imp3	4,417	3,611E-34
Efhd2	4,711	5,460E-48	Birc3	4,410	1,629E-47
Trbc1	4,706	7,699E-07	Fcf1	4,397	1,437E-22
Mrpl41	4,701	1,060E-20	Cdkn2d	4,384	2,930E-06
Fam162a	4,699	3,028E-26	Fam96b	4,379	7,562E-18
Zbtb16	4,694	1,907E-15	Lacc1	4,378	6,763E-16
Apex1	4,691	1,319E-22	Cox6b1	4,375	4,810E-26
Trim30b	4,687	1,485E-02	Neurl3	4,371	1,188E-06
Fam166c	4,686	5,144E-03	Erdr1	4,368	8,395E-26
Ncf1	4,686	2,852E-47	Vav1	4,362	1,147E-21
Mcemp1	4,680	7,532E-24	Rpf2	4,353	1,056E-15
Rps3a1	4,676	5,600E-127	Uqcrb	4,352	3,672E-19
Nudt2	4,671	3,936E-14	Ubxn1	4,347	5,347E-41
Dok2	4,664	5,245E-04	Elf3	4,342	4,526E-24
Dhrs9	4,662	9,218E-11	Klhl6	4,334	3,144E-20
Sertad1	4,658	2,616E-18	Ncr1	4,329	1,478E-08
Tmem203	4,653	6,869E-03	Coa6	4,324	1,278E-09
Ttc36	4,652	4,676E-04	Fbl	4,317	2,016E-19
Emp3	4,649	5,649E-32	Crlf2	4,311	3,232E-03
Nfkbiz	4,638	2,687E-41	Ndufc2	4,311	5,116E-34
Gm5431	4,629	1,954E-03	Polr2d	4,309	6,100E-18
Cuta	4,628	1,943E-26	Cox7a2	4,302	1,356E-28
Mrps18c	4,622	4,868E-34	Adora2a	4,296	6,016E-03
Mtln	4,620	1,400E-20	Fcgr1	4,292	5,735E-11
Gm15501	4,612	2,285E-06	H2-T-ps	4,286	2,100E-11
Selenbp1	4,611	3,738E-50	Gch1	4,284	1,369E-15
Pop7	4,604	2,784E-10	Tmed9	4,278	9,392E-50
Tbca	4,601	4,633E-44	Card19	4,272	1,434E-18
Vasp	4,599	4,679E-93	Bin3	4,266	3,444E-18
Gtf2f2	4,599	4,174E-22	Cd33	4,262	6,279E-22
Sult1a1	4,596	1,557E-31	Slc2a1	4,261	3,891E-14
Cd48	4,591	2,912E-18	Pfdn1	4,261	4,144E-35
Thoc7	4,589	1,067E-28	Ifi35	4,259	1,074E-32
Acyp2	4,587	1,038E-26	Gpx1	4,247	2,243E-14
Ndufs5	4,583	8,972E-24	Atp5l	4,246	1,262E-34
Rps2	4,582	7,390E-07	Ifi209	4,243	4,631E-13
1700007K13Rik	4,571	1,272E-13	Ccdc58	4,239	1,872E-05
Gm2427	4,571	1,030E-04	Csf2rb	4,230	4,677E-38
Rpl17	4,571	7,017E-18	G530011O06Rik	4,229	4,988E-02
Wdr55	4,562	8,476E-14	Irf1	4,227	6,271E-10
Fst	4,561	2,729E-04	Psmd10	4,226	1,481E-25
Rpl19	4,556	5,551E-32	Alox15	4,220	4,452E-02
Ffar4	4,550	8,727E-06	Ccdc113	4,214	4,690E-18
Higd2a	4,550	4,783E-22	Polr2h	4,207	1,240E-09
Tacstd2	4,541	2,940E-35	Rgs1	4,200	1,994E-06
Ubtd1	4,541	1,504E-05	Ccpg1os	4,188	2,115E-14
Lpcat2	4,541	3,817E-15	Lgals3bp	4,181	5,784E-16
Snhg12	4,538	1,164E-15	Pmaip1	4,179	1,462E-17
Mrps12	4,537	4,272E-14	S100a14	4,179	5,581E-10
Cebpd	4,528	2,344E-18	Csf2ra	4,179	1,536E-21
Wdr83os	4,528	1,445E-15	Tmem258	4,178	6,849E-23
Nxt1	4,524	5,329E-12	mt-Co3	4,173	1,401E-30
Magohb	4,521	2,604E-11	Tomm5	4,172	1,955E-21
Epsti1	4,515	3,061E-05	Ccdc85b	4,170	9,116E-06
Ccdc88b	4,509	1,908E-15	Ostc	4,168	2,061E-43
Tceal9	4,505	1,459E-53	Arf5	4,165	2,416E-15
Rhog	4,499	1,049E-31	Psmg1	4,162	4,930E-10
A2ml1	4,493	3,604E-05	Bst1	4,162	1,509E-11

Tbcc	4,147	7,181E-11	Prelid1	3,844	4,057E-29
Plek	4,145	4,813E-38	Il2rb	3,840	2,015E-08
Mrpl2	4,138	5,308E-22	Iglc2	3,838	2,114E-06
Hba-a2	4,137	1,355E-02	Ak2	3,836	2,275E-23
Fam122a	4,134	2,493E-04	Hspb1	3,833	8,488E-16
Pcgf5	4,131	9,285E-18	Il10ra	3,832	1,323E-10
Tsta3	4,120	2,180E-04	Ubald2	3,831	2,388E-25
Mrpl43	4,118	5,080E-14	Chmp2a	3,831	7,367E-36
Ccdc122	4,117	1,021E-06	Pfdn6	3,828	1,838E-19
Bax	4,113	4,529E-09	Sdc4	3,825	9,149E-34
Anxa8	4,110	9,289E-13	Tatdn1	3,825	1,757E-07
Hist1h2bl	4,097	9,793E-07	Nr2c2ap	3,823	1,136E-04
Rpl36al	4,094	1,002E-39	Grrp1	3,823	4,566E-04
Selplg	4,088	2,201E-14	Polr2g	3,818	5,058E-19
Apip	4,081	4,200E-11	Gm16136	3,818	1,531E-03
Rnasek	4,079	1,395E-16	Psme1	3,817	4,419E-18
Mcts2	4,078	1,090E-07	Timm13	3,817	8,238E-06
Znrd1	4,077	4,298E-18	Rpl41	3,803	1,267E-45
Zfp593	4,076	1,691E-02	Hspe1	3,801	2,124E-25
Dhx58	4,074	2,497E-11	Tmem176b	3,800	6,497E-41
Agr3	4,072	9,224E-06	Pik3ap1	3,799	1,529E-15
2200002D01Rik	4,068	3,122E-13	Nubp2	3,798	1,212E-09
Klrd1	4,065	1,396E-03	Cyc1	3,797	8,415E-22
Mrpl36	4,061	1,633E-07	Ranbp1	3,793	5,197E-36
Osr1	4,059	9,634E-12	Cox7c	3,792	1,012E-19
Mxd1	4,054	2,117E-28	Coa3	3,792	8,947E-08
Irf5	4,051	9,058E-16	Brms1	3,789	3,663E-11
Pinx1	4,050	1,236E-17	Fabp3	3,780	1,397E-04
Rrs1	4,044	1,485E-06	Tbcb	3,774	5,260E-18
Tomm22	4,038	9,294E-19	Ndufs8	3,774	4,884E-17
Selenow	4,037	9,264E-30	Slc25a5	3,771	1,882E-37
Hist1h4a	4,026	1,541E-06	Uqcc2	3,766	9,662E-16
Gtf2f1	4,025	5,621E-31	Acot13	3,764	7,678E-16
Sem1	4,020	2,956E-23	1810009A15Rik	3,761	6,349E-14
Exosc3	4,018	5,911E-22	Rps11	3,759	2,977E-10
Psmb8	4,017	1,763E-09	Ms4a4d	3,758	7,050E-23
Themis2	4,012	5,254E-20	Avpi1	3,751	4,557E-09
Enc1	4,012	4,975E-26	Phgdh	3,741	1,267E-06
Tmem147	4,011	7,818E-11	Eef1akmt1	3,739	1,292E-04
Nr4a1	4,003	4,144E-13	Trappc1	3,738	2,720E-14
Fdx1l	4,003	7,132E-12	Aprt	3,731	5,196E-11
Ptpn6	4,003	2,599E-23	Mat1a	3,731	6,376E-10
Tekt4	4,002	6,289E-07	Was	3,730	1,003E-12
Ftl1	3,997	5,708E-22	Chmp4b	3,728	2,701E-25
Tmsb10	3,997	1,316E-93	Uqcrfs1	3,727	1,153E-32
Gm20257	3,992	1,199E-03	Prelid3b	3,720	5,711E-21
Naa38	3,988	7,147E-20	C1qa	3,715	1,109E-12
Atf4	3,982	3,736E-71	Gm15922	3,714	4,085E-14
Daxx	3,968	7,088E-22	B230307C23Rik	3,710	4,838E-07
Il18rap	3,967	6,464E-14	Lyve1	3,703	2,138E-21
Nod2	3,959	1,633E-04	Rplp0	3,698	1,471E-28
C1qb	3,958	1,508E-05	Ccdc94	3,691	2,573E-10
Rpp30	3,952	1,047E-15	Gm10282	3,688	4,944E-26
Kcnrg	3,949	6,156E-03	Fam96a	3,677	3,086E-28
Emc4	3,940	3,238E-13	Apoo	3,676	6,033E-06
Ier2	3,936	4,872E-12	Psmd7	3,674	1,541E-19
S100a1	3,935	2,099E-23	Rpl10-ps3	3,673	3,863E-02
mt-Atp6	3,935	3,372E-17	Mrpl53	3,668	2,580E-07
Tnfaip8l2	3,922	3,322E-08	Tfpt	3,666	2,430E-09
mt-Nd1	3,922	1,672E-26	Idnk	3,662	3,442E-10
H2-M3	3,919	1,858E-11	Srfbp1	3,660	4,642E-13
Nr4a3	3,915	2,080E-03	Uqcc3	3,660	1,701E-13
Dctn3	3,915	2,371E-18	2310030G06Rik	3,656	7,094E-10
Bvht	3,915	4,635E-15	Sephs2	3,654	1,014E-19
Supt4a	3,909	1,573E-11	Arl6ip5	3,646	8,548E-20
Ngdn	3,907	4,132E-22	Nmi	3,645	5,201E-18
Serpina3c	3,907	1,150E-02	BC031181	3,640	1,667E-31
Snrnp35	3,906	1,278E-05	Tmem126a	3,621	8,169E-08
Rps21	3,894	1,728E-07	Nuak2	3,616	1,078E-05
Tmem14c	3,886	8,789E-23	Inhbb	3,616	1,093E-14
Ndufb1-ps	3,883	3,001E-21	S100a10	3,611	1,993E-21
Slc39a14	3,879	3,311E-18	Ndufa12	3,608	7,022E-22
Slc9a3r1	3,874	7,930E-26	Pawr	3,607	5,258E-24
Il34	3,868	8,508E-04	Rps28	3,606	1,562E-22
Pold4	3,865	2,948E-22	Ccdc78	3,602	1,474E-05
Klra2	3,859	4,140E-10	Hnrnpa1	3,600	2,005E-42
Pdpn	3,854	7,376E-42	Nme5	3,593	1,689E-09
Dcaf13	3,853	1,043E-30	Lamtor4	3,591	4,379E-10
Ndufa5	3,851	2,141E-35	Selenok	3,589	5,444E-27
Psmc5	3,849	2,089E-36	Dnajc17	3,589	7,275E-05
Smim12	3,849	2,534E-18	Rrad	3,586	1,289E-02
Tnfrsf26	3,847	3,069E-04	Snrpe	3,583	9,285E-15

Sema6b	3,581	1,413E-03	Ndufa3	3,371	3,861E-09
Prdx3	3,580	4,537E-23	Tm2d1	3,371	1,572E-15
Clu	3,580	1,074E-23	Rraga	3,366	7,223E-06
Mrpl40	3,574	4,777E-18	Slc39a1	3,360	5,493E-31
Thoc6	3,571	4,300E-04	Dok1	3,360	1,735E-05
Trmt112	3,570	1,859E-21	Evi2a	3,359	4,253E-13
Arhgdib	3,569	1,284E-17	Fibp	3,358	6,364E-10
Ppp1r3d	3,565	3,904E-03	Mettl1	3,354	1,799E-03
Lsm3	3,562	2,515E-14	Angptl4	3,345	3,608E-09
Nenf	3,562	1,303E-13	Emg1	3,341	3,159E-19
Cdkn2b	3,560	4,088E-25	Ripk2	3,336	1,804E-13
Jaml	3,559	1,790E-09	Cox20	3,335	6,420E-08
Svbp	3,559	1,027E-02	Glipr1	3,334	2,792E-08
Gsto1	3,557	2,346E-27	Rrp36	3,328	8,455E-14
Gpsm3	3,557	2,040E-07	Snhg5	3,327	2,450E-10
Atp5mpl	3,553	3,204E-16	Commd6	3,326	2,850E-07
Rps16	3,550	1,885E-16	H2afz	3,325	8,489E-30
Cetn3	3,549	1,362E-30	Rps27	3,323	1,808E-12
Nop10	3,541	4,552E-21	Krtcap2	3,322	1,739E-23
Immp1l	3,526	2,793E-09	Mrpl20	3,318	4,446E-07
Edf1	3,516	2,808E-20	Evi2b	3,315	4,088E-14
Mvp	3,504	7,745E-36	mt-Nd2	3,312	2,876E-11
Csf2rb2	3,498	9,513E-10	Ggct	3,312	5,526E-03
Nsmce1	3,498	1,180E-22	Mrps6	3,310	4,063E-05
Brk1	3,497	6,511E-24	Tomm6	3,308	2,469E-11
Tsr3	3,495	5,800E-10	1810055G02Rik	3,299	4,400E-11
Srp9	3,494	6,502E-13	H2-K1	3,295	2,150E-06
Isg20	3,493	1,201E-13	Tmprss4	3,293	3,492E-03
Polr2i	3,487	6,310E-09	Ap3s1	3,291	2,870E-17
Sdhd	3,484	3,038E-22	Adprh	3,288	3,321E-10
Ctss	3,482	2,054E-31	Fosl1	3,288	9,364E-05
Pgk1	3,477	3,400E-36	Hprt	3,285	1,909E-31
1810037I17Rik	3,476	4,741E-16	Trim34b	3,275	1,639E-05
3110040N11Rik	3,472	3,288E-06	Rtca	3,274	6,817E-09
C1ra	3,471	1,860E-19	Apoa1bp	3,273	4,044E-13
Znhit2	3,468	2,645E-02	Psmc6	3,272	1,646E-28
Mrpl22	3,460	4,702E-08	Sarnp	3,272	6,276E-18
Rnf113a2	3,459	2,740E-13	Lyrm2	3,270	9,245E-10
Vapa	3,458	7,636E-30	Abt1	3,262	4,299E-08
Gpatch4	3,458	1,800E-02	Trim30a	3,260	3,112E-15
Sox2	3,457	4,344E-07	Jagn1	3,260	8,360E-06
Timm23	3,454	1,620E-24	Tnfrsf1a	3,256	3,578E-28
Emc2	3,453	1,624E-24	Arpc2	3,255	1,201E-21
Pigf	3,453	6,821E-06	Emc6	3,253	9,621E-18
Clpp	3,450	1,154E-12	Mrpl14	3,251	1,662E-06
Tap2	3,445	3,501E-09	Abcb1b	3,250	8,722E-03
Rras	3,444	8,228E-08	Slc31a2	3,249	4,206E-13
Nop16	3,436	1,104E-09	Coq10b	3,249	4,387E-11
Serpina1b	3,435	2,957E-05	H2-Q4	3,249	1,953E-09
Lamtor1	3,434	2,767E-18	Rps6	3,246	6,301E-26
Gm21811	3,432	1,233E-03	Pgam1	3,244	7,178E-25
Vps25	3,431	4,999E-05	Glipr2	3,243	2,086E-25
Ap4s1	3,430	3,004E-10	Lsm10	3,243	2,130E-02
Bola2	3,420	8,854E-09	Esd	3,242	9,007E-19
Dtwd1	3,418	6,540E-03	Clec2d	3,241	4,676E-27
Asns	3,415	2,409E-14	Ctla2b	3,228	4,026E-17
AI413582	3,412	3,469E-03	Ptpn2	3,224	2,427E-26
Mrpl34	3,411	2,736E-02	Bloc1s4	3,223	1,170E-03
Ogfr	3,405	5,178E-22	Ap2s1	3,218	3,531E-08
Pigyl	3,401	4,939E-11	Rpl31	3,215	7,353E-14
Prr15	3,400	3,127E-04	Uqcrq	3,210	6,351E-08
Ndufb11	3,400	6,611E-16	Ccdc25	3,210	1,193E-18
Cfap298	3,399	1,056E-29	Dpy30	3,209	2,423E-14
Ift27	3,398	2,568E-02	Otulin	3,208	2,224E-09
Havcr2	3,398	1,056E-11	Mb	3,201	2,986E-02
Lad1	3,397	7,260E-03	Fam195b	3,200	1,712E-10
Cyp1b1	3,394	2,196E-02	Psenen	3,198	3,090E-16
Ccdc190	3,394	2,155E-12	Nipsnap3b	3,197	4,183E-06
Cfdp1	3,393	1,029E-29	Arl3	3,196	2,396E-14
A4galt	3,391	4,343E-11	Noc4l	3,196	1,493E-04
Slc15a3	3,390	7,697E-07	Itih4	3,194	2,345E-25
4930486L24Rik	3,386	5,620E-04	Slc5a1	3,186	2,768E-02
Slc10a6	3,384	5,491E-09	Adgre4	3,185	2,282E-06
Rpl35	3,382	5,859E-23	Fra10ac1	3,184	7,780E-06
Emilin2	3,382	7,208E-15	Ndufa4	3,178	2,831E-13
Nt5c	3,379	1,655E-11	Snrpd2	3,174	4,592E-08
Fam216a	3,376	6,286E-13	Prkcdbp	3,174	2,156E-12
Pcna-ps2	3,375	3,284E-13	Tma7	3,173	1,997E-13
Commd5	3,374	3,282E-07	Tlr6	3,173	1,747E-02
Smdt1	3,374	3,618E-17	Katna1	3,170	1,475E-17
Rbm3	3,373	1,310E-15	Lgals3	3,168	1,423E-17
Polr2j	3,372	2,296E-14	Plp2	3,164	4,261E-15

Uba52	3,162	1,401E-15	Med6	2,976	9,747E-15
Anp32b	3,160	6,591E-07	Calm2	2,976	5,928E-37
Sec13	3,157	8,200E-26	Adgre1	2,970	6,450E-13
Tmem60	3,155	2,857E-04	Spsb1	2,964	1,788E-03
Cisd1	3,154	2,230E-08	Nudc	2,962	3,652E-27
Ccdc12	3,152	5,662E-11	Kti12	2,958	3,970E-05
Rps17	3,149	5,035E-19	Pcbp1	2,958	6,476E-10
E130102H24Rik	3,148	5,708E-04	Srxn1	2,955	1,880E-08
Id1	3,144	4,359E-14	Rhou	2,953	8,160E-05
Spint2	3,136	3,573E-21	Ccr5	2,951	1,135E-06
Pycrl	3,131	1,215E-02	Mlf1	2,948	3,154E-05
Tmem192	3,130	2,035E-03	Psmc4	2,948	1,273E-19
mt-Cytb	3,129	3,673E-07	Gng10	2,946	2,984E-11
Apobec1	3,122	1,247E-06	Prss23	2,944	7,545E-20
Mrps34	3,121	5,289E-03	Mtres1	2,942	6,304E-07
Fstl3	3,121	1,050E-13	Itga7	2,942	2,591E-07
Rps26	3,118	9,005E-14	Capg	2,940	1,222E-12
Rbmxl1	3,116	2,691E-18	Ppie	2,939	1,946E-04
Krt18	3,111	7,371E-26	Clip4	2,939	2,376E-11
Spcs1	3,110	1,069E-10	Btf3	2,937	3,543E-27
Med29	3,108	5,758E-08	Zfp429	2,937	7,945E-04
Il2rg	3,098	2,536E-08	Hist1h1e	2,933	3,033E-06
Elof1	3,094	1,249E-10	Mcts1	2,929	4,183E-04
BC023719	3,093	7,105E-05	Mvd	2,929	1,716E-04
Cdk2ap2	3,093	2,713E-06	Ctla2a	2,928	3,197E-17
Ppan	3,092	6,805E-05	Fkbpl	2,923	2,990E-04
Rpl7a	3,092	1,593E-32	Mrpl28	2,921	2,640E-02
Cd74	3,089	2,685E-22	Rwdd1	2,918	4,169E-15
Pik3r5	3,088	7,658E-11	Dynlrb1	2,918	8,864E-08
Cdc34	3,081	2,858E-09	Bccip	2,916	2,142E-14
Pdhb	3,079	7,950E-22	Haus7	2,915	3,318E-06
Dcxr	3,078	3,346E-08	Exosc1	2,915	1,362E-08
Rbis	3,078	7,691E-20	Ccdc124	2,915	5,834E-03
Faim	3,070	2,310E-09	Tmem128	2,912	8,334E-08
Mrpl46	3,069	1,455E-07	Phpt1	2,911	4,420E-04
Clns1a	3,068	3,879E-20	Hk2	2,911	1,011E-05
Gsr	3,062	1,663E-28	Nifk	2,910	5,286E-15
Manbal	3,058	2,619E-04	Hscb	2,908	1,909E-02
Prr13	3,057	2,665E-16	Bak1	2,908	2,485E-07
Ccdc181	3,057	1,054E-17	Upk1b	2,907	1,835E-04
C1s2	3,053	7,579E-03	Gimap9	2,905	1,941E-12
Mphosph6	3,046	1,384E-06	Psma1	2,905	3,898E-22
Mrps18b	3,045	2,278E-05	Ehd1	2,901	2,085E-23
Eif5a	3,045	7,127E-27	Mfsd5	2,900	1,690E-08
Cmpk2	3,044	8,198E-05	Eci1	2,897	7,942E-06
Gabarap	3,043	2,570E-28	Epcam	2,895	2,929E-16
Tekt1	3,043	2,222E-05	Clec4a2	2,895	9,758E-05
Crcp	3,040	1,308E-10	Kars	2,890	1,677E-17
Srp14	3,040	1,903E-29	C3	2,889	6,528E-12
Crb3	3,039	9,646E-07	Srsf9	2,884	3,508E-09
Bud31	3,038	2,824E-22	Tubb2a	2,880	6,531E-17
Hn1l	3,032	5,526E-12	Ndufb10	2,879	2,621E-16
Memo1	3,031	2,024E-18	Mitd1	2,879	4,583E-11
Samm50	3,027	2,667E-14	Mrto4	2,879	1,625E-02
Cpne2	3,026	4,689E-04	Il13ra1	2,870	1,980E-20
Rpl23	3,024	1,493E-29	Nampt	2,866	1,317E-21
Txndc17	3,021	7,994E-17	Abhd17c	2,866	2,007E-14
Lrrc59	3,020	1,742E-25	Mmp14	2,866	3,900E-12
Cmbl	3,015	2,071E-06	Sar1b	2,866	1,207E-11
Med4	3,015	4,083E-13	Rps12	2,865	1,937E-07
Csf1	3,013	9,475E-15	Asna1	2,864	1,074E-12
Rsl1	3,013	3,312E-02	Rab4b	2,861	4,294E-03
Ormdl2	3,011	1,835E-07	Drap1	2,859	7,864E-06
Rnaset2b	3,010	9,508E-12	Calml4	2,858	1,455E-03
Zfp1	3,005	6,345E-05	Ndufs4	2,858	2,211E-18
Ccs	3,003	9,792E-05	Tmed1	2,855	4,082E-03
Snhg1	3,002	5,382E-09	Syngr2	2,850	1,511E-17
Clic1	3,000	1,055E-25	Pold2	2,849	1,976E-02
Kdelr2	3,000	1,213E-07	Plscr1	2,839	1,353E-11
Nutf2-ps1	3,000	8,330E-03	Nudt16l1	2,828	7,161E-03
Coro1a	2,999	5,584E-15	Rce1	2,828	1,368E-02
Taldo1	2,998	1,546E-20	Ndufaf5	2,827	3,543E-04
Rsph1	2,996	2,495E-04	Pfkfb3	2,825	2,434E-10
Gmfg	2,994	1,008E-15	Mgst1	2,821	1,618E-09
H2-DMb1	2,994	1,252E-04	Lsm7	2,818	2,659E-02
Selenos	2,993	2,015E-19	Yif1a	2,818	2,969E-04
Bcl10	2,985	1,958E-15	Tapbp	2,816	1,392E-11
Mapkapk2	2,984	1,249E-20	Sema4d	2,815	3,810E-06
Arl6ip4	2,984	4,516E-12	Rnf126	2,815	1,006E-04
Il15ra	2,983	1,496E-03	Fgl2	2,814	4,066E-12
Ndfip1	2,982	9,067E-22	Enkur	2,813	3,157E-05
Utp3	2,977	1,835E-13	March5	2,813	4,652E-18

Psmc1	2,812	7,052E-21	Smim11	2,659	6,054E-06
Gapdh	2,807	5,719E-09	Mmadhc	2,658	2,148E-07
Apobr	2,807	2,097E-06	Vamp8	2,657	3,044E-22
Creb3l1	2,806	8,733E-08	Timm21	2,656	9,546E-05
F7	2,804	3,453E-06	Sfr1	2,655	4,004E-19
Map3k6	2,804	1,215E-03	Tmed3	2,655	2,425E-10
Mrps36	2,803	2,632E-09	Etfb	2,653	2,524E-19
Clta	2,802	3,447E-30	H2-D1	2,651	2,946E-09
Arl6	2,801	1,382E-05	Tgif1	2,646	7,478E-05
Lysmd2	2,800	3,269E-12	C1s1	2,643	3,617E-09
Eif3h	2,793	6,677E-12	Rpl37a	2,643	6,482E-06
Hpcal1	2,791	3,669E-12	Rplp2	2,639	1,241E-10
Ruvbl1	2,790	2,600E-14	Fam241a	2,637	1,439E-06
G0s2	2,787	2,856E-14	Gpx8	2,636	2,990E-13
Chac2	2,783	8,304E-08	Hars	2,632	1,871E-12
Ppp3cc	2,783	6,891E-03	Tagap	2,632	3,858E-02
Il7r	2,782	6,558E-07	Trim13	2,631	8,041E-03
Snx7	2,782	7,391E-17	Ube2g2	2,629	1,357E-02
Bola1	2,781	1,790E-02	Sap30l	2,629	3,332E-05
Tst	2,779	1,826E-04	Spag7	2,628	2,199E-12
Eola1	2,777	1,025E-04	Polr3d	2,628	3,171E-05
Procr	2,776	4,980E-06	Slc7a7	2,624	2,113E-03
Ebag9	2,773	5,089E-08	Akip1	2,622	2,889E-05
Got1	2,771	8,035E-07	Clic3	2,620	2,162E-09
Cd300c2	2,771	2,049E-04	Eif6	2,619	6,049E-03
Cox7b	2,766	7,642E-06	1600014C10Rik	2,618	1,747E-04
Thyn1	2,766	1,072E-04	Papd4	2,618	9,438E-13
Lgals9	2,765	1,635E-06	Eif3l	2,614	6,017E-13
Cldn7	2,764	4,294E-04	Med9	2,612	3,422E-05
Parp9	2,764	1,359E-07	Jdp2	2,610	1,716E-08
Cwc15	2,759	4,298E-24	Rpa3	2,605	2,762E-02
Eif1a	2,755	3,081E-20	Ube2s	2,603	1,123E-10
Eif2b2	2,754	6,092E-07	Ltv1	2,602	8,961E-11
Eif3e	2,753	7,627E-20	Isyna1	2,601	4,536E-04
Map3k8	2,752	5,935E-09	Stub1	2,599	7,185E-16
Rhob	2,751	5,136E-22	Nars	2,596	2,202E-20
Alg3	2,750	2,245E-02	Sirpb1c	2,594	1,313E-02
Rpl39	2,750	3,135E-12	Lmnb1	2,593	2,529E-05
Copz1	2,749	4,834E-14	Gmppb	2,592	4,655E-03
Rnf7	2,745	1,402E-08	H2-Ab1	2,589	1,638E-09
Snrpa	2,744	1,182E-11	Gdap10	2,588	5,837E-04
Psmb6	2,743	7,715E-12	Igfbp7	2,586	3,076E-10
Ran	2,738	1,182E-18	Yeats4	2,585	4,460E-05
Prf1	2,738	4,733E-02	Psmd14	2,579	2,009E-12
Plpp1	2,733	8,662E-16	Cldn3	2,579	2,688E-11
Mrps27	2,728	3,171E-02	Oard1	2,578	3,560E-11
Mrps23	2,723	5,054E-08	Ppp2cb	2,575	1,366E-20
Aimp1	2,722	2,512E-13	Mbd1	2,574	3,832E-08
Slc25a28	2,719	2,592E-06	Mrpl18	2,573	3,122E-06
I830077J02Rik	2,718	4,298E-03	Hcfc1r1	2,572	2,770E-06
Tomm7	2,715	2,800E-07	Arid5a	2,570	1,619E-03
Tmem252	2,714	1,292E-02	Vdac3	2,568	8,289E-21
Tmem243	2,713	7,052E-10	Sh3d21	2,566	4,709E-04
Ndufa13	2,709	3,846E-17	Hif1a	2,563	1,114E-20
Pfdn2	2,708	2,152E-03	Nrbf2	2,563	2,983E-05
Arf6	2,707	3,075E-19	Foxj1	2,562	6,426E-07
Pus1	2,706	4,442E-02	Cirbp	2,562	1,958E-05
Gins4	2,702	8,934E-09	Ctdnep1	2,562	1,594E-02
Fam216b	2,701	1,999E-05	Ddit3	2,560	1,797E-05
Rps27a	2,700	3,856E-21	Bag1	2,559	1,220E-15
Dhrs4	2,700	3,429E-08	Cndp2	2,559	3,940E-14
Prps1	2,695	6,934E-07	Dbi	2,558	8,478E-08
0610040J01Rik	2,694	3,781E-03	Hyi	2,557	3,987E-02
Bop1	2,694	1,388E-06	Ptma	2,557	3,567E-16
Rab5c	2,690	2,376E-26	Hpf1	2,555	6,095E-05
Olr1	2,690	1,618E-06	Ndufc1	2,554	3,204E-05
Nop2	2,688	1,064E-04	Rasl11b	2,551	4,692E-02
Acadl	2,687	4,205E-14	Gmpr2	2,551	5,314E-04
Id2	2,686	9,073E-10	Rer1	2,549	1,734E-14
Gtf2b	2,685	3,531E-18	Vmp1	2,549	2,028E-10
Lamtor2	2,684	1,565E-04	Sema4a	2,545	3,067E-06
Edn1	2,677	5,871E-18	Arpc5	2,544	1,623E-11
Icam1	2,676	4,015E-32	Tuba1b	2,542	3,048E-20
Bri3	2,672	1,159E-04	Eif4ebp1	2,541	7,532E-05
Dcps	2,672	1,142E-03	2310011J03Rik	2,538	2,061E-03
Casp7	2,671	2,674E-07	Rps8	2,538	4,920E-10
Atp5j2	2,669	3,711E-09	Atp5g2	2,538	4,367E-13
Ccdc86	2,666	4,565E-02	Gm10184	2,534	1,792E-02
Cd40	2,665	5,173E-09	Atp5h	2,531	1,850E-09
Rtraf	2,663	1,099E-21	Wisp2	2,530	9,822E-05
Rpl28	2,660	1,273E-11	Krt8	2,530	4,371E-17
Eif1b	2,659	1,234E-08	Rsph3b	2,530	1,275E-04

Gfpt2	2,529	1,920E-02	Hebp1	2,388	3,268E-08
Fbxo4	2,525	8,456E-08	Rps14	2,387	3,891E-06
Ppp1ca	2,525	2,830E-21	Psma4	2,387	8,638E-09
Setd6	2,523	4,571E-02	Cdc42ep4	2,384	6,672E-14
Tinf2	2,522	2,719E-04	Uqcrh	2,384	1,501E-06
Cd24a	2,520	9,611E-16	Mpc1	2,383	4,709E-07
Rabggtb	2,520	2,514E-09	Tpm4	2,383	1,374E-19
Fbxo6	2,516	1,612E-04	Bloc1s1	2,381	3,534E-08
Rpl36a	2,516	2,702E-11	Phfl1d	2,381	3,912E-02
Gcsh	2,516	3,008E-05	Lox	2,380	3,768E-05
Hax1	2,516	1,580E-08	Tor1a	2,379	6,074E-04
Cib1	2,514	2,414E-02	Grap	2,376	3,652E-09
Dync2li1	2,514	2,158E-03	Slc35b1	2,372	5,935E-09
Ecscr	2,514	2,958E-10	Psmd12	2,371	1,276E-15
Ptcd2	2,508	8,947E-07	Zfpl1	2,371	1,927E-02
Rsl24d1	2,508	1,234E-13	Cfl1	2,371	1,843E-13
Fmnl2	2,507	1,619E-15	Stip1	2,370	3,413E-13
Bckdhb	2,507	1,945E-03	Ino80b	2,370	3,439E-05
Unc50	2,503	2,597E-08	Tes	2,363	8,052E-08
Polr2l	2,500	4,456E-05	Pet100	2,357	2,564E-04
Zfp52	2,500	3,222E-04	Ino80c	2,356	1,005E-06
Pirb	2,491	1,633E-05	Slc39a7	2,354	6,852E-12
Ufc1	2,483	1,656E-05	Mocs1	2,347	7,340E-03
Eif3d	2,481	1,293E-12	Tmbim4	2,344	1,010E-08
Mageh1	2,480	2,779E-06	Lmcd1	2,342	3,454E-05
Snx3	2,476	4,879E-14	Mrps30	2,342	1,823E-02
Itpa	2,476	1,457E-07	Cd38	2,340	1,689E-07
Ift57	2,476	2,691E-08	Pfdn5	2,338	2,118E-13
Atg101	2,475	9,668E-03	Arfl	2,336	1,832E-13
Sumo2	2,474	2,906E-16	Dbnl	2,336	6,503E-11
Gm4353	2,473	1,627E-03	Phlda1	2,335	4,463E-05
Tmem106a	2,473	4,472E-03	Aurkaip1	2,335	2,964E-07
Mrfap1	2,471	1,128E-15	Ddost	2,335	1,705E-13
Wdr46	2,471	1,241E-03	Mdh2	2,334	4,942E-09
Ndufb4	2,469	3,002E-03	Ndufa9	2,334	5,943E-08
Tagap1	2,467	2,516E-02	Mydgf	2,329	1,140E-02
Gm10093	2,466	1,070E-02	Arpc4	2,329	9,117E-10
Siva1	2,466	5,935E-07	Trappc3	2,329	2,659E-06
Ccl21a	2,465	1,244E-04	Spata18	2,326	1,293E-02
Zfp830	2,462	8,031E-06	Hspb8	2,325	3,153E-04
Parp10	2,462	2,149E-05	Tmem11	2,322	7,549E-06
Sp140	2,459	1,050E-04	Ptges3	2,315	1,166E-09
Dazap2	2,455	7,566E-12	Cox4i1	2,315	1,518E-08
Phyh	2,453	5,230E-10	Mettl9	2,315	5,853E-10
Bcap31	2,451	1,753E-08	Zdhhc13	2,307	2,818E-03
Pnp	2,451	4,209E-07	Arrb2	2,307	5,374E-05
Zfp36	2,451	7,855E-09	Llph	2,306	1,497E-06
Fermt3	2,449	2,918E-07	Cox7a2l	2,302	7,289E-10
Tgm2	2,447	5,390E-17	Lap3	2,299	1,267E-02
Lyar	2,446	6,810E-05	Nfam1	2,298	1,307E-06
Xdh	2,446	1,108E-02	Rsl1d1	2,296	2,229E-11
Rgs19	2,445	2,031E-05	Gars	2,296	1,680E-11
Kin	2,442	4,271E-04	Birc2	2,295	2,234E-09
Mak16	2,441	1,705E-07	Zfand2b	2,294	8,650E-03
Tinagl1	2,441	2,456E-09	Anapc13	2,291	1,374E-05
Rps4x	2,441	4,063E-13	Sfxn1	2,290	2,429E-03
Hmgn3	2,440	8,273E-03	Aldh3b1	2,290	4,118E-07
Jtb	2,438	1,684E-04	BC029722	2,284	5,868E-04
Fam49b	2,435	9,373E-13	Sh3gl1	2,282	7,737E-06
Fam204a	2,434	1,439E-08	Nop14	2,281	2,150E-05
Rpl4	2,434	8,621E-26	Ndufs3	2,280	2,030E-06
Rbfa	2,432	1,622E-02	F13a1	2,274	2,784E-05
Tipin	2,431	4,377E-03	Surf4	2,272	4,944E-14
Nucb2	2,430	2,344E-19	G6pdx	2,271	1,111E-04
Sh3bp2	2,427	2,248E-02	Tnip2	2,271	1,766E-05
Mgst3	2,425	2,239E-03	Ift20	2,270	1,064E-10
Noc2l	2,424	1,716E-08	Hist1h2bc	2,266	1,814E-03
Cyth4	2,421	6,587E-06	Trim21	2,266	2,582E-02
Rnf130	2,420	5,642E-12	Frg1	2,264	3,150E-06
Tmed2	2,418	2,439E-23	Atp1b3	2,264	1,574E-09
Rps7	2,418	8,202E-13	Psmd6	2,262	1,655E-11
H2-DMa	2,413	1,493E-03	Ssr2	2,259	1,160E-06
Ssna1	2,413	3,799E-03	Acot9	2,258	3,610E-08
Atp6v0d1	2,413	4,515E-12	Chmp5	2,256	1,648E-12
Tars	2,411	2,385E-11	Odc1	2,252	1,367E-05
Zfp869	2,411	2,119E-04	Cln5	2,252	2,717E-07
Mrpl21	2,410	2,212E-03	Ppic	2,251	7,975E-13
Gem	2,405	8,942E-05	Ssb	2,249	3,588E-17
Snx10	2,403	1,509E-08	Map1lc3a	2,245	2,967E-04
Arl8a	2,399	1,896E-08	Parp2	2,245	1,574E-03
Snapc5	2,399	1,058E-08	Cops6	2,243	9,913E-05
Hsd17b12	2,392	2,219E-15	Glul	2,236	6,665E-10

Tablas Suplementarias

S1pr1	2,233	8,513E-11	Pfdn4	2,124	1,058E-02
Pwp1	2,233	2,126E-05	Cybb	2,121	1,402E-09
Rps5	2,232	4,283E-04	Rps10	2,120	6,161E-06
Wfdc2	2,229	1,454E-08	Arhgdia	2,110	4,513E-16
Lpar1	2,223	7,016E-06	Anxa7	2,106	6,170E-12
Tubb4b	2,222	2,804E-07	Pdia4	2,105	9,877E-13
Vta1	2,221	1,914E-04	Actb	2,103	1,144E-09
Rap2c	2,218	1,006E-05	Mettl10	2,101	4,919E-03
Rps13	2,217	2,381E-04	R3hdm4	2,099	4,961E-03
Pa2g4	2,216	9,258E-08	Itgb2	2,096	1,478E-06
Zkscan6	2,216	1,534E-02	Pebp1	2,094	7,255E-03
Ppp1r11	2,213	1,374E-10	Gdpd1	2,092	1,012E-02
Fam136a	2,212	6,115E-03	Rbm42	2,089	2,719E-03
Elp5	2,206	4,717E-02	Gda	2,084	2,307E-04
Atp5g3	2,205	8,772E-04	Ttc1	2,083	2,089E-04
Irak2	2,205	4,821E-05	Sugt1	2,082	1,592E-08
Gba	2,204	8,273E-09	Rars	2,081	3,110E-07
Tmem50a	2,204	4,125E-14	Spry2	2,080	6,181E-03
Ier3ip1	2,202	7,240E-08	Susd6	2,079	8,000E-13
Mcee	2,200	8,089E-03	Tbk1	2,076	5,910E-07
Etfa	2,198	8,588E-04	Eif3j2	2,072	2,162E-07
Cript	2,193	1,786E-04	Farsb	2,066	3,316E-02
Hn1	2,192	2,092E-04	Txndc15	2,063	1,193E-04
Cct2	2,192	9,940E-14	Ifi27	2,062	3,820E-04
Rpl6	2,191	3,455E-12	Gngt2	2,057	1,042E-02
Cxcl14	2,185	1,431E-03	Cdo1	2,056	3,279E-07
Npm1	2,182	4,952E-11	Klf2	2,052	4,643E-02
Eif3g	2,182	1,731E-06	Rpl10	2,052	7,672E-05
Gatm	2,182	1,002E-03	Apoc1	2,051	4,171E-04
Tufm	2,182	3,817E-03	Ik	2,050	1,782E-07
Atpif1	2,182	1,063E-09	Rpl10a	2,050	3,743E-06
Ltbr	2,180	2,002E-08	Herpud1	2,049	1,683E-04
Ublcp1	2,179	1,851E-03	Sumo1	2,049	3,760E-06
Vti1b	2,177	2,337E-09	Hspd1	2,041	3,390E-10
Pole3	2,176	1,565E-03	Parp12	2,035	4,941E-05
H3f3b	2,172	1,510E-14	Eef1g	2,034	4,940E-05
Fez2	2,171	8,203E-07	Mgp	2,033	6,512E-06
Hopx	2,169	6,335E-05	Tspan1	2,033	9,993E-06
Tmsb4x	2,168	1,097E-14	mt-Co1	2,028	7,504E-10
Psmb3	2,160	2,565E-03	Hbegf	2,027	4,502E-02
Ccdc153	2,156	3,692E-04	Capza1	2,024	3,361E-02
Akr1c14	2,156	9,338E-03	Prps1l3	2,023	4,019E-03
Fis1	2,155	4,048E-02	Pqbp1	2,020	3,124E-04
Dtx3l	2,154	6,498E-03	Ptpn1	2,018	1,828E-07
Chmp2b	2,154	5,534E-09	Puf60	2,018	1,075E-07
Snrnp27	2,153	1,552E-04	Commd10	2,018	1,453E-02
Kat5	2,150	1,824E-04	Rbm17	2,017	6,523E-05
Manf	2,148	1,691E-06	Flot1	2,017	7,050E-03
Arf4	2,148	2,668E-08	Ndufv2	2,015	4,864E-04
Kdelr1	2,147	1,988E-04	Krcc1	2,015	6,253E-06
Laptm4a	2,146	5,545E-05	Pgm1	2,011	7,626E-03
Mrps15	2,146	9,769E-03	Sec61g	2,010	3,605E-03
Prkag1	2,137	1,850E-06	Ncf2	2,009	4,934E-04
Rbx1	2,137	2,740E-03	Dpp3	2,006	1,524E-03
Ost4	2,136	8,764E-05	Nadk	2,006	4,088E-05
Rab1b	2,134	8,570E-08	Psmc3	2,004	3,537E-10
Larp7	2,131	5,516E-04	Gtf3c6	2,003	1,429E-02
Cby1	2,126	3,900E-04	E2f4	2,001	9,588E-03
Tsr1	2,125	6,271E-03			

Table A4. Down-regulated genes in infected lungs compared to non-infected lung (2,229).

Gene name	Fold-change	p-value
Fbn2	-91,371	7,368E-03
Cntn4	-47,729	2,893E-04
Scn3a	-38,362	4,344E-79
Pik3c2g	-35,495	1,140E-03
Robo2	-30,253	1,186E-58
Colq	-29,713	1,401E-13
D430041D05Rik	-28,864	7,925E-05
Fat3	-27,758	2,915E-53
Ptprd	-26,710	1,998E-104
Hmcn1	-26,295	7,834E-126
Nrcam	-26,261	6,964E-40
Ttn	-26,009	9,437E-77
D10Wsu102e	-25,021	1,246E-34
Pclo	-24,457	6,483E-09
Macf1	-23,672	0
Ndnf	-23,326	2,209E-81
Syne1	-22,523	9,232E-161
Gm2115	-22,445	1,317E-02
Gm48662	-21,820	1,432E-03
Ros1	-21,111	6,190E-04
Pdzd2	-20,286	2,074E-173
Igsf10	-20,158	4,375E-32
Ank3	-19,835	2,726E-104
Hpcal4	-19,736	2,858E-02
Adamts17	-19,249	3,353E-09
Zbtb20	-19,243	2,556E-173
Fgfr4	-18,432	3,179E-07
Kcna2	-17,578	2,390E-22
Nrxn1	-17,241	6,090E-04
Itga8	-17,158	5,154E-163
Fras1	-16,927	2,224E-13
Tet1	-16,810	3,495E-13
Syne2	-16,484	5,647E-158
Aox3	-16,083	1,092E-95
Dnah8	-15,835	2,075E-09
Tln2	-15,657	3,599E-35
Lrp2	-15,607	9,953E-99
Stard9	-15,552	7,395E-88
Gpc5	-15,245	2,993E-05
Pgr	-15,173	1,127E-04
Fat4	-15,077	1,290E-51
Col6a3	-15,009	4,432E-93
Etv1	-14,965	2,384E-14
Lama2	-14,566	8,092E-80
Kif26b	-14,182	9,309E-05
Kcnn3	-14,130	2,690E-16
Dmd	-13,794	5,084E-65
Adam22	-13,754	6,152E-08
Nav2	-13,444	7,947E-63
Muc16	-12,997	1,312E-21
Col6a5	-12,589	1,546E-07
Tnxb	-12,583	1,334E-56
Edil3	-12,364	2,094E-18
Pde5a	-12,329	4,490E-129
Prex2	-12,142	3,557E-197
Dst	-12,112	1,112E-122
Npr3	-12,029	4,817E-85
Slit2	-11,968	2,554E-59
Myh10	-11,963	4,720E-109
Snhg11	-11,884	1,234E-06
D630045J12Rik	-11,843	5,649E-10
Mrc2	-11,668	8,870E-72
Tmem245	-11,641	2,198E-81
Tril	-11,515	2,424E-13
Foxp2	-11,331	1,131E-10
Irs1	-11,146	7,252E-46
Gria1	-10,957	1,507E-20
Adra1a	-10,857	1,515E-12
Scn7a	-10,798	1,139E-182
Rab27b	-10,636	6,054E-46
Chrdl1	-10,539	1,047E-17
Hc	-10,272	7,474E-61
Bmp3	-10,035	1,809E-86
Pde3a	-10,014	7,602E-97
Thsd4	-9,962	3,436E-35
Ackr4	-9,912	2,211E-08
Unc13b	-9,891	3,555E-64
Col12a1	-9,876	9,792E-45
Pitpnm3	-9,775	1,507E-10
Plce1	-9,662	2,956E-66
Cenpf	-9,650	1,537E-06
Abca8a	-9,614	2,777E-70
Plxdc2	-9,600	5,929E-112
Piezo2	-9,536	5,421E-28
Igsf9b	-9,535	1,193E-02
Utrn	-9,513	6,115E-174
Dock4	-9,477	1,536E-77
Cdk14	-9,430	4,318E-77
Angptl2	-9,416	2,514E-31
Sptbn1	-9,383	0
Stmn2	-9,370	7,505E-16
Atp1a2	-9,333	4,745E-67
Zfhx3	-9,314	6,501E-64
Mme	-9,299	6,564E-119
Arhgap20	-9,296	1,188E-19
Adgrg6	-9,224	6,999E-77
Pcolce2	-9,212	5,936E-132
Dnm3	-9,188	7,208E-13
Gprin3	-9,187	1,689E-70
Dlc1	-9,119	1,673E-133
Synm	-9,115	3,677E-65
Tex15	-9,076	1,123E-21
Inpp4b	-8,983	2,356E-24
Aspm	-8,967	3,100E-03
Zfp704	-8,962	1,134E-79
Ppp1r9a	-8,958	1,791E-79
Herc1	-8,936	4,609E-110
Lama3	-8,907	1,021E-100
Cacnb2	-8,899	3,801E-09
Faim2	-8,863	1,901E-06
Celf2	-8,831	6,118E-90
Frmd4a	-8,830	9,627E-61
Slc5a3	-8,827	1,162E-21
Scube2	-8,808	6,134E-24
Slc7a10	-8,723	9,739E-06
Nbea	-8,700	3,529E-71
Sox11	-8,681	1,633E-05
Lrat	-8,665	8,081E-45
Mamdc2	-8,639	4,849E-62
Vps13d	-8,635	2,052E-95
Ptgfr	-8,634	3,954E-11
Hykk	-8,534	1,814E-06
Mical3	-8,524	2,984E-17
Unc5c	-8,493	3,664E-09
Pla2r1	-8,442	1,447E-21
4932438A13Rik	-8,432	1,365E-100
Ttc3	-8,408	1,345E-84
Chd6	-8,390	9,283E-76
Pygo1	-8,347	1,233E-02
Gucy1a1	-8,344	2,200E-106
St8sia4	-8,333	8,157E-41
Kmt2c	-8,329	3,211E-115
Sema3c	-8,325	0
Ubn2	-8,309	2,175E-67
Itsn1	-8,229	9,841E-22
Tmem132c	-8,224	2,850E-07
Chst2	-8,183	5,971E-28
Nckap5	-8,113	1,038E-83
Hhip	-8,102	4,207E-45
Cacna1c	-8,085	3,134E-23
Reln	-8,047	8,700E-06
Arhgef38	-8,033	3,234E-45
Antxr1	-7,964	2,984E-76
Vezt	-7,963	2,106E-18
Ptprb	-7,954	0
Specc1l	-7,896	7,334E-116
Smad9	-7,867	3,937E-04
Gm37494	-7,855	4,447E-25
Etl4	-7,841	1,289E-70
Hspg2	-7,821	1,660E-83
Rian	-7,760	6,268E-03
Adam23	-7,748	4,345E-03
Vps13c	-7,739	7,296E-70
Cdc42bpa	-7,728	5,409E-102
D1Ertd622e	-7,726	4,725E-11
Zfp846	-7,714	4,594E-08
Ryr2	-7,703	6,280E-07

Gxylt2	-7,686	1,100E-02	Zfp652	-6,615	4,397E-92
Plcb1	-7,675	7,634E-48	Ralgps2	-6,608	2,452E-15
Bche	-7,632	5,762E-10	Pde8b	-6,607	7,847E-23
Abca8b	-7,616	6,221E-19	Rasgrf2	-6,605	5,610E-25
Plekha6	-7,596	3,163E-11	Hectd4	-6,580	5,670E-23
Tnrc6b	-7,590	1,457E-73	Ahcyl2	-6,558	2,569E-27
Cdh11	-7,570	3,230E-90	Tacc2	-6,539	1,527E-24
Ar	-7,557	8,694E-10	Phc3	-6,531	4,624E-76
Runx1t1	-7,542	3,685E-11	Kcnb1	-6,529	1,495E-04
Prrg1	-7,532	8,048E-21	Sacs	-6,526	2,223E-19
Trim2	-7,515	1,180E-19	Epha7	-6,519	1,276E-03
Vwf	-7,510	9,285E-90	Mkln1	-6,467	2,317E-44
Birc6	-7,487	1,377E-122	Amph	-6,466	1,058E-07
Svep1	-7,486	8,107E-51	Sema3a	-6,464	1,463E-48
Map2	-7,463	1,745E-62	Slc4a5	-6,463	3,495E-14
Kat6b	-7,457	2,046E-15	Mast4	-6,452	7,175E-26
Mbd5	-7,436	3,083E-21	Sned1	-6,451	8,338E-22
Ptch1	-7,430	4,841E-48	Btbd7	-6,446	2,663E-88
Col14a1	-7,395	5,598E-22	Smarca2	-6,441	4,028E-98
Mapt	-7,391	4,850E-71	Ecm2	-6,417	5,239E-17
Pkd1	-7,382	5,528E-77	Col27a1	-6,411	4,378E-04
Cadm1	-7,368	5,943E-110	Veph1	-6,399	2,677E-18
Cacna2d1	-7,347	4,425E-22	Ptprg	-6,393	2,148E-37
Psd3	-7,345	3,217E-76	Col3a1	-6,368	2,065E-111
Tmem44	-7,332	3,349E-06	Epb41l5	-6,367	1,116E-57
Tanc2	-7,329	1,725E-26	Spta1	-6,367	4,337E-08
Nbeal1	-7,295	4,472E-133	Cped1	-6,330	1,778E-107
Exph5	-7,291	8,732E-65	Kmt2d	-6,324	1,172E-73
Arhgap32	-7,269	7,612E-18	Itpr1	-6,312	4,289E-99
Nfib	-7,265	1,647E-130	Nktr	-6,303	3,295E-94
Pcdh12	-7,230	1,149E-26	Myo1b	-6,281	6,712E-119
Kcnq5	-7,209	5,402E-04	Arfgef3	-6,278	2,135E-17
Ttll5	-7,205	5,006E-10	Cdkl5	-6,269	1,995E-80
Tppp	-7,196	2,993E-18	Dnmt3a	-6,269	1,437E-23
Cttnbp2	-7,195	1,075E-06	Arhgef12	-6,260	1,798E-133
Col1a2	-7,175	3,056E-107	Nfat5	-6,259	8,346E-107
Ttc28	-7,170	2,519E-12	Usp34	-6,256	3,414E-99
Nectin3	-7,168	5,122E-101	Gtf3c1	-6,228	7,876E-58
Asph	-7,157	7,254E-51	Hip1	-6,209	3,004E-77
Ago3	-7,148	5,072E-21	Mpdz	-6,196	3,751E-22
E130308A19Rik	-7,139	3,884E-07	Foxn3	-6,188	1,332E-24
Hydin	-7,139	5,816E-09	Vldlr	-6,185	2,546E-49
Scube1	-7,124	1,430E-05	Dpp4	-6,169	3,387E-63
Chst3	-7,123	3,654E-12	Map3k20	-6,168	7,429E-104
Mtcl1	-7,118	2,044E-64	Fancc	-6,164	2,523E-03
Huwe1	-7,112	2,089E-138	Ank2	-6,151	3,021E-03
Szt2	-7,091	3,863E-14	Grb14	-6,140	6,253E-16
Nox4	-7,071	1,343E-37	Mef2c	-6,135	4,082E-22
Zbtb37	-7,052	6,465E-24	Kif26a	-6,129	1,205E-09
Brwd1	-7,030	2,857E-85	Xpr1	-6,115	9,310E-28
Rasal2	-7,023	7,399E-69	Emsy	-6,090	1,668E-29
Sgip1	-7,013	2,154E-09	Aak1	-6,088	1,077E-26
Xist	-6,990	2,443E-145	Apc	-6,084	6,603E-106
Stox2	-6,983	5,820E-17	Txndc16	-6,082	9,619E-15
Prkn	-6,947	1,257E-02	Helz	-6,080	2,485E-25
Alms1	-6,919	9,178E-15	Pkhd1l1	-6,075	3,015E-15
Myh7	-6,915	2,673E-33	Meis1	-6,069	8,030E-36
Plagl1	-6,914	1,718E-13	Trrap	-6,062	3,434E-28
Ppfibp2	-6,887	1,768E-17	Lgi3	-6,061	1,883E-21
Foxp1	-6,884	2,565E-101	Kmt2a	-6,058	1,064E-38
Frem1	-6,865	2,260E-10	Fat1	-6,051	1,597E-95
Ophn1	-6,849	1,642E-15	Spon2	-6,046	3,131E-07
Pard3b	-6,847	3,419E-21	Sfta3-ps	-6,042	1,054E-98
Strbp	-6,834	1,320E-24	Col4a4	-6,026	1,208E-54
Cdh13	-6,834	2,560E-14	Ahnak	-6,018	0
Itpr2	-6,810	2,571E-85	Ppm1l	-6,018	1,999E-15
Kif1b	-6,798	1,838E-114	Pde7b	-6,017	9,147E-12
Fndc1	-6,791	1,621E-07	Stxbp4	-6,015	8,874E-05
Sytl2	-6,780	1,718E-20	Nexmif	-6,002	2,842E-07
Fbln5	-6,778	4,725E-49	Sipa1l3	-5,995	3,258E-18
Abca9	-6,769	6,747E-09	Clasp2	-5,994	1,572E-29
Rasgrp2	-6,765	1,226E-11	Pnpla8	-5,981	1,958E-74
Reps2	-6,738	2,364E-86	Myo5c	-5,939	3,031E-64
Zfp462	-6,719	1,343E-15	Ogn	-5,937	1,996E-134
Prkdc	-6,695	1,436E-21	Clcn3	-5,931	1,556E-29
Abcc9	-6,653	2,638E-07	Nrp1	-5,906	3,725E-70
Atxn1	-6,647	2,427E-66	Cdan1	-5,889	1,789E-06
Pde4d	-6,637	5,390E-15	Acaca	-5,870	3,166E-29
Fry	-6,636	3,845E-17	Adamtsl3	-5,868	9,436E-18
Acoxl	-6,635	9,864E-18	Tspan18	-5,867	5,137E-33
Hnrnpr	-6,621	6,404E-31	Adamtsl1	-5,862	1,151E-04
Ppp1r16b	-6,618	1,403E-50	Fign	-5,859	3,153E-02

Vipr2	-5,836	4,817E-10	Arvcf	-5,339	2,094E-06
Atp8a1	-5,834	3,445E-116	Nhsl1	-5,337	7,093E-06
Herc2	-5,827	8,843E-96	Adamts10	-5,334	2,759E-21
Ntrk2	-5,827	1,664E-06	Fgfr3	-5,330	2,189E-28
Slc1a3	-5,822	4,286E-21	Tnfrsf19	-5,324	1,340E-19
Tcf4	-5,822	1,318E-98	Pbx1	-5,319	4,915E-35
Ablim1	-5,816	1,390E-100	Zhx3	-5,314	6,167E-26
Phex	-5,811	2,171E-02	Arhgef7	-5,306	8,557E-27
Aplnr	-5,793	3,148E-17	Pou2f1	-5,303	5,320E-16
Mcc	-5,791	2,506E-60	Phactr2	-5,296	2,971E-40
Fasn	-5,790	1,241E-69	Myo6	-5,295	7,864E-45
Clock	-5,784	4,461E-106	Zfp638	-5,290	1,949E-105
Dchs1	-5,779	2,925E-04	Hecw2	-5,287	7,043E-23
Atrx	-5,775	1,363E-112	Dopey1	-5,284	3,384E-27
Gria3	-5,750	4,522E-12	Acss2	-5,283	3,153E-05
Plekhh2	-5,748	1,219E-20	Myo5b	-5,273	2,416E-31
Tnik	-5,746	1,506E-20	Rabgap1l	-5,271	1,505E-42
Mapk8ip3	-5,742	7,452E-18	Dock6	-5,270	4,118E-21
Shprh	-5,729	4,597E-26	Atrn	-5,267	1,604E-32
Anapc1	-5,718	2,403E-78	Fto	-5,262	3,126E-08
Ankrd50	-5,714	1,558E-79	Myo9a	-5,258	3,447E-94
Bach2	-5,711	5,447E-05	Dicer1	-5,256	2,415E-30
Smg1	-5,699	3,823E-100	Npnt	-5,250	1,389E-110
Clmn	-5,688	4,639E-06	Mboat2	-5,248	2,682E-05
Cdh16	-5,683	6,179E-03	Slc6a2	-5,237	6,745E-03
Zfp280d	-5,679	2,315E-27	Egflam	-5,236	6,218E-17
Plxna4	-5,677	8,156E-24	Rora	-5,232	2,059E-25
Arrb1	-5,672	9,420E-108	Akap13	-5,230	1,463E-119
Dixdc1	-5,666	5,418E-06	Sox5	-5,227	2,890E-03
Dnah11	-5,657	2,285E-07	Ppp1r12b	-5,217	3,449E-29
Enpep	-5,654	4,173E-34	Arhgef40	-5,211	3,391E-10
Baz2b	-5,652	1,639E-80	Ncoa2	-5,209	2,545E-27
Senp7	-5,597	7,994E-12	Sh3rf3	-5,208	1,067E-03
Neo1	-5,597	3,699E-29	Mtss1l	-5,205	3,829E-13
Dnah7b	-5,583	9,630E-03	Olfml2a	-5,205	2,090E-10
Klhdc8b	-5,567	6,322E-03	Uggt2	-5,204	3,871E-06
Rnf144a	-5,564	5,752E-40	Mfap3l	-5,203	4,930E-19
Pikfyve	-5,556	6,319E-29	Mir99ahg	-5,199	6,394E-06
Casz1	-5,543	5,844E-28	Daam2	-5,193	6,699E-07
Nin	-5,543	1,069E-61	Fbln2	-5,190	5,145E-05
Pgap1	-5,536	1,687E-09	Slc16a7	-5,188	1,234E-14
Ccdc141	-5,518	2,674E-29	Gcn1l1	-5,179	3,340E-11
Cux1	-5,517	1,847E-79	Fgd4	-5,178	9,031E-20
Vamp1	-5,515	4,206E-04	Ubr4	-5,177	8,157E-69
Tulp4	-5,513	2,797E-30	Shroom4	-5,170	1,489E-25
Osbpl6	-5,508	8,404E-19	Raver2	-5,166	8,114E-21
Mllt3	-5,505	2,652E-15	Cers4	-5,164	8,052E-14
Zfp451	-5,496	2,082E-18	Nav1	-5,156	3,685E-15
Col4a6	-5,493	1,699E-08	Mylk	-5,154	6,431E-121
Zfp398	-5,492	1,207E-10	Tanc1	-5,134	4,911E-23
Col16a1	-5,491	8,045E-10	Clasp1	-5,128	2,801E-26
Sox4	-5,491	1,022E-18	Prkg1	-5,124	9,027E-11
Gfra2	-5,476	1,296E-05	Synpo2	-5,107	7,576E-17
Zzef1	-5,474	1,090E-31	Hace1	-5,096	1,749E-11
Stard13	-5,463	9,049E-83	Pxdn	-5,089	1,213E-47
Pard3	-5,460	5,034E-23	Lrrk2	-5,088	4,673E-52
Mical2	-5,455	5,398E-84	Bcl7a	-5,077	1,861E-04
Nfia	-5,454	8,985E-59	Asxl2	-5,077	1,179E-22
Zeb2	-5,448	8,854E-117	Scd1	-5,066	0
Ncald	-5,446	1,526E-35	Invs	-5,063	2,720E-07
Sesn3	-5,443	2,382E-21	Amot	-5,060	3,717E-04
Rev3l	-5,438	3,612E-34	Cbfa2t3	-5,060	1,580E-13
Phip	-5,436	4,871E-98	Postn	-5,055	3,807E-112
Pcdh17	-5,434	1,664E-20	Siglecf	-5,052	1,266E-06
Ctnnd2	-5,424	2,689E-02	Ltbp1	-5,032	4,049E-56
Mycbp2	-5,420	3,234E-91	Agtpbp1	-5,025	2,598E-18
Xpo7	-5,416	1,769E-16	Agmo	-5,018	6,183E-07
Rbpjl	-5,416	3,743E-09	Lrp4	-5,012	1,165E-35
Adcy8	-5,414	2,859E-08	Fryl	-5,010	1,644E-29
Thbs3	-5,390	1,830E-23	Nsd2	-4,995	2,359E-24
Sema6a	-5,374	1,371E-28	Usp15	-4,992	2,103E-43
Soat1	-5,374	2,764E-52	Slc25a36	-4,990	1,809E-32
Rftn2	-5,366	1,333E-13	Igsf3	-4,987	5,525E-05
Phactr1	-5,366	2,970E-29	Ankrd44	-4,986	1,219E-47
Heg1	-5,363	0	Fbxl20	-4,984	1,781E-13
Rnf150	-5,361	1,455E-10	Akap9	-4,984	1,668E-68
Ltbp2	-5,356	1,163E-27	Znrf3	-4,976	3,071E-07
Prkca	-5,353	1,399E-17	Mbnl1	-4,974	0
Pcnx	-5,353	1,647E-45	Map4	-4,963	6,287E-52
Tia1	-5,349	1,259E-18	Plec	-4,962	2,330E-100
Evc	-5,344	2,113E-03	Tcaf1	-4,957	1,688E-19
Ralgapa2	-5,343	4,749E-21	Kmt5b	-4,948	1,212E-32

Meis2	-4,948	1,021E-05	Agap1	-4,628	9,580E-23
Col5a2	-4,948	2,691E-64	Tpcn1	-4,627	4,765E-09
Lrba	-4,946	3,506E-31	Soga1	-4,606	2,495E-09
Mob1b	-4,946	1,395E-22	Col6a2	-4,606	1,607E-37
Ushbp1	-4,938	1,457E-20	Banp	-4,603	9,912E-09
Sort1	-4,933	5,437E-106	Zswim9	-4,599	4,982E-02
Arhgef17	-4,930	1,232E-22	Jmy	-4,594	3,509E-24
Vps13b	-4,927	9,909E-49	Prep	-4,588	2,535E-23
Dmxl1	-4,926	3,269E-36	Satb1	-4,585	3,742E-07
Limch1	-4,924	0	Nf1	-4,581	4,882E-29
Gask1b	-4,921	1,112E-18	Celsr2	-4,576	2,513E-02
Afap1	-4,920	3,551E-14	Brwd3	-4,571	7,093E-15
Usp9x	-4,916	0	Igf1r	-4,569	8,389E-25
Sugp2	-4,910	1,849E-06	Peak1	-4,566	3,259E-30
Ptpn4	-4,908	2,995E-28	Mest	-4,565	1,126E-03
Plxna1	-4,908	4,201E-70	Pcdh1	-4,564	6,175E-28
Lrp6	-4,907	1,298E-66	Rbms3	-4,564	2,967E-33
Rfx7	-4,904	5,273E-16	Gnao1	-4,564	3,123E-07
Sema3e	-4,903	2,776E-72	Cspp1	-4,564	3,322E-17
Adgrl1	-4,894	1,586E-12	Scai	-4,563	9,041E-09
C1qtnf7	-4,893	3,894E-09	Lrp1	-4,562	2,030E-78
Nptx1	-4,888	5,426E-08	Ncor1	-4,562	1,565E-70
Abca5	-4,885	4,703E-14	Glcci1	-4,553	3,279E-08
Tmbim1	-4,882	9,380E-30	Ino80d	-4,551	3,889E-25
Katnal1	-4,882	1,872E-06	Nebl	-4,545	4,872E-71
Sipa1l1	-4,881	6,295E-24	Gnb4	-4,543	4,747E-14
Tns1	-4,874	0	Iqce	-4,541	2,895E-04
Kdr	-4,871	0	Arhgap21	-4,538	2,631E-30
Npc1	-4,867	5,752E-30	Cdk6	-4,538	5,552E-23
Col4a3	-4,862	0	Map4k2	-4,536	3,666E-15
Peg3	-4,861	1,707E-16	Fmo5	-4,532	8,907E-05
Hook3	-4,857	4,005E-72	Ptpn13	-4,530	2,695E-29
Cplane1	-4,856	2,196E-11	Ttbk2	-4,529	5,461E-18
2900026A02Rik	-4,846	1,977E-12	Nipal3	-4,529	4,336E-23
Cspg4	-4,824	2,201E-02	R3hdm1	-4,523	9,069E-14
Lmo7	-4,824	0	Megf6	-4,517	4,505E-05
Pde4dip	-4,818	1,185E-17	Arhgap6	-4,495	9,244E-14
Vsnl1	-4,804	9,740E-05	Mecom	-4,494	2,086E-24
Tbc1d30	-4,796	1,545E-12	Srgap2	-4,490	8,829E-20
Wdfy3	-4,788	1,225E-30	Htt	-4,489	2,943E-17
Tet3	-4,785	5,605E-21	Ccnt2	-4,486	1,872E-26
Lama4	-4,782	3,279E-31	Atp2b4	-4,486	4,372E-19
Rb1cc1	-4,771	1,999E-93	Arid1b	-4,485	8,442E-15
Zfp950	-4,766	2,844E-11	Ston2	-4,483	5,976E-06
Cep97	-4,760	1,499E-02	Tns3	-4,469	1,106E-67
Zfyve26	-4,757	5,644E-09	Nsd1	-4,468	6,813E-76
Pgm2l1	-4,756	1,259E-10	Mprip	-4,460	0
Wnk1	-4,756	0	Mdm4	-4,459	9,230E-27
Rreb1	-4,755	2,057E-16	Bptf	-4,455	7,114E-35
Ncbp3	-4,754	3,339E-14	Cadps2	-4,445	9,933E-20
Vangl2	-4,751	2,709E-02	Ppp4r4	-4,444	2,710E-05
Naalad2	-4,745	3,383E-03	Col4a5	-4,439	1,668E-26
Steap3	-4,744	4,271E-06	Scn3b	-4,438	2,486E-20
Trp53bp1	-4,733	7,489E-13	Zfp827	-4,430	2,010E-05
Acss3	-4,732	9,176E-06	Cxcl12	-4,424	0
Raph1	-4,728	7,495E-24	Srcap	-4,420	2,334E-25
Adgrl3	-4,727	1,430E-28	Spon1	-4,420	8,824E-31
Mga	-4,723	1,187E-68	Ep400	-4,413	6,428E-25
Cep295	-4,716	1,750E-12	Top2a	-4,404	2,206E-06
Usf3	-4,714	5,622E-30	Slco2b1	-4,401	1,735E-04
Ash1l	-4,713	4,414E-66	Plekha5	-4,400	3,978E-10
Arid4b	-4,711	1,841E-29	9530026P05Rik	-4,399	7,037E-04
Elfn1	-4,711	1,303E-02	Serbp1	-4,398	0
Ptpn14	-4,709	1,162E-23	Ttc21b	-4,397	2,732E-05
Tsc22d1	-4,700	1,942E-34	Arhgap5	-4,388	0
Il17rd	-4,698	1,092E-11	Bahcc1	-4,380	2,430E-02
Creb5	-4,689	1,427E-03	Ago1	-4,377	1,157E-23
Ralgapa1	-4,687	5,705E-33	Camk2d	-4,377	3,047E-28
Olfml3	-4,687	1,352E-23	Exoc4	-4,376	1,091E-27
Dync1h1	-4,684	0	Fam160a2	-4,376	2,532E-05
Bicd1	-4,684	1,136E-04	Adcy5	-4,372	3,161E-02
Gabpb2	-4,676	8,584E-26	Tcf12	-4,372	8,269E-25
Pitpnm2	-4,672	9,957E-13	Tnrc6c	-4,372	5,722E-14
Sh3rf2	-4,672	1,044E-15	Mmp15	-4,371	8,172E-21
Dync2h1	-4,671	7,048E-12	Flt1	-4,371	0
Ralgapb	-4,665	6,401E-26	Pds5a	-4,363	8,022E-36
Zdhhc3	-4,663	1,965E-31	Cdkal1	-4,359	8,495E-13
Pik3c2b	-4,656	2,482E-05	Prrc2b	-4,359	1,907E-30
Abca3	-4,638	1,281E-119	Lifr	-4,349	0
Prc1	-4,636	1,295E-02	Zfp780b	-4,347	2,915E-05
Nisch	-4,635	1,160E-38	Tead1	-4,347	7,602E-34
Zfp26	-4,631	3,767E-16	Lpp	-4,343	3,040E-46

Wscd1	-4,342	2,399E-05	Tbc1d4	-4,091	7,379E-07
Pwwp3a	-4,341	7,039E-06	Arhgap26	-4,087	9,065E-11
Tbck	-4,326	1,453E-15	Fam210a	-4,080	4,280E-15
Patj	-4,323	1,074E-26	Dnah9	-4,074	1,137E-07
Sh3pxd2a	-4,323	4,402E-33	Tmod2	-4,074	8,294E-19
Ahnak2	-4,312	5,667E-05	Kank4	-4,070	5,528E-06
Ebf1	-4,306	2,502E-06	Adarb1	-4,070	3,404E-15
Agl	-4,302	9,702E-06	Nedd4	-4,069	0
Rasgef1b	-4,301	3,908E-08	Arrdc3	-4,069	1,497E-35
Arhgef10	-4,299	2,830E-14	Thbd	-4,065	0
Notch3	-4,299	1,519E-11	Phlpp1	-4,059	2,227E-13
1700025G04Rik	-4,293	3,772E-05	Lrp5	-4,049	6,573E-18
Hspa4l	-4,293	2,970E-23	Gan	-4,048	1,087E-12
Setd1b	-4,289	3,815E-02	Cftr	-4,047	1,381E-05
Dnajb14	-4,286	3,008E-15	Nr3c2	-4,044	1,132E-05
Kdm5a	-4,285	2,767E-26	Golim4	-4,035	5,132E-25
Dnah5	-4,284	3,291E-17	Mtm1	-4,029	1,424E-07
Nuak1	-4,283	1,123E-10	Mdn1	-4,025	1,068E-16
Tgfbrap1	-4,283	3,392E-13	Ptprs	-4,023	1,583E-15
Dock9	-4,277	0	Krit1	-4,014	7,032E-19
Slc15a2	-4,275	1,957E-09	Arap2	-4,010	3,855E-35
Tecpr1	-4,273	1,129E-08	Rbm33	-4,009	2,359E-18
Astn2	-4,273	4,168E-02	Zbtb1	-4,009	6,431E-15
Cdc14b	-4,272	9,110E-04	Abl1	-4,005	2,794E-15
Sgpp2	-4,267	6,345E-07	Iqsec1	-3,999	4,584E-17
Lamb1	-4,265	9,393E-30	Tmx4	-3,998	5,642E-17
Epb41	-4,265	1,569E-17	Gprasp1	-3,993	1,752E-15
Son	-4,260	0	Chpt1	-3,993	6,350E-23
Ankrd11	-4,260	7,391E-31	Hdac5	-3,992	2,672E-12
Dido1	-4,256	1,481E-26	Slc12a7	-3,989	1,258E-06
Fhl1	-4,246	0	Hmg20a	-3,988	7,038E-11
Bmpr2	-4,244	0	Aopep	-3,988	7,639E-14
Arhgap31	-4,238	0	Bbx	-3,987	1,276E-22
Sh3d19	-4,233	3,286E-30	Zfp169	-3,985	2,593E-02
Mbtd1	-4,229	7,026E-07	Ermp1	-3,984	3,052E-11
Rcbtb2	-4,229	2,272E-10	Jag2	-3,980	5,749E-03
Kctd12b	-4,228	4,015E-07	Zbtb44	-3,979	1,354E-17
Nynrin	-4,222	1,806E-05	Braf	-3,977	1,854E-26
Atf7	-4,220	6,041E-20	Atr	-3,973	6,678E-12
Bod1l	-4,218	1,685E-28	Pcnt	-3,972	3,904E-26
Ikbkb	-4,218	7,476E-19	Arhgap24	-3,970	3,470E-07
Frmd4b	-4,212	1,984E-18	L3mbtl3	-3,966	1,926E-07
Hmbox1	-4,207	1,731E-19	Fam126b	-3,964	2,286E-13
Tnrc18	-4,203	1,204E-18	Ubr1	-3,963	1,999E-29
Sptan1	-4,201	0	Sestd1	-3,957	3,805E-16
Specc1	-4,200	1,998E-18	Dtna	-3,957	2,715E-14
Nsd3	-4,196	2,592E-20	Plekhd1	-3,956	6,468E-04
Arhgef15	-4,195	3,298E-22	Setd7	-3,956	3,889E-21
Klhl13	-4,193	1,568E-07	Gfod1	-3,955	3,823E-07
Oip5os1	-4,192	0	Arhgef2	-3,951	3,041E-23
Rptor	-4,191	2,178E-08	Exoc6b	-3,950	2,936E-17
Pgm5	-4,190	6,640E-04	Atad2b	-3,941	3,418E-16
4930402H24Rik	-4,189	2,691E-21	Itsn2	-3,938	0
Rnf217	-4,177	4,368E-11	Megf9	-3,933	1,755E-17
Dnah6	-4,176	4,180E-13	Mbtps1	-3,929	1,147E-22
Mturn	-4,176	4,383E-08	Sipa1l2	-3,929	6,191E-18
Nhsl2	-4,170	1,453E-11	Rapgef2	-3,925	6,745E-24
Rsf1	-4,168	3,035E-20	Tmtc2	-3,924	2,799E-08
Mon2	-4,166	1,175E-23	Tbp	-3,923	9,978E-07
Mbnl3	-4,166	1,098E-03	Prdm15	-3,920	4,549E-02
Zbtb4	-4,165	4,240E-31	Syt7	-3,917	2,401E-03
Prickle1	-4,155	1,717E-20	Pds5b	-3,914	2,695E-20
Prickle2	-4,148	2,520E-22	Aff4	-3,912	0
Ro60	-4,143	6,152E-30	Kif3c	-3,911	1,043E-05
Chd3	-4,141	2,891E-22	Tcf7l2	-3,910	5,491E-04
Sik2	-4,140	6,235E-08	Colgalt2	-3,900	2,352E-04
Rps6ka5	-4,135	2,373E-02	Fn1	-3,895	0
Mib1	-4,133	8,588E-33	Etnk1	-3,893	9,893E-28
Pitpnc1	-4,130	2,072E-23	Enah	-3,890	5,404E-09
Cdk5rap2	-4,122	1,686E-05	Slc12a6	-3,887	5,977E-28
Usp46	-4,122	3,565E-18	Btbd3	-3,887	3,506E-22
Epb41l1	-4,119	1,336E-07	Kdm2a	-3,886	7,492E-27
Cep350	-4,117	6,564E-28	Hgf	-3,879	1,235E-13
Palld	-4,116	9,150E-10	Notch1	-3,873	3,646E-21
Spen	-4,115	8,298E-12	Heatr5a	-3,868	1,058E-13
Atg2b	-4,112	4,999E-11	Hivep3	-3,862	1,351E-03
Zfp266	-4,107	1,931E-31	Ddr2	-3,862	1,577E-24
Dstyk	-4,104	1,008E-12	Dpy19l3	-3,860	4,059E-03
Ube3a	-4,103	0	Dapk1	-3,860	2,370E-16
Rock2	-4,101	0	5330417C22Rik	-3,859	6,776E-16
Zbtb40	-4,100	2,503E-03	Luc7l2	-3,857	0
Yae1d1	-4,097	4,295E-14	Chd8	-3,855	1,071E-21

Tsc1	-3,854	5,613E-09	Pcdh18	-3,677	6,926E-09
Sbf2	-3,853	1,410E-21	Scd2	-3,677	0
N4bp2l2	-3,850	1,808E-24	Cdon	-3,677	1,439E-03
Wdfy4	-3,847	6,415E-12	Dnah3	-3,674	3,497E-07
Zfp60	-3,847	7,635E-05	Mrc1	-3,672	0
Gnas	-3,844	0	Sorl1	-3,669	0
Pkn1	-3,844	1,823E-22	Cnot6l	-3,667	2,785E-18
Scrn1	-3,840	1,171E-02	Ocrl	-3,664	9,468E-08
Camsap2	-3,833	1,976E-32	Arhgap29	-3,663	0
Dock10	-3,830	1,975E-22	Gls	-3,663	3,963E-20
Ssh2	-3,829	0	Wasf3	-3,662	1,652E-02
Pnisr	-3,827	4,651E-27	Slc22a23	-3,661	3,095E-14
Zmynd8	-3,826	6,550E-16	Hnrnpll	-3,656	1,502E-10
Kcne2	-3,825	3,465E-05	Prrc2c	-3,653	0
Arid2	-3,825	1,194E-23	Chka	-3,653	4,723E-14
Arhgap42	-3,822	5,121E-10	Dennd5b	-3,649	6,776E-12
Pkd2	-3,820	1,237E-24	Gm10033	-3,641	1,735E-07
Setbp1	-3,820	4,180E-18	Apbb2	-3,641	9,915E-23
Dcaf17	-3,818	3,210E-07	Ankrd12	-3,640	1,793E-20
Cnot1	-3,818	5,249E-30	Pam	-3,639	0
Dennd1a	-3,817	3,125E-08	Chid1	-3,639	5,440E-03
Ankrd33b	-3,813	4,343E-23	Ice1	-3,638	9,645E-16
Cdc73	-3,813	5,032E-13	Pag1	-3,637	4,472E-16
Ctnnal1	-3,811	5,476E-06	Cfap54	-3,634	7,060E-04
Sulf1	-3,810	1,361E-12	Hipk2	-3,630	9,362E-17
Kdm5b	-3,809	2,796E-14	Tmcc3	-3,625	1,044E-18
Qser1	-3,806	9,048E-17	Zfp319	-3,623	1,403E-04
Wfdc1	-3,805	3,079E-04	Rapgef6	-3,610	2,402E-19
Taok1	-3,803	0	Rbm5	-3,609	4,384E-28
Gpr155	-3,802	1,272E-07	Zfp101	-3,609	1,410E-04
Kalrn	-3,801	9,256E-10	Rc3h2	-3,608	2,548E-30
Atp2b1	-3,800	0	Notch4	-3,605	3,334E-09
Plcg1	-3,794	1,013E-27	Tmtc1	-3,602	1,407E-22
Magi1	-3,793	1,903E-13	Plod2	-3,601	3,615E-17
Ttc23	-3,792	9,631E-05	Dpp8	-3,600	0
Ganc	-3,791	1,705E-06	Depdc5	-3,598	7,200E-07
Itga6	-3,789	1,892E-21	Iqgap1	-3,598	0
Zmiz1	-3,786	6,597E-18	Dsp	-3,594	3,509E-23
Lrig2	-3,784	4,686E-08	Cdk13	-3,590	6,522E-25
Prkaa2	-3,781	1,066E-04	Cbx5	-3,588	7,548E-29
Cpm	-3,775	1,894E-31	Mid2	-3,588	1,549E-16
Tsga10	-3,771	2,713E-04	Pik3ca	-3,587	0
Castor2	-3,771	4,061E-03	Zfp532	-3,586	6,226E-05
Pon1	-3,768	1,067E-08	Zfp945	-3,586	4,941E-11
St6galnac3	-3,767	1,805E-03	Map3k2	-3,585	7,204E-14
Nnt	-3,766	1,802E-03	Fbn1	-3,582	0
Grb10	-3,762	6,364E-15	Ccdc93	-3,578	1,365E-10
Zbtb46	-3,762	1,588E-09	Egfr	-3,578	7,124E-17
Acox3	-3,761	2,026E-09	Inmt	-3,577	0
Aox1	-3,759	9,357E-08	Fam129a	-3,574	1,024E-13
Cds2	-3,758	8,286E-26	Rprd2	-3,573	5,392E-14
Eml5	-3,757	9,989E-03	Col5a1	-3,572	2,228E-09
Edn3	-3,750	5,600E-03	Ppip5k1	-3,570	3,701E-06
Ltbp4	-3,747	3,479E-24	Uhrf2	-3,566	1,949E-10
Pamr1	-3,746	8,483E-04	Pnpla6	-3,565	1,837E-05
Mier1	-3,745	2,043E-26	Rasgrp3	-3,564	4,357E-17
Ylpm1	-3,741	7,998E-18	Trip12	-3,564	0
Jmjd1c	-3,740	1,498E-32	Fut8	-3,562	1,234E-10
Map1b	-3,736	5,734E-14	Usp31	-3,560	6,002E-09
Cmtm4	-3,736	5,368E-19	Parva	-3,560	1,855E-26
Atp2a3	-3,735	1,270E-22	Lpin1	-3,551	1,114E-09
Thoc2	-3,730	4,344E-29	Ogt	-3,547	4,762E-20
Rc3h1	-3,728	4,133E-21	Klhl15	-3,546	2,721E-03
Snx29	-3,727	1,522E-02	Dipk2a	-3,546	3,089E-23
Abi3bp	-3,725	3,361E-12	Acer3	-3,543	2,924E-14
Arhgef6	-3,718	6,817E-17	Hivep2	-3,534	8,717E-19
Heph	-3,715	3,355E-03	Tfcp2l1	-3,533	1,080E-10
Pot1a	-3,712	3,877E-03	Ubap2l	-3,532	6,101E-23
Mphosph9	-3,709	3,514E-04	5530601H04Rik	-3,532	8,811E-03
Zkscan8	-3,708	5,697E-12	Cacna1d	-3,531	7,688E-11
Dennd1b	-3,708	1,744E-11	Smc6	-3,529	4,799E-23
Fgd6	-3,704	2,203E-11	Prrx1	-3,529	3,293E-03
Cybrd1	-3,704	6,549E-03	Nup210	-3,529	8,292E-04
Coro2b	-3,699	1,469E-04	Insr	-3,528	2,078E-10
Epha4	-3,693	1,226E-11	Srpk2	-3,525	3,206E-17
Slc38a9	-3,693	4,112E-04	Setx	-3,525	1,111E-23
Mettl16	-3,689	1,141E-06	Dip2c	-3,524	3,274E-16
Megf8	-3,686	8,026E-06	Suds3	-3,521	3,785E-14
Epb41l4b	-3,686	2,528E-11	Cobll1	-3,520	2,872E-10
Cep85l	-3,683	4,031E-22	Lepr	-3,516	1,075E-12
Ago2	-3,683	2,172E-18	Mroh1	-3,514	1,337E-07
Ets1	-3,677	0	Col1a1	-3,513	2,108E-11

Slc30a9	-3,513	8,658E-13	Gse1	-3,390	2,761E-05
Hdgfrp3	-3,511	3,316E-09	Usp37	-3,389	1,223E-07
Rfx3	-3,510	1,096E-05	Cep290	-3,386	8,112E-11
Epb41l2	-3,507	0	Hs2st1	-3,384	1,416E-23
Pogz	-3,504	5,610E-10	Fchsd2	-3,384	4,842E-15
Sbno1	-3,504	1,866E-27	Akap11	-3,383	0
Setd5	-3,502	2,993E-24	Sike1	-3,382	9,232E-17
Gpsm2	-3,499	4,458E-05	Cobl	-3,381	2,812E-10
Ubxn7	-3,498	5,328E-17	Ttll4	-3,380	4,723E-08
Daglb	-3,496	9,567E-05	Ildr2	-3,379	5,778E-03
Itfg1	-3,494	3,073E-18	Zfp148	-3,377	2,317E-20
Ttc14	-3,494	3,789E-15	Ppp2r3a	-3,377	5,754E-12
Cpsf6	-3,493	9,858E-22	Fendrr	-3,377	4,356E-07
Arid1a	-3,492	2,430E-18	Zfp111	-3,377	1,234E-04
Ppm1a	-3,489	7,934E-20	Reck	-3,374	7,246E-07
Pik3r1	-3,487	0	Thrb	-3,374	1,585E-05
Trpm7	-3,483	1,351E-25	Zfp292	-3,373	6,908E-25
Dmtf1	-3,480	5,266E-16	Zfp606	-3,373	4,885E-03
Gtf2i	-3,480	5,321E-16	Myo10	-3,368	4,670E-15
Zfp334	-3,480	2,445E-04	Vps13a	-3,365	8,729E-21
Ncor2	-3,472	1,510E-05	Mapre2	-3,364	1,354E-13
Cep128	-3,472	2,628E-02	Mtr	-3,359	6,231E-09
Stxbp5	-3,471	3,512E-09	Amotl1	-3,357	0
Rif1	-3,469	8,165E-24	Ndst1	-3,356	0
Ago4	-3,469	4,720E-03	Madd	-3,355	2,800E-08
Sept7	-3,468	0	Cc2d2a	-3,353	5,618E-08
Kif13a	-3,468	4,653E-21	Slit3	-3,348	3,016E-10
Spag9	-3,465	0	Adamts9	-3,348	3,153E-12
Daam1	-3,465	1,077E-24	Foxj3	-3,347	6,772E-09
Dnajc1	-3,463	1,025E-14	Zbtb10	-3,347	2,170E-07
Crebrf	-3,463	3,752E-26	Ipo8	-3,346	1,141E-10
Gulp1	-3,462	1,514E-10	Piezo1	-3,346	7,172E-18
Brd8	-3,453	1,556E-12	Tbc1d16	-3,345	3,219E-04
Rbbp6	-3,453	1,194E-18	Dpy19l4	-3,344	1,392E-10
Trio	-3,453	2,600E-20	Rgs3	-3,344	2,811E-12
Sema3d	-3,451	3,926E-04	Jade1	-3,343	1,694E-06
Myh14	-3,447	0	Cep250	-3,343	3,875E-07
Cecr2	-3,443	7,959E-05	St7l	-3,342	8,501E-06
Ints6l	-3,442	1,355E-17	Pik3r4	-3,340	4,291E-07
Ep300	-3,442	2,368E-21	Dock1	-3,336	7,053E-21
Nol4l	-3,441	3,528E-04	Sspn	-3,336	7,610E-03
Creb1	-3,440	8,453E-25	Kidins220	-3,335	8,530E-24
Dzip3	-3,439	4,570E-08	Arhgef18	-3,334	1,836E-13
Srrm2	-3,436	0	Gucy1b3	-3,333	1,102E-20
Gcc2	-3,434	2,039E-22	Rai1	-3,331	1,650E-03
Phf3	-3,433	1,503E-23	Gigyf2	-3,330	7,619E-15
Recql	-3,433	1,836E-03	Wdr11	-3,325	9,528E-10
Adgrf5	-3,432	0	Ppip5k2	-3,325	4,368E-10
Maml3	-3,432	2,715E-07	Taok2	-3,324	2,167E-24
Plekhm3	-3,430	1,516E-09	C2cd3	-3,323	2,040E-07
Zkscan3	-3,430	3,055E-13	Cmah	-3,322	1,708E-03
She	-3,429	2,528E-16	Kdm2b	-3,321	6,225E-03
Prkd3	-3,429	2,345E-22	Golgb1	-3,318	8,157E-21
Lcorl	-3,429	7,188E-06	Golga3	-3,318	3,989E-16
Phlpp2	-3,428	5,818E-05	Tmem260	-3,315	2,317E-04
Gja5	-3,427	4,218E-10	Zfp106	-3,314	0
Arhgap35	-3,426	3,512E-24	Cep170	-3,313	3,552E-21
Adamtsl2	-3,423	1,139E-10	Fam126a	-3,311	1,623E-11
Zfp644	-3,421	5,288E-27	Ccser2	-3,309	0
Usp24	-3,421	1,447E-19	Mtmr10	-3,308	1,631E-11
Xrn1	-3,419	4,680E-17	Dock7	-3,305	1,349E-19
Pcsk5	-3,417	1,295E-05	Ccdc88a	-3,304	7,066E-19
Guf1	-3,413	7,593E-07	Aig1	-3,302	4,721E-05
Secisbp2l	-3,413	0	Etv5	-3,301	1,019E-14
Myorg	-3,413	1,669E-03	Ift80	-3,300	2,880E-06
Trak1	-3,411	1,511E-18	Dnaja1	-3,300	0
Sh3tc2	-3,410	4,483E-03	Parp6	-3,294	1,091E-03
Igf1	-3,409	9,167E-15	Fktn	-3,293	3,491E-07
Gsk3b	-3,409	3,641E-22	Dnah12	-3,293	4,502E-06
Abhd2	-3,407	0	Cdc23	-3,292	2,525E-10
Nfix	-3,406	5,539E-12	Svil	-3,286	6,786E-22
Antxr2	-3,406	1,047E-24	Aqr	-3,285	4,461E-10
Tom1l2	-3,402	2,129E-08	Klf3	-3,284	2,144E-26
Tspan2	-3,402	3,646E-18	Dip2b	-3,280	6,600E-10
AU022252	-3,402	5,764E-04	Pten	-3,279	0
Cnst	-3,402	1,608E-09	Atf7ip	-3,276	2,093E-20
Sept6	-3,401	1,756E-03	Adgrl2	-3,274	3,238E-16
Slc25a23	-3,399	4,166E-05	Slc6a6	-3,274	1,605E-24
Ncoa1	-3,396	2,424E-12	Plekhg1	-3,262	1,075E-08
Sema6d	-3,395	1,195E-19	Rufy2	-3,261	1,374E-05
Sh3rf1	-3,394	7,546E-08	Ppp1r14c	-3,260	2,789E-08
Samd4	-3,392	1,537E-15	Arhgef28	-3,260	1,425E-12

Tspan7	-3,258	0	Gfm2	-3,130	1,782E-03
Nrip1	-3,257	1,169E-08	Fam53b	-3,128	1,875E-07
Myo18a	-3,255	3,884E-18	Creb3l2	-3,127	2,271E-13
Cyyr1	-3,253	0	Jam2	-3,126	5,079E-11
Clk1	-3,253	0	Ppp2r5a	-3,125	0
Ccdc82	-3,250	9,994E-17	Prkce	-3,124	1,203E-11
Micu1	-3,245	1,270E-08	Vps39	-3,123	3,362E-09
Zbtb38	-3,245	1,468E-20	Fmo2	-3,123	0
Jup	-3,241	0	D5Ertd579e	-3,122	1,282E-19
Dennd4c	-3,238	8,380E-24	Golga4	-3,117	0
Phkb	-3,236	8,701E-09	Brd3	-3,116	3,032E-08
Itga1	-3,236	2,302E-11	Zyg11b	-3,115	6,306E-16
Fam49a	-3,235	3,191E-19	Mars2	-3,110	3,743E-02
Rere	-3,235	1,236E-09	Dpysl2	-3,107	0
Pdk1	-3,233	8,544E-03	Rsu1	-3,105	6,582E-18
Atp7b	-3,232	1,294E-04	Ckap5	-3,101	7,976E-18
Homer1	-3,230	8,807E-05	Rbm6	-3,099	1,067E-19
Sh3kbp1	-3,228	4,142E-10	Cdc42bpg	-3,095	5,210E-17
Ednrb	-3,226	5,356E-16	Arfgef1	-3,093	7,257E-21
Atp2c1	-3,225	3,708E-25	9330182L06Rik	-3,093	3,253E-02
Auh	-3,220	1,478E-02	Ubfd1	-3,091	1,184E-07
Ppp1cb	-3,219	0	Pofut1	-3,091	1,841E-04
Lyst	-3,219	7,503E-19	Mbtps2	-3,085	2,931E-02
Tbc1d32	-3,216	3,188E-04	Crebbp	-3,084	2,962E-19
Elmod2	-3,216	1,161E-07	Esyt2	-3,082	1,308E-19
Lrrcc1	-3,213	2,352E-10	Arhgef11	-3,082	1,370E-12
Angpt1	-3,213	0	Inpp5f	-3,080	4,335E-06
Prdm16	-3,209	1,827E-02	Tspan5	-3,080	4,628E-05
Nucb1	-3,208	2,648E-22	Arl5b	-3,079	5,871E-11
Usp48	-3,206	3,691E-15	Gabbr1	-3,079	4,547E-02
Rapgef5	-3,205	0	Atm	-3,079	1,943E-11
Plod1	-3,203	4,161E-11	Alcam	-3,077	0
Lrrc8d	-3,202	1,642E-06	Snx13	-3,077	3,772E-19
Npr2	-3,201	5,257E-05	Dach1	-3,076	9,051E-08
Mkl2	-3,200	5,863E-16	Dab2ip	-3,074	7,239E-14
Pdpk1	-3,200	1,294E-17	Rassf3	-3,073	0
Clcn4	-3,199	5,163E-12	U2surp	-3,071	5,063E-19
Cntln	-3,195	1,840E-07	Baz2a	-3,070	1,039E-11
Clec16a	-3,195	1,113E-07	Rcor3	-3,069	5,404E-03
Mecp2	-3,194	4,449E-14	Ttc13	-3,069	8,265E-04
Tie1	-3,193	2,465E-13	Clic5	-3,069	0
Swt1	-3,193	3,150E-10	Dlg5	-3,067	3,140E-05
Evi5	-3,191	2,065E-19	Ankrd17	-3,066	2,073E-17
Fgd5	-3,189	3,206E-17	Sos1	-3,066	1,462E-08
Man2a2	-3,187	5,871E-14	Trappc12	-3,064	7,794E-05
Pygm	-3,186	2,770E-03	Zmym6	-3,063	2,027E-02
Rassf9	-3,186	6,560E-15	Plxnc1	-3,063	4,289E-09
Pltp	-3,185	2,912E-16	Pi4ka	-3,062	6,372E-11
Prr5l	-3,184	3,881E-04	Ccdc85a	-3,056	6,095E-12
Klhl20	-3,183	2,378E-05	Vangl1	-3,056	2,096E-04
Tmpo	-3,182	1,289E-20	Eif4g3	-3,055	1,637E-15
Mindy2	-3,179	3,420E-22	Ndrg3	-3,054	2,835E-10
Rpgrip1l	-3,178	8,517E-03	Setd2	-3,052	0
Tek	-3,178	0	Sec24a	-3,052	6,142E-08
Ppfibp1	-3,178	5,071E-20	Ptpn3	-3,050	1,394E-04
Nrf1	-3,174	1,023E-04	Cask	-3,049	7,049E-13
Ahr	-3,172	2,433E-15	Mtus1	-3,049	0
Csnk1g1	-3,170	1,917E-06	Nup214	-3,049	4,401E-06
Cbx7	-3,170	3,792E-02	Hp1bp3	-3,046	0
Mxra8	-3,170	2,121E-10	Fip1l1	-3,045	3,007E-15
Fam184a	-3,169	2,537E-02	Tnks2	-3,045	1,522E-19
Kif21b	-3,168	3,391E-02	Tsc22d2	-3,044	7,174E-08
Baz1b	-3,168	0	Ndfip2	-3,044	4,302E-06
Adamts5	-3,167	2,976E-04	Phldb1	-3,043	6,398E-11
Alkbh8	-3,166	1,608E-03	Abca2	-3,041	2,078E-08
Dhx30	-3,161	2,019E-09	Pign	-3,041	1,334E-06
Dennd5a	-3,160	0	Pola1	-3,039	3,862E-04
Gm14391	-3,154	8,800E-03	Zcchc7	-3,038	7,392E-13
C6	-3,154	7,420E-10	Dennd6a	-3,037	2,301E-15
Exd2	-3,153	3,616E-02	Zfp236	-3,036	4,747E-08
Pld1	-3,150	8,298E-10	Lpin2	-3,034	2,263E-20
Thra	-3,148	2,815E-09	Ankrd10	-3,033	1,245E-03
Ghr	-3,144	4,135E-17	Tmem131l	-3,031	4,484E-04
Fyco1	-3,144	2,231E-14	Abi2	-3,030	2,499E-08
Tpgs2	-3,144	3,026E-02	Nvl	-3,028	3,158E-07
Mef2a	-3,144	0	Mlh3	-3,024	6,919E-04
Lnpk	-3,143	8,963E-06	Crtc3	-3,023	8,868E-04
Zeb1	-3,141	6,792E-16	Trim65	-3,022	5,047E-03
Zfp329	-3,140	4,864E-07	Zfp318	-3,020	7,460E-08
Ubxn2b	-3,138	8,093E-03	Usp47	-3,020	0
Nr2c2	-3,131	6,311E-14	Ncapd3	-3,020	3,001E-02
Elmo1	-3,131	1,267E-08	Nacc2	-3,019	1,497E-04

Msi2	-3,015	5,194E-16	Nsmaf	-2,879	6,964E-12
Tnks	-3,014	3,817E-10	Mxi1	-2,877	1,257E-05
Pcgf3	-3,012	7,209E-11	Pde3b	-2,877	3,160E-04
Zkscan1	-3,012	5,538E-18	4931406P16Rik	-2,875	1,017E-15
Osbpl1a	-3,011	1,687E-04	Myrf	-2,874	5,083E-04
Rsbn1l	-3,009	1,737E-08	Cdc14a	-2,874	6,371E-08
Smg6	-3,008	2,588E-09	Prkg2	-2,874	1,088E-05
S100pbp	-3,004	2,941E-02	Abca1	-2,873	6,170E-14
Ncoa6	-3,000	1,048E-08	Trim33	-2,871	7,476E-11
Ick	-2,999	2,376E-10	Synrg	-2,870	4,036E-08
Magi3	-2,999	0	Lrrk1	-2,870	3,269E-10
Fsd1l	-2,999	1,243E-02	Nup98	-2,868	2,851E-14
Hspa12a	-2,998	1,093E-03	Zfp407	-2,867	2,745E-09
Eml1	-2,997	9,049E-13	Ptprm	-2,866	0
Firre	-2,994	8,702E-10	Aldh6a1	-2,865	3,494E-08
Chordc1	-2,993	8,118E-12	Tacc1	-2,865	0
Trps1	-2,992	2,292E-13	Sun1	-2,864	9,005E-11
Uvrag	-2,989	2,762E-10	Trip11	-2,862	0
Ankrd26	-2,982	2,718E-02	Heca	-2,862	4,981E-16
Tasor	-2,978	1,085E-20	Myh11	-2,862	0
Lss	-2,975	6,789E-03	Mtss1	-2,861	6,462E-13
Rnpepl1	-2,973	1,560E-03	Ranbp2	-2,860	0
Slc35b4	-2,973	7,485E-05	Lztfl1	-2,860	1,062E-06
Efr3a	-2,968	8,154E-15	Srek1	-2,858	2,254E-08
Nemf	-2,966	5,061E-15	Ric1	-2,857	6,443E-10
Bcl2	-2,965	1,127E-05	Fbf1	-2,853	9,124E-06
Ttll7	-2,964	4,513E-15	Zbtb41	-2,849	7,070E-12
Calcrl	-2,963	0	Uggt1	-2,846	2,050E-17
Usp40	-2,962	1,458E-04	Nbeal2	-2,845	3,781E-02
Chn1	-2,961	3,718E-03	Ccdc127	-2,845	4,664E-06
Miga1	-2,959	8,714E-05	Ints1	-2,844	2,770E-03
C2cd5	-2,958	4,523E-02	Mcm9	-2,842	4,435E-02
Eln	-2,957	8,861E-10	Sash1	-2,840	0
Dennd1l	-2,957	5,790E-06	Jcad	-2,840	0
Frs2	-2,954	1,240E-06	Kdm6a	-2,839	8,346E-12
Tmcc2	-2,953	1,610E-09	Adcy9	-2,838	2,498E-04
Afdn	-2,953	0	Cbx6	-2,837	8,425E-10
Mfsd6	-2,952	1,680E-14	Zfp91	-2,837	1,217E-16
Uhmk1	-2,951	0	Eif4ebp2	-2,837	3,761E-06
Robo1	-2,951	3,684E-02	Prkcz	-2,836	3,049E-03
Stam	-2,947	5,615E-07	Clip1	-2,834	0
Ythdc1	-2,944	7,318E-13	Mapk8	-2,833	1,776E-05
Tmtc3	-2,944	2,358E-10	Plcb4	-2,831	4,686E-14
Spg11	-2,944	2,452E-07	Kansl1l	-2,831	2,604E-07
Ltbp3	-2,939	6,608E-08	Cdk19	-2,830	6,874E-06
Atp11a	-2,937	0	Selenoi	-2,829	2,280E-05
Dock8	-2,937	4,429E-12	Fubp1	-2,829	0
Scmh1	-2,936	7,245E-03	Nrp2	-2,829	4,001E-16
Cep63	-2,935	1,909E-04	Polg	-2,827	2,095E-06
Senp1	-2,933	9,028E-07	Mcf2l	-2,827	3,559E-08
9930021J03Rik	-2,932	1,153E-10	Igf2r	-2,826	2,127E-16
Slc35a3	-2,932	5,748E-11	Mvb12b	-2,826	1,953E-05
Phf20	-2,931	1,889E-09	Cramp1l	-2,825	3,917E-04
Prr14l	-2,931	7,921E-14	Sept4	-2,825	2,302E-09
Med13l	-2,929	2,258E-10	Bcl9l	-2,824	2,544E-04
Top1	-2,924	6,859E-19	Dhdh	-2,824	5,311E-04
Cdk12	-2,922	3,970E-13	Vopp1	-2,824	8,246E-04
Nrep	-2,920	2,444E-06	Sec14l1	-2,823	7,894E-16
Stag2	-2,920	0	Usp6nl	-2,823	4,467E-10
C330007P06Rik	-2,920	3,638E-14	Rmnd5a	-2,822	4,528E-09
Ctdspl2	-2,918	2,159E-09	Dgke	-2,819	1,682E-03
Pbx3	-2,913	7,499E-03	Emcn	-2,817	5,014E-06
Zdhhc21	-2,913	1,383E-05	Gatad2b	-2,816	4,255E-13
Fam13a	-2,911	4,210E-04	Bdp1	-2,815	5,687E-18
Smurf2	-2,909	0	Gapvd1	-2,813	1,429E-14
Plxnb1	-2,906	5,064E-07	P2rx7	-2,812	1,075E-03
Fgf1	-2,905	2,302E-11	Ubr5	-2,811	0
Sox17	-2,904	5,268E-05	Axin2	-2,811	1,148E-02
Adcy7	-2,901	1,653E-11	Cic	-2,809	2,646E-05
5031439G07Rik	-2,899	3,046E-04	Txlng	-2,808	5,564E-08
Ptprk	-2,899	1,576E-17	Chd1	-2,808	3,712E-16
Zxdc	-2,898	3,355E-02	Cabin1	-2,806	1,062E-05
Phf21a	-2,897	4,371E-09	Tep1	-2,805	1,381E-03
Slco4c1	-2,896	2,550E-09	Fhdc1	-2,802	2,574E-03
Erc1	-2,891	1,534E-07	Fam20b	-2,800	3,752E-14
Tcf20	-2,889	0	Ttl	-2,800	9,547E-04
Serinc5	-2,887	6,769E-10	Yap1	-2,800	6,944E-15
Fzd7	-2,886	2,148E-05	Wwc2	-2,797	2,441E-11
Fbln1	-2,885	3,683E-02	Pfkp	-2,795	1,309E-10
Flt4	-2,882	2,305E-07	Sympk	-2,791	1,244E-04
Rab11fip1	-2,880	0	Lmtk2	-2,791	2,097E-12
Dopey2	-2,880	3,844E-08	Cstf2	-2,789	4,305E-07

Ankhd1	-2,785	1,366E-16	Gpr137b	-2,693	2,932E-03
Dnmbp	-2,785	9,805E-05	Bace1	-2,692	4,567E-06
Ptgfrn	-2,784	0	Med13	-2,691	0
Vwa8	-2,784	8,247E-07	Ttc7b	-2,690	1,240E-03
Tmem63b	-2,781	8,469E-08	Klhl42	-2,690	5,062E-03
Mettl7a1	-2,779	0	Lbh	-2,689	0
Casp2	-2,778	2,168E-05	Taf1	-2,689	4,888E-15
Prpf4b	-2,777	0	Zmym2	-2,685	5,769E-11
Wdr44	-2,776	1,536E-05	Chml	-2,685	1,092E-04
Manba	-2,776	1,700E-02	Kif1c	-2,684	0
Ctnnd1	-2,775	0	Ppp1r7	-2,683	4,699E-05
Plscr4	-2,773	3,995E-04	Gon4l	-2,683	2,928E-09
Dip2a	-2,773	6,166E-06	Nr2f2	-2,682	4,500E-07
Fam199x	-2,773	1,153E-04	Rasa1	-2,682	6,401E-16
Hnrnpu	-2,771	0	Car8	-2,681	0
Zfp629	-2,770	2,974E-02	Tent5c	-2,680	4,888E-03
Zfyve27	-2,769	1,628E-02	Xiap	-2,678	0
Wls	-2,767	2,776E-12	Ccng2	-2,678	8,401E-06
Tmem94	-2,767	1,844E-03	Atp13a3	-2,676	0
Pofut2	-2,766	1,204E-04	Clec1b	-2,676	8,309E-03
Akap5	-2,766	0	Ulk2	-2,676	1,972E-11
Klhl24	-2,766	0	Kif16b	-2,676	9,954E-08
Git2	-2,764	1,761E-08	Slc4a4	-2,675	3,538E-02
Npr1	-2,761	1,896E-11	Trim24	-2,674	1,510E-04
Fgfr2	-2,760	1,855E-17	Tubgcp5	-2,672	6,451E-06
Colec12	-2,757	0	Adgra3	-2,672	6,119E-05
Ecpas	-2,757	1,504E-14	Ncoa7	-2,672	2,114E-05
Rbl2	-2,757	5,312E-11	Kif13b	-2,672	4,285E-07
Mast2	-2,757	5,374E-05	Top3b	-2,670	6,663E-04
Diaph2	-2,756	1,344E-10	Vps50	-2,670	1,905E-05
Smim14	-2,756	1,972E-07	Cfap43	-2,669	5,573E-06
Dcaf8	-2,755	2,668E-13	Luzp1	-2,669	0
Atxn7l1	-2,755	3,049E-04	Mia2	-2,668	1,871E-15
Kat6a	-2,755	0	Gbf1	-2,665	8,742E-07
Ehmt1	-2,755	4,698E-08	Sypl	-2,665	9,533E-06
Mospd2	-2,753	1,858E-10	March2	-2,665	3,818E-05
Topbp1	-2,752	2,573E-05	Prps2	-2,663	3,037E-04
Kmt2e	-2,749	3,182E-16	Irf6	-2,660	3,811E-05
Foxo1	-2,745	6,672E-04	Ints2	-2,660	4,944E-02
Deptor	-2,745	2,244E-11	Agrn	-2,659	7,108E-10
Agpat3	-2,744	2,278E-08	Hif1an	-2,659	4,143E-03
Qk	-2,744	0	Clstn1	-2,658	0
Nr3c1	-2,742	0	C2cd2	-2,653	6,433E-05
Ccnt1	-2,742	3,079E-11	Tut4	-2,653	1,259E-06
Snapc3	-2,742	3,209E-06	Arhgef5	-2,653	6,016E-11
Mgll	-2,742	2,526E-07	Sept11	-2,651	4,925E-16
Cyhr1	-2,741	1,392E-07	Cbfa2t2	-2,651	1,671E-02
Arhgap23	-2,741	8,360E-05	Zfp646	-2,650	2,369E-07
Gpatch8	-2,740	5,885E-08	Rad54l2	-2,650	1,460E-03
Zcchc14	-2,738	6,383E-09	Mtor	-2,650	2,184E-06
Rab11fip3	-2,738	4,703E-02	Sema3b	-2,649	7,513E-08
Nup160	-2,737	1,081E-02	Gramd1b	-2,649	5,793E-03
Tpr	-2,736	0	Gm45062	-2,647	4,182E-05
Adamts2	-2,736	5,453E-08	Zzz3	-2,647	9,886E-12
Itch	-2,735	9,940E-16	Kifc3	-2,646	1,916E-02
Agps	-2,733	3,110E-09	Med14	-2,646	7,057E-08
Heyl	-2,731	4,083E-02	Podxl	-2,646	0
Mob2	-2,731	6,679E-03	Myct1	-2,643	6,307E-08
Tom1l1	-2,729	8,216E-07	Socs2	-2,643	6,418E-09
Ddi2	-2,728	6,805E-16	Usp53	-2,643	8,210E-05
Wwp1	-2,722	0	Atl2	-2,641	3,949E-07
Ppp4r3a	-2,722	1,366E-14	Ano1	-2,639	1,380E-12
Rgs12	-2,720	1,895E-05	Nek1	-2,639	7,815E-05
Tmod3	-2,718	0	Nfatc1	-2,639	3,771E-05
Shank3	-2,718	4,434E-07	Pik3cb	-2,638	1,232E-04
Map4k5	-2,715	4,572E-09	Ext1	-2,638	1,979E-09
Col4a3bp	-2,713	1,021E-13	Ciz1	-2,638	1,109E-05
Osbpl8	-2,709	4,988E-14	Chmp4c	-2,638	4,824E-04
Slc29a1	-2,709	3,609E-04	Csnk2a2	-2,633	9,935E-03
Zfp326	-2,706	3,839E-02	Ubr3	-2,633	2,947E-12
Syncrip	-2,705	1,010E-14	Nipbl	-2,632	0
Nfic	-2,704	6,241E-06	Ankmy2	-2,632	1,112E-04
Anks1	-2,704	4,319E-07	N4bp2	-2,631	3,882E-03
Mgat5	-2,703	2,827E-07	Iws1	-2,630	1,347E-10
Epb41l3	-2,702	2,210E-04	Atxn2	-2,628	9,031E-06
Zfp760	-2,701	9,475E-03	Stab1	-2,627	2,468E-06
Numa1	-2,701	0	Trp53bp2	-2,624	7,726E-12
Stim1	-2,699	4,119E-08	Rtkn2	-2,624	1,496E-10
Myo5a	-2,699	1,080E-07	Ahctf1	-2,624	4,053E-14
Slco2a1	-2,695	0	Abcb1a	-2,623	4,397E-07
Lamb2	-2,695	4,763E-11	Ldlrap1	-2,623	3,208E-02
Kmt2b	-2,693	9,109E-04	Mark3	-2,621	1,141E-13

Atg4b	-2,620	4,137E-03	Dcbld2	-2,527	3,413E-06
Appl1	-2,619	1,968E-10	Frmd6	-2,526	3,716E-09
Maml2	-2,618	5,751E-06	Tgfb1i1	-2,525	5,547E-03
Mfge8	-2,615	1,787E-10	Togaram1	-2,525	1,745E-10
Lpcat1	-2,613	0	Tubgcp3	-2,524	2,133E-03
Foxk1	-2,613	7,693E-05	Tjp1	-2,523	0
Coro1c	-2,612	3,546E-15	Large1	-2,522	3,550E-02
Pafah1b1	-2,611	0	D430042O09Rik	-2,520	2,166E-03
Hectd1	-2,607	0	Wipi2	-2,519	1,462E-05
Marf1	-2,606	1,354E-12	Zmynd11	-2,519	0
Wdr37	-2,606	2,510E-09	Lcor	-2,517	3,232E-03
Elmo2	-2,603	2,674E-05	Tmem47	-2,516	3,654E-07
Lrrc8b	-2,600	2,145E-12	Fmo1	-2,514	0
Ppp2r5c	-2,600	6,397E-13	Rbbp4	-2,514	2,114E-09
Relch	-2,596	1,781E-06	Sh3bp4	-2,513	3,782E-02
Cwf19l2	-2,594	2,585E-07	Loxl2	-2,513	7,372E-05
Runx1	-2,593	3,467E-08	Sel1l	-2,513	0
Ptprf	-2,593	0	Rrm2b	-2,513	8,979E-08
Tmem131	-2,591	3,022E-09	Csnk1e	-2,513	2,696E-05
Bmp5	-2,591	6,391E-12	Gm38394	-2,513	4,133E-02
Srpk1	-2,589	1,131E-06	Zbtb11	-2,508	1,040E-04
Ezh1	-2,589	3,044E-07	Rubcn	-2,506	2,752E-03
Nceh1	-2,587	3,609E-10	Atg16l1	-2,505	8,210E-03
Ppm1k	-2,587	1,518E-03	Rusc2	-2,503	1,316E-04
Chd2	-2,587	1,080E-14	Sdc2	-2,503	4,371E-09
Eprs	-2,586	0	Lrrc58	-2,502	1,151E-11
Ypel2	-2,585	2,108E-03	Kdm3a	-2,502	3,293E-06
Dpysl3	-2,585	7,169E-06	Ercc6l2	-2,501	1,924E-03
Tnrc6a	-2,585	8,363E-09	Strn	-2,501	1,402E-09
Fnbp1	-2,585	1,773E-05	Tshz1	-2,501	1,221E-06
Smarcad1	-2,584	1,201E-07	Trip4	-2,499	5,660E-04
Stard4	-2,583	9,522E-05	Rab3gap1	-2,498	1,868E-10
Clk3	-2,582	4,394E-06	Twsg1	-2,498	2,267E-11
Thsd1	-2,578	1,674E-03	Purb	-2,498	0
Cep68	-2,576	3,765E-04	Myh9	-2,497	0
Agpat5	-2,575	8,350E-03	Stxbp6	-2,495	2,382E-04
Abcc5	-2,575	9,879E-10	Epg5	-2,495	2,090E-02
Mysm1	-2,573	5,145E-12	Nae1	-2,495	1,055E-06
Ube3c	-2,572	3,195E-07	Ccp110	-2,493	2,463E-02
Cyth3	-2,571	0	Taok3	-2,490	9,831E-11
Zfp267	-2,568	1,055E-02	Cog5	-2,488	2,938E-09
Gm4631	-2,568	9,313E-05	AI504432	-2,488	2,840E-03
Pan3	-2,567	2,801E-13	Gne	-2,488	1,978E-03
Glg1	-2,565	1,787E-14	Lamc1	-2,487	0
Cep162	-2,565	7,305E-05	Ccdc186	-2,486	2,028E-10
Itpkb	-2,565	0	Smarcb1	-2,486	7,968E-03
Lats2	-2,563	5,823E-13	Gopc	-2,484	1,979E-05
Nfya	-2,563	1,079E-02	Csde1	-2,477	0
Pbrm1	-2,562	0	Podn	-2,476	4,363E-02
Ankfy1	-2,561	3,036E-11	Pde7a	-2,475	2,281E-05
Pcm1	-2,561	0	Pank3	-2,474	0
Slc44a3	-2,560	5,283E-03	Caprin1	-2,465	0
Man1a	-2,560	6,175E-10	Spopl	-2,465	5,326E-06
Rictor	-2,560	3,052E-11	Cdc42bpb	-2,464	5,999E-10
Phtf1	-2,559	2,020E-03	Jarid2	-2,463	3,010E-04
Tsc2	-2,559	2,532E-06	Tmem164	-2,462	3,007E-05
Phf8	-2,558	3,858E-03	Acvr2a	-2,461	2,301E-07
Myo1d	-2,555	8,949E-13	Adcy6	-2,461	9,828E-04
Arhgef26	-2,554	1,234E-07	Ccdc50	-2,459	0
Slmap	-2,552	8,015E-14	Tbx3	-2,458	9,794E-09
Sms	-2,552	1,389E-04	Setdb1	-2,457	7,311E-04
Cfh	-2,551	0	Epm2aip1	-2,457	7,025E-08
Fam171a1	-2,551	5,613E-08	Wdr48	-2,453	2,004E-07
Tln1	-2,550	0	Otud7b	-2,453	6,780E-07
Cavin2	-2,545	0	Ntn4	-2,453	1,981E-07
Atp7a	-2,545	1,035E-08	Uvssa	-2,451	1,295E-02
Efcab14	-2,544	1,618E-08	Rasa2	-2,448	4,337E-03
Ssh1	-2,542	1,808E-06	Ttc17	-2,444	5,114E-03
Csnk1a1	-2,542	0	Tpp2	-2,443	5,568E-10
Triobp	-2,541	4,671E-02	Bcr	-2,443	1,088E-05
Ube4a	-2,539	2,606E-07	Upk3b	-2,442	1,382E-02
Mapkbp1	-2,539	3,953E-06	Brd9	-2,440	2,069E-05
Mtdh	-2,537	0	Fgfr1	-2,439	4,068E-03
Usp54	-2,537	8,585E-06	Smad5	-2,439	4,295E-11
Itpripl2	-2,536	0	Bicd2	-2,438	5,552E-10
Mr1	-2,533	3,515E-03	Eps15	-2,436	0
Lratd2	-2,532	6,505E-07	Fbxo30	-2,436	6,341E-06
Fam193b	-2,532	1,669E-02	Ap3d1	-2,434	1,655E-04
Prdm2	-2,531	1,113E-07	Cdk7	-2,434	6,902E-03
Odf2	-2,530	3,151E-03	Tdrd3	-2,432	2,654E-07
Rnf141	-2,529	1,027E-13	Itgav	-2,432	9,767E-11
Rassf8	-2,529	1,447E-10	Stard8	-2,429	4,832E-10

Zfp609	-2,425	2,548E-03	Fmr1	-2,336	1,114E-07
Zfp12	-2,425	2,068E-02	Usp33	-2,334	5,125E-09
Luc7l3	-2,423	0	Atxn1l	-2,334	4,496E-07
Rassf4	-2,422	3,529E-04	Ints8	-2,333	8,304E-04
Aff3	-2,420	3,256E-04	Rabgap1	-2,333	8,926E-10
March7	-2,420	5,005E-07	Slc30a7	-2,331	2,129E-05
Nmt2	-2,420	2,116E-06	Cdip1	-2,331	5,991E-03
Aldh2	-2,419	0	Kif2a	-2,330	1,505E-03
Xpc	-2,415	2,472E-03	Dgkz	-2,329	9,577E-06
Luc7l	-2,415	2,905E-05	Fam174b	-2,325	1,069E-06
Prex1	-2,415	1,241E-04	Sptlc2	-2,323	0
Hipk1	-2,415	0	Pdgfd	-2,323	1,422E-02
Nkd1	-2,415	1,151E-11	Pcmtd1	-2,323	2,302E-11
2610507B11Rik	-2,415	0	Zfp592	-2,323	1,132E-02
Zfp367	-2,413	7,640E-04	Fam168a	-2,322	5,036E-07
Zfc3h1	-2,412	3,581E-08	Dnmt1	-2,321	2,812E-05
Abcg1	-2,412	9,206E-11	Gtf3c4	-2,321	2,310E-02
Celsr1	-2,411	8,942E-03	Dusp3	-2,320	0
Yipf6	-2,410	0	Zhx1	-2,320	4,446E-08
Prosc	-2,409	2,217E-02	Mcm3ap	-2,320	3,370E-02
Crybg3	-2,409	6,493E-10	Tfpi	-2,319	6,703E-04
Leng8	-2,408	1,004E-08	Ktn1	-2,319	0
Dgcr2	-2,408	1,337E-05	Acer2	-2,316	0
Tnpo3	-2,407	7,709E-06	Ids	-2,315	3,810E-04
Cgnl1	-2,405	0	Tmem64	-2,314	6,583E-03
Pcolce	-2,403	3,202E-05	Far1	-2,313	1,017E-07
Thada	-2,402	1,011E-03	Xpo1	-2,313	1,381E-10
Pdgfrb	-2,402	2,305E-09	Yes1	-2,312	1,350E-09
Myzap	-2,401	4,925E-09	Aqp1	-2,310	0
Dync1i2	-2,401	0	Ubr2	-2,309	1,022E-04
Ext2	-2,401	3,677E-03	Ascc3	-2,309	3,000E-08
Sgk3	-2,400	2,561E-03	Dsel	-2,309	3,813E-02
Ccdc174	-2,399	3,699E-02	Prkci	-2,308	9,794E-10
Man1a2	-2,398	2,637E-09	Sec16a	-2,307	2,689E-08
Desi2	-2,396	2,440E-02	Pkn2	-2,306	1,151E-11
Fbxo3	-2,395	5,968E-05	Zfyve16	-2,306	1,451E-03
Zmym4	-2,394	9,773E-06	Ccdc88c	-2,305	1,878E-03
Rab22a	-2,390	1,323E-06	Chd9	-2,302	1,959E-05
Brd1	-2,389	2,625E-10	Pfkfb2	-2,302	1,590E-03
Abcd2	-2,386	2,409E-03	Crebl2	-2,302	7,746E-06
Snx30	-2,383	1,150E-03	Cyfip1	-2,300	6,013E-10
Hltf	-2,383	9,349E-09	Erp29	-2,299	2,048E-05
Ipo11	-2,382	3,953E-04	Hdac4	-2,299	1,160E-02
Rnf38	-2,382	4,930E-05	Cbl	-2,298	6,738E-06
Plekhb2	-2,381	1,040E-05	Gpatch2	-2,297	4,476E-02
Sik3	-2,381	2,979E-03	Dyrk2	-2,296	4,028E-06
Nbr1	-2,380	4,868E-09	Azin1	-2,296	1,642E-08
Ehd2	-2,378	0	Als2cl	-2,294	2,418E-02
Stag1	-2,378	1,225E-11	Copg1	-2,293	8,979E-08
Sp1	-2,375	0	Pdxdc1	-2,292	3,232E-10
Fam193a	-2,374	5,084E-05	Sec63	-2,289	1,942E-09
Cep192	-2,371	7,490E-03	Rab3gap2	-2,288	6,078E-04
Hsph1	-2,370	3,183E-04	Socs6	-2,287	2,412E-04
Gpr107	-2,366	1,242E-04	Tmem170b	-2,287	1,382E-05
Myo1e	-2,366	5,551E-10	Tfdp2	-2,287	4,373E-07
Ap1ar	-2,365	4,256E-05	Tbl1x	-2,286	5,682E-10
Ccar1	-2,365	2,387E-06	Slc43a2	-2,286	3,690E-06
Hcfc1	-2,362	1,578E-08	Gsap	-2,286	1,975E-04
Atf2	-2,361	2,562E-06	Dcaf1	-2,284	7,639E-05
Mtmr3	-2,361	2,895E-08	Trpc4ap	-2,282	9,221E-04
Dennd4a	-2,360	1,016E-08	Stx8	-2,282	1,401E-02
Rad50	-2,359	3,835E-07	Tbc1d9b	-2,282	1,733E-05
Zfp608	-2,358	6,443E-09	Hdac7	-2,279	2,557E-02
Dubr	-2,357	2,755E-02	Igfbp5	-2,279	1,731E-05
Tcf21	-2,356	3,947E-04	Smchd1	-2,278	3,494E-10
Ap2b1	-2,350	6,923E-10	Slc35e2	-2,276	1,022E-02
Dcaf6	-2,349	3,279E-05	Elf2	-2,275	4,844E-05
Rsrc1	-2,347	1,303E-02	Tspan9	-2,275	2,054E-10
Kit	-2,346	1,151E-11	Stk38	-2,274	1,202E-04
Uhrf1bp1l	-2,345	8,184E-07	Med12	-2,273	6,014E-05
Glce	-2,344	4,410E-02	4930523C07Rik	-2,272	1,394E-07
Rbfox2	-2,344	5,346E-07	Maoa	-2,271	2,820E-06
Pqlc3	-2,342	5,591E-03	Nfatc3	-2,271	9,313E-06
Atp13a2	-2,341	3,036E-03	Asap2	-2,270	6,008E-04
Atad2	-2,341	3,283E-03	Vcpip1	-2,269	2,868E-07
Acin1	-2,341	4,471E-09	Notch2	-2,269	3,798E-10
Zfx	-2,339	9,514E-09	Iars2	-2,269	8,242E-05
Phldb2	-2,339	0	Ptgr2	-2,268	1,197E-04
Dlg1	-2,338	8,704E-10	Eif4g2	-2,267	0
Fbxw7	-2,337	1,214E-04	Slc23a2	-2,267	9,646E-09
Cand1	-2,337	3,646E-09	Asap1	-2,267	1,066E-03
Rbm15b	-2,336	1,838E-04	Cdc37	-2,266	1,585E-03

Ift172	-2,263	1,021E-03	Cyld	-2,173	2,901E-04
Dcaf10	-2,263	1,989E-03	Mtmr4	-2,171	8,249E-05
Med1	-2,262	3,240E-06	Mink1	-2,170	1,445E-03
Tsn	-2,256	7,222E-03	Scyl2	-2,170	1,424E-02
Fam117b	-2,254	9,047E-05	Kcnj15	-2,169	9,143E-07
Map3k4	-2,254	6,030E-03	Tgfbr2	-2,169	1,956E-10
Cav1	-2,254	0	Zc3h18	-2,169	1,015E-03
Bmpr1a	-2,254	1,052E-08	Spock2	-2,168	1,266E-10
Ppp1r12a	-2,253	0	Rnpc3	-2,167	5,815E-04
Rassf2	-2,252	1,737E-04	Cltc	-2,167	0
Rabep1	-2,249	1,266E-10	Met	-2,166	5,459E-08
Itga4	-2,248	9,521E-08	Ubn1	-2,165	1,189E-05
Kpna1	-2,247	9,622E-06	Pkia	-2,164	4,794E-02
Acss1	-2,245	1,051E-03	Kif5b	-2,164	0
Slk	-2,245	0	Ednra	-2,163	2,241E-05
Maco1	-2,243	1,095E-03	Ing4	-2,163	4,629E-03
Poglut3	-2,240	1,472E-06	Pdgfra	-2,162	1,151E-11
Fam135a	-2,240	1,346E-02	Impdh1	-2,162	7,483E-03
Dmxl2	-2,239	2,277E-04	Zfp445	-2,161	1,676E-07
Thrap3	-2,238	7,710E-10	Tc2n	-2,161	1,296E-03
Mpp7	-2,233	6,450E-03	Nfx1	-2,160	6,376E-04
Wwc1	-2,232	1,991E-09	Tle1	-2,160	2,741E-04
Pigq	-2,232	1,824E-03	Appl2	-2,159	3,720E-04
Pcyt1a	-2,231	3,310E-04	Lurap1l	-2,158	5,583E-04
Ablim3	-2,230	1,122E-06	Srebf1	-2,158	1,151E-02
Slc34a2	-2,228	0	Sh3glb1	-2,157	1,151E-11
Exoc5	-2,225	1,809E-06	Ap1g1	-2,156	1,369E-09
Ankrd13c	-2,223	5,105E-06	Copa	-2,156	2,302E-11
Add3	-2,222	2,417E-10	Stk4	-2,155	6,905E-11
Slc9a6	-2,222	1,397E-02	Socs4	-2,155	6,413E-04
Gnaq	-2,222	4,488E-10	Cd99l2	-2,153	4,293E-04
Rapgef1	-2,222	6,919E-04	Dync1li2	-2,153	7,538E-09
Lta4h	-2,222	2,449E-03	Hivep1	-2,152	1,149E-04
Vgll3	-2,221	6,148E-03	Prpf8	-2,149	7,561E-09
Arhgap44	-2,221	1,308E-04	Cdk8	-2,148	9,898E-03
Shroom3	-2,221	2,505E-06	Virma	-2,147	1,445E-05
Dock11	-2,219	5,349E-03	Sltm	-2,147	7,613E-06
Clec1a	-2,217	4,258E-10	Plekha1	-2,146	3,054E-07
Flrt3	-2,217	2,730E-08	Prxl2c	-2,146	3,608E-06
Anapc5	-2,216	6,226E-09	Rps6ka3	-2,145	1,768E-07
Uba6	-2,213	9,218E-03	Ube4b	-2,144	8,310E-03
Rsbn1	-2,211	3,718E-05	Fem1b	-2,142	5,639E-10
Tmed7	-2,209	4,569E-09	Rnf111	-2,142	1,102E-03
Tgfbr3	-2,205	1,333E-07	Cav2	-2,141	1,465E-07
Wrn	-2,202	3,139E-02	Tasor2	-2,141	3,959E-06
Ncoa3	-2,202	9,345E-08	Qrich1	-2,139	2,311E-06
Tspan12	-2,201	2,200E-05	Avl9	-2,139	1,360E-05
Il6st	-2,200	0	Map3k5	-2,138	1,539E-04
Prrc2a	-2,199	2,443E-06	Lama5	-2,135	2,845E-04
Cep170b	-2,199	1,591E-02	Add1	-2,134	7,712E-07
Gxylt1	-2,199	4,644E-05	Eif5b	-2,134	4,814E-03
Nedd4l	-2,196	1,767E-06	Acly	-2,133	1,438E-09
Epas1	-2,196	0	Arhgef1	-2,133	1,474E-02
Ddx6	-2,195	2,186E-10	Tmed8	-2,132	8,894E-03
Opa1	-2,194	9,190E-07	Tmem87b	-2,132	7,156E-04
Kansl1	-2,194	3,932E-05	Camk1	-2,130	4,106E-05
Srsf11	-2,194	7,595E-10	Lamp2	-2,129	0
Atl3	-2,193	1,542E-09	Herc4	-2,129	9,012E-05
Uaca	-2,193	3,650E-04	Plxnd1	-2,129	2,234E-04
Carmil1	-2,191	4,177E-06	Hipk3	-2,127	5,754E-11
Tmem167	-2,191	4,279E-04	Klhl5	-2,125	2,428E-09
Clk4	-2,190	2,919E-05	Ctbp2	-2,125	2,343E-03
Dnajc13	-2,189	2,544E-06	Ssr1	-2,125	3,680E-08
Kitl	-2,189	0	Atp9a	-2,124	3,423E-02
Eea1	-2,189	1,381E-10	Tmem106b	-2,124	1,599E-07
Tlk1	-2,188	6,501E-08	Chd7	-2,121	1,724E-03
Celf1	-2,186	7,039E-06	Calcoco1	-2,121	3,960E-03
Vps35l	-2,185	4,087E-02	Flna	-2,119	0
Tnpo1	-2,184	9,655E-09	Nf2	-2,119	1,362E-04
Cd36	-2,183	1,511E-07	Vps4b	-2,118	3,558E-06
Pias1	-2,183	4,341E-04	Znrf2	-2,115	2,834E-04
Fndc3a	-2,183	9,666E-10	Nid1	-2,114	9,607E-08
Orc4	-2,182	4,978E-05	Arhgap12	-2,114	7,957E-05
Palmd	-2,180	2,527E-02	Rsrc2	-2,114	3,468E-05
Cpne3	-2,180	4,730E-09	Net1	-2,113	3,488E-08
Gid4	-2,180	4,477E-05	Arfgef2	-2,113	1,637E-04
Ptpn21	-2,179	1,317E-02	Itpr3	-2,112	3,025E-02
6430548M08Rik	-2,178	1,858E-05	Slc44a1	-2,110	5,153E-08
Morf4l1	-2,177	3,341E-03	Tbc1d2b	-2,110	1,867E-03
Sertad2	-2,177	4,697E-05	Bcor	-2,109	8,065E-03
Ankib1	-2,175	5,006E-05	Prx	-2,109	3,511E-05
Mdfic	-2,174	7,245E-07	Matr3	-2,109	3,452E-11

Tablas Suplementarias

Map3k1	-2,108	1,554E-03	Trp53inp2	-2,062	7,864E-04
Dcaf11	-2,107	1,485E-04	Prpf40a	-2,062	1,154E-07
Slc25a51	-2,107	5,195E-05	Plxna2	-2,061	4,009E-04
Synj2bp	-2,106	2,604E-05	Smc4	-2,061	1,567E-06
Rnf145	-2,106	1,208E-03	Cul5	-2,061	4,312E-06
Lamb3	-2,105	6,338E-04	Klf7	-2,060	1,570E-06
Ltn1	-2,104	6,476E-05	Gsn	-2,059	0
Tardbp	-2,103	2,222E-08	Rbm26	-2,058	1,589E-05
Aplp2	-2,101	1,508E-09	Atxn7	-2,058	3,252E-04
Pik3c2a	-2,100	3,590E-09	Ivns1abp	-2,057	2,488E-04
Trak2	-2,099	1,438E-09	Arap3	-2,056	3,658E-07
Strn4	-2,098	1,675E-02	Tbl1xr1	-2,056	7,195E-04
Nbas	-2,098	9,893E-03	Sec14l3	-2,053	2,058E-08
Lima1	-2,097	6,533E-07	Ldlr	-2,049	8,640E-04
Tet2	-2,095	1,135E-05	Btaf1	-2,048	3,162E-07
Pi4k2b	-2,094	1,075E-04	Agfg1	-2,048	1,175E-08
Ctdspl	-2,094	3,608E-06	Rps6kb1	-2,048	3,023E-02
Rnf13	-2,094	3,069E-07	Tax1bp1	-2,045	2,417E-09
Afap1l1	-2,093	1,162E-06	March6	-2,045	1,307E-06
Ntn1	-2,092	1,828E-03	Mau2	-2,044	1,075E-02
Pdzrn3	-2,090	4,774E-02	Cntrl	-2,043	6,688E-06
Rhot1	-2,089	1,553E-04	Ccnd2	-2,042	8,949E-06
Vapb	-2,089	4,368E-04	Acap2	-2,042	1,631E-08
Smarce1	-2,087	1,335E-06	Fndc3b	-2,036	1,652E-06
Zfyve9	-2,087	4,269E-04	Phf20l1	-2,035	3,696E-08
Arap1	-2,087	4,426E-04	Reep3	-2,034	3,998E-08
Chic2	-2,087	1,261E-02	Ddx50	-2,031	1,364E-05
Sept8	-2,085	1,125E-04	Setd3	-2,028	5,309E-07
Tmem33	-2,085	3,458E-02	Etv3	-2,027	7,882E-03
Gns	-2,084	7,254E-08	Mapre1	-2,027	3,714E-06
Rxra	-2,083	4,963E-02	Zc3h7b	-2,025	2,248E-05
Impad1	-2,083	3,193E-05	Otud4	-2,024	7,264E-08
Serf2	-2,082	5,367E-08	Supt20	-2,022	8,776E-03
Trim37	-2,081	3,000E-02	P4ha1	-2,021	2,291E-04
Eif4a2	-2,081	2,041E-06	Bicc1	-2,021	1,267E-02
Txndc9	-2,079	1,265E-02	Cd93	-2,021	1,151E-11
Top2b	-2,078	0	Usp16	-2,019	1,832E-04
Scaf11	-2,074	6,559E-10	Arih1	-2,019	1,065E-06
Fcho2	-2,074	1,915E-06	Sgms1	-2,019	1,081E-05
Polr3f	-2,072	3,566E-02	Phf2	-2,017	2,899E-02
Pcf11	-2,070	7,455E-06	Derl2	-2,016	2,978E-02
Dyrk1a	-2,070	2,503E-05	Emc1	-2,015	2,764E-03
Extl3	-2,068	1,392E-02	Sgpp1	-2,015	1,791E-02
Pof1b	-2,068	2,542E-04	Aldh3a2	-2,014	1,127E-03
Snx25	-2,067	1,662E-05	Bclaf1	-2,013	4,615E-09
Prkar2a	-2,067	3,193E-06	Ube2h	-2,009	3,703E-06
Gab1	-2,066	2,126E-04	Kpna4	-2,005	2,143E-05
Dusp11	-2,064	4,567E-07	Scaper	-2,002	7,338E-03
Zdhhc17	-2,063	1,115E-02	Ppp3ca	-2,001	1,781E-07
Kdm7a	-2,063	3,600E-05	Ap3m1	-2,001	2,260E-03
Atp6v0a1	-2,062	2,951E-04	Ipmk	-2,000	4,052E-02
Zfp664	-2,062	5,443E-03	Tmco1	-2,000	8,968E-05

Table A5. Up-regulated *H. influenzae* genes (316) *in vivo* compared to *in vitro* in RNA-seq analysis.

Locus NTHi375	Locus RdKW20	Gene name	Fold-change	p-value	Functional category
NF38_RS04775	HI0125		30,837	1,738E-141	Transport systems / Uptake/intake systems / Purine nucleobase
NF38_RS01080	HI0773	*atoA*	26,581	2,027E-114	Metabolism / Lipid metabolism
NF38_RS09005	HI0994	*tbp1*	21,057	2,443E-154	Transport systems / Uptake/intake systems / Iron
NF38_RS01075	HI0774	*atoD*	21,050	4,227E-81	Metabolism / Lipid metabolism
NF38_RS09000	HI0995	*tbpB*, *tbp2*	19,844	3,689E-144	Transport systems / Uptake/intake systems / Iron
NF38_RS08370	HI1153	*hpt*	19,803	8,368E-152	Metabolism / Nucleotide metabolism / Purine metabolism
NF38_RS01085	HI0772	*atoE*	17,809	1,881E-94	Metabolism / Lipid metabolism
NF38_RS07020	HI1429	*purM*	16,478	7,259E-139	Metabolism / Nucleotide metabolism / Purine metabolism
NF38_RS07885	HI1615	*purE*	16,468	6,962E-113	Metabolism / Nucleotide metabolism / Purine metabolism
NF38_RS00540	HI0887	*purH*	14,895	5,979E-139	Metabolism / Nucleotide metabolism / Purine metabolism
NF38_RS04985	HI0097	*fbpA*, *hitA*	14,368	7,575E-111	Transport systems / Uptake/intake systems / Iron
NF38_RS07890	HI1616	*purK*	12,804	8,030E-62	Metabolism / Nucleotide metabolism / Purine metabolism
NF38_RS09280			12,377	1,716E-14	Hypothetical Proteins
NF38_RS07015	HI1428	*purN*	10,166	4,740E-100	Metabolism / Nucleotide metabolism / Purine metabolism
NF38_RS00635			8,947	3,603E-58	Hypothetical Proteins
NF38_RS08995			8,707	1,234E-50	Cell wall / OMP
NF38_RS06650	HI1369		8,148	2,914E-31	Cell wall / OMP
NF38_RS00535	HI0888	*purD*	7,813	2,832E-117	Metabolism / Nucleotide metabolism / Purine metabolism
NF38_RS03595	HI0359	*hfeD*	7,439	2,531E-70	Transport systems / Uptake/intake systems / Iron
NF38_RS09150			7,004	1,591E-16	Hypothetical Proteins
NF38_RS04090	HI0262	*hxuC*	6,944	1,645E-103	Transport systems / Uptake/intake systems / Iron
NF38_RS01090	HI0771	*atoB*	6,645	2,488E-101	Metabolism / Lipid metabolism
NF38_RS07330		*ftsK*	6,553	2,020E-05	Cell wall /Cell division
NF38_RS04220	HI0235	*arfA*	6,438	3,378E-10	Transcription and translation machinery / Ribosome related things
NF38_RS09025			6,295	2,524E-02	Hypothetical Proteins
NF38_RS03580	HI0362	*hfeA*	6,163	7,703E-98	Transport systems / Uptake/intake systems / Iron
NF38_RS00040	HI0986	*leuA*	6,078	8,917E-21	Metabolism / Amino acid metabolism / Leucine, isoleucine and valine
NF38_RS09160			6,043	1,921E-07	Hypothetical Proteins
NF38_RS06305			6,033	3,280E-04	Hypothetical Proteins
NF38_RS05100	HI0075	*nrdD*	6,007	3,406E-101	Metabolism / Nucleotide metabolism / Ribonucleoside-triphosphate reductases (ATP-dATP o GTP-dGTP..DNA)
NF38_RS01190	HI0752	*purL*	5,798	1,177E-100	Metabolism / Nucleotide metabolism / Purine metabolism

NF38_RS03295			5,744	4,658E-38	Hypothetical Proteins
NF38_RS08570			5,636	1,377E-06	Metabolism / Other metabolism genes
NF38_RS04085	HI0263	*hxuB*	5,599	2,353E-93	Transport systems / Uptake/intake systems / Iron
NF38_RS00030	HI0988	*leuC*	5,562	4,514E-32	Metabolism / Amino acid metabolism / Leucine, isoleucine and valine
NF38_RS04995	HI0095		5,547	1,450E-31	Nucleic acids processing, restriction and modification
NF38_RS06320			5,538	1,397E-10	Hypothetical Proteins
NF38_RS04480	HI0189	*gdhA*	5,494	1,870E-11	Metabolism / Amino acid metabolism / Glutamine
NF38_RS03590	HI0360	*hfeC*	5,487	1,075E-43	Transport systems / Uptake/intake systems / Iron
NF38_RS03585	HI0361	*hfeB*	5,482	5,529E-94	Transport systems / Uptake/intake systems / Iron
NF38_RS07530	HI1545	*sstT*	5,389	5,227E-35	Transport systems / Uptake/intake systems / Amino acids
NF38_RS01805	HI0663		5,336	3,473E-25	Transport systems / Bidirectional Transport systems or Transporters with unknown function
NF38_RS06990	HI1423		5,317	3,096E-04	Hypothetical Proteins
NF38_RS07640	HI1571		5,290	1,404E-03	Hypothetical Proteins
NF38_RS03170			4,950	5,314E-24	Hypothetical Proteins
NF38_RS03250			4,914	4,250E-22	Hypothetical Proteins
NF38_RS04975	HI0099	*fbpC2*,*hitC*	4,857	7,901E-88	Transport systems / Uptake/intake systems / Iron
NF38_RS00025	HI0989	*leuD*	4,812	1,926E-25	Metabolism / Amino acid metabolism / Leucine, isoleucine and valine
fis	HI0980	*fis*	4,805	3,447E-30	Stress response-nutrient starvation
NF38_RS03240			4,780	9,861E-22	Hypothetical Proteins
NF38_RS03225			4,762	5,487E-33	Hypothetical Proteins
NF38_RS03195			4,637	2,792E-22	Hypothetical Proteins
NF38_RS08245	HI1180	*artP*	4,625	1,256E-09	Transport systems / Uptake/intake systems / Amino acids
NF38_RS03215			4,588	6,183E-20	Hypothetical Proteins
NF38_RS03245	HI1485		4,561	2,146E-22	Transcription and translation machinery / Regulators
NF38_RS03275			4,543	2,478E-29	Hypothetical Proteins
NF38_RS04980	HI0098	*fbpB2*, *hitB*	4,519	3,269E-50	Transport systems / Uptake/intake systems / Iron
NF38_RS03185			4,455	1,150E-21	Hypothetical Proteins
NF38_RS03200			4,452	1,844E-25	Hypothetical Proteins
NF38_RS03175			4,447	1,602E-21	Hypothetical Proteins
NF38_RS06265			4,441	3,348E-04	Nucleic acids processing, restriction and modification
NF38_RS07110	HI1444	*metF*	4,419	1,534E-22	Metabolism / Vitamins biosynthesis
NF38_RS03220		*rdgC*	4,309	5,673E-27	Nucleic acids processing, restriction and modification
NF38_RS03270			4,296	2,165E-14	Hypothetical Proteins
NF38_RS06315			4,264	8,456E-06	Hypothetical Proteins
NF38_RS00035	HI0987	*leuB*	4,264	1,922E-14	Metabolism / Amino acid metabolism / Leucine, isoleucine and valine
NF38_RS09125			4,263	1,825E-17	Hypothetical Proteins
NF38_RS04150	HI0251	*tonB*	4,229	1,467E-26	Transport systems / Uptake/intake systems / Iron

NF38_RS05000	HI0094		4,229	9,214E-29	Cell wall /Cell wall biosynthesis
NF38_RS02595			4,144	7,166E-19	Hypothetical Proteins
NF38_RS00520	HI0890	*coaE*	4,137	1,083E-30	Metabolism / Coenzyme A biosynthesis
NF38_RS00075	HI0979	*dusB*	4,098	1,191E-31	Transcription and translation machinery / tRNA
NF38_RS01800	HI0664		3,980	6,307E-28	Transport systems / Bidirectional Transport systems or Transporters with unknown function
NF38_RS05715	HI1702	*metE*	3,973	5,372E-39	Metabolism / Amino acid metabolism / L-methionine, S-adenosyl -L-methionine
NF38_RS06385			3,921	1,039E-04	Hypothetical Proteins
NF38_RS09210			3,907	4,038E-27	Hypothetical Proteins
NF38_RS06645	HI1368	*pqqL*	3,858	6,386E-10	Protein degradation-stability /Protein degrading machinery
NF38_RS03280			3,853	6,912E-28	Hypothetical Proteins
NF38_RS08905	HI1035	*corA*	3,835	8,074E-25	Transport systems / Uptake/intake systems / Magnesium
NF38_RS03205			3,821	1,329E-20	Nucleic acids processing, restriction and modification
NF38_RS07720	HI1586		3,765	3,003E-29	Transport systems / Bidirectional Transport systems or Transporters with unknown function
NF38_RS03190			3,743	8,459E-23	Hypothetical Proteins
NF38_RS07310			3,719	3,165E-08	Others
NF38_RS09020			3,669	3,414E-13	Hypothetical Proteins
NF38_RS08825	HI1053		3,660	2,577E-18	Metabolism / Other metabolism genes
NF38_RS08590	HI1104		3,633	5,059E-23	Transport systems / Bidirectional Transport systems or Transporters with unknown function
NF38_RS03180			3,629	1,090E-18	Hypothetical Proteins
NF38_RS08275	HI1173	*sprT*	3,617	3,996E-15	Protein degradation-stability /Protein degrading machinery
NF38_RS03230	HI0250	*ssb*	3,596	1,880E-17	Natural competence
NF38_RS06300			3,572	2,358E-02	Hypothetical Proteins
NF38_RS02885	HI0437	*comC*	3,544	5,581E-04	Natural competence
NF38_RS03210			3,542	1,451E-14	Hypothetical Proteins
NF38_RS02890	HI0436	*comD*	3,496	2,078E-07	Natural competence
glyA	HI0889	*glyA*	3,477	1,145E-20	Metabolism / Amino acid metabolism / Glycine
NF38_RS01820	HI0660	*toxT*	3,454	3,126E-08	Natural competence
NF38_RS03300			3,433	5,154E-14	Hypothetical Proteins
NF38_RS06325			3,428	2,259E-05	Hypothetical Proteins
NF38_RS03315			3,348	2,085E-11	Hypothetical Proteins
NF38_RS01615		*tnaA*	3,325	5,114E-13	Metabolism / Amino acid metabolism / Tryptophan
NF38_RS06910			3,253	1,168E-05	Nucleic acids processing, restriction and modification
NF38_RS07430		*uupA*	3,201	6,809E-05	Transport systems / Uptake/intake systems / Other intake systems
NF38_RS04145	HI0252	*exbD*	3,199	3,158E-18	Transport systems / Uptake/intake systems / Iron
NF38_RS08565	HI1112	*xylA*	3,177	9,621E-11	Metabolism / Sugar metabolism / Pentoses metabolism
NF38_RS08095	HI1210	*mdh*	3,174	2,184E-16	Metabolism / Sugar metabolism / Krebs cycle
NF38_RS01890	HI0648	*mdaB*	3,154	2,055E-19	Metabolism / Other metabolism genes

NF38_RS08190		*queC*	3,120	5,060E-17	Metabolism / Nucleotide metabolism / Purine metabolism
NF38_RS01200	HI0750	*dapF*	3,107	2,898E-18	Metabolism / Amino acid metabolism / L-lysine biosynthesis via DAP pathway
NF38_RS03305			3,079	8,804E-10	Hypothetical Proteins
NF38_RS04905	HI0109		3,013	2,870E-02	Cell wall /Cell wall biosynthesis
NF38_RS06855	HI1410		2,969	2,124E-04	Nucleic acids processing, restriction and modification
NF38_RS09155			2,960	3,542E-08	Hypothetical Proteins
NF38_RS03310			2,946	1,876E-11	Nucleic acids processing, restriction and modification
NF38_RS00865	HI0815	*uspA*	2,929	5,350E-06	Stress response-nutrient starvation
NF38_RS00920			2,898	7,080E-09	Transcription and translation machinery / Regulators
NF38_RS07425	HI1300	*uppB*	2,895	4,182E-06	Transport systems / Uptake/intake systems / Other intake systems
NF38_RS07325			2,882	5,075E-05	Metabolism / Other metabolism genes
NF38_RS07635			2,880	8,437E-09	Hypothetical Proteins
NF38_RS04080	HI0264	*hxuA*	2,870	1,791E-23	Transport systems / Uptake/intake systems / Iron
NF38_RS07305	HI1316		2,844	2,663E-06	Hypothetical Proteins
NF38_RS00730			2,837	6,141E-20	Metabolism / Other metabolism genes
NF38_RS02900	HI0434	*comF*	2,772	8,582E-04	Natural competence
NF38_RS03325			2,767	5,894E-09	Nucleic acids processing, restriction and modification
NF38_RS05170	HI0061	*rec2*	2,760	3,425E-02	Natural competence
NF38_RS03260			2,747	3,776E-12	Others
NF38_RS04910			2,742	1,012E-03	Transport systems / Export systems
NF38_RS05005	HI0093	*cdaR*	2,740	9,974E-07	Transcription and translation machinery / Regulators
NF38_RS05605	HI1726	*purC*	2,730	9,446E-20	Metabolism / Nucleotide metabolism / Purine metabolism
NF38_RS00045	HI0985	*dprA*, *smf*	2,729	3,323E-02	Natural competence
NF38_RS02880	HI0438	*comB*	2,728	2,034E-04	Natural competence
NF38_RS01060	HI0777	*rplC*	2,716	4,196E-12	Transcription and translation machinery / Ribosome related things
NF38_RS02715	HI0468	*hisG*	2,708	1,753E-19	Metabolism / Amino acid metabolism / Histidine
NF38_RS06845	HI1407		2,698	2,080E-02	Hypothetical Proteins
NF38_RS01205	HI0749	*lexA*	2,692	1,622E-14	Transcription and translation machinery / Regulators
NF38_RS05310	HI0035		2,672	5,269E-06	Transport systems / Bidirectional Transport systems or Transporters with unknown function
NF38_RS05590	HI1729	*pxpA*	2,672	3,608E-12	Metabolism / Amino acid metabolism / Glutamate
NF38_RS00630	HI0862		2,667	1,366E-17	Transport systems / Uptake/intake systems / Queuosine (Q) precursors
moaA	HI1676	*moaA*	2,664	3,950E-15	Metabolism / Molybdopterin biosynthesis
NF38_RS01405	HI0612	*fucU*	2,663	1,658E-09	Metabolism / Sugar metabolism / Hexoses metabolism
NF38_RS01415	HI0610	*fucP*	2,647	5,708E-17	Metabolism / Sugar metabolism / Hexoses metabolism
NF38_RS05595	HI1728		2,644	1,518E-10	Transport systems / Bidirectional Transport systems or Transporters with unknown function
NF38_RS03265			2,644	1,495E-12	Hypothetical Proteins

NF38_RS01395	HI0614	*fucI*	2,625	4,167E-07	Metabolism / Sugar metabolism / Hexoses metabolism
NF38_RS01050	HI0779	*rplW*	2,614	1,986E-16	Transcription and translation machinery / Ribosome related things
NF38_RS04915			2,610	6,992E-03	Transport systems / Export systems
NF38_RS03320			2,609	1,092E-06	Nucleic acids processing, restriction and modification
NF38_RS01680	HI0692	*gpt2*	2,584	3,303E-03	Metabolism / Nucleotide metabolism / Purine metabolism
NF38_RS05585	HI1730	*pxpC*	2,580	3,326E-10	Metabolism / Amino acid metabolism / Glutamate
NF38_RS02895	HI0435	*comE*	2,560	7,202E-04	Natural competence
NF38_RS02600			2,557	8,679E-13	Hypothetical Proteins
NF38_RS01055	HI0778	*rplD*	2,548	2,097E-14	Transcription and translation machinery / Ribosome related things
NF38_RS05675			2,546	3,135E-05	Metabolism / Other metabolism genes
NF38_RS07710	HI1584	*ilvH*	2,523	2,442E-06	Metabolism / Amino acid metabolism / Leucine, isoleucine and valine
NF38_RS00655	HI0858		2,522	1,754E-03	Metabolism / Other metabolism genes
NF38_RS05690	HI1707	*qseC*	2,509	5,607E-11	Transcription and translation machinery / Regulators
NF38_RS08195	HI1190	*queD*	2,505	4,292E-10	Metabolism / Nucleotide metabolism / Purine metabolism
NF38_RS01035	HI0782	*rplV*	2,496	1,661E-13	Transcription and translation machinery / Ribosome related things
NF38_RS03290	HI1476		2,492	7,623E-12	Transcription and translation machinery / Regulators
NF38_RS06970			2,489	3,681E-10	Hypothetical Proteins
NF38_RS08110	HI1207	*purF*	2,487	1,275E-18	Metabolism / Nucleotide metabolism / Purine metabolism
NF38_RS06440	HI1284	*infB*	2,478	8,625E-14	Transcription and translation machinery / Trna
NF38_RS06880	HI1415		2,477	9,541E-05	Metabolism / Other metabolism genes
NF38_RS01410	HI0611	*fucA*	2,477	3,968E-10	Metabolism / Sugar metabolism / Hexoses metabolism
NF38_RS06340			2,476	1,044E-08	Hypothetical Proteins
oppB	HI1123	*oppB*	2,475	6,619E-09	Transport systems / Uptake/intake systems / Oligopeptides
NF38_RS02710	HI0469	*hisD*	2,474	1,707E-16	Metabolism / Amino acid metabolism / Histidine
NF38_RS02065			2,470	2,354E-08	Hypothetical Proteins
NF38_RS06345			2,463	4,044E-03	Hypothetical Proteins
NF38_RS01030	HI0783	*rpsC*	2,453	4,127E-10	Transcription and translation machinery / Ribosome related things
NF38_RS09065			2,438	9,845E-07	Hypothetical Proteins
NF38_RS01045	HI0780	*rplB*	2,433	1,603E-09	Transcription and translation machinery / Ribosome related things
NF38_RS08200	HI1189	*queE*	2,421	5,777E-09	Metabolism / Nucleotide metabolism / Purine metabolism
NF38_RS08505	HI1124	*oppA*	2,416	2,956E-13	Transport systems / Uptake/intake systems / Oligopeptides
NF38_RS05580	HI1731	*pxpB*	2,415	1,896E-13	Metabolism / Amino acid metabolism / Glutamate
oppD	HI1121	*oppD*	2,412	4,186E-10	Transport systems / Uptake/intake systems / Oligopeptides
NF38_RS01125	HI0764	*ribB*	2,412	3,335E-11	Metabolism / Vitamins biosynthesis

NF38_RS00325	HI0928	*katA*, *hktE*	2,411	1,297E-10	Stress response-nutrient starvation
NF38_RS03100	HI0390	*rnd*	2,409	1,760E-18	Nucleic acids processing, restriction and modification
NF38_RS08515	HI1122	*oppC*	2,390	1,047E-10	Transport systems / Uptake/intake systems / Oligopeptides
NF38_RS06150	HI1250		2,385	2,095E-07	Stress response-nutrient starvation
NF38_RS00515	HI0891	*yacG*	2,381	5,106E-10	Nucleic acids processing, restriction and modification
NF38_RS01430	HI0609	*folD*	2,361	2,699E-11	Metabolism / Vitamins biosynthesis
NF38_RS02705	HI0470	*hisC*	2,325	7,320E-13	Metabolism / Amino acid metabolism / Histidine
NF38_RS05870	HI1674	*moaD*	2,323	8,555E-04	Metabolism / Molybdopterin biosynthesis
NF38_RS07715	HI1585	*ilvI*	2,308	1,403E-04	Metabolism / Amino acid metabolism / Leucine, isoleucine and valine
NF38_RS01825	HI0659	*toxA*	2,262	4,278E-03	Natural competence
NF38_RS07215	HI1334	*rlmE*	2,254	3,089E-03	Transcription and translation machinery / Ribosome related things
NF38_RS01400	HI0613	*fucK*	2,252	5,841E-04	Metabolism / Sugar metabolism / Hexoses metabolism
NF38_RS08525	HI1120	*oppF*	2,244	5,533E-10	Transport systems / Uptake/intake systems / Oligopeptides
NF38_RS01900	HI0646	*asd*	2,241	4,466E-12	Metabolism / Amino acid metabolism / Threonine
NF38_RS02750	HI0462	*lon*	2,233	7,885E-11	Protein degradation-stability /Protein degrading machinery
NF38_RS07690	HI1579	*pcp*	2,232	1,372E-09	Cell wall / OMP
NF38_RS06155	HI1251		2,232	4,196E-08	Stress response-nutrient starvation
NF38_RS01815	HI0661	*hgpB*	2,230	3,918E-07	Transport systems / Uptake/intake systems, .Iron
NF38_RS00585	HI0878		2,224	7,223E-06	Transport systems / Bidirectional Transport systems or Transporters with unknown function
NF38_RS06260			2,222	6,145E-03	Hypothetical Proteins
NF38_RS08115	HI1206	*cvpA*	2,214	1,224E-11	Stress response-nutrient starvation
NF38_RS03420			2,211	1,674E-06	Transcription and translation machinery / Regulators
NF38_RS05865	HI1675	*moaC*	2,208	9,661E-09	Metabolism / Molybdopterin biosynthesis
NF38_RS04140	HI0253	*exbB*	2,192	1,189E-05	Transport systems / Uptake/intake systems / Iron
NF38_RS01020	HI0785	*rpmC*	2,192	5,652E-10	Transcription and translation machinery / Ribosome related things
NF38_RS02510	HI0511	*tehA*	2,184	4,651E-10	Transport systems / Export systems
NF38_RS01065	HI0776	*rpsJ*	2,166	7,264E-10	Transcription and translation machinery / Ribosome related things
NF38_RS03875	HI0299	*ppdD*, *pilA*	2,163	4,090E-05	Natural competence
NF38_RS03950	HI0286	*alaA*	2,160	3,214E-09	Metabolism / Amino acid metabolism / Alanine
NF38_RS06595	HI1358	*glgX*	2,154	3,490E-06	Metabolism / Sugar metabolism / Hexoses metabolism
moaE	HI1673	*moaE*	2,145	1,702E-07	Metabolism / Molybdopterin biosynthesis
NF38_RS02170	HI0581	*rpsL*	2,144	1,564E-03	Transcription and translation machinery / Ribosome related things
NF38_RS05165	HI0062	*dksA*	2,138	6,703E-05	Transcription and translation machinery / Transcription factors
NF38_RS09255			2,135	9,931E-05	Hypothetical Proteins
NF38_RS02700	HI0471	*hisB*	2,120	1,049E-10	Metabolism / Amino acid metabolism / Histidine

NF38_RS02135			2,120	2,982E-08	Transport systems / Uptake/intake systems / Iron
NF38_RS06335			2,119	5,246E-05	Hypothetical Proteins
NF38_RS01025	HI0784	*rplP*	2,116	3,393E-04	Transcription and translation machinery / Ribosome related things
NF38_RS06835	HI1401	*pyrD*	2,115	1,954E-07	Metabolism / Nucleotide metabolism / Pyrimidine metabolism
NF38_RS05600	HI1727	*argG*	2,107	2,632E-04	Metabolism / Amino acid metabolism / Arginine
NF38_RS08280	HI1172	*metK*	2,103	7,190E-07	Metabolism / Amino acid metabolism / L-methionine, S-adenosyl -L-methionine
NF38_RS01895	HI0647		2,100	2,320E-10	Others
NF38_RS03255			2,099	8,077E-08	Hypothetical Proteins
modB	HI1692	*modB*	2,096	8,510E-07	Transport systems / Uptake/intake systems / Molybdenum
NF38_RS07895	HI1617	*aspC*	2,093	6,570E-05	Metabolism / Amino acid metabolism / Aspartate
NF38_RS04180	HI0244	*tgt*	2,092	1,881E-10	Transcription and translation machinery / tRNA
NF38_RS02175	HI0580	*rpsG*	2,086	8,730E-06	Transcription and translation machinery / Ribosome related things
NF38_RS05035	HI0087	*thrC*	2,081	9,215E-10	Metabolism / Amino acid metabolism / Threonine
nusA	HI1283	*nusA*	2,071	4,132E-10	Transcription and translation machinery / Transcription factors
NF38_RS05030	HI0088	*thrB*	2,070	3,477E-09	Metabolism / Amino acid metabolism / Threonine
NF38_RS06830	HI1400	*trpH*	2,070	1,117E-06	Nucleic acids processing, restriction and modification
NF38_RS08305	HI1167	*serC*	2,070	3,922E-07	Metabolism / Amino acid metabolism / Serine
NF38_RS02990	HI0414		2,064	1,443E-02	Cell wall / OMP
NF38_RS00765	HI0835	*frdA*	2,055	5,712E-05	Metabolism / Sugar metabolism / Krebs cycle
NF38_RS05930	HI1660	*nrdB*	2,052	4,984E-08	Metabolism / Nucleotide metabolism / Ribonucleoside-triphosphate reductases (ATP-dATP o GTP-dGTP..DNA)
NF38_RS01245	HI0738	*ilvD*, *thd1*	2,045	4,268E-09	Metabolism / Amino acid metabolism / Leucine, isoleucine and valine
NF38_RS07335			2,032	5,891E-07	Hypothetical Proteins
NF38_RS05125	HI0070	*recN*	2,016	7,702E-07	Nucleic acids processing, restriction and modification
NF38_RS05205	HI0054	*uxuR*	2,015	2,771E-06	Transcription and translation machinery / Regulators
NF38_RS03895	HI0295	*rho*	2,011	2,006E-08	Transcription and translation machinery / Transcription factors
NF38_RS05215	HI0052		2,006	4,429E-02	Transport systems / Bidirectional Transport systems or Transporters with unknown function
NF38_RS08165	HI1196	*sucC*	2,002	6,373E-05	Metabolism / Sugar metabolism / Krebs cycle
NF38_RS07535	HI1546	*impA*	1,993	1,407E-03	Stress response-nutrient starvation
NF38_RS02250	HI0566	*rpe*	1,978	1,620E-05	Metabolism / Sugar metabolism / Pentoses metabolism
NF38_RS08175	HI1194	*gcvA*	1,976	1,536E-06	Transcription and translation machinery / Regulators
NF38_RS03930	HI0290		1,968	9,790E-08	Transport systems / Export systems
NF38_RS03975	HI0281		1,967	3,861E-03	Transport systems / Bidirectional Transport systems or Transporters with unknown function
NF38_RS02445	HI0526		1,966	1,662E-08	Nucleic acids processing, restriction and modification
NF38_RS08900	HI1036		1,957	5,183E-05	Hypothetical Proteins
NF38_RS03330			1,943	1,487E-03	Nucleic acids processing, restriction and modification

NF38_RS04825	HI0119	*znuA*	1,942	7,212E-08	Transport systems / Uptake/intake systems / Zinc
NF38_RS06605	HI1360	*glgA*	1,940	2,255E-04	Metabolism / Sugar metabolism / Hexoses metabolism
NF38_RS04655		*dcuB*	1,939	1,456E-02	Transport systems / Uptake/intake systems / Other intake systems
NF38_RS05685	HI1708	*qseB*	1,931	2,809E-04	Transcription and translation machinery / Regulators
NF38_RS08000	HI1636	*ppc*	1,927	3,002E-02	Metabolism / Sugar metabolism / Krebs cycle
NF38_RS06420			1,926	1,147E-02	Hypothetical Proteins
NF38_RS00885	HI0811	*argH*	1,920	8,336E-05	Metabolism / Amino acid metabolism / Arginine
NF38_RS01040	HI0781	*rpsS*	1,917	6,374E-08	Transcription and translation machinery / Ribosome related things
NF38_RS03165	HI1424		1,909	7,835E-06	Nucleic acids processing, restriction and modification
NF38_RS02450	HI0525	*pgk*	1,907	3,717E-07	Metabolism / Sugar metabolism / Hexoses metabolism
NF38_RS08170	HI1195	*rlmM*	1,904	6,373E-03	Transcription and translation machinery / Ribosome related things
obgE	HI0877	*obg*	1,898	3,106E-07	Stress response-nutrient starvation
NF38_RS01015	HI0786	*rpsQ*	1,896	1,868E-02	Transcription and translation machinery / Ribosome related things
NF38_RS08160	HI1197	*sucD*	1,885	7,567E-07	Metabolism / Sugar metabolism / Krebs cycle
NF38_RS07045	HI1434	*ybaK*	1,881	1,027E-03	Transcription and translation machinery / tRNA
NF38_RS05935	HI1659	*nrdA*	1,873	8,149E-06	Metabolism / Nucleotide metabolism / Ribonucleoside-triphosphate reductases (ATP-dATP o GTP-dGTP..DNA)
NF38_RS08495			1,871	1,190E-05	Stress response-nutrient starvation
NF38_RS07160	HI1455	*msrAB*	1,866	8,649E-06	Stress response-nutrient starvation
NF38_RS00925	HI0803	*rplQ*	1,864	2,433E-03	Transcription and translation machinery / Ribosome related things
NF38_RS04885	HI0113	*tdhA*	1,862	8,946E-08	Transport systems / Uptake/intake systems / Iron
NF38_RS00580	HI0879	*rpmA*	1,861	2,295E-03	Transcription and translation machinery / Ribosome related things
NF38_RS06600	HI1359	*glgC*	1,855	4,262E-03	Metabolism / Sugar metabolism / Hexoses metabolism
NF38_RS01985			1,853	4,291E-02	Hypothetical Proteins
NF38_RS02620	HI0487		1,848	7,689E-03	Transcription and translation machinery / Regulators
NF38_RS03415			1,843	6,485E-03	Metabolism / Other metabolism genes
NF38_RS01975	HI0634	*dusA*	1,832	5,236E-03	Transcription and translation machinery / tRNA
NF38_RS03120	HI0387	*dinG*	1,825	5,668E-06	Nucleic acids processing, restriction and modification
NF38_RS01435	HI0608		1,821	1,816E-03	Transport systems / Bidirectional Transport systems or Transporters with unknown function
NF38_RS00640	HI0861	*rnr, vacB*	1,809	5,198E-07	Nucleic acids processing, restriction and modification
NF38_RS07010	HI1427		1,800	7,948E-06	Transport systems / Bidirectional Transport systems or Transporters with unknown function
NF38_RS00135	HI0965	*rpsT*	1,797	4,066E-03	Transcription and translation machinery / Ribosome related things
NF38_RS06200	HI1263	*metXA, metX*	1,795	1,488E-03	Metabolism / Amino acid metabolism / L-methionine, S-adenosyl -L-methionine
NF38_RS01310	HI0726	*narP*	1,795	1,653E-03	Transcription and translation machinery / Regulators
NF38_RS06430	HI1282	*rimP*	1,794	1,962E-03	Transcription and translation machinery / Ribosome related things

NF38_RS04285	HI0221	*guaB*	1,776	1,991E-06	Metabolism / Nucleotide metabolism / Purine metabolism
NF38_RS00880	HI0812	*galU*	1,766	1,050E-04	Metabolism / Sugar metabolism / Hexoses metabolism
NF38_RS01570	HI0712		1,761	1,192E-05	Transport systems / Uptake/intake systems / Iron
NF38_RS09050			1,755	1,797E-02	Hypothetical Proteins
NF38_RS00930	HI0802	*rpoA*	1,754	4,853E-03	Transcription and translation machinery / RNA polimerase
NF38_RS07225	HI1331	*greA*	1,744	4,872E-04	Transcription and translation machinery / Transcription factors
NF38_RS02500	HI0515	*rpoB*	1,737	1,299E-04	Transcription and translation machinery / NA polimerase
NF38_RS02740	HI0464	*rpiA*	1,727	1,345E-03	Metabolism / Sugar metabolism / Pentoses metabolism
NF38_RS03530	HI0372	*fdx*	1,726	1,149E-03	Metabolism / Other metabolism genes
NF38_RS07340		*cobB*	1,718	1,863E-02	Others
NF38_RS03115	HI0388	*tsaB*	1,708	1,804E-04	Transcription and translation machinery / tRNA
NF38_RS05840		*hmw1A*	1,707	1,336E-04	Cell wall / OMP
NF38_RS05265	HI0044		1,704	1,958E-02	Others
NF38_RS02785		*yapH*	1,696	4,635E-03	Cell wall / OMP
NF38_RS02455	HI0524	*fba*	1,694	1,603E-04	Metabolism / Sugar metabolism / Hexoses metabolism
NF38_RS00235	HI0946	*mutM*	1,688	1,363E-03	Nucleic acids processing, restriction and modification
NF38_RS07870	HI1614	*pepN*	1,683	2,791E-04	Stress response-nutrient starvation
NF38_RS05025	HI0089	*thrA*	1,680	1,464E-04	Metabolism / Amino acid metabolism / Threonine
NF38_RS01250	HI0738	*ilvD*	1,669	3,600E-04	Metabolism / Amino acid metabolism / Leucine, isoleucine and valine
NF38_RS01105	HI0768	*ftsY*	1,667	3,092E-04	Others
ssrS			1,666	2,828E-02	Others
NF38_RS07090	HI1440	*sspB*	1,663	5,894E-04	Protein degradation-stability /Protein degrading machinery
NF38_RS06610	HI1361	*glgP*	1,663	1,010E-02	Metabolism / Sugar metabolism / Hexoses metabolism
NF38_RS02505	HI0514	*rpoC*	1,655	3,604E-03	Transcription and translation machinery / RNA polimerase
NF38_RS07760	HI1597	*radA*	1,649	2,229E-02	Nucleic acids processing, restriction and modification
NF38_RS06785	HI1391	*valS*	1,648	8,460E-04	Transcription and translation machinery / tRNA
NF38_RS05090	HI0078	*cysS*	1,646	4,480E-04	Transcription and translation machinery / tRNA
NF38_RS04185	HI0243		1,615	3,997E-03	Hypothetical Proteins
NF38_RS02685	HI0474	*hisF*	1,612	4,477E-03	Metabolism / Amino acid metabolism / Histidine
NF38_RS03755	HI0325		1,606	5,022E-03	Transport systems / Bidirectional Transport systems or Transporters with unknown function
NF38_RS07775			1,593	9,507E-03	Cell wall / OMP
NF38_RS01955	HI0639	*purB*	1,566	9,444E-04	Metabolism / Nucleotide metabolism / Purine metabolism
NF38_RS07165			1,559	9,551E-03	Transport systems / Bidirectional Transport systems or Transporters with unknown function
NF38_RS04635	HI0157	*fabH*	1,558	4,055E-02	Metabolism / Lipid metabolism
NF38_RS03075	HI0396	*ycfD*	1,554	5,524E-03	Transcription and translation machinery / Ribosome related things

NF38_RS04750	HI0136	*der*, *engA*	1,554	3,608E-03	Transcription and translation machinery / Ribosome related things
nusG	HI0717	*nusG*	1,540	7,825E-03	Transcription and translation machinery / Transcription factors

Table A6. Up-regulated genes (280) *in vitro* compared to *in vivo* in RNA-seq analysis.

Locus NTHi375	Locus RdKW20	Gene name	Fold-change	p-value	Functional category
NF38_RS03910	HI0292	*merP_1*	-186,088	7,148E-08	Protein degradation / stability / Chaperone
NF38_RS00680	HI0853	*hbpA*	-9,311	1,632E-33	Transport systems / Uptake/intake systems / Iron
NF38_RS03935	HI0289	*sdaC*	-8,147	1,537E-27	Transport systems / Uptake/intake systems / Amino acids
NF38_RS08710	HI1080	*fliY*	-7,683	0,000E+00	Transport systems / Uptake/intake systems / Amino acids
NF38_RS00750	HI0838	*bamE*, *smpA*	-6,000	2,173E-24	Cell wall / OMP
NF38_RS08715	HI1079		-5,699	1,848E-35	Transport systems / Uptake/intake systems / Amino acids
NF38_RS08935	HI1020	*thiP*	-5,260	3,484E-32	Transport systems / Uptake/intake systems / Vitamins
NF38_RS08365	HI1154		-5,158	1,143E-78	Transport systems / Uptake/intake systems / Amino acids
NF38_RS04170	HI0246		-4,883	0	Hypothetical proteins
NF38_RS08720	HI1078		-4,736	6,394E-36	Transport systems / Uptake/intake systems, / Amino acids
NF38_RS03940	HI0288	*sdaA*	-4,704	4,864E-17	Metabolism / Amino acid metabolism / Serine
NF38_RS02325	HI0550	*lex1*, *lic2*	-4,426	2,820E-13	Cell wall / LOS biosynthesis-modification-decoration
NF38_RS08940	HI1019	*thiB*	-4,228	2,473E-19	Transport systems / Uptake/intake systems / Vitamins
NF38_RS03015	HI0409	*mepM*	-4,170	3,460E-21	Cell wall / Cell wall biosynthesis
NF38_RS00755	HI0837	*cpxR*	-3,890	9,410E-17	Transcription and translation machinery / Regulators
NF38_RS02770	HI0458	*surA*	-3,890	7,247E-10	Protein degradation / stability / Chaperone
NF38_RS06740	HI1384	*ftnA*	-3,813	9,161E-12	Transport systems / Uptake/intake systems / Iron
NF38_RS07820	HI1604	*pitA*	-3,791	9,303E-22	Transport systems / Uptake/intake systems / Phosphate (Pi)
NF38_RS07825	HI1605		-3,788	3,216E-14	Hypothetical proteins
NF38_RS06180	HI1259	*htoA*	-3,754	0	Metabolism / Other metabolism genes
NF38_RS06750	HI1386		-3,562	3,811E-12	Cell wall / LOS biosynthesis-modification-decoration
NF38_RS00720	HI0845	*yihD*	-3,537	0	Hypothetical proteins
NF38_RS07815	HI1603		-3,522	1,266E-16	Hypothetical proteins
NF38_RS06745	HI1385	*ftnB*	-3,496	5,414E-11	Transport systems / Uptake/intake systems / Iron
NF38_RS08930	HI1021	*thiQ*	-3,494	2,032E-20	Transport systems / Uptake/intake systems / Vitamins
NF38_RS09070			-3,386	1,133E-16	Hypothetical proteins
NF38_RS04175	HI0245	*queA*	-3,354	0	Metabolism / Nucleotide metabolism / Purine metabolism
NF38_RS02030	HI0628	*rpoE*	-3,296	0	Stress response-nutrient starvation
NF38_RS07835	HI1607	*lolB*	-3,280	1,041E-24	Cell wal / OMP
NF38_RS00745	HI0839	*ndpA*	-3,272	3,825E-11	Stress response-nutrient starvation
NF38_RS07830	HI1606	*cca*	-3,228	3,065E-13	Transcription and translation machinery / tRNA

NF38_RS06695	HI1375		-3,164	8,907E-09	Hypothetical proteins
NF38_RS05480	HI0002		-3,125	2,058E-06	Metabolism / Lipid metabolism
NF38_RS03395			-3,079	1,511E-15	Hypothetical proteins
NF38_RS06125	HI1246		-3,072	5,744E-11	Others
NF38_RS00435	HI0908		-3,035	9,760E-14	Hypothetical proteins
NF38_RS05460			-2,962	1,241E-14	Transport systems / Bidirectional transport systems or transporters with unknown function
NF38_RS02020	HI0630	*rseB*	-2,951	0	Others
NF38_RS00740	HI0840	*yejL*	-2,910	2,200E-03	Transport systems / Uptake/intake systems / Other intake systems
NF38_RS05785	HI1688	*rnfE*	-2,904	1,451E-16	Metabolism / Other metabolism genes
NF38_RS00395	HI0916	*omp26*, *omp2*	-2,887	0	Cell wall / OMP
NF38_RS00715	HI0846	*dsbA*	-2,777	0	Stress response-nutrient starvation
lpxD	HI0915	*lpxD*	-2,768	0	Cell wall / LOS biosynthesis-modification-decoration
NF38_RS05795	HI1686	*rnfD*	-2,724	1,947E-22	Metabolism / Other metabolism genes
NF38_RS04395	HI0206	*nadN*	-2,712	2,455E-12	Metabolism / Nucleotide metabolism / Purine metabolism
NF38_RS03400			-2,711	4,311E-08	Hypothetical proteins
NF38_RS02125	HI0595	*arcC*	-2,709	8,941E-03	Metabolism / Other metabolism genes
NF38_RS03455			-2,697	5,181E-08	Hypothetical proteins
NF38_RS02200	HI0576	*tusD*	-2,679	6,171E-14	Metabolism / Other metabolism genes
NF38_RS04505	HI0185	*frmA*	-2,669	1,263E-12	Metabolism / Other metabolism genes
NF38_RS07840	HI1608	*ispE*	-2,603	1,528E-09	Metabolism / Isopentenyl diphosphate biosynthesis
NF38_RS02205	HI0575	*yheO*	-2,589	5,438E-18	Transcription and translation machinery / Regulators
NF38_RS03725	HI0331	*oapB*	-2,574	2,148E-15	Cell wall / OMP
NF38_RS03465			-2,570	8,668E-06	Hypothetical proteins
NF38_RS06700	HI1376		-2,567	1,696E-12	Transport systems / Bidirectional transport systems or transporters with unknown function
NF38_RS03620	HI0352	*lic3*	-2,565	7,025E-09	Cell wall / LOS biosynthesis-modification-decoration
NF38_RS05570	HI1734	*fabI*	-2,531	3,335E-12	Metabolism / Lipid metabolism
NF38_RS02025	HI0629	*rseA*	-2,530	00	Others
NF38_RS06060	HI1232	*aceF*	-2,511	0	Metabolism / Sugar metabolism / Hexoses metabolism
NF38_RS02560	HI0501	*rbsD*	-2,508	8,552E-04	Metabolism / Sugar metabolism / Pentoses metabolism
NF38_RS03460			-2,496	1,415E-05	Cell wall / Cell wall biosynthesis
NF38_RS03980	HI0280	*udp*	-2,492	1,814E-11	Metabolism / Nucleotide metabolism / Pyrimidine metabolism
NF38_RS08015	HI1639	*sapB*	-2,490	1,814E-14	Transport systems / Uptake/intake systems / Iron
NF38_RS00735	HI0841	*yejM*	-2,484	7,772E-16	Metabolism / Lipid metabolism
NF38_RS05790	HI1687	*rnfG*	-2,480	4,514E-14	Metabolism / Other metabolism genes
NF38_RS01785	HI0669	*mioC*	-2,472	1,546E-06	Metabolism / Vitamins biosynthesis
NF38_RS05455		*fdnG*	-2,472	1,837E-09	Metabolism / Sugar metabolism / Fermentative reactions
NF38_RS02210	HI0574	*fkbY*	-2,469	7,497E-06	Metabolism / Protein (lipoproteins) metabolism
metQ	HI0620	*metQ*	-2,468	0	Transport systems / Uptake/intake systems / Amino acids
NF38_RS07260	HI1325	*fabA*	-2,463	3,554E-04	Metabolism / Lipid metabolism

NF38_RS07315			-2,450	1,042E-08	Hypothetical proteins
NF38_RS04510	HI0184		-2,449	8,608E-11	Metabolism / Other metabolism genes
NF38_RS03540	HI0370	*yfgM*	-2,423	5,230E-09	Stress response-nutrient starvation
NF38_RS03450			-2,420	4,988E-05	Transcription and translation machinery / Regulators
NF38_RS04760	HI0134		-2,409	1,590E-12	Hypothetical proteins
NF38_RS08025	HI1641	*sapD*	-2,396	1,023E-15	Transport systems / Uptake/intake systems / Iron
NF38_RS03390			-2,390	8,500E-05	Hypothetical proteins
NF38_RS03385			-2,379	2,069E-03	Hypothetical proteins
NF38_RS06525	HI1344	*potD-B*, *potD*	-2,367	4,889E-05	Transport systems / Uptake/intake systems / Polyamines
NF38_RS06055	HI1231	*lpdA*	-2,366	2,865E-12	Metabolism / Other metabolism genes
NF38_RS01865	HI0652	*waaA, kdtA*	-2,354	5,300E-13	Cell wall / LOS biosynthesis-modification-decoration
NF38_RS08925	HI1022	*bioB*	-2,342	4,294E-14	Metabolism / Vitamins biosynthesis
NF38_RS04770	HI0132	*udk*	-2,333	2,979E-10	Metabolism / Nucleotide metabolism / Pyrimidine metabolism
NF38_RS03405			-2,325	1,475E-04	Hypothetical proteins
NF38_RS08020	HI1640	*sapC*	-2,300	4,951E-11	Transport systems / Uptake/intake systems / Iron
NF38_RS03720	HI0332	*recO*	-2,289	2,139E-09	Nucleic acids processing, restriction and modification
NF38_RS01870	HI0651	*coaD*	-2,282	1,272E-13	Metabolism / Coenzyme A biosynthesis
NF38_RS01235	HI0740	*pgmB*	-2,273	4,316E-08	Metabolism / Other metabolism genes
NF38_RS08295	HI1168		-2,272	6,439E-10	Hypothetical proteins
NF38_RS04050			-2,267	4,553E-03	Hypothetical proteins
NF38_RS08130	HI1203	*pta*	-2,265	4,911E-12	Metabolism / Sugar metabolism / Fermentative reactions
NF38_RS04055	HI0269	*rpoH*	-2,255	3,302E-06	Stress response-nutrient starvation
NF38_RS07675	HI1576	*pgi*	-2,250	1,249E-10	Metabolism / Sugar metabolism / Hexoses metabolism
NF38_RS03605	HI0357		-2,247	1,279E-03	Metabolism / Vitamins biosynthesis
NF38_RS08290	HI1169	*pabB*	-2,239	2,791E-08	Metabolism / Other metabolism genes
NF38_RS00665	HI0856	*polA*	-2,233	1,637E-10	Nucleic acids processing, restriction and modification
NF38_RS03700	HI0336	*mog*	-2,222	7,715E-12	Metabolism / Molybdopterin biosynthesis
NF38_RS03715	HI0333	*rlmD*	-2,214	6,118E-13	Transcription and translation machinery / Ribosome related things
NF38_RS04400	HI0205		-2,206	1,661E-05	Hypothetical proteins
NF38_RS03435			-2,193	3,688E-05	Hypothetical proteins
NF38_RS05915	HI1663	*gloC*	-2,186	7,387E-11	Metabolism / Other metabolism genes
NF38_RS05450	HI0007	*fdxH*	-2,179	9,836E-06	Metabolism / Sugar metabolism / Fermentative reactions
NF38_RS01880	HI0649	*rep*	-2,168	4,551E-12	Nucleic acids processing, restriction and modification
NF38_RS04545	HI0177	*bamD*	-2,152	2,236E-07	Cell wall / OMP
NF38_RS03480			-2,152	8,702E-07	Hypothetical proteins
NF38_RS05190	HI0057	*uvrC*	-2,148	4,895E-12	Nucleic acids processing, restriction and modification
NF38_RS03380			-2,140	1,279E-04	Hypothetical proteins
NF38_RS03445		*anT_1*	-2,135	4,504E-04	Transcription and translation machinery / Regulators
NF38_RS02755	HI0461	*ybjX*	-2,117	1,409E-10	Stress response-nutrient starvation

NF38_RS03850	HI0304	*yqgE*	-2,109	3,814E-09	Stress response-nutrient starvation
NF38_RS07080	HI1438	*ispA*	-2,099	6,094E-10	Metabolism / Isopentenyl diphosphate biosynthesi
NF38_RS05950	HI1656	*yraN*	-2,091	1,585E-03	Nucleic acids processing, restriction and modification
NF38_RS01585			-2,080	6,259E-10	Hypothetical proteins
NF38_RS03470			-2,059	2,287E-03	Hypothetical proteins
NF38_RS00615			-2,056	1,124E-06	Hypothetical proteins
NF38_RS06705	HI1377	*sbcB*	-2,051	5,972E-10	Nucleic acids processing, restriction and modification
NF38_RS06065	HI1233	*aceE*	-2,046	3,773E-10	Metabolism / Sugar metabolism / Hexoses metabolism
NF38_RS03485			-2,037	1,706E-04	Hypothetical proteins
NF38_RS00500	HI0894		-2,031	2,299E-09	Transport systems / Export systems
NF38_RS05740	HI1697	*lsgD*	-2,015	3,129E-06	Cell wall / LOS biosynthesis-modification-decoration
NF38_RS08445	HI1138	*murG*	-2,007	2,060E-09	Cell wall / Cell wall biosynthesis
NF38_RS03375		*ClpP*	-2,007	1,382E-02	Protein degradation / stability / Protein degrading machinery
NF38_RS05800	HI1685	*rnfC*	-2,006	2,619E-07	Metabolism / Other metabolism genes
NF38_RS05020	HI0090		-2,006	3,682E-09	Others
NF38_RS06190	HI1261	*folC*	-1,998	1,336E-05	Metabolism / Vitamins biosynthesis
NF38_RS06735	HI1383	*pstS*	-1,998	9,399E-07	Transport systems / Uptake/intake systems / Phosphate (Pi)
NF38_RS07135	HI1449	*moeB*	-1,992	9,604E-06	Metabolism / Molybdopterin biosynthesis
NF38_RS07605	HI1560		-1,988	2,949E-04	Hypothetical proteins
NF38_RS00800	HI0828	*yciI*	-1,988	6,937E-09	Cell wall / Cell division
NF38_RS05575	HI1733	*rnb*	-1,982	3,056E-05	Nucleic acids processing, restriction and modification
NF38_RS01590	HI0709	*selB*	-1,981	4,006E-08	Transcription and translation machinery / tRNA
NF38_RS02920	HI0430	*hup*	-1,979	4,866E-04	Stress response-nutrient starvation
NF38_RS08010	HI1638	*sapA*	-1,977	5,493E-09	Transport systems / Uptake/intake systems / Iron
NF38_RS00445	HI0906	*tadA*	-1,975	9,258E-08	Transcription and translation machinery / tRNA
NF38_RS00450	HI0905	*thyA*	-1,973	2,444E-08	Metabolism / Nucleotide metabolism / Pyrimidine metabolism
NF38_RS06815		*rfaI_2*	-1,972	4,285E-07	Cell wall / LOS biosynthesis-modification-decoration
NF38_RS05135	HI0068	*miaA*	-1,972	2,109E-08	Transcription and translation machinery / tRNA
NF38_RS00495	HI0895		-1,970	3,006E-09	Transport systems / Export systems
NF38_RS05650	HI1715	*orn*	-1,969	2,635E-05	Nucleic acids processing, restriction and modification
NF38_RS05945	HI1657		-1,966	4,971E-07	Cell wall / LOS biosynthesis-modification-decoration
NF38_RS06490	HI1293		-1,962	3,829E-03	Stress response-nutrient starvation
NF38_RS07120	HI1446		-1,958	2,423E-04	Hypothetical proteins
NF38_RS02470	HI0521	*yjjI*	-1,952	5,639E-04	Metabolism / Other metabolism genes
NF38_RS00675	HI0854	*hugZ*	-1,938	8,592E-05	Metabolism / Other metabolism genes
NF38_RS01360		*metI*	-1,936	1,616E-05	Transport systems / Uptake/intake systems / Amino acids
NF38_RS08125	HI1204	*ackA*	-1,930	6,865E-08	Metabolism / Sugar metabolism / Fermentative reactions
NF38_RS07560	HI1551	*bioC*	-1,926	1,029E-06	Metabolism / Lipid metabolism
NF38_RS08455	HI1136	*murD*	-1,921	7,140E-09	Cell wall / Cell wall biosynthesis

pssA	HI0425	*pssA*	-1,916	1,664E-06	Metabolism / Other metabolism genes
NF38_RS01710	HI0684	*glpB*	-1,910	4,092E-07	Metabolism / Glycerol metabolism
NF38_RS02160	HI0583	*cpdB*	-1,910	1,237E-04	Metabolism / Nucleotide metabolism / Purine metabolism
NF38_RS01455	HI0604	*cya*	-1,907	5,037E-08	Metabolism / Nucleotide metabolism / Purine metabolism
NF38_RS06690	HI1374	*mukB*	-1,907	1,859E-07	Cell wall / Cell division
NF38_RS07075	HI1437	*xseB*	-1,906	6,956E-03	Metabolism / Other metabolism genes
ppnK	HI0072	*nadK*	-1,901	9,938E-08	Metabolism / Other metabolism genes
NF38_RS01675	HI0693	*hel*	-1,900	1,483E-05	Transport systems / Uptake/intake systems / Iron
NF38_RS01165	HI0758	*rpmE*	-1,900	1,555E-03	Transcription and translation machinery / Ribosome related things
NF38_RS01885		*yafC*	-1,891	1,899E-04	Transcription and translation machinery / Regulators
NF38_RS07565	HI1552		-1,890	1,127E-04	Hypothetical proteins
NF38_RS02145	HI0587	*pepE*	-1,888	4,214E-07	Metabolism / Other metabolism genes
NF38_RS05445	HI0008	*fdxI*	-1,887	1,951E-02	Metabolism / Sugar metabolism / Fermentative reactions
NF38_RS01685	HI0691	*glpK*	-1,883	1,815E-05	Metabolism / Glycerol metabolism
NF38_RS05440	HI0009	*fdhE*	-1,883	5,101E-04	Metabolism / Sugar metabolism / Fermentative reactions
NF38_RS03030	HI0406	*accA*	-1,879	4,980E-07	Metabolism / Lipid metabolism
NF38_RS01780	HI0670	*dtd*	-1,879	6,989E-03	Metabolism / Other metabolism genes
NF38_RS01760	HI0674	*gpt1*	-1,875	5,479E-03	Metabolism / Other metabolism genes
NF38_RS00670	HI0855		-1,875	3,837E-05	Others
NF38_RS04765	HI0133	*dcd*	-1,873	1,383E-06	Metabolism / Nucleotide metabolism / Pyrimidine metabolism
NF38_RS07130	HI1448	*moeA*	-1,867	7,597E-06	Metabolism / Molybdopterin biosynthesis
NF38_RS06710	HI1378	*phoR*	-1,862	1,456E-05	Transcription and translation machinery / Regulators
NF38_RS04725	HI0139	*ompP2*	-1,861	1,668E-06	Cell wall / OMP
NF38_RS02330	HI0549	*rsmA*	-1,861	3,423E-05	Transcription and translation machinery / Ribosome related things
NF38_RS00165	HI0959	*nagZ*	-1,858	1,018E-06	Cell wall / Cell wall biosynthesis
NF38_RS01690	HI0690	*glpF*	-1,856	9,883E-04	Transport systems / Uptake/intake systems / Glycerol
NF38_RS06460	HI1287		-1,850	8,705E-06	Nucleic acids processing, restriction and modification
NF38_RS08470	HI1133	*murE*	-1,848	1,355E-06	Cell wall / Cell wall biosynthesis
NF38_RS06680			-1,847	2,939E-07	Nucleic acids processing, restriction and modification
NF38_RS08345	HI1158	*trxB*	-1,842	1,427E-04	Metabolism / Other metabolism genes
NF38_RS03855	HI0303	*rsmE*	-1,841	8,359E-06	Transcription and translation machinery / Ribosome related things
NF38_RS02280	HI0559	*cysQ*	-1,840	6,985E-03	Metabolism / Other metabolism genes
NF38_RS07195	HI1338	*sixA*	-1,835	5,296E-06	Metabolism / Other metabolism genes
NF38_RS03545	HI0369	*hisS*	-1,835	8,980E-07	Transcription and translation machinery / tRNA
NF38_RS06455	HI1286	*hsdS3*	-1,834	5,149E-05	Nucleic acids processing, restriction and modification
metG	HI1276	*metG*	-1,831	6,973E-07	Transcription and translation machinery / tRNA
NF38_RS08220	HI1186	*dppC*	-1,828	3,463E-05	Transport systems / Uptake/intake systems / Iron
NF38_RS01665	HI0695	*ppx*	-1,821	4,604E-06	Metabolism / Nucleotide metabolism / Purine metabolism
NF38_RS02035	HI0627	*sdhE*	-1,819	2,167E-06	Others

NF38_RS00415	HI0912		-1,818	2,789E-05	Nucleic acids processing, restriction and modification
NF38_RS04255	HI0227	*yhcH*	-1,818	1,863E-05	Metabolism / Other metabolism genes
NF38_RS07505	HI1540	*licD*	-1,816	1,411E-04	Cell wall / LOS biosynthesis-modification-decoration
NF38_RS04605	HI0163	*bolA*	-1,811	4,606E-03	Stress response-nutrient starvation
NF38_RS03690	HI0338	*tqsA*	-1,807	1,508E-05	Transport systems / Bidirectional transport systems or transporters with unknown function
NF38_RS09145			-1,803	8,576E-03	Hypothetical proteins
NF38_RS05140	HI0067	*mutL*	-1,803	7,253E-07	Nucleic acids processing, restriction and modification
NF38_RS00115	HI0969	*menC*	-1,802	9,509E-06	Metabolism / Quinol/quinone metabolism
NF38_RS00425	HI0910	*mutT*	-1,800	6,535E-04	Nucleic acids processing, restriction and modification
NF38_RS05780	HI1689	*nth*	-1,797	4,094E-04	Nucleic acids processing, restriction and modification
NF38_RS03550	HI0368	*ispG*	-1,793	6,301E-05	Metabolism / Isopentenyl diphosphate biosynthesis
NF38_RS03020	HI0408	*znuC*	-1,793	2,348E-05	Transport systems / Uptake/intake systems / Zinc
NF38_RS00330	HI0927	*glyQ*	-1,790	1,552E-04	Transcription and translation machinery / tRNA
NF38_RS04945			-1,786	1,245E-04	Nucleic acids processing, restriction and modification
NF38_RS01460	HI0603	*hemX*	-1,782	1,977E-05	Metabolism / Other metabolism genes
dppF	HI1184	*dppF*	-1,781	4,789E-06	Transport systems / Uptake/intake systems / Iron
NF38_RS04965	HI0102	*dapE*	-1,772	3,243E-05	Metabolism / Amino acid metabolism / L-lysine biosynthesis via DAP pathway
NF38_RS01705	HI0685	*glpA*	-1,771	1,567E-04	Metabolism / Glycerol metabolism
NF38_RS00795	HI0829	*slt*	-1,768	1,141E-05	Cell wall / Cell wall biosynthesis
NF38_RS08465	HI1134	*murF*	-1,767	5,903E-04	Cell wall / Cell wall biosynthesis
NF38_RS00810	HI0826		-1,766	2,228E-05	Cell wall / Cell division
NF38_RS04485	HI0188	*tatC*	-1,761	7,983E-06	Transport systems / Export systems
NF38_RS08225	HI1185	*dppD*	-1,759	7,802E-05	Transport systems / Uptake/intake systems / Iron
NF38_RS08815	HI1056	*sthiM*	-1,758	6,088E-05	Nucleic acids processing, restriction and modification
NF38_RS03705	HI0335	*dgkA*	-1,749	2,544E-02	Cell wall / Cell wall biosynthesis
NF38_RS08340	HI1159	*ybbN*	-1,741	7,593E-04	Protein degradation / stability / Chaperone
NF38_RS04940			-1,739	4,385E-06	Others
NF38_RS07600	HI1559	*prmC*, *hemK*	-1,739	2,174E-02	Nucleic acids processing, restriction and modification
NF38_RS01695	HI0689	*glpQ*	-1,732	3,356E-03	Cell wall / LOS biosynthesis-modification-decoration
NF38_RS00710	HI0847		-1,731	2,515E-02	Hypothetical proteins
NF38_RS06715	HI1379	*phoB*	-1,730	1,554E-04	Transcription and translation machinery / Regulators
NF38_RS06075		*ydgA*	-1,730	2,443E-04	Nucleic acids processing, restriction and modification
NF38_RS05830		*hmw2C*	-1,728	7,467E-04	Cell wall / OMP
NF38_RS00050	HI0984		-1,726	1,237E-03	Stress response-nutrient starvation
NF38_RS03845	HI0305		-1,725	6,473E-05	Transcription and translation machinery / Ribosome related things
NF38_RS00250	HI0943	*nrdR*	-1,719	6,212E-04	Transcription and translation machinery / Regulators
NF38_RS08740	HI1076	*cyoA*	-1,712	1,423E-03	Metabolism / Other metabolism genes
NF38_RS08605	HI1101	*zipA*	-1,708	3,286E-04	Cell wall / Cell division
NF38_RS07490	HI1537	*licA*	-1,699	1,230E-03	Cell wall / LOS biosynthesis-modification-decoration

NF38_RS03740	HI0328	*efp*	-1,696	2,115E-04	Metabolism / Protein (lipoproteins) metabolism
NF38_RS03780	HI0319	*cmoA*	-1,691	1,225E-03	Metabolism / Amino acid metabolism / L-methionine, S-adenosyl -L-methionine
NF38_RS08745	HI1075	*cyoB*	-1,690	1,206E-02	Metabolism / Other metabolism genes
NF38_RS07085	HI1439	*dxs*	-1,686	8,751E-05	Metabolism / Other metabolism genes
NF38_RS07500	HI1539	*licC*	-1,678	2,443E-04	Cell wall / LOS biosynthesis-modification-decoration
NF38_RS05750	HI1695	*lsgF*	-1,673	1,528E-03	Cell wall / LOS biosynthesis-modification-decoration
NF38_RS02195	HI0576	*tusC*	-1,672	4,082E-02	Metabolism / Other metabolism genes
NF38_RS06685	HI1373	*mukE*	-1,666	2,276E-04	Cell wall / Cell division
NF38_RS07570	HI1553	*bioF*	-1,660	1,962E-02	Metabolism / Vitamins biosynthesis
NF38_RS08490	HI1129	*mraZ*	-1,659	2,265E-04	Transcription and translation machinery / Regulators
NF38_RS05150	HI0065	*tsaE*	-1,657	1,439E-02	Transcription and translation machinery / tRNA
NF38_RS08460	HI1135	*mraY*	-1,655	5,242E-03	Cell wall / Cell wall biosynthesis
NF38_RS00430	HI0909	*secA*	-1,654	8,871E-04	Transport systems / Export systems
NF38_RS04340		*prrC*	-1,652	3,314E-03	Transcription and translation machinery / tRNA
NF38_RS03710	HI0334	*relA*	-1,647	2,575E-04	Stress response-nutrient starvation
NF38_RS06565	HI1352	*putP*	-1,645	1,192E-02	Transport systems / Uptake/intake systems / Amino acids
NF38_RS03050	HI0401	*ompP1*	-1,645	1,402E-04	Transport systems / Uptake/intake systems / Long chain fatty acids
NF38_RS05730	HI1699	*lsgB*	-1,641	8,345E-03	Cell wall / LOS biosynthesis-modification-decoration
NF38_RS04970		*vanY*	-1,634	4,008E-03	Cell wall / Cell wall biosynthesis
NF38_RS07455	HI1528	*parE*	-1,632	1,531E-04	Nucleic acids processing, restriction and modification
NF38_RS07445	HI1526	*hldE*	-1,627	1,233E-03	Cell wall / LOS biosynthesis-modification-decoration
NF38_RS05615	HI1724		-1,626	5,819E-03	Hypothetical proteins
NF38_RS05775	HI1690		-1,619	4,217E-03	2.Uptake/intake systems / Other intake systems
NF38_RS01130	HI0763	*nadR*	-1,616	4,922E-03	Metabolism / Other metabolism genes
NF38_RS02855	HI0443	*recR*	-1,615	4,085E-02	Nucleic acids processing, restriction and modification
NF38_RS06560	HI1351	*cmoB*	-1,612	3,054E-02	Transcription and translation machinery / tRNA
NF38_RS06450			-1,603	1,453E-02	Hypothetical proteins
NF38_RS05105	HI0074		-1,601	1,283E-02	Metabolism / Other metabolism genes
NF38_RS02940	HI0426	*fadR*	-1,598	1,107E-02	Transcription and translation machinery / Regulators
NF38_RS06140	HI1248		-1,597	1,251E-02	Transport systems / Export systems
NF38_RS06185	HI1260	*accD*	-1,596	2,533E-02	Metabolism / Lipid metabolism
NF38_RS00055	HI0983		-1,592	1,613E-02	Hypothetical proteins
NF38_RS03035	HI0404	*tilS*	-1,585	1,627E-02	Transcription and translation machinery / tRNA
NF38_RS08355	HI1156	*cydC*	-1,584	7,861E-03	Transport systems / Export systems
NF38_RS00160	HI0960	*ycfL*	-1,579	3,804E-02	Stress response-nutrient starvation
NF38_RS01595	HI0708	*selA*	-1,578	5,106E-03	Transcription and translation machinery / tRNA
NF38_RS05185	HI0058	*kdsB*	-1,578	8,657E-03	Cell wall / LOS biosynthesis-modification-decoration
NF38_RS00120	HI0968	*menB*	-1,577	1,153E-02	Metabolism / Quinol/quinone metabolism
NF38_RS06630	HI1365	*topA*	-1,575	5,361E-03	Nucleic acids processing, restriction and modification

NF38_RS04935		*hsdS1*	-1,574	1,221E-02	Nucleic acids processing, restriction and modification
NF38_RS08820		*res_1*	-1,572	8,308E-03	Others
NF38_RS01715	HI0683	*glpC*	-1,570	3,585E-02	Metabolism / Glycerol metabolism
NF38_RS00805	HI0827		-1,568	9,321E-03	Metabolism / Lipid metabolism
NF38_RS05175	HI0060	*msbA*	-1,559	3,907E-02	Cell wall / Cell wall biosynthesis
NF38_RS01240	HI0739	*dnaE*	-1,557	1,172E-02	Nucleic acids processing, restriction and modification
NF38_RS07450	HI1527	*lpxL*, *htrB*	-1,557	3,335E-02	Cell wall / LOS biosynthesis-modification-decoration
NF38_RS00505	HI0893	*acrR*	-1,549	4,406E-02	Transcription and translation machinery / Regulators
NF38_RS08795	HI1062	*fabZ*	-1,543	3,750E-02	Metabolism / Lipid metabolism
NF38_RS01620	HI0706	*lppB*	-1,538	3,664E-02	Cell wall / OMP
NF38_RS08405	HI1146		-1,537	1,169E-02	Others
NF38_RS07265	HI1324	*lonB*	-1,535	1,614E-02	Protein degradation / stability / Protein degrading machinery
NF38_RS01230	HI0743	*secB*	-1,521	2,978E-02	Transport systems / Export systems
NF38_RS07670	HI1575	*alr*	-1,517	9,814E-03	Metabolism / Amino acid metabolism / Alanine
NF38_RS02480	HI0519	*nupC*	-1,512	3,023E-02	Transport systems / Uptake/intake systems / Nucleosides

Table A7. Underrepresented genes in *output* samples compared to *input* library in Tn-seq analysis.

Locus	Gene	Product	Sample
HI0041	*xthA*	Exonuclease III	8
HI0054	*uxuR*	Uxu operon regulator	9
HI0062	*dksA*	*dnaK* suppressor protein	8, 9
HI0068	*miaA*	tRNA delta(2)-isopentenylpyrophosphate transferase	6, 7, 9
HI0086	*metB*	Cystathionine gamma-synthase	7
HI0119	*znuA*	High-affinity zinc transporter substrate-binding protein	7, 9
HI0122	*metC*	Cystathionine beta-lyase	7, 8
HI0141	*nagB*	Glucosamine-6-phosphate deaminase	6, 7
HI0159	*yceD*	Hypothetical protein	8
HI0187a	*tatA*	Sec-independent protein secretion pathway component TatA	8, 9
HI0206	*nadN*	NAD nucleotidase	7
HI0209	*dam*	DNA adenine methylase	8
HI0221	*guaB*	Inosine 5'-monophosphate dehydrogenase	7, 8, 9
HI0222	*guaA*	GMP synthase	6, 7, 8, 9
HI0229	*pnp*	Polynucleotide phosphorylase/polyadenylase	6, 7
HI0254	*bcp*	Thioredoxin-dependent thiol peroxidase	6
HI0273,1		tRNA-Ala	9
HI0274,2		tRNA-Val	6
HI0291		Mercury transport-like protein	6
HI0307	*proC*	Pyrroline-5-carboxylate reductase	6
HI0309	*xerD*	Site-specific tyrosine recombinase XerD	7, 8, 9
HI0313	*ruvA*	Holliday junction DNA helicase RuvA	6, 7, 9
HI0314	*ruvC*	Holliday junction resolvase	6
HI0328	*efp*	Elongation factor P	6, 7, 8
HI0334	*relA*	GTP pyrophosphokinase	6, 7, 8, 9
HI0351	*galE*	UDP-glucose 4-epimerase	7, 8, 9
HI0367		Hypothetical protein	9
HI0374		Hypothetical protein	8
HI0393	*ychF*	Redox-regulated ATPase *ychF*	6, 7
HI0407	*znuB*		7
HI0440	*ponA*	Penicillin-binding protein 1A	9
HI0461		Hypothetical protein	7
HI0464	*rpiA*	Ribose-5-phosphate isomerase A	7
HI0465	*serA*	D-3-phosphoglycerate dehydrogenase	7, 8, 9
HI0479	*atpD*	F0F1 ATP synthase subunit beta	6, 7, 8, 9
HI0480	*atpG*	F0F1 ATP synthase subunit gamma	6, 8
HI0482	*atpH*	F0F1 ATP synthase subunit delta	8
HI0485,1		F0F1 ATP synthase subunit I	7, 8

HI0514	*rpoC*	DNA-directed RNA polymerase subunit beta	6, 9
HI0518	*deoD*	Purine nucleoside phosphorylase	7, 8, 9
HI0523		Heptosyltransferase-like protein	7, 8, 9
HI0550	*lex1*	Lipooligosaccharide biosynthesis protein	7, 9
HI0551	*apaH*	Diadenosine tetraphosphatase	6, 7, 8, 9
HI0564	*asnA*	Asparagine synthetase AsnA	7,9
HI0578	*tufA*	Elongation factor Tu	6, 8
HI0606	*cysE*	Serine acetyltransferase	6, 8, 9
HI0609	*folD*	Bifunctional 5,10-methylene-tetrahydrofolate dehydrogenase/ 5,10-methylene-tetrahydrofolate cyclohydrolase	8
HI0621	*metN*	DL-methionine transporter ATP-binding protein	6
HI0629	*mclA*	Sigma-E factor negative regulatory protein	6
HI0632	*tufB*	Elongation factor Tu	8, 9
HI0639	*purB*	Adenylosuccinate lyase	7
HI0652	*kdtA*	3-deoxy-D-manno-octulosonic-acid transferase	6
HI0668	*zapB*	Hypothetical protein	8, 9
HI0693	*hel*	Lipoprotein E	7, 8, 9
HI0696		Hypothetical protein	7
HI0703	*lppB*	Lipoprotein B	7, 8, 9
HI0719		Hypothetical protein	9
HI0735	*lpxH*	UDP-2,3-diacylglucosamine hydrolase	6
HI0740	*yhxB*	Phosphomannomutase	6, 7, 8, 9
HI0769	*ftsE*	Cell division ATP-binding protein	8, 9
HI0770	*ftsX*	Cell division protein FtsX	8, 9
HI0812	*galU*	Glucosephosphate uridylyltransferase	7, 9
HI0836	*genX*	Lysyl-tRNA synthetase	8, 9
HI0841		Hypothetical protein	7
HI0846	*por/dsbA*	Oxidoreductase	7, 8, 9
HI0896	*ftsN*	Cell division protein	7, 8, 9
HI0905	*thyA*	Thymidylate synthase	6, 7
HI0942	*recC*	Exodeoxyribonuclease V subunit gamma	9
HI0945	*degS*	Protease	6
HI0982	*pfkA*	6-phosphofructokinase	7, 8
HI1006	*lspA*	Lipoprotein signal peptidase	8, 9
HI1033	*serB*	Phosphoserine phosphatase	7
HI1077	*pyrG*	CTP synthetase	6, 7, 8, 9
HI1078		Amino-acid ABC transporter ATP-binding protein	7
HI1082		Hypothetical protein	7, 8, 9
HI1084		ABC transpoter	7, 8, 9
HI1085	*mlaD*	ABC transporter substrate-binding protein	9
HI1086	*mlaE*	ABC transporter permease	7, 8, 9

HI1087	*mlaF*	ABC transporter ATPase	8, 9
HI1090	*ccmB*	Heme exporter protein B	6
HI1103	*cysK*	Cysteine synthetase	7
HI1125	*talB*	Transaldolase B	6
HI1130	*mraW*	S-adenosyl-methyltransferase MraW	9
HI1145	*pheA*	Chorismate mutase/prephenate dehydratase	7, 9
HI1164	*ompA*	Outer membrane protein P5	6, 9
HI1193	*ilvE*	Branched-chain amino acid aminotransferase	8
HI1220	*rpsA*	30S ribosomal protein S1	8, 9
HI1276	*metG*	Methionyl-tRNA synthetase	6, 7, 9
HI1288	*rbfA*	Ribosome-binding factor A	6
HI1290	*tyrA*		8
HI1306	*pgpA*	Phosphatidylglycerophosphatase A	8, 9
HI1313	*ihfA*	Integration host factor subunit alpha	7
HI1321	*recB*	Exodeoxyribonuclease V subunit beta	7, 8
HI1387	*trpE*	Anthranilate synthase component I	8, 9
HI1388	*trpG*	Anthranilate synthase component II	8
HI1389	*trpD*	Anthranilate phosphoribosyltransferase	7, 9
HI1389,1	*trpC*	Bifunctional indole-3-glycerol phosphate synthase/phosphoribosylanthranilate isomerase	7, 9
HI1431	*trpB*	Tryptophan synthase subunit beta	7, 8
HI1432	*trpA*	Tryptophan synthase subunit alpha	7, 8, 9
HI1441	*sspA*	Stringent starvation protein A	6
HI1444	*metF*	5,10-methylenetetrahydrofolate reductase	7, 8, 9
HI1450		dsDNA-mimic protein	7
HI1462		Hypothetical protein	6, 7, 8
HI1478	*muA*	Transposase	7
HI1485		Hypothetical protein	7
HI1493		Hypothetical protein	6
HI1587	*hns*	DNA-binding protein H-NS	8
HI1595m	*ftsK*	DNA translocase FtsK	6, 7
HI1605		Hypothetical protein	8
HI1606	*cca*	Multifunctional tRNA nucleotidyl transferase/2'3'-cyclic phosphodiesterase/2'nucleotidase/phosphatase	6, 8, 9
HI1633	*purA*	Adenylosuccinate synthetase	7
HI1640	*sapC*	Peptide ABC transporter permease	8, 9
HI1650		Hypothetical protein	8, 9
HI1678	*kpsF*	Arabinose-5-phosphate isomerase KpsF	6
HI1696		Lipopolysaccharide biosynthesis protein	7
HI1698		Lipopolysaccharide biosynthesis protein	6
HI1702	*metE*	5-methyltetrahydropteroyltriglutamate-- homocysteine S-methyltransferase	7, 8, 9
HI1711	*crr*	PTS system glucose-specific transporter subunit	7, 8

HI1715,1		tRNA-Gly	6
HI1741	*spoT*	Guanosine-3'5'-bis(diphosphate) 3'- pyrophosphohydrolase	6, 7

Tablas Suplementarias

Table A8. Primers used in Chapter 3.

Primer name	Primer ID	Sequence (5'-3')	Purpose	Reference
ackA-F1	1446	CTAATTGACTAATCACATAATTTACTAT	Gene inactivation	This study
ackA-R1	1447	GCCTGTTAATAAAATACCGCCGATTTC	Gene inactivation	This study
pflA-F1	1442	GCCTTAAACGTAATCCACTATATGCAC	Gene inactivation	This study
pflA-R1	1443	GAATTGACCGTGCTACACGTGAACAAC	Gene inactivation	This study
ackA-F2	1448	TCTTAGATGATGGATTTCTATTAACCTCAATCAAAT ATAGGGTTCCTATGATTCCGGGGATCCGTCGACC	Gene inactivation	This study
ackA-R2	1449	GCCGAAAAATTCGGCAGCTTGTTGTTAATTTAGAAA CAAAGTTTTGCGGTTGTAGGCTGGAGCTGCTTCG	Gene inactivation	This study
pflA-F2	1444	AAATATTTGGTAAAATTTAGCTATATCTAATTTTAG GAAATTTATGTATGATTCCGGGGATCCGTCGACC	Gene inactivation	This study
pflA-R2	1445	CATTATTTGCTCCTTATGTTAGCTGACATTTATTCTA GAATTTTACAGTGTGTAGGCTGGAGCTGCTTCG	Gene inactivation	This study
frdA-F1	1594	CGAAACACTTTACTGATTTGGAATATC	Gene inactivation	This study
frdA-R1	1595	CCAAATTGAGGGCAAGCGGCATAGCAT	Gene inactivation	This study
frdA-F2	1596	TGCTCAAGCAAAAGACGTTGTAGCTCG	Gene inactivation	This study
frdA-R2	1597	TATTAAATTTAAATGCACGACAACCAC	Gene inactivation	This study
HI0601.1-F1	488	GAAGTAAGAGATGAAAAGCGAAG	Gene inactivation	(Fernández-Calvet et al., 2018)
HI0601.1-R1	489	TTGGTAAAAATGGATGAAGGGGATTAC	Gene inactivation	(Fernández-Calvet et al., 2018)
ackA-COMP-XhoI-Fw	1598	CCGCTCGAGATACCGCACTTTGATTTTCTAACG	Mutant complementation	This study
ackA-HA-COMP-XhoI-Rv	1599	CCGCTCGAGTTAAGCGTAATCTGGAACATCGTATGG GTAGAAACAAAGTTTTGCGGTATCTTGTGC	Mutant complementation	This study
ackA-pta-COMP-XhoI-Fw	1853	CCGCTCGAGTTTCTAACGGCGTATTGGCACGCTTAC	Mutant complementation	This study
ackA-pta-HA-COMP-XhoI-Rv	1854	CCGCTCGAGTTAAGCGTAGTCTGGGACGTCGTATGG GTATTGTGTTGCTTGAATTGCGGTTAAGGC	Mutant complementation	This study
pSBLerm_down	1307	GGTACACGAAAAACAAGTTAAGGG	Gene inactivation	(Simon Allen et al., 2005)
ackA-qPCR-F	1543	CCAATTAAGTGAGCAGGGTTG	qRT-PCR	(Othman et al., 2014)
ackA-qPCR-R	1544	TCGTATCGTTCACGGTGGCG	qRT-PCR	(Othman et al., 2014)
pflA-qPCR-F	1541	CTCTTTACAAGCACGGAACC	qRT-PCR	(Othman et al., 2014)
pflA-qPCR-R	1542	AAAGAAGTCGTGACTTATCGC	qRT-PCR	(Othman et al., 2014)
frdA-qPCR-F	1567	GCCGTGTAAACCTGAAGATGC	qRT-PCR	(Othman et al., 2014)
frdA-qPCR-R	1568	ATCCCTGTTCGTCCAGTTGTT	qRT-PCR	(Othman et al., 2014)
aceF-qPCR-F	1539	AGCCAGCACCATTTGCTACAC	qRT-PCR	(Othman et al., 2014)
aceF-qPCR-R	1540	GTCGTAAAGGTCGTATCGTTA	qRT-PCR	(Othman et al., 2014)
ldhA-qPCR-F	1545	CTGGCGTTGCTGGGCAATGA	qRT-PCR	(Othman et al., 2014)
ldhA-qPCR-R	1546	TCTTGGCGTACGATCCTTTCA	qRT-PCR	(Othman et al., 2014)
dld-qPCR-F	1553	AGCGGAAAGGTGTCTAAACGA	qRT-PCR	(Othman et al., 2014)
dld-qPCR-R	1554	TCGTCAAGTTGATGAAGGCTC	qRT-PCR	(Othman et al., 2014)
pfkA-qPCR-F	1582	CGATATATTCACAACCGCCAG	qRT-PCR	(Othman et al., 2014)
pfkA-qPCR-R	1583	TCGACCGTTTACGTGATACAT	qRT-PCR	(Othman et al., 2014)
pykA-qPCR-F	1584	TTGCAGACATCGCAACAGATT	qRT-PCR	(Othman et al., 2014)
pykA-qPCR-R	1585	CAGTGGCAGCAATGGCTAG	qRT-PCR	(Othman et al., 2014)
zwf-qPCR-F	1586	CTCTTCCACGCCAATAGATTC	qRT-PCR	(Othman et al., 2014)
zwf-qPCR-R	1587	GAAACCGTTCAAAACTTGCTC	qRT-PCR	(Othman et al., 2014)
fdxG-qPCR-F	1547	GTGGCGGTATTAACGCATTAC	qRT-PCR	(Othman et al., 2014)

fdxG-qPCR-R	1548	CGTAAGAGGTATCTCTATCGT	qRT-PCR	(Othman et al., 2014)
nqrB-qPCR-F	1549	TGCAACTTGGGGCTCTAAAAT	qRT-PCR	(Othman et al., 2014)
nqrB-qPCR-R	1550	ACTTCGTGACCACGAACCAC	qRT-PCR	(Othman et al., 2014)
lldD-qPCR-F	1551	ATCATACGCCCAGAATGGGTG	qRT-PCR	(Othman et al., 2014)
lldD-qPCR-R	1552	ACGGTCGATATGCCTACTCCA	qRT-PCR	(Othman et al., 2014)
cydA-qPCR-F	1555	AACCAACCACACTCAATGGCA	qRT-PCR	(Othman et al., 2014)
cydA-qPCR-R	1556	ACTTACATTCGGCGCATTTGT	qRT-PCR	(Othman et al., 2014)
cydB-qPCR-F	1557	CGTGAGTGACAAGCATTGATA	qRT-PCR	(Othman et al., 2014)
cydB-qPCR-R	1558	GCGTTCCATTCCATTTTAACG	qRT-PCR	(Othman et al., 2014)
napA-qPCR-F	1561	TGGTCGCGGTCACGGTCA	qRT-PCR	(Othman et al., 2014)
napA-qPCR-R	1562	GGATCATAGCCTTCACGGTAA	qRT-PCR	(Othman et al., 2014)
mtsZ-qPCR-F	1563	AACAAACGGGTTACCACCTGC	qRT-PCR	(Othman et al., 2014)
mtsZ-qPCR-R	1564	CCATTAGCGCGTATTGCTGAT	qRT-PCR	(Othman et al., 2014)
nrfA-qPCR-F	1565	GCCGTGTAAACCTGAAGATGC	qRT-PCR	(Othman et al., 2014)
nrfA-qPCR-R	1566	ATCCCTGTTCGTCCAGTTGTT	qRT-PCR	(Othman et al., 2014)
dmsA-qPCR-F	1559	CAAGCACGAACCTGATGATCA	qRT-PCR	(Othman et al., 2014)
dmsA-qPCR-R	1560	AGTAAACTGTGGTAGCCGTTG	qRT-PCR	(Othman et al., 2014)
ndh-qPCR-F		AAATACACTTATTACCAAAGATGG	qRT-PCR	(Muda et al., 2019a)
ndh-qPCR-R		ATTGATTGATACGATTAATTTC	qRT-PCR	(Muda et al., 2019a)
pta-qPCR-F	1856	CTACATCAGCACCGCTACCA	qRT-PCR	This study
pta-qPCR-R	1857	CACCACTGCAAACACCATTC	qRT-PCR	This study
gyrA-qPCR-F2	1078	ATATGTTGGTTGATGGGCAAGG	qRT-PCR	(Moleres et al., 2018)
gyrA-qPCR-R2	1079	GGCGAGAAATTGACGGTTTCT	qRT-PCR	(Moleres et al., 2018)
il8- qPCR-F	1241	AGAGACAGCAGAGCACAC	qRT-PCR	(Euba, et al., 2015c)
il8- qPCR-R	1242	AGTTCTTTAGCACTCCTTGG	qRT-PCR	(Euba, et al., 2015c)
gapdh-qPCR-F	1237	GAAGGTGAAGGTCGGAGTC	qRT-PCR	(Euba, et al., 2015c)
gapdh-qPCR-R	1238	GAAGATGGTGATGGGATTTC	qRT-PCR	(Euba, et al., 2015c)
cxcl1- qPCR-F	1247	GCAGGGAATTCACCCCAAGA	qRT-PCR	(Euba, et al., 2015c)
cxcl1- qPCR-R	1248	CTTCAGGAACAGCCACCAGT	qRT-PCR	(Euba, et al., 2015c)
kc-qPCR-F	1404	GACAGACTGCTCTGATGGCA	qRT-PCR	(Euba et al., 2017)
kc-qPCR-R	1405	TGCACTTCTTTTCGCACAAC	qRT-PCR	(Euba et al., 2017)
mgadph- qPCR-F	1430	CCCACTAACATCAAATGGGG	qRT-PCR	(Regueiro et al., 2011)
mgadph- qPCR-R	1431	CCTTCCACAATGCCAAAGTT	qRT-PCR	(Regueiro et al., 2011)

Tablas Suplementarias

Table A9. Primers used in Chapter 4.

Primer name	Primer ID	Sequence (5'-3')	Purpose	Reference
fabH-F1	1702	AAATCAGCTTGAGCGTTTGGCGGAATC	Gene inactivation	This study
fabH-R1	1703	AAAGAAGGGAACCCAATTTGTTCT	Gene inactivation	This study
fabH-F2	1704	GATAGTCCATAGATTTTTTCCTTTTTAATCGCTTATC TTATTGAGTATGATTCCGGGGATCCGTCGACC	Gene inactivation	This study
fabH-R2	1705	GCATCTCGATATAGCCAGATTTTTCTATACCACGTTC TGGCTGAGCTAAATGTAGGCTGGAGCTGCTTCG	Gene inactivation	This study
fabH-F	1756	TTATTCGTGCAGGCAAAGTG	qRT-PCR	This study
fabH-R	1757	AAGCGTGTAAATGGGTGGAG	qRT-PCR	This study
fabH-P851-P642-F	1906	TTATTCGTGCAGGCAAGGTG	qRT-PCR	This study
fabH-P851-P642-R	1907	AAGCGTGTAAATGGGTAGAA	qRT-PCR	This study
gyrA-qPCR-F2	1078	ATATGTTGGTTGATGGGCAAGG	qRT-PCR	(Moleres et al., 2018)
gyrA-qPCR-R2	1079	GGCGAGAAATTGACGGTTTCT	qRT-PCR	(Moleres et al., 2018)

Anexo II:

Publicaciones que avalan esta Tesis Doctoral

Computational and Structural Biotechnology Journal 19 (2021) 3042–3050

ELSEVIER

COMPUTATIONAL AND STRUCTURAL BIOTECHNOLOGY JOURNAL

journal homepage: www.elsevier.com/locate/csbj

Learning from –omics strategies applied to uncover *Haemophilus influenzae* host-pathogen interactions: Current status and perspectives

Nahikari López-López [a,1], Celia Gil-Campillo [a,1], Roberto Díez-Martínez [b], Junkal Garmendia [a,c,*]

[a] *Instituto de Agrobiotecnología, Consejo Superior de Investigaciones Científicas (IdAB-CSIC)-Gobierno de Navarra, Mutilva, Spain*
[b] *Telum Therapeutics, Noain, Spain*
[c] *Centro de Investigación Biomédica en Red de Enfermedades Respiratorias (CIBERES), Madrid, Spain*

ARTICLE INFO

Article history:
Received 10 March 2021
Received in revised form 11 May 2021
Accepted 11 May 2021
Available online 15 May 2021

Keywords:
Haemophilus influenzae
Airway infection
Genome
Transcriptome
Methylome
Proteome
Metabolome
Tn-seq

ABSTRACT

Haemophilus influenzae has contributed to key bacterial genome sequencing hallmarks, as being not only the first bacterium to be genome-sequenced, but also starring the first genome-wide analysis of chromosomes directly transformed with DNA from a divergent genotype, and pioneering Tn-seq methodologies. Over the years, the phenomenal and constantly evolving development of –omic technologies applied to a whole range of biological questions of clinical relevance in the *H. influenzae*-host interplay, has greatly moved forward our understanding of this human-adapted pathogen, responsible for multiple acute and chronic infections of the respiratory tract. In this way, essential genes, virulence factors, pathoadaptive traits, and multi-layer gene expression regulatory networks with both genomic and epigenomic complexity levels are being elucidated. Likewise, the unstoppable increasing whole genome sequencing information underpinning *H. influenzae* great genomic plasticity, mainly when referring to non-capsulated strains, poses major challenges to understand the genomic basis of clinically relevant phenotypes and even more, to clearly highlight potential targets of clinical interest for diagnostic, therapeutic or vaccine development. We review here how genomic, transcriptomic, proteomic and metabolomic-based approaches are great contributors to our current understanding of the interactions between *H. influenzae* and the human airways, and point possible strategies to maximize their usefulness in the context of biomedical research and clinical needs on this human-adapted bacterial pathogen.

Contents

1. Introduction . . . 3043
2. Constantly evolving information from *H. influenzae* whole genome sequencing . . . 3043
   2.1. *H. influenzae* population structure . . . 3043
   2.2. NTHi isolates from COPD patients: genetic signatures and pathoadaptive traits . . . 3044
   2.3. WGS insights into DNA uptake, natural transformation and natural genetic variation by *H. influenzae* . . . 3045
   2.4. Single-molecule real-time (SMRT) sequencing contribution to *H. influenzae* phase-variable methylome analyses . . . 3045
   2.5. Genome-scale microevolution and genetic screening approaches shed light on NTHi adaptation and pathogenesis . . . 3046
3. Unraveling features of the *H. influenzae*-host interplay by genome-wide gene expression profiling . . . 3046
4. Update on *H. influenzae* protein and metabolite profiling . . . 3047
5. Future outlook . . . 3048
   Funding . . . 3048
   Author contributions . . . 3048

* Corresponding author at: Instituto de Agrobiotecnología, Consejo Superior de Investigaciones Científicas (IdAB-CSIC)-Gobierno de Navarra, Mutilva, Spain.
E-mail address: juncal.garmendia@csic.es (J. Garmendia).
[1] These authors contributed equally to this work.

https://doi.org/10.1016/j.csbj.2021.05.026

Declaration of Competing Interest 3048
Acknowledgment 3048
References 3048

1. Introduction

The Gram negative bacterium *Haemophilus influenzae* is a human-adapted pathogen, commonly associated with human disease in both children and adults. While asymptomatic colonisation begins in the upper airways, it can spread through the respiratory tract, and potentially lead to invasive infections. *H. influenzae* consists of capsulated strains (serotypes a to f), and non-capsulated strains designated as non-typeable (NTHi). The capsulated *H. influenzae* type b (Hib) was the predominating disease-causing serotype, with a high incidence of invasive Hib disease including meningitis and sepsis, until the introduction of the efficient polysaccharide capsule vaccine in the late 1980s/early 1990s, which has driven its almost complete disappearance in countries with established child immunisation programs [1]. In contrast, other *H. influenzae* serotypes and NTHi, which are not targeted by the Hib vaccine, are currently recognised as important causes of infections. In particular, NTHi is a common coloniser of the upper airways in healthy individuals, responsible for multiple acute and chronic infections of the respiratory tract, including otitis media (OM), conjunctivitis, sinusitis and lower respiratory infections in children; exacerbations of chronic obstructive pulmonary disease (COPD) and cystic fibrosis (CF) in adults; and sepsis in neonates, immunocompromised adults, and the elderly [1–5]. Furthermore, *H. influenzae* antimicrobial resistance presents an overall increased trend, in such a way that ampicillin-resistant *H. influenzae* is included in the WHO global priority list of bacteria for which new antibacterial agents are urgently needed [6]. Additionally, fluoroquinolone-resistant *H. influenzae* has quickly increased in recent years and spread worldwide with a variety in epidemiology [7].

The *H. influenzae* strain RdKW20 was the first free-living organism for which the complete genome sequence was established [8], the first naturally transformed organism to be genome-sequenced [9], generated the first genome-scale metabolic model [10,11], and pioneered transposon sequencing methodologies [12]. We further review the contribution of genomic, transcriptomic, proteomic and metabolomic approaches to our understanding of the interactions between *H. influenzae* and the human airways (for a summary, see Fig. 1 and Table 1).

2. Constantly evolving information from *H. influenzae* whole genome sequencing

2.1. H. influenzae population structure

On a genomic basis, a whole range of multilocus sequence typing (MLST) and core genome-single nucleotide polymorphisms (core-SNP)-based studies, performed on different *H. influenzae* strain sets encompassing capsulated and non-typeable clinical isolates, commonly share that capsulated strains concentrate into a small number of serotype-specific clusters or clonal populations, while NTHi strains display great genomic diversity [13–18]. About 779 *H. influenzae* genomes are found currently in publicly available databases (May 21st, 2021), and we expect this number to grow exponentially over time [19], making genomic information dynamic as constantly evolving data requiring regular update. In this context, *H. influenzae* competence in acquiring genomic material throughout the infection process facilitates genomic plasticity (see **Section 2.3**) leading to an open pan-genome which, for NTHi, was recently updated to 12,249 genes where the core genome accounts for about 7% [20]. The large accessory pan-genome confers diversity and is highly heterogeneous among strains. Many genes are phage-associated, leading to numerous isolates with distinct intact phages integrated in their genome [17,21].

When focusing on the capsule locus, Regions I (containing the *bexABCD* operon) and III (containing the *hcsA* and *hcsB* genes), involved in exporting the capsule polysaccharide, are conserved among all six capsular serotypes, while Region II genes, required for polysaccharide synthesis, are unique to each serotype. Notably, in the frame of transition to whole genome sequencing (WGS)-based surveillance, bioinformatics tools for *in silico* rapid determination of *H. influenzae* serotypes from WGS data have been developed [13,17]. Moreover, capsulated strains genomic closeness has been illustrated for invasive *H. influenzae* type f (Hif) and type a (Hia) isolates [22,23]. Thus, Hif may present a pattern of unique or missing genes maybe increasing the virulence, with the presence of the *sap2* operon, *aef3* fimbriae, and genes for kanamycin nucleotidyltransferase, iron-utilization and putative YadA-like trimeric autotransporters, and the absence of an operon for *de novo* histidine biosynthesis, a *hmg* locus for lipooligosaccharide (LOS) biosynthesis and biofilm formation, and a molybdate transport system [22].

Efforts to define the structure of the NTHi population and to identify groups of related strains led to strain partitioning into six or eight groups or monophyletic clades (clades I-VI / clades I-VIII) based on the core alignment, not predicted on the basis of MLST data, and supported by the composition of the accessory genome [18,20]. The clade I-VI classification allowed proposing clade-specific signatures regarding the exclusive presence/absence of genes encoding surface-associated proteins and LOS components [17,18]. This sorting was further revisited on the clade I-VIII classification by applying pan-genome-wide association studies (GWAS) tools to identify genes enriched in each specific clade [20].

On the other hand, the molecular basis underpinning NTHi transition from commensal to pathogen is not clearly understood. Clade classification did not group strains of common clinical or geographical origin [18,20], and comparative genomics, by analysing paired isogenic strains isolated from the nasopharynx (NP) and bronchoalveolar lavage (BAL) of children with chronic lung disease, did not shed light on this matter as pairs were highly genetically similar [24]. Nevertheless, and despite NTHi heterogeneity, the previously reported association between the NTHi ST14CC-PBP3IIb/A clonal group, increased clinical virulence, antimicrobial resistance and persistence over time, together with NTHi implication in clonal invasive disease, highlights that continuous surveillance and WGS in a clinical laboratory will certainly allow to rapidly address concerns of usually virulent clones or possible outbreaks, particularly in the severe immunocompromised population [25–27].

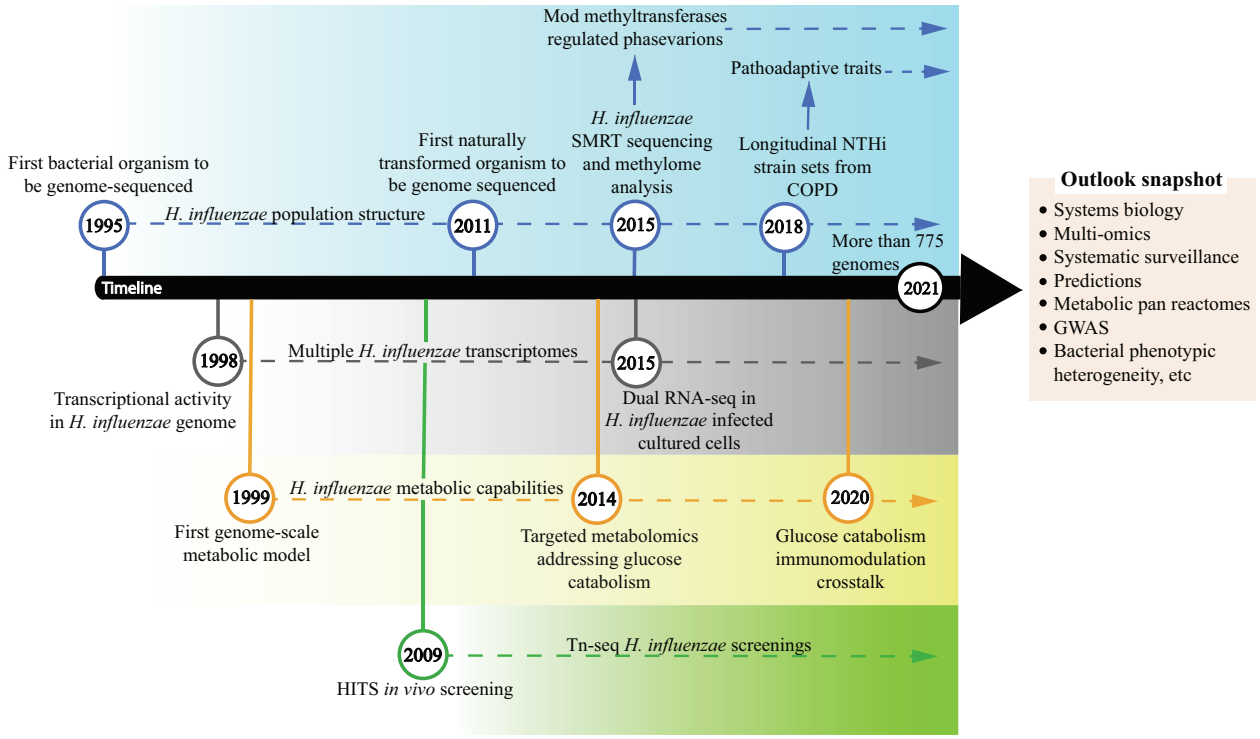

Fig. 1. Summarized landscape of –omics contribution to our understanding of the interactions between *H. influenzae* and the human host. The timeline starts when the first *H. influenzae* complete genome was sequenced, as a major breakthrough on our understanding of the biology, diversity and evolution of bacteria. We highlight key genomic (labeled in blue), transcriptomic (labeled in grey), metabolomic (labeled in yellow), and Tn-seq screening (labeled in green)-based milestones and contributions over time. Information regarding *H. influenzae* population structure, genome-wide expression profiling, metabolic capabilities, and genetic screenings keeps growing along the entire timeline (indicated with dotted arrows). SMRT, single-molecule real-time; NTHi, nontypeable *Haemophilus influenzae*; COPD, chronic obstructive pulmonary disease; dual RNA-seq, dual RNA-sequencing; HITS, high-throughput insertion tracking by deep sequencing; Tn-seq, transposon sequencing; GWAS, genome-wide association studies. (For interpretation of the references to colour in this figure legend, the reader is referred to the web version of this article.)

Table 1
Summary of –omics studies contributing to the *H. influenzae*-host interplay.

Type of study	Purpose-outcome of the study	References
A. *H. influenzae* bacterial whole genome sequencing	A1. Population structure of capsulated and non-capsulated (non-typeable) clinical isolates	[13–18,20–24]
	A2. Within-host pathoadaptive traits on longitudinally collected strain sets from chronic respiratory samples – genome evolution in natural settings	[32–34,36]
	A3. Natural transformation and recombination-driven genetic variation	[9,14,32,38–39,45–46]
	A4. Methylome profiling	[35,54]
	A5. Microevolution in experimental settings	[60–61]
B. Genome-wide genetic screening	B1. HITS* based *in vivo* genetic screenings	[12,67–68]
	B2. Tn-seq based *in vitro* genetic screenings	[69–73]
C. Genome-wide gene expression profiling	C1. Bacterial transcriptomic responses to changing environmental conditions	[75–79,82,84,87]
	C2. Bacterial transcriptomic responses to gene inactivation	[35,53–55,59,80–81,83]
	C3. Dual RNA-seq gene expression profiling	[87]
D. Proteomic profiling	D1. Bacterial responses to changing environmental conditions	[89,91–93]
	D2. Bacterial responses to gene inactivation	[54–55,81]
E. Metabolomic profiling	E1. Bacterial responses to changing environmental conditions	[99–101]
	E2. Bacterial responses to gene inactivation	[81,100]

*HITS, high-throughput insertion tracking by deep sequencing; Tn-seq, transposon sequencing; dual RNA-seq, dual RNA-sequencing.

2.2. NTHi isolates from COPD patients: genetic signatures and pathoadaptive traits

COPD is an emerging disease worldwide, and cigarette smoking is its main risk factor. The disease is characterised by dyspnea, chronic cough, sputum production and persistent airflow limitation. COPD exacerbations are often associated to bacterial pathogens, most importantly to NTHi. A main feature of COPD is, however, a chronic inflammation of the pulmonary parenchyma that is associated with bacterial persistence, and NTHi is a frequently found bacterial species in the airways of these patients [28–31]. When looking for genetic distinctions between NTHi isolates from COPD with respect to other illnesses, the distribution of core genome SNPs does not separate COPD from non-COPD strains [18,20]. However, this distinction is possible when applying discriminant analysis of principal components to the composition of

the accessory genome, further supported by pan-GWAS identification of a repertoire of unique NTHi accessory genes significantly associated with COPD, many of them with predicted roles in virulence, transmembrane transport of metal ions and nutrients, cellular respiration and maintenance of redox homeostasis [20].

Moreover, NTHi also alters its genome during persistence within the lower airways of chronic respiratory patients, as stated by the analyses of longitudinally collected NTHi strains from independent cohorts of COPD patients [32–34]. Pettigrew's group revealed frequent genetic variation due to slipped-strand mispairing in simple sequence repeats (SSR), and diversifying selection of several candidate vaccine antigens during NTHi persistence in the human airways [33]. Follow up studies on this same strain collection showed different proportions of methyltransferase-encoding *modA* alleles compared to those isolated from OM patients [35], and changes in the expression of the IgA protease variants A1, A2, B1 and B2 conferred by changes in genomes during persistent infection which, depending on the variant, could be indels or slipped-strand mispairing in mono- or heptanucleotide repeats [36]. On our part, we addressed molecular genetic changes underlying bacterial pathoadaptation by investigating genetic variants arising from within-patient evolution of NTHi in an independent cohort of COPD patients. Notably, we identified recurrent polymorphisms in several genes and provided experimental evidence for the biological significance of such convergent variation in the *ompP1-fadL* gene, whose recurrent mutations are a likely case of antagonistic pleiotropy during adaptation of NTHi to chronic lung infection associated to COPD [32].

2.3. WGS insights into DNA uptake, natural transformation and natural genetic variation by H. influenzae

Natural competence allows bacteria to respond to environmental and nutritional cues by taking up free DNA from their surroundings, gaining both nutrients and genetic information [37]. *H. influenzae* intrinsic transformable nature, self-preferences caused by the uptake machinery bias for uptake signal sequences (USS), and the high rate of homologous recombination events they can undergo, have a great impact on the evolution of the genomes of this pathogen, which seems to be higher in NTHi compared to capsulated strains [38,39].

Such frequent genetic exchange also occurs among *Haemophilus* spp., (*H. influenzae*, *H. aegyptius* and *H. haemolyticus* belong to the cluster "*Haemophilus sensu stricto*" [40,41]), causing frequent misidentifications of *H. influenzae* from clinical specimens when using selective culture methods, a limitation overcome by using matrix-assisted laser desorption/ionization time-of-flight (MALDI-TOF) mass spectrometry [42,43]. On this matter, phylogeny studies may also allow not only seeking for *H. influenzae*-specific signatures of diagnostic potential such as the *fucP* locus [16], but also speciating *Haemophilus* isolates from COPD, further supporting that the heterogeneity of NTHi may indeed provide a genetic continuum between NTHi and *H. haemolyticus* [44].

When focusing on bacterial genome shaping by natural transformation, it is noticeable that the first WGS characterization of recombination events was performed by using DNA from a clinical isolate of NTHi (strain 86-028NP) to transform competent cells of a laboratory strain (strain RdKW20), leading to the first genome-wide analysis of chromosomes directly transformed with DNA from a divergent genotype [9,45]. Such observations were independently supported by transformation of the same laboratory strain with donor DNA from a heterologous Hib strain [14]. Detailed genome-wide analyses of not only *H. influenzae* bacteria experimentally transformed with donor DNA from diverged clinical isolates, but also DNA uptake across the outer membrane of naturally competent *H. influenzae* bacteria, turned out to be extremely informative to understand the relevance and evolution of uptake sequences in the genome, and even to predict the outcome of competition between self- and non-self DNA in the respiratory tract environment [39,45]. Moreover, transformation-based experimental evolution studies showed that transformation of single competent cells is extensive, suggesting that it could be used as a tool to map traits that vary between clinical isolates. This notion was applied to develop "transformed recombinant enrichment profiling" (TREP), in which natural transformation is used to generate complex pools of recombinants, phenotypic selection is used to enrich for specific recombinants, and deep sequencing is used to survey for the genetic variation responsible. TREP was applied to investigate the genetic architecture of intracellular epithelial invasion by *H. influenzae*, and identified specific allelic variants of the HMW1 adhesin as a key factor on this matter [46]. Connecting such *in vitro* transformation studies with the high levels of natural genetic variation found in NTHi, variation within closely related genomes from clinical strains collected from COPD respiratory samples shows numerous closely spaced variants which resemble natural transformation events seen in the laboratory, i.e. recombination tracts distinguishing the clinical isolates [32].

2.4. Single-molecule real-time (SMRT) sequencing contribution to H. influenzae phase-variable methylome analyses

Formation of C-/N-methyl-cytosine and N-methyl-adenine in bacterial genomes is a postreplicative phenomenon that occurs at specific targets, has multiple roles in bacterial physiology, and can be genome-wide deciphered by using SMRT or nanopore sequencing [47–49]. DNA methyltransferases can exist as part of restriction-modification (R-M) systems and be subject to phase variation, i.e. the random and reversible switching of gene expression due to the presence of inverted repeats (IR) or SSRs in their coding regions. Phase-variable methyltransferases control the expression of multiple genes via epigenetic mechanisms [50–52]. Such systems, called phasevarions for phase-variable regulons, were originally identified in *H. influenzae*, where the DNA methyltransferase ModA is a type III R-M system component containing a variable number of SSRs within its coding sequence [53]. ModA phase variation generates ON/OFF protein variants resulting in changes in methylation patterns, and therefore in phasevarion expression profiles and phenotypic heterogeneity. Besides phase variation, ModA also undergoes allelic variation among *H. influenzae* strains contributing to a wide range of predicted DNA methylation target sequences [50–52]. By analysing *modA* allelic variation across NTHi isolates from healthy individuals, OM and COPD patients, ModA1 to ModA21 variants have been identified, whose distribution and prevalence vary depending on the strain origin, suggesting that different *modA* alleles may provide distinct advantages in the differing human body niches and even have a marker potential [35,54].

Several studies tackled phenotypic heterogeneity due to NTHi ModA2 phase variation, showing that (i) under alkaline conditions such as those in the middle ear during chronic disease, NTHi strains expressing ModA2 (*modA2* ON) form biofilms with greater biomass and less distinct architecture than those formed by a ModA2-deficient population (*modA2* OFF) [55]; (ii) ModA2 ON are more sensitive to oxidative stress than ModA2 OFF variants [56]. Regarding *in vivo* selection during infection of the middle ear in a chinchilla model of OM, *modA2* ON was preferentially selected compared to *mod2A* OFF [54], further supported by that the fact that a shift from OFF to ON within the middle ear results in increased disease severity [57], and that a unique host immune response may be mounted against each discrete *modA* subpopulation [58].

In addition, coupling of SMRT sequencing with gene and/or protein expression profiling allows combining knowledge of methylation specificity and gene expression changes proportional with methyltransferase phase variation. Thus, genome-wide gene expression profiling showed (i) differences when comparing RdKW20 WT and *modA* mutant strains for genes encoding, among others, surface-exposed proteins, transporters and heat-shock proteins [53]; (ii) differences when comparing R2866 WT and *modA10* mutant strains, including upregulation of membrane protein encoding genes such as *olpA2*, which is involved in host cell adhesion and invasion [59]; (iii) the effects of *modA2* phase variation, including those within biofilms by using an ON/OFF strain pair [54,55]; (iv) the effects of *modA15* and *modA18* phase variation, by using a single ON/OFF pair of strains for each *modA* allele. In the case of the ModA15 phasevarion, the DNA binding transcriptional regulator Fis was up-regulated in ON relative to OFF, as a likely case of regulation of a regulator [35]. Conversely, proteomic analyses (i) determined relative protein abundances within the biofilms formed by each *modA2* subpopulation, with the greatest differences occurring in alkaline conditions including a significant decrease in abundance of the DNABII DNA-binding protein HU within biofilms formed by *modA2* ON compared to those formed by *modA2* OFF bacteria [55], and (ii) showed differences related to changes in the expression of outer membrane proteins when comparing *modA* ON/OFF strain pairs [54].

2.5. Genome-scale microevolution and genetic screening approaches shed light on NTHi adaptation and pathogenesis

Unravelling pathoadaptive genome evolution related to chronicity in the natural setting is not only thrilling but also challenging, as it requires longitudinal and preferably prospective clinical isolate sampling [32,33]. This notion, when applied to well-suited experimental settings, also allows unravelling microevolution traits contributing to the pathogen persistence. This is the case of the mutation of the *icc* gene, encoding a 3́,5́-cyclic adenosine monophosphate phosphodiesterase, identified as a *H. influenzae* microevolution trait in response to transient nutrient limitation, which associates with increased development of intracellular bacterial communities (IBC) [60]. Likewise, when using a pre-clinical model of OM to assess NTHi pathoadaptation during sequential episodes of disease, microevolution of haemoglobin binding and LOS biosynthesis genes was observed in such OM-adapted strains, which in turn promoted increased biofilm formation, inflammation, stromal fibrosis, and an increased propensity to form IBCs [61].

On the other hand, sequencing and data analysis tools have also revolutionized genome-wide gene discovery aimed to determine gene disruptions differentially represented in a mutant population upon screening. Historical limitations by the labour involved in mapping the locations of the mutations, are overcome by using random transposition insertion mutagenesis followed by deep sequencing. This is achievable by high-throughput insertion tracking by deep sequencing (HITS), insertion sequencing (IN-seq), transposon sequencing (Tn-seq), or transposon-directed insertion sequencing (TraDIS), collectively referred to as Tn-seq [62–66]. *H. influenzae* pioneered genome-wide gene discovery by starring the original HITS proof of concept, developed to analyse genes required by *H. influenzae* to resist clearance from the lung in a murine pulmonary model, and identified a whole range of genes with reported or potential roles in survival during nutrient limitation, oxidative stress, and exposure to antimicrobial membrane perturbations [12]. HITS was also useful to identify *H. influenzae* genes required to colonize an influenza A virus (IAV) co-infection murine model, showing genes both exclusive or commonly shared by bacterial and IAV co-infection model systems [67], or to screen genome-wide genetic interactions to unravel epistatic interaction accounting for *H. influenzae* survival in the murine lung [68]. Tn-seq suitability has also been reported for *H. influenzae in vitro* genome-wide screening studies including the identification of (i) essential genes [69]; (ii) the carbonic anhydrase involvement in NTHi adaptation to changes in environmental CO_2 levels and intracellular survival [70]; (iii) a role for the outer membrane protein P5 in NTHi survival to complement-mediated killing [71], and for galactose-containing oligosaccharide structures in NTHi survival to complement-dependent neutrophil-mediated killing [72]; (iv) the contribution of the *mltC* and *lppB* genes to biofilm formation [73].

3. Unraveling features of the *H. influenzae*-host interplay by genome-wide gene expression profiling

Since the first high-density oligonucleotide probe array containing probes representing 106 *H. influenzae* genes [74], microarray and later on RNA sequencing (RNA-seq) technologies have greatly contributed to broaden our understanding of NTHi physiology and host interplay. Please note that profiling of gene expression changes regulated by methyltransferases and their phase variation is reviewed in **Section 2.4**. Moreover, *H. influenzae* transits between niches within the host that differ in oxygen levels, and the ArcAB two-component regulatory system controls gene expression in response to different respiratory conditions of growth. Gene expression profiling contributed not only to identify the *H. influenzae* ArcA regulon upon anaerobic growth [75], but also to decipher changes in *H. influenzae* transcriptional responses upon changes in oxygen availability, showing that, in high oxygen, arginine uptake, arginine/aspartate metabolism, and glutamate pathways leading into the Krebs cycle are commonly up-regulated [76].

Genome-wide expression profiling also identified a putative core of genes responsive to iron and heme (FeHm) availability in several NTHi strain backgrounds including RdKW20, 10810, R2866, 86-028NP or R2846. Included in the core iron/heme modulon were genes preferentially expressed under iron/heme limitation, most of which are directly involved with iron and/or heme acquisition [77–79]. The ferric uptake regulator (Fur) regulon has also been studied, which identified the first small RNA described in any *Haemophilus* species, HrrF, overexpressed in the absence of Fur and responsive to iron levels, in turn regulating the expression of molybdate uptake, and deoxyribonucleotide and amino acid synthesis genes [80]. As mentioned above, transient nutrient limitation, in particular FeHm restriction, increases the longevity of NTHi survival *in vitro* and promotes bacterial microevolution by mutation of the *icc* gene [60]. Such adaptive trait, besides increased development of IBCs [60], also relates to increased biofilm formation and gene expression changes within the *in vitro* biofilms, some of them associated to competence and therefore likely linked to the observed increased transformation efficiency of those biofilms [81].

Regarding natural competence, changes in gene expression during competence development confirmed the existence of a competence regulon characterized by a promoter-associated competence regulatory element (CRE) closely related to the cAMP receptor protein (CRP) binding consensus, and where the essential competence gene *sxy* is induced early in competence development [82]. Such observations were further extended by differential gene expression profiling of *H. influenzae* wild-type, *crp* and *sxy* mutant strains, which also shed light on the competence-regulated toxin-antitoxin ToxTA system [83]. Moreover, analysis of global transcriptional changes has also been of use when assessing *H. influenzae* response to antibiotic pressure, showing increased *ponB* (encoding PBP1b) and *acrR* (negative regulator of AcrAB-TolC efflux

pump) gene expression during heat stress, which may relate to the observed decrease in bacterial viability after incubation with imipenem at 42 °C as compared to 37 °C [84]. An effort to identify convergent molecular signatures related to lung adaptation led to comparative transcriptomic analysis of paired, isogenic NTHi strains, isolated from the NP and BAL of children with chronic lung disease, showing no convergence at the gene level, but a possible trend in terms of functional enrichment among genetically unrelated NTHi strains [24].

Although most studies have analyzed *H. influenzae* gene expression, host response to bacterial infection also needs obvious attention. Gene expression profiling identified host functions differentially expressed in NTHi-infected human type II pneumocytes, which allowed identifying a repertoire of host target candidates for pharmacological modulation [85]. In an independent study, the transcriptome of a complete episode of acute OM in mice identified sets of genes involved in regulation of immune responses, changes in epithelial and stromal cell markers, and the recruitment/function of neutrophils and macrophages [86]. Notably, a dual RNA-seq approach was undertaken for pathogen and host genome-wide expression profiling during *H. influenzae* infection of ciliated human bronchial epithelial cells. Temporal profiling of host mRNA signatures revealed significant dysregulation of the target cell cytoskeleton elicited by bacterial infection, with a profound effect on the intermediate filament network and junctional complexes. In turn, NTHi downregulated its central metabolism, and increased the expression of transporters, suggesting a change in the metabolic regime due to the availability of host substrates (see **Section 4**), and of stress-induced defense mechanisms, including the transport of exogenous glutathione and activation of toxin-antitoxin family components [87]. Currently lacking, *in vivo* dual RNA-seq would likely be of great help to gather a more comprehensive view of the *H. influenzae*-host interplay.

4. Update on *H. influenzae* protein and metabolite profiling

Proteomic studies on the *H. influenzae*-host interaction are relatively scattered. From a diagnostic perspective, *H. influenzae* species-unique peptide biomarkers discovered by tandem mass spectrometry may be a valuable tool for clinical sample proteotyping [88]. Protein profiling regulated by methyltransferase phase variation is reviewed in **Section 2.4**. Independently, proteomic expression profiling of *H. influenzae* grown in pooled human sputum revealed increased expression of antioxidant, stress-response proteins, and cofactor and nutrient uptake systems compared to media grown cells [89]. Definition of the protein content of NTHi lysates identified numerous unique *H. influenzae* proteins contributing to biofilm formation, immune evasion, or epithelial inflammation, classified as outer membrane/cell surface associated, metabolic, biosynthesis mediators, proteases, chaperones/DNA binding proteins, transporters, reductases or hydrolases [90]. Proteomic profiling was also used to demonstrate differential expression of the NTHi biofilm to planktonic samples, where ArcA showed a high level of downregulation in the biofilm [91], and whose inactivation led to ArcA-regulated proteomic changes, some of them maybe involved in serum susceptibility [92]. Proteomic profiling was also useful to prove that the two bacterial populations released from a NTHi biofilm by using antibodies directed against the type IV pilus or, alternatively, against a DNABII DNA-binding protein, are different not only from planktonically grown NTHi, but also from each other despite genetic identity. Even more, each newly released population had a distinct, increased susceptibility to antibiotic killing compared to planktonic bacteria, highlighting new clues for anti-biofilm therapeutics [93].

From the host side, proteomic and metabolomic signatures of NTHi-induced acute OM in a chinchilla model were delineated in infected middle ear tissue lysates, revealing that establishment of disease coincides with actin morphogenesis, suppression of inflammatory mediators, and bacterial aerobic respiration. As a first step toward identification of clinically meaningful metabolic biomarkers, decreased biogenic amines and sphingomyelin molecules, increased taurine, glutamine and ornithine were observed upon infection [94].

Elucidating the metabolic determinants in the lung during respiratory infection is likely to be key to develop therapeutics modulating symptom and/or disease severity [95]. Lung metabolomics have not been performed on the *H. influenzae*-human airways interplay, but currently available insights on bacterial metabolism may guide us when assessing this infectious process. The *H. influenzae* RdKW20 strain drove the first genome-scale metabolic model. Besides assessing basic structural features of the *H. influenzae* metabolic network, such model facilitated addressing minimal substrates requirements for the network to allow biomass production. Minimal requirements included fructose, a likely preferred carbon source for which a phosphotransferase system (PTS) exists in *H. influenzae* [96,97], but fructose could also be replaced by other carbon sources including glucose [10,11]. *H. influenzae* possesses complete glycolysis and pentose phosphate pathways for glucose catabolism, lacks most enzymes of the oxidative branch of the Krebs cycle, and holds a respiratory chain with several dehydrogenases transferring electrons into the menaquinone pool, and terminal reductases transferring the electrons to a variety of electron acceptors, altogether driving a so-called glucose respiration-assisted fermentation, where acetate is the main end-product under aerobic growth. When oxygen is limiting, acetate is still produced but other products arise including formate and succinate, at variable rates depending on the tested strains [98–101]. End-product excretion profiling is informative not only from the bacterial perspective, but also due to their possible immunomodulatory roles. Although lung nutritional immunity keeps low glucose levels in the airway surface liquid of healthy individuals, respiratory disease generates a glucose-rich niche favorable for pathogens able to use glucose as carbon source. As this being the case for *H. influenzae*, glucose catabolism enhances bacterial growth, but also promotes the release of end-products acting as pro-inflammatory metabolites, more specifically acetate, which may contribute to lung colonization and inflammation in chronic respiratory patients [100]. Besides the above described genomic flexibility (see **Section 2**), *H. influenzae* metabolic versatility among strains has also been reported, in terms of substrate utilization, histidine synthesis or urease activity, suggesting metabolic adaptive traits favoring differential access to throat, ear, lower airways or blood niches [101–104].

Finally, and considering that *H. influenzae* metabolic machinery adapts to the host-imposed milieu, transcriptome signatures upon cell infection showed that the genes encoding the bacterial biosynthesis pathways of carbohydrates, lipids, amino acids, nucleotides, and energy metabolism were mostly downregulated, although the shikimate pathway for precursor chorismate production and the consequent tryptophan biosynthesis pathway was upregulated after initial bacterial-cell contact [87]. Increased tryptophan biosynthetic pathway was also observed in biofilms formed by strain variants adapted to transient FeHm restriction where, moreover, amino acids and enzymes associated with central metabolism, and metabolites associated with the urea cycle were also increased [81]. Linked to the metabolic machinery, attention should also be paid to bacterial metabolite transport systems. In fact, lactate, arginine, tryptophan, cysteine/glutathione, thiamine, thiamine pyrophosphate, iron and polyamines uptake and transport systems were highly expressed during *H. influenzae* cell infec-

tion [87]. Likewise, increased production of serine, sialic acid and tryptophan transporters was observed in biofilms formed by strain variants adapted to transient FeHm restriction [81], together suggesting that changes in central metabolism combined with increased nutrient stores may help counteracting nutritional immunity at the colonizing niches.

5. Future outlook

The last twenty five years, since the *H. influenzae* RdKW20 strain was genome sequenced, have gone a long way, greatly propelled by the unstoppable –omics technologies. As a human-adapted pathogen, integrative systems biology approaches to the interactions between *H. influenzae* and the human airways, are instrumental in the discovery of specific bacterial recognition, host signal transduction or immune tolerance, together with multi-omics approaches to decipher the genetic, immunologic, (post)transcriptional, (post)translational, and metabolic mechanisms underlying the outcome of such interactions. Those approaches will be enormously enriched by bacterial single-cell resolution methodologies such as microfluidics, or single-cell sorting, microscopy and genome/RNA sequencing, to allow overlooking the remarkable bacterial phenotypic heterogeneity, and shed light on complex phenotypes such as antibiotic persistence or metabolic specialization. Guidance of such integrative work by the human specificity of the infection will provide meaningful information on *H. influenzae* patho-adaptive evolution within the human host. Furthermore, we are collecting a wealth of genomic and epigenomic data, and this will continue to grow with the introduction of routine sequencing for disease surveillance. These data will be of great use to predict how changes in genome sequence lead to different host-pathogen interaction outcomes by applying machine learning approaches, or to build genome-scale metabolic network reconstructions assessing core and pan reactomes. Also, combination of deep bacterial phenotyping and pan-GWAS methodologies will allow not only predicting bacterial genotype-phenotype associations, but also deciphering genetic determinants of resistance to antimicrobials, virulence or niche adaptation. Altogether, therapeutic/vaccination target and biomarker discovery will be moved forward, to be eventually translated to the clinical settings and reach end users.

Funding

N.L.-L. is funded by a PhD studentship from Regional Navarra Govern, Spain, reference 0011-1408-2017-000000. C.G.-C. is funded by a PhD studentship from Agencia Española de Investigación (AEI), Spain, reference PRE2019-088382. This work has been funded by grants from MINECO RTI2018-096369-B-I00, 875/2019 from SEPAR, and PC150-151–152 from Gobierno de Navarra to J. G. CIBER is an initiative from Instituto de Salud Carlos III (ISCIII), Madrid, Spain.

Author contributions

Conceptualization: J.G.; writing (original draft preparation): N. L.-L. C.G.-C. and J.G.; writing (review and editing): all authors; supervision: J.G.; funding acquisition: J.G.

Declaration of Competing Interest

The authors declare that they have no known competing financial interests or personal relationships that could have appeared to influence the work reported in this paper.

Acknowledgment

We are grateful to the Garmendia's lab for manuscript critical reading.

References

[1] Jalalvand F, Riesbeck K. Update on non-typeable *Haemophilus influenzae*-mediated disease and vaccine development. Expert Rev Vaccines 2018;17:503–12. https://doi.org/10.1080/14760584.2018.1484286.
[2] Ladhani S, Slack MPE, Heath PT, von Gottberg A, Chandra M, Ramsay ME. Invasive *Haemophilus influenzae* disease, Europe, 1996–2006. Emerg Infect Dis 2010;16:455–63. https://doi.org/10.3201/eid1603.090290.
[3] Ahearn CP, Gallo MC, Murphy TF. Insights on persistent airway infection by non-typeable *Haemophilus influenzae* in chronic obstructive pulmonary disease. Pathog Dis 2017;75:1–18. https://doi.org/10.1093/femspd/ftx042.
[4] Duell BL, Su YC, Riesbeck K. Host–pathogen interactions of nontypeable *Haemophilus influenzae*: from commensal to pathogen. FEBS Lett 2016;590:3840–53. https://doi.org/10.1002/1873-3468.12351.
[5] Su YC, Jalalvand F, Thegerström J, Riesbeck K. The interplay between immune response and bacterial infection in COPD: focus upon non-typeable *Haemophilus influenzae*. Front Immunol 2018;9:1–26. https://doi.org/10.3389/fimmu.2018.02530.
[6] Tacconelli E, Carrara E, Savoldi A, Harbarth S, Mendelson M, Monnet DL, et al. Discovery, research, and development of new antibiotics: the WHO priority list of antibiotic-resistant bacteria and tuberculosis. Lancet Infect Dis 2018;18:318–27. https://doi.org/10.1016/S1473-3099(17)30753-3.
[7] Wen S, Feng D, Chen D, Yang L, Xu Z. Molecular epidemiology and evolution of *Haemophilus influenzae*. Infect Genet Evol 2020;80. https://doi.org/10.1016/j.meegid.2020.104205.
[8] Fleischmann R.D., Adams M.D., White O., Clayton R.A., Kirkness E.F., Kerlavage A.R., et al. Whole-genome random sequencing and assembly of *Haemophilus influenzae* Rd. Science (80-) 1995;269:496–512. doi:10.1126/science.7542800.
[9] Mell JC, Shumilina S, Hall IM, Redfield RJ. Transformation of natural genetic variation into *Haemophilus influenzae* genomes. PLoS Pathog 2011;7:32–4. https://doi.org/10.1371/journal.ppat.1002151.
[10] Edwards JS, Palsson BO. Systems properties of the *Haemophilus influenzae* Rd metabolic genotype. J Biol Chem 1999;274:17410–6. https://doi.org/10.1074/jbc.274.25.17410.
[11] Schilling CH, Palsson B. Assessment of the metabolic capabilities of *Haemophilus influenzae* Rd through a genome-scale pathway analysis. J Theor Biol 2000;203:249–83. https://doi.org/10.1006/jtbi.2000.1088.
[12] Gawronski JD, Wong SMS, Giannoukos G, Ward DV, Akerley BJ. Tracking insertion mutants within libraries by deep sequencing and a genome-wide screen for *Haemophilus* genes required in the lung. Proc Natl Acad Sci U S A 2009;106:16422–7. https://doi.org/10.1073/pnas.0906627106.
[13] Potts CC, Topaz N, Rodriguez-Rivera LD, Hu F, Chang HY, Whaley MJ, et al. Genomic characterization of *Haemophilus influenzae*: a focus on the capsule locus. BMC Genomics 2019;20:1–9. https://doi.org/10.1186/s12864-019-6145-8.
[14] Power PM, Bentley SD, Parkhill J, Moxon ER, Hood DW. Investigations into genome diversity of *Haemophilus influenzae* using whole genome sequencing of clinical isolates and laboratory transformants. BMC Microbiol 2012;12:1. https://doi.org/10.1186/1471-2180-12-273.
[15] Staples M, Graham RMA, Jennison AV. Characterisation of invasive clinical *Haemophilus influenzae* isolates in Queensland. Australia using whole-genome sequencing. Epidemiol Infect 2017;145:1727–36. https://doi.org/10.1017/S0950268817000450.
[16] Price EP, Sarovich DS, Nosworthy E, Beissbarth J, Marsh RL, Pickering J, et al. *Haemophilus influenzae*: using comparative genomics to accurately identify a highly recombinogenic human pathogen. BMC Genomics 2015;16:1–10. https://doi.org/10.1186/s12864-015-1857-x.
[17] Pinto M, González-Díaz A, Machado MP, Duarte S, Vieira L, Carriço JA, et al. Insights into the population structure and pan-genome of *Haemophilus influenzae*. Infect Genet Evol 2019;67:126–35. https://doi.org/10.1016/j.meegid.2018.10.025.
[18] De Chiara M, Hood D, Muzzi A, Pickard DJ, Perkins T, Pizza M, et al. Genome sequencing of disease and carriage isolates of nontypeable *Haemophilus influenzae* identifies discrete population structure. Proc Natl Acad Sci U S A 2014;111:5439–44. https://doi.org/10.1073/pnas.1403353111.
[19] Koonin EV, Makarova KS, Wolf YI. Evolution of microbial genomics: conceptual shifts over a quarter century. Trends Microbiol 2021:1–11. https://doi.org/10.1016/j.tim.2021.01.005.
[20] Rajendra KC, Leong KWC, Harkness NM, Lachowicz J, Gautam SS, Cooley LA, et al. Whole-genome analyses reveal gene content differences between nontypeable *Haemophilus influenzae* isolates from chronic obstructive pulmonary disease compared to other clinical phenotypes. Microb Genomics 2020;6:1–12. https://doi.org/10.1099/mgen.0.000405.
[21] Tanaka E, Wajima T, Nakaminami H, Noguchi N. Whole-genome sequence of *Haemophilus influenzae* ST422 outbreak clone strain 2018–Y40 with low quinolone susceptibility isolated from a paediatric patient. J Glob Antimicrob Resist 2020;22:759–61. https://doi.org/10.1016/j.jgar.2020.06.024.

[22] Su YC, Resman F, Hörhold F, Riesbeck K. Comparative genomic analysis reveals distinct genotypic features of the emerging pathogen *Haemophilus influenzae* type f. BMC Genomics 2014;15. https://doi.org/10.1186/1471-2164-15-38.
[23] Tsang RSW, Shuel M, Ahmad T, Hayden K, Knox N, Van Domselaar G, et al. Whole genome sequencing to study the phylogenetic structure of serotype a *Haemophilus influenzae* recovered from patients in Canada. Can J Microbiol 2020;66:99–110. https://doi.org/10.1139/cjm-2019-0406.
[24] Aziz A, Sarovich DS, Nosworthy E, Beissbarth J, Chang AB, Smith-Vaughan H, et al. Molecular signatures of nontypeable *Haemophilus influenzae* lung adaptation in pediatric chronic lung disease. Front Microbiol 2019;10. https://doi.org/10.3389/fmicb.2019.01622.
[25] Månsson V, Skaare D, Riesbeck K, Resman F. The spread and clinical impact of ST14CC-PBP3 type IIb/A, a clonal group of non-typeable *Haemophilus influenzae* with chromosomally mediated β-lactam resistance—a prospective observational study. Clin Microbiol Infect 2017;23:209.e1–7. https://doi.org/10.1016/j.cmi.2016.11.006.
[26] Andersson M, Resman F, Eitrem R, Drobni P, Riesbeck K, Kahlmeter G, et al. Outbreak of a β-lactam resistant non-typeable *Haemophilus influenzae* sequence type 14 associated with severe clinical outcomes. BMC Infect Dis 2015;15. https://doi.org/10.1186/s12879-015-1319-8.
[27] John MA, Beukers A, Chan R, van Hal S. Whole genome sequencing identifies opportunistic non-typeable *Haemophilus influenzae* rather than a hypervirulent clone. Pathology 2020:10–1. https://doi.org/10.1016/j.pathol.2020.08.011.
[28] Ritchie AI, Wedzicha JA. Definition, causes, pathogenesis, and consequences of chronic obstructive pulmonary disease exacerbations. Clin Chest Med 2020;41:421–38. https://doi.org/10.1016/j.ccm.2020.06.007.
[29] Celli BR, Wedzicha JA. Update on clinical aspects of chronic obstructive pulmonary disease. N Engl J Med 2019;381:1257–66. https://doi.org/10.1056/NEJMra1900500.
[30] Hurst JR, Vestbo J, Anzueto A, Locantore N, Müllerova H, Tal-Singer R, et al. Susceptibility to exacerbation in chronic obstructive pulmonary disease. N Engl J Med 2010;363:1128–38. https://doi.org/10.1056/NEJMoa0909883.
[31] Wedzicha JA, Seemungal TAR. COPD exacerbations: defining their cause and prevention. Lancet (London, England) 2007;370:786–96. https://doi.org/10.1016/S0140-6736(07)61382-8.
[32] Moleres J, Fernandez-Calvet A, Ehrlich RL, Marti S, Perez-Regidor L, Euba B, et al. Antagonistic pleiotropy in the bifunctional surface protein FadL (OmpP1) during adaptation of *Haemophilus influenzae* to chronic lung infection associated with chronic obstructive pulmonary disease. MBio 2018;9. https://doi.org/10.1128/mBio.01176-18.
[33] Pettigrew MM, Ahearn CP, Gent JF, Kong Y, Gallo MC, Munro JB, et al. *Haemophilus influenzae* genome evolution during persistence in the human airways in chronic obstructive pulmonary disease. Proc Natl Acad Sci U S A 2018;115:E3256–65. https://doi.org/10.1073/pnas.1719654115.
[34] Garmendia J, Viadas C, Calatayud L, Mell JC, Marti-Lliteras P, Euba B, et al. Characterization of nontypeable *Haemophilus influenzae* isolates recovered from adult patients with underlying chronic lung disease reveals genotypic and phenotypic traits associated with persistent infection. PLoS ONE 2014;9:. https://doi.org/10.1371/journal.pone.0097020e97020.
[35] Atack JM, Murphy TF, Pettigrew MM, Seib KL, Jennings MP. Non-typeable *Haemophilus influenzae* isolates from patients with chronic obstructive pulmonary disease contain new phase-variable *modA* methyltransferase alleles controlling phasevarions. Sci Rep 2019;9:1–10. https://doi.org/10.1038/s41598-019-52429-6.
[36] Gallo MC, Kirkham C, Eng S, Bebawee RS, Kong Y, Pettigrew MM, et al. Changes in IgA protease expression are conferred by changes in genomes during persistent infection by nontypeable *Haemophilus influenzae* in chronic obstructive pulmonary disease. Infect Immun 2018;86:1–11. https://doi.org/10.1128/IAI.00313-18.
[37] Mell JC, Redfield RJ. Natural competence and the evolution of DNA uptake specificity. J Bacteriol 2014;196:1471–83. https://doi.org/10.1128/JB.01293-13.
[38] Connor TR, Corander J, Hanage WP. Population subdivision and the detection of recombination in non-typeable *Haemophilus influenzae*. Microbiol (United Kingdom) 2012;158:2958–64. https://doi.org/10.1099/mic.0.063073-0.
[39] Mora M, Mell JC, Ehrlich GD, Ehrlich RL, Redfield RJ. Genome-wide analysis of DNA uptake across the outer membrane of naturally competent *Haemophilus influenzae*. IScience 2021;24: https://doi.org/10.1016/j.isci.2020.102007102007.
[40] Nørskov-Lauritsen N, Bruun B, Kilian M. Multilocus sequence phylogenetic study of the genus *Haemophilus* with description of *Haemophilus pittmaniae* sp. nov. Int J Syst Evol Microbiol 2005;55:449–56. https://doi.org/10.1099/ijs.0.63325-0.
[41] Hedegaard J, Okkels H, Bruun B, Kilian M, Mortensen KK, Nørskov-Lauritsen N. Phylogeny of the genus *Haemophilus* as determined by comparison of partial *infB* sequences. Microbiology 2001;147:2599–609. https://doi.org/10.1099/00221287-147-9-2599.
[42] Marti S, Puig C, de la Campa AG, Tirado-Velez JM, Tubau F, Domenech A, et al. Identification of *Haemophilus haemolyticus* in clinical samples and characterization of their mechanisms of antimicrobial resistance. J Antimicrob Chemother 2016;71:80–4. https://doi.org/10.1093/jac/dkv307.
[43] Frickmann H, Christner M, Donat M, Berger A, Essig A, Podbielski A, et al. Rapid discrimination of *Haemophilus influenzae*, *H. parainfluenzae*, and *H. haemolyticus* by fluorescence *in situ* hybridization (FISH) and two matrix-assisted laser-desorption-ionization time-of-flight mass spectrometry (MALDI-TOF-MS) Platforms. PLoS ONE 2013;8. https://doi.org/10.1371/journal.pone.0063222.
[44] Osman KL, Jefferies JMC, Woelk CH, Devos N, Pascal TG, Mortier MC, et al. Patients with chronic obstructive pulmonary disease harbour a variation of *Haemophilus* species. Sci Rep 2018;8:1–11. https://doi.org/10.1038/s41598-018-32973-3.
[45] Mell JC, Lee JY, Firme M, Sinha S, Redfie RJ. Extensive cotransformation of natural variation into chromosomes of naturally competent *Haemophilus influenzae*. G3 Genes Genomes, Genet 2014;4:717–31. https://doi.org/10.1534/g3.113.009597.
[46] Mell JC, Viadas C, Moleres J, Sinha S, Fernández-Calvet A, Porsch EA, et al. Transformed recombinant enrichment profiling rapidly identifies HMW1 as an intracellular invasion locus in *Haemophilus influenzae*. PLoS Pathog 2016:12. https://doi.org/10.1371/journal.ppat.1005576.
[47] Flusberg BA, Webster DR, Lee JH, Travers KJ, Olivares EC, Clark TA, et al. Direct detection of DNA methylation during single-molecule, real-time sequencing. Nat Methods 2010;7:461–5. https://doi.org/10.1038/nmeth.1459.
[48] Sánchez-Romero MA, Cota I, Casadesús J. DNA methylation in bacteria: from the methyl group to the methylome. Curr Opin Microbiol 2015;25:9–16. https://doi.org/10.1016/j.mib.2015.03.004.
[49] Sánchez-Romero MA, Casadesús J. The bacterial epigenome. Nat Rev Microbiol 2020;18:7–20. https://doi.org/10.1038/s41579-019-0286-2.
[50] Atack JM, Tan A, Bakaletz LO, Jennings MP, Seib KL. Phasevarions of bacterial pathogens: methylomics sheds new light on old enemies. Trends Microbiol 2018;26:715–26. https://doi.org/10.1016/j.tim.2018.01.008.
[51] Phillips ZN, Husna AU, Jennings MP, Seib KL, Atack JM. Phasevarions of bacterial pathogens-phase-variable epigenetic regulators evolving from restriction-modification systems. Microbiol (United Kingdom) 2019;165:917–28. https://doi.org/10.1099/mic.0.000805.
[52] Seib KL, Srikhanta YN, Atack JM, Jennings MP. Epigenetic regulation of virulence and immunoevasion by phase-variable restriction-modification systems in bacterial pathogens. Annu Rev Microbiol 2020;74:655–71. https://doi.org/10.1146/annurev-micro-090817-062346.
[53] Srikhanta YN, Maguire TL, Stacey KJ, Grimmond SM, Jennings MP. The phasevarion: a genetic system controlling coordinated, random switching of expression of multiple genes. Proc Natl Acad Sci U S A 2005;102:5547–51. https://doi.org/10.1073/pnas.0501169102.
[54] Atack JM, Srikhanta YN, Fox KL, Jurcisek JA, Brockman KL, Clark TA, et al. A biphasic epigenetic switch controls immunoevasion, virulence and niche adaptation in non-typeable *Haemophilus influenzae*. Nat Commun 2015;6. https://doi.org/10.1038/ncomms8828.
[55] Brockman KL, Azzari PN, Branstool MT, Atack JM, Schulz BL, Jen FEC, et al. Epigenetic regulation alters biofilm architecture and composition in multiple clinical isolates of nontypeable *Haemophilus influenzae*. MBio 2018;9:1–15. https://doi.org/10.1128/mBio.01682-18.
[56] Brockman KL, Branstool MT, Atack JM, Robledo-Avila F, Partida-Sanchez S, Jennings MP, et al. The ModA2 phasevarion of nontypeable *Haemophilus influenzae* regulates resistance to oxidative stress and killing by human neutrophils. Sci Rep 2017;7:1–11. https://doi.org/10.1038/s41598-017-03552-9.
[57] Brockman KL, Jurcisek JA, Atack JM, Srikhanta YN, Jennings MP, Bakaletz LO. ModA2 phasevarion switching in nontypeable *Haemophilus influenzae* increases the severity of experimental otitis media. J Infect Dis 2016;214:817–24. https://doi.org/10.1093/infdis/jiw243.
[58] Robledo-Avila FH, Ruiz-Rosadode JD, Partida-Sanchez S, Brockman KL. A Bacterial epigenetic switch in non-typeable Haemophilus influenzae modifies host immune response during otitis media. Front Cell Infect Microbiol 2020;10:512743. https://doi.org/10.3389/fcimb.2020.512743.
[59] VanWagoner TM, Atack JM, Nelson KL, Smith HK, Fox KL, Jennings MP, et al. The *modA10* phasevarion of nontypeable *Haemophilus influenzae* R2866 regulates multiple virulence-associated traits. Microb Pathog 2016;92:60–7. https://doi.org/10.1016/j.micpath.2015.12.006.
[60] Hardison RL, Harrison A, Wallace RM, Heimlich DR, O'Bryan ME, Sebra RP, et al. Microevolution in response to transient heme-iron restriction enhances intracellular bacterial community development and persistence. PLoS Pathog 2018;14:1–25. https://doi.org/10.1371/journal.ppat.1007355.
[61] Harrison A, Hardison RL, Fullen AR, Wallace RM, Gordon DM, White P, et al. Continuous microevolution accelerates disease progression during sequential episodes of infection. Cell Rep 2020;30:2978–2988.e3. https://doi.org/10.1016/j.celrep.2020.02.019.
[62] van Opijnen T, Bodi KL, Camilli A. Tn-seq: High-throughput parallel sequencing for fitness and genetic interaction studies in microorganisms. Nat Methods 2009;6:767–72. https://doi.org/10.1038/nmeth.1377.
[63] Van Opijnen T, Camilli A. Transposon insertion sequencing: a new tool for systems-level analysis of microorganisms. Nat Rev Microbiol 2013;11:435–42. https://doi.org/10.1038/nrmicro3033.
[64] Cain AK, Barquist L, Goodman AL, Paulsen IT, Parkhill J, van Opijnen T. A decade of advances in transposon-insertion sequencing. Nat Rev Genet 2020;21:526–40. https://doi.org/10.1038/s41576-020-0244-x.
[65] Burby PE, Nye TM, Schroeder JW, Simmons LA. Implementation and data analysis of Tn-seq, whole-genome resequencing, and single-molecule real-time sequencing for bacterial genetics. J Bacteriol 2017;199:1–11. https://doi.org/10.1128/JB.00560-16.

[66] Wong SMS, Akerley BJ. Genome-scale approaches to identify genes essential for *Haemophilus influenzae* pathogenesis. Front Cell Infect Microbiol 2012;2:23. https://doi.org/10.3389/fcimb.2012.00023.
[67] Wong SM, Bernui M, Shen H, Akerley BJ. Genome-wide fitness profiling reveals adaptations required by *Haemophilus* in coinfection with influenza A virus in the murine lung. Proc Natl Acad Sci U S A 2013;110:15413–8. https://doi.org/10.1073/pnas.1311217110.
[68] Wong SM, Jackson MD, Akerley BJ. Suppression of alternative lipooligosaccharide glycosyltransferase activity by UDP-galactose epimerase enhances murine lung infection and evasion of serum IgM. Front Cell Infect Microbiol 2019;9:160. https://doi.org/10.3389/fcimb.2019.00160.
[69] Mobegi FM, van Hijum SAFT, Burghout P, Bootsma HJ, de Vries SPW, van der Gaast-de Jongh CE, et al. From microbial gene essentiality to novel antimicrobial drug targets. BMC Genomics 2014;15. 10.1186/1471-2164-15-958.
[70] Langereis JD, Zomer A, Stunnenberg HG, Burghout P, Hermans PWM. Nontypeable *Haemophilus influenzae* carbonic anhydrase is important for environmental and intracellular survival. J Bacteriol 2013;195:2737–46. https://doi.org/10.1128/JB.01870-12.
[71] Langereis JD, de Jonge MI, Weiser JN. Binding of human factor H to outer membrane protein P5 of non-typeable *Haemophilus influenzae* contributes to complement resistance. Mol Microbiol 2014;94:89–106. https://doi.org/10.1111/mmi.12741.
[72] Langereis JD, Weiser JN. Shielding of a lipooligosaccharide IgM epitope allows evasion of neutrophil-mediated killing of an invasive strain of nontypeable *Haemophilus influenzae*. MBio 2014;5:1–10. https://doi.org/10.1128/mBio.01478-14.
[73] Marti S, Puig C, Merlos A, Viñas M, de Jonge MI, Liñares J, et al. Bacterial lysis through interference with peptidoglycan synthesis increases biofilm formation by nontypeable *Haemophilus influenzae*. MSphere 2017;2:1–12. https://doi.org/10.1128/msphere.00329-16.
[74] De Saizieu A, Certa U, Warrington J, Gray C, Keck W, Mous J. Bacterial transcript imaging by hybridization of total RNA to oligonucleotide arrays. Nat Biotechnol 1998;16:45–8. https://doi.org/10.1038/nbt0198-45.
[75] Wong SMS, Alugupalli KR, Ram S, Akerley BJ. The ArcA regulon and oxidative stress resistance in *Haemophilus influenzae*. Mol Microbiol 2007;64:1375–90. https://doi.org/10.1111/j.1365-2958.2007.05747.x.
[76] Jiang D, Tikhomirova A, Kidd SP. *Haemophilus influenzae* strains possess variations in the global transcriptional profile in response to oxygen levels and this influences sensitivity to environmental stresses. Res Microbiol 2016;167:13–9. https://doi.org/10.1016/j.resmic.2015.08.004.
[77] Whitby PW, VanWagoner TM, Scale TW, Morton DJ, Stull TL. Transcriptional profile of *Haemophilus influenzae*: effects of iron and heme. J Bacteriol 2006;188:5640–5. https://doi.org/10.1128/JB.00417-06.
[78] Whitby PW, Seale TW, VanWagoner TM, Morton DJ, Stull TL. The iron/heme regulated genes of *Haemophilus influenzae*: comparative transcriptional profiling as a tool to define the species core modulon. BMC Genomics 2009;10:1–19. https://doi.org/10.1186/1471-2164-10-6.
[79] Whitby PW, VanWagoner TM, Seale TW, Morton DJ, Stull TL. Comparison of transcription of the *Haemophilus influenzae* iron/heme modulon genes *in vitro* and *in vivo* in the chinchilla middle ear. BMC Genomics 2013;14. https://doi.org/10.1186/1471-2164-14-925.
[80] Santana EA, Harrison A, Zhang X, Baker BD, Kelly BJ, White P, et al. HrrF is the Fur-regulated small RNA in nontypeable *Haemophilus influenzae*. PLoS One 2014;9. https://doi.org/10.1371/journal.pone.0105644.
[81] Harrison A, Hardison RL, Wallace RM, Fitch J, Heimlich DR, Bryan MO, et al. Reprioritization of biofilm metabolism is associated with nutrient adaptation and long-term survival of *Haemophilus influenzae*. Npj Biofilms Microbiomes 2019;5. https://doi.org/10.1038/s41522-019-0105-6.
[82] Redfield RJ, Cameron ADS, Qian Q, Hinds J, Ali TR, Kroll JS, et al. A novel CRP-dependent regulon controls expression of competence genes in *Haemophilus influenzae*. J Mol Biol 2005;347:735–47. https://doi.org/10.1016/j.jmb.2005.01.012.
[83] Black HF, Mastromatteo S, Sinha S, Ehrlich RL, Nislow C, Mell JC, et al. A competence-regulated toxin-antitoxin system in *Haemophilus influenzae*. PLoS ONE 2020;15:1–23. https://doi.org/10.1371/journal.pone.0217255.
[84] Cherkaoui A, Diene SM, Fischer A, Leo S, François P, Schrenzel J. Transcriptional modulation of penicillin-binding protein 1b, outer membrane protein P2 and efflux pump (AcrAB-TolC) during heat stress is correlated to enhanced bactericidal action of imipenem on non-typeable *Haemophilus influenzae*. Front Microbiol 2018;8:1–12. https://doi.org/10.3389/fmicb.2017.02676.
[85] Euba B, Moleres J, Segura V, Viadas C, Morey P, Moranta D, et al. Genome expression profiling-based identification and administration efficacy of host-directed antimicrobial drugs against respiratory infection by nontypeable *Haemophilus influenzae*. Antimicrob Agents Chemother 2015;59:7581–92. https://doi.org/10.1128/AAC.01278-15.
[86] Hernandez M, Leichtle A, Pak K, Webster NJ, Wasserman SI, Ryan AF. The transcriptome of a complete episode of acute otitis media. BMC Genomics 2015;16:1–16. https://doi.org/10.1186/s12864-015-1475-7.
[87] Baddal B, Muzzi A, Censini S, Calogero RA, Torricelli G, Guidotti S, et al. Dual RNA-seq of nontypeable *Haemophilus influenzae* and host cell transcriptomes reveals novel insights into host-pathogen cross talk. MBio 2015;6:1–14. https://doi.org/10.1128/mBio.01765-15.
[88] Karlsson R, Thorsell A, Gomila M, Salvà-Serra F, Jakobsson HE, Gonzales-Siles L, et al. Discovery of species-unique peptide biomarkers of bacterial pathogens by tandem mass spectrometry-based proteotyping. Mol Cell Proteomics 2020;19:518–28. https://doi.org/10.1074/mcp.RA119.001667.
[89] Qu J, Lesse AJ, Brauer AL, Cao J, Gill SR, Murphy TF. Proteomic expression profiling of *Haemophilus influenzae* grown in pooled human sputum from adults with chronic obstructive pulmonary disease reveal antioxidant and stress responses. BMC Microbiol 2010;10. https://doi.org/10.1186/1471-2180-10-162.
[90] Preciado D, Poley M, Tsai S, Tomney A, Brown K, Val S. A proteomic characterization of NTHi lysates. Int J Pediatr Otorhinolaryngol 2016;80:8–16. https://doi.org/10.1016/j.ijporl.2015.11.016.
[91] Post DMB, Held JM, Ketterer MR, Phillips NJ, Sahu A, Apicella MA, et al. Comparative analyses of proteins from *Haemophilus influenzae* biofilm and planktonic populations using metabolic labeling and mass spectrometry. BMC Microbiol 2014;14:329. https://doi.org/10.1186/s12866-014-0329-9.
[92] De Souza-Hart JA, Blackstock W, Di Modugno V, Holland IB, Kok M. Two-component systems in *Haemophilus influenzae*: a regulatory role for ArcA in serum resistance. Infect Immun 2003;71:163–72. https://doi.org/10.1128/iai.71.1.163-172.2003.
[93] Mokrzan EM, Ahearn CP, Buzzo JR, Novotny LA, Zhang Y, Goodman SD, et al. Nontypeable *Haemophilus influenzae* newly released (NRel) from biofilms by antibody-mediated dispersal versus antibody-mediated disruption are phenotypically distinct. Biofilm 2020;2:. https://doi.org/10.1016/j.bioflm.2020.100039100039.
[94] Harrison A, Dubois LG, John-Williams LS, Moseley MA, Hardison RL, Heimlich DR, et al. Comprehensive proteomic and metabolomic signatures of nontypeable *Haemophilus influenzae*-induced acute otitis media reveal bacterial aerobic respiration in an immunosuppressed environment. Mol Cell Proteomics 2016;15:1117–38. https://doi.org/10.1074/mcp.M115.052498.
[95] Bernatchez JA, McCall LI. Insights gained into respiratory infection pathogenesis using lung tissue metabolomics. PLoS Pathog 2020;16:1–8. https://doi.org/10.1371/journal.ppat.1008662.
[96] Macfadyen LP, Redfield RJ. Life in mucus: Sugar metabolism in *Haemophilus influenzae*. Res Microbiol 1996;147:541–51. https://doi.org/10.1016/0923-2508(96)84010-1.
[97] Macfadyen LP, Dorocicz IR, Reizer J, Saler MH, Redfield RJ. Regulation of competence development and sugar utilization in *Haemophilus influenzae* Rd by a phosphoenolpyruvate:fructose phosphotransferase system. Mol Microbiol 1996;21:941–52. https://doi.org/10.1046/j.1365-2958.1996.441420.x.
[98] Raghunathan A, Price ND, Galperin MY, Makarova KS, Purvine S, Picone AF, et al. *In silico* metabolic model and protein expression of *Haemophilus influenzae* strain Rd KW20 in rich medium. Omi A J Integr Biol 2004;8:25–41. https://doi.org/10.1089/153623104773547471.
[99] Othman DSMP, Schirra H, McEwan AG, Kappler U. Metabolic versatility in *Haemophilus influenzae*: a metabolomic and genomic analysis. Front Microbiol 2014;5:1–10. https://doi.org/10.3389/fmicb.2014.00069.
[100] López-López N, Euba B, Hill J, Dhouib R, Caballero L, Leiva J, et al. *Haemophilus influenzae* glucose catabolism leading to production of the immunometabolite acetate has a key contribution to the host airway-pathogen interplay. ACS Infect Dis 2020;6:406–21. https://doi.org/10.1021/acsinfecdis.9b00359.
[101] Muda NM, Nasreen M, Dhouib R, Hosmer J, Hill J, Mahawar M, et al. Metabolic analyses reveal common adaptations in two invasive *Haemophilus influenzae* strains. Pathog Dis 2019;77:1–12. https://doi.org/10.1093/femspd/ftz015.
[102] Juliao PC, Marrs CF, Xie J, Gilsdorf JR. Histidine auxotrophy in commensal and disease-causing nontypeable *Haemophilus influenzae*. J Bacteriol 2007;189:4994–5001. https://doi.org/10.1128/JB.00146-07.
[103] Zhang L, Patel M, Xie J, Davis GS, Marrs CF, Gilsdorf JR. Urease operon and urease activity in commensal and disease-causing nontypeable *Haemophilus influenzae*. J Clin Microbiol 2013;51:653–5. https://doi.org/10.1128/JCM.03145-12.
[104] Murphy TF, Brauer AL. Expression of urease by *Haemophilus influenzae* during human respiratory tract infection and role in survival in an acid environment. BMC Microbiol 2011;11. https://doi.org/10.1186/1471-2180-11-183.

López-López, N., Euba, B., Hill, J., Dhouib, R., Caballero, L., Leiva, J., Hosmer, J., Cuesta, S., Ramos-Vivas, J., Díez-Martínez, R., Schirra, H. J., Blank, L. M., Kappler, U., & Garmendia, J. (2020). Haemophilus influenzae glucose catabolism leading to production of the immunometabolite acetate has a key contribution to the host airway–pathogen interplay. ACS Infectious Diseases, 6(3), 406-421. https://doi.org/10.1021/acsinfecdis.9b00359

Haemophilus influenzae glucose catabolism leading to production of the immunometabolite acetate has a key contribution to the host airway-pathogen interplay

Nahikari López-López[1], Begoña Euba[1,2], Julian Hill[3], Rabeb Dhouib[3], Lucía Caballero[1], José Leiva[4,5], Jennifer Hosmer[3], Sergio Cuesta[1], José Ramos-Vivas[6,7], Roberto Díez-Martínez[8], Horst Joachim Schirra[9], Lars M. Blank[10], Ulrike Kappler[3*], Junkal Garmendia[1,2*]

[1]Instituto de Agrobiotecnología, CSIC-Gobierno Navarra, Mutilva, Spain; [2]Centro de Investigación Biomédica en Red de Enfermedades Respiratorias (CIBERES), Madrid, Spain; [3]Australian Infectious Diseases Research Centre, School of Chemistry and Molecular Biosciences, The University of Queensland, St. Lucia QLD 4072, Australia; [4]Servicio de Microbiología, Clínica Universidad de Navarra, Pamplona, Spain; [5]Instituto de Investigación Sanitaria de Navarra (IdiSNA), Pamplona, Spain; [6]Servicio Microbiología, Hospital Universitario Marqués de Valdecilla and Instituto de Investigación Marqués de Valdecilla (IDIVAL), Santander, Spain; [7]Red Española de Investigación en Patología Infecciosa (REIPI), ISCIII, Madrid, Spain; [8]Telum Therapeutics, Centro Europeo de Empresas e Innovación de Navarra (CEIN), Noáin, Spain; [9]Centre for Advanced Imaging, The University of Queensland, St Lucia, QLD 4072, Australia; [10]Institute of Applied Biotechnology, RWTH Aachen University, 52074 Aachen, Germany

Content:

Figure S1. Growth medium modifies the expression of *H. influenzae* genes involved in central carbon metabolism and respiration.

Figure S2. Changes in metabolite concentrations in cultures of *H. influenzae* NTHi411, NTHi584 and NTHi1104, grown under microaerophilic conditions.

Figure S3. Expression of genes involved in central carbon metabolism and respiration in strain NTHi411.

Figure S4. Effect of inactivating the *ackA*, *pflA* and *frdA* genes on *H. influenzae* growth and morphology.

Figure S5. Supportive information on approaches employed for *H. influenzae* Δ*ackA* mutant complementation.

Figure S6. Inactivation of the *ackA*, *pflA* and *frdA* genes modifies *H. influenzae* production of glucose catabolism endproducts.

Table S1. Plasmids used in this study.

Table S2. Primers used in this study.

Table S3. Key metabolites detected by HPLC in culture supernantants of CDM grown *H. influenzae* RdKW20 WT and mutant strains.

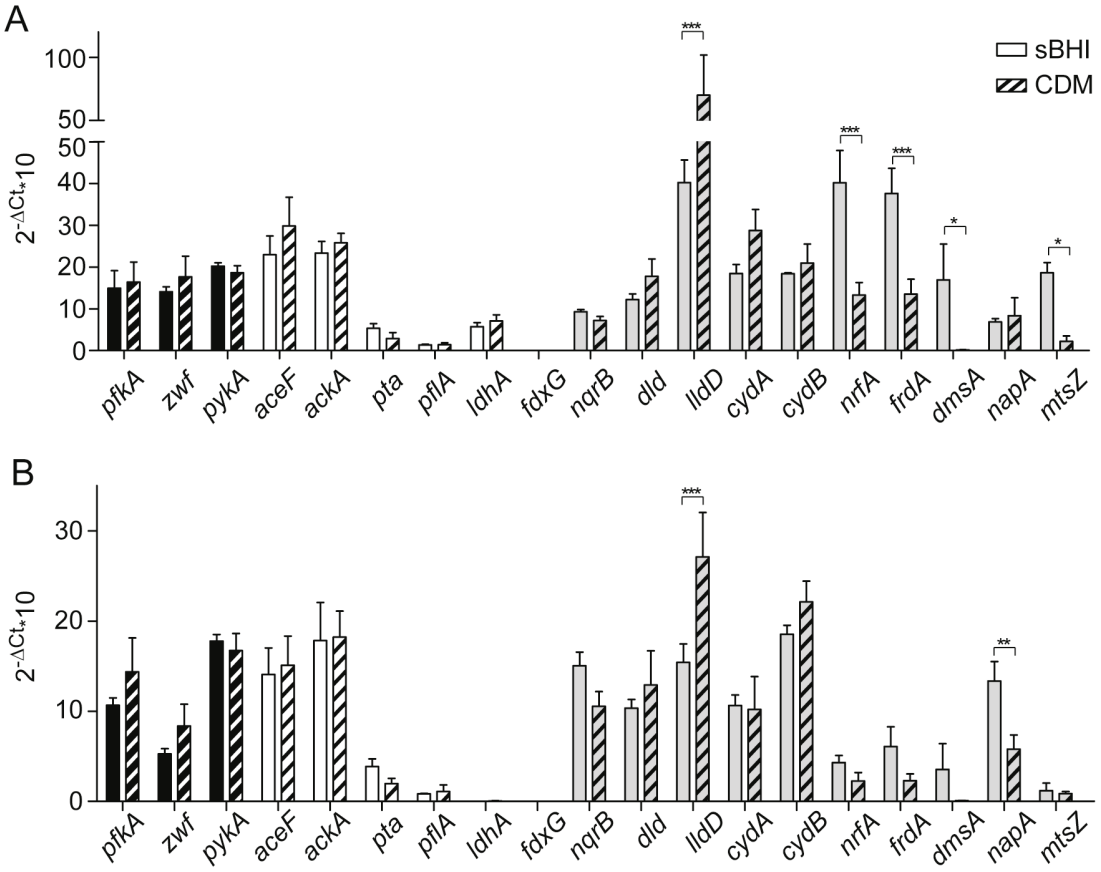

Figure S1. Growth medium modifies the expression of *H. influenzae* genes involved in central carbon metabolism and respiration. Expression of the *pfkA*, *zwf*, *pykA*, *aceF*, *ackA*, *pta*, *pflA*, *ldhA*, *fdxG*, *nqrB*, *dld*, *lldD*, *cydA*, *cydB*, *nrfA*, *frdA*, *dmsA*, *napA* and *mtsZ* genes in HiRdKW20 **(A)** and NTHi411 **(B)** strains, grown in sBHI or CDM, under aerobic conditions. Black bars: genes involved in glucose catabolism; white bars: genes relevant for pyruvate conversions; gray bars: genes relevant for respiratory metabolism. In both RdKW20 and NTHi411, the *lldD* gene expression was higher in CDM than in sBHI. In RdKW20, expression of the *nrfA*, *frdA*, *dmsA* and *mtsZ* genes was lower in CDM than in sBHI. In NTHi411, the *napA* gene expression was lower in CDM than in sBHI. Data are shown as mean±SD. Statistical comparisons of the means were performed with two-way ANOVA (Sidak´s multiple comparisons test). *$p < 0.01$, **$p < 0.001$, ***$p < 0.0001$.

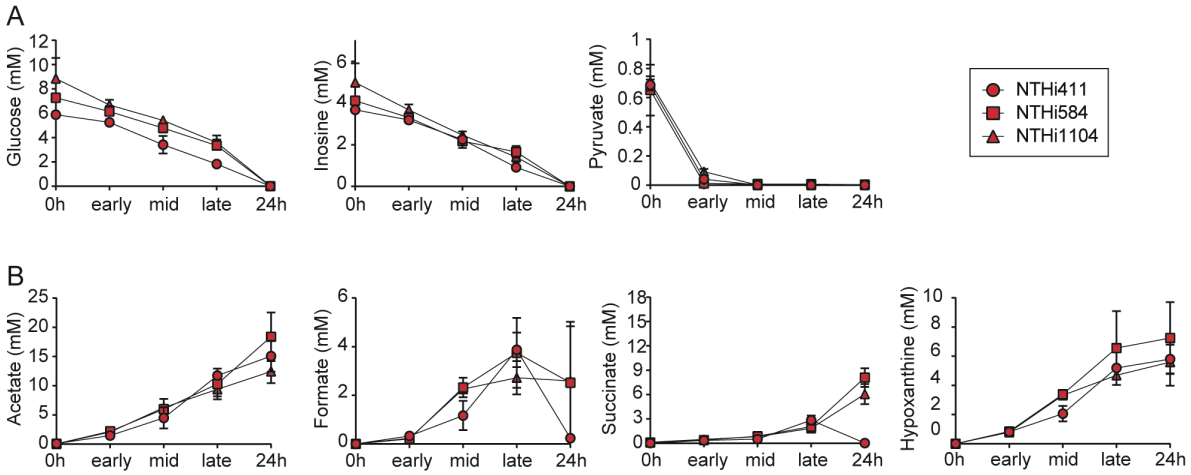

Figure S2. Changes in metabolite concentrations in cultures of *H. influenzae* NTHi411, NTHi584 and NTHi1104, grown under microaerophilic conditions. Strains are indicated in the right insert. NMR data shown is for three CDM growth substrates, glucose, inosine and pyruvate **(A)**, and for four metabolites produced during growth, acetate, formate, succinate and hypoxanthine **(B)**.

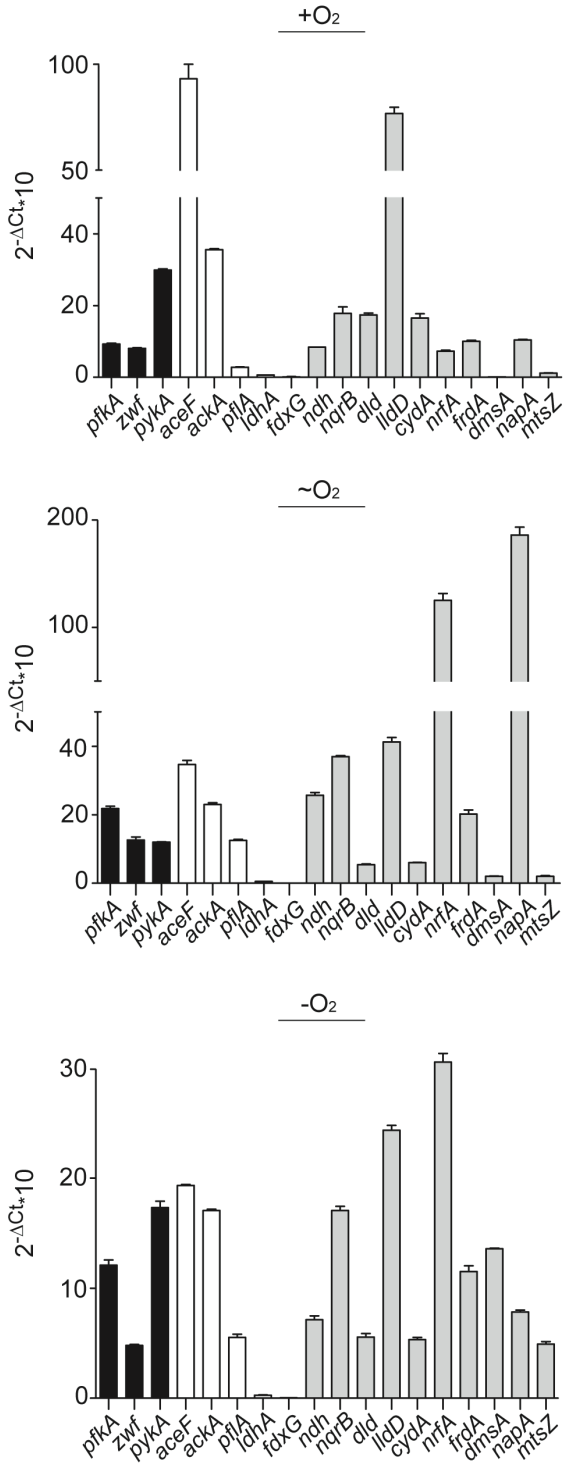

Figure S3. Expression of genes involved in central carbon metabolism and respiration in strain NTHi411. Expression of the *pfkA*, *zwf*, *pykA*, *aceF*, *ackA*, *pflA*, *ldhA*, *fdxG*, *ndh*, *nqrB*, *dld*, *lldD*, *cydA*, *nrfA*, *frdA*, *dmsA*, *napA*, *mtsZ* genes in NTHi411 grown in CDM medium under aerobic **(A)** microaerophilic **(B)** and anaerobic **(C)** conditions. Black bars: genes relevant for glucose catabolism; white bars: genes relevant for pyruvate conversion; gray bars: genes relevant for respiratory metabolism. Data are shown as mean±SD.

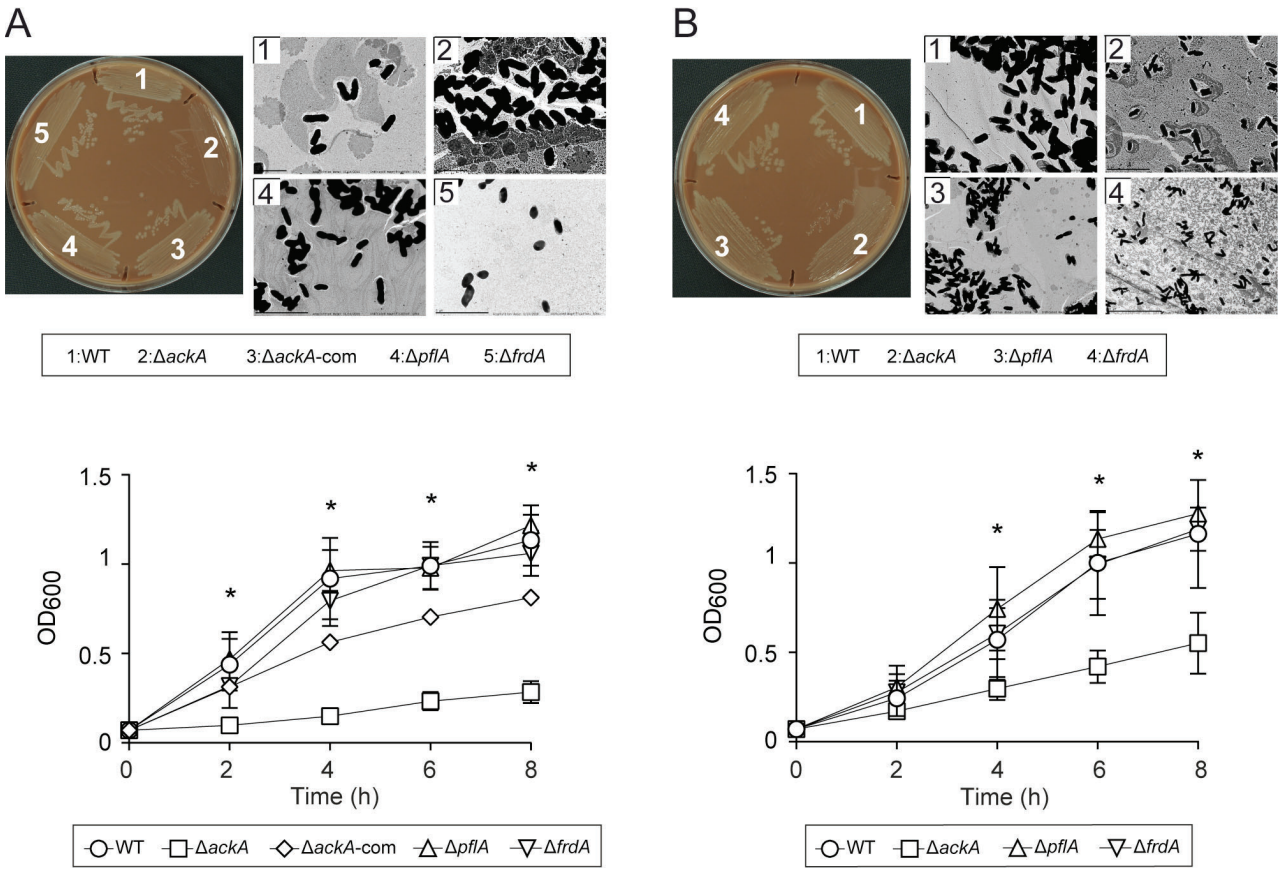

Figure S4. Effect of inactivating the *ackA*, *pflA* and *frdA* genes on *H. influenzae* growth and morphology. Data for RdKW20 and NTHi411 WT and mutant strains are shown in **(A)** and **(B)**, respectively. **(A)** Morphology at colony (left) and single bacteria (right) level, upon growth on chocolate agar. Data are shown for RdKW20 WT (1), Δ*ackA* (2), Δ*ackA*-com (3), Δ*pflA* (4), and Δ*frdA* (5) strains. Single bacterial morphology is shown by TEM. Magnification: WT, 15000x; Δ*ackA*, 15000x; Δ*pflA*, 10000x; Δ*frdA*, 10000x. Bottom panel: bacterial growth in sBHI shown as a mean of OD_{600}, at the indicated time points (mean±SD). RdKW20Δ*ackA* and Δ*frdA* showed lower OD_{600} than the WT strain (Δ*ackA*, $p<0.0001$ at all datapoints; Δ*frdA*, at 4 h, 6 h and 8 h, $p<0.005$). **(B)** Morphology at colony (left) and single bacteria (right) level, upon growth on chocolate agar. Data are shown for NTHi411 WT (1), Δ*ackA* (2), Δ*pflA* (3), and Δ*frdA* (4) strains. Single bacterial morphology is shown by TEM. Magnification: WT, 15000x; Δ*ackA*, 8000x; Δ*pflA*, 8000x; Δ*frdA*, 5000x. Bottom panel: bacterial growth in sBHI shown as a mean of OD_{600}, at the indicated time points (mean±SD). NTHi411Δ*ackA* showed lower OD_{600} than the WT strain (at 4 h $p<0.005$ and 6 h and 8 h, $p<0.0001$).

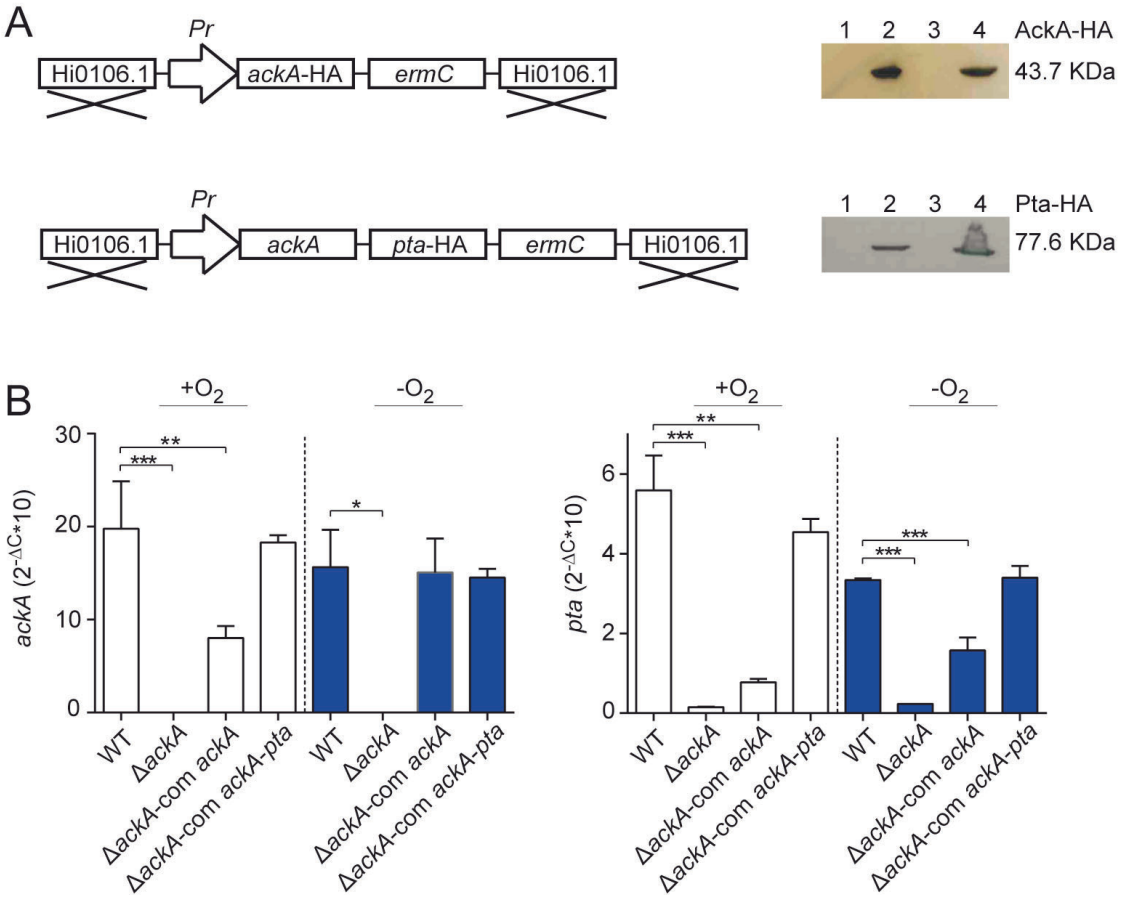

Figure S5. Supportive information on approaches employed for *H. influenzae* Δ*ackA* mutant complementation. (A) Upper panel: Δ*ackA* complementation cassette with the *ackA* gene and its promoter region, generated as it follows: the *ackA* gene with its promoter region was amplified from NTHi411 genomic DNA using primers *ackA*-COMP-*XhoI*-Fw and *ackA*-HA-COMP-*XhoI*-Rv. Primer *ackA*-HA-COMP-*XhoI*-Rv introduced a HA tail in the 3´end of the *ackA* gene. This PCR product (1,757 bp) was *Xho*I digested and cloned into *Xho*I-digested pUC19-HI0601.1-Erm [1], generating pUC19-HI0601.1-Erm-*Pr::ackA*. This plasmid was used as a template to amplify a 5,285 bp DNA fragment containing HI0601.1-flanked *Pr::ackA* by using primers HI0601.1-F1 and HI0601.1-R1, which was used to naturally transform RdKW20Δ*ackA*. Transformants were selected on sBHI agar with $Spec_{30}$ and Erm_{11}. AckA-HA (43.7 KDa) was monitored by western blot (WB). WB lanes: 1. *E. coli* Top10; 2. *E. coli* Top10 (pUC19-HI0601.1-Erm-*Pr::ackA*); 3. RdKW20 WT strain; 4. RdKW20Δ*ackA*-com *ackA*. Lower panel: RdKW20Δ*ackA* complementation cassette with the *ackA-pta* operon and its promoter region (for construct details, see Methods section). Pta-HA (77.6 KDa) was monitored by WB. WB lanes: 1. *E. coli* Top10; 2. *E. coli* Top10 (pUC19-HI0601.1::Erm-*Pr::ackA-pta*); 3. RdKW20 WT strain; 4. RdKW20Δ*ackA*-com *ackA-pta*. **(B)** Expression of the *ackA* and *pta* genes in RdKW20 WT, Δ*ackA* and Δ*ackA* complemented strains, exponentially grown in CDM, under aerobic and anaerobic conditions (mean±SEM). The *ackA* gene expression was not detected in RdKW20Δ*ackA* strain. Complementation with *Pr::ackA*-HA partially restored *ackA* gene expression in aerobiosis. The *pta* gene expression was lower in RdKW20Δ*ackA* and RdKW20Δ*ackA*-com *ackA* than in the WT strain. Complementation with *Pr::ackA-pta*-HA restored *ackA* and *pta* gene expression. RdKW20Δ*ackA*-com *ackA-pta* (from now on, named as RdKW20Δ*ackA*-com) was used in all phenotypic assays shown in this study. *p < 0.01, **p < 0.001, ***p < 0.0001.

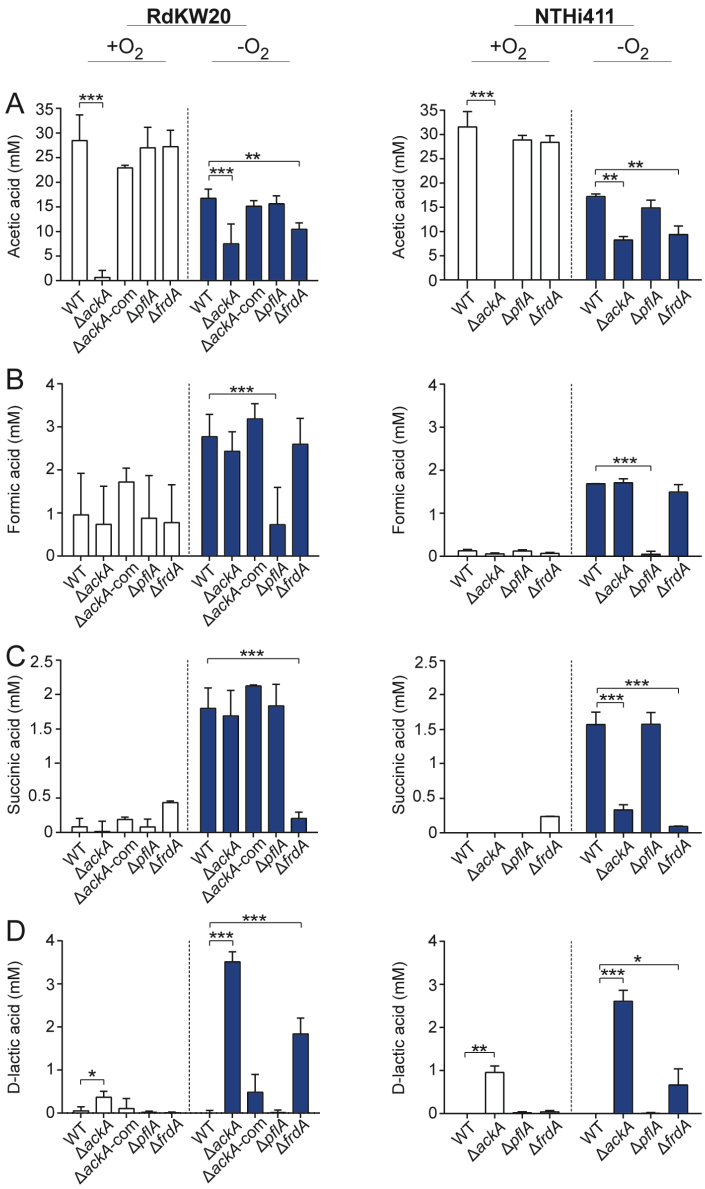

Figure S6. Inactivation of the *ackA*, *pflA* and *frdA* genes modifies *H. influenzae* production of glucose catabolism endproducts. Enzymatic measure of acetic (**A**), formic (**B**), succinic (**C**) and D-lactic (**D**) acid, determined on CDM bacterial culture supernatants grown for 24 h. Each metabolite concentration is shown as mM (mean±SD). Data for RdKW20 and NTHi411 strains are shown on the left and right columns, respectively. In RdKW20, reduced acetic acid levels were observed for the Δ*ackA* and Δ*frdA* mutants grown in aerobic and anaerobic conditions; decreased formic acid concentration was determined for Δ*pflA* grown in anaerobiosis; decreased succinic acid was found for Δ*frdA* under anaerobiosis; increased D-lactic acid level was measured for Δ*ackA*, and for Δ*frdA* (anaerobiosis) strains, compared to WT. In NTHi411, reduced acetic acid levels were measured for Δ*ackA* and Δ*frdA* mutants grown in aerobic and anaerobic conditions; decreased formic acid was quantified for Δ*pflA* bacteria grown in anaerobiosis; decreased succinic acid was measured for Δ*ackA* and Δ*frdA* mutants grown in anaerobiosis; increased D-lactic acid level was determined in Δ*ackA*, and for Δ*frdA* (anaerobiosis) strains, compared to WT. Statistical comparisons of the means with Two-way ANOVA (Dunnett's multiple comparisons test). *$p < 0.01$, **$p < 0.001$, ***$p < 0.0001$.

Table S1. Plasmids used in this study.

Plasmids	Description	Source
pJET1.2/blunt	Cloning vector	Thermofisher
pJET1.2-*ackA*	pJET1.2 derivative containing a 3,188 bp DNA fragment carrying the *ackA* gene (1,206 bp) and its upstream (1,000 bp) and downstream (982 bp) flanking regions	This study
pJET1.2-*pflA*	pJET1.2 derivative containing a 2,705 bp DNA fragment carrying the *pflA* gene (741 bp) and its upstream (964 bp) and downstream (995 bp) flanking regions	This study
pJET1.2-*frdA*	pJET1.2 derivative containing a 2,823 bp DNA fragment carrying the *frdA* gene (1800bp) and its upstream (510 bp) and downstream (513 bp) flanking regions	This study
pJET1.2-*ackA::spec*	pJET1.2-*ackA* derivative containing a 4,079 bp DNA fragment carrying an *ackA::spec* disruption cassette	This study
pJET1.2-*pflA::spec*	pJET1.2-*pflA* derivative containing a 4,050 bp DNA fragment carrying a *pflA::spec* disruption cassette	This study
pJET1.2-*frdA::ermC*	pJET1.2-*frdA* derivative containing a 3,337 bp DNA fragment carrying a *frdA::ermC* disruption cassette	This study
pUC19-HI0601.1-Erm-*Pr::ackA*	A 1,757 bp PCR fragment containing *Pr*::*ackA*-HA was *Xho*I digested and cloned into pUC19/Hi0601.1::*ermC* previously *Xho*I digested and de-P	This study
pUC19-HI0601.1-Erm	Cloning vector to generate mutant complementation cassettes to be inserted into the *H. influenzae* HI0601.1 pseudogene	[1]
pUC19-HI0601.1-Erm-*Pr::ackA-pta*	A 3,936 bp PCR fragment containing *Pr*::*ackA-pta*-HA was *Xho*I digested and cloned into pUC19/Hi0601.1::*ermC* previously *Xho*I digested and de-P	This study
pSBLerm	Source of an Erm^R cassette.	[2]
pRSM2832	pKD13 derivative carrying a cassette containing a Spec resistance gene flanked by FRT sites	[3]

Table S2. Primers used in this study.

Primer name	Primer ID	Sequence (5'-3')	Purpose	Reference
ackA-F1	1446	CTAATTGACTAATCACATAATTTACTAT	Gene inactivation	This study
ackA-R1	1447	GCCTGTTAATAAAATACCGCCGATTTC	Gene inactivation	This study
pflA-F1	1442	GCCTTAAACGTAATCCACTATATGCAC	Gene inactivation	This study
pflA-R1	1443	GAATTGACCGTGCTACACGTGAACAAC	Gene inactivation	This study
ackA-F2	1448	TCTTAGATGATGGATTTCTATTAACCTCAATCAAAT ATAGGGTTCCTATGATTCCGGGGATCCGTCGACC	Gene inactivation	This study
ackA-R2	1449	GCCGAAAAATTCGGCAGCTTGTTGTTAATTTAGAAA CAAAGTTTTGCGGTTGTAGGCTGGAGCTGCTTCG	Gene inactivation	This study
pflA-F2	1444	AAATATTTGGTAAAATTTAGCTATATCTAATTTTAG GAAATTTATGTATGATTCCGGGGATCCGTCGACC	Gene inactivation	This study
pflA-R2	1445	CATTATTTGCTCCTTATGTTAGCTGACATTTATTCTA GAATTTTACAGTGTGTAGGCTGGAGCTGCTTCG	Gene inactivation	This study
frdA-F1	1594	CGAAACACTTTACTGATTTGGAATATC	Gene inactivation	This study
frdA-R1	1595	CCAAATTGAGGGCAAGCGGCATAGCAT	Gene inactivation	This study
frdA-F2	1596	TGCTCAAGCAAAAGACGTTGTAGCTCG	Gene inactivation	This study
frdA-R2	1597	TATTAAATTTAAATGCACGACAACCAC	Gene inactivation	This study
HI0601.1-F1	488	GAAGTAAGAGATGAAAAGCGAAG	Gene inactivation	[1]
HI0601.1-R1	489	TTGGTAAAAATGGATGAAGGGGATTAC	Gene inactivation	[1]
ackA-COMP-XhoI-Fw	1598	CCGCTCGAGATACCGCACTTTGATTTTCTAACG	Mutant complementation	This study
ackA-HA-COMP-XhoI-Rv	1599	CCGCTCGAGTTAAGCGTAATCTGGAACATCGTATGG GTAGAAACAAAGTTTTGCGGTATCTTGTGC	Mutant complementation	This study
ackA-*pta*-COMP-XhoI-Fw	1853	CCGCTCGAGTTTCTAACGGCGTATTGGCACGCTTAC	Mutant complementation	This study
ackA-*pta*-HA-COMP-XhoI-Rv	1854	CCGCTCGAGTTAAGCGTAGTCTGGGACGTCGTATGG GTATTGTGTTGCTTGAATTGCGGTTAAGGC	Mutant complementation	This study
pSBLerm_down	1307	GGTACACGAAAAACAAGTTAAGGG	Gene inactivation	[2]
ackA-qPCR-F	1543	CCAATTAAGTGAGCAGGGTTG	qRT-PCR	[4]
ackA-qPCR-R	1544	TCGTATCGTTCACGGTGGCG	qRT-PCR	[4]
pflA-qPCR-F	1541	CTCTTTACAAGCACGGAACC	qRT-PCR	[4]
pflA-qPCR-R	1542	AAAGAAGTCGTGACTTATCGC	qRT-PCR	[4]
frdA-qPCR-F	1567	GCCGTGTAAACCTGAAGATGC	qRT-PCR	[4]
frdA-qPCR-R	1568	ATCCCTGTTCGTCCAGTTGTT	qRT-PCR	[4]
aceF-qPCR-F	1539	AGCCAGCACCATTTGCTACAC	qRT-PCR	[4]
aceF-qPCR-R	1540	GTCGTAAAGGTCGTATCGTTA	qRT-PCR	[4]
ldhA-qPCR-F	1545	CTGGCGTTGCTGGGCAATGA	qRT-PCR	[4]
ldhA-qPCR-R	1546	TCTTGGCGTACGATCCTTTCA	qRT-PCR	[4]
dld-qPCR-F	1553	AGCGGAAAGGTGTCTAAACGA	qRT-PCR	[4]
dld-qPCR-R	1554	TCGTCAAGTTGATGAAGGCTC	qRT-PCR	[4]
pfkA-qPCR-F	1582	CGATATATTCACAACCGCCAG	qRT-PCR	[4]
pfkA-qPCR-R	1583	TCGACCGTTTACGTGATACAT	qRT-PCR	[4]
pykA-qPCR-F	1584	TTGCAGACATCGCAACAGATT	qRT-PCR	[4]
pykA-qPCR-R	1585	CAGTGGCAGCAATGGCTAG	qRT-PCR	[4]
zwf-qPCR-F	1586	CTCTTCCACGCCAATAGATTC	qRT-PCR	[4]
zwf-qPCR-R	1587	GAAACCGTTCAAAACTTGCTC	qRT-PCR	[4]
fdxG-qPCR-F	1547	GTGGCGGTATTAACGCATTAC	qRT-PCR	[4]
fdxG-qPCR-R	1548	CGTAAGAGGTATCTCTATCGT	qRT-PCR	[4]
nqrB-qPCR-F	1549	TGCAACTTGGGGCTCTAAAAT	qRT-PCR	[4]
nqrB-qPCR-R	1550	ACTTCGTGACCACGAACCAC	qRT-PCR	[4]

lldD-qPCR-F	1551	ATCATACGCCCAGAATGGGTG	qRT-PCR	[4]
lldD-qPCR-R	1552	ACGGTCGATATGCCTACTCCA	qRT-PCR	[4]
cydA-qPCR-F	1555	AACCAACCACACTCAATGGCA	qRT-PCR	[4]
cydA-qPCR-R	1556	ACTTACATTCGGCGCATTTGT	qRT-PCR	[4]
cydB-qPCR-F	1557	CGTGAGTGACAAGCATTGATA	qRT-PCR	[4]
cydB-qPCR-R	1558	GCGTTCCATTCCATTTTAACG	qRT-PCR	[4]
napA-qPCR-F	1561	TGGTCGCGGTCACGGTCA	qRT-PCR	[4]
napA-qPCR-R	1562	GGATCATAGCCTTCACGGTAA	qRT-PCR	[4]
mtsZ-qPCR-F	1563	AACAAACGGGTTACCACCTGC	qRT-PCR	[4]
mtsZ-qPCR-R	1564	CCATTAGCGCGTATTGCTGAT	qRT-PCR	[4]
nrfA-qPCR-F	1565	GCCGTGTAAACCTGAAGATGC	qRT-PCR	[4]
nrfA-qPCR-R	1566	ATCCCTGTTCGTCCAGTTGTT	qRT-PCR	[4]
dmsA-qPCR-F	1559	CAAGCACGAACCTGATGATCA	qRT-PCR	[4]
dmsA-qPCR-R	1560	AGTAAACTGTGGTAGCCGTTG	qRT-PCR	[4]
ndh-qPCR-F		AAATACACTTATTACCAAAGATGG	qRT-PCR	[5]
ndh-qPCR-R		ATTGATTGATACGATTAATTTC	qRT-PCR	[5]
pta-qPCR-F	1856	CTACATCAGCACCGCTACCA	qRT-PCR	This study
pta-qPCR-R	1857	CACCACTGCAAACACCATTC	qRT-PCR	This study
gyrA-qPCR-F2	1078	ATATGTTGGTTGATGGGCAAGG	qRT-PCR	[6]
gyrA-qPCR-R2	1079	GGCGAGAAATTGACGGTTTCT	qRT-PCR	[6]
il8- qPCR-F	1241	AGAGACAGCAGAGCACAC	qRT-PCR	[7]
il8- qPCR-R	1242	AGTTCTTTAGCACTCCTTGG	qRT-PCR	[7]
gapdh-qPCR-F	1237	GAAGGTGAAGGTCGGAGTC	qRT-PCR	[7]
gapdh-qPCR-R	1238	GAAGATGGTGATGGGATTTC	qRT-PCR	[7]
cxcl1-qPCR-F	1247	GCAGGGAATTCACCCCAAGA	qRT-PCR	[7]
cxcl1-qPCR-R	1248	CTTCAGGAACAGCCACCAGT	qRT-PCR	[7]
kc-qPCR-F	1404	GACAGACTGCTCTGATGGCA	qRT-PCR	[8]
kc-qPCR-R	1405	TGCACTTCTTTTCGCACAAC	qRT-PCR	[8]
mgadph- qPCR-F	1430	CCCACTAACATCAAATGGGG	qRT-PCR	[9]
mgadph- qPCR-R	1431	CCTTCCACAATGCCAAAGTT	qRT-PCR	[9]

Table S3. Key metabolites detected by HPLC in culture supernatants of CDM grown *H. influenzae* RdKW20 WT and mutant strains.

Strain		**Glucose (mM)**		**Acetate (mM)**		**Succinate (mM)**		**Lactate (mM)**	
		+O_2	**-O_2**	**+O_2**	**-O_2**	**+O_2**	**-O_2**	**+O_2**	**-O_2**
RdKW20	WT	n.d.	3.05±0.07	24.35±2.19	9.2±0.04	n.d.	13.03±0.3	n.d.	n.d.
	Δ*ackA*	6.24±0.15	3.93±0.18	1.17±0.23	8.38±0.38	n.d.	5.96±0.15	1.19±0.07	3.47±0.31
	Δ*pflA*	n.d.	1.11±0.13	21.51±0.76	10.4±2.53	n.d.	14.29±1.58	n.d.	n.d.
	Δ*frdA*	n.d.	7.26±0.52	21.52±0.05	5.6±0.47	0.4±0.01	n.d.	n.d.	1.67±0.19

References

1. Fernandez-Calvet, A.; Rodriguez-Arce, I.; Almagro, G.; Moleres, J.; Euba, B.; Caballero, L.; Marti, S.; Ramos-Vivas, J.; Bartholomew, T. L.; Morales, X.; Ortiz-de-Solorzano, C.; Yuste, J. E.; Bengoechea, J. A.; Conde-Alvarez, R.; Garmendia, J., Modulation of *Haemophilus influenzae* interaction with hydrophobic molecules by the VacJ/MlaA lipoprotein impacts strongly on its interplay with the airways. *Sci Rep* **2018,** *8* (1), 6872. DOI: 10.1038/s41598-018-25232-y.
2. Allen, S.; Zaleski, A.; Johnston, J. W.; Gibson, B. W.; Apicella, M. A., Novel sialic acid transporter of *Haemophilus influenzae*. *Infect Immun* **2005,** *73* (9), 5291-300. DOI: 10.1128/IAI.73.9.5291-5300.2005.
3. Tracy, E.; Ye, F.; Baker, B. D.; Munson, R. S., Jr., Construction of non-polar mutants in *Haemophilus influenzae* using FLP recombinase technology. *BMC Mol Biol* **2008,** *9*, 101. DOI: 10.1186/1471-2199-9-101.
4. Othman, D. S. M. P.; Schirra, H.; McEwan, A. G.; Kappler, U., Metabolic versatility in *Haemophilus influenzae*: a metabolomic and genomic analysis. *Frontiers in microbiology* **2014,** *5*, 69-69. DOI: 10.3389/fmicb.2014.00069.
5. Muda, N. M.; Nasreen, M.; Dhouib, R.; Hosmer, J.; Hill, J.; Mahawar, M.; Schirra, H. J.; McEwan, A. G.; Kappler, U., Metabolic analyses reveal common adaptations in two invasive *Haemophilus influenzae* strains. *Pathog Dis* **2019,** *77* (2). DOI: 10.1093/femspd/ftz015.
6. Moleres, J.; Fernandez-Calvet, A.; Ehrlich, R. L.; Marti, S.; Perez-Regidor, L.; Euba, B.; Rodriguez-Arce, I.; Balashov, S.; Cuevas, E.; Linares, J.; Ardanuy, C.; Martin-Santamaria, S.; Ehrlich, G. D.; Mell, J. C.; Garmendia, J., Antagonistic pleiotropy in the bifunctional surface protein FadL (OmpP1) during adaptation of *Haemophilus influenzae* to chronic lung infection associated with chronic obstructive pulmonary disease. *MBio* **2018,** *9* (5). DOI: 10.1128/mBio.01176-18.
7. Euba, B.; Moleres, J.; Segura, V.; Viadas, C.; Morey, P.; Moranta, D.; Leiva, J.; de-Torres, J. P.; Bengoechea, J. A.; Garmendia, J., Genome expression profiling-based identification and administration efficacy of host-directed antimicrobial drugs against respiratory infection by nontypeable *Haemophilus influenzae*. *Antimicrob Agents Chemother* **2015,** *59* (12), 7581-92. DOI: 10.1128/AAC.01278-15.
8. Euba, B.; Lopez-Lopez, N.; Rodriguez-Arce, I.; Fernandez-Calvet, A.; Barberan, M.; Caturla, N.; Marti, S.; Diez-Martinez, R.; Garmendia, J., Resveratrol therapeutics combines both antimicrobial and immunomodulatory properties against respiratory infection by nontypeable *Haemophilus influenzae*. *Sci Rep* **2017,** *7* (1), 12860. DOI: 10.1038/s41598-017-13034-7.
9. Regueiro, V.; Moranta, D.; Frank, C. G.; Larrarte, E.; Margareto, J.; March, C.; Garmendia, J.; Bengoechea, J. A., *Klebsiella pneumoniae* subverts the activation of inflammatory responses in a NOD1-dependent manner. *Cell Microbiol* **2011,** *13* (1), 135-53. DOI: 10.1111/j.1462-5822.2010.01526.x.

Anexo III:

Otras Publicaciones en las que la Doctoranda ha participado

frontiers in Cellular and Infection Microbiology

ORIGINAL RESEARCH
published: 20 June 2017
doi: 10.3389/fcimb.2017.00266

Inactivation of the Thymidylate Synthase *thyA* in Non-typeable *Haemophilus influenzae* Modulates Antibiotic Resistance and Has a Strong Impact on Its Interplay with the Host Airways

*Irene Rodríguez-Arce[1], Sara Martí[2,3], Begoña Euba[1,2], Ariadna Fernández-Calvet[1], Javier Moleres[1], Nahikari López-López[1], Montserrat Barberán[4], José Ramos-Vivas[5,6], Fe Tubau[2,3], Carmen Losa[7], Carmen Ardanuy[2,3], José Leiva[7], José E. Yuste[2,8] and Junkal Garmendia[1,2]**

[1] Instituto de Agrobiotecnología, Consejo Superior de Investigaciones Científicas-Universidad Pública Navarra-Gobierno, Navarra, Spain, [2] Centro de Investigación Biomédica en Red de Enfermedades Respiratorias, Madrid, Spain, [3] Departamento Microbiología, Hospital Universitari Bellvitge, University of Barcelona, Institut d'Investigació Biomédica de Bellvitge, Barcelona, Spain, [4] Facultad de Veterinaria, Universidad de Zaragoza, Zaragoza, Spain, [5] Servicio Microbiología, Hospital Universitario Marqués de Valdecilla and Instituto de Investigación Marqués de Valdecilla, Santander, Spain, [6] Red Española de Investigación en Patología Infecciosa, Instituto de Salud Carlos III, Madrid, Spain, [7] Servicio de Microbiología, Clínica Universidad de Navarra, Navarra, Spain, [8] Centro Nacional de Microbiología, Instituto de Salud Carlos III, Madrid, Spain

OPEN ACCESS

Edited by:
W. Edward Swords, Wake Forest University, United States

Reviewed by:
Sandy Wong, University of Mississippi Medical Center School of Dentistry, United States
Christian Berens, Friedrich Loeffler Institute Greifswald, Germany

***Correspondence:**
Junkal Garmendia
juncal.garmendia@unavarra.es

Received: *01 December 2016*
Accepted: *02 June 2017*
Published: *20 June 2017*

Citation:
Rodríguez-Arce I, Martí S, Euba B, Fernández-Calvet A, Moleres J, López-López N, Barberán M, Ramos-Vivas J, Tubau F, Losa C, Ardanuy C, Leiva J, Yuste JE and Garmendia J (2017) Inactivation of the Thymidylate Synthase thyA in Non-typeable Haemophilus influenzae Modulates Antibiotic Resistance and Has a Strong Impact on Its Interplay with the Host Airways. Front. Cell. Infect. Microbiol. 7:266. doi: 10.3389/fcimb.2017.00266

Antibacterial treatment with cotrimoxazol (TxS), a combination of trimethoprim and sulfamethoxazole, generates resistance by, among others, acquisition of thymidine auxotrophy associated with mutations in the thymidylate synthase gene *thyA*, which can modify the biology of infection. The opportunistic pathogen non-typeable *Haemophilus influenzae* (NTHi) is frequently encountered in the lower airways of chronic obstructive pulmonary disease (COPD) patients, and associated with acute exacerbation of COPD symptoms. Increasing resistance of NTHi to TxS limits its suitability as initial antibacterial against COPD exacerbation, although its relationship with thymidine auxotrophy is unknown. In this study, the analysis of 2,542 NTHi isolates recovered at Bellvitge University Hospital (Spain) in the period 2010–2014 revealed 119 strains forming slow-growing colonies on the thymidine low concentration medium Mueller Hinton Fastidious, including one strain isolated from a COPD patient undergoing TxS therapy that was a reversible thymidine auxotroph. To assess the impact of thymidine auxotrophy in the NTHi-host interplay during respiratory infection, *thyA* mutants were generated in both the clinical isolate NTHi375 and the reference strain RdKW20. Inactivation of the *thyA* gene increased TxS resistance, but also promoted morphological changes consistent with elongation and impaired bacterial division, which altered *H. influenzae* self-aggregation, phosphorylcholine level, C3b deposition, and airway epithelial infection patterns. Availability of external thymidine contributed to overcome such auxotrophy and TxS effect, potentially facilitated by the nucleoside transporter *nupC*. Although, *thyA* inactivation resulted in bacterial attenuation in a lung infection mouse model, it

also rendered a lower clearance upon a TxS challenge *in vivo*. Thus, our results show that thymidine auxotrophy modulates both the NTHi host airway interplay and antibiotic resistance, which should be considered at the clinical setting for the consequences of TxS administration.

Keywords: *Haemophilus influenzae*, thymidylate synthase, thymidine auxotrophy, thymidine uptake, bacterial morphology, antibiotic resistance, airway infection

INTRODUCTION

Non-typeable (non-capsulated) *Haemophilus influenzae* (NTHi) is a Gram negative coccobacillus that is a common commensal in the nasopharynx of healthy humans, and also an opportunistic pathogen causing respiratory infections such as acute otitis media, otitis media with effusion, community-acquired pneumonia, and exacerbations of chronic obstructive pulmonary disease (COPD; Agrawal and Murphy, 2011). COPD is characterized by a progressive and not fully reversible airflow limitation, accompanied by infiltration of the airways by neutrophils and mucus hypersecretion (Barnes, 2016). The chronic course and evolution of COPD is often characterized by periods of symptom exacerbation with a negative impact on the patient's quality of life and evolution of the disease, and represent a significant cause of medical intervention and hospitalization. Given that acute exacerbations of COPD (AECOPD) are mostly caused by bacterial and viral infections (Sethi, 2010), antibiotic therapy is routinely prescribed. Use of amoxicillin, tetracyclines, or cotrimoxazole (TxS), a combination of trimethoprim (TMP) and sulfamethoxazole (SMX), has long been regarded as standard therapy for patients with AECOPD, which has contributed to the increasing emergence of resistance to these antibiotics in common respiratory pathogens such as NTHi, and become a real challenge in the choice of adequate antibacterials (Nouira et al., 2010).

The treatment of respiratory infections has been a very important field of use of TxS, as a first-line agent against *H. influenzae* infected respiratory patients (Iyer Parameswaran and Murphy, 2009), and has also been considered as a prophylactic option in HIV-infected children therefore having an impact on *H. influenzae* carriage (Grant et al., 2009; Mwenya et al., 2010), altogether increasing TxS resistance levels in this pathogen. TxS interferes with the bacterial metabolism and replication by blocking the production of tetrahydrofolic acid (THF). THF is a co-factor for the thymidylate synthase, an essential protein encoded by the *thyA* gene, required for the conversion of thymidine from uracil (Stryer, 1995). During normal metabolism, dihydrofolate is reduced to THF by the dihydrofolate reductase (DHFR), encoded by the *folH* gene, also known as *drfA* and *folA*. TMP is a substrate analog of dihydrofolate and blocks its reduction to THF. Conversely, SMX is a substrate analog of *para*-aminobenzoic acid, and blocks the *folP* gene encoding the dihydropteroate synthetase DHPS, which is involved in production of dihydropteroate, a precursor of dihydrofolate. Both TMP and SMX have little toxicity to humans because humans do not synthesize folic acid but obtain it from dietary sources (Tristram et al., 2007). Inhibiting the production of THF prevents thymine synthesis and, hence, DNA replication, causing bacterial death and TxS susceptibility. However, if external thymidine is available, as shown in infected tissues (Besier et al., 2008), thymidine-dependent TxS resistance may emerge upon treatment. This aspect has been long reported (Maskell et al., 1978), and extensively analyzed in *Staphylococcus aureus*, where the underlying mechanism for thymidine dependency relies on mutations of the *thyA* gene. Thus, inactivation of the *thyA* gene generates thymidine auxotroph small colony variants (SCVs) with a strong impact in this pathogen's physiology, virulence, and persistence, and uptake of external thymidine by the *S. aureus* NupC nucleoside transporter seems to bypass the effect of TxS (Kriegeskorte et al., 2014).

In NTHi, resistance to TxS is associated to polymorphisms and/or short insertions in the *folH* and *folP* genes, DHFR overproduction, or acquisition of the sulfonamide (SUL) genes *sul1* and *sul2* (de Groot et al., 1988, 1996; Enne et al., 2002). Existing evidence also relates *H. influenzae* TMP resistance to transient thymidine auxotrophy in isolates from sputum samples of chronic bronchitis patients receiving TMP (Platt et al., 1983). Despite this observation, little is known about thymidine-dependent antibiotic resistance and its underlying consequences for NTHi pathogenesis. Following this notion, we observed that among 2,542 NTHi strains isolated between 2010 and 2014 from clinical samples at Bellvitge University Hospital (Spain), 119 strains formed slow-growing colonies on Mueller Hinton Fastidious (MH-F) agar, a thymidine low concentration medium. This observation prompted us to hypothesize that such slow-growth could relate to thymidine auxotrophy, rendering TxS resistance due to the antibiotic administration. If so, such auxotrophy could also modify the dynamics of the NTHi-host interplay. To address these hypotheses, we screened the available NTHi isolates with a slow growth on MH-F agar and identified one thymidine auxotroph, easily reversible to the normal phenotype. Moreover, to question the relationship between thymidine auxotrophy and respiratory infection by NTHi, we employed two genome sequenced strains, NTHi strain 375, hereafter NTHi375, and *H. influenzae* (Hi) RdKW20 (Fleischmann et al., 1995; Mell et al., 2014), to generate thymidine auxotrophs by mutating the *thyA* gene, and systematically evaluated its effect on (i) bacterial resistance to TxS, morphology, growth, self-aggregation, and gene expression; (ii) NTHi-host interplay by assessing bacterial binding to a panel of components of the complement system, adhesion to- and invasion of cultured airway epithelia; (iii) NTHi respiratory infection *in vivo* by using a murine intranasal infection model upon TxS treatment. This work provides further evidence of the emergence of NTHi TxS resistance upon its administration, and shows for the first time

that mutation of the thymidylate synthase encoding gene *thyA* in NTHi leads to a strong impact on its physiology and virulence, but also provides a survival advantage during TxS challenge. Our results provide a context for a better understanding of the potential effects of TxS treatment against NTHi respiratory infection.

MATERIALS AND METHODS

Bacterial Strains and Growth Conditions

Strains used in this study are described in **Table 1**. NTHi strains were grown at 37°C, 5% CO_2 on chocolate agar (Biomérieux), MH-F agar (Biomérieux), or brain-heart infusion (BHI) agar supplemented with 10 μg/ml hemin and 10 μg/ml nicotinamide adenine dinucleotide (NAD), referred to as sBHI. NTHi liquid cultures were grown in sBHI (37°C, 5% CO_2). Thymidine (Sigma-Aldrich) was dissolved in sterile distilled water (stock solution, 10 mg/ml). When necessary, media were supplemented with thymidine by (i) using sterile paper discs soaked on thymidine 300 μg/ml or 10 mg/ml, (ii) thymidine 300 μg/ml spreading on 20 ml chocolate agar or MH-F agar plates, (iii) thymidine 300 μg/ml addition into sBHI. Erythromycin 11 μg/ml (Erm_{11}) or spectinomycin 50 μg/ml ($Spec_{50}$) were used when required. *Escherichia coli* was grown on Luria Bertani (LB) agar at 37°C, supplemented with ampicillin 100 μg/ml (Amp_{100}), erythromycin 150 μg/ml (Erm_{150}) or $Spec_{50}$, when necessary.

For *thyA* disruption, a DNA fragment containing the *thyA* gene and its respective adjacent regions (2,852 bp), was PCR amplified with *Phusion* polymerase (Thermofisher) using NTHi375 genomic DNA as template and primers thyA-F1 (5′-TGCCTGAATATTCGCTCGGTTACATTTA) and thyA-R1 (5′-CGATGATACTTAAAAGTAATCGCGACCAAAAATTCGG). The gene-containing fragment was cloned into pJET1.2 (Thermofisher), generating pJET1.2-*thyA*. This cloned PCR product was disrupted by inverse PCR with *Phusion* polymerase, using primers thyA-F2 (5′-CGTTCCTGTGATGTTCCGCTTGGA) and thyA-R2 (5′-ATATCATCAACGCCTCTACGATGC). An internal 226-bp fragment (nucleotides 312–537 in the *thyA* coding sequence) was replaced by a blunt-ended erythromycin resistance cassette excised by *Sma*I digestion from pBSLerm (Allen et al., 2005), generating pJET1.2-*thyA::ermC*. This plasmid was used as a template to amplify the *thyA::ermC* disruption cassette with primers thyA-F1 and thyA-R1, which was used to transform NTHi375 using the MIV method (Herriott et al., 1970). Transformants were screened by plating bacteria on sBHI agar with Erm_{11} to obtain NTHi375Δ*thyA*. Same approach and disruption cassette were used to generate RdKW20Δ*thyA*. For mutant confirmation, NTHi375Δ*thyA* and RdKW20Δ*thyA* genomic DNA were used as template to be PCR amplified with four primer pairs: (i) thyA-F1 and thyA-R1, rendering a 3,814 bp product; (ii) thyA-F1 and pBSLerm-down (5′-GGTACACGAAAAACAAGTTAAGGG), rendering a 2,421 bp product; (iii) pBSLerm-up (5′-ATAAAGAGGGTTATAATGAACGAG) and thyA-R1, rendering a 2,190 bp product; (iv) pBSLerm-up and pBSLerm-down, rendering a 797 bp product (data not shown). Recombination events resulting from integration of the *thyA* disruption

TABLE 1 | Strains and plasmids used in this study.

	Description	Source
STRAINS		
Haemophilus influenzae		
NTHi375	Wild-type, otitis media clinical isolate	Hood et al., 1999
NTHi375Δ*thyA*	*thyA::ermC*, Erm^R	This study
NTHi375Δ*nupC*	*nupC::spec*, $Spec^R$	This study
RdKW20	Laboratory strain, capsule-deficient serotype d	Fleischmann et al., 1995
RdKW20Δ*thyA*	*thyA::ermC*, Erm^R	This study
RdKW20Δ*nupC*	*nupC::spec*, $Spec^R$	This study
NTHi8233	COPD isolate from a sputum sample, thymidine auxotroph	This study
Escherichia coli		
TOP 10	Used for cloning assays	Thermofisher scientific
SW102	Derived from DY380, it contains a defective λ prophage with the recombination proteins *exo*, *bet*, and *gam* being controlled by the temperature-sensitive repressor *cI*857	Tracy et al., 2008
PLASMIDS		
pJET1.2	Cloning vector	Thermofisher scientific
pBSLerm	Source of an Erm^R cassette	Allen et al., 2005
pJET1.2-*thyA*	pJET1.2 with a 2,852 bp insert containing the $thyA_{NTHi375}$ gene (852 bp) and 1 kb flanking regions	This study
pJET1.2-*thyA::ermC*	pJET1.2 with a 3,814 bp insert containing a $thyA_{NTHi375}$*::ermC* disruption cassette	This study
pJET1.2-*nupC*	pJET1.2 with a 2,664 bp insert containing the $nupC_{RdKW20}$ gene (1,254 bp) gene and ∼700 bp flanking regions	This study
pJET1.2-*nupC::spec*	pJET1.2 with a 3,501 bp insert containing a $nupC_{RdKW20}$*::spec* disruption cassette	This study
pRSM2832	pKD13 derivative carrying a cassette containing a spectinomycin resistance gene flanked by FRT sites	Tracy et al., 2008

cassette in the NTHi375 and RdKW20 genomes were further verified by NTHi375Δ*thyA* and RdKW20Δ*thyA* genomic DNA PCR amplification with primers thyA-F1 and thyA-R1, and PCR product sequencing with primers thyA-F1, pBSLerm-up, pBSLerm-down and thyA-R1. When necessary, the *thyA* gene was PCR amplified with primers ThyA_Pro_F (5′-TGCGCCTTTGATTCCGTTTG) and ThyA_R2 (5′-TCACCTAACGCTTCCGCTTT) for DNA sequencing.

The *nupC* gene and its respective adjacent regions (2,664 bp) was amplified by PCR with *Phusion* polymerase using RdKW20 genomic DNA as template and primers nupC-F1 (5′-ATGAACAGGTTATGGAGGCAGTTCCAT) and nupC-R1 (5′-GTGAGTACGAATATGGTCAGACACGGT). The gene-containing fragment was cloned into pJET1.2, generating pJET1.2-*nupC*. A Spec^r cassette was PCR amplified from pRSM2832 using gene-specific mutagenic primers nupC-F2 (5′-GTAGAATAAGCCGAATTTTATTAACTTAACTAAT CTAGGGGAATCAAATGATTCCGGGGATCCGTCGACC) and nupC-R2 (5′-TACCGCACTTTTTAATTGATTAAGATA AATTAAAGTGCTGCAGCACCTAAGCCTGTAGGCTGG AGCTGCTTCG), as described previously (Tracy et al., 2008). Primers were designed to delete sequences between the start codon and the last seven codons of *nupC*. *E. coli* SW102 cells were prepared for recombineering, co-electroporated with pJET1.2-*nupC* (Amp^r; 50 ng) and the *nupC*-specific mutagenic cassette (Spec^r; 200 ng) as previously described (Sinha et al., 2012), and mutagenized clones containing pJET1.2-*nupC::spec* were selected on LB agar with Amp_{100}, $Spec_{50}$. This plasmid was used as a template to amplify the *nupC::spec* disruption cassette with primers nupC-F1 and nupC-R1, which was used to transform NTHi375 and RdKW20 using the MIV method. Transformants were selected on sBHI agar with $Spec_{50}$, to obtain NTHi375Δ*nupC* and RdKW20Δ*nupC* mutant strains.

Screening for NTHi Thymidine Auxotroph Clinical Isolates

Laboratory records of Microbiology Department at the Bellvitge University Hospital (Spain) regarding the difficulties of some NTHi isolates to growth on conventional antimicrobial susceptibility testing medium (Mueller-Hinton agar+5% defibrinated horse blood and 20 mg/l β-NAD, MH-F) were reviewed from 2010 to 2014. Screening for thymidine auxotrophs among NTHi clinical isolates was based on the interpretation of their growth characteristics. Isolates identified as having growth problems were further screened for thymidine auxotrophy by comparative growth on chocolate agar plates and low-thymidine MH-F agar plates. Thymidine auxotrophy was confirmed by testing strain growth on MH-F agar in the absence or presence of discs soaked with thymidine.

Susceptibility Testing under Non-standard Conditions

TxS susceptibility testing of NTHi thymidine auxotrophs failed to produce results by disc diffusion (Becton Dickinson), *E*-test (Biomérieux) or broth microdilution when inoculated on MH-F and incubated for 24 h, as specified by the European Committee on Antimicrobial Susceptibility Testing (EUCAST; http://www.eucast.org/clinical_breakpoints). Given that chocolate agar supported growth for all strains after 24 h of incubation, this medium was used for *E*-test- or TxS discs-based determination of minimal inhibitory concentrations (MIC). Strains were grown on chocolate agar, to generate bacterial suspensions normalized in phosphate-buffered saline (PBS) to $OD_{600} = 1$. Normalized suspensions were spread on chocolate agar or, when necessary, on MH-F agar, in the presence of *E*-test or TxS discs (23.75 mg/1.25 mg SMX:TMP) and incubated for 24 h before assessing the diameter of the growth inhibition zones.

Growth Curves

To monitor growth, NTHi strains grown on chocolate agar for 16 h were inoculated (2–5 colonies) in 20 ml sBHI, with or without thymidine, and incubated for 11 h with shaking. Cultures were diluted in 40 ml sBHI, with or without thymidine, to $OD_{600} = 0.01$ (RdKW20) or $OD_{600} = 0.05$ (NTHi375), incubated with agitation, and OD_{600} was recorded every hour for 8 h. Every 2 h, culture samples were serially diluted and plated on sBHI agar. Data are shown both as OD_{600} and c.f.u./ml. At the final time point, 10 μl of the bacterial cultures were placed on glass coverslips and fixed with 3.7% paraformaldehyde (PFA) in PBS pH 7.4 for 15 min at room temperature. Bacteria were labeled with a polyclonal rabbit anti-NTHi primary antibody diluted 1:600 and a donkey anti-rabbit conjugated to Cy2 (Jackson Immunological) secondary antibody diluted 1:100. Samples were analyzed with a Carl Zeiss Axioskop 2 plus fluorescence microscope and a Carl Zeiss Axio Cam MRm monochrome camera.

Confocal Microscopy

NTHi strains were grown on chocolate agar for 16 h, in the absence or presence of thymidine, and a colony was aseptically spread with an inoculation loop over a drop of distilled water on a microscopy slide. Samples were air-dried and stained for 15 min in the darkness with the cell-permeable fluorescent nucleic acid stain SYTO 9 (Life Technologies), following the manufacturer's instructions. Samples were washed twice with distilled water and fluorescence was observed by confocal laser microscopy. Images were acquired using a Leica TCS-SL filter-free spectral confocal laser-scanning microscope (Leica Microsystems) equipped with a 488 nm argon laser, 543 nm and 633 nm He/Ne lasers (Centres Científics i Tecnològics-Campus de Bellvitge, Universitat de Barcelona, Spain) using a 63× magnification oil immersion objective (1.4 numerical aperture), and an image resolution of 1024 × 1024 pixels. Images were acquired randomly and analyzed using the Leica Confocal Software 2.5 (Leica Microsystems).

Transmission Electron Microscopy (TEM)

H. influenzae strains were examined by TEM after growth on chocolate agar following established procedures (Remuzgo-Martinez et al., 2015). Briefly, bacteria were applied to Formvar-coated grids, air dried, negatively stained with 1% phosphotungstic acid in distilled water for 10 s, and examined with a JEM-1011 transmission electron microscope (JEOL)

operating at 80 kV and equipped with an Orius SC1000 charge-coupled device (CCD) camera (Gatan).

RNA Extraction and Real-Time Quantitative PCR (RT-qPCR) Analysis

NTHi strains were grown for 16 h on chocolate agar. Bacteria (2–5 colonies) were inoculated into 20 ml sBHI, grown for 11 h, with or without thymidine, diluted into 40 ml fresh sBHI to $OD_{600} = 0.05$, in the absence or presence of thymidine, and grown to $OD_{600} = 0.6$. Bacterial total RNA was isolated using TRIzol reagent (Invitrogen). Total RNA quality was evaluated using RNA 6000 Nano LabChips (Agilent 2100 Bioanalyzer). All samples had intact 16S and 23S ribosomal RNA. Complementary DNA (cDNA) was synthesized from total RNA (1 μg) using SuperScript II Reverse Transcriptase reagents (Invitrogen). Real-time quantitative PCR was performed using Thermo Scientific Luminaris HiGreen qPCR Master Mix (Thermo Scientific) and fluorescence data were analyzed with BioRad CFX96 qPCR System (Bio-Rad). Relative quantities of mRNAs were calculated using the comparative threshold cycle (Ct) method and normalized using 16S ribosomal RNA (*16SrRNA*) as an endogenous control. Primer pairs were designed with Primer3 software: for *nupC*, nupC-RT-Fw (5′-ATGTTAATCGCATTCGTTGGTT) and nupC-RT-Rv (5′-ATTTGTCCTGCAATACCTGCTT); for *tdk*, tdk-RT-Fw (5′-TGTGCTTTGTTATGGCTTGC) and tdk-RT-Rv (5′-CTTTAATGACCTCGCCCTGA); for *16SrRNA*, 16S-Fw (5′-GGCGTTGATGACCGTGAAAC) and 16S-Rv (5′-GCCAGTAATAATCGCCCTCTTCTAG). Data are expressed as relative expression on mutant strains compared to their parental wild-type strains, considered to be 1. All measures were carried out in duplicate and at least three times ($n \geq 6$).

Bacterial Aggregation Assay

Three to four colonies of NTHi grown on chocolate agar for 16 h were inoculated into 20 ml sBHI, grown for 11 h, diluted in sBHI to $OD_{600} = 1$ and left standing at room temperature for 5 h (starting volume ∼25 ml). The viability of each culture was tested by serial dilution and plating on sBHI agar at the beginning of each experiment ($t = 0$; data not shown). OD_{600} readings were performed at regular time intervals on 700 μl aliquots collected from the top of each bacterial suspension. At least four independent experiments ($n \geq 4$) were performed for each strain.

Phosphorylcholine (PCho) Quantification

Three to four colonies of NTHi grown on chocolate agar for 16 h were inoculated into 20 ml sBHI, grown for 11 h, diluted into 40 ml sBHI to $OD_{600} = 0.05$, grown to $OD_{600} = 0.6$ in the absence or presence of thymidine, serially diluted, plated on sBHI agar for c.f.u. determination, and used to generate stocks stored at −80°C in sBHI with 20% glycerol as single use aliquots for further experiments. For PCho determination, ∼1 × 10^7 c.f.u. were incubated for 1 h at 37°C with TEPC-15, a mouse monoclonal antibody specific for PCho (Sigma-Aldrich) diluted 1:25 in PBS-0.05% Tween 20. Samples were washed twice with PBS-0.05% Tween 20, and incubated with a fluorescein isothiocyanate (FITC)-conjugated rabbit anti-mouse (Serotec) diluted 1:300 in PBS-0.05% Tween 20 for 30 min at 4°C under dark conditions. Bacteria were washed with PBS-0.05% Tween 20, fixed in 3% paraformaldehyde (PFA) for 2–3 min at room temperature, and analyzed on a FACSCalibur flow cytometer (BD Biosciences) using forward and side scatter parameters to gate on at least 25,000 bacteria. Results are expressed as a relative percent fluorescence index (RFI), to measure both the proportion of fluorescent bacteria positive for PCho and the intensity of fluorescence (Ramos-Sevillano et al., 2015). Assays were performed in quadruplicate in at least three independent occassions ($n \geq 12$).

Binding of Complement Factors to NTHi

Bacterial strains were grown as indicated for PCho determination. C3b deposition was analyzed as explained previously (Ramos-Sevillano et al., 2015). Briefly, a bacterial suspension containing ∼1 × 10^7 c.f.u. was opsonized with human serum diluted 1:4 in PBS-0.05% Tween 20, and detected with a FITC-conjugated polyclonal goat anti-human C3b antibody (ICN-Cappel) diluted 1:300 in PBS-0.05% Tween 20 for 30 min at 4°C under dark conditions. CRP binding was measured as previously described (Ramos-Sevillano et al., 2015), by incubating ∼1 × 10^7 c.f.u. with human serum diluted 1:4 in PBS-0.05% Tween 20 and detected with a polyclonal rabbit anti-human CRP antibody (Calbiochem) for 1 h at 37°C, followed by two washes with PBS-0.05% Tween 20. Bacterial suspensions were then incubated for 30 min with a FITC-conjugated polyclonal goat anti-rabbit antibody in PBS-0.05% Tween 20 for 1 h at 37°C. For both C3b and CRP binding, bacteria were finally washed with PBS-0.05% Tween 20, fixed in 3% PFA, and analyzed on a FACSCalibur flow cytometer as described above. Results are expressed as a RFI. Assays were performed in quadruplicate in at least three independent occassions ($n \geq 12$).

Cell Culture and Bacterial Infection

A549 human alveolar basal epithelial cells (ATCC CCL-185) were maintained as described (Morey et al., 2011), seeded to 6 × 10^4 cells/well for 32 h, and serum-starved 16 h before infection. NCI H-292 mucoepidermoid pulmonary human carcinoma epithelial cells (ATCC CRL-1848) were maintained as described (Euba et al., 2015c), and seeded to 4 × 10^5 cells/well 16 h before infection. Adhesion and invasion assays were performed and processed as described (Morey et al., 2011; Lopez-Gomez et al., 2012; Euba et al., 2015a,c). For infection, PBS-normalized bacterial suspensions ($OD_{600} = 1$) were prepared by using NTHi strains grown on chocolate agar for 16 h, or in 20 ml sBHI for 11 h in the absence or presence of thymidine. A multiplicity of infection (MOI) of ∼100:1 was used. To monitor adhesion, cells were infected for 30 min. Although this assay does not completely exclude a possible internalization of some bacteria, experimental conditions were previously set to mainly monitor adhesion (Morey et al., 2011; data not shown). For invasion assays, cells were incubated with bacteria for 2 h, washed three times with PBS, incubated for 1 h with RPMI 1640 medium containing 10% FCS, Hepes 10 mM, and gentamicin 200 μg/ml to kill extracellular bacteria.

When necessary, A549 cells were infected for 30 min with bacterial suspensions ($OD_{600} = 1$) generated with bacteria grown on chocolate agar, in the absence or presence of thymidine; infections were performed in RPMI 1640, and in the absence or presence of purified C3 (16 μg/ml), 2% C3-deficient human serum (HS), or C3-depleted HS reconstituted with purified C3. Human C3-deficient serum and human complement C3 were purchased from Sigma-Aldrich. Cells were then washed three times with PBS, lysed with 300 μl of PBS-saponin 0.025% for 10 min at room temperature, and serial dilutions were plated on sBHI agar. All infections were performed in triplicate at least three independent times ($n \geq 9$). Results are expressed as c.f.u./ml.

Secretion of IL-8

For A549 cell stimulation by NTHi, bacteria grown on chocolate agar, in the absence or presence of thymidine, were collected with PBS, suspensions were normalized to $OD_{600} = 1$, and used for a 2 h infection with a MOI of ∼100:1. Cells were washed three times with PBS, and incubated for 6 h in RPMI 1640 medium containing 10% FCS, Hepes 10 mM and gentamicin 100 μg/ml. Supernatants were collected from the wells, cell debris removed by centrifugation and samples frozen at –80°C. IL-8 levels in the supernatants were measured by ELISA (Abnova KA0115) with sensitivity <2 pg/ml. Infections were performed in duplicate and at least twice ($n \geq 4$). Results are expressed as IL-8 pg/ml.

Scanning Electron Microscopy (SEM)

A549 cells were seeded on glass coverslips and infected as described above, by using bacteria previously grown on chocolate agar. Coverslips were fixed in ice-cold 3% glutaraldehyde for 20 min at 4°C. Samples were dehydrated in a series of graded acetone, dried by the critical point method, coated with gold in a Fine coat ion sputter JFC-1100 226 (JEOL, Ltd) and observed with an Inspect S microscope (FEI Company) working at 15 or 20 kV (Lazaro-Diez et al., 2016).

NTHi Mouse Lung Infection

A CD1 mouse model of NTHi lung infection was used, as described previously (Morey et al., 2013; Euba et al., 2015a,b,c). CD1 female mice (18–20 g) aged 4–5 weeks were purchased from Charles River Laboratories (France), housed under pathogen-free conditions at the Institute of Agrobiotechnology facilities (registration number ES/31-2016-000002-CR-SU-US), and used at 22–25 g. Animal handling and procedures were in accordance with the current European (Directive 86/609/EEC) and National (Real Decreto 53/2013) legislations, following the FELASA and ARRIVE guidelines, and with the approval of the Universidad Pública de Navarra (UPNa) Animal Experimentation Committee (Comité de Ética, Experimentación Animal y Bioseguridad) and the local Government authorization. NTHi375 and NTHi375Δ*thyA* were used for lung infection, and mice were randomly divided into two groups ($n = 5$): (i) control, vehicle solution (0.1 ml PBS) administered by oroesophageal gavage (Popper & Sons Inc.); (ii) one dose of TxS each 6 h administered by oroesophageal gavage, starting at 6 h post-infection (hpi). TxS (Septrin, 8 mg/40 mg/ml TMP:SMX) treatment was performed at a dose of 960 mg/kg of body weight in 0.1 ml PBS. Infecting bacteria were previously grown on chocolate agar, in the absence or presence of thymidine. For NTHi intranasal infection, 40 μl of a NTHi suspension containing $\sim 5 \times 10^8$ c.f.u./ml ($\sim 2 \times 10^7$ c.f.u./mouse) were placed at the entrance of the nostrils until complete inhalation, in mice previously anesthetized with ketamine-xylazine (3:1). At 12, 24, or 48 hpi, mice were euthanized using cervical dislocation. BALF samples were obtained by perfusion and collection of 0.7 ml of PBS, with help of a sterile 20G (1.1 mm diameter) Vialon™ intravenous catheter (Becton-Dickinson) inserted into the trachea. An aliquot of each recovered BALF was serially 10-fold diluted in PBS, and plated on sBHI agar to determine the number of viable bacteria. Results are expressed as mean ± *SD* of individual $\log_{10}$ c.f.u./BALF. In parallel, lungs were removed; the left one was processed for viable bacterial counts (as detailed above), and the right lung was fixed in 10% neutral buffered formalin for histological purposes. Heads and necks containing upper airways, larynx, and tracheas were fixed in the same buffered formalin for histology. Uninfected mice receiving PBS or TxS were used as controls when necessary.

For cell counting, the remaining volume of each BALF sample was centrifuged at 5,000 r.p.m. for 3 min at 4°C. Each pellet was resuspended in 1 ml RPMI 1640 with 10% FCS and Hepes 10 mM, and total cell count determined using a hemocytometer. $\sim 5x10^4$ cells in 200 μl RPMI 1640 with 10% FCS and Hepes 10 mM were used for cytospin preparation (1,500 r.p.m. for 10 min at room temperature, Thermo Shandon Cytospin). Giemsa stains were performed with an automated hematology slide preparation unit (SP-10, Sysmex Cosporation) according to the manufacturer's instructions. Preparations were examined in a double-blinded manner with an optical microscope (BX, Olympus).

Histopathology and Lesion Score

Heads and necks were rinsed in running tap water for 1 h, immersed in 5% nitric acid for 24–36 h until complete decalcification, and 7–8 transaxial slices were made every 3–4 mm beginning at the nostrils and finishing in the caudal tracheas. Transaxial slices and lungs were embedded in paraffin, and 4–6 μm sections were stained with hematoxylin and eosin (H&E) by standard procedures, and examined by microscopy to determine the presence and extent of inflammatory lesions. Sections were examined blind as sets by a trained veterinary pathologist (Dr. M. Barberán). Parameters characterizing an acute inflammatory reaction in upper airways, larynx, trachea, and lung, including hemorrhages, hyperemia, polymorphonuclear cell infiltrates (PMNs), and alveolar macrophages, were subjectively scored on a scale of 0–3 (0: absent, 1: mild, 2: moderate, 3: severe). For tissue control, similar organs obtained from non-infected control and TxS treated mice were processed in an identical manner to the infected tissues.

Statistical Analysis

For self-aggregation, gene expression, diameter of growth or inhibition zones, PCho level, complement deposition, cell

infection, bacterial loads in lungs and BALF samples, and inflammatory cells in BALF samples, mean ± *SD* were calculated and statistical comparison of means performed using the two-tail *t*-test. For histopathology scoring, means ± *SD* were also calculated and statistical comparisons performed using one-way analysis of variance (ANOVA) followed by Fisher's protected least significant difference (PLSD) multiple-comparison test. In all cases, a $p < 0.05$ value was considered statistically significant. Analyzes were performed using Prism software, version 6 for Mac (GraphPad Software) statistical package.

RESULTS

Isolation of a Thymidine Dependent NTHi Strain from the Sputum of a COPD Patient Receiving TxS

Among 2,542 clinical NTHi isolated between 2010 and 2014 at Bellvitge University Hospital (Spain), 119 (4.7%) isolates formed slow-growing colonies on MH-F agar. Thymidine auxotrophy was screened on the 119 isolates by comparative growth on chocolate agar and on low-thymidine MH-F agar. Thymidine auxotrophy was confirmed by absence of bacterial growth on MH-F agar, and further growth on MH-F agar in the presence of discs soaked in thymidine. One thymidine auxotroph NTHi isolate, named strain 8233, was identified in a sputum sample recovered from a COPD patient who had received TxS for 36 days to treat an acute exacerbation by *Stenotrophomonas maltophilia*. NTHi8233 produced small colonies on chocolate agar (data not shown) and did not grow on MH-F agar, except when discs soaked with thymidine 300 μg/ml or 10 mg/ml were added to the plate. Bacterial growth showed to be dependent on thymidine concentration (**Figure 1A**). The thymidylate synthase encoding gene $thyA_{NTHi8233}$ was sequenced, and a 6 nt duplication 267GAAAAT rendering a two-amino acid insertion (E90N91) was found, when compared to that of the RdKW20 genome sequenced reference strain (Fleischmann et al., 1995). A prediction of $ThyA_{H.influenzae}$ tertiary structure, based on *Burkholderia thailandensis* ThyA protein (PDB: 3V8H), was generated by the automated modeling tool of the Swiss Model web service (http://swissmodel.expasy.org). $ThyA_{NTHi8233}$ displayed 11 α-helices, 6 β-sheet strands and several coil connecting segments (Figure S1A). Homology between $ThyA_{NTHi8233}$ and $ThyA_{RdKW20}$ predicted structures is shown by structural alignment (Figure S1D).

NTHi8233 morphology was analyzed by confocal microscopy, and showed non-septated bacterial filaments ∼5–10 times longer than the average NTHi bacteria (**Figure 1A**, right). The absence of NTHi8233 growth on MH-F agar did not allow assessing its antibiotic susceptibility following standard procedures (http://www.eucast.org/clinical_breakpoints), and TxS resistance was tested by *E*-test on bacteria grown on chocolate agar. The MIC of TxS for NTHi8233 was >32 μg/ml. NTHi8233 thymidine auxotrophy was found to be easily reversible, as described for other pathogens (Kahl, 2014). Thymidine prototroph reverted NTHi8233 strain did not present a filamented morphology (data not shown) and the sequence of the *thyA* gene did not present the 6 nt duplication described above, even though its MIC of TxS remained unchanged.

Identification of NTHi8233 supports the notion that thymidine auxotrophy may be a bacterial response to TxS treatment that could be underestimated due to the lack of growth on MH-F agar and given that, as previously stated for other NTHi isolates (Platt et al., 1983), was shown to be reversible. This observation prompted us to generate mutant strains lacking the *thyA* gene on previously characterized NTHi genetic backgrounds for a detailed study of the impact of thymidine auxotrophy for this pathogen.

Generation and Characterization of Thymidine Dependent *H. influenzae* strains

H. influenzae genome sequenced strains NTHi375 and RdKW20 were employed to generate thymidine dependent mutants by disruption of the *thyA* gene (*thyA* accession numbers NF38_0045 and HI0905, respectively). At the protein level, $ThyA_{NTHi375}$ and $ThyA_{RdKW20}$ displayed 98.2% identity (Figure S1E). NTHi mutants lacking the *thyA* gene were selected on sBHI agar and rendered normal size colonies (data not shown), did not grow on MH-F agar, and grew around discs soaked with thymidine on MH-F agar. Growth was dependent on the thymidine concentration present on the discs (**Figure 1B** and **Table 2**). Thus, the *thyA* mutants displayed a larger growth zone around discs soaked with thymidine 10 mg/ml than around discs soaked with thymidine 300 μg/ml (NTHi375Δ*thyA*, $p < 0.005$; RdKW20Δ*thyA*, $p < 0.05$). In contrast, wild-type (WT) bacteria presented a normal growth on MH-F agar. For NTHi375 WT and Δ*thyA* strains, the MICs of TxS were 0.25 and 0.38–0.5 μg/ml, respectively. For RdKW20 WT and *thyA* mutant strains, the MICs of TxS were 0.12 and 0.5–0.75 μg/ml, respectively. For purpose of illustration, larger growth inhibition zones were observed for WT than for *thyA* mutant strains on chocolate agar around TxS discs (**Figure 1B**). The morphology of NTHi375Δ*thyA* and RdKW20Δ*thyA* strains was assessed by confocal microscopy, showing non-septated filaments longer than their respective WT bacteria. Bacterial median length, measured by TEM in ∼70 bacteria per strain, was (i) 1.42 ± 0.56 and 3.78 ± 2.86 μm for NTHi375 WT and Δ*thyA* strains, respectively ($p < 0.0001$); (ii) 1.43 ± 0.24 and 4.6 ± 4.98 μm for RdKW20 WT and Δ*thyA* strains, respectively ($p < 0.0001$). In agreement, SEM showed enlarged thymidine dependent bacteria on the surface of infected A549 human airway epithelial cells, which may modify the infectious process, compared to that shown by the WT strains (**Figure 1B**).

NTHi self-aggregates, which may promote microcolony formation on host cell surfaces (Meng et al., 2011; Mell et al., 2016). We asked whether the observed thymidine auxotrophy-driven increased bacterial size differs in its self-aggregation, by using tube-settling assays and monitoring the optical density of bacterial suspensions over time. Thymidine dependent mutants self-aggregated faster than their respective WT strains (**Figure 1C**).

Together, inactivation of the *thyA* gene in NTHi (i) impaired bacterial growth on MH-F agar, compensated by addition of

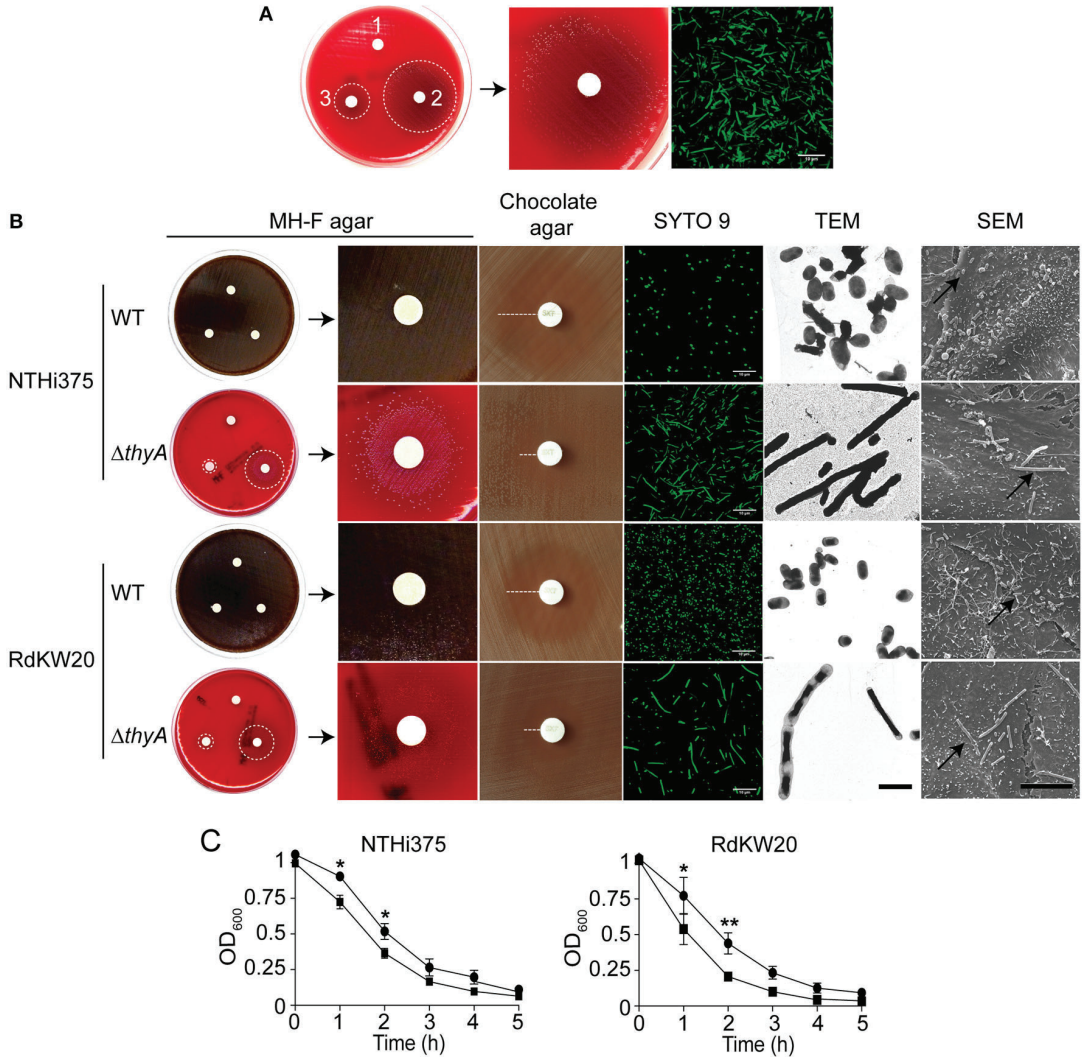

FIGURE 1 | Thymidine auxotrophy modifies *H. influenzae* growth and morphology. **(A)** Growth of clinical isolate NTHi8233 on MH-F agar with sterile discs soaked in water (1), thymidine 10 mg/ml, thymidine 300 μg/ml (3). Dotted circles indicate the growth zone around discs (left). A zoom of bacterial growth around a disc soaked in thymidine 10 mg/ml is shown (middle). NTHi8233 morphology observed by SYTO 9 staining and confocal microscopy (scale bar, 10 μm; right). **(B)** Growth of NTHi375 and RdKW20 WT and Δ*thyA* strains on MH-F agar with sterile discs soaked in water (1), thymidine 10 mg/ml (2), thymidine 300 μg/ml (3). Bacterial growth rendering a lawn switches color of the MH-F agar medium from red to brown. Dotted circles indicate the growth zone around thymidine discs; zooms of bacterial growth around a disc soaked in thymidine 10 mg/ml are shown. Growth inhibition of NTHi375 and RdKW20 WT and Δ*thyA* strains on chocolate agar around TxS discs; dotted lanes indicate growth inhibition. Bacterial morphology observed by SYTO 9 staining and confocal microscopy (scale bar, 10 μm), TEM (scale bar, 2 μm; magnification 25000×), and SEM (scale bar, 10 μm; magnification 6000×). In SEM panels, black arrows indicate infecting bacteria. **(C)** Effect of thymidine auxotrophy on *H. influenzae* self-aggregation. Tube-settling experiment of bacterial cultures previously grown for 11 h on sBHI, after incubation at room temperature for 5 h. Left, NTHi375 WT and Δ*thyA* strains; right, RdKW20 WT and Δ*thyA* strains; WT strains, black circle; Δ*thyA* mutants, black square. Bacterial aggregation was quantified by measuring the decrease of absorbance at OD_{600}. The *thyA* mutants self-aggregated faster than their isogenic WT strains (for NTHi375, $p < 0.05$ at 1 and 2 h; for RdKW20, $p < 0.05$ at 1 h, and $p < 0.0005$ at 2 h). All significant differences are indicated with *.

external thymidine, (ii) triggered enlarged bacilli which self-aggregate faster than their isogenic WT strains, (iii) increased resistance to TxS.

Thymidine Auxotrophy Causes Growth Defects in *H. influenzae*

Growth in sBHI was analyzed for WT and *thyA* mutant strains. NTHi375Δ*thyA* had an extended lag phase and lower final OD_{600} than the WT strain, which correlated with a reduced viability, measured as c.f.u./ml at the indicated time points (**Figure 2A**). Although not as pronounced, RdKW20Δ*thyA* also had a slightly extended lag phase and lower numbers of viable bacteria than those of the WT strain (**Figure 2B**). In both *thyA* mutants, the observed growth defects were partially restored by sBHI supplementation with thymidine 300 μg/ml, independently of its addition in the pre-culture used for further dilution in sBHI and

TABLE 2 | Bacterial growth in different media and conditions.

H. influenzae strain	Chocolate agar	MH-F agar	Diameter of bacterial growth on MH-F agar around Thy[a] disc (cm)	
			Thy 300 μg/ml	Thy 10 mg/ml
NTHi375	Yes	Yes	Yes	Yes
NTHi375Δ*thyA*	Yes	No[b]	0.65 ± 0.05	1.83 ± 0.025
NTHi375Δ*thyA*+Thy[c]	Yes	No	1.25 ± 0.05	2.9 ± 0.1
RdKW20	Yes	Yes	Yes	Yes
RdKW20Δ*thyA*	Yes	No	0.9 ± 0.1	1.83 ± 0.08
RdKW20Δ*thyA*+Thy	Yes	No	1.4 ± 0.1	3.35 ± 0.05

[a] *Thy, thymidine.*
[b] *Total absence of bacterial growth.*
[c] *NTHi375ΔthyA+Thy, bacteria previously grown on chocolate+Thy were used to inoculate chocolate agar or MH-F agar plates.*

OD_{600} recording, or in the actual sBHI culture used for growth monitoring over time (**Figures 2A,B**). Immunofluorescence microscopy at the final time point of the growth curve showed non-septated long bacterial filaments for NTHi375Δ*thyA* grown in sBHI, but a mixture of non-septated filaments and bacteria with the average NTHi WT size for NTHi375Δ*thyA* pre-grown in sBHI supplemented with thymidine 300 μg/ml (**Figure 2A**, right). This could relate to the observed restoration of final OD_{600} but not of final bacterial counts for NTHi375Δ*thyA* when pre-cultured in sBHI supplemented with thymidine.

The *thyA* mutants, previously grown on chocolate agar with thymidine (chocolate+Thy), grew on MH-F agar around discs in a thymidine dependent manner, displaying a larger growth zone around discs soaked with thymidine 10 mg/ml than with thymidine 300 μg/ml (NTHi375Δ*thyA*, $p < 0.005$; RdKW20Δ*thyA*, $p < 0.005$). Of note, *thyA* mutants previously grown on chocolate+Thy rendered a better growth on MH-F agar around discs soaked in thymidine than that of the same strains previously grown on chocolate agar (for thymidine 300 μg/ml, NTHi375Δ*thyA*, $p < 0.05$; for thymidine 10 mg/ml, NTHi375Δ*thyA*, $p < 0.05$, RdKW20Δ*thyA*, $p < 0.005$; **Figures 1B**, **2** bottom and **Table 2**). Similarly, external thymidine (chocolate+Thy) rendered *thyA* bacterial length and morphology similar to those shown by their respective isogenic WT strains (**Figures 1B**, **2** bottom).

Thymidine Auxotrophy Modifies the Expression of the Nucleoside Transporter Encoding *nupC* Gene in *H. influenzae*

Both *thyA* mutants growth on MH-F agar around discs soaked in thymidine, and morphology/growth restoration in the presence of external thymidine, prompted us to speculate that these mutants may use external thymidine to overcome their nucleoside dependency. It has been previously shown that the nucleoside transporter encoding gene *nupC* is overexpressed in *S. aureus* thymidine dependent-SCVs, and that a Δ*nupC* mutant fails to use external thymidine for growth under TxS challenge (Chatterjee et al., 2008; Kriegeskorte et al., 2014). HI0519 and NF38_02480 are annotated as *nupC* in the RdKW20 and NTHi375 genomes, respectively (Fleischmann et al., 1995; Mell et al., 2014). Expression of the *nupC* gene in *H. influenzae* was assessed by RT-qPCR, showing a trend to be higher in the Δ*thyA* than in their isogenic WT strains grown in sBHI, with stronger evidence in NTHi375 (Figure S2A). As shown in **Figure 2**, sBHI supplementation with thymidine partially restored the growth defects shown by the *thyA* mutants. Following the notion that thymidine supplementation may restore mutant-related phenotypes, expression of the *nupC* gene was analyzed in Δ*thyA* bacteria when pre-cultured in sBHI with thymidine and then grown in sBHI, or when grown in sBHI supplemented with thymidine. Unexpectedly, when mutant bacteria were pre-cultured in sBHI supplemented with thymidine 300 μg/ml and then grown in sBHI, expression of the *nupC* gene was even higher than when pre-cultured and grown in sBHI (Figure S2A). Of note, a total absence of growth inhibition was observed for *thyA* mutant strains on chocolate agar around TxS discs, when pre-grown on chocolate+Thy (data not shown).

Next, NTHi375Δ*nupC* and RdKW20Δ*nupC* strains were generated, showing growth rates comparable to those of their respective WT strains in sBHI (Figure S2B), chocolate agar and MH-F agar (data not shown). To assess the biological function of *nupC* as a pyrimidine transporter responsible for the uptake of extracellular thymidine in *H. influenzae*, we tested the *nupC* mutants for their ability to use external thymidine for growth under TxS challenge in a TxS disc diffusion assay. Inhibition zones on chocolate agar and MH-F agar were comparable for WT and Δ*nupC* strains. Growth inhibition around TxS discs was also tested on chocolate agar and MH-F agar plates supplemented with thymidine. Unfortunately, no conclusive differences were observed because, as already described, bacterial growth on plates with high concentration of thymidine may produce haze or fine growth areas (Lorian, 1996). Following this notion, we performed a search for pyrimidine transporters in all available genome sequenced *H. influenzae* strains, which did not reveal the presence of nucleoside transporters additional to NupC in this bacterial species. We also unsuccessfully attempted to generate a NTHi double mutant strain lacking both the *thyA* and *nupC* genes (data not shown), further supporting a role for NupC in the uptake of external thymidine.

Moreover, thymidylate is synthesized either by the thymidylate synthase ThyA or by the thymidine kinase TK, and inactivation of the former has been shown to result in upregulated expression of the later one in *Mycoplasma pneumoniae* (Wang et al., 2010). HI0529 and NF38_02430 are annotated as a *tdk* thymidine kinase in the RdKW20 and NTHi375 genomes, respectively (Fleischmann et al., 1995; Mell et al., 2014). Different to *nupC*, the *tdk* gene expression was shown to be similar in WT and Δ*thyA* strains grown in sBHI, independently of thymidine addition (Figure S2C).

Together, these results suggest that *nupC* may be a transporter for external thymidine in *H. influenzae*, whose increased expression could contribute to bypass the effects of TxS upon *de novo* thymidylate biosynthesis.

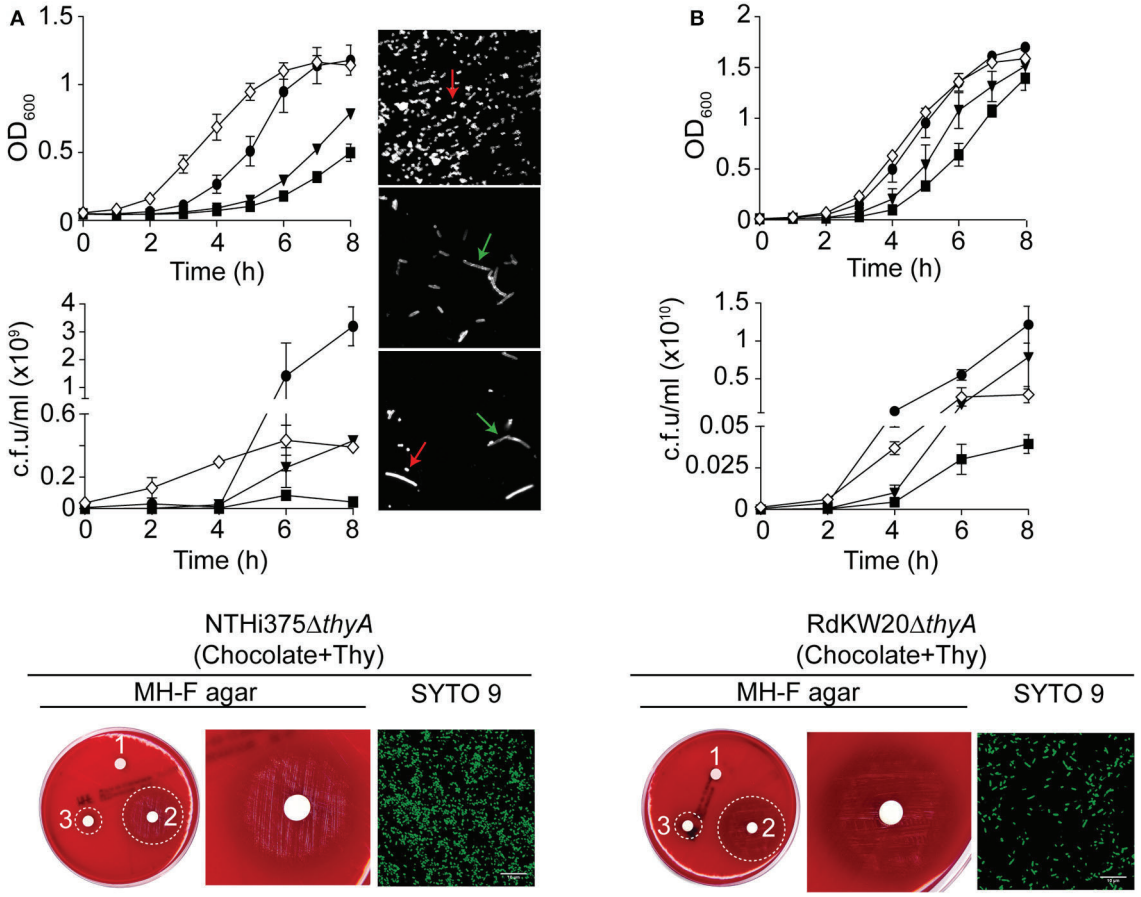

FIGURE 2 | *H. influenzae* growth is modified by thymidine availability. Bacterial growth, in the absence or presence of supplemented thymidine is shown for NTHi375 **(A)** and RdKW20 **(B)** WT and Δ*thyA* strains. Growth in sBHI is shown as a means of OD_{600} (upper) and c.f.u./ml (middle) at the indicated time points. WT strains were grown in sBHI (black circle); Δ*thyA* strains were (i) grown in sBHI (black square), (ii) grown in sBHI+thymidine 300 μg/ml (inverted black triangle), (iii) pre-grown in sBHI+thymidine 300 μg/ml and further diluted in sBHI for growth recording (white diamond). **(A,B)** bottom: growth of Δ*thyA* mutants, pre-grown on chocolate agar with thymidine 300 μg/ml (chocolate+Thy) and inoculated on MH-F agar with sterile discs soaked in water (1), thymidine 10 mg/ml (2), thymidine 300 μg/ml (3). Dotted circles indicate the growth zone around discs; bacterial morphology is shown by SYTO 9 staining and confocal microscopy (scale bar, 10 μm). Immunofluorescence microscopy at the final time point of the growth curve is shown for NTHi375 WT, Δ*thyA*, and Δ*thyA* pre-grown in sBHI supplemented with thymidine 300 μg/ml (top, middle, and bottom images in **A**, right, respectively). Red arrows indicate the average NTHi WT size; green arrows indicate non-septated bacterial filaments. Bacteria were labeled with rabbit anti-NTHi primary—and a donkey anti-rabbit conjugated to Cy2 secondary antibodies.

Thymidine Auxotrophy Reduces PCho Expression and C3b Deposition in *H. influenzae*

We have previously reported that bacteria lacking PCho self-aggregate slightly faster (Morey et al., 2013). Thymidine auxotroph mutants showed faster self-aggregation compared to that of their WT strains (**Figure 1C**), which could relate to changes in cellular morphology (i.e., elongation) or, alternatively, to a different amount of PCho residues on the bacterial surface. The level of PCho was measured on NTHi375 and RdKW20 WT and *thyA* mutant strains by flow cytometry using bacteria grown in sBHI. Thymidine auxotrophy was associated with a decreased detection of PCho in both NTHi375Δ*thyA* and RdKW20Δ*thyA* mutants, which was restored in NTHi375Δ*thyA* by bacterial growth in sBHI in the presence of thymidine. Indeed, PCho detection was higher in the thymidine dependent mutants grown in sBHI supplemented with thymidine than in their isogenic WT strains (**Figure 3A** and Figure S3A). Decreased levels of PCho in the *thyA* mutants may modify the bacterial ability to bind C-reactive protein (CRP; Weiser et al., 1998). However, CRP deposition on the bacterial surface was similar in WT and *thyA* mutant strains (**Figure 3B** and Figure S3B). Finally, to assess the possibility that cellular morphology may affect complement interaction, C3b deposition was analyzed. Thymidine auxotrophy was associated with decreased detection of C3b in NTHi375Δ*thyA*, which was restored by bacterial growth in sBHI supplemented with thymidine (**Figure 3C**). No differences were observed for C3b deposition between RdKW20 strains (Figure S3C).

Together, inactivation of the *thyA* gene caused a reduction in the amount of PCho residues on *H. influenzae* surface, leading to impaired C3b deposition in at least NTHi375, which suggests that

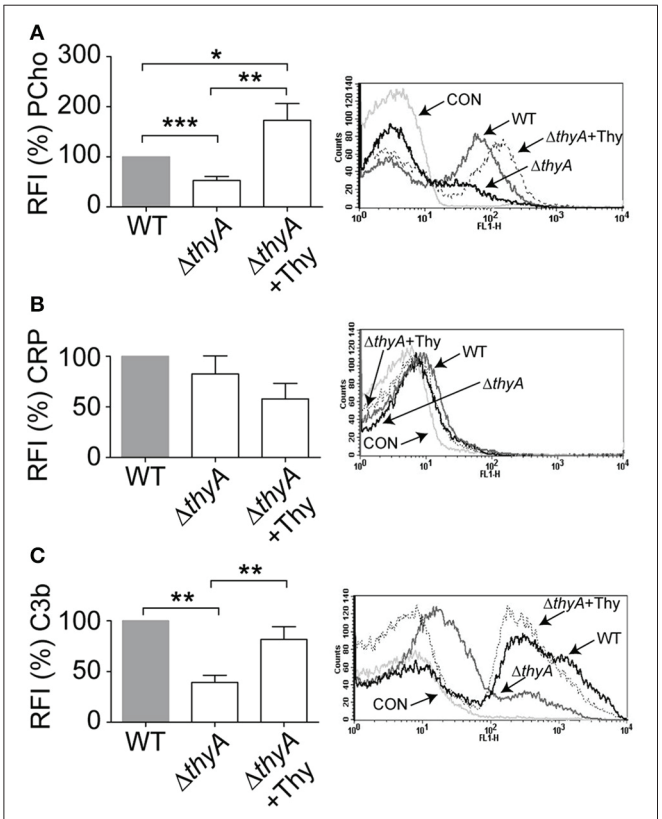

FIGURE 3 | Thymidine auxotrophy reduces PCho level and C3b binding on NTHi375. NTHi375 WT and Δ*thyA* strains were exponentially grown in sBHI, in the absence or presence of thymidine 300 μg/ml, and incubated with anti-PCho **(A)**, human serum and anti-CRP **(B)** or human serum and anti-C3b **(C)** antibodies. Binding was analyzed by flow cytometry. Representative flow cytometry histograms for each assay are shown (right). Color code: light gray, control (CON) buffer; gray, NTHi375; black, NTHi375Δ*thyA*; dotted lane, NTHi375Δ*thyA* grown in sBHI+Thy. NTHi375Δ*thyA* showed significantly lower PCho level ($p < 0.0001$) and C3b deposition ($p < 0.01$) than the WT strain, which was restored by mutant bacterial growth in sBHI with thymidine 300 μg/ml (PCho, $p < 0.01$; C3b, $p < 0.01$). PCho detection was significantly higher in NTHi375Δ*thyA* grown in sBHI supplemented with thymidine than in the WT strain ($p < 0.05$). *$p < 0.05$, **$p < 0.01$, ***$p < 0.0001$.

thymidine dependency may trigger changes affecting bacterial recognition by this key complement component by a CRP-independent mechanism.

Thymidine Auxotrophy Modifies *H. influenzae* Interaction with Human Airway Epithelia

The interplay of NTHi with the human respiratory epithelium plays a determinant role in the progression of infection (Clementi and Murphy, 2011). Next, we assessed if auxotrophy-related bacterial morphology changes could alter such interplay, by infecting A549 human type II pneumocytes with WT and *thyA* mutant strains (Morey et al., 2011; Lopez-Gomez et al., 2012; Euba et al., 2015c). Invasion by RdKW20 WT and *thyA* mutant strains was not assayed given the poor invasiveness of this genetic background (Mell et al., 2016). A549 cell adhesion and invasion by NTHi375Δ*thyA* was lower than that shown by the WT strain (**Figure 4A**). We also asked if external thymidine could restore such deficiency by using mutant bacteria grown in sBHI, in the absence or presence of thymidine (sBHI±Thy). A549 cell adhesion of NTHi375Δ*thyA* grown in sBHI was lower than that shown by the WT strain, which was restored by thymidine addition (**Figure 4A**, right). Similar results were obtained for RdKW20Δ*thyA* grown in sBHI, when compared to the WT strain, and to growth in sBHI with thymidine (Figure S4A). Given the impaired host cell interaction due to thymidine auxotrophy, we asked if inactivation of the *thyA* gene modifies the epithelial cell inflammatory response upon NTHi infection. Of note, the amount of secreted IL-8 was higher in A549 cells infected by NTHi375Δ*thyA* than by the WT strain, and such increase was reduced to WT levels upon infection by NTHi375Δ*thyA* previously grown on chocolate+Thy (**Figure 4C**). NTHi375Δ*thyA* lower epithelial infection rate was also observed during infection of NCI H-292 human bronchial epithelial cells (Euba et al., 2015c), for both adhesion and invasion (**Figure 4B**). NTHi375Δ*thyA* grown in sBHI showed lower adhesion to NCI H-292 cells than the WT strain, which was restored by thymidine supplementation, and adhesion by NTHi375Δ*thyA* grown in sBHI+Thy was higher than that shown by the WT strain (**Figure 4B**, right).

Complement opsonization, specifically C3, has been shown to enhance the bacterium-epithelial cell interaction for poorly encapsulated strains (de Astorza et al., 2004). Based on the observed differential C3b deposition by NTHi375 WT and Δ*thyA* strains, we next tested the effect of C3 in NTHi infection of A549 cells. NTHi375 and NTHi375Δ*thyA* strains were grown on chocolate agar (Δ*thyA*) or chocolate+Thy (Δ*thyA*+Thy), and A549 cells were infected in the presence of human purified C3, C3-deficient serum, or C3-deficient serum reconstituted with human purified C3. The level of bacterial attachment did not change in the presence of C3, compared to that observed in control untreated cells (CON) or cells co-incubated with C3-deficient serum (Figure S4B).

In summary, thymidine auxotrophy modified NTHi ability to infect airway epithelial cells in terms of bacterial location and triggered inflammatory response. Changes in adhesion and IL-8 secretion could be restored by addition of external thymidine in the bacterial growth medium. The presence of C3 at the onset of infection did not modulate bacterial adhesion.

Inactivation of the *thyA* Gene Attenuates *H. influenzae* Virulence and Confers Advantage under TxS Treatment *In vivo*

Finally, we sought to determine the impact of thymidine auxotrophy *in vivo*, by using a mouse NTHi respiratory infection model system previously used for NTHi375 (Morey et al., 2013; Euba et al., 2015a,b). Mice were infected with NTHi375 WT and *thyA* mutant strains grown on chocolate agar, and bacterial loads were quantified in lungs and BALF samples at 12, 24, and 48 hpi. In lungs, NTHi375Δ*thyA* bacterial numbers were lower than those recovered for the WT strain at the three infection time

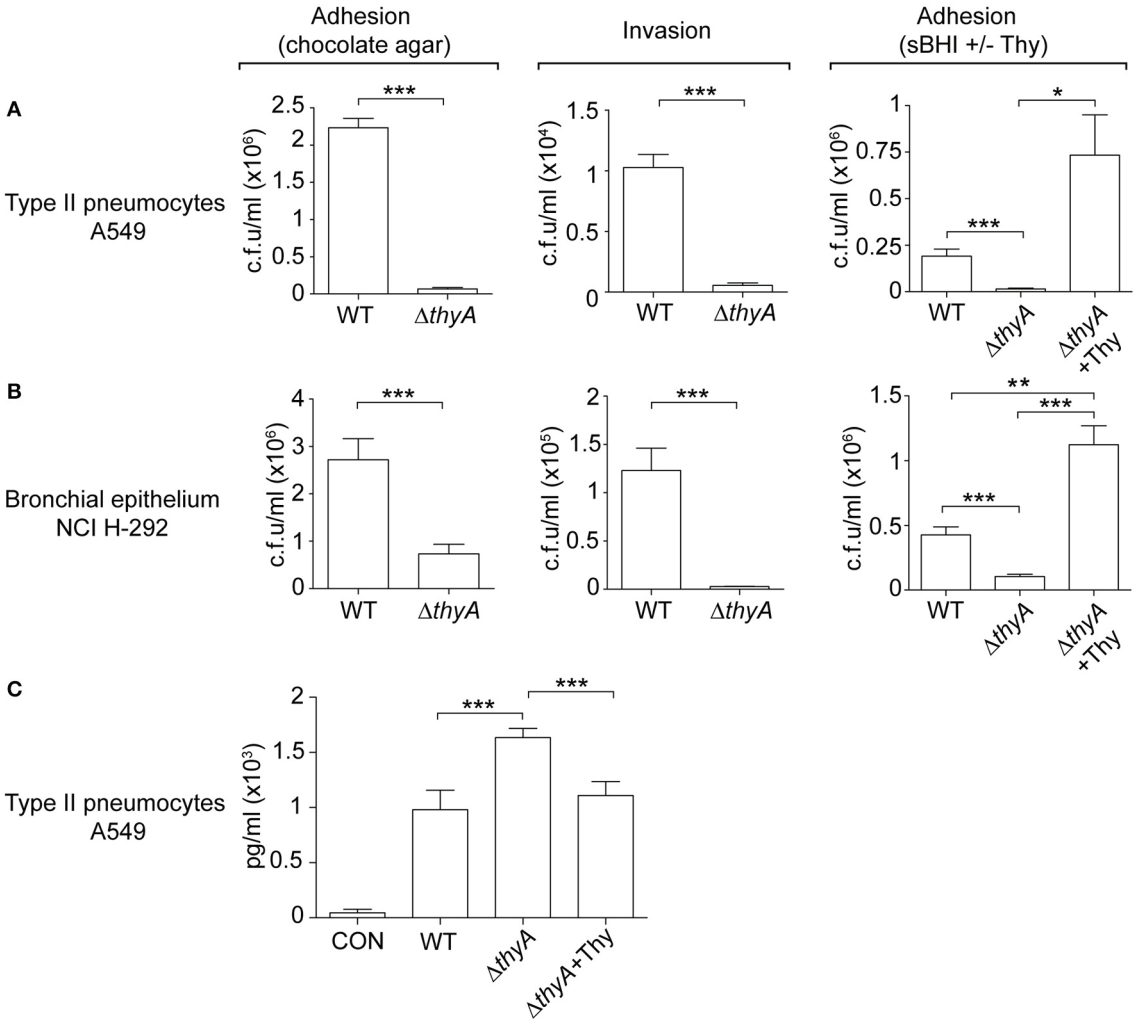

FIGURE 4 | The *thyA* gene inactivation modulates *H. influenzae* interplay with cultured human airway epithelia. A549 type II pneumocytes **(A)** and NCI H-292 bronchial epithelial cells **(B)** were used to quantify adhesion and invasion by NTHi375 WT and Δ*thyA* strains. For adhesion, infecting inocula were prepared by using bacteria previously grown on chocolate agar following previously established methods (Morey et al., 2011; left). Alternatively, bacteria previously grown on sBHI, in the absence or presence of thymidine (sBHI±Thy), were used (right). NTHi375Δ*thyA* showed significantly lower adhesion to A549 (chocolate agar, $p < 0.005$; sBHI, $p < 0.005$) and NCI H-292 (chocolate agar, $p < 0.005$; sBHI, $p < 0.005$) cells than the WT strain, which was restored by mutant pre-growth in sBHI with thymidine 300 μg/ml (A549, $p < 0.05$; NCI H-292, $p < 0.005$). NTHi375Δ*thyA* showed significantly lower entry into A549 ($p < 0.005$) and NCI H-292 ($p < 0.005$) cells than the WT strain. **(C)** IL-8 release was higher in cells infected by NTHi375Δ*thyA* than by the WT strain ($p < 0.005$); NTHi375Δ*thyA* growth on chocolate+Thy reduced IL-8 secretion to WT levels ($p < 0.005$). *$p < 0.05$, **$p < 0.005$, ***$p < 0.005$.

points tested. Thymidine dependency was also associated with significantly reduced bacterial counts in BALF at 12 and 24 hpi (**Figures 5A,B**).

To further investigate if thymidine auxotrophy, despite attenuation, confers an advantage to *H. influenzae* under TxS treatment, we used a therapeutic regimen consisting of one TxS dose (960 mg/kg, 1:5 TMP:SMX) every 6 h, starting at 6 hpi. Results indicate that TxS treatment was more efficient in reducing bacterial counts of the WT than of the *thyA* mutant strain. Thus, a significant reduction of the WT population in lungs at 12, 24, and 48 hpi, and BALF samples at 24 hpi, was observed under treated—compared to that of untreated conditions. In contrast, bacterial counts of NTHi375Δ*thyA* were unchanged at 12 and 24 hpi in both lungs and BALFs, despite TxS administration. The protective effect of *thyA* mutation against TxS was not observed at 48 hpi, maybe due to NTHi375Δ*thyA* severe clearance at this post-infection time point.

Based on the differences observed at 24 hpi, we attempted to restore the *thyA* mutant phenotypes by infecting with mutant bacteria previously grown in the presence of thymidine. However, intranasal inoculation of NTHi375Δ*thyA* grown on chocolate+Thy did not restore bacterial counts, and lung and BALF counts for NTHi375 WT were higher than those obtained for Δ*thyA* grown on chocolate+Thy. Unexpectedly, NTHi375Δ*thyA* previous growth on chocolate+Thy increased TxS efficiency, i.e., in TxS treated animals, lung, and BALF counts

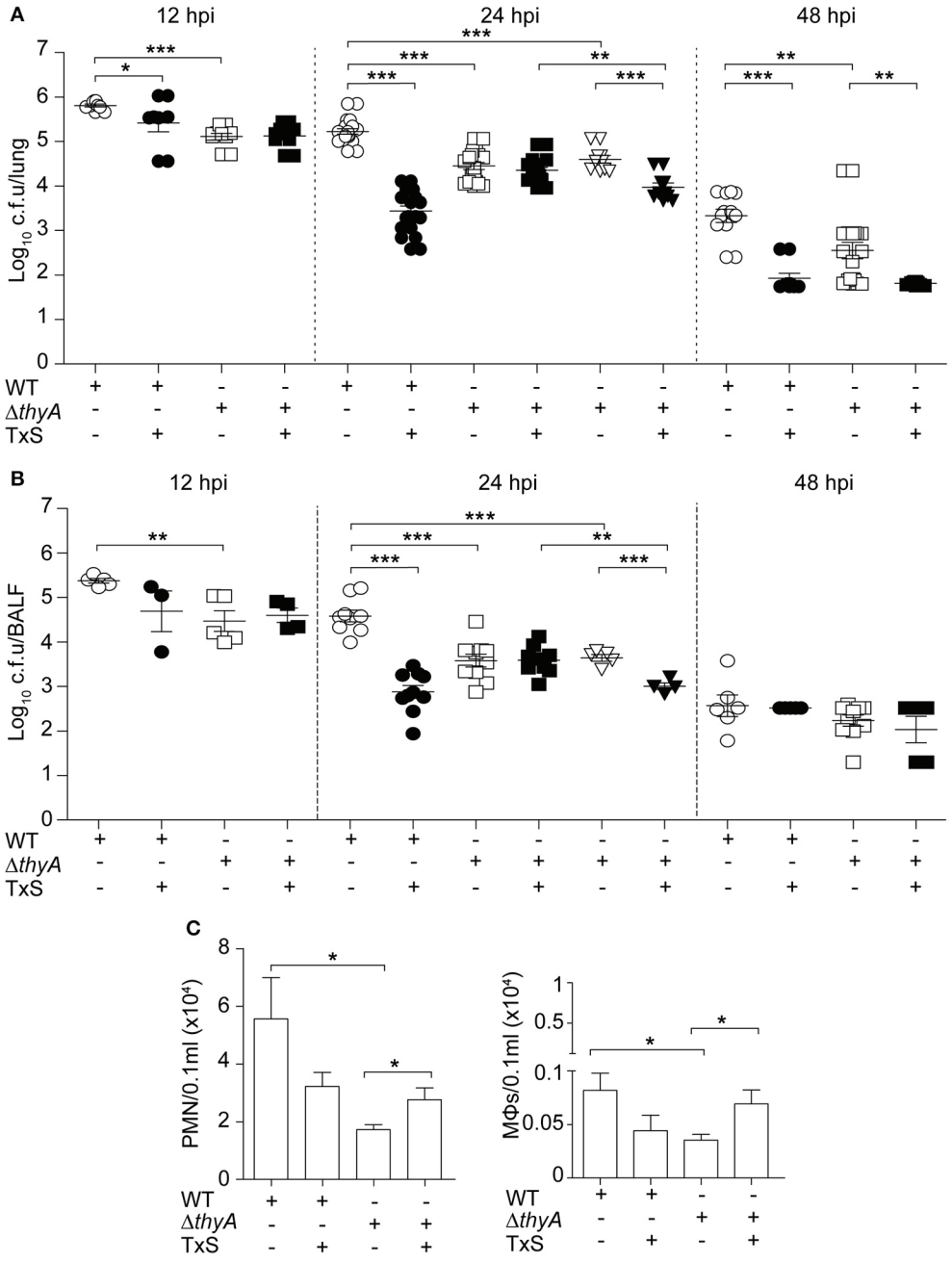

FIGURE 5 | Inactivation of the *thyA* gene attenuates *H. influenzae* virulence and confers advantage under TxS treatment *in vivo*. CD1 mice were infected with ~2 × 10^7 bacteria/mouse of NTHi375 WT (circle) or Δ*thyA* (square) strains. When necessary, a therapeutic regimen consisting of 960 mg/kg TxS (1:5 TMP:SMX) was administered orally each 6 h (dark symbols). Mice were euthanized at 12, 24, and 48 hpi, and bacterial loads were quantified in lungs (log_{10} c.f.u./lung) **(A)** and BALF (log_{10} c.f.u./BALF) **(B)**. NTHi375Δ*thyA* showed significantly lower loads in lungs and BALFs at 12 (lung, $p < 0.001$; BALF, $p < 0.01$), 24 (lung, $p < 0.001$; BALF, $p < 0.001$), and 48 (lung, $p < 0.01$) hpi than those shown by the WT strain. TxS administration significantly reduced WT strain recovery from lungs and BALF samples at 12 (lung, $p < 0.05$), 24 (lung, $p < 0.001$; BALF, $p < 0.001$), and 48 (lung, $p < 0.001$) hpi, compared to WT infected untreated mice. Inverted triangles: CD1 mice were infected with ~2 × 10^7 bacteria/mouse of Δ*thyA* strain previously grown on chocolate+Thy for 16 h; when necessary, a therapeutic regime consisting of 960 mg/kg TxS was administered orally each 6 h (dark inverted triangles). NTHi375Δ*thyA* previously grown on chocolate+Thy rendered significantly lower loads in lungs and BALFs than the WT strain ($p < 0.001$); NTHi375Δ*thyA* previously grown on chocolate+Thy showed significantly lower loads in lungs and BALFs of TxS treated—than in those of untreated mice ($p < 0.001$); in TxS treated mice, NTHi375Δ*thyA* previously grown on chocolate+Thy showed lower loads in lungs and BALFs than NTHi375Δ*thyA* previously grown on chocolate agar ($p < 0.01$). **(C)** BALF samples were analyzed for PMN (left) and alveolar macrophage (MΦ; right) counts at 12 hpi. Significantly higher numbers were observed in NTHi375 WT than in Δ*thyA* infected samples for both PMN ($p < 0.05$) and MΦs ($p < 0.05$). *$p < 0.05$, **$p < 0.01$, ***$p < 0.001$.

were higher for NTHi375Δ*thyA* grown on chocolate agar than for NTHi375Δ*thyA* grown on chocolate+Thy. Also, lung and BALF counts for NTHi375Δ*thyA* grown on chocolate+Thy were higher in untreated—than in TxS treated animals (**Figures 5A,B**).

Microscopy score of the average histopathological lesion in samples of mice infected with WT or Δ*thyA* strains was also determined along the respiratory tract, and compared for untreated and TxS-treated mice (**Table 3**). Histopathological analysis of upper airways, larynxes, tracheas, and lungs from mice intranasally infected with WT or with Δ*thyA* rendered inflammatory lesions. Lungs and airways from control mice instilled with PBS did not show significant inflammation or pathological changes, independently of TxS administration. In both WT and Δ*thyA*-infected mice, the upper airways showed PMN infiltration of the lamina propria and lumens. PMN infiltration was found in larger numbers in the lumens of Δ*thyA* infected mice than in those infected with WT bacteria, at both 12 and 24 hpi. Conversely, PMN infiltration of the upper airway lamina propria was found to be larger in WT—than in Δ*thyA* infected mice at 24 hpi. Mild PMN infiltration of the lamina propria and lumens containing red blood cells and PMNs were the main findings in larynxes and tracheas. A tendency towards increased red blood cells containing lumens in WT-infected compared to Δ*thyA* infected mice was apparent at 24 hpi, although the differences did not reach statistical significance. As previously described (Euba et al., 2015b), lungs in infected mice showed areas of acute bronchopneumonia where alveolar septa were thickened with edema and hyperemic septal capillaries. Neutrophils, alveolar macrophages and scattered small hemorrhages were observed in alveolar spaces. Comparison of scored lesions at 12 hpi showed significantly more hemorrhages at the lower airway of mice infected with WT than at those infected with Δ*thyA* bacteria in control untreated mice. Hemorrhages were also found in larger proportions at the alveoli of mice infected with NTHi375 at 12 than at 24 hpi, but a lower proportion of alveolar macrophages was found at the lower airway of mice infected with NTHi375 at 12 than at 24 hpi. Significant differences were not found at the alveoli of Δ*thyA* infected mice between post-infection time points. Analysis of scored lesions in the airways of WT infected mice showed differences between control untreated- and TxS treated-mice. We observed a higher proportion of PMN infiltration in (i) the upper airway lumens at 24 hpi in TxS treated—than in control untreated mice, and (ii) the alveoli in control untreated—than in TxS treated mice at 12 hpi. Conversely, Δ*thyA* infection caused comparable lesions in both untreated- and TxS treated-mice (**Table 3**). Intranasal inoculation of NTHi375Δ*thyA* previously grown on chocolate+Thy rendered similar inflammatory lesions in both untreated- and TxS treated-animals; as a sole difference, a higher proportion of PMN infiltration was observed in the alveoli of TxS treated—than of control untreated mice ($p < 0.05$).

Last, we quantified accumulation of immune cells in the collected BALF samples at 12 hpi. NTHi375 WT pulmonary infection increased the accumulation of PMNs and alveolar macrophages, compared to that observed in the BALF of Δ*thyA* infected mice. TxS treatment showed a trend to reduce immune cell accumulation in BALF samples of WT infected mice. Unexpectedly, TxS treatment increased immune cell accumulation in BALF samples of Δ*thyA* infected mice (for both PMNs and alveolar macrophages; **Figure 5C**).

In summary, thymidine auxotrophy reduces NTHi virulence but, concomitantly, it confers an advantage under TxS treatment *in vivo*, suggesting that uptake of external thymidine from the infected tissue may contribute to bypass the bactericidal effect of TxS. Moreover, overall higher inflammatory traits were observed in WT—than in Δ*thyA* infected mice.

DISCUSSION

First-line antimicrobial agents must be effective, reliable, widely available and affordable in resource-poor settings (Grant et al., 2009). Following this notion, oral TxS has been recommended for years as initial antibacterial for acute otitis media, non-severe pneumonia or AECOPD because of its effectiveness and reasonable price, which, in turn, has resulted in increased resistance patterns by frequent respiratory pathogens such as *H. influenzae*. Thus, *H. influenzae* increased TxS resistance has been reported in clinical isolates from serotypes b, e, and f, and non-typeable strains from various pathological origins (Rowe et al., 2000; Leiberman et al., 2001; Campos et al., 2003a,b; Arguedas et al., 2005; Mohd-Zain et al., 2012; Puig et al., 2014; Greenhill et al., 2015). Besides *H. influenzae* TxS resistance due to changes in the sequence and/or expression of the *folH* and *folP* genes, or acquisition of the *sul* genes (de Groot et al., 1988, 1996; Enne et al., 2002), TMP resistance has been reported to arise in this pathogen as an indirect result of mutation to thymidine/thymine auxotrophy (Platt et al., 1983). Standard procedures for determination of *H. influenzae* antibiotic susceptibility at diagnostic laboratories involve the use of the low thymidine containing medium MH-F, which could underestimate the frequency of thymidine-dependent TMP/TxS resistance. Indeed, the routine evaluation of NTHi clinical isolates carried out in this study reported a proportion of strains designated as forming slow-growing colonies, which prompted us to screen their thymidine dependency, leading to identification of the thymidine auxotroph NTHi8233. Compared to $ThyA_{RdKW20}$, $ThyA_{NTHi8233}$ has a two-amino acid insertion at positions 90 and 91, which slightly modifies its predicted structure (Figure S1). Inactive *thyA* gene alleles have been reported for *S. aureus* due to in-frame deletions, deletions resulting in a frameshift, or point mutations resulting in amino acid transitions or non-sense mutations (Chatterjee et al., 2008; Kriegeskorte et al., 2014). In this study, we identified a NTHi *thyA* allele with an in-frame insertion compared to previously genome sequenced strains, which could alter its enzymatic activity. The ThyA canonical active site tryptophan (W83) proposed for bacterial sequences (Baugh et al., 2013) is conserved in $ThyA_{NTHi8233}$, and future work will attempt to purify $ThyA_{NTHi8233}$ and further assess its thymidylate synthase activity.

Moreover, NTHi8233 thymidine auxotrophy was found to be reversible, and such reversion was associated to disappearance

TABLE 3 | Score of histopathological lesions found in the airways of control untreated or TxS treated mice, intranasally infected with NTHi375 WT or Δ*thyA* strains.

		Score (mean ± *SD*)[b]								
		Upper airways			Larynx-trachea		Lung			
Strain	**Treatment[a]/hpi**	**PMNs[c] lumen**	**PMNs lamina propria**	**Hyperemia**	**Red blood cells lumen**	**PMNs lamina propria**	**Hyperemia**	**Hemorrhage**	**Bronchial-alveolar PMNs**	**Alveolar macrophages**
NTHi375	Control/12 h	[d,f]1.5 ± 0.9	1.2 ± 0.4	0.8 ± 0.2	1.1 ± 1.3	0.8 ± 0.4	1.3 ± 0.3	[f,i]0.7 ± 0.3	[h]2 ± 0.5	[j]0.7 ± 0.2
	TxS/12 h	1.1 ± 0.6	1	1.1 ± 0.4	0.5 ± 1	0.7 ± 0.3	1.5 ± 0.7	0.3 ± 0.5	[h]1.3 ± 0.2	0.5 ± 0.4
	Control/24 h	[d,g]0.6 ± 0.6	[e]1.1 ± 0.3	1.1 ± 0.2	1.4 ± 0.9	0.7 ± 0.2	1.7 ± 0.6	[i]0.2 ± 0.2	1.8 ± 0.4	[j]1.4 ± 0.3
	TxS/24 h	[g]2.1 ± 1.9	1 ± 0.5	1.1 ± 0.5	1.7 ± 1.2	0.4 ± 0.2	1.7 ± 0.4	0.6 ± 0.6	1.8 ± 0.5	1.7 ± 0.2
NTHi375Δ*thyA*	Control/12 h	[d]2.5 ± 0.3	0.9 ± 0.2	0.9 ± 0.2	1.5 ± 0.8	0.7 ± 0.3	1.1 ± 0.4	[f]0.3 ± 0.2	1.7 ± 0.2	0.4 ± 0.2
	TxS/12 h	2.1 ± 0.4	0.9 ± 0.2	0.6 ± 0.2	0.8 ± 1.1	0.8 ± 0.4	0.9 ± 0.4	0.1 ± 0.2	1.7 ± 0.5	0.8 ± 0.4
	Control/24 h	[d]1.7 ± 1.1	[e]0.6 ± 0.2	1 ± 0.3	0.5 ± 0.8	0.7 ± 0.2	1.6 ± 0.4	0.2 ± 0.2	2 ± 0.3	1.1 ± 0.4
	TxS/24 h	1.8 ± 0.2	0.8 ± 0.2	0.8 ± 0.3	0.5 ± 1	0.6 ± 0.4	1 ± 0.4	0.1 ± 0.2	1.9 ± 0.4	1.1 ± 0.2

[a]*Control, animals administered vehicle solution; TxS, postinfection, one TxS dose was administered each 6 h.*

[b]*Statistical comparisons of mean values were performed using one-way ANOVA followed by Fisher's PLSD multiple-comparison test.*

[c]*PMNs: infiltrates of polymorphonuclear cells.*

[d]*More recruitment of PMNs at the upper airway lumen of mice infected with NTHi375ΔthyA than with WT at 12 and 24 hpi (both, $p < 0.05$).*

[e]*More recruitment of PMNs at the upper airway lamina propria of mice infected with WT than with ΔthyA bacteria at 24 hpi ($p < 0.05$).*

[f]*Higher alveolar hemorrhage in the lungs of mice infected with WT than with ΔthyA bacteria at 12 hpi ($p < 0.05$).*

[g]*Lower proportion of PMNs at the upper airway lumen (24 hpi) of WT bacteria infected mice untreated than TxS treated ($p < 0.05$).*

[h]*Larger proportion of PMNs at the alveoli (12 hpi) of WT bacteria infected mice untreated than TxS treated ($p < 0.05$).*

[i]*Higher alveolar hemorrhage in the lungs of mice infected with WT bacteria at 12 than at 24 hpi ($p < 0.01$).*

[j]*Lower numbers of alveolar macrophages at the alveoli of mice infected with WT bacteria at 12 than at 24 hpi ($p < 0.01$).*

of the in-frame insertion in the *thyA*$_{NTHi8233}$ gene. This transient phenotype, in agreement with previous observations (Platt et al., 1983), prompts us to speculate that reversible thymidine auxotrophy may lead into the infrequent isolation of thymidine dependent NTHi strains from respiratory samples. In contrast, TxS resistance level remained unchanged in NTHi8233, independent of auxotrophy reversion. Of note, increased TMP resistance has been previously found in *H. influenzae* thymidine prototrophs isolated soon after isogenic thymidine auxotrophs recovery from sputum samples exposed to subinhibitory TMP concentrations, suggesting that TMP resistance could be the result of a suppressor mutation (Platt et al., 1983). Following this observation, the MIC of TMP for NTHi8233 was >32 μg/ml, independent of auxotrophy reversion. The mechanism(s) underlying TMP/TxS resistance in NTHi8233 is currently unknown and will be subject of future study.

Reversible thymidine auxotrophy has been widely shown for *S. aureus* thymidine dependent-SCVs (Kahl, 2014), and made NTHi8233 inadequate for analysis of the impact of thymidine dependency on NTHi pathogenesis. For this purpose, the *thyA* gene was inactivated in strains NTHi375 and RdKW20. NTHi *thyA* mutants displayed alterations in morphology and growth, and dependence on external thymidine, comparable to those shown by *S. aureus*, *Salmonella typhimurium*, or *S. maltophilia* thymidine auxotrophs (Kok et al., 2001; Kahl et al., 2003, 2005; Anderson et al., 2007; Chatterjee et al., 2008). Moreover, NTHi *thyA* gene disruption caused a reduced PCho level and C3b deposition, impaired airway epithelial adhesion and invasion, and enhanced secretion of IL-8 by cultured epithelial cells. In some cases, minor phenotypic differences were observed between NTHi375 and RdKW20 *thyA* mutants, likely to be related to the known NTHi genomic heterogeneity (De Chiara et al., 2014). Altogether, the observed *in vitro* phenotypes, such as a deficient interaction with—and an increased inflammatory response by cultured airway epithelial cells upon infection by Δ*thyA* mutant strains, are likely to contribute to NTHi thymidine auxotroph attenuation upon murine lung infection. Modification of the biology of infection due to thymidine auxotrophy has been reported for other bacterial pathogens including *S. aureus*, *S. typhimurium*, *Shigella flexneri*, or *Vibrio cholerae* (Attridge, 1995; Cersini et al., 1998; Kok et al., 2001; Kriegeskorte et al., 2014). We acknowledge that a limitation of this study is the lack of genetic complementation for the *thyA* gene inactivation. Several approaches were unsuccessfully undertaken for plasmid-encoded *thyA*$_{RdKW20}$ gene complementation into RdKW20Δ*thyA*, and plasmid-encoded heterologous expression of the *thyA*$_{NTHi8233}$ allele into RdKW20Δ*thyA* (data not shown). Of note, we exclude a relationship between the *thyA* gene-related phenotypes shown in this study and overexpression of the immediately downstream gene, a putative homolog of the *tadA* gene encoding a tRNA-specific adenosine deaminase, in the *thyA* mutants (data not shown). Overexpression of the *tadA* gene has been shown to confer resistance to the bactericidal natural product xanthorrhizol in *E. coli* (Yogiara et al., 2015). Importantly, addition of external thymidine in the growth media restored, partial or totally, all analyzed *in vitro* phenotypes. Attenuation of NTHi375Δ*thyA* *in vivo* was not restored by infecting bacteria previously grown in the presence of external thymidine, which could be due to the observed partial restoration of thymidine prototrophy by available external thymidine, shown to be dependent on thymidine concentration on MH-F agar.

In addition to the impact of thymidine auxotrophy by inactivation of the *thyA* gene on NTHi virulence, TxS resistance was shown to increase in the Δ*thyA* mutant strains. Disruption of the *thyA* gene has been related to increased TMP resistance in other bacteria (Song et al., 2016). In agreement, the MIC of TMP was 1 and >32 μg/ml for NTHi375 WT and Δ*thyA* strains, respectively, and was 0.75 and >32 μg/ml for RdKW20 WT and Δ*thyA* strains, respectively. NTHi375Δ*thyA* pre-grown in chocolate+Thy was cleared faster in TxS-treated than in untreated mice, and the reason(s) for this observation is currently unknown. Although, originally intended to restore the observed increased expression of the *nupC* gene upon *thyA* inactivation, mutant pre-growth in sBHI with thymidine further amplified *nupC* expression, compared to sBHI. It should be noted that increased *nupC* gene expression by a *thyA* mutant in *S. aureus* was previously restored by complementing *thyA* gene disruption (Chatterjee et al., 2008). Our observation was unexpected and formally incomparable to that made for *S. aureus*. We speculate that it could be associated with the lack of growth inhibition around TxS discs observed for *thyA* mutant strains when pre-grown in chocolate+Thy, therefore suggesting that uptake of external thymidine by the NupC nucleoside transporter could contribute to circumvent the effects of TxS upon *de novo* thymidylate biosynthesis in NTHi. We suggest here for the first time that NupC could function as a primary thymidine transporter in NTHi if *de novo* thymidylate synthesis is blocked. Search in all available genome sequenced *H. influenzae* strains did not reveal the presence of additional nucleoside transporters in this bacterial species. As expected, we unsuccessfully attempted to generate a NTHi double mutant strain lacking both the *thyA* and *nupC* genes (data not shown), further supporting the proposed role for NupC.

Three additional aspects deserve further discussion. First, *S. aureus* thymidine dependent SCVs grow on Columbia blood agar (Kriegeskorte et al., 2014); *S. maltophilia* thymidine dependent SCVs grow on sheep blood-, brucella-, and chocolate-agar (Anderson et al., 2007), but neither grow on MacConkey agar and M9 minimal medium (Anderson et al., 2007), nor *S. typhimurium thyA* mutants grow on LB agar (Kok et al., 2001). Our results show that NTHiΔ*thyA* thymidine auxotrophs grow rendering normal size colonies on chocolate—and sBHI-agar, but fail to grow on MH-F agar. Therefore, we may not consider the term thymidine dependent SCVs for *H. influenzae*. Second, *S. aureus* SCVs are recovered from several human and animal specimens, and are a highly dynamic subpopulation optimized for persistence, enabling the bacteria to hide inside the host cell without eliciting a strong host response (Kahl, 2014; Kahl et al., 2016). This may be unlikely for NTHi thymidine auxotrophs, given that we observed a significantly impaired airway epithelial cell invasion by the NTHi375Δ*thyA* mutant strain. Third, this study does not tackle the induction of NTHi thymidine auxotrophy by TxS challenge, and we therefore cannot speculate on the selection for thymine auxotrophs and TxS resistance due to prolonged antibiotic exposure. Unexpectedly, no statistically significant connection has been found between

regional TxS use and resistance among *H. influenzae* isolates (Karpanoja et al., 2008). We should also consider the potential emergence of mutations in the *thyA* gene as a consequence of treatment with other antibiotics with mutagenic activity such as ciprofloxacin, which concomitantly increases TMP resistance (Song et al., 2016). Hence, emergence of TxS resistance in response to exposure to antibiotics needs further analysis and continuous monitoring.

In conclusion, this study shows for the first time the impact of thymidine auxotrophy by disruption of the thymidylate synthase *thyA* on *H. influenzae* morphology and interplay with the host airway and, indirectly, on its resistance to TxS. We also show NupC as a potential facilitator of external thymidine uptake upon inhibition of thymidylate *de novo* synthesis. Thymidine auxotrophy lowers NTHi virulence, but also provides an advantage under TxS exposure. Thus, our results should be considered for the consequences of TxS administration in the clinical settings. Further studies will contribute to better assess the emergence of NTHi thymidine auxotrophs in clinical samples, likely to be currently underestimated, and to understand if NTHi thymidine dependency may be a response to antibiotic treatment with a survival advantage in specific environments.

AUTHOR CONTRIBUTIONS

IR, SM, BE, AF, JM, NL, MB, JR, FT, and CL have participated in the design and fulfillment of the experimental work. IR, SM, CA, JL, JY, and JG carried out in the conceptual design of the study. IR, SM, JL, JY, and JG have written the manuscript (text, tables, and figures). All authors have participated in the correction of the manuscript to its final version.

ACKNOWLEDGMENTS

We wish to thank the staff of the Microbiology Laboratory of Bellvitge University Hospital who contributed to this project on a daily basis. IR is funded by a Ph.D. studentship from Universidad Pública de Navarra, Spain; JM is funded by Ph.D. studentship BES-2013-062644 from Ministerio Economía y Competitividad-MINECO, Spain; SM is funded by a postdoctoral contract from CIBER Enfermedades Respiratorias (CIBERES); NL is funded by a contract from Department of Economy, Regional Govern from Navarra, Spain, reference 0011-1307-2015-000037. This work has been funded by grants from MINECO SAF2012-31166 and SAF2015-66520-R, Health Department, Regional Govern from Navarra, Spain, reference 03/2016, and SEPAR 31/2015 to JG. CIBERES is an initiative from Instituto de Salud Carlos III (ISCIII), Madrid, Spain. We acknowledge support of the publication fee by the CSIC Open Access Publication Support Initiative through its Unit of Information Resources for Research (URICI).

SUPPLEMENTARY MATERIAL

The Supplementary Material for this article can be found online at: http://journal.frontiersin.org/article/10.3389/fcimb.2017.00266/full#supplementary-material

REFERENCES

Agrawal, A., and Murphy, T. F. (2011). *Haemophilus influenzae* infections in the *H. influenzae* type b conjugate vaccine era. *J. Clin. Microbiol.* 49, 3728–3732. doi: 10.1128/JCM.05476-11

Allen, S., Zaleski, A., Johnston, J. W., Gibson, B. W., and Apicella, M. A. (2005). Novel sialic acid transporter of *Haemophilus influenzae*. *Infect. Immun.* 73, 5291–5300. doi: 10.1128/IAI.73.9.5291-5300.2005

Anderson, S. W., Stapp, J. R., Burns, J. L., and Qin, X. (2007). Characterization of small-colony-variant *Stenotrophomonas maltophilia* isolated from the sputum specimens of five patients with cystic fibrosis. *J. Clin. Microbiol.* 45, 529–535. doi: 10.1128/JCM.01444-06

Arguedas, A., Sierra, H., Soley, C., Guevara, S., and Brilla, E. (2005). Activity of trimethoprim-sulfamethoxazole against middle ear fluid pathogens obtained from Costa Rican children with otitis media. *Pediatr. Infect. Dis. J.* 24, 839–841. doi: 10.1097/01.inf.0000177286.40817.10

Attridge, S. R. (1995). Thymine auxotrophy as an attenuating marker in *Vibrio cholerae*. *Microb. Pathog.* 19, 11–18. doi: 10.1006/mpat.1995.0040

Barnes, P. J. (2016). Inflammatory mechanisms in patients with chronic obstructive pulmonary disease. *J. Allergy Clin. Immunol.* 138, 16–27. doi: 10.1016/j.jaci.2016.05.011

Baugh, L., Gallagher, L. A., Patrapuvich, R., Clifton, M. C., Gardberg, A. S., Edwards, T. E., et al. (2013). Combining functional and structural genomics to sample the essential Burkholderia structome. *PLoS ONE* 8:e53851. doi: 10.1371/journal.pone.0053851

Besier, S., Zander, J., Siegel, E., Saum, S. H., Hunfeld, K. P., Ehrhart, A., et al. (2008). Thymidine-dependent *Staphylococcus aureus* small-colony variants: human pathogens that are relevant not only in cases of cystic fibrosis lung disease. *J. Clin. Microbiol.* 46, 3829–3832. doi: 10.1128/JCM.01440-08

Campos, J., Roman, F., Perez-Vazquez, M., Aracil, B., Oteo, J., Cercenado, E., et al. (2003a). Antibiotic resistance and clinical significance of *Haemophilus influenzae* type f. *J. Antimicrob. Chemother.* 52, 961–966. doi: 10.1093/jac/dkh004

Campos, J., Roman, F., Perez-Vazquez, M., Oteo, J., Aracil, B., Cercenado, E., et al. (2003b). Infections due to *Haemophilus influenzae* serotype E: microbiological, clinical, and epidemiological features. *Clin. Infect. Dis.* 37, 841–845. doi: 10.1086/377232

Cersini, A., Salvia, A. M., and Bernardini, M. L. (1998). Intracellular multiplication and virulence of *Shigella flexneri* auxotrophic mutants. *Infect. Immun.* 66, 549–557.

Chatterjee, I., Kriegeskorte, A., Fischer, A., Deiwick, S., Theimann, N., Proctor, R. A., et al. (2008). *In vivo* mutations of thymidylate synthase (encoded by thyA) are responsible for thymidine dependency in clinical small-colony variants of *Staphylococcus aureus*. *J. Bacteriol.* 190, 834–842. doi: 10.1128/JB.00912-07

Clementi, C. F., and Murphy, T. F. (2011). Non-typeable *Haemophilus influenzae* invasion and persistence in the human respiratory tract. *Front. Cell Infect. Microbiol.* 1:1. doi: 10.3389/fcimb.2011.00001

de Astorza, B., Cortes, G., Crespi, C., Saus, C., Rojo, J. M., and Alberti, S. (2004). C3 promotes clearance of *Klebsiella pneumoniae* by A549 epithelial cells. *Infect. Immun.* 72, 1767–1774. doi: 10.1128/IAI.72.3.1767-1774.2004

De Chiara, M., Hood, D., Muzzi, A., Pickard, D. J., Perkins, T., Pizza, M., et al. (2014). Genome sequencing of disease and carriage isolates of nontypeable *Haemophilus influenzae* identifies discrete population structure. *Proc. Natl. Acad. Sci. U.S.A.* 111, 5439–5444. doi: 10.1073/pnas.1403353111

de Groot, R., Campos, J., Moseley, S. L., and Smith, A. L. (1988). Molecular cloning and mechanism of trimethoprim resistance in *Haemophilus influenzae*. *Antimicrob. Agents Chemother.* 32, 477–484. doi: 10.1128/AAC.32.4.477

de Groot, R., Sluijter, M., de Bruyn, A., Campos, J., Goessens, W. H., Smith, A. L., et al. (1996). Genetic characterization of trimethoprim resistance in *Haemophilus influenzae*. *Antimicrob. Agents Chemother.* 40, 2131–2136.

Enne, V. I., King, A., Livermore, D. M., and Hall, L. M. (2002). Sulfonamide resistance in *Haemophilus influenzae* mediated by acquisition of sul2 or a short insertion in chromosomal folP. *Antimicrob. Agents Chemother.* 46, 1934–1939. doi: 10.1128/AAC.46.6.1934-1939.2002

Euba, B., Moleres, J., Segura, V., Viadas, C., Morey, P., Moranta, D., et al. (2015a). Genome expression profiling-based identification and administration efficacy of host-directed antimicrobial drugs against respiratory infection by nontypeable *Haemophilus influenzae*. *Antimicrob. Agents Chemother.* 59, 7581–7592. doi: 10.1128/AAC.01278-15

Euba, B., Moleres, J., Viadas, C., Barberan, M., Caballero, L., Grillo, M. J., et al. (2015b). Relationship between azithromycin susceptibility and administration efficacy for nontypeable *Haemophilus influenzae* respiratory infection. *Antimicrob. Agents Chemother.* 59, 2700–2712. doi: 10.1128/AAC.04447-14

Euba, B., Moleres, J., Viadas, C., Ruiz de los Mozos, I., Valle, J., Bengoechea, J. A., et al. (2015c). Relative contribution of P5 and Hap surface proteins to nontypeable *Haemophilus influenzae* interplay with the host upper and lower airways. *PLoS ONE* 10:e0123154. doi: 10.1371/journal.pone.0123154

Fleischmann, R. D., Adams, M. D., White, O., Clayton, R. A., Kirkness, E. F., Kerlavage, A. R., et al. (1995). Whole-genome random sequencing and assembly of *Haemophilus influenzae* Rd. *Science* 269, 496–512. doi: 10.1126/science.7542800

Grant, G. B., Campbell, H., Dowell, S. F., Graham, S. M., Klugman, K. P., Mulholland, E. K., et al. (2009). Recommendations for treatment of childhood non-severe pneumonia. *Lancet Infect. Dis.* 9, 185–196. doi: 10.1016/S1473-3099(09)70044-1

Greenhill, A. R., Phuanukoonnon, S., Michael, A., Yoannes, M., Orami, T., Smith, H., et al. (2015). *Streptococcus pneumoniae* and *Haemophilus influenzae* in paediatric meningitis patients at Goroka General Hospital, Papua New Guinea: serotype distribution and antimicrobial susceptibility in the pre-vaccine era. *BMC Infect. Dis.* 15:485. doi: 10.1186/s12879-015-1197-0

Herriott, R. M., Meyer, E. Y., Vogt, M., and Modan, M. (1970). Defined medium for growth of *Haemophilus influenzae*. *J. Bacteriol.* 101, 513–516.

Hood, D. W., Makepeace, K., Deadman, M. E., Rest, R. F., Thibault, P., Martin, A., et al. (1999). Sialic acid in the lipopolysaccharide of *Haemophilus influenzae*: strain distribution, influence on serum resistance and structural characterization. *Mol. Microbiol.* 33, 679–692. doi: 10.1046/j.1365-2958.1999.01509.x

Iyer Parameswaran, G., and Murphy, T. F. (2009). Chronic obstructive pulmonary disease: role of bacteria and updated guide to antibacterial selection in the older patient. *Drugs Aging* 26, 985–995. doi: 10.2165/11315700-000000000-00000

Kahl, B. C. (2014). Small colony variants (SCVs) of *Staphylococcus aureus*-a bacterial survival strategy. *Infect. Genet. Evol.* 21, 515–522. doi: 10.1016/j.meegid.2013.05.016

Kahl, B. C., Becker, K., and Loffler, B. (2016). Clinical significance and pathogenesis of staphylococcal small colony variants in persistent infections. *Clin. Microbiol. Rev.* 29, 401–427. doi: 10.1128/CMR.00069-15

Kahl, B. C., Belling, G., Becker, P., Chatterjee, I., Wardecki, K., Hilgert, K., et al. (2005). Thymidine-dependent *Staphylococcus aureus* small-colony variants are associated with extensive alterations in regulator and virulence gene expression profiles. *Infect. Immun.* 73, 4119–4126. doi: 10.1128/IAI.73.7.4119-4126.2005

Kahl, B. C., Belling, G., Reichelt, R., Herrmann, M., Proctor, R. A., and Peters, G. (2003). Thymidine-dependent small-colony variants of *Staphylococcus aureus* exhibit gross morphological and ultrastructural changes consistent with impaired cell separation. *J. Clin. Microbiol.* 41, 410–413. doi: 10.1128/JCM.41.1.410-413.2003

Karpanoja, P., Nyberg, S. T., Bergman, M., Voipio, T., Paakkari, P., Huovinen, P., et al. (2008). Connection between trimethoprim-sulfamethoxazole use and resistance in *Streptococcus pneumoniae*, *Haemophilus influenzae*, and *Moraxella catarrhalis*. *Antimicrob. Agents Chemother.* 52, 2480–2485. doi: 10.1128/AAC.01118-07

Kok, M., Bühlmann, E., and Pechère, J.-C. (2001). *Salmonella typhimurium* thyA mutants fail to grow intracellularly *in vitro* and are attenuated in mice. *Microbiology* 147, 727–733. doi: 10.1099/00221287-147-3-727

Kriegeskorte, A., Block, D., Drescher, M., Windmüller, N., Mellmann, A., Baum, C., et al. (2014). Inactivation of thyA in *Staphylococcus aureus* attenuates virulence and has a strong impact on metabolism and virulence gene expression. *mBio* 5:e01447-14. doi: 10.1128/mBio.01447-14

Lazaro-Diez, M., Navascues-Lejarza, T., Remuzgo-Martinez, S., Navas, J., Icardo, J. M., Acosta, F., et al. (2016). *Acinetobacter baumannii* and *A. pittii* clinical isolates lack adherence and cytotoxicity to lung epithelial cells *in vitro*. *Microbes Infect.* 18, 559–564. doi: 10.1016/j.micinf.2016.05.002

Leiberman, A., Leibovitz, E., Piglansky, L., Raiz, S., Press, J., Yagupsky, P., et al. (2001). Bacteriologic and clinical efficacy of trimethoprim-sulfamethoxazole for treatment of acute otitis media. *Pediatr. Infect. Dis. J.* 20, 260–264. doi: 10.1097/00006454-200103000-00009

Lopez-Gomez, A., Cano, V., Moranta, D., Morey, P., Garcia del Portillo, F., Bengoechea, J. A., et al. (2012). Host cell kinases, α5 and β1 integrins, and Rac1 signalling on the microtubule cytoskeleton are important for non-typeable *Haemophilus influenzae* invasion of respiratory epithelial cells. *Microbiology* 158(Pt 9), 2384–2398. doi: 10.1099/mic.0.059972-0

Lorian, V. (1996). *Antibiotics in Laboratory Medicine*. Philadelphia, PA: Williams and Wilkins.

Maskell, R., Okubadejo, O. A., Payne, R. H., and Pead, L. (1978). Human infections with thymine-requiring bacteria. *J. Med. Microbiol.* 11, 33–45. doi: 10.1099/00222615-11-1-33

Mell, J. C., Sinha, S., Balashov, S., Viadas, C., Grassa, C. J., Ehrlich, G. D., et al. (2014). Complete genome sequence of *Haemophilus influenzae* strain 375 from the middle ear of a pediatric patient with otitis media. *Genome Announc.* 2:e01245-14. doi: 10.1128/genomeA.01245-14

Mell, J. C., Viadas, C., Moleres, J., Sinha, S., Fernandez-Calvet, A., Porsch, E. A., et al. (2016). Transformed recombinant enrichment profiling rapidly edentifies HMW1 as an intracellular invasion locus in *Haemophilus influenzae*. *PLoS Pathog.* 12:e1005576. doi: 10.1371/journal.ppat.1005576

Meng, G., Spahich, N., Kenjale, R., Waksman, G., and St Geme, J. W. III. (2011). Crystal structure of the *Haemophilus influenzae* Hap adhesin reveals an intercellular oligomerization mechanism for bacterial aggregation. *EMBO J.* 30, 3864–3874. doi: 10.1038/emboj.2011.279

Mohd-Zain, Z., Kamsani, N. H., Ismail, I. S., and Ahmad, N. (2012). Antibiotic susceptibility profile of *Haemophilus influenzae* and transfer of co-trimoxazole resistance determinants. *Trop. Biomed.* 29, 372–380. Available online at: https://drive.google.com/file/d/0B75lcx0mfp2OckRZZHdtVXRUWHM/view

Morey, P., Cano, V., Marti-Lliteras, P., Lopez-Gomez, A., Regueiro, V., Saus, C., et al. (2011). Evidence for a non-replicative intracellular stage of nontypable *Haemophilus influenzae* in epithelial cells. *Microbiology* 157(Pt 1), 234–250. doi: 10.1099/mic.0.040451-0

Morey, P., Viadas, C., Euba, B., Hood, D. W., Barberan, M., Gil, C., et al. (2013). Relative contributions of lipooligosaccharide inner and outer core modifications to nontypeable *Haemophilus influenzae* pathogenesis. *Infect. Immun.* 81, 4100–4111. doi: 10.1128/IAI.00492-13

Mwenya, D. M., Charalambous, B. M., Phillips, P. P. J., Mwansa, J. C. L., Batt, S. L., Nunn, A. J., et al. (2010). Impact of cotrimoxazole on carriage and antibiotic resistance of *Streptococcus pneumoniae* and *Haemophilus influenzae* in HIV-infected children in Zambia. *Antimicrob. Agents Chemother.* 54, 3756–3762. doi: 10.1128/AAC.01409-09

Nouira, S., Marghli, S., Besbes, L., Boukef, R., Daami, M., Nciri, N., et al. (2010). Standard versus newer antibacterial agents in the treatment of severe acute exacerbation of hronic Obstructive Pulmonary Disease: a randomized trial of trimethoprim-sulfamethoxazole versus ciprofloxacin. *Clin. Infect. Dis.* 51, 143–149. doi: 10.1086/653527

Platt, D. J., Guthrie, A. J., and Langan, C. F. (1983). The isolation of thymidine–requiring *Haemophilus influenzae* from the sputum of chronic bronchitic patients receiving trimethoprim. *J. Antimicrob. Chemother.* 11, 281–286. doi: 10.1093/jac/11.3.281

Puig, C., Grau, I., Marti, S., Tubau, F., Calatayud, L., Pallares, R., et al. (2014). Clinical and molecular epidemiology of *Haemophilus influenzae* causing invasive disease in adult patients. *PLoS ONE* 9:e112711. doi: 10.1371/journal.pone.0112711

Ramos-Sevillano, E., Urzainqui, A., Campuzano, S., Moscoso, M., Gonzalez-Camacho, F., Domenech, M., et al. (2015). Pleiotropic effects of cell wall amidase LytA on *Streptococcus pneumoniae* sensitivity to the host immune response. *Infect. Immun.* 83, 591–603. doi: 10.1128/IAI.02811-14

Remuzgo-Martinez, S., Lazaro-Diez, M., Mayer, C., Aranzamendi-Zaldumbide, M., Padilla, D., Calvo, J., et al. (2015). Biofilm formation and quorum-sensing-molecule production by clinical isolates of *Serratia liquefaciens*. *Appl. Environ. Microbiol.* 81, 3306–3315. doi: 10.1128/AEM.00088-15

Rowe, A. K., Deming, M. S., Schwartz, B., Wasas, A., Rolka, D., Rolka, H., et al. (2000). Antimicrobial resistance of nasopharyngeal isolates of *Streptococcus pneumoniae* and *Haemophilus influenzae* from children in the Central African Republic. *Pediatr. Infect. Dis. J.* 19, 438–444. doi: 10.1097/00006454-200005000-00009

Sethi, S. (2010). Infection as a comorbidity of COPD. *Eur. Respir. J.* 35, 1209–1215. doi: 10.1183/09031936.00081409

Sinha, S., Mell, J. C., and Redfield, R. J. (2012). Seventeen Sxy-dependent cyclic AMP receptor protein site-regulated genes are needed for natural transformation in *Haemophilus influenzae*. *J. Bacteriol.* 194, 5245–5254. doi: 10.1128/JB.00671-12

Song, L. Y., Goff, M., Davidian, C., Mao, Z., London, M., Lam, K., et al. (2016). Mutational consequences of ciprofloxacin in *Escherichia coli*. *Antimicrob. Agents Chemother.* 60, 6165–6172. doi: 10.1128/AAC.01415-16

Stryer, L. (1995). "Biosynthesis of nucleotides," in *Biochemistry*, ed L. Stryer (New York, NY: W.H. Freemann and Company), 739–762.

Tracy, E., Ye, F., Baker, B. D., and Munson, R. S. Jr. (2008). Construction of non-polar mutants in *Haemophilus influenzae* using FLP recombinase technology. *BMC Mol. Biol.* 9:101. doi: 10.1186/1471-2199-9-101

Tristram, S., Jacobs, M. R., and Appelbaum, P. C. (2007). Antimicrobial resistance in *Haemophilus influenzae*. *Clin. Microbiol. Rev.* 20, 368–389. doi: 10.1128/CMR.00040-06

Wang, L., Hames, C., Schmidl, S. R., and Stülke, J. (2010). Upregulation of thymidine kinase activity compensates for loss of thymidylate synthase activity in *Mycoplasma pneumoniae*. *Mol. Microbiol.* 77, 1502–1511. doi: 10.1111/j.1365-2958.2010.07298.x

Weiser, J. N., Pan, N., McGowan, K. L., Musher, D., Martin, A., and Richards, J. (1998). Phosphorylcholine on the lipopolysaccharide of *Haemophilus influenzae* contributes to persistence in the respiratory tract and sensitivity to serum killing mediated by C-reactive protein. *J. Exp. Med.* 187, 631–640. doi: 10.1084/jem.187.4.631

Yogiara., Kim, D., Hwang, J. K., and Pan, J. G. (2015). *Escherichia coli* ASKA clone library harboring tRNA-specific adenosine deaminase (tadA) reveals resistance towards Xanthorrhizol. *Molecules* 20, 16290–16305. doi: 10.3390/molecules200916290

Conflict of Interest Statement: The authors declare that the research was conducted in the absence of any commercial or financial relationships that could be construed as a potential conflict of interest.

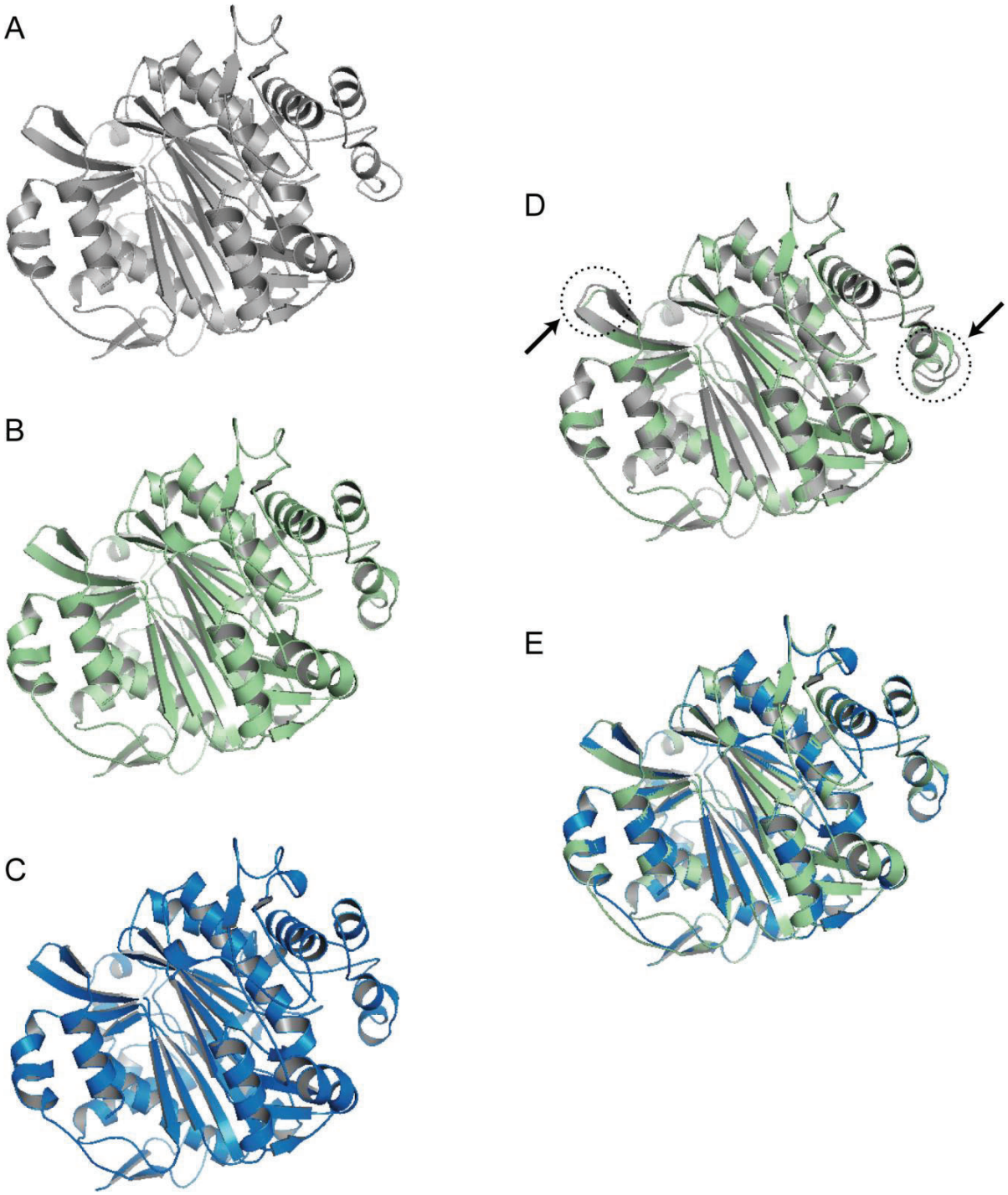

Figure S1. Predicted protein structure for ThyA$_{Hi8233}$(A), ThyA$_{RdKW20}$ (B) and ThyA$_{NTHi375}$ (C), generated by the automated modeling tool of the Swiss Model web service (http://swissmodel.expasy.org). Protein structural alignments and representation were generated with the molecular visualization software Open PyMOL (http://www.pymol.org). Superpositions of ThyA$_{NTHi8233}$ and ThyA$_{RdKW20}$ **(D)**, and of ThyA$_{RdKW20}$ and ThyA$_{NTHi375}$ proteins **(E)** are shown. Structural changes between ThyA$_{NTHi8233}$ and ThyA$_{RdKW20}$ are circled and arrow pointed. Right arrow indicates amino acids E90 and N91 in ThyA$_{NTHi8233}$ (absent in ThyA$_{RdKW20}$).

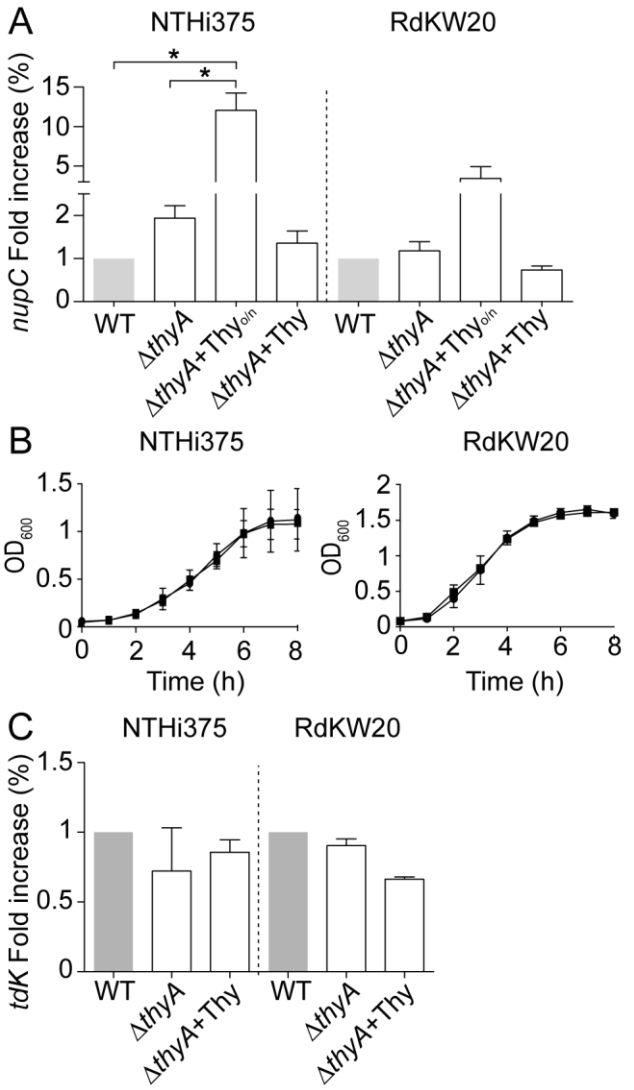

Figure S2. (A) *H. influenzae* thymidine auxothrophy modulates expression of the nucleoside transporter *nupC*. Expression of the nucleoside transporter encoding *nupC* gene upon bacterial growth in sBHI, in the absence or presence of thymidine, is shown for NTHi375 and RdKW20 WT and *thyA* strains. WT strains were grown in sBHI; Δ*thyA* strains were grown in sBHI (Δ*thyA*), sBHI+thymidine 300 µg/ml (ΔthyA+Thy), or were o/n pre-cultured in sBHI+thymidine 300µg/ml and grown in sBHI (Δ *thyA*+Thy$_{o/n}$). Expression of the *nupC* gene was higher in the *thyA* mutants pre-cultured in sBHI+thymidine (Δ *thyA*+Thy$_{o/n}$) than in the *thyA* mutants grown in sBHI (Δ*thyA*) (for NTHi375, $p<0.05$). **(B) Mutation of the *nupC* gene does not modify NTHi growth.** Bacterial growth in sBHI is shown for NTHi375 and RdKW20 WT and Δ*nupC* strains. **(C) *H. influenzae* thymidine auxothrophy does not modulate expression of the thymidine kinase *tdk*.** Expression of the thymidine kinase *tdK* gene upon bacterial growth in sBHI, in the absence or presence of thymidine, is shown for NTHi375 and RdKW20 WT and *thyA* mutant strains. WT strains were grown in sBHI; Δ*thyA* strains were grown in sBHI (Δ*thyA*) or sBHI+thymidine 300 µg/ml (Δ *thyA*+Thy)

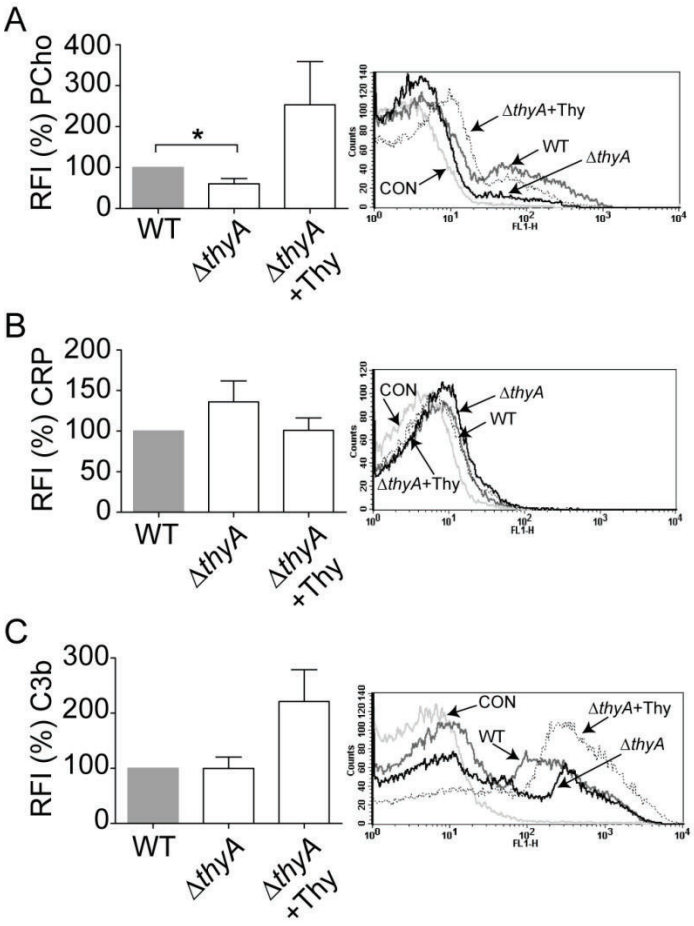

Figure S3. Thymidine auxotrophy reduces PCho level in RdW20. RdKW20 WT and Δ*thyA* strains were exponentially grown in sBHI, in the absence or presence of thymidine 300 µg/ml, and incubated with anti-PCho (A), human serum and anti-CRP (B) or human serum and anti-C3b (C) antibodies. Binding was analyzed by flow cytometry. Representative flow cytometry histograms for each assay are shown (right panels). Color code: light gray, control (CON) buffer; gray, RdKW20; black, RdKW20 Δ*thyA*; dotted lane, RdKW20Δ*thyA* grown in sBHI+Thy. RdKW20Δ*thyA* showed significantly lower PCho level ($p<0.05$) than the WT strain, which was restored by mutant bacterial growth in sBHI with thymidine 300 µg/ml.

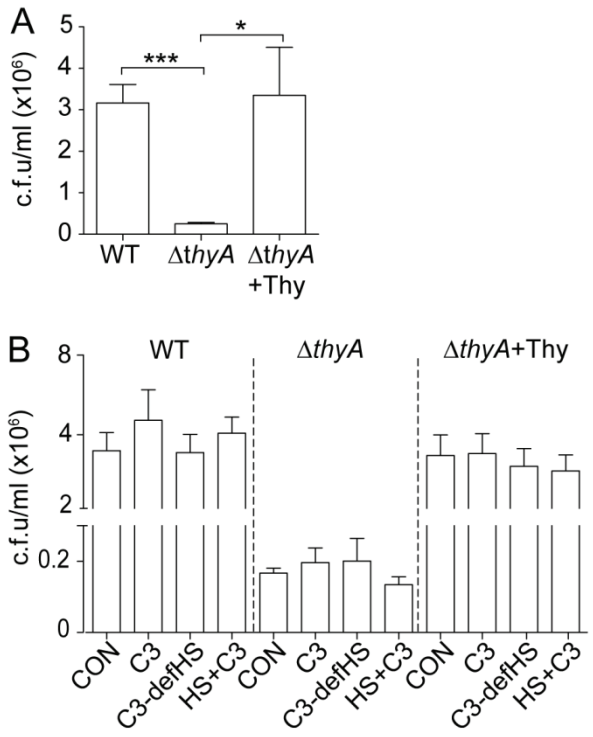

Figure S4. Modulation of *H. influenzae* cell infection by thymidine dependency and host complement. (A) Inactivation of the *thyA* gene reduces adhesion o*f H. influenzae* RdKW20 to epithelial cells. A549 cells were used to quantify adhesion of RdKW20 WT and Δ*thyA* strains. Bacteria pre-grown in sBHI, in the absence or presence of thymidine 300 µg/ml, were used. NTHi375Δ*thyA* showed significantly lower adhesion to A549 cells ($p<0.0001$) than the WT strain, which was restored by mutant pre-growth in sBHI with thymidine ($p<0.05$). **(B)** NTHi375 WT and Δ*thyA* strains were grown on chocolate agar (Δ*thyA*) or chocolate+Thy (Δ*thyA*+Thy) and A549 cells were infected in the presence of human purified C3, C3-deficient serum, or C3-deficient serum reconstituted with human purified C3. Bacterial attachment remained unchanged in the tested conditions.

SCIENTIFIC REPORTS

OPEN

Received: 30 June 2017
Accepted: 12 September 2017
Published online: 16 October 2017

Resveratrol therapeutics combines both antimicrobial and immunomodulatory properties against respiratory infection by nontypeable *Haemophilus influenzae*

Begoña Euba[1,2], Nahikari López-López[2], Irene Rodríguez-Arce[2], Ariadna Fernández-Calvet[2], Montserrat Barberán[3], Nuria Caturla[4], Sara Martí[1,5], Roberto Díez-Martínez[6] & Junkal Garmendia[1,2]

The respiratory pathogen nontypeable *Haemophilus influenzae* (NTHi) is an important cause of acute exacerbation of chronic obstructive pulmonary disease (AECOPD) that requires efficient treatments. A previous screening for host genes differentially expressed upon NTHi infection identified sirtuin-1, which encodes a NAD-dependent deacetylase protective against emphysema and is activated by resveratrol. This polyphenol concomitantly reduces NTHi viability, therefore highlighting its therapeutic potential against NTHi infection at the COPD airway. In this study, resveratrol antimicrobial effect on NTHi was shown to be bacteriostatic and did not induce resistance development *in vitro*. Analysis of modulatory properties on the NTHi-host airway epithelial interplay showed that resveratrol modulates bacterial invasion but not subcellular location, reduces inflammation without targeting phosphodiesterase 4B gene expression, and dampens β defensin-2 gene expression in infected cells. Moreover, resveratrol therapeutics against NTHi was evaluated *in vivo* on mouse respiratory and zebrafish septicemia infection model systems, showing to decrease NTHi viability in a dose-dependent manner and reduce airway inflammation upon infection, and to have a significant bacterial clearing effect without signs of host toxicity, respectively. This study presents resveratrol as a therapeutic of particular translational significance due to the attractiveness of targeting both infection and overactive inflammation at the COPD airway.

Though typically a commensal of the nasopharynx, the Gram negative bacterium *H. influenzae*, especially in its noncapsulated or nontypeable form (NTHi), is also an opportunistic pathogen causing middle ear infections (otitis media), conjunctivitis, community-acquired pneumonia, exacerbations of chronic obstructive pulmonary disease (COPD) and, occasionally, invasive disease[1,2].

COPD is an airway inflammatory disease characterized by a progressive and not fully reversible airflow limitation accompanied by emphysema, fibrosis, chronic overactive inflammation and mucus hypersecretion[3]. COPD is a main leading cause of death, is predicted by the World Health Organization to become the fifth most

[1]Centro de Investigación Biomédica en Red de Enfermedades Respiratorias (CIBERES), Madrid, Spain. [2]Instituto de Agrobiotecnología, CSIC-Universidad Pública Navarra-Gobierno Navarra, Mutilva, Spain. [3]Facultad de Veterinaria, Universidad de Zaragoza, Zaragoza, Spain. [4]Monteloeder, Elche Parque Empresarial, Elche, Alicante, Spain. [5]Departamento Microbiología, Hospital Universitari Bellvitge, University of Barcelona, IDIBELL, Barcelona, Spain. [6]Ikan Biotech SL, The Zebrafish Lab, Centro Europeo de Empresas e Innovación de Navarra (CEIN), Noáin, Spain. Begoña Euba and Nahikari López-López contributed equally to this work. Correspondence and requests for materials should be addressed to J.G. (email: juncal.garmendia@unavarra.es)

significant contributor to the worldwide burden of disease by 2020, and it greatly contributes to the economic burden of healthcare costs[4]. Although cigarette smoking is the most common instigating factor in the development of COPD, bacterial colonization of these damaged airways may contribute to disease progression, being NTHi the most common colonizing bacterium in COPD[5]. Moreover, the chronic course and evolution of COPD is often characterized by periods of symptom exacerbation caused by respiratory pathogens such as NTHi (acute exacerbation of COPD, i.e. AECOPD), with a negative impact on the patient's quality of life and evolution of the disease[6,7].

Despite the routine therapeutic use of antibiotics, NTHi persists and recurs at the COPD airways, and the numbers of antibiotic-resistant strains increase. NTHi is a facultative intracellular pathogen[8–16], and subcellular location may allow bacterial cells to temporarily evade the immune system and/or antibiotic-based therapeutic interventions[17,18]. Moreover, given its inflammatory properties, common pharmaceuticals used to manage the symptoms of COPD include β2-agonists, inhaled corticosteroids and phosphodiesterase 4 (PDE4) inhibitors[4,19]. Of note, NTHi infection is also an inflammatory process, and those pharmaceuticals may influence the infectious process[20,21], as observed for glucocorticoids such as dexamethasone, which attenuate NTHi-triggered inflammation but may also compromise bacterial clearance in mice[22], or for nonbactericidal PDE4 inhibitors such as roflumilast N-oxide or rolipram, which dampen NTHi-triggered inflammation[23], dampen NTHi intracellular invasion and enhance mice lung clearance[24], but may also synergize with NTHi to up-regulate PDE4B2 expression therefore contributing to chemokine induction[25]. Together, success of current therapeutics is limited due to resistance, adverse side effects, tolerance and/or cost[4]. Therefore, novel treatments being safe, effective and not vulnerable to developing resistance are needed to counteract NTHi respiratory infection.

Previous global expression profiling revealed SIRT1, encoding the NAD-dependent deacetylase sirtuin 1, as a host cell gene differentially expressed upon NTHi infection[24]. Emphysema relates to accelerated aging of the lungs, and accelerated aging might be due to defective function of endogenous antiaging molecules such as sirtuins[3]. SIRT1 is a negative regulator of matrix metalloproteinase-9[26] and protects against emphysema[27], but its expression is reduced in the peripheral lungs of patients with COPD[26]. Thus, SIRT1 activation may be an attractive therapeutic approach for COPD[28]. Of note, the SIRT1 activator resveratrol (3,5,4′-trihydroxystilbene), a naturally occuring polyphenolic phytoalexin produced by a variety of flowering plants in response to unfavourable environmental conditions and found in dietary products including peanuts, grapes and red wine, reduces NTHi viability[24,29]. Besides NTHi, resveratrol antimicrobial effect has been shown for several Gram positive and negative bacteria[30–33]. Next to its proposed geroprotector role[3,28], pathway candidates affected by resveratrol exposure in humans are anti-inflammatory mechanisms, cell cycle and programmed cell death pathways, calorie restriction mimetic via energy-sensing metabolic regulators, and anti-oxidant properties[34]. In fact, evidence supports a protective role of resveratrol in respiratory disease as an anti-inflammatory and antioxidant agent[35]. Mechanistically, resveratrol targets are molecules that bind directly with the polyphenol and whose activity, structure, and/or stability is altered as a consequence, or molecules whose expression or activity is altered via an indirect mechanism[34].

Besides its antimicrobial effect, resveratrol anti-inflammatory action is known to occur during NTHi infection by suppression of extracellular signal-regulated kinases (ERK)-mediated down-regulation of an alternative spliced variant of the adaptor protein myeloid differentiation factor 88 (MyD88) named MyD88 short (MyD88s)[36]. However, both resveratrol antimicrobial and immunomodulatory therapeutic properties have not been jointly considered. The existing body of evidence prompted us to hypothesize that resveratrol effectiveness for the treatment of NTHi respiratory infection may rely on the combined action of its antimicrobial and host cell modulatory effects. Based on this notion, we further analyzed resveratrol antimicrobial properties, its effect on bacterial intracellular location and host gene expression in infected cells, and evaluated resveratrol therapeutic potential *in vivo*. Here we show that resveratrol (i) is bacteriostatic and does not induce resistance development in NTHi, (ii) reduces NTHi airway epithelial invasion but does not alter its subcellular location, (iii) has an anti-inflammatory effect without targeting PDE4B gene expression and dampens human β defensing-2 (hBD2) gene expression in NTHi infected airway epithelial cells, (iv) decreases NTHi viability and reduces airway inflammation in lung infected mice, and (v) has a bacterial clearing effect without signs of host toxicity in a newly established septicemia model system by zebrafish infection with NTHi. Together, this work presents preclinical evidence for resveratrol therapeutic potential against NTHi infection.

Results

Resveratrol effect on NTHi is bacteriostatic and does not induce resistance. Exposure of NTHi strain 375, hereafter NTHi375, cells in sBHI to increasing concentrations of resveratrol previously revealed bacterial growth inhibition[24]. Resveratrol has been shown to be bacteriostatic on *E. coli* and *Bacillus subtilis*[31,32]. To evaluate if resveratrol is bactericidal or bacteriostatic on NTHi, we incubated pre-grown NTHi375 cells with resveratrol 112.5 or 56.25 μg/ml (concentrations selected based on previous observations[24]), and monitored the OD_{600} and number of viable cells by serial dilution and plating at the indicated time intervals. After 4 h, resveratrol 112.5 or 56.25 μg/ml-treated cultures showed lower OD_{600} and number of viable cells than the control untreated and vehicle solution ones. Moreover, results of both time and dose dependent assays did not show a reduction in OD_{600} and in the number of viable cells due to resveratrol treatment through time, suggesting it to be bacteriostatic (Fig. 1). We next assessed the ability of NTHi to become resistant to resveratrol through serial passage of strain NTHi375 in sBHI broth containing increasing polyphenol concentrations. A range of resveratrol inhibitory concentrations consisting of 250, 225, 175, 130, 120 and 112.5 μg/ml were employed. After 15 consecutive overnight passages, no resistant bacteria were isolated (Fig. S1). In summary, resveratrol is likely to have a bacteriostatic effect on NTHi and, under the conditions tested, it does not induce resistance on strain NTHi375.

Resveratrol has an antimicrobial effect on a panel of NTHi COPD clinical isolates. Genomic heterogeneity is a known feature for NTHi[37], which may lead to variable resveratrol susceptibility among strains,

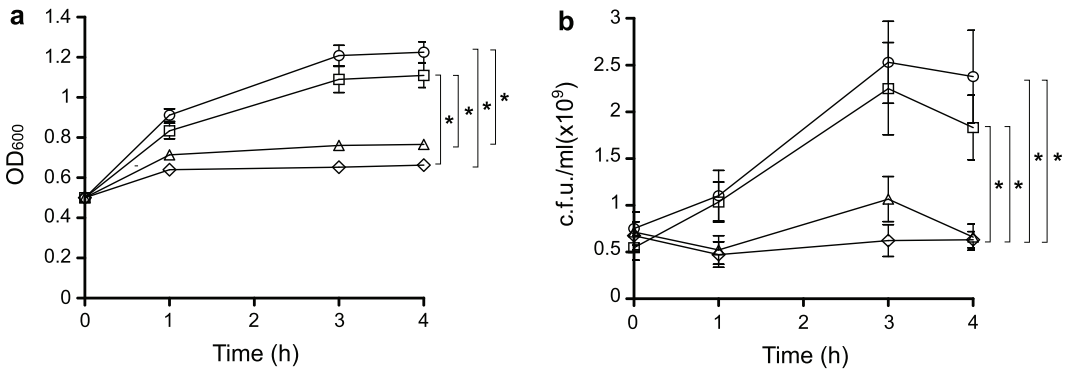

Figure 1. Resveratrol has a bacteriostatic effect on pre-grown NTHi cells. OD_{600}-normalized sBHI cultures of NTHi375 were divided into control untreated (circle); resveratrol 112.5 μg/ml (diamond); resveratrol 56.25 μg/ml (triangle); vehicle solution (square), and incubated for 4 h. At the indicated time points, OD_{600} was recorded **(a)**, and samples were serially diluted and plated on sBHI agar for c.f.u./ml determination **(b)**. After 4 h, NTHi375 cells treated with both resveratrol 56.25 and 112.5 μg/ml showed a reduction in OD_{600} and in the number of viable cells compared to control untreated ($p < 0.0001$) and vehicle solution cultures ($p < 0.0001$ and $p < 0.001$, respectively) cultures. Both OD_{600} and number of viable cells were maintained through time in resveratrol treated cultures.

	Resveratrol (μg/ml)			
NTHi strain	**175**	**75**	**25**	**8.33**
P617–9224	35 ± 11	62.8 ± 14.6	87.9 ± 16.9	98.9 ± 2
P621–7028	24.6 ± 15.2	56 ± 8.3	72.6 ± 19.1	80.8 ± 19.4
P636–8296	23.4 ± 6.9	47.5 ± 22.9	79.7 ± 21	95.6 ± 5.5
P642–4396	22.4 ± 4.5	46.2 ± 6.4	56.4 ± 11.5	73 ± 16.5
P595–8370	31.5 ± 15.5	65.8 ± 9.8	86.2 ± 14.8	90 ± 11.5
P615–8618	11 ± 8	40.3 ± 11.7	52.2 ± 16.5	82 ± 18.5
P650–8603	10.8 ± 4.3	50.8 ± 15.4	81.7 ± 18.3	95.5 ± 7.2
P652–8881	4.8 ± 9.5	42.5 ± 18.4	73.7 ± 19.5	88.3 ± 16.4
P662–7189	15 ± 8.4	40 ± 5.9	61.1 ± 11.7	79.2 ± 12.1
P657–8759	23.6 ± 12.3	60 ± 18.9	83.1 ± 16.3	86 ± 14.1
P665–7858	1.1 ± 2.7	70.7 ± 25	90.1 ± 17	88.5 ± 17.5
P669–6977	24 ± 8.9	57.8 ± 9.6	76.7 ± 10.7	89.8 ± 10.4
P672–7661	2.6 ± 3.2	34.3 ± 10.2	87.4 ± 14.5	96.6 ± 6.8
P679–2791	38.4 ± 10.6	62.4 ± 20.3	74.9 ± 17.8	87 ± 13.2

Table 1. Percentage of survival by a panel of 14 NTHi COPD clinical isolates, when incubated with increasing concentrations of resveratrol. Values denoted are mean ± SD.

as shown for other antimicrobials[38]. To further expand our observations on NTHi375, we evaluated the effect of resveratrol on NTHi viability by using a panel of 14 clinical strains isolated from COPD sputum samples rendering different typing profiles by PFGE (data not shown). We found that viability decreased for all strains tested in a resveratrol dose-dependent manner (Table 1). As observed for NTHi375, bacterial survival was less than 50% at a resveratrol concentration of 175 μg/ml; for 5 of the isolates analyzed, bacterial survival was less or equal to 10% when incubated with resveratrol 175 μg/ml (Table 1). These results further support resveratrol antimicrobial effect on NTHi. Given that NTHi375 has been previously used in host-pathogen interaction studies[13–15,24,38], it was next used to assess resveratrol modulatory effect on the NTHi-host airway interplay.

Resveratrol efficacy against NTHi infection of cultured airway epithelial cells. In agreement with our previous host expression profiling[24], NTHi infection increased SIRT1 protein levels in A549 cells. As expected, resveratrol addition also increased SIRT1 protein levels, as already seen in uninfected cells; a synergistic effect between NTHi infection and resveratrol addition on SIRT1 protein levels was not observed (Fig. S2). Conversely, sirtuin-1 siRNA did not modify NTHi epithelial invasion[24], suggesting that SIRT1 expression/activity and NTHi cell entry may be uncoupled events.

Resveratrol modulates other molecules within the host cell besides SIRT1[39]. Intracellular cAMP increase has been reported to reduce NTHi cell invasion[13,24]. Given that resveratrol inhibits cAMP-degrading PDEs leading to elevated cAMP levels[40], host cell treatment with this polyphenol should be likely to reduce bacterial infection. However, previous evaluation of resveratrol effect on NTHi airway epithelial infection, performed by A549 cell

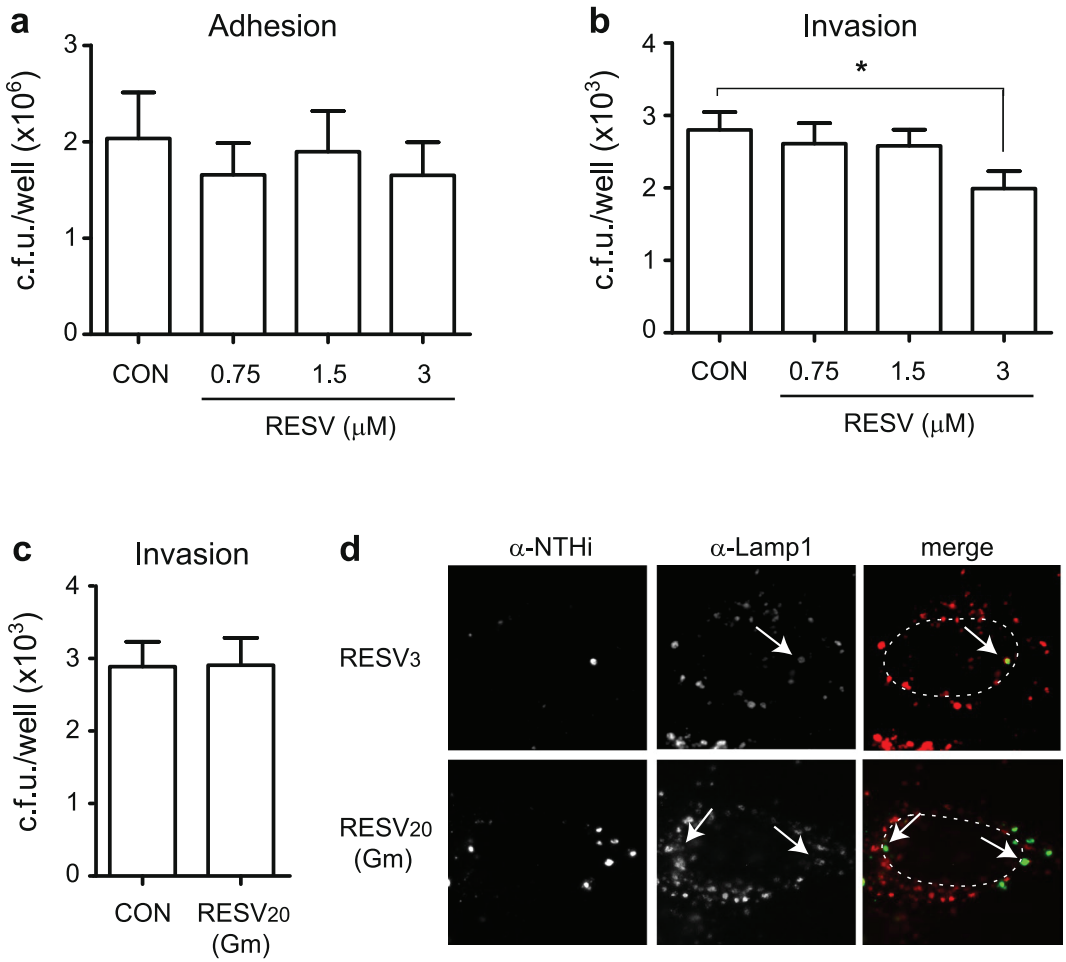

Figure 2. A resveratrol sub-inhibitory concentration lowers NTHi375 invasion of A549 human respiratory epithelial cells. Controls (CON): in adhesion and invasion assays (**a** and **b**, respectively), cells did not receive resveratrol (RESV), but did receive vehicle solution (DMSO) prior and during bacterial contact; in invasion assay (**c**), cells received vehicle solution during gentamicin treatment. Effect of resveratrol sub-inhibitory concentrations on NTHi375 adhesion to- **(a)** and invasion of **(b)** A549 cells. Cells were pre-treated with resveratrol 0.75, 1.5, or 3 μM for 4 h, and the polyphenol was maintained during infection. Bacterial adhesion was comparable for resveratrol-treated and control (CON) cells. Mean numbers of NTHi375 entry into cells treated with resveratrol 3 μM were significantly lower than those obtained for control (CON) cells ($p < 0.05$). **(c)** Resveratrol effect on intracellular NTHi375. A549 cells were infected and resveratrol 20 μM was added during cell incubation with gentamicin (Gm). Resveratrol did not reduce the number of intracellular bacteria. **(d)** Subcellular location of NTHi375 inside A549 cells shows co-localization with Lamp-1 endosomal marker. NTHi was stained with rabbit α-NTHi and Alexa 488-conjugated donkey α-rabbit (green) antibodies. Lamp-1 was stained with mouse α-Lamp-1 and donkey α-mouse conjugated to RRX (red) antibodies. A549 cells were pre-treated with resveratrol 3 μM for 4 h, which was maintained during infection (upper panels); alternatively, A549 cells were infected for 2 h and resveratrol 20 μM was added during cell incubation with Gm (lower panels). Representative images are shown, taken at 1 h post-Gm. Host cell nuclei location is indicated with dashed lines. Bacteria:Lamp-1 co-localization is indicated with arrows.

pre-treatment with resveratrol 20 μM and drug removal before infection, rendered comparable NTHi375 infection levels for both control and resveratrol pre-treated cells[24]. Such assays were performed with resveratrol concentrations reducing bacterial viability, and drug removal prior to infection was necessary to allow quantifying infection rates, which could limit observing a potential resveratrol effect on bacterial location upon infection.

Following this notion, we assessed NTHi adhesion to- and invasion of A549 cells pre-treated with resveratrol sub-inhibitory concentrations maintained during bacterial-cell contact. Bacterial adhesion to A549 cells treated with increasing resveratrol concentrations (0.75; 1.5; 3 μM) was comparable to that observed for control untreated cells (Fig. 2a). Differently, a significant decrease on NTHi375 invasion was observed upon cell treatment with resveratrol 3 μM (0.68 μg/ml) ($p < 0.05$) (Fig. 2b); this resveratrol concentration did not affect NTHi375 bacterial or A549 cell viability (data not shown).

Resveratrol penetration into host cells may occur by a passive diffusion mechanism[41], and antimicrobial molecules likely to penetrate epithelial cells can reduce intracellular NTHi viability[38]. We next asked if resveratrol

could reduce the viability of intracellular bacteria. To do so, A549 cell infection with NTHi375 was performed in culture medium without drug supplementation, followed by subsequent incubation in fresh medium supplemented with gentamicin to kill extracellular bacteria, and without (CON) or with resveratrol 20 μM. Under these conditions, resveratrol did not reduce the number of intracellular bacteria (Fig. 2c). We and others have previously described that NTHi invades epithelial cells and locates inside a non-proliferative compartment with late endosome features[10,13–15]. In agreement, resveratrol pre-treatment or addition during the gentamicin incubation period did not alter such subcellular location (Fig. 2d).

Together, these results show that resveratrol sub-inhibitory concentrations reduce NTHi375 airway epithelial cell invasion and, under the conditions tested, this polyphenol does not modify intracellular bacterial numbers and/or subcellular location.

Resveratrol modulates NTHi-induced IL-8 and hBD2 expression on A549 airway epithelial cells. Despite previous reports on resveratrol antimicrobial and immunomodulatory properties upon NTHi infection[24,36], the therapeutic potential of this dual effect has not been jointly considered. Thus, resveratrol has been shown to reduce NTHi-induced expression of IL-1β, IL-6, CCL-2 and GM-CSF proinflammatory cytokines in BEAS-2B bronchial epithelial cells[36]. Separately, IL-8 enhanced expression has been observed in NTHi infected A549 cells[24]. Resveratrol effect on NTHi-induced expression of IL-8 in A549 cells was next assessed by cell pre-treatment with resveratrol 20 μM and drug removal before infection, which did not render an anti-inflammatory effect at the gene expression or protein secretion levels (Fig. 3b). This lack of effect could be related to resveratrol removal prior to infection. To maintain resveratrol at the onset of the infectious inflammatory stimulus without jeopardizing bacterial viability, we assessed IL-8 expression and secretion by A549 cells incubated with heat killed (HK) bacteria. Under these conditions, IL-8 expression and secretion were stimulated, compared to control non-infected cells. Indeed, IL-8 expression/secretion levels were higher in cells incubated with HK bacteria than in NTHi infected cells. Moreover, IL-8 gene expression showed a non statistically significant but reproducible trend to be lower in resveratrol-treated cells at 2 and 4 h post-incubation with HK bacteria (Fig. 3a); likewise, IL-8 protein secretion showed the same decreasing trend in resveratrol-treated cells at 8 h post-incubation with HK bacteria (Fig. 3b), compared to control cells receiving vehicle solution.

Resveratrol is known to directly inhibit PDE1, 3 and 4 by competitive inhibition with cAMP in their binding sites[40]. Resveratrol anti-inflammatory effect on NTHi-infected cells may be mediated by MKP-1 phosphatase dependent up-regulation of MyD88s expression via a cAMP-PKA-dependent mechanism[36]. Given that NTHi airway epithelial infection stimulates differential expression for several PDEs including PDE4B (the major PDE isoform expressed in lung)[24], we asked if resveratrol anti-inflammatory effect on NTHi-infected cells could be also mediated by modulation of NTHi-induced PDE4B gene expression. PDE4B gene expression was assessed in A549 infected cells, in the absence or presence of resveratrol 20 μM. As previously stated, resveratrol removal prior- or maintenance during infection was dependent on the use of intact or HK bacteria, respectively. As shown in Fig. 3c, PDE4B gene expression was increased in NTHi infected- when compared to control uninfected cells (in cells incubated with HK bacteria for 2 and 4 h, $p < 0.005$ and $p < 0.05$, respectively). Under these conditions, resveratrol treatment did not modify PDE4B gene expression.

Bacteria-induced human β-defensin-2 (hBD2) antimicrobial peptide expression in lung epithelial cells has also been shown to be differently modulated by resveratrol[42,43]. Based on this notion, we investigated whether NTHi could induce the expression of hBD2 in A549 cells. hBD2 gene expression was higher in NTHi infected than in control uninfected cells (for 1 h infected cells, $p = 0.001$). Such hBD2 gene expression was lowered to control levels upon resveratrol cell pre-treatment (for 1 h infected cells, $p < 0.01$) (Fig. 3d). HK bacteria did not modify hBD2 expression on A549 cells, therefore excluding evaluation of a resveratrol-mediated effect under these conditions (data not shown).

These results show that, under the conditions tested, resveratrol anti-inflammatory effect is observed when maintained at the onset of the infectious inflammatory stimulus. Resveratrol treatment of NTHi-infected lung epithelial cells lowers IL-8 gene expression and protein secretion, hBD2 gene expression, and does not interfere PDE4B gene expression.

Antimicrobial and anti-inflammatory effects of resveratrol administration on mouse pulmonary infection with NTHi. Next, we sought to determine the impact of resveratrol oral administration *in vivo* by using a mouse model system of NTHi respiratory infection. We used two regimens of oral resveratrol (100 or 150 mg/kg) consisting of three administrations prior to infection (48, 24, 1 h before infection) and three administrations at 6, 12 and 18 h post-infection (hpi). Fewer NTHi375 bacteria were recovered at 12 hpi from lung and BALF samples of mice treated with resveratrol 150 mg/kg than from mice receiving vehicle solution (for lung, $p < 0.01$; for BALF, $p = 0.01$), or receiving resveratrol 100 mg/kg (for lung, $p = 0.01$; for BALF, $p < 0.05$) (Fig. 4a,b). Bacterial loads on lung and BALF samples were comparable for resveratrol 100 mg/kg-treated and untreated infected mice. No differences in terms of bacterial counts were observed at 24 hpi among the three conditions tested. Treatment with resveratrol has been shown before to decrease NTHi-induced expression of IL-1β and IL-6 in mice lung tissue[36]. In this study, analysis of NTHi-induced expression of KC and TNF-α pro-inflammatory mediators in mice lung tissue euthanized at 12 hpi rendered higher numbers than those obtained for control non-infected animals (for KC and TNF-α, $p = 0.01$); moreover, treatment with resveratrol 150 mg/kg decreased NTHi-induced expression of KC and TNF-α in infected mice lung tissue at 12 hpi (for KC, $p < 0.01$; for TNF-α, $p < 0.05$) (Fig. 4c,d). No differences in terms of KC and TNF-α expression were observed in resveratrol treated and control untreated non-infected animals.

Microscopy score of average histopathological lesions in samples from mice infected with NTHi375 was also determined along the respiratory tract and compared for untreated and resveratrol 150 mg/kg-treated mice, euthanized at 12 hpi. Overall comparison of scored lesions in the lower airways of NTHi infected mice showed lower

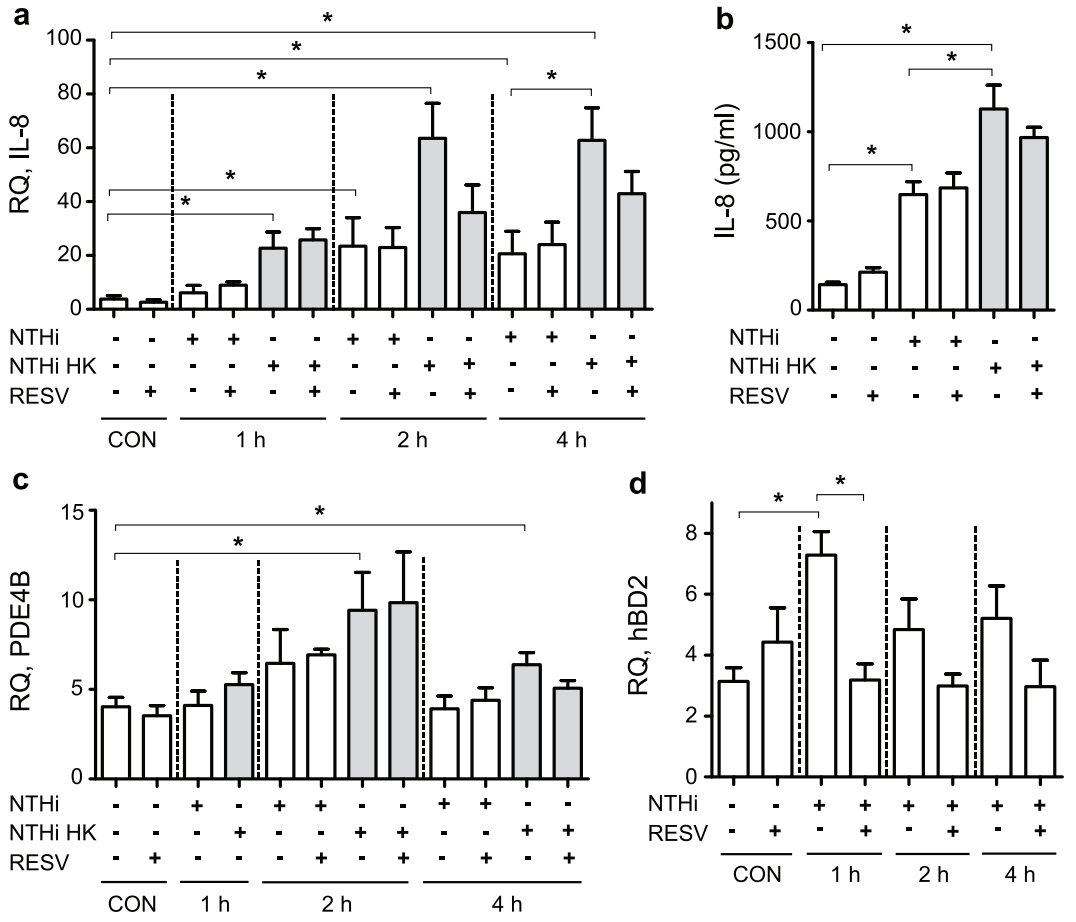

Figure 3. Resveratrol modulates NTHi-induced A549 cell gene expression. Controls (CON): non-infected cells. A549 cells were treated with resveratrol (RESV) 20 μM or DMSO for 4 h, removed prior to bacterial addition (NTHi), or maintained when HK bacteria were used as an inflammatory stimulus (NTHi HK). To monitor gene expression, bacteria were added for 1, 2 or 4 h. Relative quantity (RQ) of human IL-8 ($2^{-\Delta Ct} \times 100$) **(a)**, PDE4B ($2^{-\Delta Ct} \times 100$) **(c)**, and hBD2 ($2^{-\Delta Ct} \times 1000000$) **(d)** mRNA were measured by qRT-PCR. **(b)** Quantification of IL-8 protein secretion by A549 cells, measured by ELISA at 8 h post-infection (hpi). NTHi375 induced IL-8 expression in A549 cells, being significant at 1 (for HK stimulated cells, $p < 0.0005$), 2 (for NTHi and HK stimulated cells, $p < 0.01$ and $p < 0.0001$, respectively) and 4 hpi (for NTHi and HK stimulated cells, $p < 0.005$ and $p < 0.0001$, respectively). IL-8 expression was higher in A549 cells incubated with HK bacteria than in NTHi infected cells (for 4 hpi, $p < 0.05$). NTHi375 induced PDE4B expression in A549 cells, being significant at 2 and 4 hpi (for HK incubated cells, $p < 0.005$ and $p < 0.05$, respectively). NTHi375 induced hBD2 expression at 1 hpi ($p = 0.001$). NTHi triggered IL-8 secretion by A549 cells at 8 hpi (for NTHi and HK stimulated cells, $p < 0.0005$). IL-8 secretion was higher in cells incubated with HK bacteria than in NTHi infected cells ($p < 0.05$). Under these conditions, resveratrol shows a trend to reduce IL-8 gene expression and protein secretion, and lowers hBD2 gene expression ($p < 0.01$). White bars correspond to non-infected (CON) or to NTHi infected cells (NTHi); gray bars correspond to cells stimulated with HK bacteria (NTHi HK).

inflammatory reaction scores for resveratrol-treated mice. This reduction was significant for PMNs at the bronchi and alveoli in infected mice treated with resveratrol, compared to control untreated mice ($p = 0.01$) (Table 2). As an exception, the upper airways of resveratrol-treated infected mice showed a significant increase for PMNs at the nasal cavity compared to control untreated animals ($p < 0.05$) (Table 2).

In sum, these results show that resveratrol 150 mg/kg reduces bacterial load and whole-lung inflammatory markers such as KC and TNF-α. This is in turn reflected by lower PMN in the broncho-alveolar space.

Resveratrol has an antimicrobial protective effect on zebrafish infection with NTHi. Zebrafish has been used for over a decade to study the mechanisms of a variety of inflammatory disorders and infectious diseases. Zebrafish presents adaptive immunity 4–6 weeks after birth, when it becomes a suitable model to analyze novel antimicrobial agents[44]. Thus, aiming to validate the *in vivo* data shown above in an alternative animal model of infection, we tested *H. influenzae* infection on adult zebrafish by bacterial intraperitoneal injection[45,46]. The infection dose was first optimized by injection of 6 animal groups ($n = 10$) with 10 μl of a NTHi375 suspension containing 5×10^5, 5×10^6, 5×10^7, 5×10^8 or 5×10^9 c.f.u./ml, or saline solution 0.9% as a control. NTHi375 severely reduced zebrafish survival. An infection dose consisting of $\sim 5 \times 10^7$ c.f.u./zebrafish caused progressive

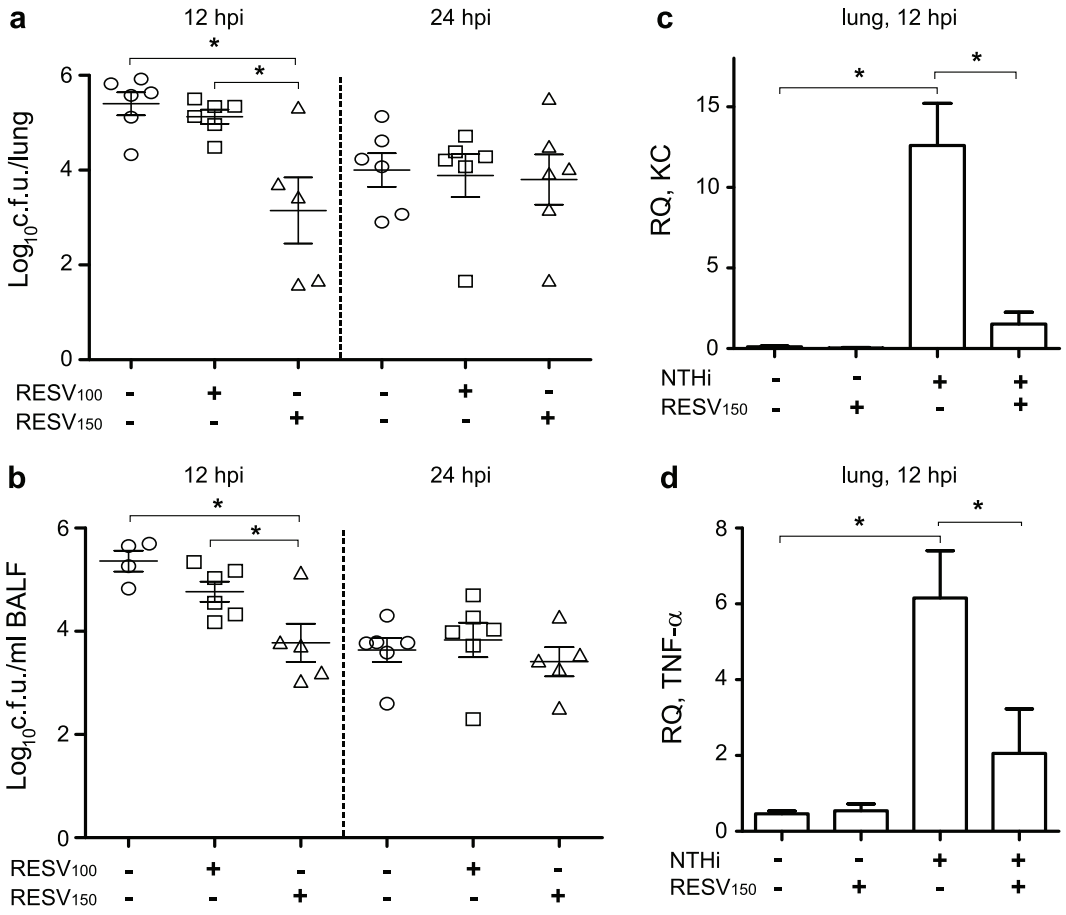

Figure 4. Effect of resveratrol administration on bacterial loads and pro-inflammatory markers in CD1 mice infected by NTHi. Mice were infected intranasally with $\sim 10^8$ bacteria/mouse. Resveratrol (100 or 150 mg/kg/dose) was administered orally ($RESV_{100}$ or $RESV_{150}$). Controls: animals were administered vehicle solution but did not receive resveratrol. Bacterial counts were determined at 12 and 24 hpi for lungs (log_{10} c.f.u./lung) **(a)** and BALF (log_{10} c.f.u./ml BALF) samples (**b**). At 12 hpi, NTHi375 counts were significantly lower in mice treated with resveratrol 150 mg/kg (triangle) than in control mice treated with vehicle solution (circle) (for lung, $p < 0.01$; for BALF, $p = 0.01$), and than in mice treated with resveratrol 100 mg/kg (square) (for lung, $p = 0.01$; for BALF, $p < 0.05$). Relative quantities of mouse KC ($2^{-\Delta Ct} \times 100$) **(c)** and TNF-α ($2^{-\Delta Ct} \times 100$) **(d)** mRNA were measured by RT-qPCR analysis on lung samples corresponding to non-infected untreated, non-infected resveratrol 150 mg/kg treated, NTHi375 infected untreated, and NTHi375 infected resveratrol 150 mg/kg treated groups. At 12 hpi, KC and TNF-α gene expression was increased in infected compared to non-infected mice (for KC and TNF-α, $p = 0.01$). Both KC and TNF-α gene expression was lower in NTHi infected resveratrol treated- than in untreated mice (for KC, $p < 0.01$, for TNF-α, $p < 0.05$).

death of the animals after injection (data not shown), therefore presenting a novel preclinical sepsis model system suitable for further use.

Before performing a resveratrol protective assay in adult zebrafish, a resveratrol acute toxicity assay was carried out in zebrafish embryos following the OECD TG 236 "Fish embryo acute toxicity (FET) test". Results showed that resveratrol was not toxic, being 1 mg/ml the highest dose tested (data not shown). Next, we assessed resveratrol antimicrobial effect on NTHi375 infected zebrafish by using a therapeutic regimen of intraperitoneal resveratrol (0.1 mg/g) consisting of two administrations at 29 and 53 hpi. Survival rate for resveratrol-treated and control untreated groups was monitored up to 5 days post-infection. Mortality rate in resveratrol-treated infected zebrafish was significantly lower than in control animals receiving vehicle solution ($p < 0.0001$); indeed, survival was similar for infected zebrafish receiving resveratrol than for control non-infected animals (Fig. 5a). To quantify resveratrol protective effect, we determined the number of bacterial c.f.u. by collecting blood from the caudal fin of NTHi infected zebrafish at 1 and 2 days post-challenge, corresponding to 5 h before- and 19 h post-resveratrol treatment. Significantly fewer NTHi375 bacteria were recovered at 19 h post-treatment from zebrafish treated with resveratrol than from those receiving perfusion solution-DMSO (1:1) ($p < 0.0001$) (Fig. 5b).

Altogether, these results present zebrafish as a preclinical sepsis model system useful for *in vivo* therapeutic evaluation against NTHi infection. By using this system, we observed both significant resveratrol-mediated NTHi clearing effect upon zebrafish infection and subsequent increased survival.

		[b]Score (mean ± SD)							
		Upper airways				Lung			
Infecting NTHi strain	[a]Treatment	Secretion and erythrocytes in lumen	PMNs lumen	Hyperemia	PMNs lamina propria	Haemorrhage	Alveolar macrophages	Hyperemia	Bronchial-alveolar PMNs
NTHi375	Control untreated	1.7 ± 0.4	1.6 ± 0.2	1 ± 0.2	1.4 ± 0.2	0.2 ± 0.2	0.5 ± 0	0.7 ± 0.1	0.9 ± 0.1
NTHi375	$RESV_{150}$	1 ± 0.3	[c]2.5 ± 0.2	0.8 ± 0.1	1 ± 0.2	0.1 ± 0.1	0.5 ± 0	0.8 ± 0.1	[d]0.3 ± 0.1

Table 2. Score of histopathological lesions found in the airways of untreated or resveratrol treated mice, intranasally infected with NTHi375. [a]Control untreated animals were administered vehicle solution (PBS:DMSO, 1:1). RESV treated animals were administered three RESV doses (150 mg/kg) at 48, 24, and 1 h before infection and one RESV (150 mg/kg) dose at 6 hpi. Mice were euthanized at 12 hpi. [b]Statistical comparisons of mean values were performed using the two-tail *t* test. [c]Larger numbers of PMNs in the upper airways lumen of RESV treated than control untreated animals ($p < 0.05$) infected by NTHi375. [d]Lower PMNs numbers at the bronchi and alveoli of mice treated with RESV, compared to controls ($p = 0.01$) infected by NTHi375.

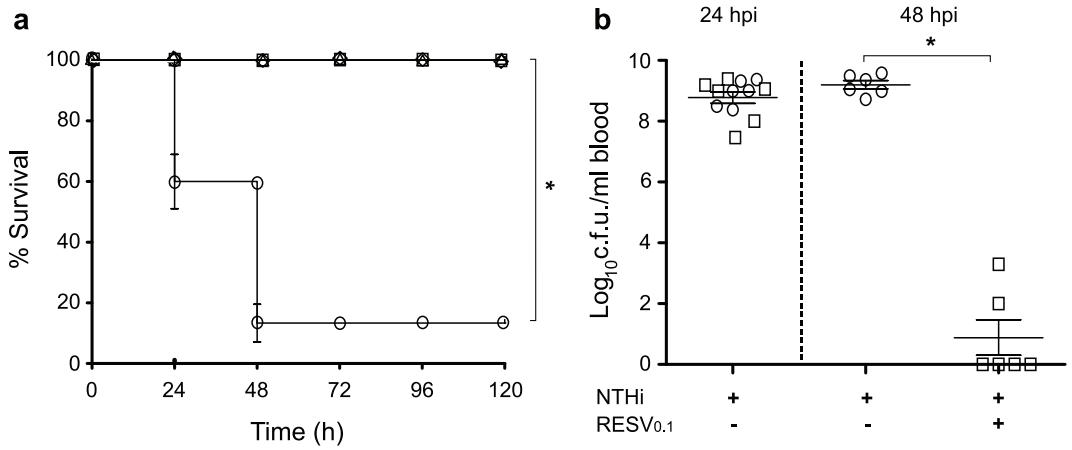

Figure 5. Effect of resveratrol administration on zebrafish infected by NTHi. Zebrafish were infected intraperitoneally with $\sim 5 \times 10^7$ bacteria/individual. When necessary, resveratrol 0.1 mg/g/dose ($RESV_{0.1}$) was administered intraperitoneally at 29 and 53 hpi. **(a)** Effect of resveratrol administration on adult zebrafish survival upon NTHi375 infection. Non-infected groups were administered perfusion solution-DMSO (1:1) (triangle) or saline solution 0.9% (diamond); infected groups were administered perfusion solution-DMSO (1:1) (circle) or resveratrol (square). Survival rate is reported as percentage (mean ± SD) of adult individuals survival at 120 hpi. Survival of NTHi infected zebrafish was significantly higher in resveratrol treated- and in untreated animals ($p < 0.0001$). **(b)** Bacterial counts on zebrafish blood samples from the caudal fin were determined at 24 and 48 hpi ($\log_{10}$ c.f.u./ml blood), corresponding to 5 h before- and 19 h post-resveratrol treatment, respectively. At 48 hpi, NTHi375 counts were lower in resveratrol treated (square) than in control vehicle administered (circle) zebrafish ($p < 0.0001$). Perfusion solution-DMSO (1:1) was used as vehicle solution.

Discussion

This study delineates the effect of resveratrol administration on infection by NTHi. By using conditions mimicking therapeutic resveratrol administration *in vitro*, in cultured respiratory epithelial cells and *in vivo*, we established the impact of this natural polyphenol on a number of properties related to NTHi viability, host-pathogen interplay and progression of infection. Given that NTHi is largely associated with COPD chronic infection and AECOPD frequency[47], therapeutics targeting both infection and overactive inflammation at the COPD airway are of particular interest. Preventive and therapeutic benefits of this antimicrobial/anti-inflammatory duality have been exploited for the macrolide antibiotic azithromycin. Thus, clinical studies suggest that azithromycin long-term low-dose use to prevent and/or manage chronic inflammatory airway disorders such as AECOPD may be beneficial, but could also increase the rate of macrolide resistance by colonising opportunistic pathogens. In fact, adverse effects of long-term azithromycin use in patients with chronic lung diseases have been suggested[48], and its use for AECOPD prevention is under debate. Following this notion, this study assessed resveratrol therapeutic potential against NTHi infection, which may also rely on its antimicrobial/anti-inflammatory duality. Previous work has been separately performed on resveratrol antibacterial and anti-inflammatory activities against NTHi infection[24,36]. This is, to our knowledge, the first study jointly considering the therapeutic benefits of both

properties. Thus, our use of *in vitro* and *in vivo* model systems has allowed establishing associations between resveratrol effects, doses, bacterial inhibitory concentrations and antimicrobial/host modulatory properties.

Resveratrol has demonstrated antibacterial activity against several Gram-negative and Gram-positive bacterial pathogens[30–33,49,50]. Mechanistically, it is thought to work by inhibiting bacterial ATP synthase[51], and by site-specific oxidative damage to the bacterial cell, resulting in a bacteriostatic effect[31,32]. Our results show that resveratrol is likely to be bacteriostatic on NTHi, it has a comparable effect on a whole range of genomically unrelated NTHi clinical isolates, and resistance is not induced *in vitro*; as a counterpoint to these likely beneficial therapeutic properties, and different to macrolides[38,52], resveratrol does not seem to reduce NTHi intracellular numbers despite using working concentrations shown to reduce viability for the infecting strain.

At the cellular level, our results indicate that each experimental setting is crucial to properly address resveratrol effects during infection. Thus, resveratrol concentrations inhibiting NTHi viability or being sub-inhibitory determine drug removal prior to- or drug maintenance during infection, respectively. Of note, although evaluation of resveratrol impact on the NTHi-airway epithelia interface by cell pre-treatment with a resveratrol bactericidal concentration did not modify NTHi invasion rate[24], a maintained sub-inhibitory dose is able to lower NTHi epithelial invasion. We speculate that resveratrol effects could be transitory and/or reversible, and this aspect should be further elucidated and taken into consideration when designing any administration regimen. Consequently, this notion may also apply when assessing resveratrol immunomodulatory effects on infected cells. Resveratrol has been shown to suppress the inflammatory response of host cells infected by several bacterial pathogens including *Porphyromonas gingivalis* and *Streptococcus pneumoniae*[43,53], and also to reduce inflammation on NTHi-infected cells[36]; of note, such observation did not consider resveratrol antimicrobial effect therefore maintaining the polyphenol upon cell infection with NTHi strain 12. In practical terms, the use of HK bacteria is likely to mimic the inflammatory stimulus and allow assessing resveratrol immunomodulatory properties on cells infected by susceptible pathogens without jeopardizing their viability. This approach previously allowed addressing resveratrol-based suppression of inflammatory responses on *P. gingivalis* infected human gingival epithelia[53], and has been used in the present study, showing a trend to reduce IL-8 expression in NTHi HK infected human airway epithelial cells. Resveratrol also modulates positive or negatively antimicrobial peptide (AMP) expression in cells infected by *S. pneumoniae* or *Pseudomonas aeruginosa*, respectively[42,43]. NTHi has been shown to induce AMP expression in primary bronchial epithelial cells[54], and we show here that resveratrol reduces hBD2 expression on A549 cells infected by NTHi. In addition, resveratrol has anti-oxidant properties in cultured epithelial cells infected by respiratory pathogens inducing oxidative stress, such as *S. pneumoniae* and *P. aeruginosa*[42,55]. NTHi has been shown to induce lung oxidative stress mainly in phagocytic cells[56]; however, we could not detect this stress in infected cultured epithelia (data not shown), therefore excluding the possibility of assessing a potential resveratrol antioxidant effect on NTHi infected cells. Given that oxidative stress is intimately associated to COPD progression and exacerbation, therapeutic intervention with antioxidants may have a beneficial outcome in the treatment of COPD[57].

Future work will tackle alternative host cell infection model systems to monitor resveratrol antioxidant properties upon NTHi infection.

Resveratrol effectiveness has been shown by reducing bacterial loads in lungs and BALF samples during NTHi mouse respiratory infection, with a clearing effect dependent on resveratrol dose. Resveratrol antimicrobial potential has been previously proven in rat and mouse models infected by *Serratia marcescens* or respiratory syncytial virus, respectively[58,59]. In this study, we further support resveratrol antimicrobial effect by presenting a newly established preclinical sepsis model system by NTHi zebrafish infection. Moreover, testing resveratrol toxicity in zebrafish supports previous evidences for its low cytotoxicity in human cells[33]. Besides its antibacterial effect, evidence suggests that resveratrol has anti-inflammatory properties *in vivo*[59,60]. This is also the case in the lungs of NTHi infected mice[36]. Our results revealed parallel bacterial clearance and reduction of inflammation in resveratrol treated NTHi infected lungs. Of note, the upper airways of resveratrol-treated infected mice showed increased PMN numbers at the nasal cavity compared to untreated animals, which could somehow contribute to reduce bacterial load and inflammation at the lower airway, even though the reasons for such increase are currently unknown. Likewise, we acknowledge that the observed suppression of lung inflammation could be not only due to resveratrol anti-inflammatory properties, but also to its bacterial clearing effect, actively reducing the inflammatory stimulus by lowering bacterial viability. Importantly, this aspect should be taken into consideration when analyzing and concluding on potential immunomodulatory properties by antimicrobial therapeutic agents. The use of anti-inflammatory therapeutics against NTHi respiratory infection has been previously tested *in vivo* for dexamethasone, azithromycin and the non-bactericidal PDE4 inhibitors roflumilast N-oxide and rolipram, highlighting the benefits of PDE4 inhibition[22–24,38]. Resveratrol is known to inhibit PDE4, but our PDE4B expression data did not show a resveratrol inhibitory effect at the gene expression level, leading us to speculate that it may occur by competitive inhibition with cAMP, as previously stated[40].

Overall, plant polyphenols are important components of human diet, and a number of them are considered to possess chemopreventive and therapeutic properties. Numerous dietary plants contain polyphenols, resveratrol belonging to the non-flavonoid family. Although no studies have specifically examined resveratrol concentrations in relation to respiratory disease risk, a number of epidemiologic studies identified that consumption of various antioxidant-rich foods, many of which known to contain resveratrol, are protective against asthma outcomes[35]. Resveratrol-driven inflammatory reduction in COPD[28,61–63] and its potential to slow aging-related deterioration of lung function and structure by maintaining alveolar cell integrity[64], support a resveratrol protective role against chronic airway disease. The present study sheds light on resveratrol as an attractive therapy that timely combines anti-inflammatory and antimicrobial properties, therefore targeting both infection and overactive inflammation at the COPD airway. Future research will consider the efficacy and toxicity of resveratrol when present in the human airways, and explore the therapeutic potential of other plant polyphenols against respiratory infection.

Methods

Bacterial strains, media, growth conditions, interfering drugs. NTHi strains were grown at 37 °C, 5% CO_2 on chocolate agar (Biomérieux) or on brain heart infusion (BHI) agar supplemented with 10 μg/ml hemin and 10 μg/ml nicotinamide adenine dinucleotide (NAD), referred to as sBHI. NTHi liquid cultures were grown in sBHI. When necessary, heat killed (HK) bacteria were used; for this purpose, a bacterial suspension recovered with 1 ml PBS from a freshly grown chocolate agar plate was adjusted to $OD_{600} = 1$ ($\sim 10^9$ c.f.u./ml) and incubated at 80 °C for 30 min. NTHi375 is a genome sequenced clinical isolate previously used in host-pathogen interplay studies[13,15,65,66]. NTHi clinical strains shown Table 1 were isolated from COPD sputum samples during independent AECOPD episodes at Bellvitge University Hospital, Spain. Strain relatedness was determined by pulse field gel electrophoresis (PFGE)[67]. Resveratrol was purchased from Sigma-Aldrich, and was also kindly supplied by Monteloeder (Elche, Spain). Resveratrol (20 mM, i.e. 4.56 mg/ml) stock solutions were prepared in dimethyl sulfoxide (DMSO) and diluted to the required working concentrations in Earle's balanced salt solution (EBSS; Gibco), sBHI or PBS, depending on the assay type (see below).

Resveratrol susceptibility assays. NTHi susceptibility to resveratrol was assessed as described before[24]. To assess if resveratrol effect on NTHi is bactericidal or bacteriostatic, bacteria grown on chocolate agar for 16 h were inoculated (2 to 5 colonies) in 20 ml sBHI and incubated for 11 h under shaking. Cultures were then diluted in 100 ml sBHI to $OD_{600} = 0.05$, incubated with agitation to $OD_{600} = 0.5$ and divided into 4 flasks (20 ml/flask) as it follows: (i) control untreated; (ii) resveratrol 112.5 μg/ml; (iii) resveratrol 56.25 μg/ml; (iv) DMSO, by adding a volume identical to that used in (ii). Cultures were incubated with agitation for 4 h. When indicated, OD_{600} was recorded and culture samples were serially diluted and plated on sBHI agar. Data are shown as OD_{600} and c.f.u./ml. Experiments were performed in duplicate at least four times ($n \geq 8$).

NTHi serial passage in the presence of resveratrol. Bacteria grown on chocolate agar for 16 h were inoculated (1 colony) in 3 ml sBHI and incubated for 11 h under shaking; starting inocula were prepared in quadruplicate (cultures 1 to 4, CL1 to CL4). Resveratrol 20 mM stock solution was diluted in sBHI (250; 225; 175; 130; 120; 112.5 μg/ml). One hundred μl of each resveratrol dilution were transferred to individual wells in 96-well microtiter plates; a vehicle solution control consisting of a DMSO volume equivalent to that used for the highest resveratrol concentration tested was performed in parallel. The assay was initiated by inoculating 1 μl of the previously grown bacterial cultures in each well, and further incubation for 24 h at 37 °C shaking. Cultures were then passaged (10 μl in 100 μl fresh sBHI with resveratrol or vehicle solution) every day for 15 days. At various time points throughout the cycling, culture samples were serially diluted and plated on sBHI agar. The assay was performed in duplicate ($n \geq 8$).

Infection of cultured epithelial cells. Carcinomic human alveolar basal epithelial cells (A549, ATTC CCL-185) were maintained, and NTHi infected to quantify bacterial adhesion and invasion, as described previously[15]. When indicated, cells were pre-treated with resveratrol (0.75; 1.5; 3 μM) or vehicle solution (DMSO) for 4 h in 1 ml EBSS, and drug exposure was maintained during bacterium-cell contact. Alternatively, cells were infected, and resveratrol 20 μM or DMSO was added during the gentamicin incubation period. These treatments did not induce A549 cytotoxicity, verified by measuring the release of lactate dehydrogenase and by microscopy (data not shown). Controls (CON) were performed by using a DMSO volume corresponding to that of the highest resveratrol concentration tested in each assay. Results are expressed as c.f.u./well. Experiments were performed in triplicate and at least in three independent occasions ($n \geq 9$).

Immunofluorescence microscopy. A549 cells were seeded on 13 mm circular coverslips in 24-well tissue culture plates and NTHi infected for 2 h as previously described[15]. Infected cells were incubated in RPMI 1640 containing 10% FCS, Hepes 10 mM and gentamicin 200 μg/ml for 1 h. When necessary, cells were pre-treated with resveratrol 3 μM or DMSO for 4 h in 1 ml EBSS, maintained during bacterium-cell contact; alternatively, cells were infected, and resveratrol 20 μM or DMSO was added during the gentamicin incubation period. Cells were washed three times with PBS and fixed with 3.7% paraformaldehyde (PFA) in PBS pH 7.4 for 15 min at room temperature. Bacteria were stained with rabbit anti-NTHi serum[15] diluted 1:600. Late endosomes were stained with mouse monoclonal anti-human Lamp-1 H4A3 antibody (Developmental Studies Hybridoma Bank) diluted 1:70. Donkey anti-rabbit conjugated to Alexa 488 and donkey anti-mouse conjugated to Rhodamine Red-X (RRX) secondary antibodies (Jackson Immunological) were diluted 1:100. Samples were analyzed with a Carl Zeiss Axioskop 2 plus fluorescence microscope and a Carl Zeiss Axio Cam MRm monochrome camera.

RNA extraction and real-time quantitative PCR. A549 cells were seeded on 24-well tissue culture plates, and infected for 1, 2 or 4 h in EBSS. When indicated, cells were pre-treated with resveratrol 20 μM or DMSO for 4 h in 1 ml EBSS, and removed prior to bacterial addition. Alternatively, cells were pre-treated with resveratrol 20 μM or DMSO for 4 h in 1 ml EBSS, and a suspension containing HK bacteria (equivalent in numbers to that of the infecting dose) was added for 1, 2 or 4 h, without removal of resveratrol or DMSO. Following treatment and/or NTHi stimulation, total RNA was isolated from A549 cells using a Nucleospin RNAII kit (Macherey-Nagel) as recommended by the manufacturer and including an on column DNase treatment step. When necessary, total RNA was isolated from mouse lungs using TRIzol reagent (Invitrogen). Total RNA quality was evaluated using RNA 6000 Nano LabChips (Agilent 2100 Bioanalyzer, Santa Clara, CA). All samples had intact 18 S and 28 S ribosomal RNA bands with RNA integrity numbers (RIN) between 9.3 to 10. Reverse transcription was performed using 1 μg of RNA by PrimerScript RT Reagent kit (Takara). To amplify human *il-8*, *pde4b*, and mouse *kc*, *tnf-α*, *gapdh* genes, 6 ng of cDNA were used; to amplify human *hbd2*, 50 ng of cDNA were used as template. In all cases, 20 μl reaction mixtures containing 1X SYBR Premix Ex Taq II (Tli RNaseH Plus) (Takara) and the adequate primer mix were used. When necessary, human *gapdh* was amplified using 6

or 50 ng of cDNA as template. Fluorescence data were analyzed with AriaMx Real-Time PCR System (Agilent Technologies). The comparative threshold cycle (Ct) method was used to obtain relative quantities of mRNAs that were normalized using human or mouse *gapdh* as an endogenous control. Intron-spanning primers were designed with Primer-BLAST software (NCBI)[24,68] (Table S1). All measures were performed in triplicate and at least four times ($n \geq 12$).

Western Blot. A549 cells were seeded before each experiment on 6-well tissue culture plates at 2.8×10^6 cells per well. Cells were pre-treated with resveratrol 20 μM for 4 h in 4 ml EBSS per well, and then infected for 10, 20, 30, 50, 70, 90, 100 or 120 min with NTHi375. Next, wells were washed 3 times with cold PBS, scrapped and lysed with 100 μl of lysis buffer (62.5 mM Tris-HCl pH 6.8, 2% w/v SDS, 10% glycerol, 50 mM DTT, 0.01% w/v bromophenol blue) on ice. Samples were sonicated, boiled at 100 °C for 10 min and cooled on ice before 10% SDS-PAGE and western blotting. SIRT1 was detected with primary rabbit anti-SIRT1 antibody (sc-15404, Santa Cruz Biotechnology) diluted 1:1,000; tubulin, used as a loading control, was detected with primary mouse anti-tubulin antibody (Sigma-Aldrich) diluted 1:3,000. Secondary goat anti-rabbit IgG and anti-mouse IgG (whole molecule, Sigma-Aldrich) antibodies, conjugated to horseradish peroxidase, were diluted 1:1,000. ECL AdvanceTM Western Blotting Detection Kit (GE HealthCare) was used for detection. Western blots were performed at least three times by using independently generated A549 cell extracts. Densitometry analysis on scanned images was performed using ImageJ software (http://rsb.info.nih.gov/ij/download.html). Bands in each lane were analyzed using the label peaks tool, and the mean intensity was recorded. Results are expressed as relative level of protein (mean intensity of protein SIRT1/mean intensity of tubulin).

Secretion of IL-8. A549 cells were maintained, seeded on 24-well tissue culture plates, and infected for 2 h. When necessary, cells were pre-treated with resveratrol 20 μM or DMSO for 4 h in 1 ml EBSS, and removed prior to bacterial addition. Alternatively, cells were pre-treated with resveratrol 20 μM or DMSO for 4 h in 1 ml EBSS, and a suspension containing HK bacteria was added for 2 h, without removal of resveratrol or DMSO. Cells were washed 3 times with PBS and incubated for 6 h in RPMI 1640 containing 10% FCS, Hepes 10 mM, gentamicin 100 μg/ml, and resveratrol 20 μM or DMSO. Supernatants were collected from the wells, cell debris was removed by centrifugation and samples were frozen at −80 °C until use. IL-8 levels in the supernatants were measured by ELISA (Abnova KA0115) with sensitivity <2 pg/ml. Results are expressed as IL-8 pg/ml. Infections were performed in duplicate and at least twice ($n \geq 4$).

NTHi mouse lung infection. A previously described mouse model of NTHi respiratory infection was used[24,38,67,69,70] at the Institute of Agrobiotechnology facilities (registration number ES/31–2016–000002-CR-SU-US). Animal handling and procedures were in accordance with the current European (Directive 86/609/EEC) and National (Real Decreto 53/2013) legislations, following the FELASA and ARRIVE guidelines, and with the approval of the Universidad Pública de Navarra (UPNa) Animal Experimentation Committee (Comité de Ética, Experimentación Animal y Bioseguridad) and the local Government authorization. Resveratrol treatment was performed at doses of 100 or 150 mg/kg of body weight in 0.1 ml PBS-DMSO (1:1) and administered by oroesophageal gavage (Popper&Sons Inc.). Administrations were performed at 48, 24, 1 h before infection and at 6, 12 and 18 h post-infection (hpi) (resveratrol administrations at 12 and 18 hpi were performed in mice euthanized at 24 hpi). NTHi375 was used for lung infection, and mice were randomly divided into 6 infected ($n = 6$) and 2 control non-infected ($n = 3$) groups: (i) treated with 100 mg/kg resveratrol, euthanized at 12 hpi; (ii) treated with 100 mg/kg resveratrol, euthanized at 24 hpi; (iii) treated with 150 mg/kg resveratrol, euthanized at 12 hpi; (iv) treated with 150 mg/kg resveratrol, euthanized at 24 hpi; (v) treated with vehicle solution (PBS-DMSO, 1:1), euthanized at 12 hpi; (vi) treated with vehicle solution, euthanized at 24 hpi; (vii) control, administered 150 mg/kg resveratrol; (viii) control, administered vehicle solution. For NTHi intranasal infection, 20 μl of a NTHi375 suspension containing $\sim 5 \times 10^9$ c.f.u./ml (1×10^8 c.f.u./mouse) was placed at the entrance of the nostrils until complete inhalation by the mouse, previously anesthetized (ketamine-xylazine, 3:1). At 12- or 24 hpi, mice were euthanized and lungs were aseptically removed. The left lung was individually weighed in sterile bags (Stomacher80, Seward Medical) and homogenized 1:10 (wt/vol) in PBS. Each homogenate was serially 10-fold diluted in PBS and plated in triplicate on sBHI agar to determine the number of viable bacteria. Results are shown as $\log_{10}$ c.f.u./lung. The right lung was fixed in 10% neutral buffered formalin. Heads and necks, containing upper airways, larynxes, and tracheas, were fixed in the same buffered formalin for histology. In parallel, BALF samples were obtained by perfusion and collection of 0.7 ml of PBS, with the help of a sterile 20 G (1.1-mm diameter) Vialon intravenous catheter (Becton-Dickinson) inserted into the trachea. Each recovered BALF fraction was serially 10-fold diluted and plated on sBHI agar as described above. Results are shown as $\log_{10}$ c.f.u./ml BALF.

Histopathology and lesions score was performed as it follows. Heads and necks were rinsed in running tap water for 1 h, immersed in 5% nitric acid for 24–36 h until complete decalcification, and 7–8 transaxial slices were made every 3–4 mm beginning at the nostrils and finishing in the caudal tracheas. Transaxial slices and lungs were embedded in paraffin, and 4- to 6 μm sections were stained with hematoxylin and eosin (H&E) by standard procedures, and examined by microscopy to determine the presence and extent of inflammatory lesions. Sections were examined blind as sets by a trained veterinary pathologist (Dr. M. Barberán). Parameters characterizing an acute inflammatory reaction in upper airways and lung, including hemorrhages, hyperemia, polymorphonuclear cell infiltrates (PMNs) and alveolar macrophages, were subjectively scored on a scale of 0 to 3 (0: absent, 1: mild, 2: moderate, 3: severe). For tissue control, similar organs obtained from non-infected control and resveratrol treated mice were processed in an identical manner to the infected tissues. Images were observed and digitalized using an Olympus Vanox AHBS3 microscope coupled to an Olympus DP12 digital camera.

NTHi adult zebrafish infection. Animal experiments conducted at The Zebrafish Lab (http://www.thezebrafishlab.com) animal housing facility were performed according to EU guidelines (http://ec.europa.eu/environment/chemicals/lab_animals/home_en.htm), and the approval of the Universidad de Navarra (UNAV) Ethics Committee for Animal Experimentation (Protocol 03417). Once lack of resveratrol toxicity in zebrafish was confirmed (data not shown), adult zebrafish (n = 10 per group) were randomly divided into 2 infected and 2 non-infected groups. Infected groups were injected with 10 μl of a NTHi375 suspension containing $\sim 5 \times 10^9$ c.f.u./ml, i.e. $\sim 5 \times 10^7$ c.f.u./zebrafish, prepared in perfusion solution (Grifols, Spain). At 29 and 53 hpi, an infected group was intraperitoneally administered resveratrol at a dosis of 0.1 mg/g of body weight in 10 μl of perfusion solution-DMSO (1:1); the other groups were administered perfusion solution-DMSO (1:1) or saline solution 0.9% as a control. Survival rate for each group was monitored three times per day during 5 days after infection. To quantify resveratrol protective effect, the numbers of bacterial c.f.u. in blood samples collected from zebrafish caudal fin were quantified at 24 and 48 hpi, i.e. 5 h before- and 19 h post-treatment. Each recovered blood fraction was serially 10-fold diluted in PBS and spread on BHI agar to determine the number of viable bacteria. Results are shown as $\log_{10}$ c.f.u./ml blood.

Statistical analysis. For bacterial viability, cell infection, gene expression, IL-8 secretion and bacterial loads in lungs and BALF samples, mean±SD were calculated and statistical comparisons of means were performed using the two-tail Student's *t* test. For zebrafish assays, statistical analysis were performed by using the two-tailed Student's *t* test (for two groups), analysis of variance (ANOVA) was chosen for multiple comparisons, and the log-rank (Mantel–Cox) and Gehan–Breslow–Wilcoxon tests were used to draw, analyze and compare survival curves. In all cases, a $p < 0.05$ value was considered statistically significant. Analyses were performed using the Prism software, version 7 for Mac (GraphPad Software) statistical package.

References

1. Agrawal, A. & Murphy, T. F. *Haemophilus influenzae* infections in the *H. influenzae* type b conjugate vaccine era. *J Clin Microbiol* **49**, 3728–3732, https://doi.org/10.1128/JCM.05476-11 (2011).
2. Duell, B. L., Su, Y. C. & Riesbeck, K. Host-pathogen interactions of nontypeable *Haemophilus influenzae*: from commensal to pathogen. *FEBS letters* **590**, 3840–3853, https://doi.org/10.1002/1873-3468.12351 (2016).
3. Barnes, P. J. Inflammatory mechanisms in patients with chronic obstructive pulmonary disease. *J Allergy Clin Immunol* **138**, 16–27, https://doi.org/10.1016/j.jaci.2016.05.011 (2016).
4. Hassett, D. J., Borchers, M. T. & Panos, R. J. Chronic obstructive pulmonary disease (COPD): evaluation from clinical, immunological and bacterial pathogenesis perspectives. *J Microbiol* **52**, 211–226, https://doi.org/10.1007/s12275-014-4068-2 (2014).
5. Alikhan, M. M. & Lee, F. E. Understanding nontypeable *Haemophilus influenzae* and chronic obstructive pulmonary disease. *Curr Opin Pulm Med* **20**, 159–164, https://doi.org/10.1097/MCP.0000000000000023 (2014).
6. Huang, Y. J. *et al.* Airway microbiome dynamics in exacerbations of chronic obstructive pulmonary disease. *J Clin Microbiol* **52**, 2813–2823, https://doi.org/10.1128/JCM.00035-14 (2014).
7. Sethi, S. Infection as a comorbidity of COPD. *Eur Resp J* **35**, 1209–1215, https://doi.org/10.1183/09031936.00081409 (2010).
8. Ahren, I. L., Williams, D. L., Rice, P. J., Forsgren, A. & Riesbeck, K. The importance of a β-glucan receptor in the nonopsonic entry of nontypeable *Haemophilus influenzae* into human monocytic and epithelial cells. *J Infect Dis* **184**, 150–158, https://doi.org/10.1086/322016 (2001).
9. Bandi, V. *et al.* Nontypeable *Haemophilus influenzae* in the lower respiratory tract of patients with chronic bronchitis. *Am J Resp Crit Care Med* **164**, 2114–2119, https://doi.org/10.1164/ajrccm.164.11.2104093 (2001).
10. Clementi, C. F., Hakansson, A. P. & Murphy, T. F. Internalization and trafficking of nontypeable *Haemophilus influenzae* in human respiratory epithelial cells and roles of IgA1 proteases for optimal invasion and persistence. *Infect Immun* **82**, 433–444, https://doi.org/10.1128/IAI.00864-13 (2014).
11. Forsgren, J. *et al. Haemophilus influenzae* resides and multiplies intracellularly in human adenoid tissue as demonstrated by *in situ* hybridization and bacterial viability assay. *Infect Immun* **62**, 673–679 (1994).
12. Ketterer, M. R. *et al.* Infection of primary human bronchial epithelial cells by *Haemophilus influenzae*: macropinocytosis as a mechanism of airway epithelial cell entry. *Infect Immun* **67**, 4161–4170 (1999).
13. Lopez-Gomez, A. *et al.* Host cell kinases, α5 and β1 integrins, and Rac1 signalling on the microtubule cytoskeleton are important for non-typeable *Haemophilus influenzae* invasion of respiratory epithelial cells. *Microbiology* **158**, 2384–2398, https://doi.org/10.1099/mic.0.059972-0 (2012).
14. Mell, J. C. *et al.* Transformed recombinant enrichment profiling rapidly identifies HMW1 as an intracellular invasion locus in *Haemophilus influenzae*. *PLoS Pathogens* **12**, e1005576, https://doi.org/10.1371/journal.ppat.1005576 (2016).
15. Morey, P. *et al.* Evidence for a non-replicative intracellular stage of nontypeable *Haemophilus influenzae* in epithelial cells. *Microbiology* **157**, 234–250, https://doi.org/10.1099/mic.0.040451-0 (2011).
16. Swords, W. E. *et al.* Non-typeable *Haemophilus influenzae* adhere to and invade human bronchial epithelial cells via an interaction of lipooligosaccharide with the PAF receptor. *Mol Microbiol* **37**, 13–27 (2000).
17. Clementi, C. F. & Murphy, T. F. Non-typeable *Haemophilus influenzae* invasion and persistence in the human respiratory tract. *Front Cell Infect Microbiol* **1**, 1, https://doi.org/10.3389/fcimb.2011.00001 (2011).
18. Garmendia, J., Marti-Lliteras, P., Moleres, J., Puig, C. & Bengoechea, J. A. Genotypic and phenotypic diversity of the noncapsulated *Haemophilus influenzae*: adaptation and pathogenesis in the human airways. *Int Microbiol* **15**, 159–172 (2012).
19. Miravitlles, M., D'Urzo, A., Singh, D. & Koblizek, V. Pharmacological strategies to reduce exacerbation risk in COPD: a narrative review. *Resp Res* **17**, 112, https://doi.org/10.1186/s12931-016-0425-5 (2016).
20. Sethi, S. *et al.* Inflammation in COPD: implications for management. *Am J Med* **125**, 1162–1170, https://doi.org/10.1016/j.amjmed.2012.06.024 (2012).
21. Wang, W. Y., Lim, J. H. & Li, J. D. Synergistic and feedback signaling mechanisms in the regulation of inflammation in respiratory infections. *Cell & Mol Immunol* **9**, 131–135, https://doi.org/10.1038/cmi.2011.65 (2012).
22. Gaschler, G. J. *et al.* Bacteria challenge in smoke-exposed mice exacerbates inflammation and skews the inflammatory profile. *Am J Resp Crit Care Med* **179**, 666–675, https://doi.org/10.1164/rccm.200808-1306OC (2009).
23. Komatsu, K. *et al.* Inhibition of PDE4B suppresses inflammation by increasing expression of the deubiquitinase CYLD. *Nature Comm* **4**, 1684, https://doi.org/10.1038/ncomms2674 (2013).
24. Euba, B. *et al.* Genome expression profiling-based identification and administration efficacy of host-directed antimicrobial drugs against respiratory infection by nontypeable *Haemophilus influenzae*. *Antimicrob Ag Chemother* **59**, 7581–7592, https://doi.org/10.1128/AAC.01278-15 (2015).
25. Susuki-Miyata, S. *et al.* Cross-talk between PKA-Cβ and p65 mediates synergistic induction of PDE4B by roflumilast and NTHi. *Proc Nat Acad Sci USA* **112**, E1800–1809, https://doi.org/10.1073/pnas.1418716112 (2015).

26. Nakamaru, Y. *et al*. A protein deacetylase SIRT1 is a negative regulator of metalloproteinase-9. *FASEB J* **23**, 2810–2819, https://doi.org/10.1096/fj.08-125468 (2009).
27. Yao, H. *et al*. SIRT1 protects against emphysema via FOXO3-mediated reduction of premature senescence in mice. *J Clin Invest* **122**, 2032–2045, https://doi.org/10.1172/JCI60132 (2012).
28. Ito, K., Colley, T. & Mercado, N. Geroprotectors as a novel therapeutic strategy for COPD, an accelerating aging disease. *Int J COPD* **7**, 641–652, https://doi.org/10.2147/COPD.S28250 (2012).
29. Agrawal, M. Natural polyphenols based new therapeutic avenues for advanced biomedical applications. *Drug Metab Rev* **47**, 420–430, https://doi.org/10.3109/03602532.2015.1102933 (2015).
30. Nawrocki, E. M., Bedell, H. W. & Humphreys, T. L. Resveratrol is cidal to both classes of *Haemophilus ducreyi*. *Int J Antimicrob Ag* **41**, 477–479, https://doi.org/10.1016/j.ijantimicag.2013.02.008 (2013).
31. Paulo, L., Ferreira, S., Gallardo, E., Queiroz, J. A. & Domingues, F. Antimicrobial activity and effects of resveratrol on human pathogenic bacteria. *World J Microbiol Biotechnol* **26**, 1533–1538, https://doi.org/10.1007/s11274-010-0325-7 (2010).
32. Subramanian, M., Goswami, M., Chakraborty, S. & Jawali, N. Resveratrol induced inhibition of *Escherichia coli* proceeds via membrane oxidation and independent of diffusible reactive oxygen species generation. *Redox. Biol* **2**, 865–872, https://doi.org/10.1016/j.redox.2014.06.007 (2014).
33. Taylor, E. J. M., Yu, Y., Champer, J. & Kim, J. Resveratrol demonstrates antimicrobial effects against *Propionibacterium acnes in vitro*. *Dermatol Ther* **4**, 249–257, https://doi.org/10.1007/s13555-014-0063-0 (2014).
34. Britton, R. G., Kovoor, C. & Brown, K. Direct molecular targets of resveratrol: identifying key interactions to unlock complex mechanisms. *Ann N Y Acad Sci* **1348**, 124–133, https://doi.org/10.1111/nyas.12796 (2015).
35. Wood, L. G., Wark, P. A. & Garg, M. L. Antioxidant and anti-inflammatory effects of resveratrol in airway disease. *Antioxid Redox Signal* **13**, 1535–1548, https://doi.org/10.1089/ars.2009.3064 (2010).
36. Andrews, C. S., Matsuyama, S., Lee, B.-C. & Li, J.-D. Resveratrol suppresses NTHi-induced inflammation via up-regulation of the negative regulator MyD88 short. *Sci Rep* **6**, 34445, https://doi.org/10.1038/srep34445 (2016).
37. De Chiara, M. *et al*. Genome sequencing of disease and carriage isolates of nontypeable *Haemophilus influenzae* identifies discrete population structure. *Proc Nat Acad Sci USA* **111**, 5439–5444, https://doi.org/10.1073/pnas.1403353111 (2014).
38. Euba, B. *et al*. Relationship between azithromycin susceptibility and administration efficacy for nontypeable *Haemophilus influenzae* respiratory infection. *Antimicrob Ag Chemother* **59**, 2700–2712, https://doi.org/10.1128/AAC.04447-14 (2015).
39. Bonkowski, M. S. & Sinclair, D. A. Slowing ageing by design: the rise of NAD + and sirtuin-activating compounds. *Nat Rev Mol Cell Biol* **17**, 679–690, https://doi.org/10.1038/nrm.2016.93 (2016).
40. Park, S. J. *et al*. Resveratrol ameliorates aging-related metabolic phenotypes by inhibiting cAMP phosphodiesterases. *Cell* **148**, 421–433, https://doi.org/10.1016/j.cell.2012.01.017 (2012).
41. Frombaum, M. *et al*. Penetration of resveratrol into bovine aortic endothelial cells (BAEC): a possible passive diffusion. *C R Biol* **335**, 247–252, https://doi.org/10.1016/j.crvi.2012.03.013 (2012).
42. Cerqueira, A. M., Khaper, N., Lees, S. J. & Ulanova, M. The antioxidant resveratrol down-regulates inflammation in an *in vitro* model of *Pseudomonas aeruginosa* infection of lung epithelial cells. *Can J Physiol Pharmacol* **91**, 248–255, https://doi.org/10.1139/cjpp-2012-0268 (2013).
43. Lin, L. *et al*. Role of SIRT1 in *Streptococcus pneumoniae*-induced human β-defensin-2 and interleukin-8 expression in A549 cell. *Mol Cell Biochem* **394**, 199–208, https://doi.org/10.1007/s11010-014-2095-2 (2014).
44. Sullivan, C. *et al*. Infectious disease models in zebrafish. *Methods Cell Biol* **138**, 101–136, https://doi.org/10.1016/bs.mcb.2016.10.005 (2017).
45. Saralahti, A. *et al*. Adult zebrafish model for pneumococcal pathogenesis. *Dev Comp Immunol* **42**, 345–353, https://doi.org/10.1016/j.dci.2013.09.009 (2014).
46. Xie, J. *et al*. An adult zebrafish model for *Laribacter hongkongensis* infection: Koch's postulates fulfilled. *Emerg Microbes Infect* **3**, e73, https://doi.org/10.1038/emi.2014.73 (2014).
47. Sethi, S. Molecular diagnosis of respiratory tract infection in acute exacerbations of chronic obstructive pulmonary disease. *Clin Infect Dis* **52**(Suppl 4), S290–295, https://doi.org/10.1093/cid/cir044 (2011).
48. Li, H. *et al*. Meta-analysis of the adverse effects of long-term azithromycin use in patients with chronic lung diseases. *Antimicrob Ag Chemother* **58**, 511–517, https://doi.org/10.1128/AAC.02067-13 (2014).
49. Lee, S. Y., Shin, Y. W. & Hahm, K. B. Phytoceuticals: mighty but ignored weapons against *Helicobacter pylori* infection. *J Digestive Dis* **9**, 129–139 (2008).
50. O'Connor, D. J., Wong, R. W. K. & Rabie, A. B. M. Resveratrol inhibits periodontal pathogens *in vitro*. *Phytother Res* **25**, 1727–1731, https://doi.org/10.1002/ptr.3501 (2011).
51. Dadi, P. K., Ahmad, M. & Ahmad, Z. Inhibition of ATPase activity of *Escherichia coli* ATP synthase by polyphenols. *Int J Biol Macromol* **45**, 72–79, https://doi.org/10.1016/j.ijbiomac.2009.04.004 (2009).
52. Nakamura, S. *et al*. Efficacy of clarithromycin against experimentally induced pneumonia caused by clarithromycin-resistant *Haemophilus influenzae* in mice. *Antimicrob Ag Chemother* **54**, 757–762, https://doi.org/10.1128/AAC.00524-09 (2010).
53. Minagawa, T. *et al*. Resveratrol suppresses the inflammatory responses of human gingival epithelial cells in a SIRT1 independent manner. *J Periodontal Res* **50**, 586–593, https://doi.org/10.1111/jre.12238 (2015).
54. Zarcone, M. C., van Schadewijk, A., Duistermaat, E., Hiemstra, P. S. & Kooter, I. M. Diesel exhaust alters the response of cultured primary bronchial epithelial cells from patients with chronic obstructive pulmonary disease (COPD) to non-typeable *Haemophilus influenzae*. *Resp Res* **18**, 27, https://doi.org/10.1186/s12931-017-0510-4 (2017).
55. Zahlten, J. *et al*. *Streptococcus pneumoniae*–induced oxidative stress in lung epithelial cells depends on pneumococcal autolysis and is reversible by resveratrol. *J Infect Dis* **211**, 1822–1830, https://doi.org/10.1093/infdis/jiu806 (2015).
56. King, P. T. *et al*. Nontypeable *Haemophilus influenzae* induces sustained lung oxidative stress and protease expression. *PloS One* **10**, e0120371, https://doi.org/10.1371/journal.pone.0120371 (2015).
57. Rahman, I. Antioxidant therapeutic advances in COPD. *Ther Adv Resp Dis* **2**, 351–374, https://doi.org/10.1177/1753465808098224 (2008).
58. Lu, C.-C., Lai, H.-C., Hsieh, S.-C. & Chen, J.-K. Resveratrol ameliorates *Serratia marcescens*-induced acute pneumonia in rats. *J Leuk Biol* **83**, 1028–1037, https://doi.org/10.1189/jlb.0907647 (2008).
59. Zang, N. *et al*. Resveratrol-mediated γ-interferon reduction prevents airway inflammation and airway hyperresponsiveness in respiratory syncytial virus-infected immunocompromised mice. *J Virol* **85**, 13061–13068, https://doi.org/10.1128/JVI.05869-11 (2011).
60. Rieder, S. A., Nagarkatti, P. & Nagarkatti, M. Multiple anti-inflammatory pathways triggered by resveratrol lead to amelioration of staphylococcal enterotoxin B-induced lung injury. *British J Pharmacol* **167**, 1244–1258, https://doi.org/10.1111/j.1476-5381.2012.02063.x (2012).
61. Chen, J. *et al*. Therapeutic effects of resveratrol in a mouse model of LPS and cigarette smoke-induced COPD. *Inflammation* **39**, 1949–1959, https://doi.org/10.1007/s10753-016-0430-3 (2016).
62. Culpitt, S. *et al*. Inhibition by red wine extract, resveratrol, of cytokine release by alveolar macrophages in COPD. *Thorax* **58**, 942–946, https://doi.org/10.1136/thorax.58.11.942 (2003).

63. Knobloch, J. *et al*. Resveratrol attenuates the release of inflammatory cytokines from human bronchial smooth muscle cells exposed to lipoteichoic acid in Chronic Obstructive Pulmonary Disease. *Basic & Clin Pharmacol & Toxicol* **114**, 202–209, https://doi.org/10.1111/bcpt.12129 (2014).
64. Navarro, S., Reddy, R., Lee, J., Warburton, D. & Driscoll, B. Inhaled resveratrol treatments slow ageing-related degenerative changes in mouse lung. *Thorax* **72**, 451–459, https://doi.org/10.1136/thoraxjnl-2016-208964 (2017).
65. Bouchet, V. *et al*. Host-derived sialic acid is incorporated into *Haemophilus influenzae* lipopolysaccharide and is a major virulence factor in experimental otitis media. *Proc Nat Acad Sci USA* **100**, 8898–8903, https://doi.org/10.1073/pnas.1432026100 (2003).
66. Mell, J. C. *et al*. Complete genome sequence of *Haemophilus influenzae* strain 375 from the middle ear of a pediatric patient with otitis media. *Genome Announc* **2**, https://doi.org/10.1128/genomeA.01245-14 (2014).
67. Garmendia, J. *et al*. Characterization of nontypeable *Haemophilus influenzae* isolates recovered from adult patients with underlying chronic lung disease reveals genotypic and phenotypic traits associated with persistent infection. *PloS One* **9**, e97020, https://doi.org/10.1371/journal.pone.0097020 (2014).
68. Regueiro, V. *et al*. *Klebsiella pneumoniae* subverts the activation of inflammatory responses in a NOD1-dependent manner. *Cell Microbiol* **13**, 135–153, https://doi.org/10.1111/j.1462-5822.2010.01526.x (2011).
69. Morey, P. *et al*. Relative contributions of lipooligosaccharide inner and outer core modifications to nontypeable *Haemophilus influenzae* pathogenesis. *Infect Immun* **81**, 4100–4111, https://doi.org/10.1128/IAI.00492-13 (2013).
70. Euba, B. *et al*. Relative contribution of P5 and Hap surface proteins to nontypeable *Haemophilus influenzae* interplay with the host upper and lower airways. *PloS One* **10**, e0123154, https://doi.org/10.1371/journal.pone.0123154 (2015).

Acknowledgements

We thank Javier Moleres for his technical support. N.L.L. was funded by a contract from Department of Economy, Regional Govern from Navarra, Spain, reference 0011–1307; I.R.A. is funded by a PhD studentship from Universidad Pública de Navarra, Spain. This work has been funded by grants from MINECO SAF2012-31166 and SAF2015-66520-R, Health Department, Regional Govern from Navarra, Spain, reference 3/2016, and SEPAR 31/2015 to J.G. CIBERES is an initiative from Instituto de Salud Carlos III (ISCIII), Madrid, Spain.

Author Contributions

Study design: B.E., R.D.-M., J.G. Experimental work: B.E., N.L.-L., I.R.-A., A.F.-C., M.B., N.C., S.M., R.D.-M. Manuscript preparation and writing: B.E., R.D.-M., J.G. Manuscript correction: all authors.

Additional Information

Supplementary information accompanies this paper at https://doi.org/10.1038/s41598-017-13034-7.

Competing Interests: The authors declare that they have no competing interests.

Publisher's note: Springer Nature remains neutral with regard to jurisdictional claims in published maps and institutional affiliations.

Supplementary information

Resveratrol therapeutics combines both antimicrobial and immunomodulatory properties against respiratory infection by nontypeable *Haemophilus influenzae*

Begoña Euba[1,2+], Nahikari López-López[2+], Irene Rodríguez-Arce[2], Ariadna Fernández-Calvet[2], Montserrat Barberán[3], Nuria Caturla[4], Sara Martí[1,5], Roberto Díez-Martínez[6], Junkal Garmendia[1,2*]

[1]Centro de Investigación Biomédica en Red de Enfermedades Respiratorias (CIBERES), Madrid, Spain; [2]Instituto de Agrobiotecnología, CSIC-Universidad Pública Navarra-Gobierno Navarra, Mutilva, Spain; [3]Facultad de Veterinaria, Universidad de Zaragoza, Spain; [4]Monteloeder, Elche Parque Empresarial, Elche, Alicante, Spain; [5]Departamento Microbiología, Hospital Universitari Bellvitge, University of Barcelona, IDIBELL, Barcelona, Spain; [6]Ikan Biotech SL, The Zebrafish Lab, Centro Europeo de Empresas e Innovación de Navarra (CEIN), Noáin, Spain

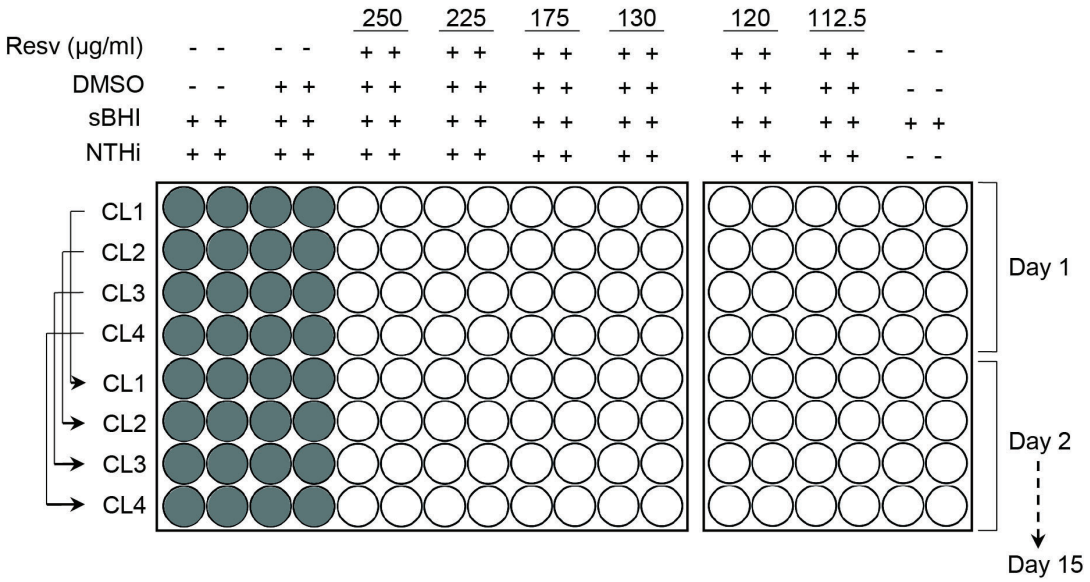

Figure S1. NTHi serial passage in the presence of resveratrol does not induce resistance. Four independently grown NTHi375 cultures (CL), CL1 to CL4, were exposed to a range of resveratrol inhibitory concentrations consisting of 250, 225, 175, 130 and 112.5 µg/ml. sBHI without/with DMSO were used as positive controls for NTHi growth. After 15 serial overnight passages, lack of growth, i.e. no resistant bacteria, was observed under the conditions tested. Lack of growth is represented by white empty wells; turbidity and growth is represented by gray filled wells.

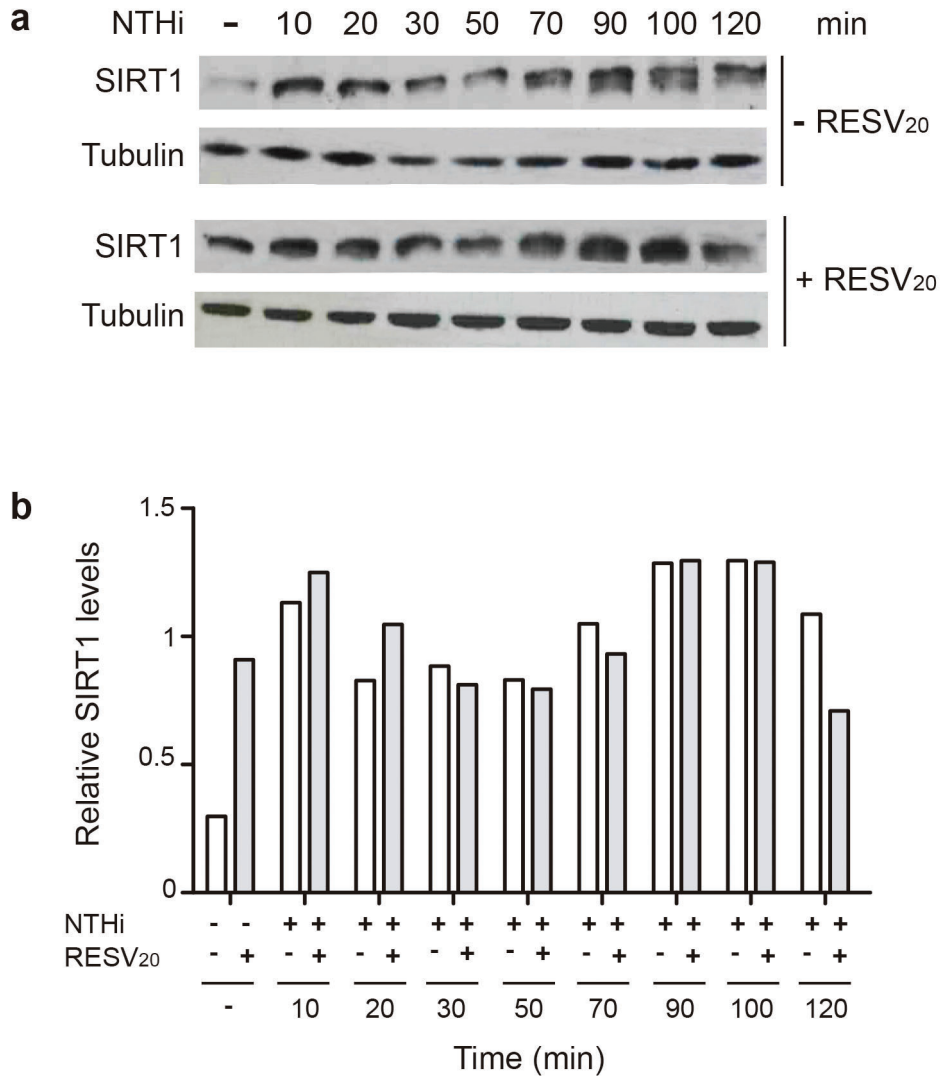

Figure S2. NTHi infection and resveratrol treatment increase SIRT1 protein levels on A549 cells. A549 cells were treated with resveratrol 20 μM for 4 h, and then infected with NTHi375 for 10, 20, 30, 50, 70, 90, 100 or 120 min. **(a)** SIRT1 protein was detected in host cell lysates by western blot analysis with rabbit anti-SIRT1 and goat anti-rabbit IgG antibodies. Tubulin was monitored as a loading control, by using mouse anti-tubulin and goat anti-mouse IgG antibodies. Representative immunoblots are shown. Bands corresponding to SIRT1 (bands ~120 KDa) or tubulin (~55 KDa) were cropped by using Adobe Illustrator CS5. Full-length blots are presented in "Expanded data for Figure S1" (see below). **(b)** Relative level of protein (mean intensity of SIRT1/mean intensity of tubulin) obtained after

densitometry analysis of western blot protein bands at each indicated time point. Please note that samples derive from the same experiment and blots were processed in parallel.

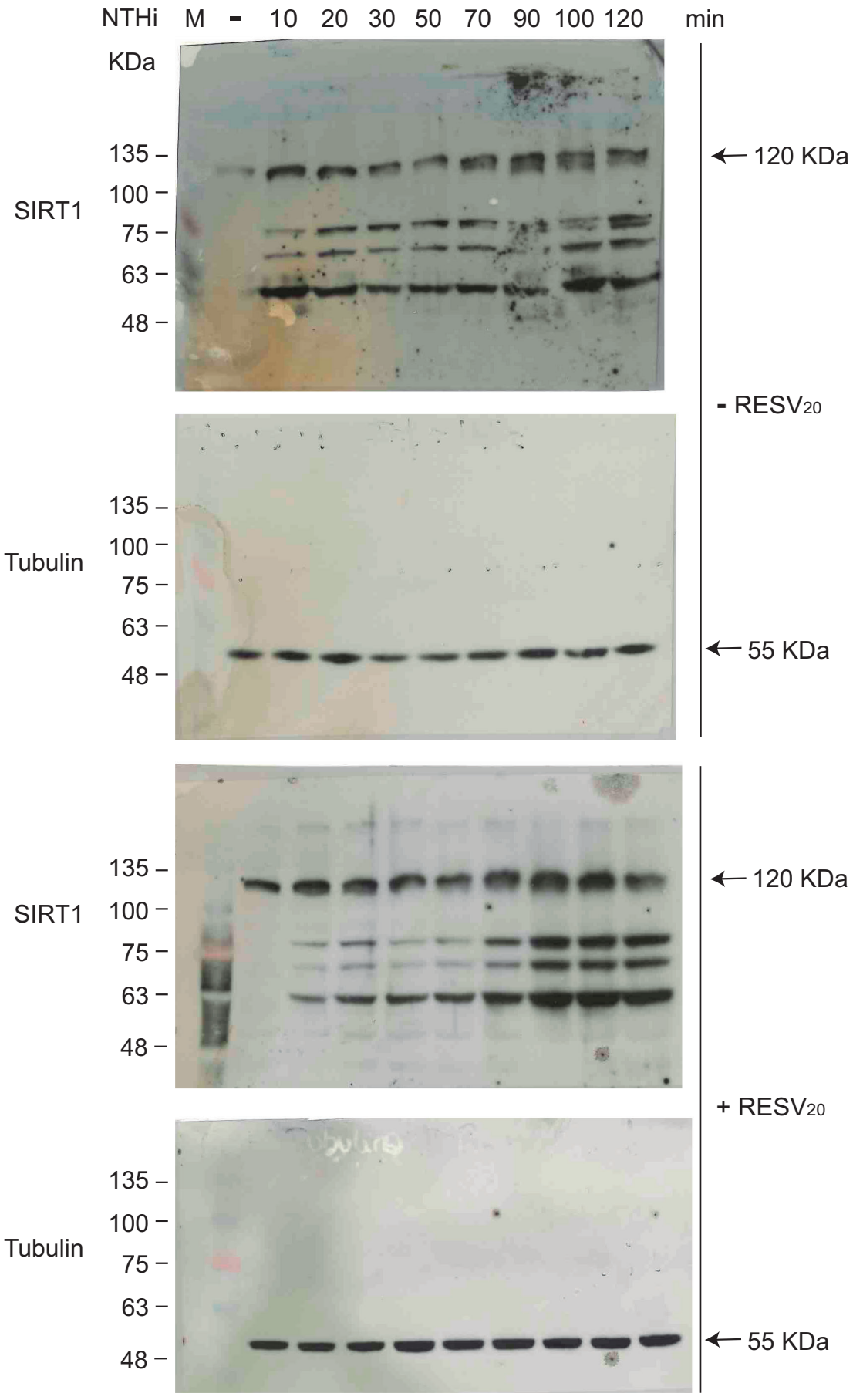
NTHi M - 10 20 30 50 70 90 100 120 min
KDa
135 –
100 –
75 –
63 –
48 –
SIRT1
← 120 KDa
- RESV20
Tubulin
← 55 KDa
+ RESV20

Expanded data for Figure S2. Full length blots. Protein extracts loaded in the four blots contain samples generated in parallel in the same experiment (both infection time course and non-infected controls). Similarly, samples were processed in parallel, in terms of protein extract preparation, electrophoretic separation and blotting. Each blot was scanned by using a MP C3503 scanner (Ricoh), with a 300 dpi resolution, in color. Scanned images were processed with Adobe Photoshop CS5. Brightness and contrast controlling tools were used across each entire blot to match the color tone of the four images. Bands corresponding to SIRT1 (bands ~120 KDa) or tubulin (~55 KDa) were cropped to improve clarity and conciseness of the presentation in Fig. S1, and combined into one figure with four separate panels (Fig. S1a) by using Adobe Illustrator CS5. Please note that complete experiments were performed at least three times, and blots corresponding to a representative one are shown here. The anti-SIRT1 antibody used in these assays was a rabbit polyclonal antibody raised against amino acids 448-747 of SIRT1 of human origin (sc-15404, Santa Cruz Biotechnology). The anti-tubulin antibody (T5168, Sigma-Aldrich) used in these assays was a mouse monoclonal antibody derived from the B-5-1-2 hybridome; it recognizes an epitope located in the C-terminal end of the α-tubulin isoform.

Table S1. Primers used in this study.

Primer name	Sequence (5´-3´)	Organism	Source
IL8-F-1241	AGAGACAGCAGAGCACAC	Human	[1]
IL8-R-1242	AGTTCTTTAGCACTCCTTGG	Human	[1]
hBD2-F3-1619	TGGCTGAATTCTAACCTCTGTAATGA	Human	This study
hBD2-R3-1620	GGACATCAAGCCTTCCACCTTATA	Human	This study
PDE4B-F-1259	GAGACAAAGAGCGGGAGAGG	Human	This study
PDE4B-R-1260	GGTGGTGAGGGACTTTGAGG	Human	This study
GAPDH-F-1237	GAAGGTGAAGGTCGGAGTC	Human	[1]
GAPDH-R-1238	GAAGATGGTGATGGGATTTC	Human	[1]
KC-F-1404	GACAGACTGCTCTGATGGCA	Mouse	This study
KC-R-1405	TGCACTTCTTTTCGCACAAC	Mouse	This study
mTNFα-F-1592	AGGCACTCCCCCAAAAGATG	Mouse	This study
mTNFα-R-1593	GCTCCTCCACTTGGTGGTTT	Mouse	This study
mGAPDH-F-1430	CCCACTAACATCAAATGGGG	Mouse	[2]
mGAPDH-R-1431	CCTTCCACAATGCCAAAGTT	Mouse	[2]

References

1 Euba, B. *et al*. Genome expression profiling-based identification and administration efficacy of host-directed antimicrobial drugs against respiratory infection by nontypeable *Haemophilus influenzae*. *Antimicrob Ag Chemother* **59**, 7581-7592, doi:10.1128/AAC.01278-15 (2015).

2 Regueiro, V. *et al*. *Klebsiella pneumoniae* subverts the activation of inflammatory responses in a NOD1-dependent manner. *Cell Microbiol* **13**, 135-153, doi:10.1111/j.1462-5822.2010.01526.x (2011).

VIRULENCE
2021, VOL. 12, NO. 1, 1672–1688
https://doi.org/10.1080/21505594.2021.1937883

Taylor & Francis
Taylor & Francis Group

RESEARCH PAPER

OPEN ACCESS Check for updates

Development and multimodal characterization of an elastase-induced emphysema mouse disease model for the COPD frequent bacterial exacerbator phenotype

Irene Rodríguez-Arce[a], Xabier Morales[b,c], Mikel Ariz[b,c], Begoña Euba [a], Nahikari López-López[a], Maider Esparza[b,c], Derek W. Hood[d], José Leiva[e,f], Carlos Ortíz-de-Solórzano[e,b,c], and Junkal Garmendia [g,a]

[a]Instituto De Agrobiotecnología, CSIC (IdAB-CSIC)-Gobierno de Navarra, Mutilva, Spain; [b]Department of Solid Tumors and Biomarkers, Center for Applied Medical Research (CIMA), Laboratory of Preclinical Models and Analytical Tools, Pamplona, Spain; [c]Laboratory of Preclinical Models and Analytical Tools, Division of Solid Tumors and Biomarkers, Center for Applied Medical Research (CIMA), Pamplona, Spain; [d]Mammalian Genetics Unit, MRC Harwell Institute, Oxfordshire, UK; [e]Instituto De Investigación Sanitaria De Navarra (IdiSNA), Pamplona, Spain; [f]Servicio De Microbiología, Clínica Universidad De Navarra, Pamplona, Spain; [g]Centro De Investigación Biomédica En Red De Enfermedades Respiratorias (CIBERES), Madrid, Spain

ABSTRACT

Chronic obstructive pulmonary disease (COPD) patients undergo infectious exacerbations whose frequency identifies a clinically meaningful phenotype. Mouse models have been mostly used to separately study both COPD and the infectious processes, but a reliable model of the COPD frequent exacerbator phenotype is still lacking. Accordingly, we first established a model of single bacterial exacerbation by nontypeable *Haemophilus influenzae* (NTHi) infection on mice with emphysema-like lesions. We characterized this single exacerbation model combining both non-invasive *in vivo* imaging and *ex vivo* techniques, obtaining longitudinal information about bacterial load and the extent of the developing lesions and host responses. Bacterial load disappeared 48 hours post-infection (hpi). However, lung recovery, measured using tests of pulmonary function and the disappearance of lung inflammation as revealed by micro-computed X-ray tomography, was delayed until 3 weeks post-infection (wpi). Then, to emulate the frequent exacerbator phenotype, we performed two recurrent episodes of NTHi infection on the emphysematous murine lung. Consistent with the amplified infectious insult, bacterial load reduction was now observed 96 hpi, and lung function recovery and disappearance of lesions on anatomical lung images did not happen until 12 wpi. Finally, as a proof of principle of the use of the model, we showed that azithromycin successfully cleared the recurrent infection, confirming this macrolide utility to ameliorate infectious exacerbation. In conclusion, we present a mouse model of recurrent bacterial infection of the emphysematous lung, aimed to facilitate investigating the COPD frequent exacerbator phenotype by providing complementary, dynamic information of both infectious and inflammatory processes.

ARTICLE HISTORY
Received 14 December 2020
Revised 20 May 2021
Accepted 30 May 2021

KEYWORDS
Lung emphysema; bacterial exacerbation; inflammation; test of pulmonary function; micro-CT

Introduction

Chronic obstructive pulmonary disease (COPD) is a clinical syndrome characterized by chronic respiratory symptoms, structural pulmonary abnormalities (airway disease, emphysema, or both), lung function impairment (poorly reversible airflow limitation), or any combination of these [1]. COPD patients undergo episodes of acute deterioration in respiratory health termed exacerbations, described as the acute worsening of respiratory symptoms associated with a variable degree of physiological deterioration. Exacerbations are associated with increased systemic and airway inflammation, worsening of lung function (according to post-bronchodilator FEV1), greater impairment in health status (quality of life), and increased white-cell count [2,3]. Most exacerbations have an infectious origin and are triggered by respiratory bacterial and viral infections. Approximately one half of these infectious exacerbations are triggered by bacteria, whereas the other half is triggered by viral infections [4]. In particular, bacterial exacerbations are characterized by increased dyspnea and sputum production, and by changes in the sputum color [5]. *Haemophilus influenzae*, in its nontypeable (NTHi) form, is one of the most common bacterial species isolated from respiratory

CONTACT Junkal Garmendia juncal.garmendia@csic.es Instituto de Agrobiotecnología, CSIC-Gobierno de Navarra, 31192 Mutilva, Navarra, Spain; Carlos Ortiz de Solórzano codesolorzano@unav.es Laboratory of Preclinical Models and Analytical Tools, Division of Solid Tumors and Biomarkers, Center for Applied Medical Research, Pamplona, Spain
Supplemental data for this article can be accessed here

samples in COPD exacerbations [6–11]. One clinically meaningful COPD phenotype is termed frequent exacerbator, characterized by the occurrence of two or more exacerbations per year [1,2,12]. Frequent exacerbations lead to increased risk of depressive symptoms, decline in lung function, poorer quality of life, decreased physical activity, increased health-care utilization, and up to a threefold increase in mortality [12].

Animal models allow investigating the pathobiology of a disease, to anticipate the value of biological markers, and can be used as platforms for in-depth analysis of possible therapeutic intervention of pathways involved in the disease. As long-term exposure to cigarette smoke is a main risk for COPD, cigarette smoke murine models have been used on their own or combined with inactivated NTHi bacteria, to study the disease [13–15]. However, the complexity of these models, and the difficulty to faithfully reproduce the heterogeneity of COPD, has shifted the focus of animal models toward one of its hallmarks, parenchymal lung tissue destruction by neutrophil-produced elastase, resulting in pulmonary fibrin deposition and decreased lung volume. Indeed, mice treated with elastase exhibit lung damage consistent with several COPD features, including parenchymal collapse, enlargement of airspaces, and fibrotic deposits within the lung alveolar spaces [16]. The clinical relevance of infectious COPD exacerbations has also promoted the use of animal models of bacterial (NTHi, *Streptococcus pneumoniae, Staphylococcus aureus*) or viral (flu virus) infection-induced exacerbations, showing that infections increase inflammation, remodeling, and emphysema, and that COPD increases susceptibility to respiratory infection [17]. Regarding NTHi, pulmonary infection in cigarette smoke-exposed or emphysematous mice, and in emphysematous hamsters [16,18–22] has been reported. However, despite its relevance, animal models resembling features of the COPD frequent exacerbator phenotype are currently lacking. Here, we report the development and longitudinal, multimodal characterization of a disease model based on recurrent NTHi pulmonary infection of a murine emphysematous lung, which could be of use to obtain novel insights on the COPD frequent exacerbator phenotype and its response to therapies.

Microbial load quantification by colony-forming units (CFU) count after tissue homogenization and serial dilution plating, and microscopic observation of infected tissue sections, are the gold standard techniques used to evaluate infections in small animal models [23]. Based on our prior experience quantifying lung damage in an elastase-induced mouse model of emphysema [24–27], here we put forward the notion that modeling bacterial exacerbations will also benefit from the use of noninvasive *in vivo* techniques to study the dynamic process of infection, thus obtaining longitudinal, correlative information about the extent of both lung damage and microbial load. This involves a multimodal approach that combines pulmonary function tests (PFT) to quantify alterations of the pulmonary physiology, with noninvasive micro-computed X-ray tomography (micro-CT), for the longitudinal visualization and quantification of imaging-derived biomarkers such as the lung tissue volume, low-density areas typical of emphysema, or ground-glass opacity regions associated to inflammation [23,28]. In summary, we present a multimodal, longitudinal characterization of the bacterial dynamics and host responses to emphysema lung infection by NTHi when occurring in an acute or repeated manner, and show its utility for antimicrobial efficacy testing.

Methods and materials

Animal handling

The assays performed are described next and the Methods used in each assay are detailed in the Supplementary Material.

A. NTHi infection conditions (pilot assay). Eighty-four CD1 female mice were randomly divided into four groups: (i) intranasally infected with stationary grown NTHi RdKW20; (ii) intranasally infected with stationary grown NTHi Xen21; (iii) intranasally infected with exponentially grown Xen21; (iv) oropharyngeally infected with exponentially grown Xen21. Mice in each group (n = 7) were sampled 12, 24, and 30 hours post-infection (hpi) and underwent lung processing for CFU counts.

B. NTHi infection in an emphysematous background to model COPD bacterial exacerbation. Two assays were performed. In the first one, aimed at determining the baseline effect of the emphysematous background in the bacterial load, 94 CD1 female mice were divided into four groups: (i) mice instilled with a vehicle solution (V+/I-); (ii) mice instilled with a vehicle solution, NTHi infected (V+/I+); (iii) mice with lung emphysema (E+/I-); (iv) mice with lung emphysema, NTHi infected (E+/I+). Mice in each group (V+/I- and E+/I-, n = 5; V+/I+ and E+/I+, n = 5) were sampled 6, 12, 24, 30, and 48 hpi, and 1 week post-infection (wpi). In detail, V+/I+ and E+/I + groups were sampled 6, 12, 24, 30, and 48 hpi and underwent lung processing for CFU counts; mice from all groups were sampled for gene expression and histopathology analyses 24 and 48 hpi, and 1 wpi. In

the second assay, aimed at complementing the *ex vivo* made measurements with *in vivo* longitudinal evaluation of pulmonary function and radiological status, 50 CD1 female mice were divided into five groups: (i) healthy control mice (CON); (ii) mice instilled with a vehicle solution (V+/I-); (iii) mice with lung emphysema (E+/I-), and NTHi infected groups as those in the first assay, (iv) V+/I+ and (v) E+/I+. Mice in each group (n = 10) were sampled as follows: (i) 24 and 48 hpi, 1, 2, and 3 wpi, all animals underwent PFT, and at least 3 mice per group underwent micro-CT imaging; (ii) 1, 3, 6, 9, 12, and 24 hpi, bioluminescence was measured.

C. NTHi recurrent infection in an emphysematous background to model COPD frequent exacerbation. Three separate assays were performed. In all three assays, the infected groups were infected twice (I2+). The first infection was performed 17 days (d) after vehicle solution or elastase administration; re-infection was performed 24 d after vehicle solution or elastase administration. In the first assay, aimed at determining the baseline effect of the emphysematous background in bacterial load after recurrent infection, 56 CD1 female mice were randomly divided into two groups: (i) V+/I2+; (ii) E+/I2+. In the second assay, aimed at completing the measurements of bacterial load in the frequent exacerbation phenotype with *in vivo* evaluation of pulmonary function and the radiological status, 28 CD1 female mice were randomly divided into four groups: (i) V+/I2-; (ii) E+/I2-; (iii) V+/I2+; (iv) E+/I2+. In the third assay, aimed at determining the clearing effect of azithromycin dehydrate (AZM) treatment in mice after recurrent infection, 84 CD1 female mice were randomly divided into four groups: (i) mice instilled with a vehicle solution, NTHi infected, and treated with water, vehicle solution where the macrolide dissolves (V+/I2+); (ii) mice instilled with a vehicle solution, NTHi infected, and treated with AZM (V+/I2+/AZM); (iii) mice with lung emphysema, NTHi infected, and water treated (E+/I2+); (iv) mice with lung emphysema, NTHi infected, and AZM treated (E+/I2+/AZM). In this first assay, mice in each group (n = 7) were sampled 24, 48, 72, and 96 h post re-infection, underwent lung processing for CFU counts, and samples were also collected for histopathology analyses. In the second assay, mice in each group (n = 7) underwent PFTs 24 and 48 h, and 1, 2, 3, 6, 9, and 12 weeks post re-infection, and at least two animals per group underwent micro-CT thoracic imaging. In the third assay, mice in each group (n = 7) were sampled 24, 30, and 36 h post re-infection and underwent lung processing for CFU counts.

Results

Multimodal dynamic analysis of a model of COPD exacerbation by bacterial infection in a murine emphysematous lung

The protocol used for the generation and longitudinal analysis of a mouse model of infectious exacerbation (E+/I+) is presented in Figure 1a that shows all the assays performed and sampling time points. We next describe the E+/I+ model and its controls, i.e. the emphysema only (E+/I-) and respiratory infection only (V+/I+) models.

Emphysema model (E+/I-)

To elicit pulmonary damage consistent with emphysema, mice were treated with pancreatic porcine elastase (PPE) delivered via nonsurgical oropharyngeal instillation. As previously reported [18,24], emphysema-like patho-physiological features were confirmed 17 d after elastase instillation, while vehicle-treated mice (V+/I-) displayed pulmonary function parameters similar to those of control mice with normal lung function (CON). Specifically, elastase-treated mice (E+/I-) showed significant decrease in resistance (R) and elastance (E), and increased compliance (C) at all time points tested (**Figure S1A-C**). Similarly, the complex, broadband-forced oscillation model revealed significantly lower airways (Rn) as well as parenchymal resistance (G), reduced tissue elasticity (H), and a significant increase in tissue resistance to airflow deformation (inertance, I) compared to vehicle-treated (V+/I-) and control (CON) mice, at all times tested (**Figure S1D-G**). These values confirm an abnormal distension of alveolar lung parenchyma and the lung airway walls during tidal breathing, as well as impaired elastic recoil of the parenchyma. Altogether, they suggest that the instillation of elastase elicits a reduction in airflow resistance, caused both by pathological changes in the central airways and lung tissue, consistent with elastolytic parenchymal degradation and airway remodeling. Furthermore, visual analysis of micro-CT image scans revealed lower X-ray density, and swollen lungs in E+/I- animals compared to the V+/I- and CON groups (**Figure S1H-I**). These observations were further confirmed by automatic quantification of the micro-CT scans. Indeed, quantified lung volumes were significantly higher in E+/I- compared to V+/I- and CON animals (**Figure S1J**). Moreover, lung volumes in E+/I- mice increased over time contrasting with the flat, constant trend measured in both V+/I- and CON groups. Regarding the extent of emphysema, measured as the percentage of lung voxels below −900 Hounsfield units (RVB −900 HU) [24], the obtained values were

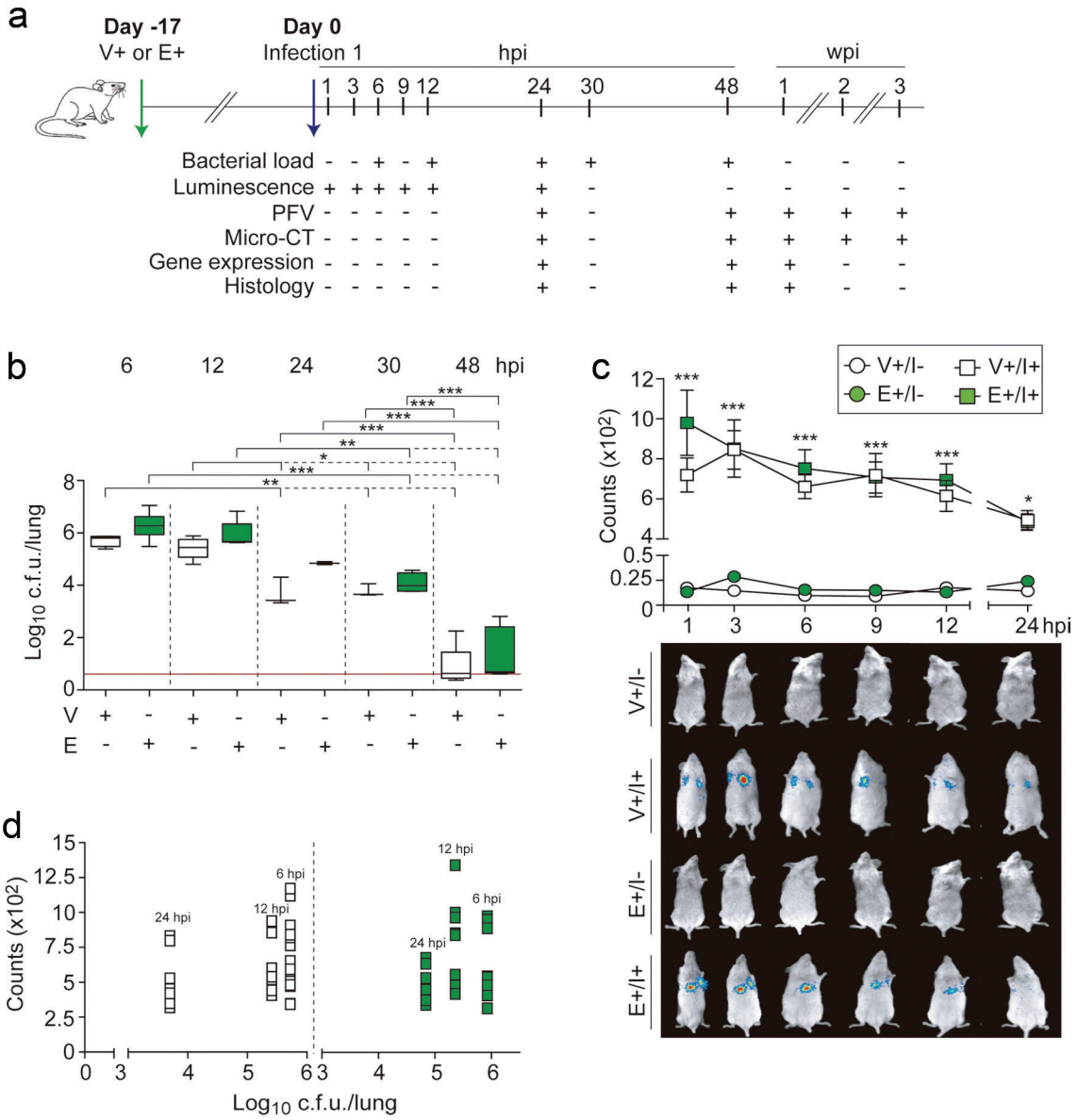

Figure 1. A mouse model of lung emphysematous infection: experimental design and characterization. (a) Experimental design: lung emphysema was induced by oropharyngeal instillation of PPE in CD1 mice (Day −17). Elastase instillation induces pulmonary damage compatible with emphysema-like lesions. Mice were instilled with PPE (E+/I-) or received physiological saline solution (V+/I-). Animals were infected with ~10^8 CFU/mouse of *H. influenzae* Xen21 (Day 0), V+/I+ and E+/I+ groups. Assay types and sampling time points are indicated. (b) Longitudinal analysis of lung bacterial loads. Mice were infected as indicated in (a), euthanized 6, 12, 24, 30 and 48 hpi, and bacterial loads quantified in homogenized lungs. No significant differences were observed between V+/I+ (white) and E+/I+ (green) groups at any of the indicated time points. V+/I+ groups: bacterial counts were lower 24, 30 and 48- than 6 hpi ($p < 0.005$); bacterial counts were lower 24, 30 and 48- than 12 hpi ($p < 0.05$); bacterial counts were lower 48- than 24 and 30 hpi ($p < 0.0001$). E+/I+ animals: bacterial counts were lower 30 and 48- than 6 hpi ($p < 0.0001$); bacterial counts were lower 30 and 48- than 12 hpi ($p < 0.005$); bacterial counts were lower 48- than 24 and 30 hpi ($p < 0.0001$). Results are reported as $\log_{10}$ CFU/lung and represented as box plot graphs (lines inside boxes represent median values). Statistical comparisons were performed using one-way ANOVA and Tukey's multiple comparison test. *** $p < 0.001$; ** $p < 0.01$; * $p < 0.05$. (c) Bacterial bioluminescence was determined 1, 3, 6, 9, 12 and 24 hpi, representative animals are shown (bottom panel). Results are shown as mean ± SEM. Statistical comparisons were performed using one-way ANOVA and Tukey's multiple comparison test. *** $p < 0.001$; * $p < 0.05$. (d) *H. influenzae* Xen21 light levels and bacterial numbers *in vivo*. Bacterial counts and animal luminescence determined at different time points post-inoculation (6, 12 and 24 h). Spearman's correlation coefficient was determined.

significantly higher in E+/I- compared to V+/I- and CON mice, suggesting the prevalence of low X-ray density areas, consistent with emphysema-like lesions (**Figure S1K**). Accordingly, Mean Lung Voxel Intensity (MLVI) values, that describe the average intensity of the lung in HU, and are expected to be lower in emphysematous compared to healthy lungs, were lower in E+/I- than in V+/I- and CON mice (**Figure S1L**). These results are clearly reflected in the 3D volume renders shown in **Figures S1M, 3e,** and **3jJ**.

Histological images of lung sections were also analyzed 24 d after elastase instillation, to measure the main histopathological descriptors of emphysema (i.e. the alveolar space, measured through the mean linear intercept (MLI), a weighted mean measure of alveolar size (D2), and the ratio of alveolar space with respect to the whole lung tissue ($R_{alv/tissue}$)). The five lung lobes were quantified independently. All three parameters were significantly higher in E+/I- than in V+/I-, confirming the presence of emphysema. No significant differences were found between lobes, meaning that the presence of emphysema was homogeneous across the lung (**Figure S2)**. Caspase-3 staining on these same lungs revealed a clear, though not statistically significant increase in apoptotic cell density (Caspase-3^+/mm^2 ($p > 0.075$) in mice treated with elastase (E+/I-) compared to control (V+/I-) mice (**Figure S3**). These results suggest that elastase treatment elicits the apoptosis of alveolar cells. This is consistent with the parenchymal destruction and airspace enlargement observed in IHC by H&E sections (**Figure S2**), and the low lung X-ray density observed in the micro-CT images (**Figure S1I-L**).

Furthermore, matrix metalloproteinases (MMPs), which are crucial for extracellular matrix remodeling following tissue damage, and are elevated in sputum, bronchoalveolar lavage, and lung tissue specimens from animals and patients with COPD [29,30], were quantified in our models. Notably, the expression of the *mmp-2* and *mmp-12* genes in emphysematous (E+/I-) lungs was higher than in control (V+/I-) uninfected lung tissue (**Figure S4C-D**).

Altogether, these findings demonstrate degradation of the alveolar walls and enlargement of the airspace induced by elastase activity, which strongly agrees with the physiological parameters detected by PFT.

Respiratory infection model (V+/I+)

The *H. influenzae* RdKW20 strain has been previously used in mouse models of lung infection [31,32]. Both RdKW20 and Xen21 (RdKW20 derivative with a *luxCDABE* insert [33]) strains showed similar growth dynamics, while Xen21 bioluminescence accurately reflected the measured bacterial numbers (**Figure S5A**). Likewise, RdKW20 and Xen21 lung bacterial counts were comparable upon CD1 mice intranasal infection, supporting our use of Xen21 for subsequent experiments (**Figure S5B**). Lung infection with similar inocula of exponential or stationary phase grown Xen21 bacteria rendered comparable results, although lower variability was observed in the counts obtained when using exponentially grown bacteria (**Figure S5C**). Finally, we compared lung bacterial loads after intranasal or oropharyngeal administration, obtaining similar results. However, the bioluminescent signal detected in the lungs of oropharyngeally infected mice was higher than the one obtained in the lungs of intranasally infected animals (**Figure S5D**). Together, these results supported our use of oropharyngeal administration of the exponentially grown *H. influenzae* strain Xen21 to generate a mouse model of lung infection.

Bacterial loads were quantified in V+/I+ lungs. Bacterial counts remained comparable 6 and 12 hpi (~10^6 CFU/lung), decreased reaching a second plateau between 24 and 30 hpi (~10^4 CFU/lung), and became barely detectable 48 hpi (Figure 1b). In parallel, we used bacterial bioluminescence for real-time noninvasive detection of NTHi dynamics *in vivo*. Here, the lungs of infected mice were found to emit low bioluminescent signals (6–10 × 10^2 photonic counts), decreasing with time as expected (Figure 1c). However, no significant correlation coefficients (Spearman r = 1 in V+/I+ mice) were found between photon counts and bacterial loads at the sampled times (Figure 1d). Furthermore, isolated lung lobes of the same mice exhibited also low bioluminescence signals (data not shown), altogether suggesting that bioluminescence emission was not a good indicator of NTHi pulmonary infection in this model.

The dynamics of pulmonary infection by *H. influenzae* were also examined by PFT and micro-CT. During the first 48 hpi, PFT values obtained by single-frequency-forced oscillation revealed that V+/I+ lungs display higher resistance (R) and elastance (E) and lower compliance (C), compared to non-infected V+/I- and CON mice. However, these differences disappear 1 week after infection, consistent with the remission of the effects of the infection (Figure 2a-c). Similarly, PFT values obtained using a broadband-forced maneuver revealed a significant decrease in tissue inertance (I), compared to non-infected mice during the first 48 h, suggesting an increment of parenchymal rigidity. On the contrary, tissue elasticity (H) displayed significantly higher values during the first 48 h compared to non-infected mice. Likewise, airways (Rn) and parenchymal (G) resistance were also higher in V+/I+ compared to V+/I- and CON mice 24 and 48 hpi, consistent with the higher stiffness of both

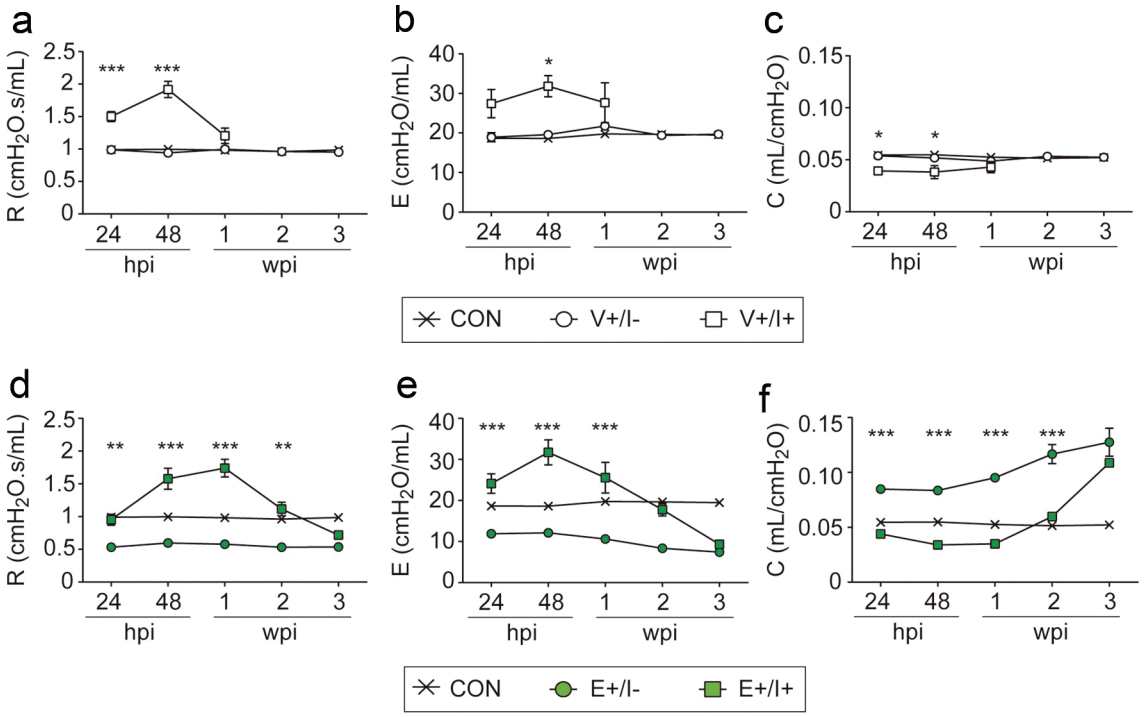

Figure 2. Pulmonary NTHi infection modifies lung physiology in the murine model. Evolution of pulmonary physiological parameters at the indicatedpost-infection time points by PFT (24 and 48 hpi; 1, 2 and 3 wpi). Mice groups: non-infected control animals with normal lung function (CON, black cross); V+/I- and E+/I-, white and green circles, respectively; V+/I+ and E+/I+, white and green squares, respectively. (a and d) Lung resistance (R, $cmH_2O.s/mL$), (b and e) elastance (E, cmH_2O/mL), (c and f) compliance (C, mL/cmH_2O), measured by the single-frequency forced oscillation maneuver. Results are shown as mean ± SEM, statistical differences were analyzed using a two-way ANOVA followed by Bonferroni´s post-hoc test. *** $p < 0.001$; ** $p < 0.01$; * $p < 0.05$.

compartments (**Figure S6**, upper panels). These results suggest altered pulmonary function as early as 24 hpi, worsening 48 hpi, when the parenchyma displays lower distention capacity and increased level of resistance, i.e. constriction in the lungs, both in the airways and alveolar areas, that recovers 1 week after infection. Visual analysis of micro-CT images reveals evident inflammatory signs 24 and 48 hpi in all lung lobes (Figure 3a). Indeed, chest scans showed densely radiopaque areas, as well as consolidated and ground-glass opacity regions, which disappear 1 week after infection. This observation was confirmed by quantification of the corresponding micro-CT images. In particular, the MLVI parameter, indicative of the parenchymal opacity compatible with the inflammatory process, increased significantly 48 hpi, as also observed in the three-dimensional reconstruction (Figure 3d-e). Finally, as expected, no significant differences in total lung volume and RVB −900 HU were detected among groups (Figure 3b-c). These results reveal parenchymal obstruction happening during the first 48 h after infection, disappearing 1 wpi, confirming the alterations in pulmonary physiology detected by PFT.

For completion, inflammation was also analyzed at the molecular level. The expression of *kc* and *tnf-α* pro-inflammatory mediators in lung tissue of V+/I+ mice was higher 24 and 48 hpi than in non-infected V+/I- animals, and this increase was restored to basal levels 1 wpi. In contrast, the expression of the *mmp-2* and *mmp-12* genes in lung tissue of V+/I+ mice was lower at 24 and 48 hpi than in V+/I- animals, and such decrease was restored to basal levels 1 wpi (**Figure S4**). A microscopy-based score of the lower airway histopathological lesions in samples from infected mice was also quantified. No significant differences in terms of lymphocyte counts were observed between V+/I- and V+/I+ groups. In contrast, scoring of alveolar macrophages and bronchiolar recruitment of polymorphonuclear cells (PMN) showed higher numbers in V+/I+ than in V+/I- animals. PMN recruitment was higher 24 and 48 hpi, and decreased after 1 wpi (Table 1, upper panels). In summary, the inflammatory response, measured by the expression of pro-inflammatory cytokines and recruitment of PMNs and macrophages nicely correlates with the damage quantified by means of PFT and radiological measurements.

Model of COPD bacterial exacerbation by single-dose NTHi infection in emphysematous mice (E+/I+)

COPD bacterial exacerbation was elicited by oropharyngeal administration of exponentially grown

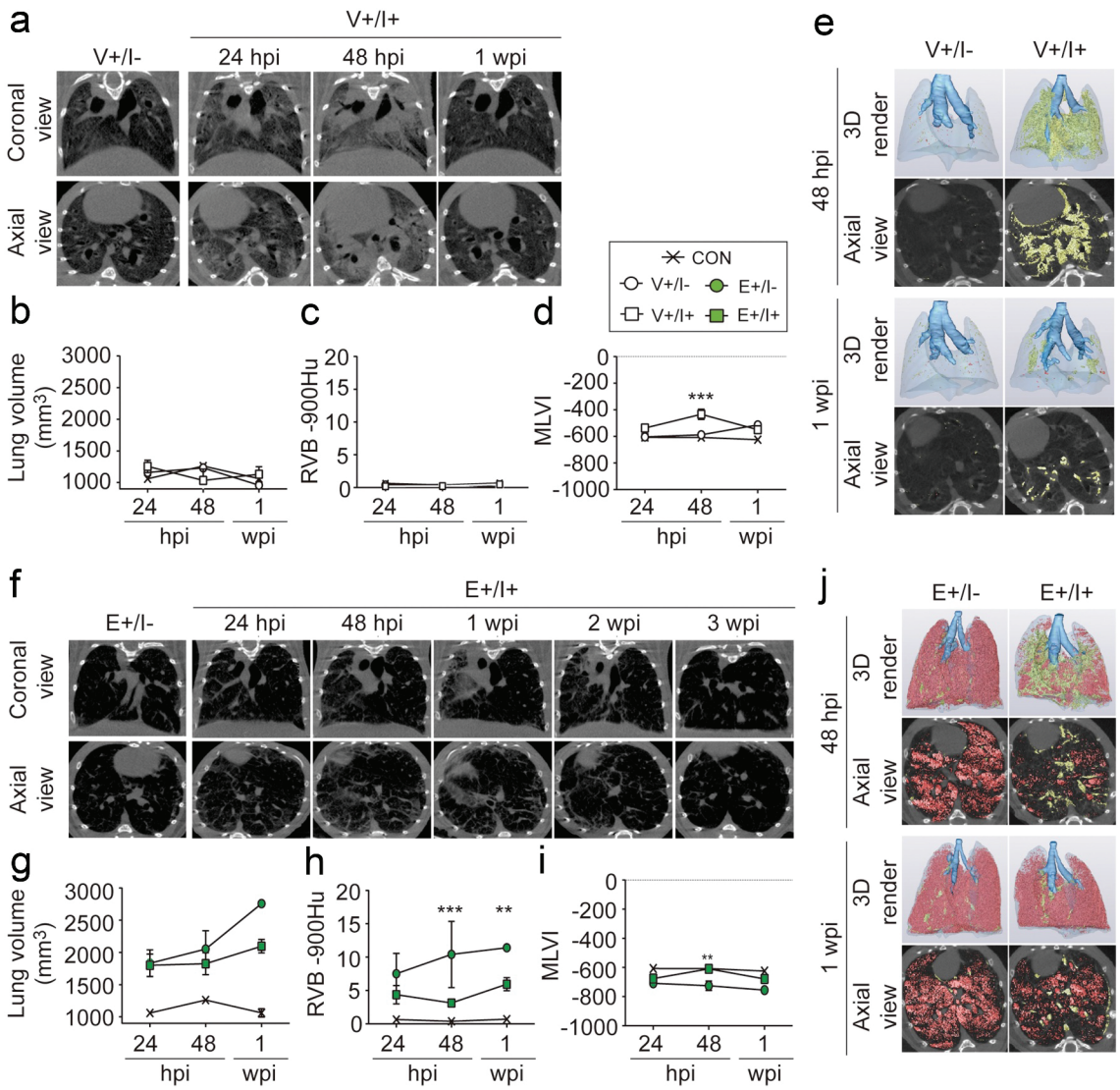

Figure 3. Pulmonary NTHi infection induces lung inflammation in the murine model. (a and f) Representative micro-CT images in the longitudinal section (upper row) and cross-section (bottom row) acquired from the chest of the V+/I- and V+/I+ (a), and E+/I- and E+/I+ (f) mice, at the indicated time points. Evolution of the image parameters calculated from the micro-CT scans at the indicated time points (number of images, n ≥ 3). Mice groups: non-infected control animals with normal lung function (CON, black cross); V+/I- and E+/I-, white and green circles, respectively; V+/I+ and E+/I+, white and green squares, respectively. (b and g) Total lung volume (mm^3). (c and h) Relative lung volume below −900 HU (RVB −900 HU). (d and i) Mean lung voxel intensity (MLVI). (e) Representative rendered views, and 2D axial micro-CT slices of a lung from V+/I- and V+/I+ models, 48 hpi and 1 wpi. Yellow areas indicate hyperintense regions corresponding with infection. (f) Representative 3D rendered views, and 2D axial micro-CT slices of a lung from E+/I- and E+/I+ models, 48 hpi and 1 wpi. Yellow areas indicate hyperintense regions corresponding with infection. Red areas indicate areas of low X-ray absorption corresponding with emphysema. In (e) and (j), lung reconstructions show the main airways in solid blue, the lungs in transparent blue, the low-density areas in red (RVB −900 HU), and the high-density areas in yellow (RV −30/-150 HU). Axial micro-CT slices show RVB −900 HU and RV −30/-150 HU parameters merged on the radiographic image. Results are shown as mean ± SEM, statistical differences were analyzed using a two-way ANOVA followed by Bonferroni´s post-hoc test. *** $p < 0.001$; ** $p < 0.01$; * $p < 0.05$.

H. influenzae strain Xen21 in emphysematous mice. As observed in V+/I+ animals, bacterial counts remained comparable 6 and 12 hpi (~10^6 CFU/lung), decreased reaching a second plateau between 24 and 30 hpi (~10^4 CFU/lung), and became barely detectable 48 hpi. Even if the trend was similar, bacterial counts were consistently higher in E+/I+ than in V+/I+ groups (Figure 1b). As indicated, the lungs of infected mice were found to emit very low bioluminescent signals (Figure 1c), resulting in no significant correlation coefficients (Spearman r = 0.5000 in E+/I+ mice) between photon counts and bacterial loads (Figure 1d).

PFT values obtained by single-frequency-forced oscillation revealed lower compliance (C) and higher

Table 1. Score of histopathology lesions found in the airways of V+ or E+ administered mice, infected with the strain *H. influenzae* Xen21.

		Score (mean ± SD)[a]			
		hpi	Bronchioli PMNs[b]	Alveolar macrophages	Lymphocytes
	V+/I-	-	0.2 ± 0.27	0	0
	E+/I-	-	0.4 ± 0.25	0.5	0
Single infection	**V+/I+**	**24**	[f]1.8 ± 0.5	[c]1 ± 0.3	0
		48	[f]2.5 ± 0.4	[c]1.5	0.1 ± 0.4
		168 (1 week)	[f]1.1 ± 0.75	[c]1.3 ± 0.28	0
	E+/I+	**24**	[f]1.9 ± 0.5	[c,d]1.4 ± 0.2	0
		48	[f,i]2.1 ± 0.4	[c]1.4 ± 0.2	0.4 ± 0.5
		168 (1 week)	[g]0.4 ± 0.39	[c]1.1 ± 0.41	0.4 ± 0.52
Recurrent infection	**V+/I2+**	**24**	1.25 ± 0.29	[e]1.38 ± 0.48	0.13 ± 0.25
		48	1.63 ± 0.85	[e]1.38 ± 0.48	0.38 ± 0.48
		72	0.75 ± 0.65	[e]2 ± 0.71	[h]1 ± 0.41
		96	0.5 ± 0.7	[e]2.25 ± 0.35	[h]1.5
	E+/I2+	**24**	1 ± 0.84	[e]1.42 ± 0.58	0.33 ± 0.26
		48	0.25 ± 0.86	[e]2 ± 0.74	[h]0.75 ± 0.27
		72	0.25 ± 0.29	1.25 ± 0.65	[h]0.88 ± 0.25
		96	0.17 ± 0.41	[e]1.30 ± 0.67	[h]1.33 ± 0.41

[a]Statistical comparisons of mean values were performed using two-way ANOVA followed by Tukey's multiple-comparison test.
[b]PMNs: infiltrates of polymorphonuclear cells.
[c]Single infection: Higher proportion of alveolar macrophages in infected- than in non-infected mice, compared to their respective non-infected controls ($p<0.001$).
[d]Single infection: Higher proportion of alveolar macrophages in E+/I+ than in V+/I+ mice, 24 hpi ($p<0.05$).
[e]Recurrent infection: Higher proportion of alveolar macrophages in infected- than in non-infected mice, compared to their respective non-infected controls ($p<0.05$).
[f]Single infection: Higher proportion of PMNs in infected- than in non-infected mice, compared to their respective non-infected controls ($p<0.0001$).
[g]Single infection: Lower proportion of PMNs in E+/I+ than in V+/I+ mice, 1 wpi ($p<0.0005$).

resistance (R) and elastance (E) in E+/I+ mice compared to their non-infected controls. This is similar to what was observed in V+/I+ mice. Strikingly however, in E+/I+ animals, pulmonary dysfunction remained until 3 weeks post-infection (Figure 2d-f). Similarly, PFT values obtained using a broadband-forced maneuver showed a significant increase in tissue elasticity (H), as well as in parenchymal (G) and airway resistance (Rn), and significantly lower inertance (I) values in E+/I+ compared to E+/I- mice, during the first 2 weeks post-infection, and a return to baseline levels 3 wpi (**Figure S6**, lower panels). Altogether, these results clearly point to higher rigidity of both lung parenchyma and central airways, exacerbated due to the emphysematous background, since the measured increment in all physiology parameters, relative to their respective controls, was higher in E+/I+ than in V+/I+ mice (**Figure S6**). Indeed, the peak of parenchymal inflammation in E+/I+ mice, measured from most PFT parameters, raised relative to its control (E+/I-) levels, and was shifted from 48 hpi to 1 wpi, while the recovery of the PFT parameters back to the level of the emphysematous non-infected E+/I- background levels was delayed 2 weeks. Thus, from the standpoint of lung function, the existence of an emphysematous background exacerbates the intensity and duration of the effects of the NTHi infection.

Consistent with the PFT measurements, visual analysis of micro-CT images revealed higher X-ray density areas in E+/I+ lungs 48 hpi compared to E+/I- mice. This increment became more evident 1 wpi, while full recovery of E+/I+ lungs also occurred 3 weeks after NTHi infection (figure 3f). Despite this, radiological signs of inflammation were less well defined in E+/I+ than in V+/I+ mice, maybe due to preexisting alveolar wall degradation caused by elastase activity that reduces bacterial target cell types or tissues. Quantitative analysis of E+/I+ lungs revealed significant differences in the MLVI index compared to E+/I- mice, 48 h after infection (Figure 3i), and significantly lower RVB −900 HU values were detected 48 hpi and 1 wpi, consistent with the described inflammatory peak (Figure 3h). These results are clearly reflected in the 3D renders shown in Figure 3j. Bearing these findings in mind, NTHi infection modifies lung physiology and induces parenchymal inflammation regardless of lung status. However, the inflammatory process is longer and more acute in the emphysematous-like background. For completion, expression of *kc* and *tnf-α* pro-inflammatory genes in lung tissue of E+/I+ mice

was higher 24 and 48 hpi than in E+/I- animals, and such increase was restored to basal levels 1 wpi. In addition, expression of the *mmp-2* and *mmp-12* genes in lung tissue of E+/I+ mice was lower at 24 and 48 hpi than in E+/I- animals (**Figure S4**).

The extent of emphysema in histological images of infected lung sections was also analyzed using the MLI, D2, and $R_{alv/tissue}$ descriptors. All three parameters were higher in E+/I+ than in V+/I+, confirming a clear enlargement of alveolar spaces and, thus, the presence of emphysema (**Figure S2**). No significant differences were found between lobes, showing a homogeneous extent of emphysema across the lung. Caspase-3 staining showed significant increase in apoptotic cell density (Caspase-$3^+/mm^2$) 24 d after elastase treatment in E+/I+ mice compared to the V+/I+ group (**Figure S3**), pointing to a higher apoptosis rate within the lung parenchyma of animals instilled both with elastase and NTHi.

Conversely, no significant differences in terms of lymphocyte counts were observed between E+/I- and E+/I+ groups. Contrarily, scoring of alveolar macrophages and bronchiolar recruitment of PMNs showed higher numbers in E+/I+ than in E+/I- animals, and scores of PMNs recruitment were higher 24 and 48 hpi, and decreased after 1 wpi. Furthermore, we observed higher alveolar macrophage scoring 24 hpi and lower PMN recruitment 1 wpi in those animals treated with elastase (E+/I+) compared to V+/I+ mice (Table 1, upper panels).

Summarizing, these results suggest an increased infectious response caused by NTHi in mice undergoing emphysema lesions promoted by altered expression of pro-inflammatory cytokines and the consequent infiltration of cells with inflammatory activity (macrophages and PMN), which seem to cause longer persistence of parenchymal lesions detected by X-ray imaging, as well as alteration of physiological lung parameters in the E+/I+ animals compared to V+/I+ ones.

Modeling the COPD frequent exacerbator phenotype by NTHi recurrent infection in emphysematous mouse lung

We next reasoned that recurrent NTHi infections in a background of lung emphysema might faithfully recapitulate features of the COPD frequent exacerbator phenotype. The generation of this model (E+/I2+) and its multimodal longitudinal analysis is presented in Figure 4a. We inoculated *H. influenzae* Xen21 (day −7) and allowed 1 week for the infection to clear. Then, we performed a second identical inoculation (day 0). In non-emphysematous, re-infected V+/I2+ animals, the bacterial load measured was almost undetectable 48 h after re-infection, similar to what was observed in singly infected V+/I+ animals. However, clearance after bacterial re-infection was slower in E+/I2+ mice, taking almost 96 h (Figures 4B and 1b).

The dynamics of recurrent pulmonary infection by *H. influenzae* were also examined by PFT and micro-CT. Namely, PFT values obtained by single-frequency-forced oscillation displayed lower compliance (C) and increased resistance (R) and elastance (E) during the first 6 weeks after re-infection (V+/I2+), compared to non-infected V+/I2- mice (Figure 5a). This trend was similar in those animals with an emphysematous-like background (E+/I2+), which also displayed significantly lower compliance (C) and higher resistance (R) and elastance (E) than E+/I2- mice. However, pulmonary lesions were sustained in E+/I2+ mice up to 9 weeks after re-infection, and full recovery did not occur until week 12 post re-infection (Figure 5b). Similarly, pulmonary function values obtained using a broadband-forced maneuver showed a significant increase in tissue elasticity (H), as well as in parenchymal (G) and airway resistance (Rn), and significantly lower tissue inertance (I) values in V+/I2+ and E+/I2+ mice compared to their respective non-infected groups. Functional parameters, as observed in the single-frequency-forced maneuver, displayed the same time recovery gap, i.e. 9 and 12 weeks for V+/I2+ and E+/I2+, respectively (**Figure S7**). These results highlight that recurrent NTHi infection causes chronic pulmonary lesions and delays parenchymal recovery regardless of lung status, although the recovery time needed is longer in the emphysematous lung. In this sense, micro-CT images visual analysis revealed evident higher X-ray density areas both in V+/I2+ and E+/I2+ lungs during the first week after re-infection compared to the non-infected groups, consistent with the inflammatory peak (Figure 5c-d). These densely radiopaque areas disappeared in V+/I2+ mice 9 weeks after re-infection, while they subsided in E+/I2+ mice week 12 post re-infection. Summarizing, recurrent NTHi infection elicits a synergistic effect of the pulmonary lesion and reveals circular infection dynamics that compromise lung recovery, further exacerbated by the parenchymal degradation developed in elastase-treated mice E+/I2+.

Likewise, microscopy scoring of lower airway histopathological lesions in samples from V+/I2+ and E+/I2+ groups, euthanized 24, 48, 72, and 96 h after re-infection, showed no differences in terms of PMN recruitment when comparing the V+/I2+ and E+/I2+ groups. Scoring of alveolar macrophages and lymphocytes showed higher numbers in infected than in

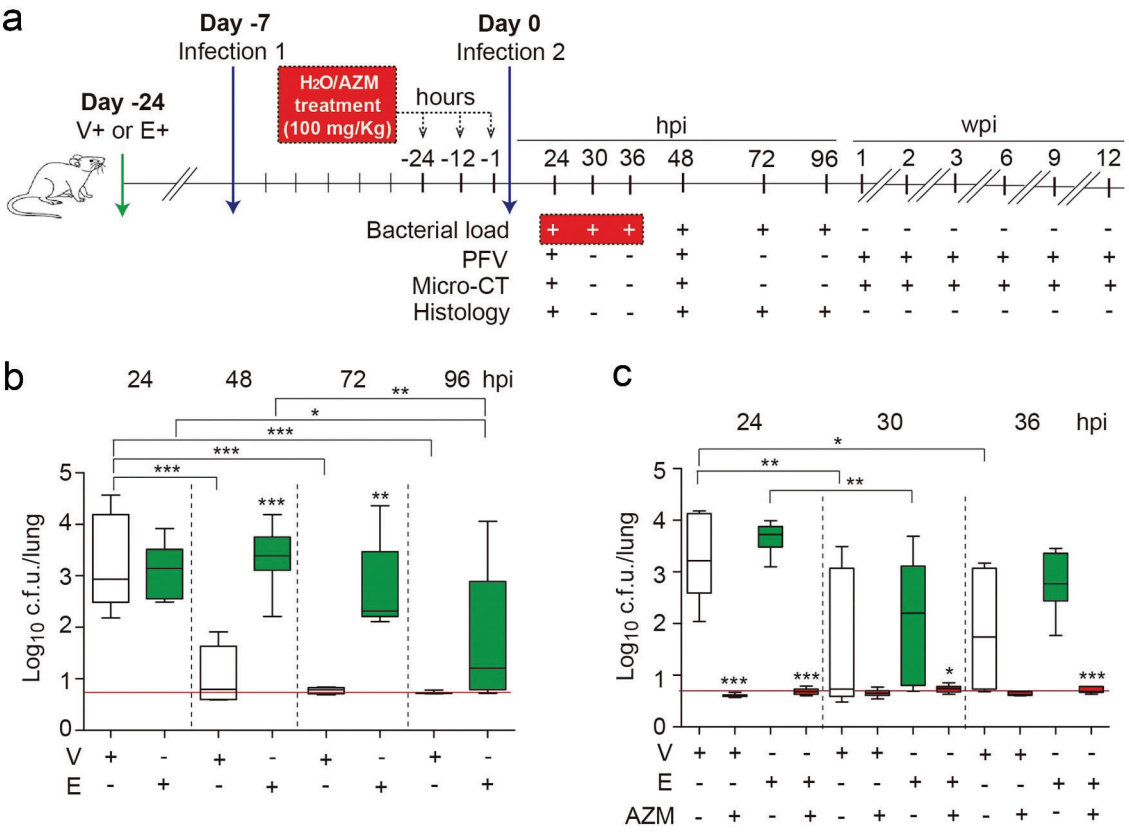

Figure 4. Emphysema mice recurrent pulmonary infection by NTHi, experimental design and analysis of lung bacterial loads. (a) Experimental design: lung emphysema was induced by oropharyngeal instillation of PPE (Day −24). Controls: animals were administered vehicle solution (V+/I-) but did not receive elastase (E+/I-). Animals were infected with ~10^8 CFU/mouse of *H. influenzae* Xen21 (Day −7, infection 1). Same animals were infected with ~10^8 CFU/mouse of *H. influenzae* Xen21 (Day 0, infection 2), V+/I2+ and E+/I2+ groups. Assay types and sampling time points are indicated. (b) Mice were infected as indicated in (a), euthanized 24, 48, 72 and 96 hpi, and bacterial loads quantified in lungs (log_{10} CFU/lung). Infection took longer to clear in emphysema mice, significant differences were observed between V+ (white) and E+ (green) mice 48 ($p < 0.0001$) and 72 ($p < 0.01$) hpi. V+/I2+ mice: bacterial counts were lower 48, 72 and 96- than 24 hpi ($p < 0.001$). E+/I2+ mice: bacterial counts were lower 96- than 24 and 48 hpi ($p < 0.05$ and $p < 0.01$, respectively). (c) Effect of AZM administration on bacterial loads in NTHi infected mice. AZM (100 mg/kg/dose) was administered oroesophageally as indicated in (a). Control animals were administered water. Bacterial counts were determined 24, 30 and 36 hpi. V+ infected animals: 24 hpi, Xen21 counts were significantly lower in V+/I2+/AZM than in V+/I2+ animals ($p < 0.0001$). Also, bacterial counts were lower 30 and 36 than 24 hpi ($p < 0.01$ and $p < 0.05$, respectively). E + infected mice: bacterial counts were lower in E+/I2+/AZM than in E+/I2+ animals 24 ($p < 0.0001$), 30 ($p < 0.05$) and 36 ($p < 0.0001$) hpi. Also, bacterial counts were lower 30 than 24 hpi ($p < 0.01$). Results are reported as log_{10} CFU/lung and represented as box plot graphs (lines inside boxes represent median values). Statistical comparisons were performed using one-way ANOVA and Tukey's multiple comparison test. *** $p < 0.001$; ** $p < 0.01$; * $p < 0.05$.

non-infected animal groups. Scoring of lymphocytes was initially low but increased over time in the same manner in both infected groups. Finally, when comparing single and recurrent infection, higher proportion of PMN was observed in E+/I+ than in E+/I2+ mice, at 48 hpi (Table 1).

In conclusion, our analysis shows that the E+/I2+ phenotype could represent a suitable model system for the COPD frequent exacerbator phenotype, as it displays a longer time for bacterial clearance, together with a synergistic effect of the infectious and emphysematous attacks that produces inflammatory lesions observed to remain in the lung until 12 weeks post re-infection.

Azithromycin clears NTHi infection in a COPD frequent exacerbator mouse model

Antibiotics are indicated in patients with severe COPD who suffer frequent exacerbations despite optimal inhaler therapy, as being beneficial by reducing hospital readmissions and frequency of acute exacerbations [34,35]. Based on its clinical interest, our model was used to assess the efficacy of AZM. The minimal inhibitory concentration (MIC) of AZM for the NTHi Xen21 strain is 4 µg/ml. We sought to determine the impact of AZM oroesophageal administration on NTHi recurrent pulmonary infection, by using a regimen

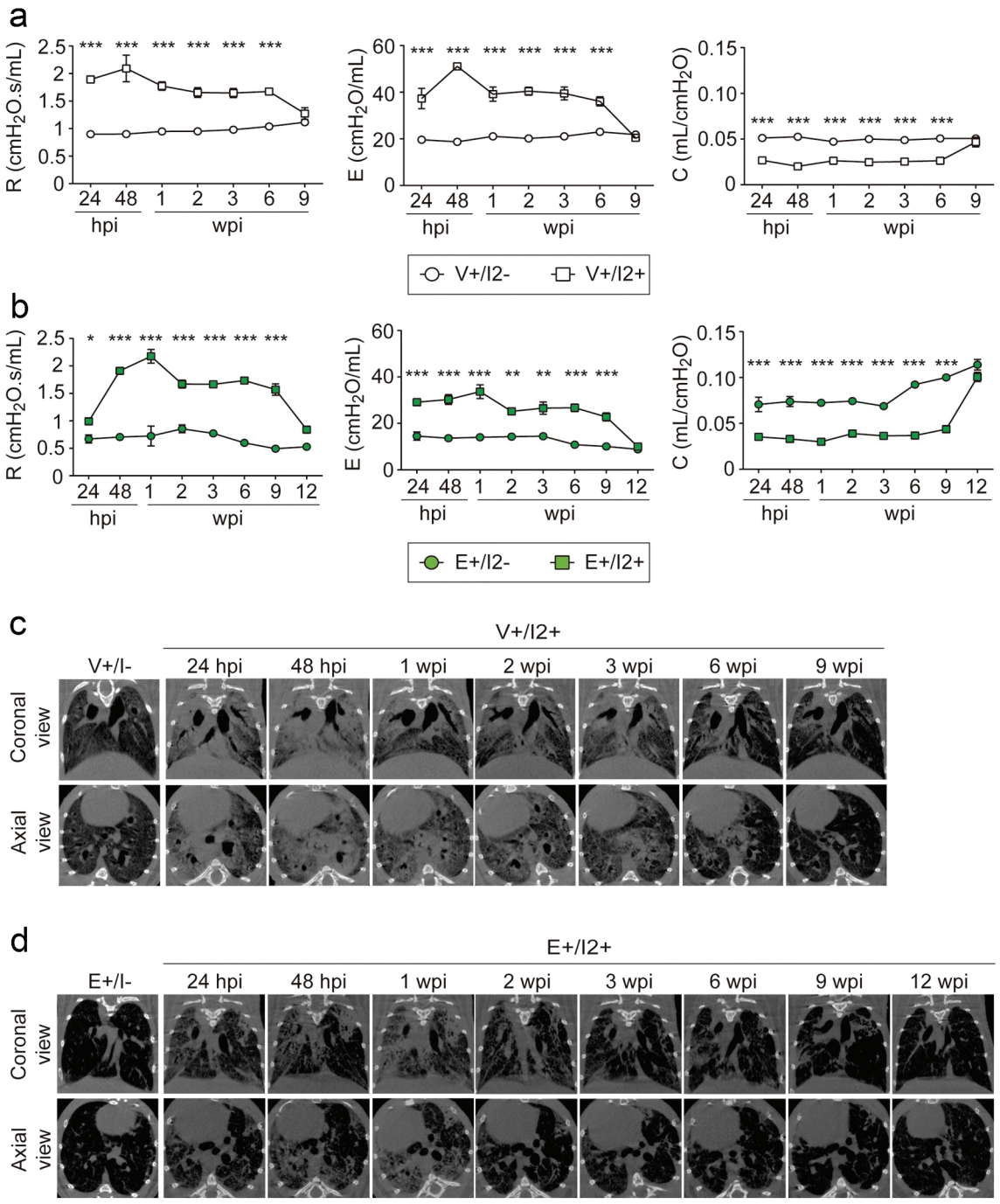

Figure 5. Recurrent NTHi infection exacerbates lung damage and renders chronic lung lesions in mice. CD1 mice were infected with NTHi Xen21 on days −7 and 0, after instillation of physiological saline solution (V+/I2+) or PPE (E+/I2+), as indicated in Figure 4a. (a-b) Evolution of physiological parameters at the indicated time points, measured in V+/I2+ and E+/I2+ mice, in comparison with their respective non-infected groups (V+/I2- and E+/I2-). Mice groups: V+/I2- and E+/I2-, white and green circles, respectively; V+/I2+ and E+/I2+, white and green squares, respectively. (a, b) Lung resistance (R, $cmH_2O.s/mL$), elastance (E, cmH_2O/mL) and compliance (C, mL/cmH_2O) measured by the single-frequency forced oscillation maneuver. (c, d) Representative micro-CT images (n = 2) in the longitudinal section (upper row) and cross-section (bottom row) acquired from the chest of the V+/I2+ and E+/I2+ mice at the indicated time points. V+/I- and E+/I- animals are shown as controls. Results are shown as mean ± SEM, statistical differences were analyzed using a two-way ANOVA followed by Bonferroni´s post-hoc test. *** $p < 0.001$; ** $p < 0.01$; * $p < 0.05$.

consisting of repeated AZM administrations (Figure 4a), by adapting a previously used approach [36]. The results indicated that this AZM treatment was effective providing clearance of NTHi infection at the three post-infection time points tested when comparing V+/I2+/AZM to V+/I2+, and E+/I2+/AZM to E+/I2+. Such clearing effect was independent of previous emphysema development (Figure 4c). AZM has dual antimicrobial and anti-inflammatory properties [37]. Histopathology score was not performed on AZM-treated groups precluding us from assessing its effect on leukocyte recruitment. Nevertheless, we quantified the expression of *kc* and *tnf-α* pro-inflammatory genes in lung tissue of E+/2I+ mice upon AZM treatment, and observed a decrease to basal levels comparable to those in uninfected animals (**Figure S8**). AZM cleared NTHi infection; therefore, the observed effect may be the outcome of both AZM immunomodulatory and antibiotic effects.

Discussion

Understanding the nature and frequency of COPD exacerbations is instrumental to identify individuals at high risk for such events, and for the delineation of specific clinical phenotypes. Four phenotypes of exacerbations have been described: bacterial, viral, inflammatory (eosinophilic), and pauci-inflammatory, being more than 50% of them of microbial nature. Bacterial exacerbations can be explained by (i) the "fall and rise" hypothesis, suggesting a primary chronic bronchial infection as a result of impaired local defenses. The increase in bronchial bacterial load and associated increase in inflammation in a chronically infected patient may cause the symptoms of exacerbation; (ii) newly acquired infecting strains against which no immune protection exists may explain the occurrence of an exacerbation; (iii) a viral infection may impair the local defenses thus facilitating bacterial infection [5]. Furthermore, the Global Initiative for Chronic Obstructive Lung Disease (GOLD) therapeutic strategy requires a history of two or more exacerbations in the previous year as a key component to define frequent exacerbators [38,39]. In this context, we addressed the need for a disease model of such frequent exacerbator phenotype with bacterial origin, by presenting a novel mouse model of recurrent bacterial pulmonary infections in an emphysematous lung. Several groups have established animal models of bacterial exacerbation in COPD [15,40,41], and cigarette smoke and elastase/LPS treatment have been shown to exacerbate the inflammatory responses to NTHi in mice [13,14,16,19–21]. However, to the best of our knowledge, our model recapitulates, for the first time, the inflammatory component of the frequent exacerbator situation observed in COPD patients, by using two recurrent bacterial inoculations in a damaged murine lung undergoing emphysema lesions. From a mechanistic perspective, we may recall a situation half-way between the above cited "fall and rise" and newly infecting strain hypotheses, by generating recurrent infection by repeated inoculation of clonal bacteria.

The standard techniques used to evaluate infection in preclinical settings, i.e. microbial load quantification in homogenized tissues and microscopic observation, are severely limited by their invasive character, thus precluding the longitudinal evaluation of the disease in the same animal, and requiring sampling of high number of animals. Conversely, X-ray micro-CT imaging allows noninvasive longitudinal monitoring of disease progression. This technique was previously applied to the study of invasive pulmonary aspergillosis, cryptococcosis, *S. aureus* pneumonia, or lung lesions by *Streptococcus pyogenes* [23,28,42–44], and also to track emphysematous lesions over time in living mice and evaluate the progression of the associated alveolar destruction [24,27]. Indeed, the extent of emphysema in a mouse lung has been shown to correlate with the mean X-ray intensity, the prevalence of low-density areas, and/or the total lung volume. More relevant to our work, this imaging approach has been previously used to characterize a model of exacerbation in COPD, generated by administering a single dose of LPS into the trachea of mice with established emphysematous lung disease instigated by prior exposure to elastase [45]. Here, we go one step further, by using micro-CT to evaluate disease progression in a model consisting of a single or recurrent *H. influenzae* pulmonary infection in an emphysematous mouse lung, as a means of modeling COPD baseline and frequent exacerbation. Our quantitative micro-CT-based results show that the models of single (E+/I+), and especially of recurrent (E+/I2+) infection display clear radiological signs of lung inflammation that are higher in intensity and take longer to clear (3 weeks in the E+/I+ and 12 weeks in the E+/I2+ model) than the control model of infection on a non-emphysematous lung (V+/I+), clearing all radiological signs of inflammation in 1 week.

COPD clinical management normally includes pulmonary function tests, to measure the amount of air inhaled and exhaled, and whether the lungs deliver enough oxygen to the blood (spirometry, measurement of lung volumes and diffusing capacity, 6-minute walk test, pulse oximetry). Accordingly, we quantitatively characterized lung function in our mouse models

using passive tests of pulmonary function. By using both a single frequency and a more complex broad-band-forced oscillation model, we quantified the effect of the infectious process in the function of the lungs, observing in all cases (V+/I+, E+/I+, V+/I2+, E+/I2+), temporal trends in the main parameters tracked that closely parallel those observed by micro-CT imaging. This highlights the complementary value of both techniques that faithfully capture the lung damage caused by the inflammatory and elastolytic damage inflicted on the lungs, both at radiological and physiological levels. To further correlate our radiological findings with *in situ* measurements of inflammation, we measured the expression of pro-inflammatory cytokines associated with bacterial infection and inflammatory cell recruitment, supported by previous studies reporting how PMNs play key roles in parenchymal elastolytic degradation and actively contribute to emphysema progression [46,47]. These results suggest that the inflammatory response takes place immediately after instillation of NTHi and correlates over time with the development of inflammation areas on radiographic images as well as their effect on pulmonary function. In summary, our findings highlight the potential of micro-CT to perform longitudinal studies and provide accurate information on emphysema progression and inflammation development and clearance.

Another interesting outcome of this study is that recovery times for bacterial load clearance from the murine lungs and airways return to baseline symptoms, were uncoupled, and such uncoupling is different and amplified after recurrent infection. Thus, bacteria are cleared 48 h post-single infection but return to baseline symptoms takes up to 3 weeks in the exacerbator (E+/I+) model; even more, bacteria are cleared 96 h post-recurrent infection and return to baseline symptoms takes up to 12 weeks in the frequent exacerbator (E+/I2+) model. When translating into humans, patients recover to baseline symptoms after 7 d in half of exacerbations, but in about 14% of events patients do not return to baseline symptoms within 35 d of onset, and in a small proportion, symptoms never return to the baseline level. In fact, ~30% of exacerbated patients are seen again and possibly readmitted with another event within 8 weeks, and ~20% of moderate-severe COPD patients followed-up after exacerbation have a recurrent event within 50 d of the first one. Thus, an initial exacerbation increases susceptibility to a subsequent one, and patients with a history of frequent exacerbations have increased airway inflammation likely contributing to disease progression [2]. Overall, we put forward the notion that the E+/I2+ phenotype may nicely emulate several features of the COPD frequent exacerbator phenotype. The observed delays in both bacterial clearance and inflammatory lung recovery after re-infection, compared to single infection and non-infected control groups, are aligned with clinical observations, and with the notion of recurrent infection contributing to disease progression in a circular manner (Figure 6, upper graphs).

Our multimodal approach based on quantifying bacterial and host lung parameters, has shown to be highly complementary. However, we acknowledge several drawbacks and considerations. First, we initially considered bioluminescence imaging to obtain longitudinal information on the extent of bacterial load, but could not be reliably used. Bioluminescence was previously used by other groups to monitor NTHi infection within the nasopharynges, eustachian tubes and middle ear of chinchilla after intranasal and transbullar infections [48–50], but did not allow direct monitoring of bacterial movement from the nasopharynx to the middle ear in a *Junbo* mouse model of otitis media due to insufficient signal [33]. Bioluminesce monitoring of lung infection renders dissimilar results depending on mouse models, pathogens and strains [51]. Here, correlation of bioluminescence signal with bacterial loads was poor, maybe due to spread and dilution of the non-multiplying inoculum rendering insufficient signal for an imaging of the lower airways *in vivo*. This type of limitation was previously reported for *S. pneumoniae* and *Pseudomonas aeruginosa* [52,53]. Second, the number of recurrent infections in the same animal may be a limiting factor. Here, we performed two identical recurrent infections 1 week apart. After the second infection, the bacterial load recovered 24 hpi was lower than after the first one, maybe due to the increased animal weight or immune system insensitivity. This issue could be amplified in subsequent infections. Third, the quantification of alveolar cell destruction by Caspase-3 immunostaining showed a trend, but not a significant difference between the V+/I- and E+/I- groups. This is most likely due to the relatively low number of animals analyzed (n = 5), and the analysis time point. Indeed, 24 d after elastase instillation, which is an appropriate time point to evaluate the extent of emphysematous lesion, might be a late time to evaluate the level of alveolar destruction by means of the quantification of apoptotic cells. A future time course assay, including earlier times would allow investigating the apoptotic effect of elastase on alveolar cells from the time of elastase instillation on. Fourth, elastase-induced emphysema, which we acknowledge may have limitations when resembling the pathology seen in COPD, did not allow consistent sampling of bronchoalveolar lavage fluid, impairing the

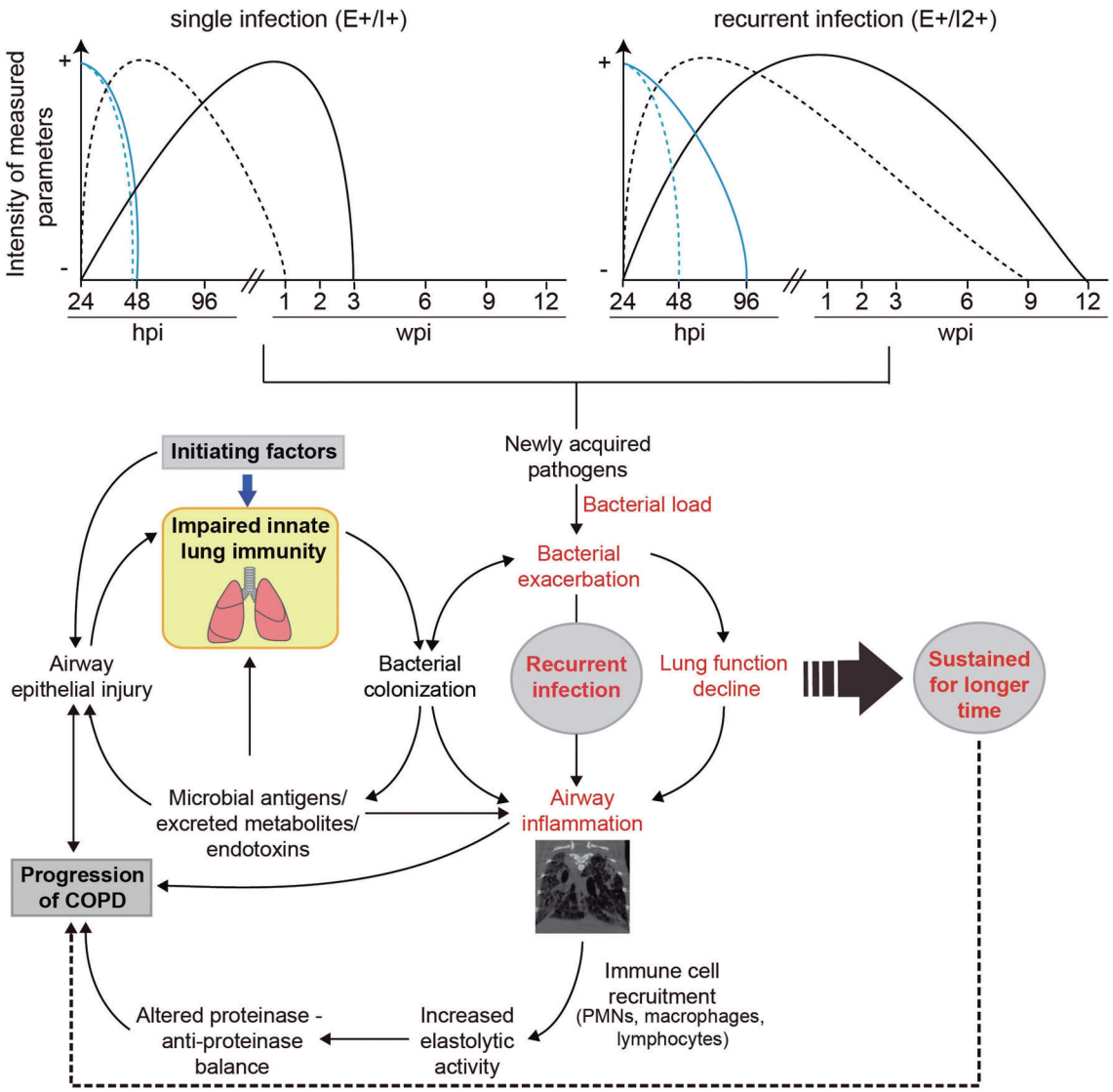

Figure 6. A disease model based on murine emphysematous lung recurrent bacterial infection in the context of the COPD vicious circle hypothesis. Alterations in innate defenses induced by inhalational exposure due to cigarette or biomass smoke allow pathogenic bacteria initiating the endless vicious circle that contributes to disease progression. By modeling increased elastolytic activity by elastase administration and combined use of longitudinal approaches, we observed that newly acquired opportunistic pathogenic bacteria contribute to the decline of pulmonary function and to airway inflammation. Respiratory parameters return to the baseline after bacterial clearance, but such return is much slower than bacterial clearance as such, and this delay is further amplified in the damaged lungs (single infection summary, upper left representation: E+/I+, continuous lines; V+/I+, dashed lines; bacterial load, blue lines; PFT and X-ray data, black lines). Recurrent infection exacerbates such gaps, heavily increasing lung recovery times, i.e. from 3 to 12 weeks after re-infection of emphysema lungs (recurrent infection summary, upper right representation: E+/I2+, continuous lines; V+/I2+, dashed lines; bacterial load, blue lines; PFT and X-ray data, black lines). This E+/I2+ situation may emulate features of the COPD frequent exacerbator phenotype.

analysis of inflammatory cells present in this type of samples. This could relate to the use of CD1 mice, in contrast to previous studies exposing C57BL/6 animals to LPS/elastase [19,45]. Along these lines, the choice of murine models and procedures to generate COPD-type lesions is likely to be a key factor in some aspects of the outcome. In fact, our data regarding bacterial load align nicely with those presented by Pang and coauthors [16], who observed that NTHi pulmonary clearance was impaired in elastase-treated mice. This is in conflict with Gaschler and coauthors [21], who observed accelerated clearance of NTHi from cigarette smoke-exposed mice. This discrepancy could be due to a higher NTHi-specific IgA in the cigarette smoke animals, or even to an inhibitory/cytotoxic effect of the cigarette smoke on NTHi. Finally, our decision to terminate the experiment at 12 weeks was based on the observation that at that time, we could not see

significant differences between double infected (E+/I2+) and non-infected (E+/I2-) animals, based on the PFT values and a qualitative visual examination of the micro-CT images. Therefore, we focused only in the short-term effect of emphysema in the duration and strength of the infection, monitored after each infectious attack, but not in the long-term effect of the exacerbation on the underlying emphysematous lung. It would be interesting to extend the study to look at the long-term effects of the infection on the baseline emphysema. The expected results of such a long-term study, based on our preliminary results, point to an exacerbation of emphysema in mice that undergo both NTHi infection and emphysema, compared to the non-infected emphysematous mice. This observation agrees with what is reported in the literature after LPS administration in elastase-treated mice [45] .

To conclude, the information presented here is integrated in the so-called COPD vicious-circle hypothesis [11], where the gradual lung damage and loss of function are consequences of successive rounds of microbial dysbiosis with anomalous inflammation, where new strains of opportunistic bacteria may account for about one-half of exacerbations. E+/I2+ modeled increased elastolytic activity and recurrent bacterial infection. This way, and by comparing E+/I2+ data with those obtained from E+/I+ and V+/I2+ animal groups through time, we could model the deleterious impact of recurrent lung infection, by sustaining bacterial load, lung function decline, and airway inflammation for longer time (Figure 6). Currently, COPD patients and their physicians face significant clinical challenges, including determining the bases for identifying the biological and clinical implications of the presence of pathogenic bacteria in the airways according to the COPD phenotype, next to exploring suitable treatments. Aligned with those needs, the mouse model presented here aims to provide an *in vivo* tool to facilitate investigating the COPD frequent exacerbator phenotype.

Acknowledgments

We thank Dr. Montserrat Barberán, Facultad de Veterinaria, Universidad de Zaragoza, Spain, for sample processing and scoring of histopathology lesions. This work has been funded by grants from MICIU (UE FEDER) SAF2015-66520-R, RTI2018-096369-B-I00, and RED2018-102469-T, from Health Department, Regional Navarra Govern, Spain, reference 03/2016, and from SEPAR 31/2015 to J.G.; from MICIU (UE FEDER) RTI2018-094494-B-C222 to C.O.S; from University, Innovation and Digital Transformation Department, Regional Navarra Govern, Spain, reference PC150-151-152 to J.G. and C.O.S. CIBER is an initiative from Instituto de Salud Carlos III (ISCIII), Madrid, Spain.

Disclosure of potential conflicts of interest

The authors declare no competing (financial or non-financial) interests.

Funding

This work was supported by the Departamento de Universidad, Innovación y Transformación Digital, Gobierno de Navarra [PC150-151-152]; Ministerio de Ciencia, Innovación y Universidades (MICIU), Gobierno de España [RTI2018-096369-B-I00]; MICIU, Gobierno de España [RED2018-102469-T]; MICIU , Gobierno de España [SAF2015-66520-R]; MICIU , Gobierno de España [RTI2018-094494-B-C222]; Departamento de Salud, Gobierno de Navarra [03/2016]; Sociedad Española de Neumología y Cirugía Torácica [31/2015].

ORCID

Begoña Euba http://orcid.org/0000-0001-5620-596X
Junkal Garmendia http://orcid.org/0000-0002-7440-2737

References

[1] Celli BR, Wedzicha JA. Update on clinical aspects of chronic obstructive pulmonary disease. N Engl J Med. 2019;381(13):1257–1266. Available from: https://www.ncbi.nlm.nih.gov/pubmed/31553837
[2] Wedzicha JA, Seemungal TA. COPD exacerbations: defining their cause and prevention. Lancet. 2007;370(9589):786–796. Available from: https://www.ncbi.nlm.nih.gov/pubmed/17765528
[3] Hurst JR, Vestbo J, Anzueto A, et al. Susceptibility to exacerbation in chronic obstructive pulmonary disease. N Engl J Med. 2010;363(12):1128–1138. Available from. https://www.ncbi.nlm.nih.gov/pubmed/20843247
[4] Waeijen-Smit K, Houben-Wilke S, DiGiandomenico A, et al. Unmet needs in the management of exacerbations of chronic obstructive pulmonary disease. Intern Emerg Med. 2021;16(1):1–11.
[5] Lopez-Campos JL, Miravitlles M, De La Rosa Carrillo D, et al. Current challenges in chronic bronchial infection in patients with chronic obstructive pulmonary disease. J Clin Med. 2020;9(6):1639. Available from: https://www.ncbi.nlm.nih.gov/pubmed/32481769
[6] Ahearn CP, Gallo MC, Murphy TF. Insights on persistent airway infection by non-typeable *Haemophilus influenzae* in chronic obstructive pulmonary disease. Pathog Dis. 2017;75(4):75.
[7] Chin CL, Manzel LJ, Lehman EE, et al. *Haemophilus influenzae* from patients with chronic obstructive pulmonary disease exacerbation induce more inflammation than colonizers. Am J Respir Crit Care Med. 2005;172(1):85–91.
[8] Duell BL, Su YC, Riesbeck K. Host-pathogen interactions of nontypeable *Haemophilus influenzae*: from commensal to pathogen. FEBS Lett. 2016;590

(21):3840–3853. Available from: https://www.ncbi.nlm.nih.gov/pubmed/27508518
[9] Look DC, Chin CL, Manzel LJ, et al. Modulation of airway inflammation by *Haemophilus influenzae* isolates associated with chronic obstructive pulmonary disease exacerbation. Proc Am Thorac Soc. 2006;3(6):482–483.
[10] Murphy TF, Brauer AL, Schiffmacher AT, et al. Persistent colonization by *Haemophilus influenzae* in chronic obstructive pulmonary disease. Am J Respir Crit Care Med. 2004;170(3):266–272. Available from: http://www.ncbi.nlm.nih.gov/pubmed/15117742
[11] Rangelov K, Sethi S. Role of infections. Clin Chest Med. 2014;35(1):87–100. Available from: https://www.ncbi.nlm.nih.gov/pubmed/24507839
[12] Mirza S, Benzo R. Chronic obstructive pulmonary disease phenotypes: implications for care. Mayo Clin Proc. 2017;92(7):1104–1112. Available from: https://www.ncbi.nlm.nih.gov/pubmed/28688465
[13] Ganesan S, Comstock AT, Kinker B, et al. Combined exposure to cigarette smoke and nontypeable *Haemophilus influenzae* drives development of a COPD phenotype in mice. Respir Res. 2014;15(1):11. Available from: https://www.ncbi.nlm.nih.gov/pubmed/24495712
[14] Herr C, Han G, Li D, et al. Combined exposure to bacteria and cigarette smoke resembles characteristic phenotypes of human COPD in a murine disease model. Exp Toxicol Pathol. 2015;67(3):261–269. Available from: https://www.ncbi.nlm.nih.gov/pubmed/25601416
[15] Perez-Rial S, Giron-Martinez A, Peces-Barba G. Animal models of chronic obstructive pulmonary disease. Arch Bronconeumol. 2015;51(3):121–127. Available from: https://www.ncbi.nlm.nih.gov/pubmed/25201221
[16] Pang B, Hong W, West-Barnette SL, et al. Diminished ICAM-1 expression and impaired pulmonary clearance of nontypeable *Haemophilus influenzae* in a mouse model of chronic obstructive pulmonary disease/emphysema. Infect Immun. 2008;76(11):4959–4967. Available from: https://www.ncbi.nlm.nih.gov/pubmed/18794286
[17] Starkey MR, Jarnicki AG, Essilfie A-T, et al. Murine models of infectious exacerbations of airway inflammation. Curr Opin Pharmacol. 2013;13(3):337–344.
[18] Fernandez-Calvet A, Rodriguez-Arce I, Almagro G, et al. Modulation of *Haemophilus influenzae* interaction with hydrophobic molecules by the VacJ/MlaA lipoprotein impacts strongly on its interplay with the airways. Sci Rep. 2018;8(1):6872.
[19] Ganesan S, Faris AN, Comstock AT, et al. Elastase/LPS-exposed mice exhibit impaired innate immune responses to bacterial challenge: role of scavenger receptor A. Am J Pathol. 2012;180(1):61–72. Available from: https://www.ncbi.nlm.nih.gov/pubmed/22079429
[20] Gaschler GJ, Skrtic M, Zavitz CC, et al. Bacteria challenge in smoke-exposed mice exacerbates inflammation and skews the inflammatory profile. Am J Respir Crit Care Med. 2009;179(8):666–675. Available from: http://www.ncbi.nlm.nih.gov/pubmed/19179487
[21] Gaschler GJ, Zavitz CCJ, Bauer CMT, et al. Mechanisms of clearance of nontypeable *Haemophilus influenzae* from cigarette smoke-exposed mouse lungs. Eur Respir J. 2010;36(5):1131–1142. Available from: http://erj.ersjournals.com/content/36/5/1131.abstract
[22] Wang D, Wang Y, Liu YN. Experimental pulmonary infection and colonization of *Haemophilus influenzae* in emphysematous hamsters. Pulm Pharmacol Ther. 2010;23(4):292–299. Available from: https://www.ncbi.nlm.nih.gov/pubmed/20211751
[23] Poelmans J, Hillen A, Vanherp L, et al. Longitudinal, *in vivo* assessment of invasive pulmonary aspergillosis in mice by computed tomography and magnetic resonance imaging. Lab Invest. 2016;96(6):692–704. Available from: https://www.ncbi.nlm.nih.gov/pubmed/27019389
[24] Artaechevarria X, Blanco D, De Biurrun G, et al. Evaluation of micro-CT for emphysema assessment in mice: comparison with non-radiological techniques. Eur Radiol. 2011;21(5):954–962. Available from. https://www.ncbi.nlm.nih.gov/pubmed/20953986
[25] Artaechevarria X, Munoz-Barrutia A, Ortiz-de-solorzano C. Combination strategies in multi-atlas image segmentation: application to brain MR data. IEEE Trans Med Imaging. 2009;28(8):1266–1277. Available from: https://www.ncbi.nlm.nih.gov/pubmed/19228554
[26] Artaechevarria X, Perez-Martin D, Ceresa M, et al. Airway segmentation and analysis for the study of mouse models of lung disease using micro-CT. Phys Med Biol. 2009;54(22):7009–7024. Available from: https://www.ncbi.nlm.nih.gov/pubmed/19887716
[27] Munoz-Barrutia A, Ceresa M, Artaechevarria X, et al. Quantification of lung damage in an elastase-induced mouse model of emphysema. Int J Biomed Imaging. 2012;2012:734734. Available from https://www.ncbi.nlm.nih.gov/pubmed/23197972
[28] Poelmans J, Himmelreich U, Vanherp L, et al. A multimodal imaging approach enables *in vivo* assessment of antifungal treatment in a mouse model of invasive pulmonary aspergillosis. Antimicrob Agents Chemother. 2018;62(7):62. Available from. https://www.ncbi.nlm.nih.gov/pubmed/29760132
[29] Löffek S, Schilling O, Franzke C-W. Series "matrix metalloproteinases in lung health and disease": biological role of matrix metalloproteinases: a critical balance. Eur Respir J. 2011;38(1):191–208.
[30] Koo H-K, Hong Y, Lim MN, et al. Relationship between plasma matrix metalloproteinase levels, pulmonary function, bronchodilator response, and emphysema severity. Int J Chron Obstruct Pulmon Dis. 2016;11:1129–1137.
[31] Lopez-Lopez N, Euba B, Hill J, et al. *Haemophilus influenzae* glucose catabolism leading to production of the immunometabolite acetate has a key contribution to the host airway–pathogen interplay. ACS Infect Dis. 2020;6(3):406–421. Available from. https://www.ncbi.nlm.nih.gov/pubmed/31933358
[32] Moleres J, Fernandez-Calvet A, Ehrlich RL, et al. Antagonistic pleiotropy in the bifunctional surface protein FadL (OmpP1) during adaptation of *Haemophilus influenzae* to chronic lung infection associated with

chronic obstructive pulmonary disease. MBio. 2018;9 (5). doi:10.1128/mBio.01176-18.

[33] Hood D, Moxon R, Purnell T, et al. A new model for non-typeable *Haemophilus influenzae* middle ear infection in the *Junbo* mutant mouse. Dis Model Mech. 2016;9(1):69–79. Available from. https://www.ncbi.nlm.nih.gov/pubmed/26611891

[34] Al-Hasan MN, Al-Jaghbeer MJ. Use of antibiotics in chronic obstructive pulmonary disease: what is their current role in older patients? Drugs Aging. 2020;37 (9):627–633. Available from: https://www.ncbi.nlm.nih.gov/pubmed/32691330

[35] Plusa T. Azithromycin in the treatment of patients with exacerbation of chronic obstructive pulmonary disease. Pol Merkur Lek 2020; 48:65–68. Available from: https://www.ncbi.nlm.nih.gov/pubmed/32218410.

[36] Euba B, Moleres J, Viadas C, et al. Relationship between azithromycin susceptibility and administration efficacy for nontypeable *Haemophilus influenzae* respiratory infection. Antimicrob Agents Chemother. 2015;59(5):2700–2712. Available from. http://www.ncbi.nlm.nih.gov/pubmed/25712355

[37] Huckle AW, Fairclough LC, Todd I. Prophylactic antibiotic use in COPD and the potential anti-inflammatory activities of antibiotics. Respir Care. 2018;63(5):609–619. Available from: https://www.ncbi.nlm.nih.gov/pubmed/29463692

[38] Labaki WW, Martinez FJ. Time to understand the infrequency of the frequent exacerbator phenotype in COPD. Chest. 2018;153(5):1087–1088. Available from: https://www.ncbi.nlm.nih.gov/pubmed/29731034

[39] Le Rouzic O, Roche N, Cortot AB, et al. Defining the "frequent exacerbator" phenotype in COPD: a hypothesis-free approach. Chest. 2018;153 (5):1106–1115. Available from. https://www.ncbi.nlm.nih.gov/pubmed/29054347

[40] Gaschler GJ, Bauer CMT, Zavitz CCJ, et al. Animal models of chronic obstructive pulmonary disease exacerbations. Contrib Microbiol. 2007;14:126–141. Available from https://www.ncbi.nlm.nih.gov/pubmed/17684337

[41] Wright JL, Cosio M, Churg A. Animal models of chronic obstructive pulmonary disease. Am J Physiol Lung Cell Mol Physiol. 2008;295(1):L1–15. Available from: https://www.ncbi.nlm.nih.gov/pubmed/18456796

[42] Mason WJ, Skaar EP. Assessing the contribution of heme-iron acquisition to *Staphylococcus aureus* pneumonia using computed tomography. PLoS One. 2009;4 (8):e6668. Available from: https://www.ncbi.nlm.nih.gov/pubmed/19688098

[43] Minami M, Sobue S, Ichihara M, et al. Analysis of the pathological lesions of the lung in a mouse model of cutaneous infection with *Streptococcus pyogenes*. Pathol Int. 2012;62(2):99–104. Available from: https://www.ncbi.nlm.nih.gov/pubmed/22243779

[44] Vanherp L, Ristani A, Poelmans J, et al. Sensitive bioluminescence imaging of fungal dissemination to the brain in mouse models of cryptococcosis. Dis Model Mech. 2019;12(6): Available from https://www.ncbi.nlm.nih.gov/pubmed/31101657

[45] Kobayashi S, Fujinawa R, Ota F, et al. A single dose of lipopolysaccharide into mice with emphysema mimics human chronic obstructive pulmonary disease exacerbation as assessed by micro-computed tomography. Am J Respir Cell Mol Biol. 2013;49(6):971–977. Available from. https://www.ncbi.nlm.nih.gov/pubmed/23822858

[46] Jasper AE, Sapey E, Walton GMMWJ. Understanding the role of neutrophils in chronic inflammatory airway disease. F1000Res. 2019;8:F1000Faculty Rev–557.

[47] Meijer M, Fj Rgt VO. Neutrophils and emerging targets for treatment in chronic obstructive pulmonary disease. Expert Rev Clin Immunol. 2013;9(11):1055–1068.

[48] Bookwalter JE, Jurcisek JA, Gray-Owen SD, et al. A carcinoembryonic antigen-related cell adhesion molecule 1 homologue plays a pivotal role in nontypeable *Haemophilus influenzae* colonization of the chinchilla nasopharynx via the outer membrane protein P5-homologous adhesin. Infect Immun [Internet] 2008; 76(1):48–55. Available from: https://www.ncbi.nlm.nih.gov/pubmed/17938212

[49] Mason KM, Munson JRS, Bakaletz LO. A mutation in the *sap* operon attenuates survival of nontypeable *Haemophilus influenzae* in a chinchilla model of otitis media. Infect Immun. 2005;73(1):599–608. Available from: https://www.ncbi.nlm.nih.gov/pubmed/15618200

[50] Novotny LA, Mason KM, Bakaletz LO. Development of a chinchilla model to allow direct, continuous, biophotonic imaging of bioluminescent nontypeable *Haemophilus influenzae* during experimental otitis media. Infect Immun. 2005;73(1):609–611. Available from: https://www.ncbi.nlm.nih.gov/pubmed/15618201

[51] Avci P, Karimi M, Sadasivam M, et al. *In vivo* monitoring of infectious diseases in living animals using bioluminescence imaging. Virulence. 2018;9(1):28–63. Available from: https://www.ncbi.nlm.nih.gov/pubmed/28960132

[52] Henken S, Bohling J, Ogunniyi AD, et al. Evaluation of biophotonic imaging to estimate bacterial burden in mice infected with highly virulent compared to less virulent *Streptococcus pneumoniae* serotypes. Antimicrob Agents Chemother. 2010;54(8):3155–3160. Available from: https://www.ncbi.nlm.nih.gov/pubmed/20530224

[53] Munder A, Wolbeling F, Klockgether J, et al. *In vivo* imaging of bioluminescent *Pseudomonas aeruginosa* in an acute murine airway infection model. Pathog Dis. 2014;72(1):74–77. Available from: https://www.ncbi.nlm.nih.gov/pubmed/24833236

Supplementary Material

Development and multimodal characterization of an elastase-induced emphysema disease mouse model for the COPD frequent bacterial exacerbator phenotype

Irene Rodríguez-Arce[1], Xabier Morales[2,3], Mikel Ariz[2,3], Begoña Euba[1], Nahikari López-López[1], Maider Esparza[2,3], Derek W. Hood[4], José Leiva[5-6], Carlos Ortíz-de-Solórzano[2,3,6#], Junkal Garmendia[1,7#]

[1]Instituto de Agrobiotecnología, CSIC (IdAB-CSIC)-Gobierno Navarra, Spain; [2]Laboratory of Preclinical Models and Analytical Tools, Division of Solid Tumors and Biomarkers, Center for Applied Medical Research (CIMA), Pamplona, Spain; [3]Centro de Investigación Biomédica en Red de Enfermedades Oncológicas (CIBERONC), Madrid, Spain; [4]Mammalian Genetics Unit, MRC Harwell Institute, Oxfordshire, United Kingdom; [5]Servicio de Microbiología, Clínica Universidad de Navarra, Pamplona, Spain; [6]Instituto de Investigación Sanitaria de Navarra (IdiSNA), Pamplona, Spain; [7]Centro de Investigación Biomédica en Red de Enfermedades Respiratorias (CIBERES), Madrid, Spain

Methods and Materials

Animal handling. CD1 female mice (18-20 g) aged 4 to 5 weeks (Charles River Laboratories) were housed under pathogen-free conditions at the IdAB-CSIC or CIMA animal facilities (registration numbers ES/31-2016-000002-CR-SU-US and ES31-2010000132). Animal handling and procedures were in accordance with European (Directive 2010/63/EU) and National (RD-53/2013) legislation, with the approval of the Universidad Pública de Navarra (UPNa), CIMA and CSIC Animal Experimentation Committees and local Government authorization (Protocols 141-16E1, E36-17/141-16E1, PI007/19).

Animal procedures. For emphysema induction, mice were anesthetized (isoflurane, Iso Vet) and placed supine on an upward inclined platform [1]. Then the appropriate solution was instilled oropharyngeally at the entrance of the throat using a Hamilton pipette (Hamilton) until its complete inhalation. The vehicle groups (V+) were instilled with 90 µl of physiological saline serum (Braun, Hessen, Germany). The emphysema groups (E+) were administered porcine pancreatic elastase (PPE, Elastin Products Company) as previously described [2]. Specifically, a 90 µl dose containing 6 PPE units/mouse (25 g) was administered to each animal. After elastase installation, mice were housed 17 days to wait for the stabilization of the emphysematous lesion.

The *H. influenzae* RdKW20 [3] and Xen21 (Caliper, PerkinElmer, [4]) strains were used for mouse lung infection (I+ and I2+ groups). Bacteria were grown at 37ºC, 5% CO_2 on chocolate agar (Biomérieux) or brain-heart infusion (BHI) agar supplemented with 10 µg/ml hemin and 10 µg/ml nicotinamide adenine dinucleotide (NAD), referred to as sBHI. NTHi liquid cultures were grown in sBHI at 37ºC, 5% CO_2. Infecting bacteria were previously grown on chocolate agar (stationary phase prior infection) [5–10]. Alternatively, bacteria were grown in sBHI with shaking (180 r.p.m.) and collected to OD_{600}=0.5-0.6 (exponential phase prior infection). For intranasal infection, 20 µl of a bacterial suspension containing ~$2x10^8$ CFU was placed at the

entrance of the nostrils until complete inhalation by each mouse, previously anesthetized with ketamine (Imalgene®, Merial) and xylazine (Rompun®, Bayer AG) (3:1). For oropharyngeal infection, 20 µl of a bacterial suspension containing ~2x10^8 CFU was administered with a Hamilton pipette to animals previously anesthetized with isoflurane.

When indicated, mice were euthanized by cervical dislocation, and lungs were aseptically removed. The left lung was individually weighed in sterile bags (Stomacher80, Seward Medical) and homogenized 1:10 (w/v) in PBS. Each homogenate was serially 10-fold diluted in PBS and plated in triplicate on sBHI agar to determine the number of viable bacteria. Results are shown as $\log_{10}$ CFU/lung. When indicated, the right lung was homogenized with TRIzol reagent (Invitrogen) for subsequent RNA extraction, or fixed in 10% neutral buffered formalin for histology.

When needed, AZM (Zytromax) treatment was performed at doses of 100 mg/kg of body weight in 0.1 ml water at 24, 12 and 1 hour before intranasal infection and administered by oroesophageal gavage (Popper&Sons Inc.), as described previously [8].

Detection of bacterial bioluminescence. Two assays were performed. In the first one, aimed at optimizing the NTHi administration route, 6 CD1 female mice were randomly divided into two groups (n=3, intranasal instillation; n=3 oropharyngeal instillation). All groups were sampled 5 minutes post-infection (mpi), 1, 6 and 24 hpi, and the bioluminescence signal was measured in both the nostrils and the lungs, with 15 min exposure time. Representative images for this assay are shown in **Figure S2D**, right panel. In second assay, aimed at determining the bacterial load after the oropharyngeal instillation, 32 CD1 female mice were randomly divided into five groups (three groups with n=4, control non-infected mice; two groups with n=10, NTHi infected mice): (i) healthy control mice (CON); (ii) mice instilled with a vehicle solution (V+/I-); (iii) mice with lung emphysema (E+/I-); (iv) mice instilled with a vehicle solution, and NTHi infected (V+/I+); (v) mice with lung emphysema, and

NTHi infected (E+/I+). Mice were sampled 1, 3, 6, 9, 12 and 24 hpi and the bioluminescence signal was measured over the lungs. Results for this assay are shown in **Figure 1C**. In all cases, animals were anesthetized with an intraperitoneal injection of ketamine (Imalgene®, Merial):xylazine (Rompun®, Bayer AG) (3:1), and placed in the ventro-dorsal position on the imaging tray of the PhotonImager Optima *in vivo* system (Biospace laboratory). Bioluminescence signal was captured using the Photoacquisition software (v3.5) using an exposure time of 15 min. For bioluminescence post-processing, the M3 Vision software (v1.1) was used. To do so, a region of interest (ROI) containing the bioluminescence signal was drawn manually around the lungs or on the nostrils. In parallel, a ROI surrounding the lower limbs was defined as the background signal. Bioluminescence measurements of these ROIs are expressed as mean ± SEM of photonic counts.

Pulmonary function tests (PFT). Animals were anesthetized with an intraperitoneal injection of ketamine (Imalgene®, Merial):xylazine (Rompun®, Bayer AG) (3:1), intratracheally cannulated, and connected to a flexiVent Legacy rodent ventilator (Scireq) at a rate of 200 breaths/min and a tidal volume of 10 ml/kg. Animals were kept breathing 2% isoflurane until completely anesthetized. Once the animals showed neither swallowing reflexes nor spontaneous breathing, lung physiological parameters were assessed using two maneuvers: (i) a single-frequency-forced oscillation technique (FOT) and (ii) a broadband-forced oscillation technique (BFOT). Briefly, the FOT maneuver consists of a single frequency (2.5 Hz), 1.25 second long volume-driven perturbation, which matches the mouse's ventilation rate (breaths/minute) and its tidal volume (mL/kg). Lung volume and pressure values measured during the perturbation are fitted to the classical lung single-compartment model by linear regression to obtain the overall lung resistance (R, $cmH_2O.s/mL$), compliance (C, mL/cmH_2O), and elastance (E, cmH_2O/mL). On the other hand, the BFOT consists of 8 seconds of complex-frequency perturbations ranging from 1 to 20.5 Hz, and the mouse lung

tidal volume (mL/kg). In this case, the lung volume and pressure values measured during the perturbation are fitted to a multi-compartment model that discriminates the response of the airways and lung tissue, to obtain the resistance of the central or conducting airways (Rn, $cmH_2O.s/mL$), as well as the resistance of the parenchyma (G, cmH_2O/mL), tissue elastance (H, cmH_2O/mL), and its inertance (I, $cmH_2O.s.s/mL$). All measurements were repeated at five times and averaged [11,12].

Breath-hold gated micro-CT imaging. Full thorax 3D tomographic images were acquired using an X-ray micro-CT (Micro-CAT II, Siemens PreClinical Solutions) with the following parameters: 80 kVp X-ray source voltage, 500 μA current, 450 ms camera exposure time per projection and 43×43 mm field of view. Seven hundred projections were acquired during forced, 12 cm H_2O iso-pressure 650 ms breath-holds. Normal breathing was induced during two respiratory cycles between breath-holds [13]. A total lung capacity (TLC) perturbation was performed every 20 breath-holds to prevent lung atelectasis [14]. The tomographic three-dimensional images obtained had a total of 640 slices with isotropic 46 μm voxel size and a resolution of 1024×1024 pixels per slice. The estimated X-ray dosage irradiated to the animal was 71.6 cGy per scan. Three-dimensional (3D) lung images were automatically reconstructed using the Cobra software (Exxim Computing Corporation) and processed using the Amira 3D Software for preclinical analysis (Thermo Scientific). A water phantom was used to calibrate the image to Hounsfield Units (HU).

Micro-CT 3D image reconstruction and quantification. 3D micro-CT images were processed using fully automated 3D image analysis tools. The lungs were first extracted following the next steps [15]: (i) a preliminary lung and airway tree segmentation is calculated using an automatic adaptive thresholding [16]; (ii) a convex hull containing the ribcage is obtained through a region growing algorithm using 900 HU seed voxels; (iii) a connectivity and topological analysis is performed to segment the lung tissue and discard other structures

with similar intensity in the image; (iv) a fine airway tree segmentation is carried out using the method by [17], based on a wavefront propagating through the trachea; (v) a final refinement process, including morphological filters and level sets, is applied to exclude the fuzzy boundaries produced by the respiratory motion artifact from the final segmentation. After removing the airway tree mask from the final lung segmentation mask, emphysema and infection quantification parameters were calculated using a home-made Fiji [18] plugin. Total lung volume and mean lung voxel intensity (MLVI) were obtained after applying the final segmentation mask to the original 3D image, together with the relative volume below -900 HU (RVB -900 HU). Finally, 3D renders were generated from the segmented masks using Amira V5.2 software (Thermo Fischer Scientific). To that aim, the RVB -900 HU values, that represent the extent of emphysema as indicated above, and the relative volume in the range of -30 HU to -150 HU, which encompasses areas of high inflammation damage as reported [19], were merged on the entire lung volume.

Histopathology. After fixation in 10% formalin, dissected lungs were embedded in paraffin, and 4- to 6 μm sections were stained with hematoxylin and eosin (H&E) by standard procedures, and examined by microscopy to determine the presence and extent of inflammatory lesions. Sections were examined blind as sets by a trained veterinary pathologist (Dr. M. Barberán). Parameters characterizing an acute inflammatory reaction in lower airways, including polymorphonuclear cell infiltrates (PMNs), alveolar macrophages, and lymphocytes were subjectively scored on a scale of 0 to 3 (0: absent, 1: mild, 2: moderate, 3: severe). For tissue control, similar organs obtained from V+/I- and E+/I- mice were processed in an identical manner. Images were observed and digitalized using an Olympus Vanox AHBS3 microscope coupled to an Olympus DP12 digital camera.

In parallel, to evaluate the main histopathological descriptors of emphysema, 20 CD1 female mice were randomly divided into four groups: (i) V+/I-; (ii) E+/I-; (iii) V+/I+; (iv) E+/I+.

Mice were anesthetized and subsequently sacrificed by exsanguination 1 wpi. Then, lungs were fixed at a constant pressure of 20 cm H_2O in 4% formalin in phosphate buffer for 1 h and subsequently immersed in formalin for 48 h. Lung lobes were disaggregated along their main bronchial axis and embedded in three paraffin blocks: (i) the first block contained the two halves of the left lung lobe (L1); (ii) the second block contained the upper and middle right lobes (L2 and L3, respectively); (iii) and the third block contained the lower and post-caval right lobes (L4 and L5, respectively). Two consecutive 3-micron sections were cut from each block maintaining the same orientation and height between the lobes and stained with H&E and Caspase-3 (Cell Signaling), respectively. Images were acquired at 20X magnification using a digital slide scanner (Aperio CS2, Leica). Images were analyzed using automated home-made plugins developed for Fiji/ImageJ. The five lung lobes of each section were quantified independently. Alveolar spaces were automatically segmented from the luminance component of the H&E images, by means of an image enhancement operation (i.e., a morphological opening filter) followed by image thresholding, and some image post-processing for refining the resulting binary mask. This mask was used to measure three histopathological descriptors of emphysema: (i) the mean linear intercept (MLI); (ii) a weighted mean measure of alveolar size (i.e., D2) using the distribution of equivalent diameters of individual alveolar spaces [20]; (iii) and the ratio of area of alveolar space with respect to the total lung tissue area (i.e., $R_{alv/tissue}$), calculated also automatically from the images. Similarly, Caspase-3 stained images were automatically quantified using the following image processing pipeline: a color deconvolution plugin [21] was first used to separate H&E and diaminobenzedine (DAB) staining. Then Caspase-3^+ cells were detected by thresholding the DAB component, followed by a sequence of post-processing operations: binary hole filling, median filtering, watershed algorithm for aggregated cell separation, and size filtering for artifact removal. Caspase-3^+ cell density 24 days after elastase instillation

was calculated by normalizing the number of Caspase-3^+ cells with respect to the total tissue area.

RNA extraction and RT-qPCR. Total RNA was isolated from mouse lungs using TRIzol reagent, and its quality was evaluated using RNA 6000 Nano LabChips (Agilent 2100 Bioanalyzer). All samples had intact 18S and 28S ribosomal RNA bands with RNA integrity numbers (RIN) between 9.3 to 10. Reverse transcription was performed using 1 µg of RNA by PrimerScript RT Reagent kit (Takara). To amplify mouse *kc*, *tnf-α* and *gapdh* genes, 1:10 diluted cDNA was used as template. In all cases, 20 µl reaction mixtures containing 1X SYBR Premix Ex Taq II (Tli RNaseH Plus) (Takara) and the adequate primer mix were used. Fluorescence data were analyzed with AriaMx Real-Time PCR System (Agilent Technologies). The comparative threshold cycle (Ct) method was used to obtain relative quantities of mRNAs that were normalized using mouse *gapdh* as an endogenous control. Intron-spanning primers were designed with Primer-BLAST software (NCBI) as described (**Table S1**) [22]. All measures were performed in triplicate and at least four times ($n \geq 4$).

Statistical analysis. In all cases, $p<0.05$ value was considered statistically significant. Analyses were performed using GraphPad Prism software, version 7 for Mac statistical package, and WRS2 R package [23] in RStudio for non-parametric robust ANOVAs. All analyses are detailed in each Figure caption.

Table S1. Primers used in this study

Primer name	Primer ID	Sequence (5'-3')	Purpose	Reference
kc-qPCR-F	1404	GACAGACTGCTCTGATGGCA	qRT-PCR	[7]
kc-qPCR-R	1405	TGCACTTCTTTTCGCACAAC	qRT-PCR	[7]
mgadph-qPCR-F	1430	CCCACTAACATCAAATGGGG	qRT-PCR	[24]
mgadph-qPCR-R	1431	CCTTCCACAATGCCAAAGTT	qRT-PCR	[24]
mTNFα-F	1592	AGGCACTCCCCCAAAAGATG	qRT-PCR	[7]
mTNFα-R	1593	GCTCCTCCACTTGGTGGTTT	qRT-PCR	[7]
mmp2-qPCR-F	1709	CGATGTCGCCCCTAAAACAG	qRT-PCR	In this study
mmp2-qPCR-R	1710	CTTGAGGGTATCTTTCAGCACAAA	qRT-PCR	In this study
mmp12-qPCR-F	1713	TGAGGCAGAAACGTGGACTAAA	qRT-PCR	In this study
mmp12-qPCR-R	1714	ATTGACTTTGGATTATTGGAATGCT	qRT-PCR	In this study

Supplementary Figures

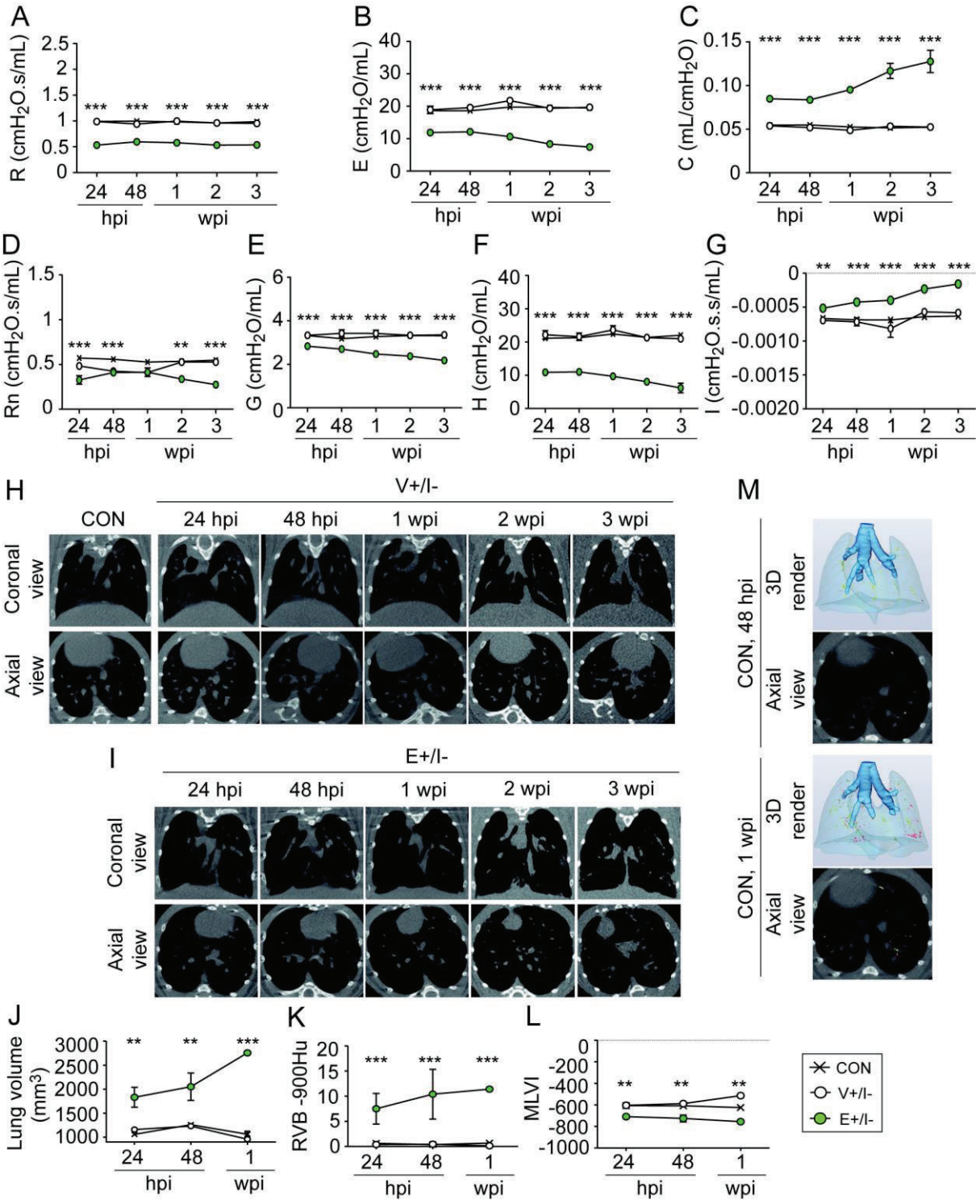

Figure S1. Elastase instillation induces pulmonary damage compatible with emphysema-like lesions. Mice were instilled with physiological saline solution (V+/I-) or received PPE (E+/I-). Pulmonary damage was evaluated 17 days after elastase instillation by pulmonary function tests (PFT) and micro-CT imaging at the indicated time points (24 and 48 hours; 1, 2 and 3 weeks). Mice groups: non-infected control with normal lung function (CON, black cross); V+/I- and E+/I-, white and green circles, respectively. **(A-G)** Evolution of pulmonary physiological parameters: **(A-C)** Lung resistance (R, cmH_2O.s/mL), elastance (E, cmH_2O

/mL) and compliance (C, mL/cmH_2O) measured by the single-frequency forced oscillation maneuver. **(D-G)** Airways (Rn, cmH_2O.s/mL) and parenchymal resistance (G, cmH_2O/mL), as well as tissue elasticity (H, cmH_2O/mL) and inertance (I, cmH_2O.s.s/mL) quantified by the broadband-forced oscillation technique. **(H-I)** Representative micro-CT images in the longitudinal section (upper row) and cross-section (bottom row) acquired from the chest of V+/I- and E+/I- mice. Mice with normal lung function are shown as control (CON). **(J-L)** Evolution of image parameters calculated from the micro-CT scans at the indicated time points (number of images, n≥ 3): **(J)** total lung volume (mm^3); **(K)** relative lung volume below -900 HU (RVB -900 HU); **(L)** mean lung voxel intensity (MLVI). **(M)** Representative 3D renders in the front view (upper row) and axial micro-CT slices (lower row) from the lungs of CON mice at the indicated times. Lung reconstructions show the main airways in solid blue, the lungs in transparent blue, the low-density areas in red (RVB -900 HU), and the high-density areas in yellow (RV -30/-150 HU). Axial micro-CT slices show RVB -900 HU and RV -30/-150 HU parameters merged on the radiographic image. Results are shown as mean ± SEM, statistical differences were analyzed using a two-way ANOVA and Bonferroni´s multiple comparisons test. *** $p<0.001$; ** $p<0.01$; * $p<0.05$.

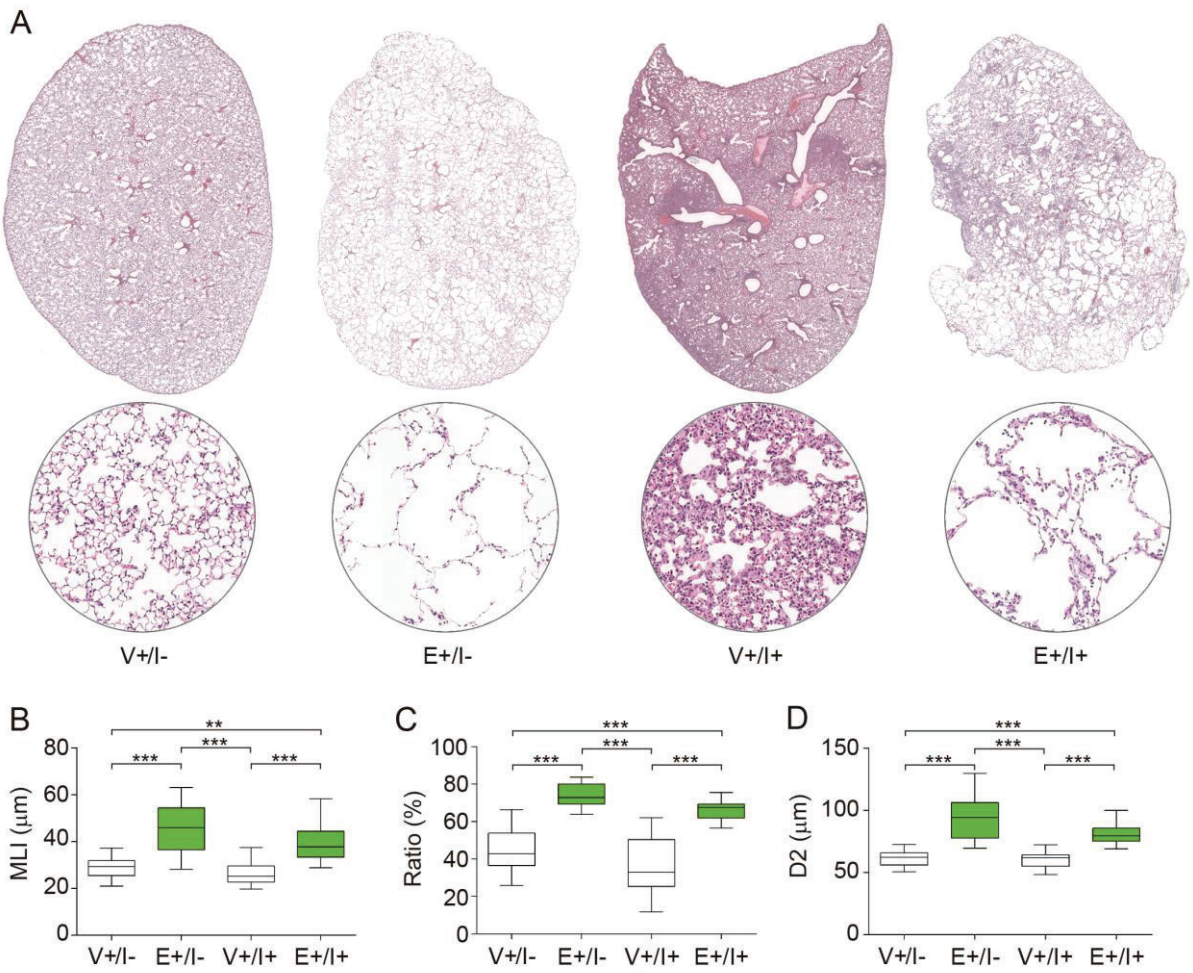

Figure S2. Quantitative histomorphological evaluation of emphysema severity from H&E tissue sections. (A) Representative 20X H&E sections showing the entire right upper lobe in both non-infected and infected vehicle (V+) and elastase-treated (E+) mice. The bottom row shows enlarged areas detailing the air spaces and the structure of the parenchyma for each group. **(B-D)** Automated quantification of the main histological descriptors of emphysema lesion: **(B)** MLI, **(C)** $R_{alv/tissue\ ratio}$ (%), and **(D)** D2 from images shown in A (number of mice, n=5 per group). The five lung lobes of each animal: right lobe (L1), upper (L2), middle (L3), lower (L4), and post-caval (L5) left lobes were quantified independently. Results are represented as box plot graphs (lines inside boxes represent median values). Statistical differences were analyzed using a two-way robust mixed ANOVA to evaluate both the effect of treatment (elastase or NTHi infection) and lobes. No effects between lobes were observed for all descriptors ($p=0.807$, $p=0.185$, and $p=0.413$ respectively), whereas treatment effect was confirmed between groups ($p<0.05$, $p<0.001$, and $p<0.01$ respectively). Differences between groups were further analyzed by Friedman test and Tukey's multiple comparisons test. *** $p<001$.

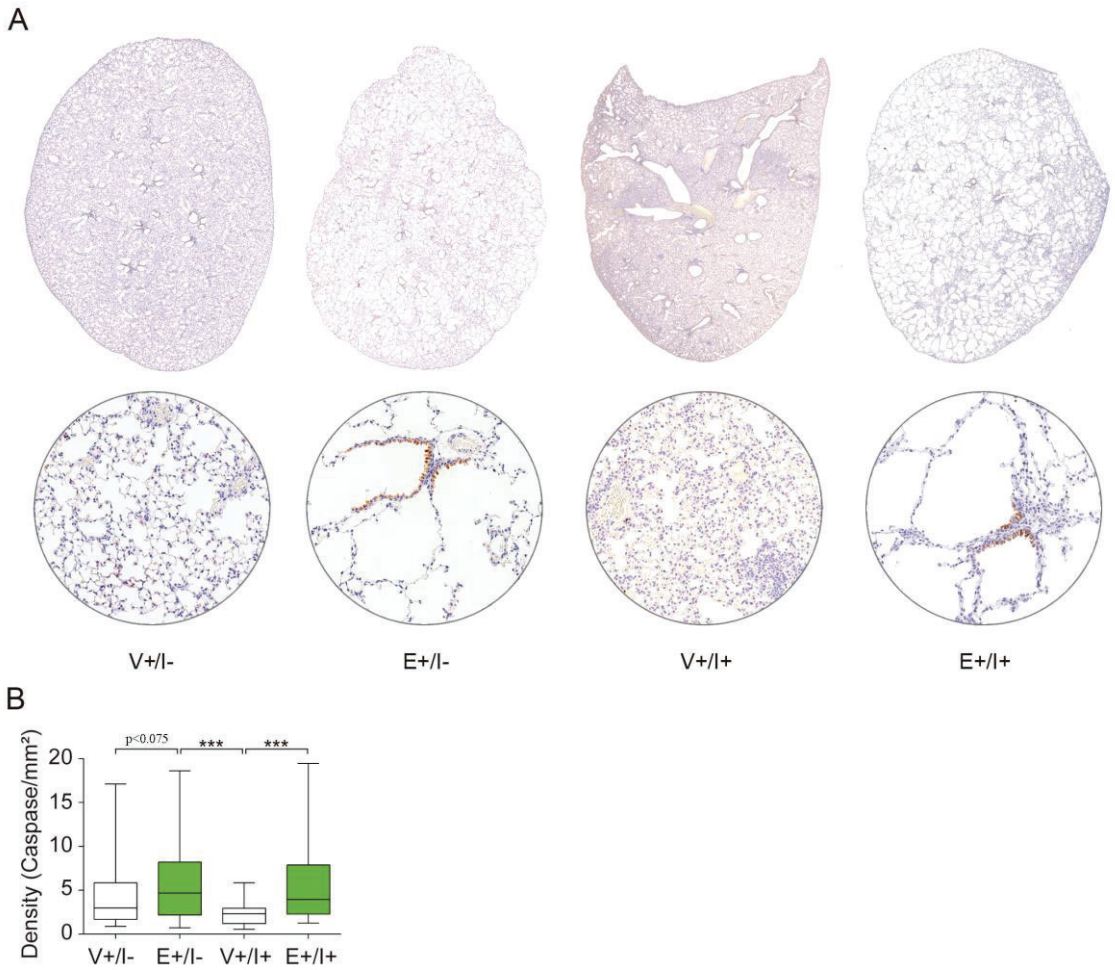

Figure S3. Evaluation of alveolar cell death within the lung parenchyma in mice exposed to elastase and NHTi infection. (A) Representative 20X Caspase-3 stained sections showing the entire right upper lobe in both non-infected and infected vehicle (V+) and elastase-treated (E+) mice, 24 days after elastase installation. The bottom row shows enlarged regions detailing apoptotic areas rich in Caspase-3^+ cells. **(B)** Automated quantification of Caspase-3^+ cells from images shown in **A** (number of mice, n=5 per group). The five lung lobes of each animal: right lobe (L1), upper (L2), middle (L3), lower (L4), and post-caval (L5) left lobes were quantified independently. Results are represented as box plot graphs as the density of Caspase-3^+ cells normalized per mm^2 (Caspase-3/mm^2) (lines inside boxes represent median values). Statistical differences were analyzed by the Friedman test and Tukey's multiple comparisons test. *** p<001.

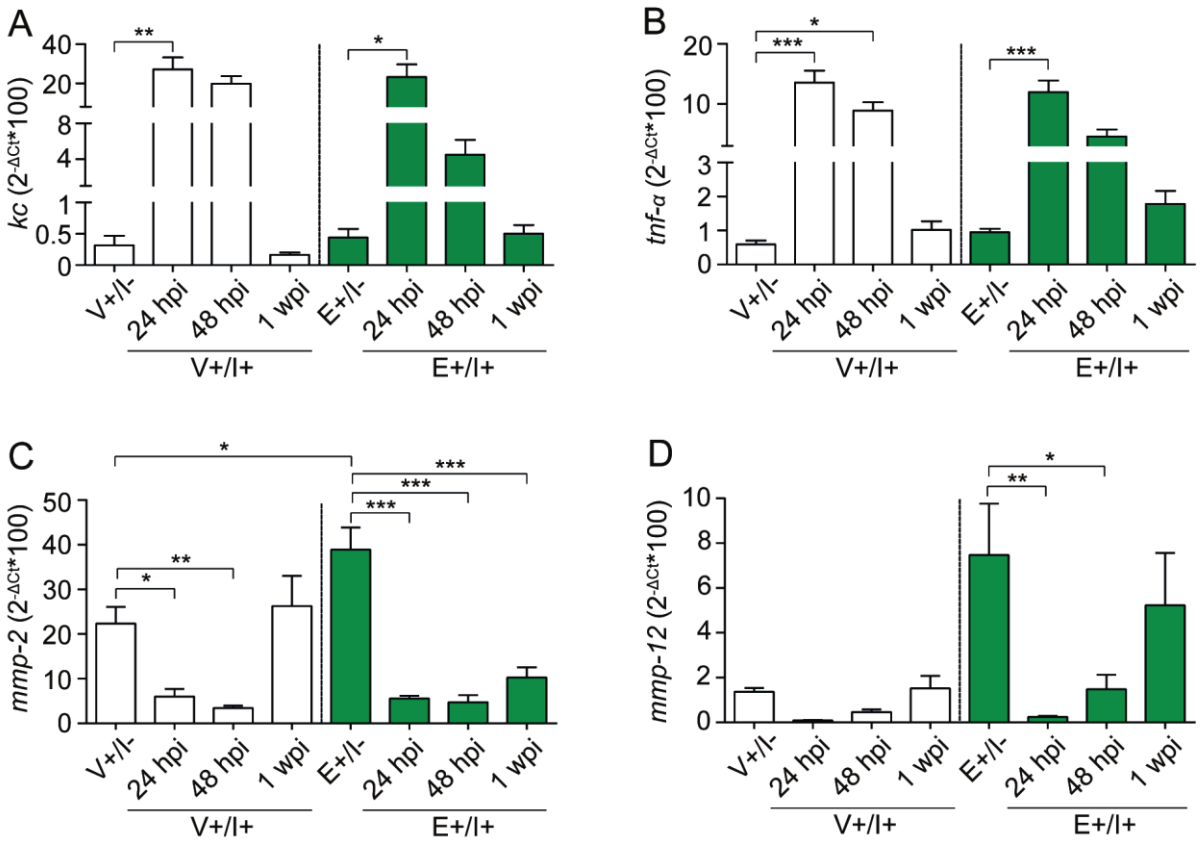

Figure S4. NTHi infection modulates the expression of molecular markers in the murine model. Relative quantities of mouse *kc*, *tnf-α*, *mmp-2*, and *mmp-12* mRNA were measured by RT-qPCR analysis on lung samples corresponding to V+/I- and V+/I+ (white bars); E+/I- and E+/I+ (green bars) groups. Results are shown as the relative quantity of each gene (mean ± SEM), statistical comparisons of the means were performed with one-way ANOVA and Tukey's multiple comparisons test. *** $p<0.001$; ** $p<0.01$; * $p<0.05$.

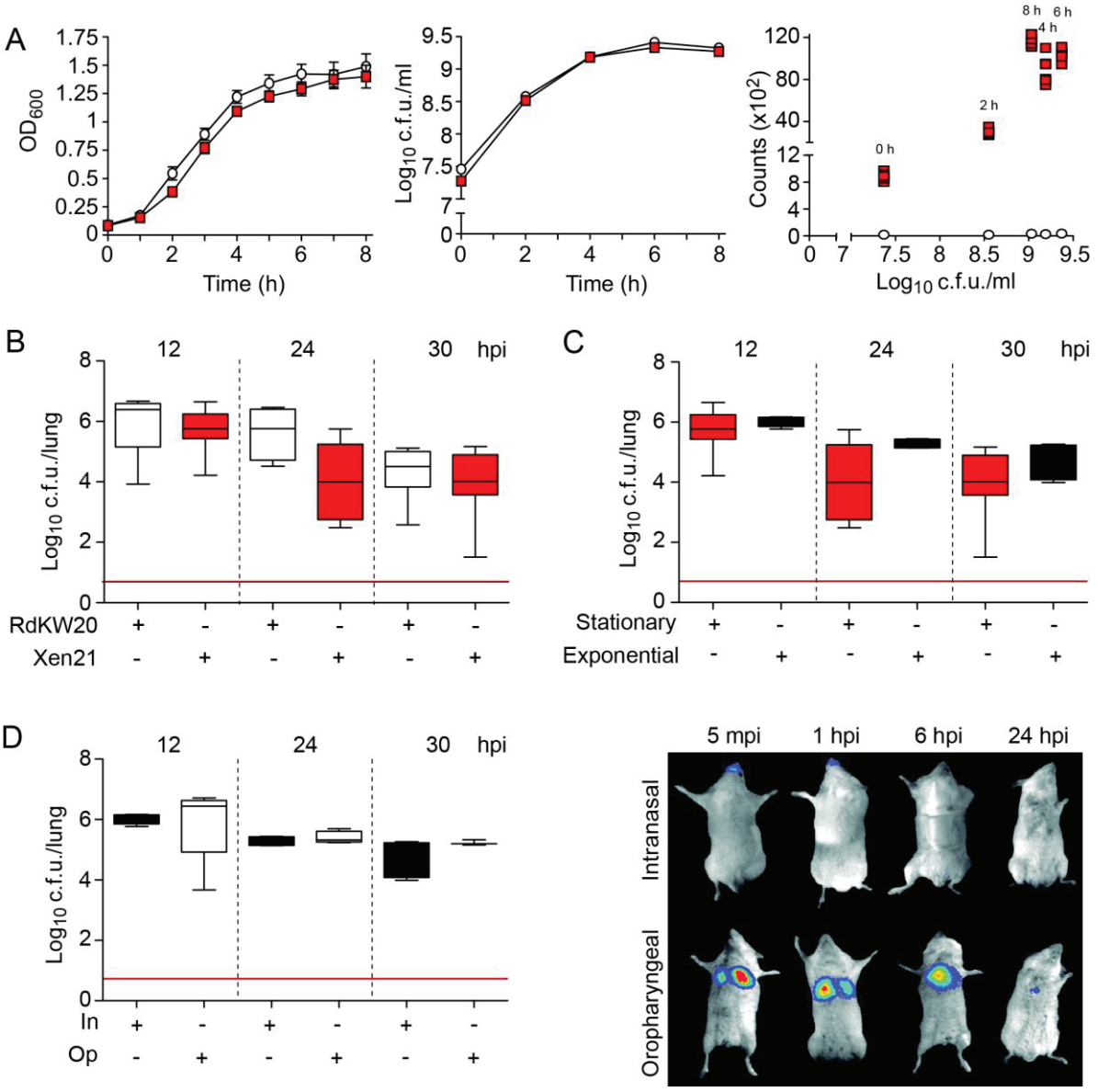

Figure S5. Optimizing experimental conditions for NTHi mouse emphysematous lung infection. (A) Bacterial growth is shown for *H. influenzae* RdKW20 (white circle) and its bioluminescent derivative Xen21 (red square) strains. Growth in sBHI is shown as a means of OD_{600} (left), log_{10} CFU/ml (middle), and bioluminescence (right), at the indicated time points. **(B)** CD1 mice were intranasally infected with 10^8 CFU of RdKW20 (white box) or Xen21 (red box), euthanized 12, 24 and 30 hpi, and bacterial loads were quantified in lungs (log_{10} CFU/lung). **(C)** Mice were intranasally infected with 10^8 CFU of Xen21, previously grown stationary (red box) or exponentially (black box), euthanized at 12, 24 and 30 hpi, and bacterial loads were quantified in lungs (log_{10} CFU/lung). **(D)** Mice were infected by the intranasal (In, black box) or oropharyngeal (Op, white box) route with 10^8 CFU of exponentially grown Xen21, euthanized at 12, 24 and 30 hpi, and bacterial loads were quantified in lungs (log_{10} CFU/lung) (left panel). Results are represented as box plot graphs (lines inside boxes represent median values). Statistical comparisons were performed using one-way ANOVA and Tukey's multiple comparison test. Bioluminescence was determined at 5 min, and at 1, 6 and 24 h post-infection, representative animals are shown (right panel).

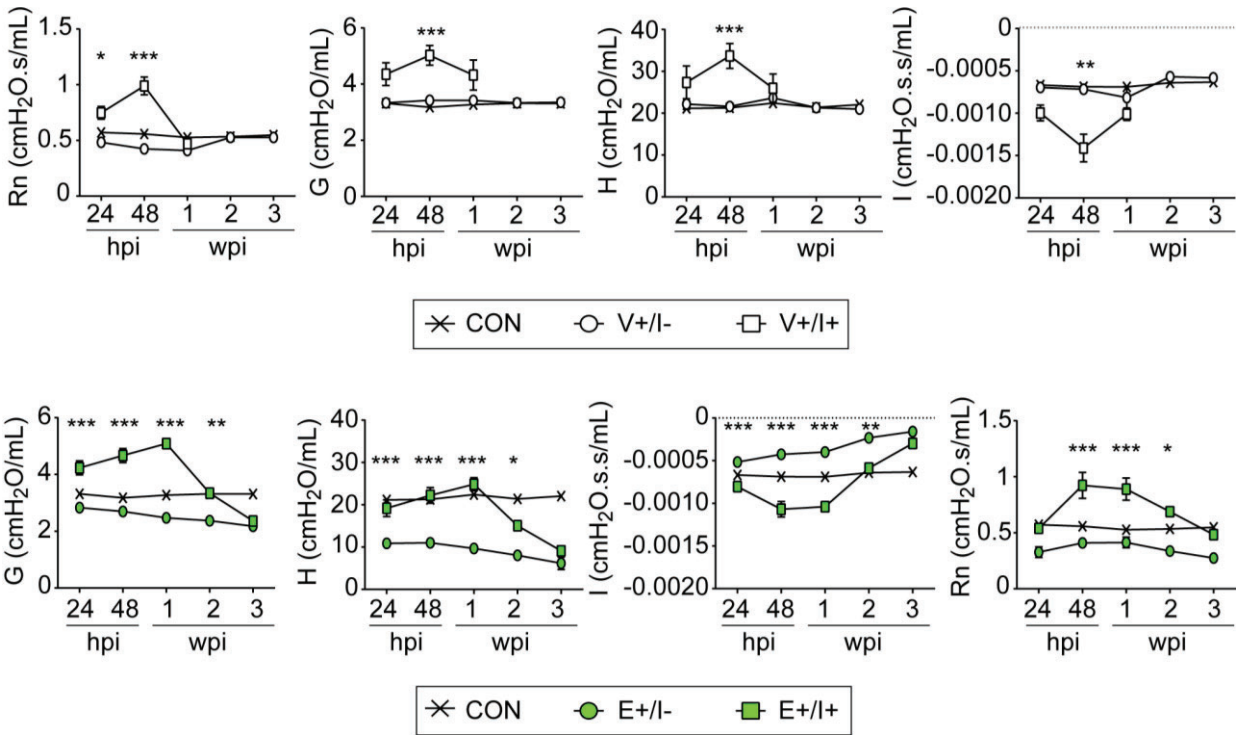

Figure S6. NTHi infection modifies lung physiology in the murine model. Evolution of pulmonary physiological parameters at the indicated after infection time points by PFT (24 and 48 hours; 1, 2 and 3 weeks). Mice groups: non-infected control with normal lung function (CON, black cross); V+/I- and E+/I-, white and green circles, respectively; V+/I+ and E+/I+, white and green squares, respectively. Airways resistance (Rn, $cmH_2O.s/mL$), parenchymal resistance (G, cmH_2O/mL), tissue elasticity (H, cmH_2O/mL), inertance (I, $mH_2O.s.s/mL$), quantified by the broadband-forced oscillation technique. Results are shown as mean ± SEM, statistical differences were analyzed using a two-way ANOVA and Bonferroni´s multiple comparisons test. *** $p<0.001$; ** $p<0.01$; * $p<0.05$.

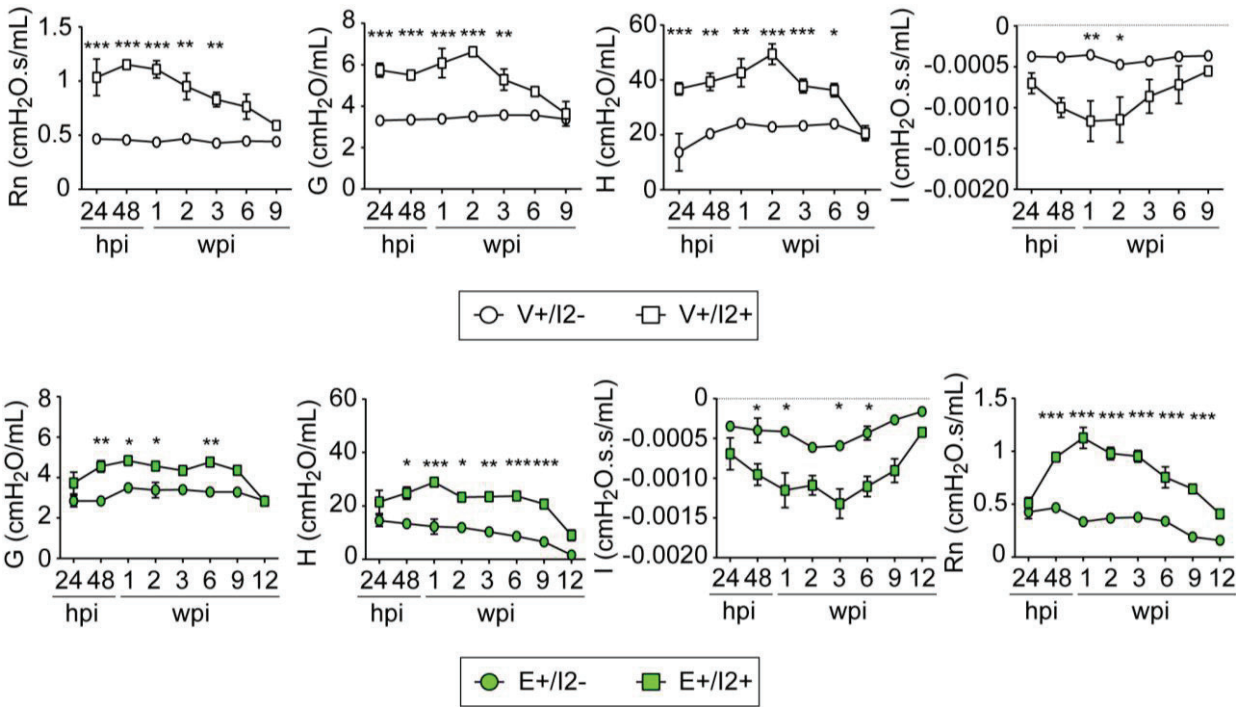

Figure S7. Recurrent NTHi infection exacerbates lung damage in mice. CD1 mice were infected with NTHi Xen21 on days -7 and 0, after instillation of physiological saline solution (V+/I2+) or PPE (E+/I2+), as indicated in **Figure 4A**. Evolution of physiological parameters at the indicated time points. Mice groups: V+/I2- and E+/I2-, white and green circles, respectively; V+/I2+ and E+/I2+, white and green squares, respectively (number of mice, n=7). Airways (Rn, $cmH_2O.s/mL$) and parenchymal resistance (G, cmH_2O/mL), as well as tissue elasticity (H, cmH_2O/mL) and inertance (I, $cmH_2O.s.s/mL$) quantified by the broadband-forced oscillation technique. Results are shown as mean ± SEM, statistical differences were analyzed using a two-way ANOVA and by Bonferroni´s multiple comparisons test. *** $p<0.001$; ** $p<0.01$; * $p<0.05$.

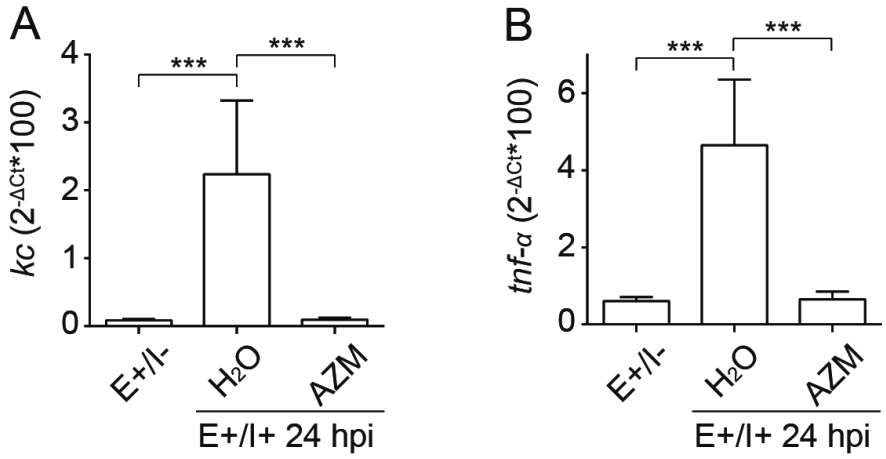

Figure S8. Expression of pro-inflammatory genes upon azithromycin treatment on NTHi infected mice. AZM (100 mg/kg/dose) or water, were administered oroesophageally to non-infected and infected animals, E+/I- and E+/I+ groups. Relative quantities of mouse *kc* and *tnf-α* mRNA were measured by RT-qPCR on lung samples. Results are shown as the relative quantity of each gene (mean ± SEM), statistical comparisons of the means were performed with one-way ANOVA and Tukey's multiple comparisons test. *** $p<0.001$.

References

1. Walters DM KSR. Mouse models of bleomycin-induced pulmonary fibrosis. Curr Protoc Pharmacol 2008; 5.46:1–17.
2. Lakatos HF, Burgess HA, Thatcher TH, Redonnet MR, Hernady E, Williams JP, Sime PJ. Oropharyngeal aspiration of a silica suspension produces a superior model of silicosis in the mouse when compared to intratracheal instillation. Exp Lung Res 2006; 32:181–99. Available from: https://www.ncbi.nlm.nih.gov/pubmed/16908446
3. Fleischmann RD, Adams MD, White O, Clayton RA, Kirkness EF, Kerlavage AR, Bult CJ, Tomb JF, Dougherty BA, Merrick JM, et al. Whole-genome random sequencing and assembly of *Haemophilus influenzae* Rd. Science (80-) 1995; 269:496–512. Available from: https://www.ncbi.nlm.nih.gov/pubmed/7542800
4. Hood D, Moxon R, Purnell T, Richter C, Williams D, Azar A, Crompton M, Wells S, Fray M, Brown SD, et al. A new model for non-typeable *Haemophilus influenzae* middle ear infection in the Junbo mutant mouse. Dis Model Mech 2016; 9:69–79. Available from: https://www.ncbi.nlm.nih.gov/pubmed/26611891
5. Rodriguez-Arce I, Marti S, Euba B, Fernandez-Calvet A, Moleres J, Lopez-Lopez N, Barberan M, Ramos-Vivas J, Tubau F, Losa C, et al. Inactivation of the thymidylate synthase thyA in non-typeable *Haemophilus influenzae* modulates antibiotic resistance and has a strong impact on its interplay with the host airways. Front Cell Infect Microbiol 2017; 7:266. Available from: https://www.ncbi.nlm.nih.gov/pubmed/28676846
6. Rodriguez-Arce I, Al-Jubair T, Euba B, Fernandez-Calvet A, Gil-Campillo C, Marti S, Tornroth-Horsefield S, Riesbeck K, Garmendia J. Moonlighting of *Haemophilus influenzae* heme acquisition systems contributes to the host airway-pathogen interplay in a coordinated manner. Virulence 2019; 10:315–33.
7. Euba B, Lopez-Lopez N, Rodriguez-Arce I, Fernandez-Calvet A, Barberan M, Caturla N, Marti S, Diez-Martinez R, Garmendia J. Resveratrol therapeutics

combines both antimicrobial and immunomodulatory properties against respiratory infection by nontypeable *Haemophilus influenzae*. Sci Rep 2017; 7:12860. Available from: https://www.ncbi.nlm.nih.gov/pubmed/29038519
8. Euba B, Moleres J, Viadas C, Barberan M, Caballero L, Grillo MJ, Bengoechea JA, de-Torres JP, Linares J, Leiva J, et al. Relationship between azithromycin susceptibility and administration efficacy for nontypeable *Haemophilus influenzae* respiratory infection. Antimicrob Agents Chemother [Internet] 2015; 59:2700–12. Available from: http://www.ncbi.nlm.nih.gov/pubmed/25712355
9. Euba B, Moleres J, Segura V, Viadas C, Morey P, Moranta D, Leiva J, De-Torres JP, Bengoechea JA, Garmendia J. Genome expression profiling-based identification and administration efficacy of host-directed antimicrobial drugs against respiratory infection by nontypeable *Haemophilus influenzae*. Antimicrob Agents Chemother 2015; 59:7581–92.
10. Fernandez-Calvet A, Rodriguez-Arce I, Almagro G, Moleres J, Euba B, Caballero L, Marti S, Ramos-Vivas J, Bartholomew TL, Morales X, et al. Modulation of *Haemophilus influenzae* interaction with hydrophobic molecules by the VacJ/MlaA lipoprotein impacts strongly on its interplay with the airways. Sci Rep 2018; 8:6872.
11. Hantos Z, Daroczy B, Suki B, Nagy S, Fredberg JJ. Input impedance and peripheral inhomogeneity of dog lungs. J Appl Physiol 1992; 72:168–78. Available from: https://www.ncbi.nlm.nih.gov/pubmed/1537711
12. Bates JH, Irvin CG. Measuring lung function in mice: the phenotyping uncertainty principle. J Appl Physiol 2003; 94:1297–306. Available from: https://www.ncbi.nlm.nih.gov/pubmed/12626466
13. Namati E, Chon D, Thiesse J, Hoffman EA, de Ryk J, Ross A, McLennan G. In vivo micro-CT lung imaging via a computer-controlled intermittent iso-pressure breath hold (IIBH) technique. Phys Med Biol 2006; 51:6061–75. Available from: https://www.ncbi.nlm.nih.gov/pubmed/17110770
14. Allen GB, Suratt BT, Rinaldi L, Petty JM, Bates JH. Choosing the frequency of deep inflation in mice: balancing recruitment against ventilator-induced lung injury. Am J Physiol Lung Cell Mol Physiol 2006; 291:L710-7. Available from: https://www.ncbi.nlm.nih.gov/pubmed/16698851
15. Gordaliza PM, Munoz-Barrutia A, Abella M, Desco M, Sharpe S, Vaquero JJ. Unsupervised CT lung image segmentation of a *Mycobacterium tuberculosis* infection model. Sci Rep 2018; 8:9802. Available from: https://www.ncbi.nlm.nih.gov/pubmed/29955159
16. Hu S, Hoffman EA, Reinhardt JM. Automatic lung segmentation for accurate quantitation of volumetric X-ray CT images. IEEE Trans Med Imaging 2001; 20:490–8. Available from: https://www.ncbi.nlm.nih.gov/pubmed/11437109
17. Artaechevarria X, Perez-Martin D, Ceresa M, de Biurrun G, Blanco D, Montuenga LM, van Ginneken B, Ortiz-de-Solorzano C, Munoz-Barrutia A. Airway segmentation and analysis for the study of mouse models of lung disease using micro-CT. Phys Med Biol 2009; 54:7009–24. Available from: https://www.ncbi.nlm.nih.gov/pubmed/19887716
18. Schindelin J, Arganda-Carreras I, Frise E, Kaynig V, Longair M, Pietzsch T, Preibisch S, Rueden C, Saalfeld S, Schmid B, et al. Fiji: an open-source platform for biological-image analysis. Nat Methods 2012; 9:676–82. Available from: https://www.ncbi.nlm.nih.gov/pubmed/22743772
19. Malherbe ST, Dupont P, Kant I, Ahlers P, Kriel M, Loxton AG, Chen RY, Via LE, Thienemann F, Wilkinson RJ, et al. A semi-automatic technique to quantify

complex tuberculous lung lesions on 18 F-fluorodeoxyglucose positron emission tomography/computerised tomography images. EJNMMI Res 2018; 8:55.
20. Parameswaran H, Majumdar A, Ito S, Alencar AM, Suki B. Quantitative characterization of airspace enlargement in emphysema. J Appl Physiol 2006; 100:186–93.
21. Ruifrok AC, Johnston DA. Quantification of histochemical staining by color deconvolution. Anal Quant Cytol Histol 2001; 23:291–9.
22. Fernández-Calvet A, Euba B, Caballero L, Díez-Martínez R, Menéndez M, Ortiz de Solórzano C, Leiva J, Micol V, Barrajón-Catalán E, Garmendia J. Preclinical evaluation of the antimicrobial-immunomodulatory dual action of xenohormetic molecules against *Haemophilus influenzae* respiratory infection. Biomolecules 2019; 9:891. Available from: https://www.mdpi.com/2218-273X/9/12/891
23. Mair P, Wilcox R. Robust statistical methods in R using the WRS2 package. Behav Res Methods 2020; 52:464–88.
24. Regueiro V, Moranta D, Frank CG, Larrarte E, Margareto J, March C, Garmendia J, Bengoechea JA. *Klebsiella pneumoniae* subverts the activation of inflammatory responses in a NOD1-dependent manner. Cell Microbiol 2011; 13:135–53.